UNIVERSITÉ DU QUÉBEC À MONTRÉAL

DÉVELOPPEMENT D'INHIBITEURS DE TEAD, PB1 ET BPTF, TROIS RÉGULATEURS DE L'EXPRESSION GÉNIQUE.

THÈSE

PRÉSENTÉE

COMME EXIGENCE PARTIELLE

DU DOCTORAT EN CHIMIE

PAR

LÉA MÉLIN

OCTOBRE 2021

REMERCIEMENTS

Dans un premier temps, je souhaite remercier mon superviseur, le professeur Alexandre Gagnon, pour m'avoir donné l'occasion d'effectuer ma thèse de doctorat au sein de son groupe de recherche. Nombre de réunions, de projets, de congrès et d'opportunités m'ont été offerts grâce à toi et je t'en suis extrêmement reconnaissante. Merci d'avoir cru en moi dès le début et de m'avoir encouragée jusqu'à la fin.

Les travaux de cette thèse n'auraient pas pu voir le jour sans la collaboration du Structural Genomics Consortium (SGC) de Toronto et de Zenith Epigenetics, Ltd. Un grand merci à vous tous ! Je remercie tout particulièrement Vijayaratnam Santhakumar, pour avoir coordonné les échanges avec l'ensemble des personnes travaillant au SGC et avoir toujours pris le temps de répondre à nos questions, ainsi que Matthieu Shapira, pour son accueil et sa supervision au sein de son groupe de recherche en chimie computationnelle. Merci aux membres de son équipe, surtout Renato Freitas, sans qui le chapitre III de cette thèse n'existerait pas. Ta patience et tes explications claires ont ouvert un tout nouveau pan de la chimie pour moi. J'aimerais également remercier Ahmed Aman et Michael Prakesch pour m'avoir pris sous votre aile au Ontario Institute for Cancer Research (OICR) le temps d'un été. Du côté de Zenith, je tiens à exprimer ma gratitude envers Henrik Hansen pour m'avoir fait entièrement confiance sur nos différents projets. Je remercie également Emily Gesner, Sarah Attwell, Olesya Kharenko, Cyrus Calosing et Edward van der Horst pour leur bienveillance constante à mon égard et leur accueil des plus chaleureux lors de mon séjour à Zenith. Une pensée toute particulière pour Emily Gesner qui m'aura initié à la réalisation des différents tests biochimiques. Merci aussi à Eric Campeau pour m'avoir donné l'enrichissante opportunité d'écrire un chapitre de livre.

Certains travaux ont nécessité la contribution d'autres groupes de recherche, c'est pourquoi je souhaite remercier les professeurs Borhane Annabi et Steven LaPlante ainsi que leurs équipes de recherche respectives pour les échanges stimulants que nous avons pu avoir ainsi que pour leurs apports non négligeables à cette thèse.

Bien entendu, ces remerciements ne seraient pas complets sans une mention spéciale à chacun de mes collèges. Ces années n'auraient vraiment pas été les mêmes sans vous ! Emeline, tu as été la première à qui j'ai parlé et, déjà à ce moment là, je savais que tu allais être spéciale pour moi. Des milliers d'heures de labo, des centaines de fous rires, des dizaines de coups de blues et un nombre incalculable de discussions plus tard, je ne sais même pas comment formuler ma reconnaissance à ton égard. Merci d'avoir été là, pour tout, tout le temps. Puis j'ai rencontré Adrien et Maxime. Que de souvenirs ! Entre vos musiques, vos chamailleries et vos conseils, votre duo de choc m'a accueilli à bras ouverts dès le début. Merci d'avoir rendu mes débuts au labo aussi faciles et agréables ! Ahmed, ta force tranquille et ton écoute ont également été précieuses pendant toutes ces années. Hwai-Chien, ta bonne humeur et ton énergie sans faille ont définitivement égayé mon quotidien, merci d'avoir toujours le mot pour rire. Bianca, ta touche de folie a apporté beaucoup à mes journées, merci pour ton enthousiasme et ton support inébranlable ! Yarelys, ta bienveillance et ton accent chantant ont participé à la bonne ambiance du labo et m'ont permis de tenir le coup quand on était juste toutes les deux au labo l'été dernier. Et Annabelle, même si on n'aura fait que se croiser au labo, saches que j'attendais toujours avec impatience nos petits points potins pendant que je faisais mes colonnes. Pour finir, Myriam, même si tu n'as été qu'une « Gagnon » le temps d'un été et ce avant même que j'arrive, je suis ravie d'avoir pu compter sur toi à l'UQAM et en dehors, merci pour tous ces moments !

Finalement, je tiens à remercier mes amis et ma famille, qui m'ont épaulé dans cette aventure du début à la fin. Tout particulièrement Alban, qui m'a écouté inlassablement raconter mes journées, qu'elles soient bonnes ou mauvaises. Merci de m'avoir supporté

sans broncher, ou presque, et d'avoir toujours cru en moi. Une grosse pensée aussi pour mes parents, qui ont été les premiers à m'encourager à commencer, et à finir, cette thèse de doctorat. Même à distance, je vous suis extrêmement reconnaissante de votre soutien inconditionnel.

TABLE DES MATIÈRES

LISTE DES FIGURES

LISTE DES TABLEAUX

LISTE DES ABRÉVIATIONS, DES SIGLES ET DES ACRONYMES

AACR : association américaine de la recherche contre le cancer

ADN : acide désoxyribonucléique

ADP : adénosine diphosphate

ARN : acide ribonucléique

ARNm : acide ribonucléique messager

ATP : adénosine triphosphate

BAF : *BRG1/BRM-associated factor*

BCP : protéine contenant des domaines bromés

BLI : *biolayer interferometry*

BPMC : *biased probability Monte Carlo*

BPTF : *bromodomain and PHD-finger containing transcription factor*

BPTFBrD : domaine bromé de BPTF

ccRCC : carcinomes rénaux à cellules claires

CHD : *chromodomain/helicase/DNA-binding domain*

CHD7 : *chromodomain-helicase-DNA-binding protein 7*

CSC : cellules souches cancéreuses

DBD : *DNA-binding domain*

DNA : *deoxyribonucleic acid*

DNMT : *DNA methyltransferase*

DPB : *DNA-binding protein*

DSF : *differential scanning fluorimetry*

ECEPP/3 : *empirical conformational energy program for peptides 3*

EMT : transition épithéliale-mésenchymateuse

FA : acide flufénamique

FALZ : *fetal alzheimer antigen*

FAS : *first apoptosis signal*

FEP : *free energy pertubation*

FP : polarisation de fluorescence

HAT : histone acétyltransférase

HB : *hydrogen bond*

HDAC : histone désacétylase

HMT : histone méthyltransférase

HSA : *helicase-SANT*

HTH : *helix-turn-helix*

HTRF : *homogenous time-resolved fluorescence resonance energy transfer*

HTS : *high-throughput screening*

HTVS : *high-throughput virtual screening*

INO80 : *inositol requiring 80*

ISWI : *imitation switch*

ITC : *isothermal titration calorimetry*

Lats1/2 : *large tumor suppressor kinase 1*

LE : *ligand efficiency*

LR : ligand de référence

LT : ligand à tester

MAZ : *Myc-associated zinc-finger protein*

MBT : *malignant brain tumor*

MMFF : *merck molecular force field*

Mst1/2 : *macrophage stimulating ½*

NA : acide niflumique

NCI : *National Cancer Institute*

NF2 : *neurofibromin 2*

NK : *natural killers*

NURF : *nucleosome-remodeling factor*

PB1 : *polybromo-1 protein*

PCNA : *proliferating cell nuclear antigen*

PBAF : *polybromo-associated BAF*

PHD : *plant homeodomain*

PRR : *prolin-rich region*

PWWP : proline – tryptophane – tryptophane – proline

RASSF : *Ras association domain family*

RMSD : écart quadratique moyen

RMSF : fluctuation moyenne pondérée

RUNX : *Runt related transcription factor*

SANT : Swi3, Ada2, N-Cor et TFIIIB

SMARCA2/4 : *SWI/SNF-related, matrix-associated actin-dependent regulator of chromatin, subfamily A2/4*

SP : *standard-precision docking*

SPR : *surface plasmon resonance*

SWH : Salvador-Warts-Hippo

SWI/SNF : *switch/sucrose non-fermentable*

TAF : *TBP-associated factors*

TAZ : *transcriptional co-activator with PDZ-binding motif*

TBD : domaine de liaison à TEAD N-terminal (*N-terminal TEAD-binding domain*)

TEAD : *transcriptional enhancer factor with TEA/ATTS domain*

TFIIIB : *transcription factor III B*

TGCA : *The Cancer Genome Atlas*

TNF-α : facteur de nécrose tumorale alpha aussi appelé cachectine

WWTR1 : *WW domain containing transcription regulator 1*

XP : *extra-precision docking*

YAP : *yes-associated protein*

YBD : *YAP-binding domain*

LISTE DES SYMBOLES ET DES UNITÉS

ΔG : énergie libre de Gibbs

G : énergie libre

k_B : constante de Boltzmann

kcal : kilocalories

mol : moles

T : température

RÉSUMÉ

Une expression génique spécifique permet à chaque cellule de se différencier et de participer au phénotype sain ou malade de tout individu. Le contrôle de l'expression de nombreux gènes s'effectuant lors de l'initiation de la transcription de l'ADN (acide désoxyribonucléique), les facteurs de transcription, les modificateurs épigénétiques ainsi que les remodeleurs de chromatine se retrouvent en première ligne de cette machinerie complexe. En raison de leur rôle primordial, des mutations au niveau de ces protéines sont fréquemment associées à diverses maladies, notamment le cancer. Ces liens de plus en plus nombreux mettent en évidence l'importance de développer des sondes chimiques puissantes et sélectives afin d'aider à comprendre la fonction exacte de chacun de ces points de contrôle et, potentiellement, d'aboutir au développement de nouvelles thérapies contre le cancer.

Dans ce contexte, les travaux de cette thèse de doctorat ont principalement porté sur la conception et la synthèse d'inhibiteurs de trois régulateurs de l'expression génique. Tout d'abord, des inhibiteurs du facteur de transcription TEAD (*transcriptional enhancer factor with TEA/ATTS domain*). Dans le cadre de son interaction avec son co-facteur YAP (*yes-associated protein*), ce complexe est responsable de l'expression de gènes contribuant principalement à la croissance cellulaire et à la prolifération. Les travaux menés ont conduit sur de nouveaux dérivés de l'acide flufénamique comme **LM98** se liant de façon réversible dans la poche palmitique de TEAD, permettant ainsi une inhibition de l'auto-palmitoylation de TEAD et une réduction de l'activité transcriptionnelle associée à YAP-TEAD. Différentes modélisations moléculaires et des criblages virtuels à haut débit ont également été réalisés afin de faciliter les efforts de conception. Par la suite, des inhibiteurs sélectifs des domaines bromés de PB1 (*polybromo-1 protein*) ont été développés. PB1 est une protéine unique contenant six domaines bromés qui agit comme lecteur épigénétique pour le compte du remodeleur de chromatine PBAF (*polybromo-associated BAF*). Les travaux réalisés ont permis l'obtention de **LM146**, une sonde chimique puissante présentant une sélectivité accrue contre les autres domaines bromés existants, y compris SMARCA2. Pour finir, des études sur BPTF (*bromodomain and PHD-finger containing transcription factor*), une protéine multidomaines servant de sous-unité principale pour le remodeleur de chromatine NURF (*nucleosome-remodeling factor*), ont été entreprises. Cette thèse de doctorat aura ainsi permis de rapporter pour la première fois la synthèse de **NVS-BPTF-1**, un inhibiteur sélectif du domaine bromé de BPTF.

Mots clés : chimie médicinale, sonde chimique, inhibiteur, TEAD, YAP-TEAD, facteur de transcription, modélisation moléculaire, criblage virtuel à haut débit, PB1, domaine bromé, lecteur épigénétique, PBAF, remodeleur de chromatine, BPTF, NURF, NVS-BPTF-1.

ABSTRACT

Specific gene expression allows cells to differentiate and participate to the phenotype of each healthy or sick individual. The expression checkpoint of many genes occurs during the DNA transcription initiation, which implies that transcription factors, epigenetic modifiers, and chromatin remodelers are key proteins involved. Because of their essential role for gene expression regulation, mutations within any of these proteins is often associated with numerous types of diseases, including cancer. As increasing evidence is being discovered, the importance of developing potent and selective chemical probes against these targets is being highlighted. These inhibitors would help to better understand the exact function of these proteins and, hopefully, would pave the way to new therapies against cancer.

In this context, this thesis has mainly focused on the design and synthesis of inhibitors of gene expression regulators. First, inhibitors of TEAD transcription factor were probed. When interacting with its co-factor YAP, this complex is responsible for gene expression associated with cell growth and proliferation. The work accomplished led to new fluflenamic acid derivatives such as **LM98** that binds in a reversible fashion to the palmitic pocket of TEAD, therefore inhibiting TEAD's autopalmitoylation and reducing YAP-TEAD transcriptional activity. Diverse molecular modeling and high-throughput virtual screening were performed in order to facilitate the design process. Then, the focus was switched to PB1 inhibitors. PB1 is a unique protein that contains six distinct bromodomains and acts as an epigenetic reader for the chromatin remodeler PBAF. **LM146**, a potent chemical probe with unprecedented selectivity against other bromodomains, including SMARCA2, was obtained at the end of this project. Finally, studies on BPTF, a multidomain protein serving as the major subunit for the chromatin remodeler NURF, were performed. This led to the first report of **NVS-BPTF-1** synthesis, a selective inhibitor of BPTF bromodomain.

Keywords : medicinal chemistry, chemical probe, inhibitor, TEAD, YAP-TEAD, transcription factor, molecular modeling, high-throughput virtual screening, PB1, bromodomain, epigenetic reader, PBAF, chromatin remodeler, BPTF, NURF, NVS-BPTF-1.

CHAPITRE I

INTRODUCTION

Ce chapitre commencera par une courte présentation des mécanismes de régulation de l'expression génique chez les eucaryotes. Les acteurs responsables de la régulation de la transcription seront ensuite abordés plus en détail, incluant notamment les facteurs de transcription, les modificateurs épigénétiques ainsi que les remodeleurs de chromatine. Enfin, trois cas spécifiques seront étudiés : (1) le facteur de transcription TEAD (*transcriptional enhancer factor with TEA/ATTS domain*), tout particulièrement dans le cadre de son interaction avec son co-facteur YAP (*yes-associated protein*), (2) la protéine contenant des domaines bromés PB1 (*polybromo-1 protein*), sous-unité du remodeleur de chromatine PBAF (*polybromo-associated BAF*), (3) la protéine multidomaines BPTF (*bromodomain and PHD-finger containing transcription factor*), sous-unité du remodeleur de chromatine NURF (*nucleosome-remodeling factor*). Les travaux de recherche de cette thèse, à savoir le développement d'inhibiteurs des trois régulateurs de l'expression génique cités au-dessus, seront par la suite abordés chapitre par chapitre.

Le phénotype de tout être vivant, y compris les traits caractéristiques d'individus malades, est un savant mélange entre causes génétiques et environnementales. Chez l'humain, l'information génétique contenue dans le noyau cellulaire réside au sein de 46 chromosomes, soit 22 paires d'autosomes et deux gonosomes. Avec près de 20 000 gènes,[1] contenus dans presque chacune des 37.2 trillions de cellules qui constituent le corps humain,[2] comment expliquer la diversité de types cellulaires ?

1.1 Régulation de l'expression génique

En dépit du fait que chaque cellule contienne un génome identique, de nombreuses études ont montré le lien entre morphologie/fonction cellulaire et expression génique spécifique.[3] L'expression d'une partie seulement des gènes encodés par l'acide désoxyribonucléique (ADN) permet ainsi à chaque cellule de se différencier. L'expression des gènes passe par deux étapes clefs chez les eucaryotes, à savoir la transcription et la traduction, et, comme illustré au niveau de la Figure 1.1, de nombreux points de contrôle existent tout le long de cette machinerie.[4,5] La transcription est par exemple régulée par les facteurs de transcription, les marques épigénétiques et l'accessibilité à la chromatine.[6,7] Il est également possible d'agir sur la transformation de l'ARNm (notamment via l'épissage, la polyadénylation ou l'ajout d'une coiffe), son transport ou sa dégradation.[8] La traduction peut quant à elle être facilement activée ou inhibée.[9] Pour finir, l'activité d'une protéine reste modulable via les multiples modifications post-traductionnelles qu'elle peut encore subir.[10] En prenant également en compte la régulation des différentes voies de dégradation protéasomique, il est indéniable que ces nombreuses étapes permettent d'ajuster avec précision l'expression des gènes dans chaque cellule.

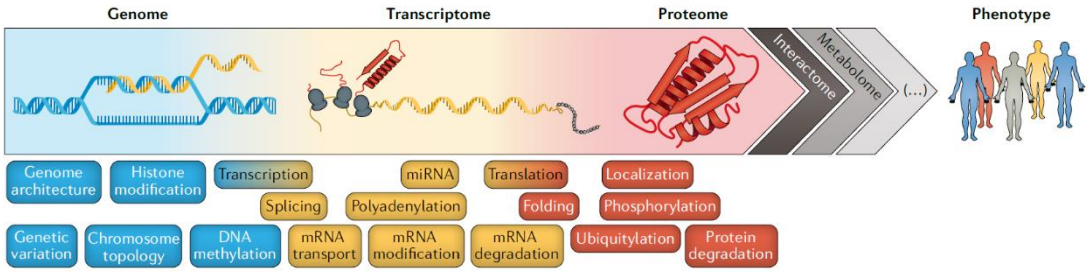

Figure 1.1 Du génome au phénotype, de nombreuses étapes pour réguler l'expression des gènes[4]

Différents gènes peuvent être régulés à différentes étapes et, à l'inverse, certains gènes importants sont quant à eux soumis à plusieurs points de contrôle. Malgré tout, les études convergent pour dire que la régulation de la transcription, tout particulièrement son étape d'initiation, est clef pour le contrôle de l'expression de nombre d'entre eux.[11] Pour cette raison, la suite des travaux présents dans cette thèse se concentrera sur cette partie.

1.2 Régulation de la transcription

Comme vu précédemment, la transcription est essentiellement contrôlée par les facteurs de transcription, le marquage épigénétique et la topologie de la chromatine. S'il est évident que des facteurs extrinsèques à la cellule (température, niveau d'oxygène, protéines/molécules envoyées par d'autres cellules ou par l'environnement du sujet, etc.) ont un impact sur certains des régulateurs transcriptionnels,[12,13] les facteurs intrinsèques seront priorisés pour des raisons de clarté.

1.2.1 Facteurs de transcription

Les facteurs de transcription sont des protéines qui se lient à des séquences de régulation de l'ADN, également appelées séquences-*cis*, afin de moduler le niveau de transcription d'un gène.[14] En contrôlant quand, où et avec quelle efficacité l'ARN polymérase II agit, ils jouent un rôle crucial dans la régulation de l'expression génique

chez les eucaryotes.[15] Aussi divers soient-ils, il est possible de les séparer en trois grandes familles basées sur leur fonction :

- Les facteurs de transcription généraux.[16] Ils permettent à l'ARN polymérase II de se lier au promoteur du gène et sont donc nécessaires à l'initiation de la transcription. Par conséquent, ils sont omniprésents dans l'ensemble des cellules.[17]
- Les activateurs de transcription.[18] Ils stimulent l'expression génétique en favorisant la formation du complexe de transcription. L'amplificateur sur lequel ils se lient peut se situer jusqu'à des centaines de paires de base de l'ADN en amont du promoteur.[19]
- Les inhibiteurs de transcription.[20] Plus rares, ils réduisent, voire abolissent, l'expression génique en gênant la formation du complexe de transcription de façon directe ou indirecte.

Bien entendu, d'autres systèmes de classement existent, le plus commun étant établi sur l'homologie du domaine se liant à l'ADN (*DNA-binding domain*, soit DBD). Bien qu'une grande diversité structurale existe, 4 grandes familles se distinguent : les facteurs de transcription qui possèdent des DBD (1) basiques, (2) se coordonnant au zinc, (3) hélices-coude-hélices (*helix-turn-helix*, soit HTH), (4) de type *β-scaffold factors with minor groove contacts* (Figure 1.2).[21] Une cinquième famille a également été créée afin de regrouper les facteurs de transcription dont le manque de données structurales ne permet pas encore le classement dans l'une des quatre catégories citées précédemment.[22]

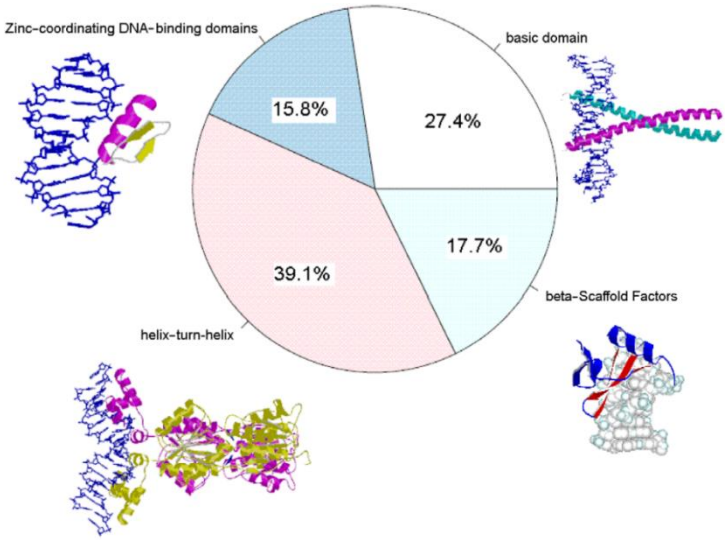

Figure 1.2 Classification des facteurs de transcription[21]

Chaque DBD reconnaît des séquences spécifiques de l'ADN (allant souvent de 4 à 12 paires de bases) avec une affinité jusqu'à 10^6 fois supérieure pour la séquence ciblée par rapport au reste du brin de l'ADN.[23] En raison de leurs fonctions, la majorité des facteurs de transcription possèdent deux domaines clefs : un ou plusieurs DBD leur permettant de se lier spécifiquement à l'ADN et une autre région aidant à l'activation de la transcription. Si les DBD ont été largement étudiés au cours des dernières décennies, les données sur les domaines d'activation de la transcription sont moins nombreuses et impliquent encore certains modèles prédictifs.[24] Ce sont des régions intrinsèquement désordonnées qui ont par conséquent été classées en fonction des acides aminés majoritairement présents. Il existe ainsi des domaines d'activation dits « acides », c'est-à-dire composés principalement de résidus chargés négativement comme l'aspartate ou le glutamate. D'autres sont quant à eux riches en prolines, sérines/thréonines ou encore en glutamines.[25] Quelle que soit leur structure, ces domaines interagissent avec les facteurs de transcription généraux ou des co-activateurs de transcription, permettant ainsi de faciliter la formation du complexe de transcription avec l'ARN polymérase II au niveau du promoteur. Surprenamment, différents facteurs de transcription avec des domaines d'activation variés sont capables

de se lier aux mêmes protéines, par exemple à TAF (*TBP-associated factors*) appartenant au complexe général de transcription II D[11] ou bien à des protéines du complexe Mediator,[26] à d'autres de l'histone acétyltransférase p300,[27] voire même à certaines des protéines formant les homologues humains du remodeleur de chromatine SWI2/SNF2.[28] Cette caractéristique permet ainsi une approche combinatoire où l'action conjointe de différents facteurs de transcription est requise pour amorcer la transcription.[29] Cette synergie est essentielle pour la régulation des gènes chez les eucaryotes et passe fréquemment par une homo- ou hétérodimérisation.[30]

Malgré tout, une question subsiste : si les facteurs de transcription sont capables de réguler l'expression génique de par leurs structures et leurs capacités à recruter de multiples co-facteurs transcriptionnels ainsi que l'ARN polymérase II, comment sont-ils eux-mêmes contrôlés ? Premièrement, il est important de rappeler que les facteurs de transcription restent des protéines. Ce constat implique que pour exister, les facteurs de transcription ont eux-mêmes dû être transcrits puis traduits. Par conséquent, il est possible de limiter leur production, notamment via certaines boucles de rétroaction négatives incluant soit eux-mêmes soit d'autres facteurs de transcription,[31] ou bien il est possible de jouer sur la localisation sous-cellulaire du dit facteur de transcription.[32] En effet, pour pouvoir exercer sa fonction, un facteur de transcription doit se trouver dans le noyau cellulaire et donc migrer hors du cytoplasme dans lequel il se trouve après sa traduction. Deuxièmement, un facteur de transcription est rarement activé directement après son entrée dans le noyau ; il peut avoir besoin de se lier préalablement à un ligand,[33] d'être phosphorylé,[34] ou bien d'interagir avec des co-facteurs[35] ou d'autres facteurs de transcription.[36] Pour finir, en remaniant la structure

de la chromatine, l'accès à la portion du gène à transcrire peut tout simplement lui être rendu impossible.

1.2.2 Topologies de la chromatine et marquage épigénétique

Chez les eucaryotes, l'ADN, présent sous forme d'hélice à double brin, interagit avec des octamères d'histones (deux copies respectives de H2A, H2B, H3 et H4) afin de former des nucléosomes. Cette structure, souvent décrite en « collier de perles », est peu condensée et permet la transcription des gènes; il s'agit de l'euchromatine. Chaque nucléosome va ensuite se lier à une histone H1, donnant ainsi des chromatosomes qui vont se joindre pour créer une fibre.[37] Cette fibre va alors s'enrouler sur elle-même, constituant l'hétérochromatine. À l'inverse de l'euchromatine, l'hétérochromatine est hautement compactée et est considérée inactive vis-à-vis de la transcription (Figure 1.3).[38]

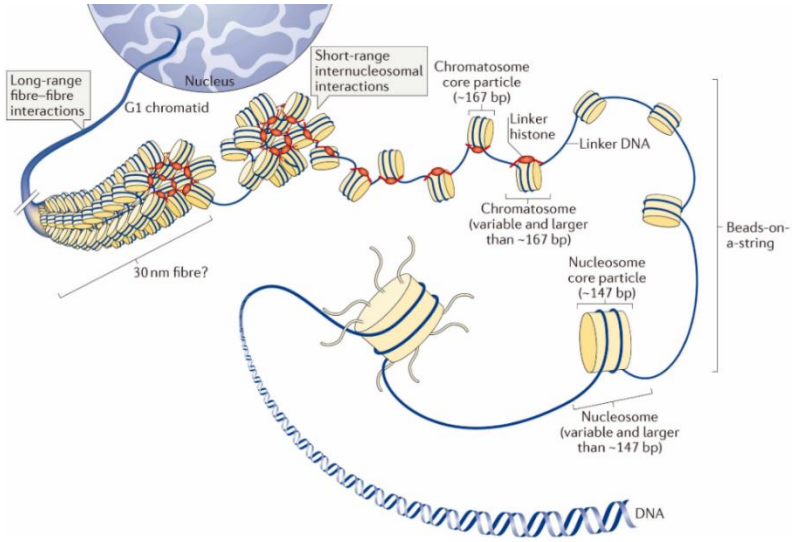

Figure 1.3 Topologies de la chromatine[37]

Même à l'état d'euchromatine, la transcription reste difficile et nécessite plusieurs sous-étapes. En effet, à partir du moment où l'ADN s'est enroulé autour du complexe d'histones, les séquences-*cis* demeurent inaccessibles pour tout facteur de transcription

n'étant pas « pionnier ». La majorité des facteurs de transcription doivent donc attendre l'intervention conjointe de complexes permettant des modifications covalentes sur la chromatine et de remodeleurs de chromatine (*chromatin remodelers*) avant de pouvoir se lier à l'ADN.

1.2.2.1 Marquage épigénétique

Les modifications covalentes sur les histones, voire directement sur l'ADN, vont influencer la topologie de la chromatine et donc, par extension, l'expression génique.[39] Ces marquages dits épigénétiques sont réversibles et transmissibles de génération en génération, régulant ainsi la transcription sans pour autant changer la séquence nucléosidique. S'il existe de nombreuses modifications possibles (méthylation, acétylation, phosphorylation, ubiquitination, etc.) et s'il est clair que certaines combinaisons peuvent agir de manière synergique ou antagoniste,[40] deux d'entres elles sont tout particulièrement importantes pour la modulation de la chromatine: l'acétylation et la méthylation.

Tout d'abord, l'acétylation.[41] Chaque histone est susceptible d'être acétylée au niveau de lysines spécifiques de leur domaine N-terminal par des histones acétyltransférases (HAT). Ce marquage épigénétique neutralise ainsi la charge positive de la lysine (normalement ionisée sous forme d'ammonium à pH physiologique), diminuant ainsi les interactions ioniques avec les groupes phosphates de l'ADN, les interactions nucléosomes/nucléosomes et les contacts de certaines protéines stabilisant l'hétérochromatine.[42] L'ensemble de ces modifications entraîne une flexibilité accrue de la chromatine, exposant finalement l'ADN aux facteurs de transcription. Une hyperacétylation globale des histones est donc généralement associée aux régions actives en transcription, tandis que la désacétylation catalysée par les histones désacétylases (HDAC) est quant à elle affiliée à une répression, voire un silençage de l'expression génique.[43]

Ensuite, la méthylation. La méthylation de certaines lysines ou arginines, principalement sur les extrémités N-terminales des histones H3 et H4, par des histones méthyltransférases (HMT) peut mener soit à l'activation, soit à la répression de la transcription en fonction du résidu ciblé et du nombre de groupements méthyles avoisinants.[44] Contrairement aux HAT, les HMT présentent une spécificité accrue et modifient généralement un seul résidu sur une seule histone.[45] De façon intéressante, le silençage des gènes a souvent été corrélé avec une méthylation de l'ADN dans la région de leurs promoteurs.[46] Cette méthylation s'effectue principalement sur la cytosine d'îlots CpG via l'action d'ADN méthyltransférases (DNMT) et est associée à l'hétérochromatine.[47] S'il ne fait aucun doute que la méthylation de l'ADN et celle des histones sont étroitement liées,[48] il est important de préciser que les DNMT peuvent également agir de concert avec d'autres enzymes épigénétiques, notamment les HDAC, afin d'inhiber la transcription génique.[49]

Si l'ensemble de ces marques épigénétiques module parfois la structure de la chromatine de façon directe, la majeure partie du temps leur impact est indirect et passe par le recrutement de co-facteurs ou de remodeleurs de chromatine.[50]

1.2.2.2 Remodeleurs de chromatine

Les remodeleurs de chromatine sont des complexes multiprotéiques possédant un domaine catalytique ATPase capable d'altérer la structure, la composition ou le positionnement des nucléosomes. Il existe quatre grandes familles basées sur les domaines adjacents à celui permettant l'hydrolyse de l'ATP : (1) la famille *switch/sucrose non-fermenting* SWI/SNF avec ses domaines bromés (*bromodomains*) et HSA (*helicase-SANT*), (2) la famille *imitation switch* ISWI avec ses domaines HAND, SANT et SLIDE, (3) la famille *chromodomain/helicase/DNA-binding domain* CHD avec ses domaines chromés en tandem (*tandem chromodomains*) et (4) la famille *inositol requiring 80* INO80 qui possède un domaine HSA (Figure 1.4).[51]

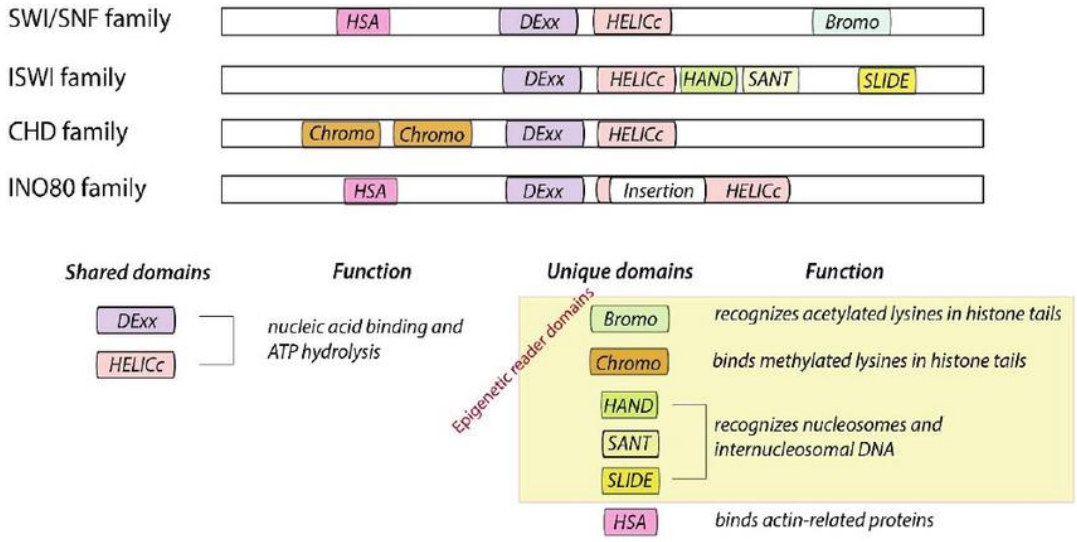

Figure 1.4 Les quatre familles de remodeleurs de chromatine[51]

Nombre de remodeleurs de chromatine possèdent des domaines considérés comme des lecteurs épigénétiques, c'est-à-dire capables de reconnaître sélectivement les marques épigénétiques énumérées dans la partie précédente. Il est cependant à noter que ces lecteurs épigénétiques ne sont pas un attribut exclusif des remodeleurs de chromatine et que les domaines présents dans les différentes familles citées ci-dessus ne constituent pas une liste exhaustive des lecteurs épigénétiques existants.[52] Par exemple, la méthylation des lysines est entre autres reconnue par différents modules de la famille Royal (domaines chromés (*chromodomains*), domaines tudor, domaines MBT, domaines PWWP) ainsi que par des domaines PHD.[53]

Les remodeleurs de chromatine sont impliqués dans de nombreux procédés biologiques, incluant notamment l'assemblage de la chromatine, la compensation de dose du chromosome X, la réplication, réparation et recombinaison de l'ADN, la ségrégation des chromosomes, le développement embryonique, la pluripotence et, bien entendu, la régulation de l'expression génique.[54] Chaque famille possède un rôle spécifique permettant d'équilibrer l'accès aux gènes. Certains remodeleurs aident par exemple l'assemblage de la chromatine en permettant la déposition de nouveaux nucléosomes

tout en favorisant leur espacement adéquat. D'autres remodeleurs rendent accessibles les séquences-*cis* de l'ADN afin d'activer le recrutement des facteurs de transcription. Pour ce faire, le remodeleur peut : (1) faire glisser les nucléosomes afin que la partie désirée de l'ADN se retrouve entre les nucléosomes, (2) éjecter le nuclésome en question pour que l'ADN n'interagisse plus avec l'octamère d'histones, (3) dérouler une portion de l'ADN localement, directement sur le nucléosome. Pour finir, certains remodeleurs qui participent à la réparation et recombinaison de l'ADN modulent la composition des nucléosomes en échangeant le dimère H2A-H2B par d'autres dimères d'histones ou en supprimant certains dimères du dit nucléosome (Figure 1.5).[54]

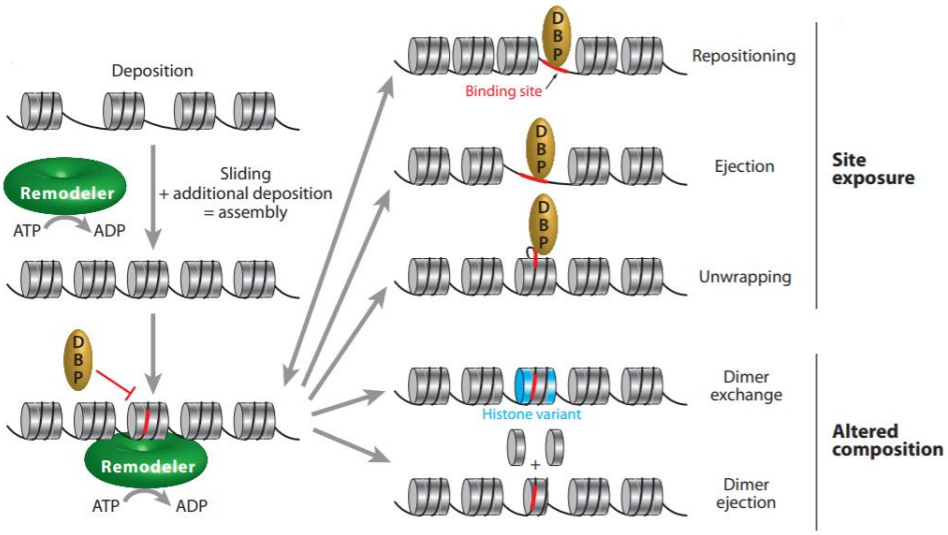

Figure 1.5 Mécanismes d'action généraux des remodeleurs de chromatine[54]

Au vu du nombre de membres que chaque famille contient, il est difficile de catégoriser une famille comme étant responsable d'une action biologique en particulier. Malgré tout, les études semblent indiquer que la famille SWI/SNF a tendance à promouvoir l'expression génique en augmentant l'exposition de l'ADN nu tandis que la majorité des membres de la famille ISWI permettent davantage l'assemblage et l'organisation des nucléosomes.[55] Plus précisément, les homologues SWI/SNF de l'humain ont entre

autres été associés à la suppression des tumeurs,[56] à la différentiation,[57] au développement,[58] à l'élongation[59] ainsi qu'à l'épissage.[60]

S'il est évident que les remodeleurs de chromatine utilisent les lecteurs épigénétiques afin de reconnaître les histones et les nucléosomes, leurs interactions dynamiques avec les facteurs de transcription pionniers semblent également jouer un rôle dans l'accessibilité de l'ADN.[61]

1.2.2.3 Facteurs de transcription pionniers

Les facteurs de transcription dits « pionniers » correspondent à la catégorie des facteurs de transcription capable de se lier directement à l'ADN nucléosomal.[62] Ils peuvent agir de façon directe, en ouvrant localement la chromatine afin de permettre à d'autres facteurs de transcription d'accéder à l'ADN,[63] ou bien de manière indirecte, en se liant à des séquences de régulation de l'ADN, menant ainsi à l'initiation rapide de la transcription de gènes spécifiques lors du développement ou à la suite de signaux hormonaux.[64] Les facteurs pionniers peuvent aussi recruter des remodeleurs de chromatine ou moduler le marquage épigénétique.[65] Il a par exemple été démontré que les facteurs pionniers peuvent notamment protéger certaines cystéines de la méthylation, évitant ainsi le silençage des gènes en question.[66]

Maintenant que les mécanismes principaux de régulation de l'expression génique ont été mis en lumière, les prochaines parties de ce chapitre traiteront au cas par cas de trois acteurs spécifiques : (1) le complexe de transcription YAP-TEAD (*yes-associated protein - transcriptional enhancer factor with TEA/ATTS domain*), (2) la protéine contenant des domaines bromés PB1 (*polybromo-1 protein*), sous-unité du remodeleur de chromatine PBAF (*polybromo-associated BAF*), (3) la protéine multidomaines BPTF (*bromodomain and PHD-finger containing transcription factor*), sous-unité du remodeleur de chromatine NURF (*nucleosome-remodeling factor*).

1.3 Complexe transcriptionnel YAP-TEAD

Chez les mammifères, le complexe transcriptionnel YAP-TEAD est considéré comme étant l'effecteur principal de la voie de signalisation Hippo.

1.3.1 Voie de signalisation Hippo

Initialement découverte lors d'un criblage génétique sur des mutants *Drosophila melanogaster* présentant une surcroissance tissulaire, la voie de signalisation Salvador-Warts-Hippo (SWH ou plus simplement Hippo) régule la prolifération cellulaire et l'apoptose chez les organismes multicellulaires afin d'assurer un développement normal des tissus ainsi qu'une croissance adéquate des organes.[67] Pour ce faire, cette voie de signalisation est tout particulièrement sensible à l'organisation spatiale et physique des cellules, coordonnant notamment l'inhibition de contact.[68] Chez les mammifères, des facteurs extracellulaires tels que les signaux hormonaux, les jonctions cellulaires, la matrice extracellulaire ou encore les protéines RASSF et NF2/Merlin vont ainsi pouvoir activer la voie Hippo et déclencher une cascade de kinases.[69,70] À la suite des phosphorylations séquentielles des complexes Mst1/2 – Sav et Lats1/2 – Mob permettant d'activer les kinases en question, le co-activateur transcriptionnel YAP (*yes-associated protein*) et son unique paralogue TAZ (*transcriptional co-activator with PDZ-binding motif*, également connu sous le nom de WWTR1) vont à leur tour être phosphorylés, entraînant alors leur liaison avec la protéine 14-3-3, suivie ultimement de leur dégradation.[71] Il est à noter que la dégradation de YAP/TAZ dans le cytoplasme s'effectue à la fois par la voie ubiquitine/protéasome via le recrutement de l'ubiquitine ligase E3 $SCF^{\beta\text{-}TRCP}$,[72] ainsi que par l'autophagie.[73] En revanche, lorsque la voie de signalisation Hippo est inactive, YAP/TAZ non phosphorylés translocalisent dans le noyau où ils interagissent avec de nombreux facteurs de transcription, parmi lesquels se trouvent p73, RUNXs (*runt related transcription factor*), SMADS ou encore les 4 isoformes de la famille TEAD (*transcriptional*

enhancer factor with TEA/ATTS domain),[74] afin d'initier la transcription de gènes divers favorisant la prolifération cellulaire et la croissance des organes (Figure 1.6). Il est intéressant de mentionner que YAP et TAZ, bien que présents sur différents chromosomes (11q22 et 3q23-q24 respectivement) et codant pour des protéines de différentes tailles (approximativement 488 acides aminés versus 400 pour TAZ), partagent 46% de leur séquence d'acides aminés et possèdent des topologies presque identiques.[75] Ces caractéristiques structurales partagées leur confèrent des fonctions souvent similaires et la suite des travaux de cette thèse se concentrera sur YAP pour des raisons de clarté d'écriture.[76]

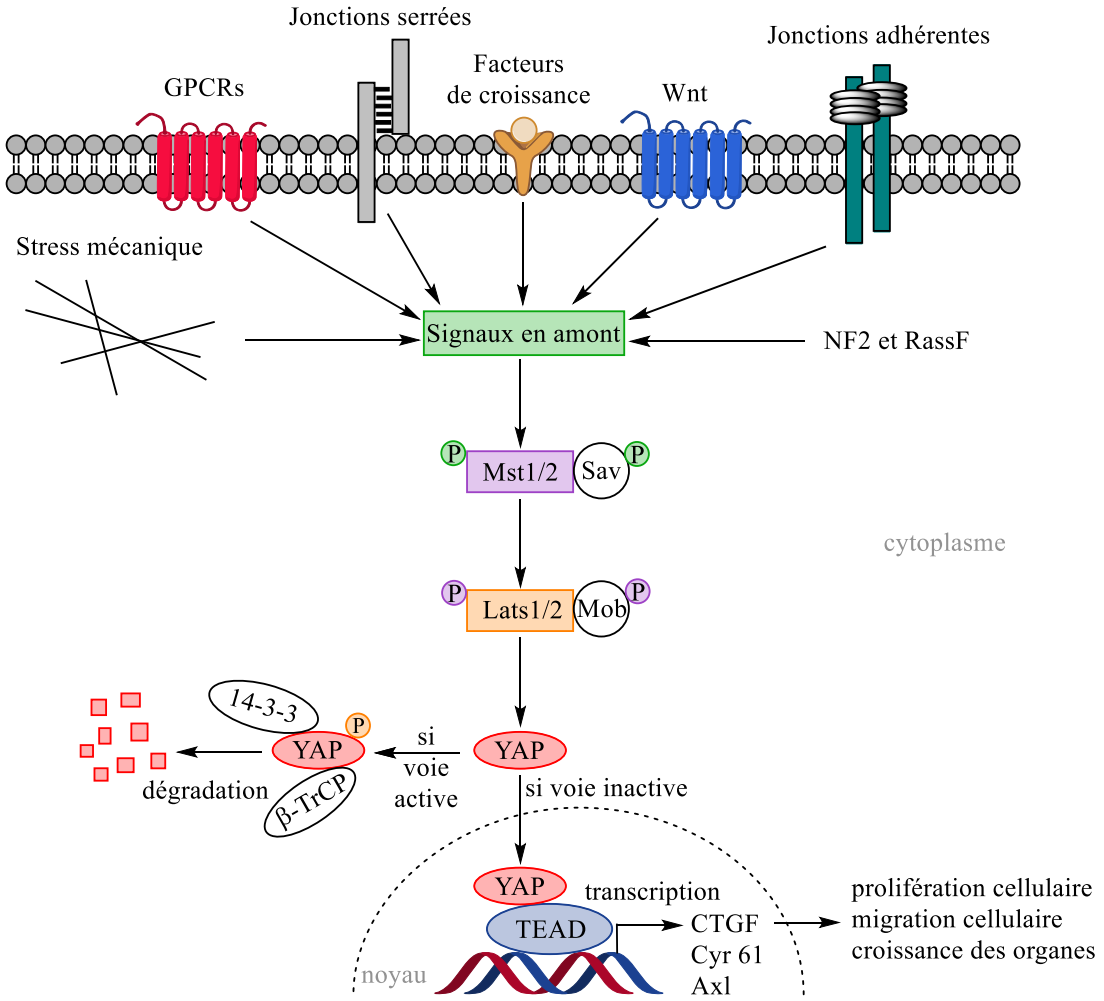

Figure 1.6 Voie de signalisation Hippo

En temps normal, la voie Hippo contrôle la taille des organes en régulant l'expansion des cellules souches par inhibition de YAP. Une fois passé le stade développemental, la voie Hippo reste impliquée dans de nombreux processus biologiques, notamment l'homéostasie, la différenciation cellulaire et la régénération/réparation des tissus. En cas de mutation au sein de la voie de signalisation entraînant, directement ou indirectement, une hyperactivation de YAP, une surcroissance des organes est généralement observée ainsi qu'un risque élevé de tumorigénèse.[77] Il est à noter que, même si moins souvent abordée et étudiée, une telle hyperactivation a également été

impliquée dans d'autres maladies telles que la douleur neuropathique[78] ou la fibrose,[79] mais que cette thèse se cantonnera au cancer pour davantage de concision.

1.3.2 Dérégulations et implications dans le cancer

De nombreuses études ont démontré l'implication de dérégulations de la voie Hippo dans diverses formes de cancer.[80,81] Les analyses de l'Atlas du génome du cancer ont permis de mettre en lumière l'importance de l'effecteur en aval de la voie de signalisation en révélant que parmi 33 types de cancer, YAP est le facteur le plus fréquemment amplifié de la voie Hippo, tout particulièrement dans les cancers squameux.[82]

1.3.2.1 YAP, une protéine proto-oncogénique

En particulier, la surexpression de YAP et sa présence accrue dans le noyau cellulaire ont été observées dans de nombreux cas, incluant notamment, mais non exclusivement, les cancers du foie,[83] du colon,[84] des ovaires,[85] des poumons[86], de la prostate[87] ainsi que les tumeurs solides.[88] Une surexpression de YAP induit par exemple une augmentation des transitions épithéliale-mésenchymateuses (EMT), caractéristique de certaines progressions tumorales et métastatiques, dans diverses lignées cellulaires.[89,90] Chez la souris, des niveaux élevés de YAP dans le noyau ont été associés à une sur-croissance du foie associée à des carcinomes.[91] Il est cependant important de préciser que YAP ne possède pas de domaine lui permettant de se lier directement à l'ADN, son impact provenant donc principalement de ses interactions avec ses partenaires de transcription. Il a ainsi été démontré que le caractère proto-oncogénique de YAP est essentiellement lié à son association avec TEAD.[92]

1.3.2.2 YAP-TEAD interdépendance et dérégulations

En formant un complexe transcriptionnel avec TEAD, tout en recrutant l'activateur de transcription Mediator,[93] YAP active l'expression des gènes responsables de la

prolifération cellulaire tout en inhibant celle des gènes codant pour l'apoptose. Les principaux gènes régulés sont *Cyr61*, *CTGF* (*Connective Tissue Growth Factor*), *c-myc*,[94] *AXL*,[95] *AREG* et *survivin*.[96] À ce jour, de nombreuses études indiquent que YAP agit comme principal co-activateur de TEAD et, réciproquement, TEAD paraît indispensable à l'activation et à l'accumulation de YAP dans le noyau cellulaire.[97] Le séquençage ChIP-Seq a notamment permis de découvrir que (1) YAP et TEAD co-occupent plus de 80% des promoteurs détectés dans des cellules MCF10A,[98] (2) dans des cellules MDA-MB-231 génétiquement modifiées pour présenter une voie Hippo inactive, 80% des protéines TEAD liées à des séquences-*cis* de l'ADN forment des hétéromères avec YAP et, inversement, 75% des protéines YAP liés à l'ADN le sont via leurs interactions avec TEAD,[99] (3) 86% des pics associés à YAP indiquent une association avec TEAD dans des cellules du glioblastome.[100] Il a également été démontré que, dans le cas où TEAD serait absent du noyau cellulaire (en raison d'une translocation cytoplasmique induite ou d'un *knock-out*), YAP ne migre pas dans le noyau, peu importe son état de phosphorylation ou les stimuli appliqués.[101] D'une façon similaire, une étude avec des *knockdowns* de TEAD a établi que les cellules présentent un silençage de la majorité des gènes associés à YAP ainsi qu'une atténuation de la surcroissance.[98] À l'inverse, une surexpression de TEAD induit une accumulation de YAP dans le noyau, suivi par l'expression de gènes essentiels pour l'EMT et la métastase.[102] Cette interdépendance entre YAP et TEAD permet d'expliquer en partie qu'une surexpression de TEAD a également été associée à de nombreux types de cancer dont les cancers de l'estomac, des seins, du colon ou de la prostate,[103,104] généralement accompagnés d'une faible survie pour les patients atteints.[105]

L'ensemble de ces études reliant YAP et/ou TEAD au cancer révèlent que ce complexe est non seulement impliqué dans l'activation et la transcription de gènes de croissance mais aussi dans celles de gènes qui confèrent des propriétés souvent associées aux cellules cancéreuses.

1.3.2.3 Implication de YAP-TEAD dans les propriétés des cellules cancéreuses

Si une hyperactivation de YAP-TEAD entraîne de façon logique une prolifération aberrante des cellules menant souvent à l'initiation de tumeurs, le complexe transcriptionnel joue également un rôle important dans leur progression et leur résistance aux thérapies anti-cancéreuses.[106]

Premièrement, un niveau surélevé de YAP permet aux cellules cancéreuses de prévenir leur mort programmée. Il a par exemple été démontré qu'une surexpression de YAP permet aux cellules d'éviter l'anoïkose (processus qui peut être réversible comme illustré par la restauration de cette forme d'apoptose dans des *knockdowns* de YAP).[107] YAP est aussi responsable de la suppression des formes d'apoptose mitochondriale.[108] En activant l'expression de gènes inhibiteurs de l'apoptose, tels que *Survivin*, YAP-TEAD perturbe également les voies d'apoptose extrinsèques initiées par TNF-α et FAS.[109] En plus d'aider les tumeurs à échapper à la mort cellulaire, YAP-TEAD favorise leur croissance en induisant l'expression de gènes de facteurs de croissance comme *AREG*, de gènes oncogéniques comme *c-myc* ou encore de gènes activant l'angiogenèse comme *CTGF*.[110]

Deuxièmement, il faut savoir que YAP est non seulement actif dans les cellules souches cancéreuses (CSC) mais est également nécessaire pour l'expansion de ces dernières. YAP est ainsi capable de reprogrammer des cellules tumorales normales en cellules présentant des propriétés caractéristiques des CSC, incluant la résistance aux traitements[111] et l'induction de métastases.[112] Le développement de mécanismes de résistance aux thérapies anti-cancéreuses causé par YAP est puissant et varié et inclu une résistance à la chimiothérapie, à la thérapie moléculaire ciblée, à l'immunothérapie ainsi qu'aux radiations.[113,114] Ceci s'explique partiellement par une augmentation de la tension du cytosquelette de la cellule cancéreuse, activant davantage la mécanotransduction et par conséquent, l'accumulation de YAP dans le noyau ; YAP va ensuite permettre d'augmenter le dépôt de la matrice extracellulaire, qui va alors

avoir tendance à se rigidifier, réinitialisant ainsi la boucle. Ce processus de rigidification de la matrice extracellulaire induit par YAP abroge également l'inhibition de contacts qui permet normalement de limiter la prolifération cellulaire.[115] Pour ce qui est de l'induction de métastases, YAP-TEAD promeut plusieurs étapes de leurs formations : (1) perturbation des jonctions cellulaires, impact sur la polarité de la cellule, activation de l'expression de gènes mésenchymateux, en d'autres termes : activation de l'EMT, (2) migration et intravasation, (3) survie dans différents milieux, (4) croissance des métastases.[116]

L'ensemble de ces résultats explique que la formation du complexe fonctionnel YAP-TEAD est un véritable enjeu pour le développement de médicaments efficaces contre le cancer, que ce soit comme agents seuls ou en combinaison avec des thérapies existantes.

1.3.3 Développement d'inhibiteurs de YAP-TEAD

De nombreuses stratégies peuvent être mises au point afin d'inhiber l'activité du complexe fonctionnel YAP-TEAD.[117]

1.3.3.1 Inhibiteurs non spécifiques

Puisqu'il s'agit des effecteurs finaux de la voie Hippo, l'une des options envisageables est d'activer les membres en amont dans la voie de signalisation afin d'induire une phosphorylation accrue de YAP, empêchant ainsi sa translocalisation dans le noyau et par conséquent son interaction avec TEAD. Par exemple, les statines, le Dasatinib ou le Pazopanib sont connus pour être des régulateurs non spécifiques de YAP-TEAD en agissant sur de multiples cibles en amont du complexe.[118] Malheureusement, cette stratégie pose plusieurs problèmes : (1) les kinases ciblées sont impliquées dans d'autres processus biologiques, ce qui augmente le risque de causer des effets indésirables et (2) le développement d'activateurs reste un défi avec peu d'approches

rationnelles connues. L'option la plus viable est donc de s'attaquer directement au complexe YAP-TEAD, soit en inhibant directement l'un des deux partenaires, soit en empêchant l'interaction protéine-protéine.

1.3.3.2 Inhibiteurs de YAP

Pour ce qui est de l'inhibition de YAP, il faut savoir qu'il existe 8 variants d'épissages séparés en deux isoformes majeurs : YAP1, contenant un unique domaine WW, et YAP2, possédant deux domaines WW.[119] YAP interagit avec TEAD via un domaine de liaison à TEAD N-terminal (*N-terminal TEAD-binding domain*, TBD) connecté à un domaine de transactivation C-terminal par le(s) domaine(s) WW (Figure 1.7).[120]

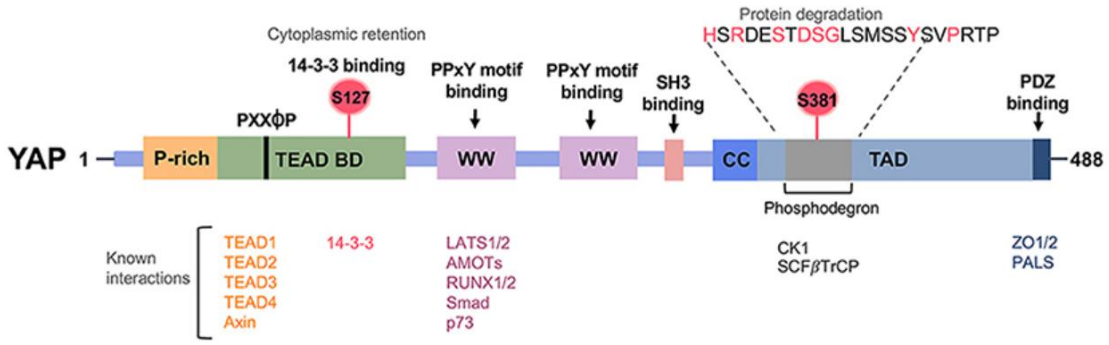

Figure 1.7 Structure de YAP2-γ[120]

YAP est une protéine intrinsèquement désordonnée qui, de ce fait, est difficile à cibler avec de petites molécules. À ce jour, la Vertéporfine est considérée comme inhibiteur de référence de YAP (Figure 1.8). Actuellement prescrit comme agent photosensibilisant dans les cas de dégénérescence maculaire, cette porphyrine agit en augmentant l'activité de la protéine chaperonne 14-3-3 et donc par conséquent en accroissant la séquestration puis la dégradation protéasomique de YAP, empêchant ainsi la formation du complexe YAP-TEAD.[121] Le seul autre candidat en lice des inhibiteurs de YAP est le composé CA3 (Figure 1.8). Cette fluorénone oxime a été

rapportée comme capable de diminuer l'expression de YAP ainsi que l'activité transcriptionnelle de YAP-TEAD.[122]

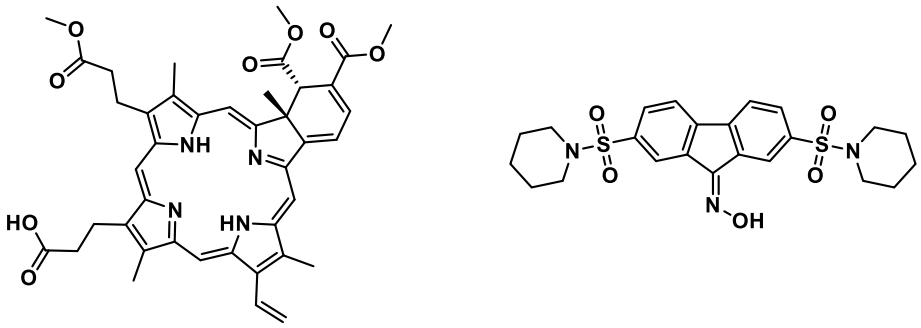

Figure 1.8 Inhibiteurs de YAP

Bien que l'activité antitumorale de ces deux agents ait été démontrée,[123] la Vertéporfine reste un inhibiteur non spécifique de YAP, donc non idéal.[124] Quant à CA3, son mode d'interaction et d'inhibition de YAP demeure inconnu. Considérant également que YAP peut parfois jouer le rôle de suppresseur de tumeurs lorsqu'il n'interagit pas avec TEAD,[125] il semble plus judicieux d'agir soit en perturbant la formation du complexe YAP-TEAD, soit en inhibant TEAD directement.

1.3.3.3 Inhibiteurs pertubant l'interaction protéine-protéine

La structure cristalline de YAP2 interagissant avec TEAD1 (code PDB : 3KYS) montre que trois surfaces d'interaction entrent en jeu lorsque YAP s'enroule autour de TEAD. L'interface 1 est régie par sept liaisons hydrogènes entre le squelette peptidique de YAP et les feuillets β1 et β7 de TEAD, formant ainsi un feuillet β antiparallèle. L'interface 2 est créée par la proximité de l'hélice α1 de YAP avec les hélices α3 et α4 de TEAD. Cette liaison est conditionnée par des interactions hydrophobes. Dans l'interface 3, la boucle Ω de YAP interagit avec une poche profonde de TEAD, formée par ses feuillets β4, β11, β12 et ses hélices α1 et α4 (Figure 1.9).[126] De ces trois surfaces

d'interaction, l'interface 3 a été rapportée comme étant la plus importante pour la formation de l'hétérodimère.[127]

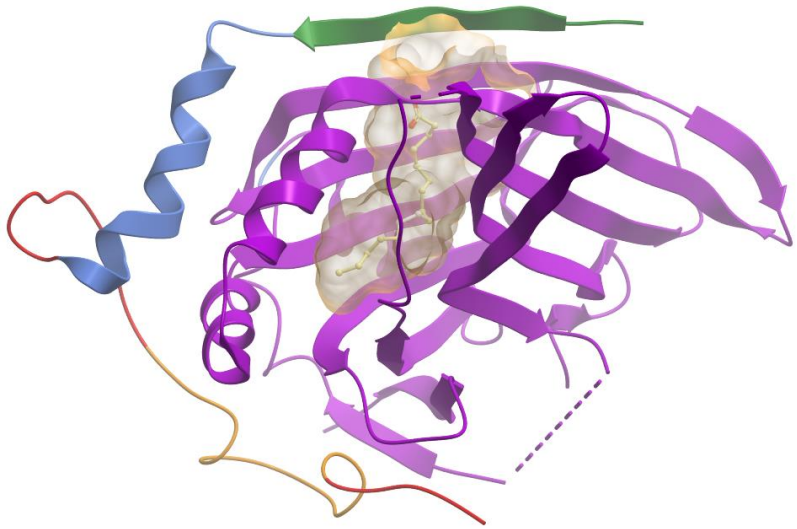

Figure 1.9 Interactions entre hYAP et hYBD de TEAD1 en présence d'acide palmitique (beige) (PDB: 3KYS et 5HGU). hTEAD YBD en violet, YAP en vert (interface 1), bleu (interface 2), rouge et orange (interface 3)

Après avoir mis en lumière les résidus clefs présents dans les sites de liaison des deux protéines, de nombreux groupes de recherche se sont penchés sur le développement de peptides pour empêcher ces interactions. Des peptides similaires à YAP, sous forme cyclique[128] et linéaire,[129] des peptides denses en cystéines[130] ainsi que des peptides mimant VGLL4[131] ont par exemple été étudiés. De façon intéressante, ces découvertes ont été menées autant par de grands groupes pharmaceutiques, comme Roche et Novartis, que par des laboratoires académiques, démontrant bien le potentiel thérapeutique et l'intérêt croissant pour YAP-TEAD. Cependant, aucun de ces composés n'a pour le moment été amené en phase clinique en raison de problèmes associés à des profils pharmacocinétiques non optimaux, une faible stabilité plasmatique ainsi qu'une perméabilité cellulaire moindre. Afin de s'éloigner des difficultés souvent inhérentes aux peptides, d'autres groupes se sont tournés vers le

développement de petites molécules. À la suite de campagnes de criblage virtuel ont donc été rapportés le composé **1** qui se lie avec un IC_{50} de 6.5 µM dans une cavité formée par la région C-terminale de hTEAD1 en périphérie de l'interface 3[132] et CPD3.1, une molécule tétracylique qui bloque l'interaction de YAP avec TEAD1 en inhibant l'activité de TEAD avec un IC_{50} de 110 µM (Figure 1.10).[133] Finalement, deux campagnes de criblage parallèle (l'une basée sur des fragments, l'autre étant un HTS), ont permis à Inventiva de breveter le composé **2** et ses dérivés.[134] Le composé **2** déplace YAP avec un IC_{50} de 886 nM et permet d'inhiber la prolifération dans des cellules du mésothéliome NCIH2052.[135]

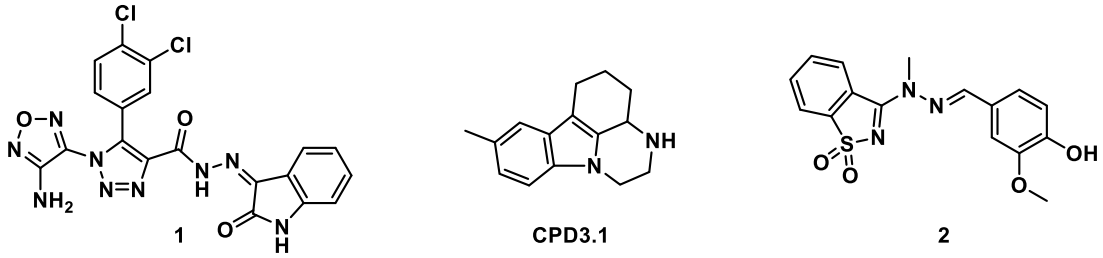

Figure 1.10 Petites molécules pertubant l'interaction protéine-protéine

Malgré tout, l'optimisation de composés se liant d'un côté ou de l'autre de l'interface YAP-TEAD reste un défi de taille en raison de l'absence de véritable poche définie au niveau des différentes interfaces. La dernière approche stratégique est donc de venir inhiber directement le deuxième partenaire du complexe, à savoir TEAD.

1.3.3.4 Inhibiteurs de TEAD

La famille TEAD est composée chez les mammifères de quatre paralogues nommés TEAD1, TEAD2, TEAD3 et TEAD4 avec une homologie de séquence variant de 61 à 73%. L'ensemble de ces protéines partage un domaine de liaison à l'ADN N-terminal (DBD), lié par une région riche en proline (PRR) d'environ 100 acides aminés à un domaine de liaison de YAP/TAZ/VGLL C-terminal (fréquemment référé simplement par YBD pour *YAP-binding domain*). Les DBD et YBD sont hautement conservés

parmi les quatre membres avec une homologie de séquence minimale de 87.9% et de 72.0%, respectivement (Figure 1.11).[104]

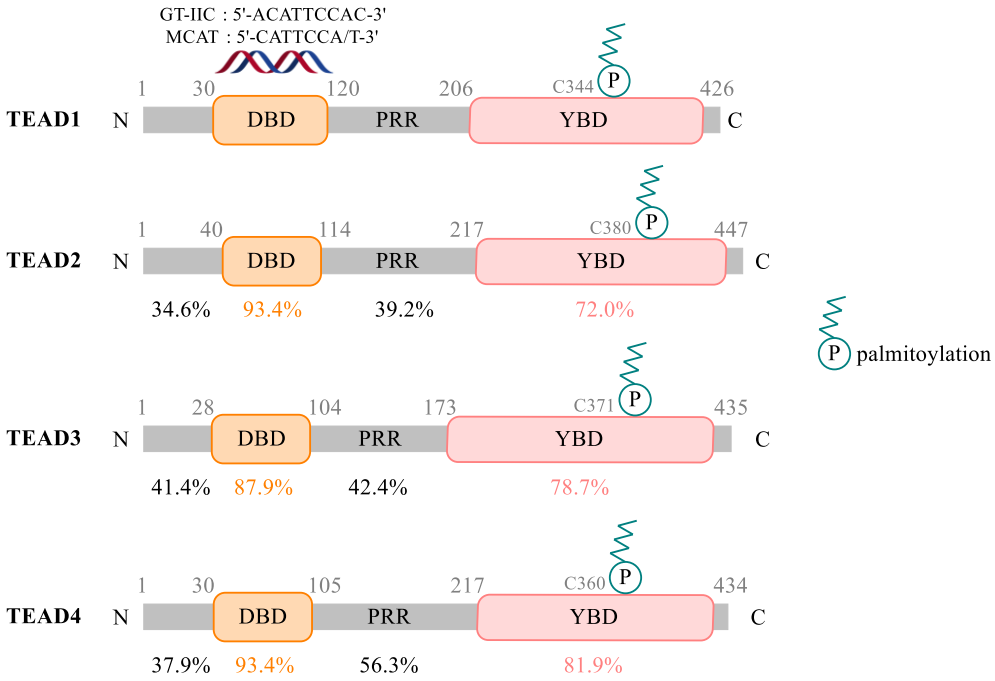

Figure 1.11 Structures et homologies de la famille TEAD

Alors que les formes complètes de TEAD sont exclusivement présentes dans le noyau cellulaire, certaines isoformes d'épissage composées uniquement de la partie C-terminale avec le PRR et le YBD ont été détectés à la fois dans le cytoplasme et le noyau, servant apparemment de régulateurs additionnels de YAP.[136] Malgré la forte homologie de séquence des formes complètes de TEAD, il semblerait que chaque paralogue possède une fonction distincte. Ainsi chaque membre de la famille TEAD est exprimé différemment selon le tissu et le stade de développement, même s'il est à noter que presque tous les tissus expriment au moins l'un des gènes de TEAD, si ce n'est les quatre. TEAD1 semble nécessaire pour la différenciation et le développement des muscles cardiaques,[137] tandis qu'un *knockout* de TEAD2 est viable mais augmente les risques d'exencéphalies.[138] Selon toute vraisemblance, TEAD1 et TEAD2 partagent

certaines fonctions encore non définies lors du développement de l'embryon.[139] TEAD4 semble quant à lui être lié à l'implantation de l'embryon et est largement exprimé dans les muscles squelettiques.[140] Finalement, la fonction exacte de TEAD3 reste un mystère, mais la protéine serait principalement exprimée dans le placenta[141] et d'autres tissus (système nerveux et muscles notamment) lors du développement.[142] En dehors du stade développemental, peu est encore connu sur le rôle de chaque paralogue. Étant donné leurs fonctions distinctes et leurs niveaux d'expression variables selon les tissus, il est donc difficile de prévoir si un inhibiteur à large spectre (*pan-inhibitor*) sera nécessaire pour inhiber le caractère oncogénique du complexe YAP-TEAD ou si un inhibiteur sélectif de certains membres de la famille TEAD serait plus favorable. Quoi qu'il en soit, développer un antagoniste de TEAD semble une stratégie moins risquée qu'inhiber YAP puisque TEAD apparaît comme non essentiel à l'homéostasie chez les adultes, diminuant ainsi les risques d'effets secondaires majeurs potentiels.[96,143]

Théoriquement, le développement de tels inhibiteurs pourrait se concentrer soit sur le DBD, soit sur le YBD, deux régions hautement conservées chez les différents paralogues.

1.3.3.4.1 Inhibiteurs du DBD de TEAD

Des études par mutations géniques démontrent que des altérations du DBD de TEAD mènent à une diminution du taux d'occupation des promoteurs de TEAD, une perte de spécificité de reconnaissance de l'ADN, une réduction de la transcription associée au complexe YAP-TEAD et donc une croissance réduite des cellules.[144] Bien que la preuve de concept soit prometteuse, il n'existe à ce jour aucun inhibiteur du DBD de TEAD. Ceci peut s'expliquer par deux raisons principales. Premièrement, les interactions sont principalement générées par des hélices α de TEAD avec des sillons de l'ADN. Il n'existe donc pas de poche bien définie pour favoriser le développement de petites molécules, bien que des pseudo-cavitées aient été identifiées (Figure 1.12).[118] Deuxièmement, empêcher une interaction protéine/ADN requiert généralement une

molécule chargée, ce qui peut devenir problématique pour passer la membrane nucléaire.

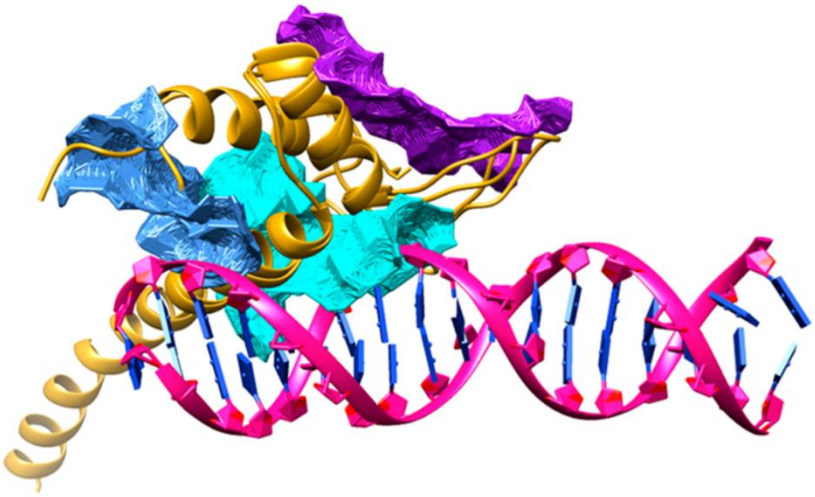

Figure 1.12 Pseudo-cavités potentiellement ciblables pour l'inhibition du DBD de TEAD[118]

La découverte d'une poche centrale hydrophobe dans le YBD où s'effectue la palmitoylation post-traductionnelle de TEAD permet une autre approche.

1.3.3.4.2 Inhibiteurs de la palmitoylation de TEAD dans le YBD

La formation d'une liaison covalente entre un résidu d'acide palmitique et une cystéine conservée chez tous les paralogues de TEAD induit l'auto-palmitoylation de la protéine au niveau d'une poche centrale hydrophobe présente dans son YBD. Cette cavité est bien définie et conservée au sein de la famille TEAD. En prenant l'exemple de TEAD2, il est possible de remarquer que l'interaction principale s'effectue à l'entrée de la cavité via les résidus C380 et K357 tandis que l'hydrophobicité provient à la fois de groupements aromatiques (3 phénylalanines, 1 tyrosine) et aliphatiques (1 méthionine, 1 isoleucine, 4 leucines, 4 valines et 2 alanines). Il est également intéressant de noter

que la cavité s'étend directement vers l'interface 1 entre YAP et TEAD avec le feuillet β1 de TEAD qui en masque l'entrée.

L'influence exacte de cette palmitoylation sur l'interaction entre YAP et TEAD reste débattue au sein de la communauté scientifique. Certaines études montrent que l'affinité avec YAP est drastiquement réduite lorsqu'il y a absence de palmitoylation,[145] tandis que d'autres études par mutations partielles semblent indiquer que l'interaction entre YAP et TEAD est maintenue, mais avec une plus faible affinité.[146,147] Une rigidification de TEAD semble être à l'origine de ces résultats.[148] Si l'effet allostérique est encore questionné, tous s'accordent à dire que la palmitoylation augmente la stabilité de TEAD, ce qui lui permet d'acquérir et/ou de maintenir sa conformation active.[149] Le niveau d'expression et d'activité transcriptionnelle de TEAD est également directement modulé par son état de palmitoylation.[150]

L'ensemble de ces données, combiné au fait qu'une poche définie et hydrophobe constitue un environnement idéal pour la liaison de petites molécules, explique que cette stratégie est actuellement la plus couramment exploitée pour le développement d'inhibiteurs de YAP-TEAD.[151] L'acide flufénamique et l'acide niflumique ont été les premiers inhibiteurs de la palmitoylation de TEAD à être rapporté en 2015. Bien que leur liaison n'empêche pas la formation du complexe fonctionnel à proprement parler, elle mène malgré tout à une réduction du niveau d'expression des gènes associés à YAP-TEAD dans la lignée cellulaire MCF10A avec un K_D de 73 μM pour l'acide flufénamique.[152] En 2017, MGH-CP1 fut breveté par l'hôpital général du Massachusetts (Mass General) à Boston comme ligand se liant dans la poche palmitique de TEAD2, réduisant l'activation des gènes avec un IC_{50} de 83 nM dans un test cellulaire de reporteur Gal4-TEAD1 ainsi que l'expression de *CTGF* et *Cyr61*.[148] Une subvention (R01CA238270) accordée par le National Cancer Institute (NCI) est actuellement en cours et devrait se poursuivre jusqu'en 2024, mais à ce jour aucun résultat concernant l'optimisation ou le statut de MGH-CP1 n'a été publié. Un autre

brevet, mais cette fois-ci déposé par Inventiva en France, rapporte le composé **3** qui, aussi par test cellulaire de reporteur Gal4-TEAD, diminue l'activation de TEAD avec un IC_{50} de 260 nM.[153] Une fois de plus, le stade de développement de **3** et de ses dérivés reste inconnu. L'intérêt croissant pour YAP-TEAD comme cible thérapeutique, et pour cette approche qui est d'inhiber la palmitoylation de TEAD en particulier, s'illustre par la publication récente des inhibiteurs **4** (issue d'une collaboration entre Genentech et Roche)[154] et **5** (projet en partenariat entre plusieurs facultés de Dortmund en Allemagne et AstraZeneca)[155] ainsi que par la présentation au meeting annuel de l'association américaine de la recherche contre le cancer (AACR) 2020 de deux autres inhibiteurs réversibles, dont les structures n'ont pas été divulguées, actuellement en phases pré-cliniques (développés par la biotech Ikena Oncology[156] et par le centre de conception et de découverte de médicaments à Louvain en Belgique,[157] respectivement). Finalement, divers inhibiteurs covalents sont également en cours de développement. Ces dérivés DC-TEADin02,[158] TED-347[159] et K-975[160] se lient avec la cystéine présente à l'entrée de la cavité et présentent des activités anti-tumorales dûes à l'inhibition de l'auto-palmitoylation de TEAD. Il est cependant important de constater qu'une exception existe : l'interaction de la quinolinole **Q2** avec la poche palmitique de TEAD mène quant à elle à une augmentation de l'activité transcriptionnelle du complexe YAP-TEAD (Figure 1.13).[161] Ainsi, **Q2** n'agit donc pas comme un inhibiteur de TEAD mais plutôt comme un activateur de ce dernier.

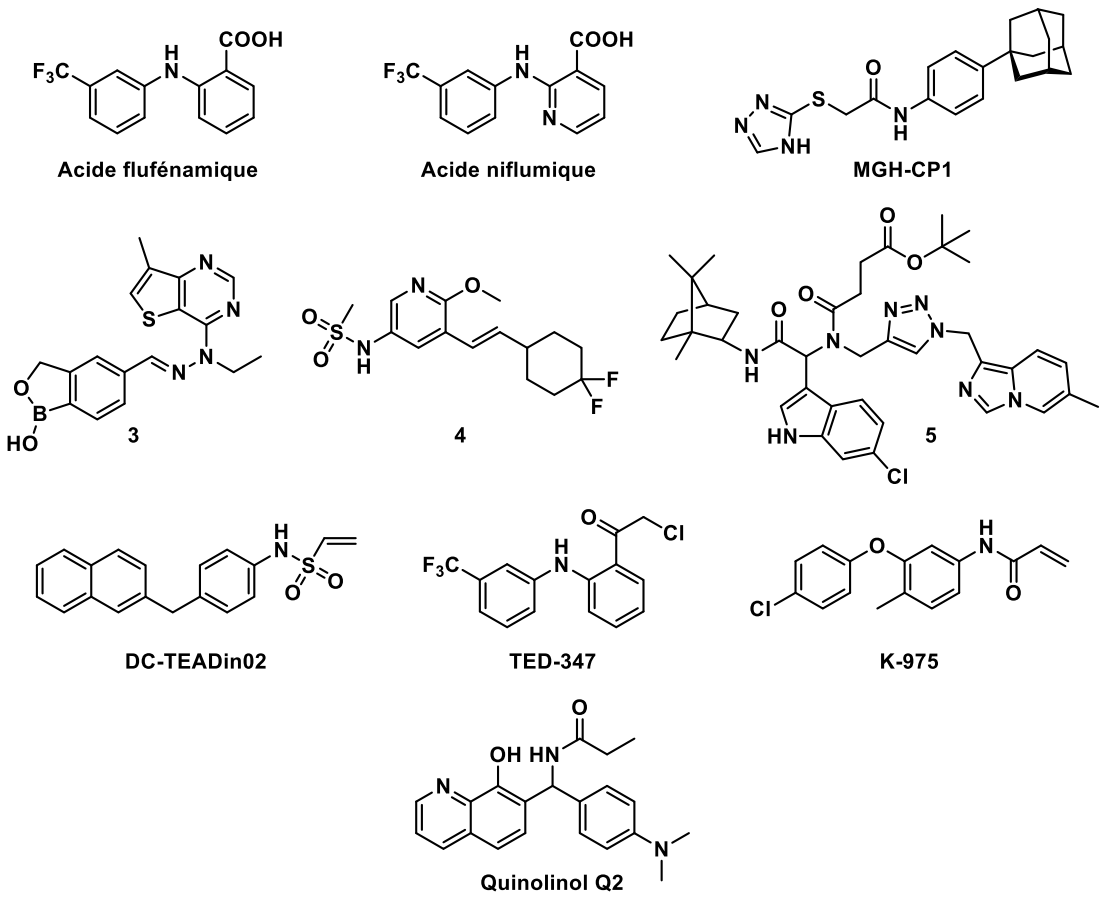

Figure 1.13 Inhibiteurs de la palmitoylation de TEAD dans le YBD

L'ensemble des approches citées précédemment révèlent un intérêt croissant et indéniable pour le développement d'antagonistes de l'activité transcriptionnelle du complexe YAP-TEAD. Véritable enjeu dans la lutte contre le cancer, il n'existe à ce jour aucun inhibiteur approuvé, ni même en phases cliniques connues. Les travaux du chapitre II de cette thèse feront donc état de la conception, de la synthèse et de l'évaluation biologique de nouveaux dérivés de l'acide flufénamique se liant de façon réversible dans la poche palmitique de TEAD afin d'inhiber l'auto-palmitoylation ainsi que l'activité transcriptionnelle associée à YAP-TEAD. Par la suite, le chapitre III présentera divers outils informatiques employés afin soit de guider l'optimisation de la série présentée au chapitre II, soit d'identifier de nouveaux inhibiteurs de TEAD.

1.4 Lecteur épigénétique PB1

PB1 (*polybromo-1 protein*), parfois également mentionné sous le nom de PBRM1 ou BAF180 dans la littérature, est une protéine contenant des domaines bromés (*bromodomain containing protein*, c'est-à-dire BCP) qui agit comme lecteur épigénétique pour le compte du remodeleur de chromatine PBAF (*polybromo-associated BAF*).

1.4.1 PB1 : une protéine contenant six domaines bromés distincts

Afin de mieux comprendre le rôle de PB1, il est important de se rappeler de l'importance de la topologie de la chromatine et du marquage épigénétique dans la régulation de l'expression génique, tel que mentionné dans la partie 1.2.2.

1.4.1.1 Domaines bromés et reconnaissance des lysines acétylées

Les domaines bromés sont des motifs d'approximativement 110 acides aminés qui gèrent des interactions protéine-protéine. Capables de reconnaître et de se lier sélectivement aux lysines ε-N-acétylées des histones, ces modules jouent le rôle de médiateur entre la chromatine marquée et divers régulateurs de la transcription, bien souvent des remodeleurs/modificateurs de chromatine ou des co-facteurs de transcription.[162] La structure des domaines bromés est hautement conservée et est définie par quatre hélices α (αA, αB, αC et αZ) liées par deux boucles flexibles (ZA et BC) de longueur variable, délimitant le site de liaison de la lysine acétylée. Cette cavité hydrophobe est profonde et permet l'interaction avec la lysine acétylée (K_{Ac}) via une liaison hydrogène entre l'oxygène du groupement carbonyle de l'acétyle et l'azote de la chaîne latérale d'une asparagine conservée dans la plupart des domaines bromés.[163,164] La liaison est renforcée par des interactions supplémentaires avec deux tyrosines également conservées, ainsi que par un réseau de liaisons hydrogènes, médiées par des molécules d'eau, avec divers groupements carbonyles du squelette

peptidique situés au niveau de l'entrée de la cavité.[165] Au sein de la poche, l'absence de résidus possédant une chaîne latérale capable de stabiliser des charges positives semble participer à la sélectivité des lysines acétylées par rapport aux lysines non modifiées.[166] La spécificité de reconnaissance de chaque domaine bromé paraît quant à elle provenir des acides aminés délimitant l'entrée de la poche. En effet, si le repliement structural est hautement conservé, il a en revanche été démontré que les séquences des boucles ZA et BC sont extrêmement variables,[167] ce qui implique que le potentiel électrostatique de la surface limitrophe au site de liaison de K_{Ac} est assez versatile, pouvant fluctuer d'une forte charge négative à une charge hautement positive.[168]

Ces lecteurs épigénétiques peuvent se retrouver dans de multiples protéines, le protéome humain exprimant par exemple 61 domaines bromés distribués parmi 46 protéines, incluant PB1, et répartis dans huit familles en fonction de leurs homologies de structure et de séquence.[168]

1.4.1.2 Structure unique de PB1

Les BCP servant essentiellement d'intermédiaires entre le marquage épigénétique et les régulateurs de l'expression génique. Ce sont des acteurs clefs qui se retrouvent souvent au sein de HAT et d'autres complexes protéiques importants (Figure 1.14).[169]

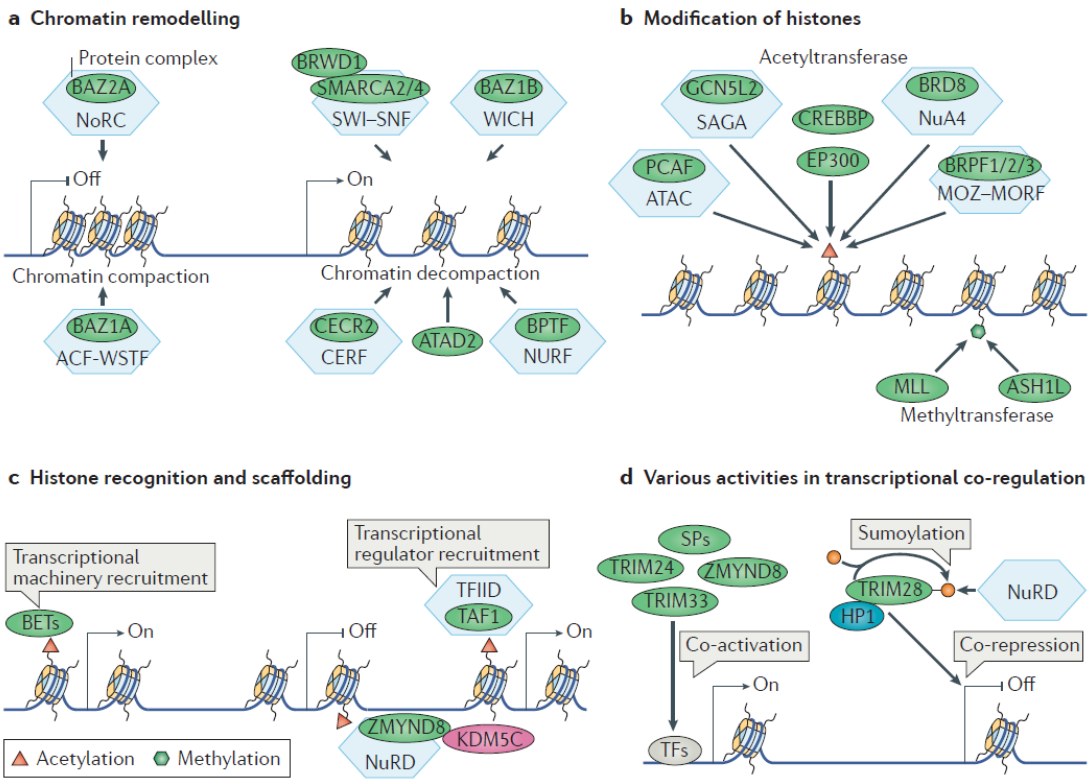

Figure 1.14 Rôles des BCP dans la régulation des gènes[169]

De ce fait, il n'est pas rare qu'une BCP possède d'autres domaines de reconnaissance de la chromatine et des marques épigénétiques, tels que des doigts PHD (*PHD fingers*), des modules PWWP, ou tout simplement plusieurs domaines bromés.[170] Malgré tout, PB1 demeure une protéine unique en son genre puisqu'il s'agit de la seule BCP constituée de six domaines bromés distincts (nommés PB1(1), PB1(2), etc. jusqu'à PB1(6)) tandis que les autres BCP contiennent deux domaines bromés tout au plus. En plus de ses six domaines bromés en tandem situés du côté N-terminal, PB1 comprend deux domaines BAH (*bromo-adjacent homology*) responsables d'autres interactions protéine-protéine, notamment la reconnaissance des histones méthylées, ainsi qu'un groupement à haute mobilité (*high-mobility group*, HMG) permettant sa liaison aux nucléosomes (Figure 1.15).[171]

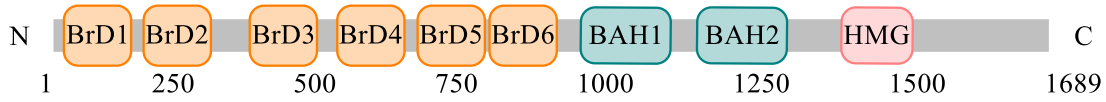

Figure 1.15 Structure de PB1 canonique

Plusieurs études réalisées par polarisation de fluorescence (FP) rapportent que chaque domaine bromé de PB1 se lie à des K_{Ac} situées à des positions spécifiques de la queue de l'histone 3 des nucléosomes, démontrant leur sensibilité unique à l'environnement entourant la lysine acétylée (Tableau 1.1).

Tableau 1.1 Interactions entre les domaines bromés de PB1 et les lysines acétylées

	K_{Ac} reconnue	Séquence reconnue	Affinité (µM)	Méthode utilisée	Ref
PB1 entier	H3K4	ART**K_{Ac}**QTARKSTGGKAPRKQLATKAA	1.1 - 34	FP	[172]
	H3K9	ARTKQTAR**K_{Ac}**STGGKAPRKQLATKAA			
	H3K14	ARTKQTARKSTGG**K_{Ac}**APRKQLATKAA			
	H3K18	ARTKQTARKSTGGKAPR**K_{Ac}**QLATKAA			
	H3K23	ARTKQTARKSTGGKAPRKQLAT**K_{Ac}**AA			
PB1(1)	H3K4	ART**K_{Ac}**QTARKSTGGKAPRKQLATKAA	0.39	FP	[173]
PB1(2)	H3K9	ARTKQTAR**K_{Ac}**STGGKAPRKQLATKAA	0.36		
PB1(3)	H3K9	ARTKQTAR**K_{Ac}**STGGKAPRKQLATKAA	0.71		
PB1(4)	H3K23	ARTKQTARKSTGGKAPRKQLAT**K_{Ac}**AA	0.12		
PB1(5)	H3K14	ARTKQTARKSTGG**K_{Ac}**APRKQLATKAA	0.79		

Il semblerait donc que chaque domaine bromé participe et oriente la spécificité de reconnaissance globale de PB1 entier. Récemment, certains groupes de recherche se sont attelés à déterminer l'importance de chaque domaine bromé afin de découvrir si tous sont nécessaires au bon fonctionnement de PB1, s'ils agissent de façon coopérative ou si, au contraire, ils permettent simplement une plus grande versatilité de reconnaissance. Des études utilisant des micro-réseaux d'histones (*histone microarrays*) et des nucléosomes intactes indiquent que PB1(2) et PB1(4) sont essentiels pour que PB1 puisse se lier autant à des peptides d'histones acétylés qu'à des nucléosomes, modifiés ou cellulaires. De façon intéressante, ces études mettent également en avant l'impact de chaque domaine bromé sur ses voisins avec par

exemple PB1(1) et PB1(5), exhausteurs des activités de PB1(2) et PB1(4), tandis que PB1(3) servirait à réduire ces mêmes interactions.[174] S'il est indéniable qu'il reste encore énormément à découvrir, mieux comprendre la complexité et la variabilité des fonctions de chaque domaine bromé, et de PB1 en général, demande de remettre la protéine dans son milieu cellulaire, c'est-à-dire comme sous-unité du remodeleur de chromatine PBAF (initialement nommé SWI/SNF-B).

1.4.2 PB1 : sous-unité du remodeleur de chromatine PBAF

Comme vu dans la partie 1.2.2.2, SWI/SNF est l'une des quatre grandes familles qui constitue les remodeleurs de la chromatine. Chez les humains, deux formes majeures hautement conservées de SWI/SNF existent : BAF (*BRG1/BRM-associated factor*) et PBAF (*polybromo-associated BAF)*. Ces complexes sont constitués d'une seule composante centrale ATPase (BRG = BRG1 = SMARCA4 dans le cas de PBAF, et soit SMARCA4, soit SMARCA2 = BRM pour BAF) entourée de multiples sous-unités. Tandis que les formes humaines de SWI/SNF partagent 9 de leurs membres, la différence entre les deux réside principalement dans la présence ou l'absence de certaines sous-unités spécifiques. PBAF contient ainsi PB1, possède ARID2 (= BAF200) à la place de ARID1A/B (= BAF250A/B), BRD7 à la place de BRD9, BAF45A (= PHF10) à la place de BAF45B/D/C (= DPF1/2/3), et manque SS18 (Figure 1.16).[175]

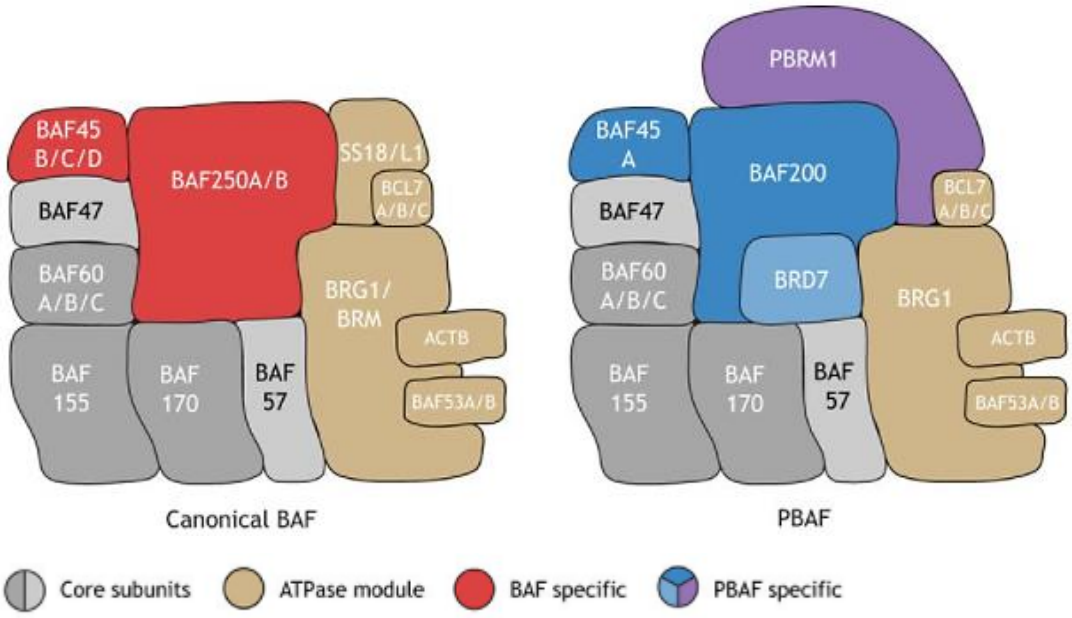

Figure 1.16 Structure des complexes BAF et PBAF[175]

Comme tout remodeleur de chromatine, PBAF joue un rôle important dans la régulation de la transcription génique en contrôlant l'accessibilité à l'ADN nucléosomal, en l'occurrence par repositionnement des nucléosomes via hydrolyse de l'ATP. Plus particulièrement, en migrant au niveau des kinétochores lors de la mitose, PBAF serait requis pour maintenir l'intégrité du génome lors de cette étape de division cellulaire.[176] PBAF est également engagé dans la régulation de gènes impliqués dans plusieurs processus du développement : formation du cœur,[177] développement de l'embryon,[178] métabolisation du glucose[179] et différenciation des ostéoblastes notamment.[180] Il a par exemple été rapporté que ce remodeleur de la chromatine coopère avec CHD7 afin de promouvoir l'expression des gènes de la crête neurale et la migration cellulaire lors de l'embryogenèse.[181]

Malgré leurs fortes similitudes, il a été démontré que BAF et PBAF peuvent autant co-exister[182] que se retrouver dans certaines régions distinctes de la chromatine, entraînant ainsi des réponses variables aux stimuli et potentiellement une transcription de gènes

différents.[183,184] Par exemple, PBAF est nécessaire à l'activation transcriptionnelle médiée par les récepteurs nucléaires d'hormone tandis que BAF échoue à induire une quelconque transcription dans le même contexte.[185] PBAF a ainsi été associé à la transcription de gènes répondant à l'oestrogène.[186] De façon intéressante, des études menées par extraction séquentielle du sel (*sequential salt extraction*) indiquent que PBAF se lie avec une plus grande affinité à la chromatine que son homologue, probablement en raison de ses 8 domaines bromés versus les 2 domaines bromés de BAF.[187] L'ensemble de ces résultats démontre que BAF et PBAF possèdent certaines fonctions biologiques distinctes probablement dues à leur liaison à des motifs uniques de la chromatine. S'il est important de noter que le rôle exact de chacun des membres formant ces complexes reste ambigu, plusieurs hypothèses se détachent petit à petit. Étant donné que la majorité des sous-unités sont partagées entre ces deux complexes, il apparaît par exemple fort probable que la reconnaissance spécifique de la chromatine soit l'une des fonctions associées aux membres distincts de l'un et l'autre.

C'est ici qu'intervient PB1 : avec ses six domaines bromés, ce lecteur épigénétique coordonne la reconnaissance des nucléosomes pour PBAF. Il est tout de même important de noter que PB1 n'est pas la seule BCP du complexe puisque BRD7 et SMARCA4 possèdent également des domaines bromés, rendant ainsi difficile l'évaluation de la fonction exacte de PB1. Malgré tout, il semblerait que PB1 joue un rôle central dans le ciblage des nucléosomes en étant par exemple nécessaire pour orienter PBAF au niveau des kinétochores des chromosomes mitotiques.[176] PB1 contribue aussi à la stabilité du génome et à la réparation de l'ADN en régulant la migration dépendante de l'actine des chromosomes,[188] en contrôlant la cohésion des centromères[189] et en participant au réamorçage des fourches de réplication abimées (*stalled replication forks*) par ubiquitination des antigènes nucléaires cellulaires proliférants (PCNA).[190,191] PB1 se révèle également clef pour le silençage transcriptionnel au voisinage des ruptures double brin de l'ADN, permettant ainsi d'induire la réparation rapide de l'ADN endommagé.[192] Quant à l'importance de PBAF

dans la maturation de la chambre cardiaque, elle a été attribuée à PB1.[193] En effet, des *knock-outs* de PB1 chez la souris indiquent que les embryons succombent de déficiences cardiaques sévères vers les jours 12.5-15.[177]

Même s'il reste encore beaucoup à découvrir sur les fonctions exactes de PBAF et de ses sous-unités, l'impact de ce remodeleur de chromatine sur la régulation des gènes et la réparation de l'ADN est indéniable. Ces deux procédés étant souvent dérégulés lors de l'initiation de tumeurs, des mutations au sein du complexe PBAF, et tout particulièrement au niveau de PB1, ont très souvent été associées au développement de diverses formes de cancer.[194,195]

1.4.3 PB1 et le cancer

Tout type de cancer confondu, les complexes hSWI-SNF font partis des régulateurs de la chromatine les plus fréquemment mutés avec approximativement 20% des tumeurs cancéreuses humaines comportant des dérégulations dans BAF et/ou PBAF.[196] Les mutations ont le plus souvent lieu au niveau des membres conférant des fonctionnalités spécifiques à chaque complexe, PB1 représentant la deuxième sous-unité la plus fréquemment mutée d'après cBioPortal 2016 (Figure 1.17).[197]

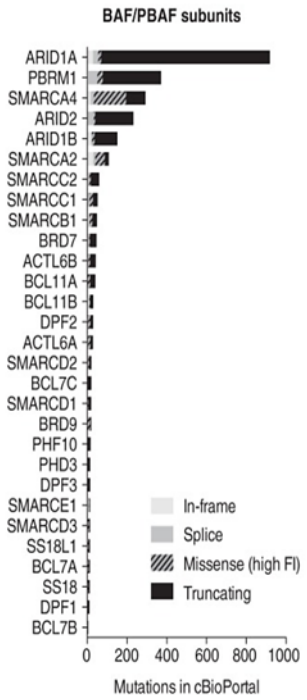

Figure 1.17 Nombre de cas de cancers présentant des mutations au sein des sous-unités de BAF et PBAF[197]

Si des mutations somatiques de PB1 ont été observées dans de nombreux types de cancer, leur occurrence dans les cas de carcinomes rénaux à cellules claires (ccRCC) est tout particulièrement significative, avec 41% des patients souffrant de ccRCC atteints de mutations tronquées au niveau de PB1.[198] D'autres études confirment que la mutation ou la suppression du gène sont à l'origine de ces résultats puisqu'aucune hyperméthylation du promoteur de PB1 n'a été observée chez les patients ccRCC.[199] Il est à noter qu'en raison de sa localisation au niveau du chromosome 3p21, l'inactivation de PB1 dans les cas de ccRCC coïncide souvent avec des altérations au niveau d'autres gènes suppresseurs de tumeurs comme VHL (von Hipper-Lindau, le seul gène plus fréquemment muté que PB1 dans les cas de ccRCC), SETD2 et BAP1.[200]

En raison de sa prévalence dans les cas de ccRCC, les mutations de PB1 ont principalement été étudiées dans ce contexte. Malgré tout, les scientifiques ont

récemment commencé à s'intéresser à l'impact de PB1 sur d'autres types de cancer. Une perte de PB1 a globalement été liée à une prolifération cellulaire accentuée, ainsi qu'une dérégulation de l'expression génique, notamment au niveau des gènes contrôlant l'apoptose et la division cellulaire.[201] Sans surprise, une analyse des données TGCA sur cBioPortal (Février 2021) indique que PB1 est désormais lié à plus de 30 types de cancer, incluant le cholangiocarcinome (cancer du canal biliaire),[202,203] les cancers du sein,[204,205] le cancer de la vessie,[206] et différents types de mésothéliomes[207] (Figure 1.18).

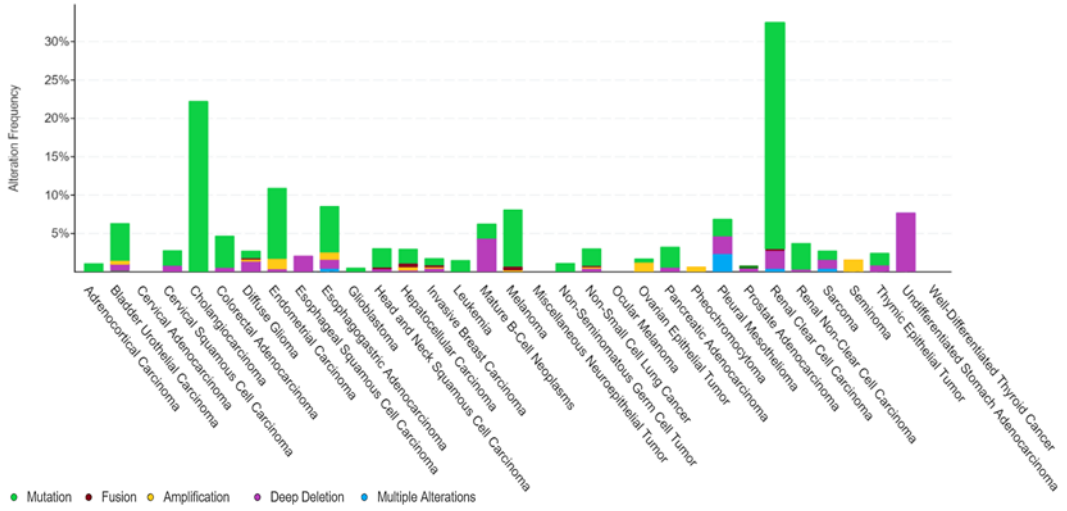

Figure 1.18 Fréquence d'altérations de PB1 dans différents types de cancer (cBioPortal, Février 2021)

L'impact des altérations de PB1 sur le cancer provient fort probablement de son rôle dans la stabilisation du génome et la réparation de l'ADN.[208] Il est cependant à noter que les différents domaines de PB1 ne sont pas tous mutés avec la même fréquence ou le même schéma de modifications (Figure 1.19). Plusieurs études s'intéressant à l'impact des différents domaines bromés de PB1 sur sa fonction de suppresseur de tumeurs indiquent notamment que PB1(2) joue un rôle tout particulièrement critique, bien que la collaboration de PB1(2), PB1(4) et PB1(5) soit généralement requise pour une fonction optimale.[187,209]

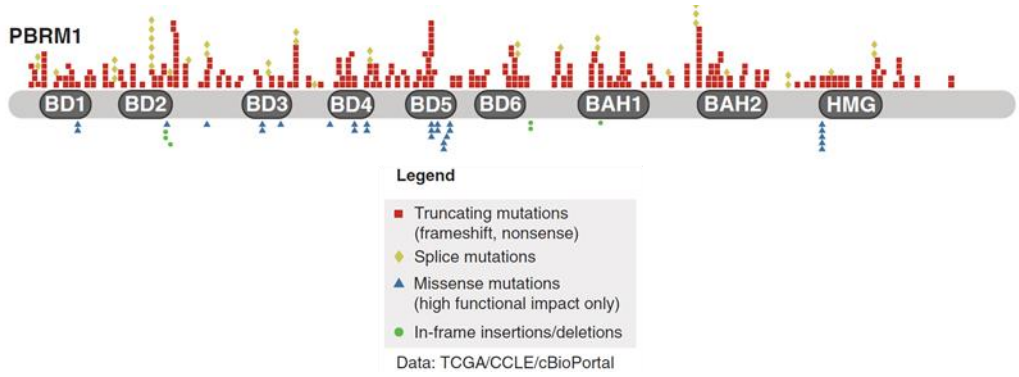

Figure 1.19 Types de mutations de PB1 dans les cas de cancer[197]

À la lumière de l'importance de plus en plus flagrante de PBAF en général, et de PB1 en particulier, dans le cancer, le développement de sondes chimiques visant les différents lecteurs épigénétiques du complexe permettrait d'aider à l'élucidation de leurs fonctions exactes afin de confirmer leurs pertinences thérapeutiques relatives. Nul doute qu'avec l'augmentation de preuves liant les domaines bromés de PB1 à différents types de cancer, ces études mèneront au lancement de campagnes de développement de nouveaux traitements.

1.4.4 Inhibiteurs des domaines bromés de PB1

Comme mentionné précédemment, PBAF contient au total huit domaines bromés : BRD7, SMARCA4 et les six domaines bromés de PB1. Si BRD7 appartient à la sous-famille IV, les autres présentent une forte homologie et sont donc tous regroupés au niveau de la sous-famille VIII. Cette sous-famille inclue également SMARCA2, l'un des domaines bromés présents dans BAF (Figure 1.20).[210]

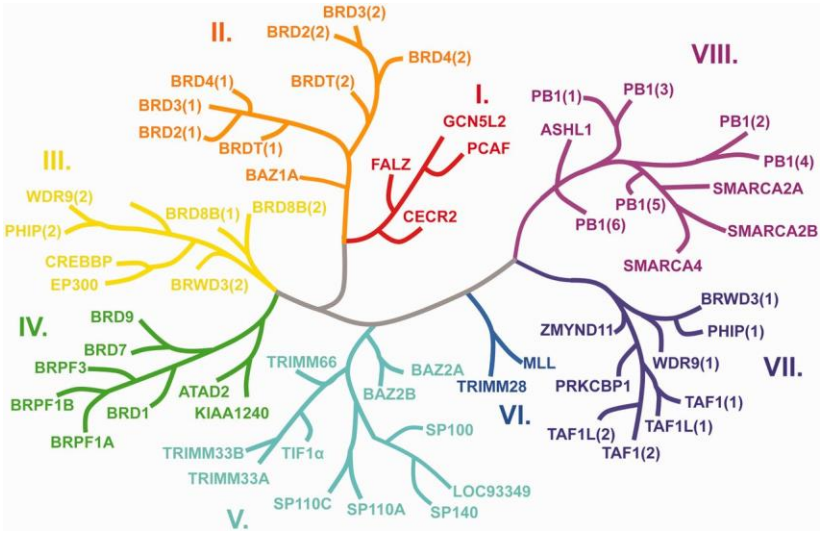

Figure 1.20 Arbre phylogénétique basé sur les domaines bromés humains[210]

À ce jour, il n'existe que peu de sondes chimiques visant les domaines bromés du groupe VIII et toutes manquent de sélectivité au sein de la famille. La première sonde disponible, et probablement celle encore la plus couramment employée, fut PFI-3. Développée par Pfizer en 2015, PFI-3 dérive de l'acide salicylique avec un bicyle di-azoté et inhibe efficacement les domaines bromés de SMARCA2A/B (deux isoformes obtenus par épissage alternatif : SMARCA2A provient d'une transcription longue tandis que SMARCA2B est issu d'une transcription courte), SMARCA4 et PB1(5) avec des K_d de 81, 86, 97 et 54 nM, respectivement.[211] Le mode de liaison de PFI-3 est peu usuel et permet une excellente sélectivité pour la sous-famille VIII : la molécule déplace des particules d'eau conservées situées au sein de la poche de liaison de la lysine acétylée, particules d'eau plus fortement liées dans les domaines bromés des autres sous-familles.[212] Malheureusement, le motif prop-2-én-1-one lié à une amine tertiaire entraîne une certaine instabilité du composé et limite donc son application à des tests cellulaires rapides. Le composé **6**, un analogue de PFI-3, a également été rapporté comme visant simultanément SMARCA2, SMARCA4, PB1(5) et PB1(2) avec des K_d respectifs de 37, 53, 30 et 190 nM.[213] En 2016, le SGC d'Oxford en Angleterre ajouta à la liste des inhibiteurs de PB1 la quinazolinone **7** qui se lie à PB1(5),

SMARCA2B et SMARCA4 avec des K_d de 124, 262 et 417 nM,[214] ainsi que le tricycle **8**, qui lui semble présenter un profil assez sélectif de PB1(5) mais qui manque toutefois d'affinité avec un K_d de 3.3 µM.[215] La même année, des dérivés de pyridazines tels qu'illustrés par la structure **9** furent brevetés par les compagnies Constellation Pharmaceuticals et Genentech sous le nom d'inhibiteurs à large spectre de SMARCA2/4 et PB1(5).[216] En 2020, ces mêmes dérivés furent finalement re-synthétisés par le SGC de Francfort en Allemagne qui en poussa la caractérisation afin de déterminer que le composé **10** se lie à SMARCA2, SMARCA4 et PB1(5) avec des K_d de 35, 36 et 13 nM, respectivement (Figure 1.21).[217]

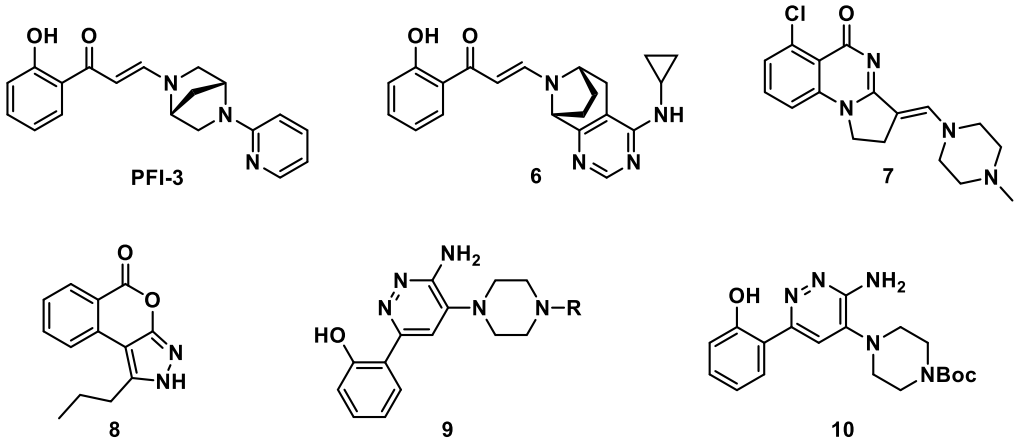

Figure 1.21 Inhibiteurs de PB1 à spectre large

Malgré toutes ces études, il n'existe à ce jour aucun inhibiteur efficace sélectif des domaines bromés de PB1 par rapport aux autres membres de la sous-famille VIII. Les travaux du chapitre IV de cette thèse feront donc état du développement et de la caractérisation d'inhibiteurs puissants présentant une sélectivité jusqu'alors non atteinte pour les domaines bromés clefs de PB1.

1.5 Protéine multidomaines BPTF

BPTF (*bromodomain and PHD-finger containing transcription factor*), parfois également mentionné sous le nom de FALZ dans la littérature, est la sous-unité principale du remodeleur de chromatine NURF (*nucleosome-remodeling factor*).

1.5.1 Rôles et structure de BPTF

Afin de mieux appréhender les fonctions de BPTF, il peut être utile de se souvenir de l'implication des protéines contenant des domaines bromés (BCP) dans la régulation de l'expression génique, tel que présenté précédemment dans la partie 1.4.1.

1.5.1.1 BPTF, sous-unité essentielle de NURF

NURF est un remodeleur de chromatine appartenant à la famille ISWI. Comme la majorité des membres appartenant à cette famille, NURF est principalement impliqué dans l'organisation des nucléosomes, son activité ATPase n'étant stimulée que par ces derniers, et non par l'ADN nu ou par l'ADN nucléosomal.[218] En interagissant avec la queue positivement chargée du côté N-terminal des histones,[219] NURF catalyse le glissement des nucléosomes tout en maintenant leur intégrité, décompactant ainsi la chromatine.[220] Mais NURF n'est pas seulement responsable d'exposer les séquences-*cis* de l'ADN, il participe également au recrutement de différents facteurs de transcription.[221] L'ensemble de ces caractéristiques font de NURF un complexe clef de l'étape d'initiation de la transcription génique.[222]

Chez l'humain, NURF (hNURF) est composé de trois sous-unités : le cœur catalytique ATPase SNF2L avec ses domaines C-terminaux caractéristiques HAND, SANT et SLIDE conservés chez l'ensemble des membres de la famille ISWI et deux orthologues respectifs de NURF301 et NURF55 présents chez les mammifères, à savoir le co-

facteur de transcription BPTF et la protéine associée au rétinoblastome RbAP48/46, (Figure 1.22).[223]

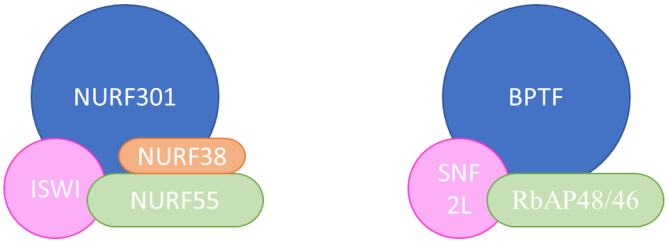

Figure 1.22 Structure de NURF chez la mouche et l'humain

Tandis que RbAP48/46 et SNF2L se retrouvent chez d'autres remodeleurs de chromatine, BPTF, en plus d'être la sous-unité la plus imposante du complexe, constitue la partie spécifique de NURF.[224] Nombre des fonctions de NURF sont donc naturellement dues à BPTF, avec plusieurs études démontrant notamment que BPTF est essentiel à l'activité de régulation de la transcription de NURF *in vivo*.[223,225] Si BPTF joue un rôle important pour la régulation transcriptionnelle à l'âge adulte, il devient absolument déterminant lors de l'embryogénèse durant laquelle il participe au développement des lignées cellulaires du mésoderme, de l'endoderme et de l'ectoderme via la répression ou l'activation de nombreux gènes.[226] D'autres analyses confirment qu'une perte de fonction de BPTF est fatale chez les embryons, alors incapables de développer des lignées extra-embryonnaires appropriées.[227] En raison de son implication lors du développement embryonnaire, peu d'études ont pu être réalisées chez les adultes. Il semblerait cependant que BPTF reste requis pour maintenir l'accessibilité à de nombreux promoteurs, jouant ainsi un rôle prépondérant lors de la différenciation des cellules souches adultes. Il a notamment été démontré que BPTF permet l'auto-renouvellement des cellules souches mammaires et la différenciation des cellules épithéliales mammaires,[228] ainsi que la différenciation des cellules souches mélanocytaires adultes.[229] Il est à noter que BPTF est omniprésent dans le corps humain

et s'avère vital pour le développement des thymocytes,[230] ainsi que pour la fonction adéquate et l'homéostasie des cellules T du système immunitaire.[231]

L'ensemble de ces fonctions n'est rendu possible que grâce aux multiples domaines qui constituent BPTF.

1.5.1.2 BPTF, une protéine multidomaines

En effet, BPTF est une protéine multidomaines comprenant plusieurs lecteurs épigénétiques : un domaine bromé (FALZ) appartenant à la sous-famille I, deux domaines PHD ainsi qu'un domaine riche en glutamine (Figure 1.23).[232]

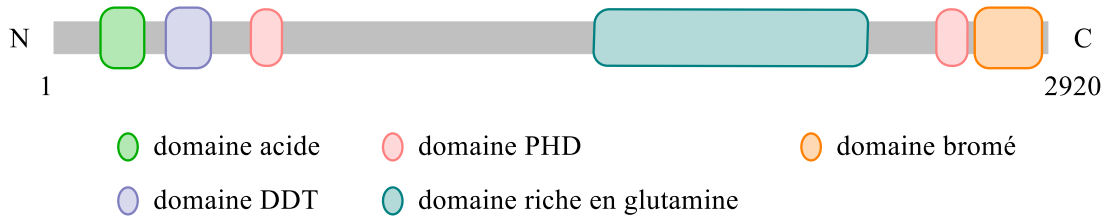

Figure 1.23 Structure de BPTF

Si la région N-terminale est reconnue pour être responsable des interactions avec différents facteurs de transcription, incluant GAGA,[224] MAZ (*Myc-associated zinc-finger protein*)[233] et hKeap1 (*human Kelch-like Ech-Associated Protein 1*),[234] les lecteurs épigénétiques de BPTF servent quant à eux à reconnaître les lysines acétylées ou méthylées présentes au niveau N-terminal des histones. Plusieurs études ont ainsi démontré que BPTF se lie aux histones acétylées H2 et H4 (notamment H4K16Ac) via son domaine bromé tandis que son domaine PHD C-terminal est capable d'interagir avec H3K3Me3.[235] Cette reconnaissance nucléosomale bivalente permet un recrutement spécifique de BPTF au niveau des gènes homéotiques à activer,[236] laissant penser que ces domaines participent activement au maintien de l'activité cellulaire normale de BPTF.

En raison de l'importance de BPTF au niveau de la régulation de l'expression génique, il n'est pas surprenant qu'une dérégulation de sa propre expression ait été associée à de multiples maladies, incluant des anomalies neurodéveloppementales,[237] ainsi que différents types de cancer.

1.5.2 Implications de BPTF dans le cancer

Une analyse des données TGCA sur cBioPortal (Mars 2021) indique qu'une expression aberrante de BPTF a été recensée dans plus d'une trentaine de types de cancer, avec une amplification du gène souvent présente, notamment chez les patients atteints de mésothéliomes (Figure 1.24).

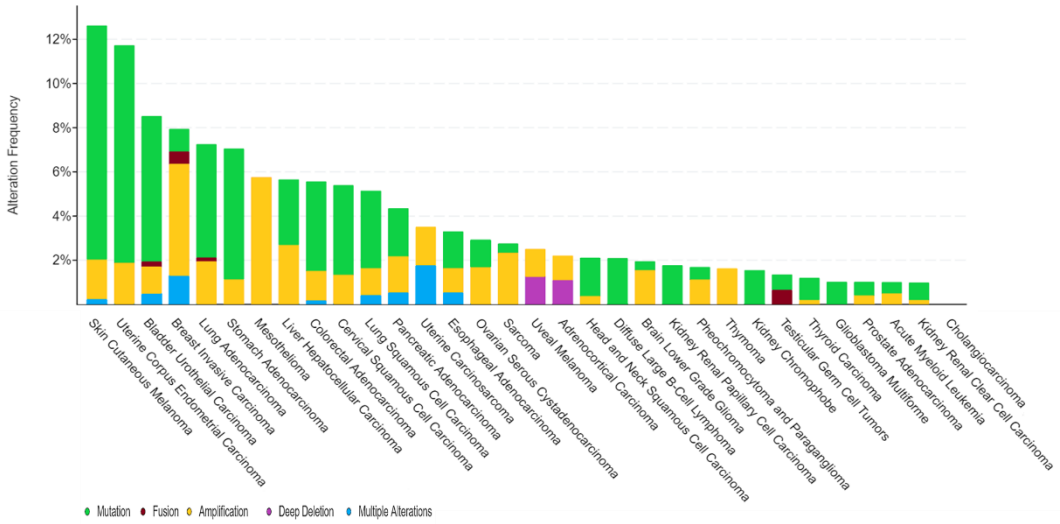

Figure 1.24 Fréquence d'altérations de BPTF dans différents types de cancer (cBioPortal, Mars 2021)

BPTF réside sur le chromosome 17q, un morceau fréquemment dupliqué dans de nombreux cancers.[238] Une surexpression de BPTF a ainsi été associée au développement et à la progression du cancer colorectal,[239] des adénocarcinomes des poumons,[240] des mélanomes,[241,242] et des neuroblastomes.[243] Des études menées sur des tissus présentant un carcinome hépatocellulaire semblent indiquer qu'une forte

expression de BPTF se traduit par une augmentation des différents processus liés à l'EMT (invasion vasculaire, récurrence, etc), entraînant un pronostic de survie assez bas.[244] Des *knockdowns* de BPTF dans différentes lignées cancéreuses montrent quant à eux une réduction de la prolifération cellulaire.[245,246] L'implication de BPTF dans ces multiples cancers proviendrait en partie de sa participation requise pour l'activation de la transcription et le bon fonctionnement du gène oncogène *c-myc*.[247,248] En effet, le silençage de BPTF diminue l'expression de c-MYC, nuit à son recrutement au niveau de la chromatine et réduit l'accès à l'ADN des gènes cibles de c-MYC.[249] Émergeant ainsi comme une cible potentielle pour le développement de nouvelles thérapies contre le cancer,[250] il a également été constaté que des *knockdowns* de BPTF améliorent l'immunité antitumorale médiée par les lymphocytes T $CD8^+$ et NK (*natural killers*).[251,252] Ces résultats laissent présager que des inhibiteurs de BPTF pourraient également être investigés dans le cadre d'immunothérapies.

Sachant que l'inhibition des domaines bromés de nombreuses BCP s'est déjà révélée une stratégie payante pour le traitement de plusieurs maladies reliées à ces BCP en question,[253] l'intérêt croissant pour le développement d'inhibiteurs du domaine bromé de BPTF s'explique aisément.

1.5.3 Inhibiteurs du domaine bromé de BPTF

Bien qu'en 2012 le domaine bromé de BPTF (BPTFBrD) ait été rapporté comme hautement *druggable,*[254] il faudra attendre trois ans de plus pour que soit développé le premier inhibiteur de BPTFBrD. AU1 fut découvert lors d'un criblage par RMN-^{19}F visant à la fois BPTFBrD et BRD4. Des mesures par titrage calorimétrique isotherme (ITC) révèlent que *rac*-AU1 interagit avec BPTFBrD avec un K_d de 2.8 μM tandis qu'aucune liaison avec BRD4 n'est observée.[255] Malheureusement, des études ultérieures démontrent que *rac*-AU1 interagit également avec certaines kinases, inhibant notamment CDKL2 et TRKC à 82% lorsque testé à 1 μM.[256] Dans une tentative d'améliorer la sélectivité, les deux isomères de AU1 furent isolés en 2020,

permettant ainsi de déterminer que l'activité provient uniquement de l'énantiomère *S*. Le manque de sélectivité relativement aux kinases CDKL2 et TRKC est cependant confirmé pour l'énantiomère (S) avec des K_d de 260 et 200 nM, respectivement.[257] En 2019, un nouveau dérivé dialkoxyiodobenzamide DCB29 fut rapporté. Conçu à la suite d'un criblage virtuel basé sur la structure, DCB29 inhibe BPTFBrD avec un IC_{50} de 13.2 μM dans un test de transfert d'énergie de résonance de fluorescence à résolution temporelle homogène (HTRF) et un K_d de 17.9 μM mesuré par résonance plasmonique de surface (SPR).[258] La même année, C620-0696 fut publié avec un K_d de 35.5 μM pour BPTFBrD déterminé cette fois-ci par interférométrie biocouche (BLI). En inhibant l'interaction entre BPTFBrD et H4K16Ac, C620-0696 entraîne une répression de l'activation de la transcription de *c-myc* et conduit à une diminution de la prolifération de cellules du cancer du poumon sur-exprimant BPTF.[259] TP-238 fut finalement la première sonde avec une activité biochimique envers BPTFBrD de l'ordre du bas nanomolaire. Issu d'une collaboration entre Takeda et le SGC, TP-238 est cependant un inhibiteur double de CECR2, un domaine bromé appartenant également à la sous-famille I, et de BPTFBrD avec des IC_{50} mesurés par test alphascreen de 30 nM et 350 nM, respectivement, et des K_d de 10 nM et 120 nM, respectivement.[260] Palliant ce problème, NVS-BPTF-1 fut la première petite molécule à être à la fois fortement active et sélective de BPTFBrD. Issu cette fois-ci d'une collaboration entre le SGC et Novartis, NVS-BPTF-1 possède un IC_{50} de 56 nM dans un test alphascreen et un K_d de 71 nM par test BLI. Des études supplémentaires par analyse fluorimétrique différentielle (DSF) et par BROMOscan permettent d'affirmer que NVS-BPTF-1 ne cible aucun autre domaine bromé de façon significative.[261] Récemment, un nouveau composé **11** fut également rapporté comme inhibiteur puissant de BPTFBrD avec un K_d de 428 nM déterminé par ITC. **11** réduit l'expression de c-MYC et BPTF dans des cellules de l'adénocarcinome humain A549 (Figure 1.25).[262]

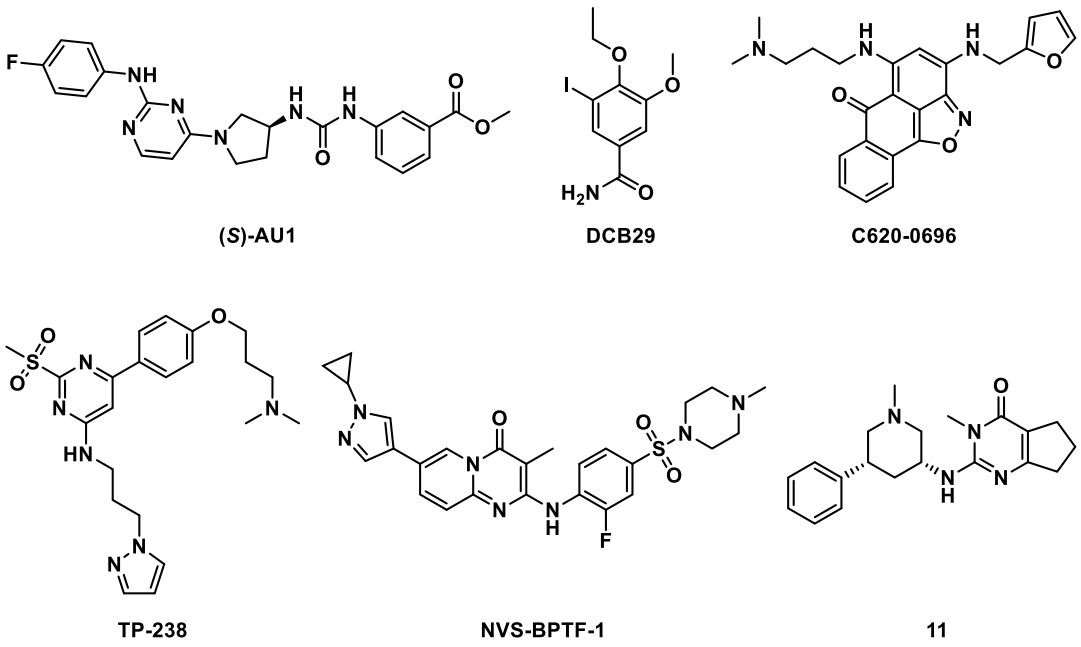

Figure 1.25 Inhibiteurs du domaine bromé de BPTF

S'il ne fait aucun doute que NVS-BPTF-1 demeure à ce jour la sonde chimique la plus efficace et sélective pour BPTFBrD, sa synthèse n'a encore jamais été rapportée. Les travaux du chapitre V de cette thèse présenteront donc la première voie de synthèse divulguée, permettant ainsi un accès rapide à cet inhibiteur et potentiellement différents dérivés. Afin d'évaluer le potentiel en immunothérapie de BPTFBrD, des études concernant l'impact de son inhibition sélective grâce à NVS-BPTF-1 seront également exposées.

CHAPITRE II

DÉVELOPPEMENT D'INHIBITEURS DE TEAD DÉRIVÉS DE L'ACIDE FLUFÉNAMIQUE

2.1 Introduction

Responsable de l'expression de gènes contribuant entre autres à la croissance cellulaire et à la prolifération, le contrôle de l'activité du complexe fonctionnel YAP-TEAD est devenu un véritable enjeu dans la lutte contre le cancer. Pourtant, il n'existe à ce jour aucun inhibiteur approuvé, ni même en phases cliniques connues. Cet article rapporte donc la conception, la synthèse et l'évaluation biologique de nouveaux dérivés de l'acide flufénamique se liant de façon réversible dans la poche palmitique de TEAD afin d'inhiber l'auto-palmitoylation ainsi que l'activité transcriptionnelle associée au complexe.

2.2 Article issu de ces travaux

ChemMedChem | Full Papers
doi.org/10.1002/cmdc.202100432

Development of LM98, a Small-Molecule TEAD Inhibitor Derived from Flufenamic Acid

Léa Mélin,[a] Shuay Abdullayev,[a] Ahmed Fnaiche,[a] Victoria Vu,[b] Narjara González Suárez,[a] Hong Zeng,[b] Magdalena M. Szewczyk,[b] Fengling Li,[b] Guillermo Senisterra,[b] Abdellah Allali-Hassani,[b] Irene Chau,[b] Aiping Dong,[b] Simon Woo,[c] Borhane Annabi,[a] Levon Halabelian,[b] Steven R. LaPlante,[c] Masoud Vedadi,[b, d] Dalia Barsyte-Lovejoy,[b, d] Vijayaratnam Santhakumar,[b] and Alexandre Gagnon*[a]

Dedicated to our dear friend and colleague Prof. Eric Marsault, who passed away on January 13th, 2021

The YAP-TEAD transcriptional complex is responsible for the expression of genes that regulate cancer cell growth and proliferation. Dysregulation of the Hippo pathway due to overexpression of TEAD has been reported in a wide range of cancers. Inhibition of TEAD represses the expression of associated genes, demonstrating the value of this transcription factor for the development of novel anti-cancer therapies. We report herein the design, synthesis and biological evaluation of LM98, a flufenamic acid analogue. LM98 shows strong affinity to TEAD, inhibits its autopalmitoylation and reduces the YAP-TEAD transcriptional activity. Binding of LM98 to TEAD was supported by ^{19}F-NMR studies while co-crystallization experiments confirmed that LM98 is anchored within the palmitic acid pocket of TEAD. LM98 reduces the expression of *CTGF* and *Cyr61*, inhibits MDA-MB-231 breast cancer cell migration and arrests cell cycling in the S phase during cell division.

Introduction

The Hippo signaling pathway plays a crucial role in organ size by controlling the balance between cell proliferation and apoptosis.[1] TEAD (transcriptional enhancer factor with TEA/ATTS domain), the downstream effector of the Hippo pathway, is composed of an N-terminal DNA binding domain and a C-terminal YAP-binding domain (YBD) that binds to co-regulator YAP (Yes-associated protein) or its paralog TAZ (transcriptional co-activator with PDZ-binding motif). Since TEAD does not possess an activation domain and because YAP and TAZ do not have a DNA binding domain, TEAD and coactivators YAP or TAZ must associate in the nucleus to form a transcriptionally active YAP/TAZ-TEAD complex. In the active Hippo pathway, external signals such as hormonal cues, cell junctions, extracellular matrix as well as proteins RASSF and NF2/Merlin trigger a cascade of kinases involving Mst1/2, Sav, Mob1 and Lats1/2 which ultimately results in the phosphorylation of YAP. Subsequent recruitment of phosphorylated YAP by protein 14-3-3 then leads to its retention and degradation in the cytoplasm, therefore precluding its interaction with TEAD and preventing the transcription of associated genes.[2,3] Conversely, in the inactive Hippo pathway, unphosphorylated YAP translocates to the nucleus where it binds to one of the four paralogs of TEAD[4,5] to initiate the transcription of target genes such as *Cyr61*, *CTGF* (Connective Tissue Growth Factor), *c-myc*, receptor tyrosine kinase *Axl* and *Survivin*.[6,7,8,9]

Numerous studies have shown that the dysregulation of the Hippo pathway can lead to various forms of cancer.[10,11] For instance, increased YAP expression and nuclear localization have been observed in liver, colon, ovarian, lung and prostate cancer[12,13] while upregulation of TEAD and poor patients survival were correlated with gastric, breast and prostate cancers.[14–17] Aberrant Hippo can lead to organ overgrowth and tumorigenesis, as demonstrated in mouse models where elevated nuclear YAP induced by a double Mst mutation resulted in an oversized liver with carcinoma.[18] The proto-oncogenic nature of YAP comes from its interaction with TEAD[19,20] which leads to the activation of genes that confer cancer-associated traits to cells such as the ability to induce chemoresistance and metastasis.[21–23] Silencing of the majority of YAP-inducible genes and attenuation of YAP-induced overgrowth in TEAD knockdowns suggest that TEAD is a highly valuable target for drug development.[19] Furthermore, TEAD

[a] L. Mélin, S. Abdullayev, A. Fnaiche, N. González Suárez, Prof. B. Annabi, Prof. A. Gagnon
Département de chimie, Université du Québec à Montréal
C.P. 8888, Succ. Centre-Ville, Montréal QC,
H3C 3P8 (Canada)
E-mail: gagnon.alexandre@uqam.ca
[b] Dr. V. Vu, H. Zeng, Dr. M. M. Szewczyk, Dr. F. Li, Dr. G. Senisterra, Dr. A. Allali-Hassani, I. Chau, Dr. A. Dong, Dr. L. Halabelian, Prof. M. Vedadi, Dr. D. Barsyte-Lovejoy, Dr. V. Santhakumar
Structural Genomics Consortium, University of Toronto
101 College St. MaRS South Tower, Toronto, ON, M5G 1 L7 (Canada)
[c] Dr. S. Woo, Prof. S. R. LaPlante
INRS-Centre Armand Frappier Santé Biotechnologie,
Université du Québec
531 Boulevard des Prairies, Laval, QC,
H7V 1B7 (Canada)
[d] Prof. M. Vedadi, Dr. D. Barsyte-Lovejoy
Department of Pharmacology and Toxicology
University of Toronto, Toronto, ON,
M5S 1 A8 (Canada)

Supporting information for this article is available on the WWW under https://doi.org/10.1002/cmdc.202100432

ChemMedChem
Full Papers
doi.org/10.1002/cmdc.202100432
Chemistry Europe
European Chemical Societies Publishing

appears to be dispensable for tissue homeostasis in adults, therefore decreasing the risks of major adverse side effects.[24] Taken together, these results indicate that blocking the formation of the YAP-TEAD transcription complex can abolish the oncogenic function of YAP.[20]

The crystal structure of YAP2 with TEAD1 (PDB: 3KYS) shows that YAP wraps itself around the surface of TEAD via three distinct interaction surfaces that are composed of an antiparallel β-strand (interface 1), an α-helix (interface 2) and a twisted-coil region (interface 3) (Figure 1). Studies have demonstrated that out of these three interfaces, interface 3 is the most critical for heterodimer formation.[25] Disruption of the YAP-TEAD complex by cyclic or linear YAP-like peptides, cysteine-dense peptides or VGLL4-mimicking peptides has been reported.[26–30] However, the development of these compounds is compromised by poor pharmacokinetic profiles, low plasmatic stability and poor cell permeability that are commonly associated with peptides. Compounds that bind in a cavity formed by the C-terminal hTEAD1 region close to interface 3 were identified following a virtual screen of the ZINC database and their activity was confirmed by biophysical and *in cellulo* assays.[31] Similarly, CPD3.1, a tetracyclic molecule that blocks the interaction of YAP with TEAD1 and inhibits TEAD activity with an IC_{50} of 110 μM as well as TEAD targeted gene expression, cell proliferation and cell migration, was recently disclosed.[32] However, binding of small molecules to one of the interfaces between YAP and TEAD remains challenging due to the absence of well-defined druggable pockets.[33]

One way to circumvent that problem consists in indirectly disrupting the YAP-TEAD functional complex. Because they are highly disordered, YAP and TAZ are not suitable targets for medicinal chemistry endeavors. On the other hand, TEAD is much more attractive due to the presence of a well-defined hydrophobic pocket that is occupied by a palmitic acid (PA) molecule (shown in beige in Figure 1) and that is conserved within the TEAD family. Studies have shown that TEAD undergoes auto-palmitoylation through covalent bond formation between a conserved cysteine residue and palmitic acid. Some reports indicate that the absence of TEAD palmitoylation results in a drastic reduction of the affinity with YAP while other studies conclude that TEAD containing partial mutations retains its ability to interact with YAP, albeit with a lower affinity.[33–37] TEAD rigidification appears to be at the origin of these results.[38] The expression level and transcriptional activity of TEAD are also directly modulated by its palmitoylation status[39] and numerous studies agree on a loss of stability for non-palmitoylated TEAD.[38]

Small molecules inhibitors that bind to TEAD's palmitate pocket have been reported. For example, Pobbati and Poulsen reported that flufenamic acid (FA) **1** and niflumic acid (NA) **2**, two commercialized non-steroidal anti-inflammatory drugs (NSAID), inhibit TEAD's palmitoylation by binding inside the TEAD palmitate pocket (Figure 2).[40] Although this binding did not prevent the formation of the YAP-TEAD complex, it nevertheless resulted in a reduction in the expression of the Hippo-associated genes in MCF10 A breast cancer cells, suggesting that the YAP-TEAD complex was transcriptionally inactive. Compound MGH-CP1 **3**, reported by a team from Boston General Hospital, binds in the central pocket of TEAD2, reduces gene activation with an IC_{50} of 83 nM in a cell based Gal4-TEAD1 reporter assay, disrupts the YAP-TEAD complex and diminishes the expression of YAP-TEAD responsive genes *CTGF* and *Cyr61*.[38] Although many derivatives were disclosed, the

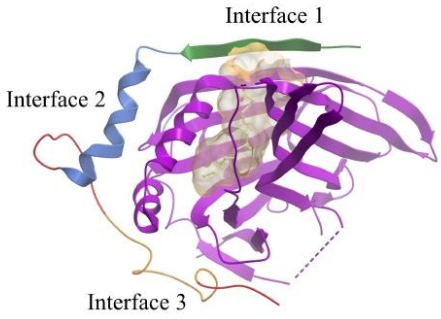

Figure 1. hYAP-hYBD of TEAD1 in the presence of palmitic acid (PA) (beige) (PDB: 3KYS and 5HGU). TEAD1's hYBD in purple, YAP in green (interface 1), blue (interface 2), red and orange (interface 3).

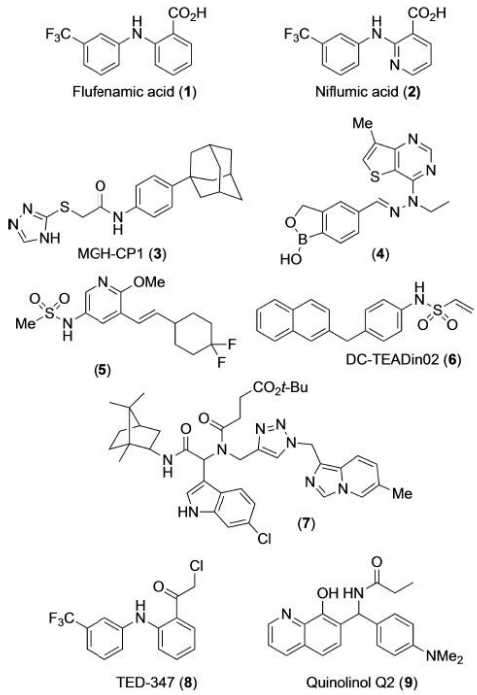

Figure 2. Examples of reported TEAD inhibitors and activators.

ChemMedChem
Full Papers
doi.org/10.1002/cmdc.202100432
Chemistry Europe
European Chemical Societies Publishing

current development stage for **3** is not known. Similarly, compound **4**, recently reported by Inventiva, showed an IC_{50} of 260 nM in a cell-based TEAD-GAL4 transactivation reporter assay. Even though many analogues were reported, to the best of our knowledge, its development status has not been disclosed yet.[41] While preparing this manuscript, compound **5** and **7**, two reversible inhibitors targeting the TEAD palmitate binding pocket, have been published.[42,43]

Covalent TEAD inhibitors that react with the cysteine located at the entry of the palmitate pocket such as **6** and **8** have also been developed, further emphasizing the growing interest for compounds that bind in that pocket.[44,45] Although covalent inhibitor **6** inhibited TEAD autopalmitoylation with an IC_{50} value of 197 nM, it showed only minimal effect on YAP-TEAD interaction, contrary to inhibitor **8** which was found to disrupt the YAP-TEAD complex.[44,45] It should be noted that, similar to covalent inhibitor **6**, non-covalent inhibitors **2** and **5** also did not inhibit YAP-TEAD interaction, suggesting that the inhibition of TEAD activity is not due to the inability of TEAD to form a complex with YAP in cells.[40,42] Interestingly, binding of compounds inside TEAD's palmitate pocket can also, in some cases, result in increased TEAD activity, as demonstrated by quinolinol **9**.[46]

Although an increasing number of studies highlight the relevance of TEAD in the development of cancer, to our knowledge, there are currently no TEAD inhibitors on the market or in the clinic. Therefore, there is an urgent need for efficient small-molecule inhibitors targeting these oncogenic proteins. In light of the drug-like properties and modular structure of flufenamic acid **1**, its reversible mode of inhibition and its decent affinity to TEAD, we initiated a program aimed at thoroughly studying its SAR and improving its activity. While preliminary SAR studies have been reported for FA **1** and for the analogous covalent compound TED-347 (**8**), to the best of our knowledge, extensive and systematic SAR investigations around FA series **1** have not been reported. Herein, we would like to disclose our results on the design, synthesis and biological evaluation of new derivatives of flufenamic acid **1** that bind in the palmitate pocket of TEAD, inhibit TEAD's autopalmitoylation and reduce YAP-TEAD's transcriptional activity.

Results and Discussion

Synthesis of flufenamic acid derivatives and evaluation of their binding to TEAD. The aim of our initial medicinal chemistry efforts was to systematically study the structure-activity landscape of flufenamic acid (FA) **1** and to expand on the limited existing knowledge from the literature.[40,45] To do so, we divided FA **1** into four key sections: the left-hand side (LHS) aromatic ring, the central linker, the right-hand side (RHS) aromatic ring and the carboxylic acid (Figure 3a). To guide our SAR efforts, we superimposed the high-resolution co-crystal structures of palmitic acid (PA) (PDB: 5HGU, resolution: 2,05 Å; structure of PA shown in Figure 3b) with FA (PDB: 5DQ8, resolution: 2,3 Å) complexed to hTEAD2-YBD (Figure 3c). Preliminary observations suggested the presence of an internal H-bond interaction between the carboxylate and the NH functions of FA. As previously reported, the X-ray structures also revealed that FA and PA are anchored within the pocket via an H-bond interaction between their respective carboxylate functions and Cys380 as well as through an ionic interaction with the terminal amine of Lys357.[39] The overlay of the FA and PA co-crystal structures highlighted the presence of an empty hydrophobic space inside the pocket which appeared suitable for extensive diversification at the CF_3 position of FA, the most logical being the direct transposition of the palmitic acid alkyl chain onto the core of FA. Meroueh *et al* showed the value of this approach by replacing the trifluoromethyl moiety with a methoxyethoxy group in the covalent TED series **8**.[45]

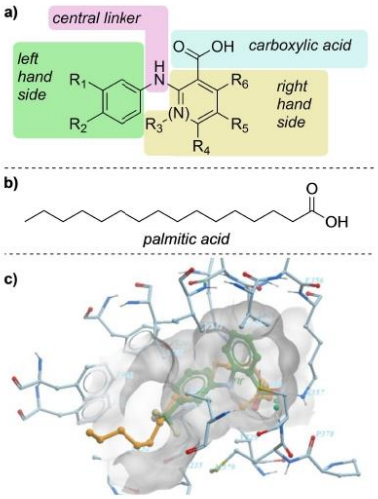

Figure 3. a) Subdivision of flufenamic acid (FA) in four key sections for SAR activities. **b)** Palmitic acid (PA). **c)** Superposition of PA (yellow; PBD 5HGU) and FA (green; PDB 5DQ8) in TEAD2's hYBD.

To explore the importance of the putative internal H-bond between the carboxylate and the NH of FA, we resynthesized FA (**1**) and prepared compounds where the central amino function of FA **1** is replaced by an ether (**10**), a thioether (**11**), a methylene (**12**) and an N-methylamine (**13**) (Table 1, see experimental section for the syntheses). Evaluation of the binding of compounds to TEAD4 by differential scanning fluorimetry (DSF), a fluorescence-based method that monitors the changes in melting temperature (T_m) upon ligand binding, was attempted.[48] However, some compounds interfered with the fluorescence read out, leading us to use differential static light scattering (DSLS) thermal shift assay instead.[47] In this assay, the increase in temperature of aggregation (ΔT_{agg}) of TEAD4 YBD upon compound binding, which is unaffected by fluorescence properties of the compounds, is monitored. We were pleased to see that resynthesized FA **1** showed weak but

ChemMedChem | Full Papers
doi.org/10.1002/cmdc.202100432
Chemistry Europe
European Chemical Societies Publishing

Table 1. Replacement of the central NH linker in flufenamic acid (FA) **1**.

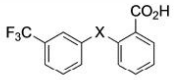

Compounds	X	ΔT_{agg} [a]
1 (FA)	NH	1.3
10	O	0.7
11	S	0.4
12	CH_2	0.4
13	NMe	0.3

[a] ΔT_{agg} values are the average of three DSLS measurements at 25 μM of compound (n = 3).

Table 2. Structure-activity relationships of R_1 substituted FA derivatives.

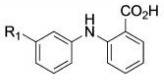

Compounds	R_1	ΔT_{agg} [a]
16	H	0.2
17	Me	0.1
18	Et	−0.1
19	*n*-Pr	2.9
20	*n*-Bu	3.4
21	*n*-Pent	4.4
22	*n*-Hex	5.2
23	*n*-Hept	6.0
24	*i*-Pr	2.6
25	*t*-Bu	1.5
26	Ph	2.1

[a] ΔT_{agg} values are the average of three DSLS measurements at 25 μM of compound (n = 3).

measurable stabilization of TEAD by DSLS (ΔT_{agg} = 1.3 °C), a value which is similar to the differential scanning fluorimetry (DSF) results previously published by Pobatti *et al.*[40] However, none of the NH replacements improved the affinity of compounds. NA **2** and MGH-CP1 **3** were also resynthesized in our laboratory as reference compounds. MGH-CP1 **3** was synthesized according to patent WO 2017/053706 A1.[38] Resynthesized NA **2** showed an almost negligible ΔT_{agg} value of 0.3 °C while resynthesized MGH-CP1 **3** afforded a higher shift of 3.0 °C.

Pobbati *et al* demonstrated that replacement of the trifluoromethyl group in FA **1** with a bromide or a hydrogen leads to drastic loss of affinity to TEAD while Meroueh *et al* showed that an ethoxymethoxy chain or a thiophene are valid CF_3 replacements.[40,45] To get a more complete picture, we designed a modular synthetic route that allows the rapid preparation of analogues of FA **1** with various groups at the CF_3 position (R_1 in Scheme 1a). Compounds **16**–**26** were prepared through a Buchwald-Hartwig N-arylation reaction between aniline **14** and 2-bromomethyl benzoate followed by saponification of the methyl ester. A similar palladium-catalyzed N-arylation reaction was used by Meroueh *et al* for the synthesis of covalent TED compounds **8**.[45] Anilines **14** were either obtained commercially or were prepared via Wittig olefination reaction between 3-nitrobenzaldehyde and phosphonium iodides **28** followed by reduction of the nitro group of **29** under Béchamp's conditions and reduction of the alkene in **30** under hydrogenation conditions (Scheme 1b). Phosphonium iodides **28** were prepared by reacting the corresponding alkyl iodides **27** with triphenylphosphine.

DSLS results indicate that the unsubstituted compound **16** lacking the CF_3 group, as previously shown by Pobbati *et al*, does not stabilize TEAD4 significantly (Table 2). Similarly, the methyl and ethyl derivatives **17** and **18** showed no protein stabilization. However, a gradual increase in ΔT_{agg} was observed with compounds **19** to **23** as the carbon chain increased from 3 to 7 carbons, demonstrating that the more an analogue resembles palmitic acid, the better its affinity to TEAD is. Furthermore, the pocket appeared to be large enough to accommodate an isopropyl or *tert*-butyl group on the upper West side as well as a phenyl ring, as shown by compounds **24**, **25** and **26**, respectively. To our knowledge, this is the first time that the tolerability of the TEAD's PA pocket towards bulky tertiary or secondary alkyl groups is demonstrated.

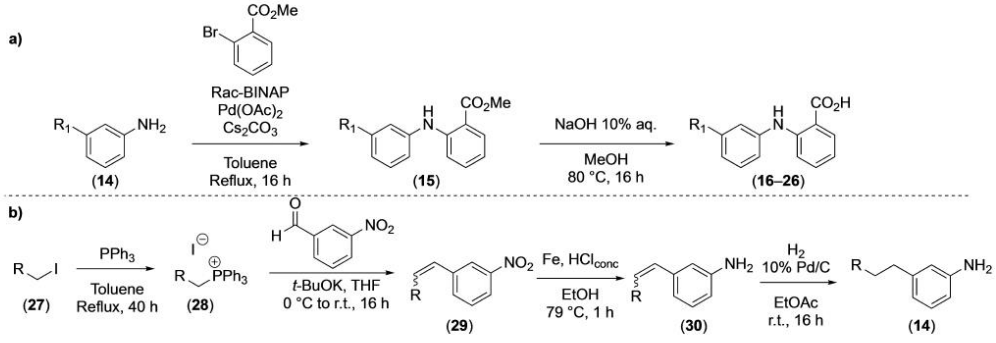

Scheme 1. a) General synthetic route for the synthesis of flufenamic acid derivatives **16**–**26**. **b)** Preparation of anilines **14**.

To assess the structure activity relationship (SAR) more accurately, we attempted to determine the affinities of our compounds for binding to TEAD4 by surface plasmon resonance (SPR). We used MGH-CP1 (compound **3**) as a control. However, we could not reliably detect binding of any of them including the control compound to TEAD4 by SPR (Supporting Information figure 1). We were also not successful in assessing the affinities of any of these compounds including compound **3** by isothermal titration calorimetry (ITC) due to poor solubility of compounds (Supporting Information figure 2). While DSLS is not an ideal quantitative assay for rank-ordering compounds for SAR studies, it has been shown that thermal shift data could meaningfully correlate with binding affinities of compounds measured by other methods.[49–52] Our DSLS data on compounds in this study also showed a wide range of stabilization effects with $\triangle T_{agg}$ values up to 10 °C. Therefore, we concluded that the DSLS data are valuable in rank-ordering our compounds, where other methods failed.

Using compound **22**, which showed one of the highest ΔT_{agg}, as a new lead compound, we next proceeded to explore the tolerance of the RHS towards the introduction of substituents. To our knowledge, the only derivative exploring modifications on the East side of the molecule is the C4-methoxy, reported by Meroueh *et al* in the covalent series **8**.[45] Because the co-crystal structure of FA with TEAD2 showed limited space in the pocket around the RHS, we began by walking a fluorine around the right-hand side aromatic ring, resulting in compounds **31** to **34** (Table 3). DSLS results show that this additional fluorine is well tolerated at every position and even leads, in some cases, to a non-negligible increase in affinity to TEAD. Substitution at C6 is of particular interest as it is pointing towards interface 1 between YAP and TEAD. We hypothesized that in addition to inhibiting TEAD's palmitoylation, directly disrupting one of the interaction surfaces could result in more potent inhibitors of the YAP-TEAD complex and thus stronger reduction of gene expression. Consequently, compound **35** with a C6-methyl group was prepared and was found to be well tolerated, thus providing an additional vector for future SAR investigations.

Table 3. Structure-activity relationships of compounds substituted on the right-hand side (RHS) aromatic group.

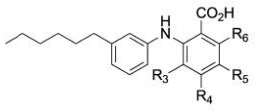

Compound	R_3	R_4	R_5	R_6	ΔT_{agg} [a]
22	H	H	H	H	5.2
31	F	H	H	H	5.2
32	H	F	H	H	6.4
33	H	H	F	H	6.2
34 (**LM98**)	H	H	H	F	6.4
35	H	H	H	Me	5.2

[a] ΔT_{agg} values are the average of three DSLS measurements at 25 μM of compound (n = 3).

As an orthogonal method to confirm binding, we used ^{19}F-NMR spectroscopy, where differences in the linewidth and/or intensity of the signal(s) of the compound in the free state (SF) and in the presence of protein (SP) may be used to monitor binding.[53,54] Before initiating the binding studies, an evaluation by ^{1}H-NMR of the compounds' free state behavior in aqueous buffer (10 mM HEPES-d_{18}, 150 mM NaCl, 0.5 mM TCEP-d_{15}, 10% D_2O, pH 7.4, 1% DMSO-d_6) was performed to minimize the chances of misleading results stemming from poor compound solubility. **LM98**, FA **1** and NA **2** showed measured concentrations by the ERETIC method[55] of 54, 53 and 47 μM, respectively, for a nominal concentration of 50 μM, demonstrating sufficient solubility for the ligand binding studies (Figure 4a–c). In the presence of TEAD (50 μM compound:15 μM TEAD, a 3.33:1 compound:TEAD ratio), **LM98** showed clear evidence of binding based on the differential line broadening and signal intensity change of the ^{19}F-NMR signal of the SP sample compared to the SF sample (Figure 4d). Under the same conditions, FA **1** and NA **2** also showed evidence of binding based on the change in the ^{19}F-NMR signal intensity for the SP versus the SF sample (Figure 4e–f). In agreement with the results from the DSLS thermal shift assay, **LM98** appeared to be a much stronger binder to TEAD4 than the hit compounds FA and NA based on the greater change in the peak shape of the ^{19}F-NMR signal. With binding confirmed for all three compounds by ^{19}F-NMR spectroscopy, we moved to the next set of experiments to further characterize the binding of our compounds to TEAD.

To further elucidate the binding mode of our compounds and to identify additional opportunities for improvement in activity and physicochemical properties, we co-crystallized the

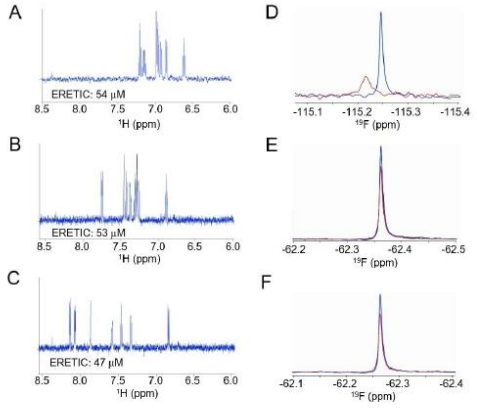

Figure 4. a) Aromatic region of free state ^{1}H-NMR spectrum of **LM98** (50 μM) in buffer. **b)** Aromatic region of free state ^{1}H-NMR spectrum of FA **1** (50 μM) in buffer. **c)** Aromatic region of free state ^{1}H-NMR spectrum of NA **2** (50 μM) in buffer. **d)** ^{19}F-NMR spectrum of **LM98** (50 μM): Free state in buffer (blue) and in presence of 15 μM TEAD4 (red). **e)** ^{19}F-NMR spectrum of FA **1** (50 μM): Free state in buffer (blue) and in presence of 15 μM TEAD4 (red). **f)** ^{19}F-NMR spectrum of NA **2** (50 μM): Free state in buffer (blue) and in presence of 15 μM TEAD4 (red).

ChemMedChem | Full Papers doi.org/10.1002/cmdc.202100432 | Chemistry Europe European Chemical Societies Publishing

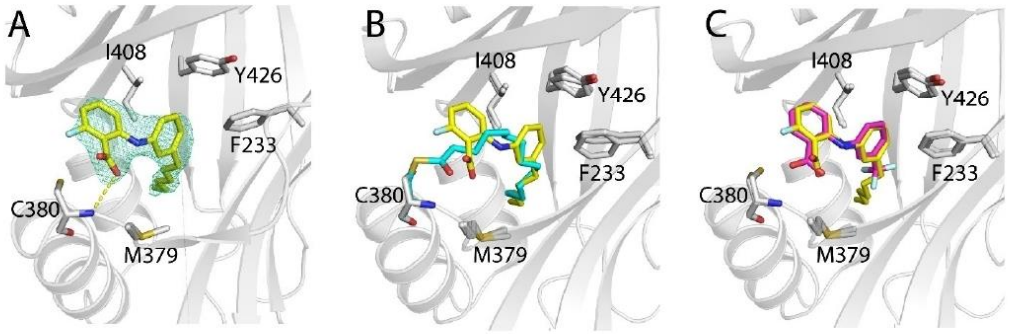

Figure 5. LM98 interaction with human TEAD2 YAP-binding domain. **a)** Co-crystal structure of *h*TEAD2 in complex with compound **LM98** (PDB ID: 6VAH). Compound **LM98** is shown in sticks and colored yellow. TEAD2 is shown in cartoon representation in grey with key hydrophobic pocket residues highlighted in sticks. The mFo-DFc electron density omit-map for compound **LM98** is displayed as green mesh contoured at 2.5σ. The polar interaction is displayed as a yellow dashed line. **b)** Overlay of TEAD2 bound to compound **LM98** (yellow) and palmitate (cyan) cross-linked to Cys380 (PDB: 5EMV). **c)** Overlay of TEAD2 bound to compound **LM98** (yellow) and FA (magenta) (PDB: 5DQ8).

human TEAD2 YAP-binding domain (residue range 221-451) in complex with **LM98**. As expected, the structure shows that **LM98** is anchored within the same palmitic acid binding pocket of TEAD2 as palmitate and flufenamic acid (Figure 5a–c). No significant structural changes were observed in the overall fold of TEAD2 upon binding to **LM98** compared to palmitate- and flufenamic acid-bound TEAD2 structures, with root-mean-square deviation (R.M.S.D.) of 0.56 Å over 194 Cα atoms between TEAD2-**LM98** (chain-A) and TEAD2-palmitate (chain-A) (PDB: 5EMV) and 0.66 Å over 192 Cα atoms between TEAD2-**LM98** (chain-A) and TEAD2-flufenamic (chain-A) (PDB: 5DQ8). The interaction between TEAD2 and **LM98** is mainly hydrophobic in nature with residues lining the palmitate-binding pocket. The hexyl chain moiety of **LM98** is docked into the same TEAD2 hydrophobic pocket as observed previously in palmitate-bound TEAD2 structure (PDB ID: 5EMV) (Figure 5b). **LM98** anchors itself into a hydrophobic pocket through H-bond interaction between the carboxylate group and main-chain amide nitrogen of Cys380 (Figure 5a), as well as via T-shaped pi-stacking interaction between the LHS phenyl ring of **LM98** and Phe233 of TEAD2, resembling the FA interaction with TEAD2 (PDB: 5DQ8) (Figure 5a–c).

Pobbati *et al* showed that substituents such as a methyl or difluoromethyl on the West side ring in *para* position relative to the NH are well tolerated.[40] In the covalent TED series **8**, Meroueh *et al* found that the introduction of a thiophene at that position is also tolerated.[45] With the objective of better understanding the impact of introducing groups at the *para* position (R_2), we prepared a small ensemble of compounds as shown in Table 4 and found that the *para* derivatives are not only well tolerated but that they even display higher thermal stabilization of TEAD4 than their *meta* counterparts. For instance, *para*-hexyl **36**, *para*-*tert*-butyl **37** and *para*-phenyl **38** gave ΔT_{agg} values of 6.6, 7.2 and 6.0 °C, respectively compared to 5.2, 1.5 and 2.1 °C for their *meta* analogues **22**, **25** and **26**. To the best of our knowledge, this unambiguous demonstration of an increase in affinity following the introduction of substituents on the West aryl ring of FA is unprecedented. Inspired by compound **3**, we prepared compound **39** that incorporates an adamantyl group in the R_2 position and observed a significant stabilization of the protein. Encouraged by this result, we then prepared the cyclohexyl derivative **40** which gave the highest ΔT_{agg} amongst all our FA derivatives.

Table 4. Structure-activity relationships of R_2 substituted derivatives on the left-hand side aryl group.

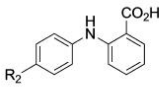

Compound	R_2	ΔT_{agg} [a]
36	*n*-Hex	6.6
37	*t*-Bu	7.2
38	Ph	6.0
39	Adamantyl	5.5
40	*c*-Hex	10

[a] Values shown are the average of three replicates by DSLS assay, with a compound concentration of 25 μM.

To explain these unexpected results, we performed docking studies on compound **36**, **39** and **40** in the hYBD of TEAD2 using the co-crystal structure of **LM98** (Figure 6). Our studies suggest that the central amine can rotate around the C–N–C bonds to accommodate the *para* substituent. Because the hexyl chain is flexible, it can easily adapt to the shape of the pocket, requiring small conformational changes to reach a conformation similar to the *meta*-substituted counterparts. However, for more voluminous groups such as the adamantyl and the cyclohexyl, the left-hand side aromatic ring needs to rotate. Our model suggests that this conformational change could allow the creation of new pi-stacking interactions, for example with Phe233, which could explain why these analogues show higher stabilization of TEAD.

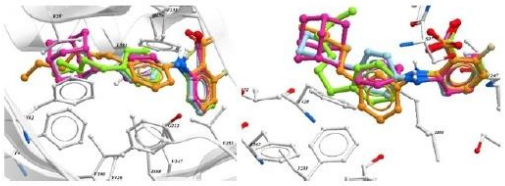

Figure 6. Docking studies of compound **36** (green), **39** (pink) and **40** (blue) in hYBD of TEAD2 overlaid with co-crystal structure of hDEAT2 in complex with **LM98** (orange) (PDB ID: 6VAH).

Being aware that these compounds are designed for optimal interactions with the hydrophobic palmitate pocket, we then proceeded with the incorporation of an oxygen atom in the R_1 and R_2 groups in order to improve their physicochemical properties. To do so, the general synthetic route was adapted, starting either with an *ipso*-hydroxylation on (3-nitrophenyl) boronic acid **41** or with a reduction of the carbonyl of 3-nitrobenzaldehyde **44** (Scheme 2). Phenol **42** and benzylic alcohol **45** thus obtained were then reacted via an S_N2 reaction with the corresponding iodoalkanes to yield key nitro-intermediates **43** and **46** which were converted into compounds **47**–**54** following the general synthetic route from Scheme 1. To further lower the lipophilicity of the compounds, we also prepared derivatives based on the NA scaffold where a nitrogen atom is present in the RHS ring *ortho* to the central NH linker.

DSLS results indicate that the replacement of the first methylene unit by an oxygen atom is well tolerated, as indicated by compound **47** which gave a ΔT_{agg} of 7.0 °C compared to 5.2 °C for the corresponding carbon analogue **22** (Table 5). However, replacing the second methylene unit in **22** with an oxygen led to a drastic loss of affinity with TEAD, as indicated by compound **48**. The addition of a nitrogen atom on the RHS was well tolerated, as shown by compound **49** which is the NA analogue of **22**. Combining the beneficial features of **47** and **49** afforded compound **50** which unexpectedly showed a reduced ability to stabilize TEAD. Introduction of a nitrogen in the *para*-adamantyl compound **39** provided a substantial increase in the temperature of aggregation (8.4 °C for **51** vs 5.5 °C for **39**). A complete loss of affinity to TEAD was observed with compound **52**, an oxygenated version of **36**. However, some of the affinity could be re-established with the NA counterpart **53**. Finally, the impact of moving the carboxylic acid group to the *meta* position of the RHS relative to the NH connector was investigated with compound **54**. The fact that **54** retains its affinity to TEAD is interesting as well as unprecedented and supports our hypothesis that compounds can adapt inside the pocket by undergoing conformational changes.

Inhibition of palmitoylation. As co-crystals structure of **LM98** with TEAD2 confirmed our hypothesis that our compounds occupy central pocket of TEAD, we further wished to

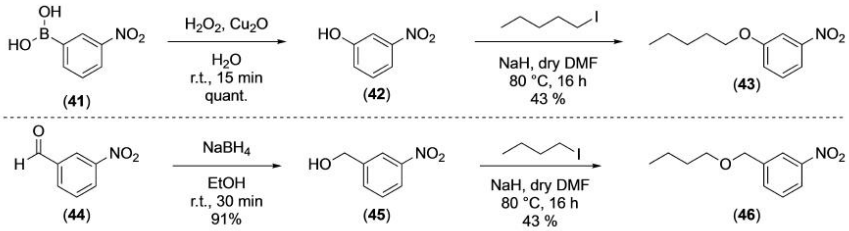

Scheme 2. General routes for the synthesis of key intermediates incorporating an ether side chain on the LHS.

Table 5. Analogues with polar atoms in the LHS alkyl chains and the RHS ring.

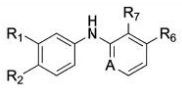

Compound	R_1	R_2	A	R_6	R_7	ΔT_{agg} [a]
47	$CH_3(CH_2)_4O$	H	CH	H	CO_2H	7.0
48	$CH_3(CH_2)_3OCH_2$	H	CH	H	CO_2H	2.3
49	*n*-Hex	H	N	H	CO_2H	6.0
50	$CH_3(CH_2)_4O$	H	N	H	CO_2H	3.4
51	H	Adamantyl	N	H	CO_2H	8.4
52	H	$CH_3(CH_2)_4O$	CH	H	CO_2H	0.5
53	H	$CH_3(CH_2)_4O$	N	H	CO_2H	3.2
54	$CH_3(CH_2)_4O$	H	CH	CO_2H	H	4.5

[a] Values shown are the average of three replicates by DSLS assay, with a compound concentration of 25 μM.

demonstrate whether they can compete with palmityl CoA or not. Therefore, we treated TEAD4 with different concentrations of **LM98** (**34**) and six other representative compounds (**22**, **32**, **40**, **47**, **49** and **50**) as well as flufenamic acid (**1**) in the presence of palmityl CoA according to a protocol reported by Li and coworkers.[34] The formation of TEAD4-palmityl CoA covalent adduct was then monitored by mass spectrometry. Results indicate that all compounds dose-dependently reduce the covalent palmitoylation of TEAD4 (Supporting Information figure S3), confirming that our compounds can indeed compete with palmityl CoA. Compounds **40**, **49** and **50** showed less reduction of palmitoylation at the highest concentrations of the compounds probably due to their limited solubility at the highest concentrations.

Evaluation of YAP-TEAD interaction in cells. We established a cellular nano-BRET assay to evaluate whether our TEAD inhibitors would inhibit YAP-TEAD interaction.[56] In this assay, we measured the inhibition of interaction between C-terminally NanoLuc® (NL) tagged TEAD1 and C-terminally HaloTag® (HT) tagged YAP1 by our compounds by comparing the nano-BRET ratio in the presence and absence of compounds. None of the three compounds tested, **LM98** (**34**), **36** and **40**, reduced nano-BRET ratio indicating that our TEAD inhibitors do not inhibit YAP-TEAD interaction up to 30 μM compound concentration (Figure 7). This is not surprising; as discussed in the introduction section, while some TEAD inhibitors such as **3** and **8** inhibit YAP-TEAD interaction, others TEAD inhibitors, including niflumic acid **2** as well as compounds **5** and **6**, do not.

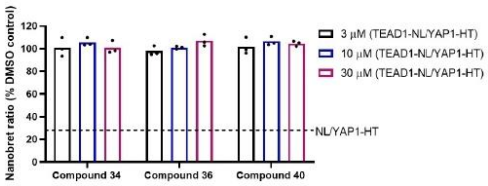

Figure 7. Compounds do not affect YAP1 and TEAD1 interaction in cells – NanoBRET assay. HEK293T were transfected with C-terminally NanoLuc® (NL) tagged TEAD1 or NL alone and C-terminally HaloTag® (HT) tagged YAP1. The following day cells were treated with compounds for 4 h. The interaction was measured using NanoBRET assay. The results are MEAN of 3 technical replicates. The line indicates the background NanoBRET signal from unspecific interaction between NL and YAP1-HT.

Inhibition of TEAD activation in cells. Having demonstrated that our compounds can compete with palmityl CoA *in vitro*, we next assessed whether they could inhibit TEAD mediated effects in cells. To examine the effects of our TEAD inhibitors, a dual-luciferase assay was used to measure TEAD activation through a YAP/TAZ-responsive synthetic promoter, the 8x-GTIIC TEAD reporter, which drives luciferase expression.[57] After 24 hours of treatment with increasing concentrations of NA (**2**) and **LM98** (**34**), HEK293 cells expressing the 8x-GTIIC TEAD reporter showed a significantly lower level of TEAD activation with **LM98** than with NA (Figure 8a). **LM98** also showed greater potency at inhibiting TEAD activation at lower concentrations, registering lower TEAD activation levels at 3 μM than NA (Figure 8a), without any increased toxicity in cells compared to NA (Figure 8b). Furthermore, compounds **23** and **33**, which showed comparable ΔT_{agg} to **LM98**, also showed similar reduction of TEAD activation. Compound **40**, which showed significantly better $\Delta T_{agg} = 10\,^{\circ}C$, showed almost a complete inhibition of TEAD activation at 30 μM while compound **35** which showed lower ΔT_{agg} of 5.2 °C showed no significant inhibition up to 30 μM (Supporting Information figure S4).

Inhibition of TEAD responsive genes and breast cancer cell migration. To determine the effect of our compounds on endogenous TEAD-mediated expression of Hippo-responsive genes, we then measured the levels of well-established TEAD responsive *CTGF* and *Cyr61* genes by RT-qPCR (Figure 9a). Compound **3** was selected as a reference compound since it was previously found to reduce the expression of *CTGF* and *Cyr61* and since we confirmed its binding in our DSLS assay.

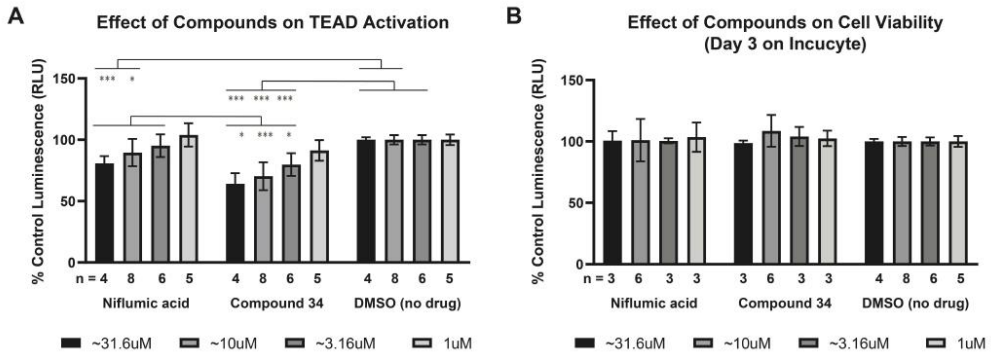

Figure 8. **a)** Effect of **LM98** (**34**) on TEAD activation in cells measured by dual-luciferase reporter assay. **b)** Effect of **LM98** (**34**) on cell viability. The toxicity of compounds on cell viability was measured using the Incucyte to measure cell confluence over a 3-day period. Results were generated by training the Incucyte analysis software to optimally detect cell confluence for HEK293 cells, averaging across technical replicates and normalizing to control "DMSO (no drug)" treatment.

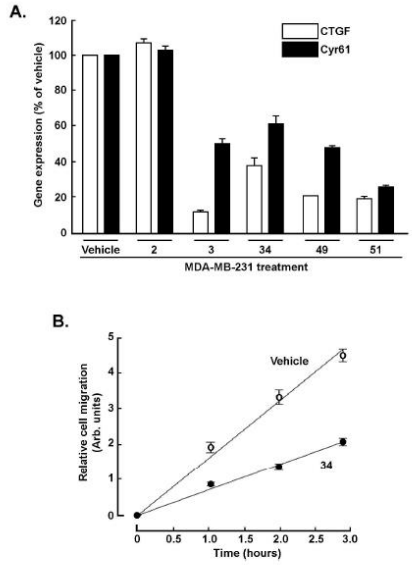

Figure 9. a) *CTGF* and *Cyr61* gene expression levels are altered by compounds **3**, **LM98** (**34**), **49** and **51**, but not by NA (**2**). Serum-starved MDA-MB-231 breast cancer cells were treated either with 10 μM of compounds or vehicle (DMSO) for 48 hours. Total RNA was isolated from cell monolayers. *CTGF* and *Cyr61* gene expression was then assessed by RT-qPCR as described in the Supporting Information. **b) LM98** (**34**) inhibits MDA-MB-231 breast cancer cell migration. Real-time cell migration was next performed using the xCELLigence system as described in the Supporting Information section. Serum-starved MDA-MB-231 breast cancer cells were treated either with 10 μM **LM98** (**34**) or vehicle (DMSO) for 48 hours. Data are representative of two independent experiments that were performed in triplicates (SEM is represented).

LM98 (**34**) was chosen because of its high affinity to TEAD in the DSLS assay, since its binding in the palmitic acid pocket was confirmed by X-ray crystallization, and because it reduced TEAD activation in the Luciferase assay. Compound **49** was selected as a niflumic acid version of **LM98** while compound **51** was chosen for the presence of the adamantyl group in the *para*-position of the left-hand side ring, and thus its structural resemblance to **3**. Niflumic acid **2**, which in our hands showed no binding in the DSLS assay and weak binding by ^{19}F-NMR, was selected as the negative control compound.

Treatment of human triple-negative MDA-MB-231 breast cancer cells with 10 μM **LM98** (**34**), **49** and **51**, significantly reduced *CTGF* and *Cyr61* transcript levels after 48 hours comparable to the levels of the published compound **3** at the same concentration while reference compound NA (**2**) did not show any significant effect at the same concentration. Since the Hippo-associated genes promote cell migration, we then studied the impact **LM98** (**34**) on MDA-MB-231 breast cancer cells migration using the real-time xCELLigence system and observed strong inhibition of cell migration compared to vehicle (Figure 9b).

Evaluation of the impact of LM98 on cell cycle division and wound healing. Given its capacity to alter cell migration, we also addressed whether **LM98** could impact cell cycle division by assessing G0/G1, S, and G2/M phases in MDA-MB-231 cells (Figure 10a). Cells were found trapped in the S phase upon treatment with 10 μM of **LM98** (Figure 10b). These results suggest that **LM98** can alter molecular events regulating cell division processes and cell proliferation.

The effect of **LM98** on the ability of cells to migrate in response to a wound was next assessed (Figure 10c). While vehicle-treated cells were able to partly rescue wounding, **LM98** treatment at 10 μM in MDA-MB-231 cells prevented migration of the wound region (Figure 10d). This property suggests that **LM98** can halt MDA-MB-231 cell migration.

Conclusion

We prepared flufenamic acid derivatives that target the central hydrophobic palmitate pocket of TEAD. A modular synthetic

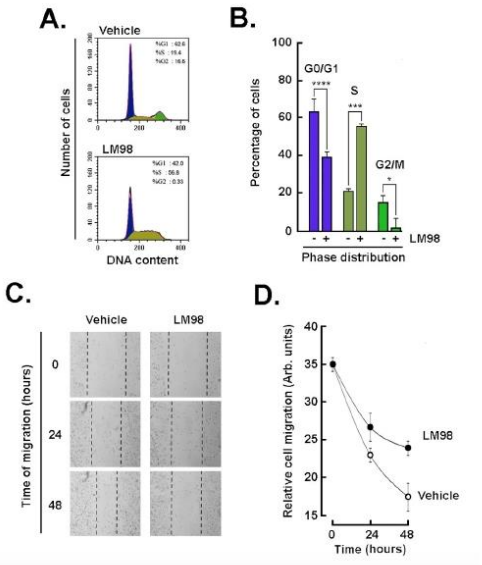

Figure 10. LM98 alters MDA-MB-231 breast cancer cell cycle division and wound healing. Human TNBC-derived MDA-MB-231 cells were cultured, followed by treatments with 10 μM **LM98** in serum-free media for 48 hours, fixation, and PI staining as described in the Supporting Information. **a)** Data acquisition was performed by flow cytometry in order to assess cell cycle phases. **b)** Data analysis was performed in order to assess the levels of cells in G0/G1, S, and G2/M phases. Significance: $*p<0.05$, $***p<0.01$, $****p<0.001$ versus the vehicle (0.1% DMSO). **c)** Photomicrographs of cell migration, in the presence or absence of 10 μM **LM98**, to the scratched zone at different time points (magnification, ×20). **d)** Quantitative assessment of cells that migrated into the scratched zone. For each condition, representative fields within the scratch were photographed. Data are representative of two independent experiments. Data are representative of two independent experiments that were performed in triplicates (SEM is represented).

ChemMedChem | Full Papers doi.org/10.1002/cmdc.202100432 | Chemistry Europe European Chemical Societies Publishing

route was established that allow the expedient access to derivatives of flufenamic acid. Rational design combined with systematic SAR studies led to the discovery of **LM98** (**34**), a FA derivative that shows high affinity to TEAD in a DSLS biophysical assay. ^{19}F-NMR studies confirmed that **LM98** binds more strongly to TEAD than flufenamic or niflumic acid. Co-crystal structure showed that **LM98** binds in the palmitate pocket of TEAD while mass spectrometry measurements confirmed that this compound acts as a TEAD autopalmitoylation inhibitor. Although **LM98** did not disrupt the YAP-TEAD complex, it was found to interfere with the transcriptional activity of TEAD at concentrations that are not toxic to cells in a dual luciferase assay. Treatment of MDA-MB-231 cells with **LM98** resulted in a decrease in the expression of associated genes *CTGF* and *Cyr61* as shown by RT-qPCR. **LM98** displayed strong inhibition of MDA-MB-231 cancer cell migration and arrested cells in the S phase.

Experimental Section

General Chemistry Methods. Unless otherwise stated, reactions were performed in non-flame dried glassware and commercial reagents were used without further purification. Anhydrous solvents were obtained using an encapsulated solvent purification system and were further dried over 4 Å molecular sieves. The evolution of reactions was monitored by analytical thin-layer chromatography (TLC) using silica gel 60 F254 precoated plates visualized by ultraviolet radiation (254 nm). Flash chromatography was performed employing 230–400 mesh silica using the indicated solvent system according to standard techniques. ^{1}H-NMR spectra were recorded on a Bruker Avance-III 300 MHz, 500 MHz or 600 MHz. ^{13}C-NMR spectra were recorded on a Bruker Avance-III 75 MHz, 126 MHz or 151 MHz spectrometer. ^{19}F-NMR were recorded on a Bruker Avance-III 282 MHz. Chemical shifts for ^{1}H-NMR spectra are recorded in parts per million from tetramethyl silane with the solvent resonance as the internal standard (chloroform-d, δ 7.26 ppm; methanol-d4, δ 3.34 ppm; dimethysulfoxide-d6, δ 2.54 ppm; acetone-d6, δ 2.09 ppm). Data is reported as follows: chemical shift, multiplicity (s = singlet, s(br) = broad singlet, d = doublet, t = triplet, q = quartet, quint = quintet, sext = sextet, sept = septet, m = multiplet, dd = doublet of doublet, dt = doublet of triplet, ddd = doublet of doublet of doublet), coupling constant *J* in Hz and integration. Chemical shifts for ^{13}C-NMR spectra are recorded in parts per million from tetramethyl silane using the solvent resonance as the internal standard (chloroform-d, δ 77.36 ppm; methanol-d4, δ 49.86 ppm; dimethysulfoxide-d6, δ 40.45 ppm; acetone-d6, δ 30.60 ppm). Purity was assessed on an Agilent 1260 infinity HPLC system equipped with an Agilent Eclipse Plus C18 (3.5 μM, 4.6×100 mm) column using a 20-minute gradient method (0 to 100% MeCN + 0.06% TFA in water + 0.06% TFA; the absorbance was measured at 254 nm). Purity is greater than 95% for all final compounds. HRMS were performed on a TOF LCMS analyzer using the electrospray (ESI) mode. MGH-CP1 **3** was synthesized according to WO 2017/053706 A1.[37]

Accession Codes. Coordinates and structure factors of *h*TEAD2-**34** complex are available in the Protein Data Bank (PDB) under accession code 6VAH. Coordinates for X-ray structure of **40** have been deposited in the Cambridge Crystallographic Date Centre (CCDC) under the number 2054155.

General Procedure A: nitro reduction. Metallic iron (4 equiv) was added to a solution of the appropriate nitro substrate (1.0 equiv) in 3:1 EtOH/$HCl_{conc.}$ (5 mL per mmol of substrate). After heating at 79 °C for 1 h, the reaction mixture was cooled down to room temperature and quenched with a slow addition of saturated aqueous solution of $NaHCO_3$ (50 mL). The aqueous phase was extracted with EtOAc (3×50 mL). Combined organic phases were washed with water (1×50 mL), brine (1×50 mL), dried over Na_2SO_4, filtered and concentrated under reduced pressure. If needed, the crude material was purified by flash column chromatography to provide the desired compound.

General Procedure B: Ullmann coupling. To a solution of the appropriate aniline substrate (1 equiv) in dry DMF (10 mL per mmol of substrate) were added K_2CO_3 (3 equiv), the appropriate benzoic acid derivative (1.1 equiv), Cu (0.2 equiv) and Cu_2O (0.1 equiv). The reaction mixture was stirred at 153 °C for 16 h, cooled down to room temperature, after which H_2O was added. The mixture was filtered over a plug a celite, rinsed with DCM and acidified with $HCl_{conc.}$ until pH < 3. If formation of a precipitate, filtration was performed. Otherwise, the aqueous phase was extracted with DCM (3×20 mL), combined organic phases were dried over Na_2SO_4, filtered and concentrated under reduced pressure to yield directly to the title compound.

General Procedure C: Buchwald-Hartwig coupling. To a solution of the appropriate amine substrate (1.0 equiv) in dry toluene (7 mL per mmol of substrate) was added the appropriate halogen benzoate (1.1 equiv), cesium carbonate (2.4 equiv) and a freshly prepared solution of $Pd(OAc)_2$/*Rac*-BINAP in dry toluene. This solution was obtained by stirring $Pd(OAc)_2$ (0.06 equiv) and *Rac*-BINAP (0.09 equiv) in dry toluene (3 mL per mmol of substrate) for 15 min with argon bubbling through the mixture. The main reaction mixture was heated at 120 °C for 16 h, cooled down to room temperature, filtered over a plug of celite and concentrated under reduced pressure. Purification by flash column chromatography provided the title compound.

General Procedure D: saponification. To a solution of the appropriate ester substrate (1.0 equiv) in MeOH (20 mL per mmol of substrate) was added an aqueous solution of NaOH at 10% (20 mL per mmol of substrate). The reaction mixture was stirred at 80 °C until completion as indicated by TLC, cooled down to room temperature after which the mixture was diluted with DCM and quenched with aqueous solution of HCl 1 M (20 mL). The aqueous phase was extracted with DCM (3×20 mL), combined organic phases were dried over Na_2SO_4, filtered and concentrated under reduced pressure. If not pure enough, the crude material was purified by flash column chromatography to provide the title compound.

General Procedure E: esterification. To a solution of the appropriate acid substrate (1.0 equiv) in MeOH (2 mL per mmol of substrate) was added H_2SO_4 (0.2 mL per mmol of substrate). The reaction mixture was stirred at 65 °C until completion as indicated by TLC, cooled down to room temperature after which the mixture was diluted with DCM and H_2O. The aqueous phase was extracted with DCM (3×20 mL). Combined organic phases were washed with saturated aqueous solution of $NaHCO_3$ (3×20 mL), brine (1×20 mL), dried over Na_2SO_4, filtered and concentrated under reduced pressure. If not pure enough, the crude material was purified by flash column chromatography to provide the title compound.

General Procedure F: Ullmann coupling. To a solution of the appropriate benzoic acid substrate (1.0 equiv) in *n*-butanol (0.5 mL per mmol of substrate) were added the appropriate aniline substrate (1.4 equiv), K_2CO_3 (1.4 equiv) and Cu (0.9 equiv). The reaction mixture was heated at 120 °C for 4 h and then allowed to cool down to room temperature. After removal of *n*-butanol under high vacuum, hot water (15 mL) was added to the residue. The

mixture was filtered through a pad of celite and washed with water. The filtrate was acidified with $HCl_{conc.}$ until pH < 3. The precipitate obtained was filtered on Büchner and then recrystallized in chloroform to yield the title compound.

2-((3-(Trifluoromethyl)phenyl)amino)benzoic acid (1) (Flufenamic acid; FA). 2-Bromobenzoic acid (605 mg, 3.00 mmol) was reacted with 3-aminobenzotrifluoride (678 mg, 4.20 mmol) according to general procedure F, affording flufenamic acid (FA) **1** (323 mg, 1.14 mmol, 38%) as a white solid. ^{1}H-NMR (300 MHz, $CDCl_3$) δ 9.42 (s, 1H), 8.07 (dd, *J* = 8.1, 1.7 Hz, 1H), 7.51 (s, 1H), 7.46 (d, *J* = 7.0 Hz, 2H), 7.43–7.39 (m, 1H), 7.35 (d, *J* = 6.9 Hz, 1H), 7.27–7.25 (m, 1H), 6.85 (ddd, *J* = 8.2, 7.1, 1.1 Hz, 1H); ^{13}C-NMR (75 MHz, $CDCl_3$) δ 173.52, 147.88, 141.34, 135.59, 132.96, 132.33, 131.90, 130.13, 125.51, 120.39, 119.06, 119.01, 118.52, 114.36; ^{19}F-NMR (282 MHz, $CDCl_3$) δ −62.80; HRMS (ESI) $[M+H]^+$ calcd for $C_{14}H_{10}F_3NO_2$: 282.0736, found 282.0740, HPLC purity: 98%.

2-(3-(Trifluoromethyl)phenoxy)benzoic acid (10). To a solution of 3-(trifluoromethyl)phenol (1.755 g, 10.82 mmol) in water (10 mL) were added K_2CO_3 (2.995 g, 21.66 mmol), 2-chloro-benzoic acid (3.389 g, 21.65 mmol), pyridine (882 μL, 10.9 mmol), Cu (104 mg, 1.63 mmol) and CuI (104 mg, 0.55 mmol). The reaction mixture was stirred at 100 °C for 16 h, then cooled down to room temperature. The reaction mixture was extracted with Et_2O, then the aqueous phases was acidified with $HCl_{conc.}$ until pH < 3. The precipitate formed was filtered on Büchner. Purification of 32 mg of crude by preparative reverse phase HPLC (H_2O + 0.01% TFA/MeCN + 0.01% TFA 100:0 to 0:100) provided **10** (13 mg, 0.071 mmol) as a white solid. ^{1}H-NMR (300 MHz, $CDCl_3$) δ 8.14 (dd, *J* = 7.9, 1.8 Hz, 1H), 7.56 (ddd, *J* = 8.3, 7.4, 1.8 Hz, 1H), 7.48 (t, *J* = 7.9 Hz, 1H), 7.41 (d, *J* = 7.8 Hz, 1H), 7.31–7.26 (m, 2H), 7.18 (d, *J* = 7.9 Hz, 1H), 6.96 (dd, *J* = 8.3, 0.8 Hz, 1H); ^{13}C-NMR (75 MHz, $CDCl_3$) δ 168.45, 156.90, 156.29, 135.14, 133.47, 132.87, 130.72, 125.48, 124.65, 122.10, 121.41, 120.79, 120.25, 115.93.; ^{19}F-NMR (282 MHz, $CDCl_3$) δ −62.73; HRMS (ESI) calcd for $C_{14}H_9F_3O_3$: 282.0504, found 305.0403 $[M+Na]^+$; HPLC purity: 96%.

2-((3-(Trifluoromethyl)phenyl)thio)benzoic acid (11). To a solution of thiosalicylic acid (886 mg, 5.74 mmol) in DMF (10 mL) were added 3-bromobenzotrifluoride (1.44 g, 6.64 mmol), K_2CO_3 (1.21 g, 8.72 mmol) and CuCl (89 mg, 0.90 mmol). The reaction mixture was stirred at 153 °C for 7 h and cooled down to room temperature. The precipitate formed was filtered on Büchner and the solid was dissolved in water. The aqueous phase was acidified with $HCl_{conc.}$ until pH < 3, then extracted with EtOAc (3 × 15 mL). Purification by preparative reverse phase HPLC (H_2O + 0.01% TFA/MeCN + 0.01% TFA 100:0 to 0:100) provided **11** (16 mg, 0.053 mmol, 1%) as a white solid. ^{1}H-NMR (300 MHz, $CDCl_3$) δ 8.13 (d, *J* = 7.9 Hz, 1H), 7.83 (s, 1H), 7.71 (dd, *J* = 15.6, 7.7 Hz, 2H), 7.56 (t, *J* = 7.9 Hz, 1H), 7.34 (t, *J* = 7.6 Hz, 1H), 7.22 (t, *J* = 9.0 Hz, 1H), 6.82 (d, *J* = 7.7 Hz, 1H); ^{13}C-NMR (75 MHz, $CDCl_3$) δ 171.09, 143.00, 138.76, 134.28, 133.57, 132.41, 132.18, 132.11, 132.06, 130.36, 129.88, 127.81, 126.01, 125.19;^{19}F-NMR (282 MHz, $CDCl_3$) δ −62.75; HRMS (ESI) $[M+H]^+$ calcd for $C_{14}H_9F_3O_2S$: 299.0348, found 299.0336; HPLC purity: 97%.

Ethyl 2-methylbenzoate (55). *o*-Toluic acid (2.050 g, 15.06 mmol) was dissolved in ethanol (20 mL) and $H_2SO_{4conc.}$ (1 mL) was added. The reaction was heated 78 °C for 16 h, cooled down to room temperature. After evaporation of the solvent, the residue was redissolved in Et_2O. The organic phase was washed with aqueous 1 N NaOH aqueous solution (1 × 20 mL), aqueous $NaHCO_3$ saturated solution (1 × 20 mL), dried over Na_2SO_4, filtered and evaporated under reduced pressure to give ethyl 2-methylbenzoate **55** (2.290 g, 13,58 mmol, 90%) as a colorless oil. ^{1}H-NMR (300 MHz, $CDCl_3$) δ 7.92 (dd, *J* = 8.1, 1.4 Hz, 1H), 7.40–7.33 (m, 1H), 7.22 (t, *J* = 6.9 Hz, 2H), 4.35 (q, *J* = 7.1 Hz, 2H), 2.61 (s, 3H), 1.38 (t, *J* = 7.1 Hz, 3H); ^{13}C-NMR (75 MHz, $CDCl_3$) δ 167.59, 139.97, 131.77, 131.61, 130.47, 129.93, 125.63, 60.61, 21.67, 14.29.

Ethyl 2-(bromomethyl)benzoate (56). To a solution of ethyl 2-methylbenzoate **55** (1.45 g, 8.81 mmol) in CCl_4 (20 mL) were added *N*-bromosuccinimide (NBS) (1.57 g, 8.81 mmol) and benzoyl peroxide (58 mg, 0.24 mmol) under argon atmosphere. The reaction mixture was stirred at 80 °C for 4 h and then stirred at room temperature for 16 h. After filtration over a pad of celite, the filtrate was concentrated under vacuum. Purification by flash column chromatography (hexanes/EtOAc 90:10) provided ethyl 2-(bromomethyl)benzoate **56** (1.95 g, 8.03 mmol, 91%) as a colorless oil. Spectral data are consistent with literature values.[58] ^{1}H-NMR (300 MHz, $CDCl_3$) δ 7.90–7.85 (m, 1H), 7.42–7.33 (m, 2H), 7.30–7.23 (m, 1H), 4.86 (s, 2H), 4.36–4.26 (m, 2H), 1.33 (t, *J* = 7.1 Hz, 3H).

Ethyl 2-(3-(trifluoromethyl)benzyl)benzoate (12). To a solution of ethyl 2-(bromomethyl)benzoate **56** (296 mg, 1.22 mmol) in toluene (3 mL) were added 3-trifluoromethylphenylboronic acid (342 mg, 1.80 mmol), $Pd(OAc)_2$ (14 mg, 0.062 mmol), PPh_3 (48 mg, 0.18 mmol) and K_3PO_4 (518 mg, 2.44 mmol). The reaction mixture was stirred at 80 °C for 16 h, cooled down to room temperature and concentrated under vacuum. The crude compound was used in the following step without any purification. Its saponification was performed according to general procedure D, providing **12** (126 mg, 0.450 mmol, 37%) without any need for purification as a white solid. ^{1}H-NMR (600 MHz, $CDCl_3$) δ 8.11 (d, *J* = 7.8 Hz, 1H), 7.53 (t, *J* = 7.5 Hz, 1H), 7.45 (d, *J* = 8.2 Hz, 2H), 7.37 (t, *J* = 7.8 Hz, 2H), 7.32 (d, *J* = 7.7 Hz, 1H), 7.24 (d, *J* = 7.7 Hz, 1H), 4.50 (s, 2H); ^{13}C-NMR (151 MHz, $CDCl_3$) δ 172.69, 142.53, 141.83, 133.44, 132.44, 132.19, 132.00, 131.06, 130.84, 130.63, 130.42, 128.86, 127.01, 125.89, 125.87, 125.84, 125.82, 125.26, 123.46, 123.09, 123.06, 123.04, 123.01, 39.69; ^{19}F-NMR (282 MHz, $CDCl_3$) δ −62.54; HRMS (ESI) $[M+H]^+$ calcd for $C_{15}H_{11}F_3O_2$: 281.0784, found 281.0795; HPLC purity: 99%.

Methyl 2-(methyl(3-(trifluoromethyl)phenyl)amino)benzoate (57). To a solution of **1** (48 mg, 0.17 mmol) in DMF (1 mL) was added NaH dry 90% (12 mg, 0.45 mmol). The reaction mixture was stirred for 40 min, after which a solution of MeI (85 mg, 0.60 mmol) in DMF (1 mL) was added. The reaction mixture was stirred at 80 °C for 16 h, then cooled down to room temperature. Purification by column chromatography (hexanes/EtOAc 95:5) provided methyl 2-(methyl(3-(trifluoromethyl)phenyl)amino)benzoate **57** (42 mg, 0.14 mmol, 80%) as a transparent oil. ^{1}H-NMR (300 MHz, $CDCl_3$) δ 7.89 (dd, *J* = 7.8, 1.6 Hz, 1H), 7.59 (td, *J* = 7.7, 1.7 Hz, 1H), 7.35 (td, *J* = 7.6, 1.2 Hz, 1H), 7.30 (dd, *J* = 8.0, 1.0 Hz, 1H), 7.22 (t, *J* = 8.0 Hz, 1H), 6.99–6.93 (m, 1H), 6.83 (t, *J* = 2.2 Hz, 1H), 6.69 (dd, *J* = 8.3, 2.4 Hz, 1H), 3.63 (s, 3H), 3.30 (s, 3H); ^{13}C-NMR (75 MHz, $CDCl_3$) δ 166.96, 149.47, 147.24, 133.82, 131.93, 129.89, 129.58, 129.36, 126.53, 116.71, 116.70, 114.06, 114.01, 113.96, 113.90, 109.59, 109.53, 109.48, 109.43, 52.24, 40.35; ^{19}F-NMR (282 MHz, $CDCl_3$) δ −62.76.

2-(Methyl(3-(trifluoromethyl)phenyl)amino)benzoic acid (13). Methyl 2-(methyl(3-(trifluoromethyl)phenyl)amino)benzoate **57** (39 mg, 0.13 mmol) was saponified according to general procedure D to afford **13** (29 mg, 0.098 mmol, 76%) as a yellow solid without the need for any purification. ^{1}H-NMR (300 MHz, $CDCl_3$) δ 8.29 (dd, *J* = 7.9, 1.6 Hz, 1H), 7.62 (td, *J* = 7.8, 1.7 Hz, 1H), 7.46 (td, *J* = 7.7, 1.2 Hz, 1H), 7.33 (t, *J* = 8.0 Hz, 1H), 7.20 (d, *J* = 7.8 Hz, 1H), 7.16 (dd, *J* = 8.0, 0.9 Hz, 1H), 7.07 (s, 1H), 6.90 (dd, *J* = 8.2, 2.2 Hz, 1H), 3.27 (s, 3H); ^{13}C-NMR (75 MHz, $CDCl_3$) δ 167.31, 149.34, 149.09, 135.23, 133.02, 132.43, 132.00, 131.58, 131.15, 129.87, 128.07, 128.00, 126.87, 122.25, 120.48, 118.02, 112.92, 41.61; ^{19}F-NMR (282 MHz, $CDCl_3$) δ −62.75; HRMS (ESI) $[M+H]^+$ calcd for $C_{15}H_{12}F_3NO_2$: 296.0893, found 296.0887; HPLC purity: 99%.

2-(Phenylamino)benzoic acid (16). 2-Bromobenzoic acid (206 mg, 1.02 mmol) was reacted with aniline (138 mg, 1.48 mmol) according to general procedure F to afford **16** (92 mg, 0.43 mmol, 42%) as a white solid. ^{1}H-NMR (300 MHz, $CDCl_3$) δ 9.32 (s(br), 1H), 8.04 (dd, J= 8.1, 1.6 Hz, 1H), 7.41–7.32 (m, 3H), 7.28 (d, J=1.3 Hz, 1H), 7.23 (dd, J=8.6, 0.8 Hz, 1H), 7.17–7.10 (m, 1H), 6.76 (ddd, J=8.1, 7.0, 1.1 Hz, 1H); ^{13}C-NMR (75 MHz, $CDCl_3$) δ 173.37, 149.07, 140.48, 135.35, 132.74, 129.58, 124.26, 123.30, 117.33, 114.19, 110.49; HRMS (ESI) $[M+H]^+$ calcd for $C_{13}H_{11}NO_2$: 214.0863, found 214.0865; HPLC purity: 99%.

2-(m-Tolylamino)benzoic acid (17). 2-Bromobenzoic acid (201 mg, 1.00 mmol) was reacted with *m*-toluidine (157 mg, 1.46 mmol) according to general procedure F to afford **17** (30 mg, 0.13 mmol, 13%) as a greenish solid. ^{1}H-NMR (300 MHz, $CDCl_3$) δ 9.27 (s(br), 1H), 8.04 (dd, J=8.1, 1.5 Hz, 1H), 7.39–7.30 (m, 1H), 7.25–7.20 (m, 2H), 7.11–7.06 (m, 2H), 6.95 (d, J=7.5 Hz, 1H), 6.75 (t, J=7.5 Hz, 1H), 2.36 (s, 3H); ^{13}C-NMR (75 MHz, $CDCl_3$) δ 174.04, 149.20, 140.38, 139.54, 135.35, 132.75, 129.35, 125.08, 124.01, 120.27, 117.18, 114.31, 110.47, 21.57; HRMS (ESI) $[M+H]^+$ calcd for $C_{14}H_{13}NO_2$: 228.2710, found 228.1053; HPLC purity: 99%.

1-Nitro-3-vinylbenzene (58). Methyltriphenylphosphonium iodide (4.06 g, 10.0 mmol) and potassium *tert*-butoxide (1.12 g, 10.0 mmol) were stirred at 70°C for 30 min in toluene (19 mL) under argon atmosphere. Then 3-nitrobenzaldehyde (756 mg, 5.00 mmol) was added. The reaction mixture was stirred at 110°C for 3 h 30 under argon atmosphere, cooled down to room temperature and diluted with water. The aqueous phase was extracted with EtOAc (3× 20 mL). Combined organic phases were dried over Na_2SO_4, filtered and concentrated under reduced pressure. The crude material was purified by flash column chromatography (hexanes/EtOAc 95:5) to give 1-nitro-3-vinylbenzene **58** (541 mg, 3,62 mmol, 72%) as a yellow oil. ^{1}H-NMR (300 MHz, $CDCl_3$) δ 8.09 (t, J=1.9 Hz, 1H), 7.97 (ddd, J=8.2, 2.1, 0.8 Hz, 1H), 7.60 (d, J=7.7 Hz, 1H), 7.39 (t, J= 7.9 Hz, 1H), 6.66 (dd, J=17.6, 10.9 Hz, 1H), 5.79 (d, J=17.6 Hz, 1H), 5.34 (d, J=10.9 Hz, 1H); ^{13}C-NMR (75 MHz, $CDCl_3$) δ 148.36, 139.05, 134.54, 131.92, 129.31, 122.17, 120.57, 116.83..

3-Ethylaniline (59). To a solution of 1-nitro-3-vinylbenzene **58** (515 mg, 3.45 mmol) in EtOAc (10 mL) was added Pd/C 10% (1 mg). The reaction vessel was evacuated under vacuum and filled with hydrogen. The cycle was repeated twice and the suspension was stirred at room temperature for 16 h under H_2 atmosphere. The mixture was then filtered over a plug of celite, rinsed with DCM and concentrated under reduced pressure to afford 3-ethylaniline **59** (343 mg, 2.83 mmol, 82%) as a yellow oil which was used directly in the next step. ^{1}H-NMR (300 MHz, $CDCl_3$) δ 7.22 (t, J=7.6 Hz, 1H), 6.77 (d, J=7.4 Hz, 1H), 6.65–6.58 (m, 2H), 3.69 (s(br), 2H), 2.71 (q, J= 7.6 Hz, 2H), 1.38 (t, J=7.6 Hz, 3H); ^{13}C-NMR (75 MHz, $CDCl_3$) δ 146.43, 145.33, 129.07, 117.97, 114.59, 112.40, 28.74, 15.41.

2-((3-Ethylphenyl)amino)benzoic acid (18). 2-Bromobenzoic acid (291 mg, 1.45 mmol) was reacted with 3-ethylaniline **59** (240 mg, 1.98 mmol) according to general procedure F to afford **18** (132 mg, 0.547 mmol, 38%) as a brown solid. ^{1}H-NMR (300 MHz, $CDCl_3$) δ 9.31 (s(br), 1H), 8.04 (dd, J=8.1, 1.6 Hz, 1H), 7.35 (ddd, J=8.6, 7.0, 1.7 Hz, 1H), 7.30 (d, J=8.4 Hz, 1H), 7.23 (d, J=7.8 Hz, 1H), 7.14–7.08 (m, 2H), 6.98 (d, J=7.6 Hz, 1H), 6.78–6.71 (m, 1H), 2.66 (q, J=7.6 Hz, 2H), 1.26 (t, J=7.6 Hz, 3H); ^{13}C-NMR (75 MHz, $CDCl_3$) δ 173.59, 149.24, 145.97, 140.41, 135.33, 132.73, 129.42, 123.94, 122.91, 120.57, 117.15, 114.28, 110.38, 28.96, 15.68; HRMS (ESI) $[M+H]^+$ calcd for $C_{15}H_{15}NO_2$: 242.1176, found 242.1179; HPLC purity: >99%.

1-Nitro-3-(prop-1-en-1-yl)benzene (60). To a suspension of ethyltriphenylphosphonium bromide (140 mg, 0.377 mmol) and potassium carbonate (130 mg, 0.941 mmol) in toluene (3.1 mL) was added 3-nitrobenzaldehyde (47 mg, 0.31 mmol). The reaction mixture was heated at reflux for 48 h, then cooled down to room temperature and concentrated under reduced pressure. The residue was dissolved in CH_2Cl_2. The organic phase was washed with H_2O (3×10 mL), brine (1×10 mL), dried over Na_2SO_4, filtered and concentrated under reduced pressure. Purification by flash column chromatography (hexanes/EtOAc 95:5) provided 1-nitro-3-(prop-1-en-1-yl)benzene **60** (32 mg, 0.20 mmol, 65%) as a colorless oil. A mixture of E/Z isomers in a 1:1 ratio was obtained. ^{1}H-NMR (300 MHz, $CDCl_3$) δ 8.15 (dt, J=6.5, 2.0 Hz, 1H), 8.04 (dddd, J=15.0, 8.2, 2.3, 1.1 Hz, 1H), 7.60 (ddt, J=7.5, 4.7, 1.4 Hz, 1H), 7.46 (dt, J= 17.3, 7.9 Hz, 1H), 6.50–6.37 (m, 1H), 5.95 (dq, J=11.6, 7.2 Hz, 1H), 1.94–1.89 (m, 3H); ^{13}C-NMR (75 MHz, $CDCl_3$) δ 139.78, 139.26, 134.88, 131.80, 129.86, 129.42, 129.14, 129.12, 127.86, 123.53, 121.46, 121.39, 120.49, 18.62, 14.68.

3-Propylaniline (61). To a solution of 1-nitro-3-(prop-1-en-1-yl) benzene **60** (570 mg, 3.49 mmol) in EtOAc (10 mL) was added Pd/C 10% (2.8 mg). The reaction vessel was evacuated under vacuum and filled back with hydrogen. The cycle was repeated twice and the suspension was stirred at room temperature for 16 h under H_2 atmosphere. The mixture was then filtered over a plug of celite, rinsed with DCM and concentrated under reduced pressure. Purification by flash column chromatography (hexanes/EtOAc 80:20) provided 3-propylaniline **61** (158 mg, 1.17 mmol, 33%) as a brown oil. ^{1}H-NMR (300 MHz, $CDCl_3$) δ 7.18–7.10 (m, 1H), 6.67 (d, J= 7.6 Hz, 1H), 6.59–6.54 (m, 2H), 3.61 (s(br), 2H), 2.57 (t, J=9.0 Hz, 2H), 1.70 (sext, J=6.0 Hz, 2H), 1.02 (t, J=7.3 Hz, 3H). ^{13}C-NMR (75 MHz, $CDCl_3$) δ 146.34, 143.96, 129.10, 118.90, 115.38, 112.60, 38.10, 24.46, 13.93.

2-((3-Propylphenyl)amino)benzoic acid (19). 3-Propylaniline **61** (106 mg, 0.784 mmol) was reacted with methyl 2-bromobenzoate (327 mg, 1.52 mmol) according to general procedure C. The crude compound was used without any purification. Its saponification was performed according to general procedure D to afford **19** (160 mg, 0.627 mmol, 80%) as a yellow solid without the need of any purification. ^{1}H-NMR (300 MHz, $CDCl_3$) δ 9.29 (s(br), 1H), 8.03 (dd, J=8.1, 1.6 Hz, 1H), 7.35 (ddd, J=8.6, 7.0, 1.6 Hz, 1H), 7.31–7.27 (m, 1H), 7.25–7.20 (m, 1H), 7.09 (d, J=7.4 Hz, 2H), 6.96 (d, J=7.6 Hz, 1H), 6.78–6.71 (m, 1H), 2.59 (t, J=9.0 Hz, 2H), 1.66 (sext, J=7.4 Hz, 2H), 0.96 (t, J=7.3 Hz, 3H); ^{13}C-NMR (75 MHz, $CDCl_3$) δ 173.67, 149.27, 144.40, 140.32, 135.31, 132.74, 129.32, 124.55, 123.49, 120.62, 117.12, 114.25, 38.12, 24.64, 13.99; HRMS (ESI) $[M+H]^+$ calcd for $C_{16}H_{17}NO_2$: 256.13321, found 256.13422; HPLC purity: >99%..

1-(Buta-1,3-dien-1-yl)-3-nitrobenzene (62). To a solution of 3-nitrobenzaldehyde (1.02 g, 6.75 mmol) in dry THF (25 mL) was added allyltriphenylphosphonium bromide (3.10 g, 8.09 mmol) under argon atmosphere. Potassium *tert*-butoxide (960 mg, 8.56 mmol) was added portionwise at 0°C. The mixture was stirred at 0°C for 15 min and then was allowed to warm up to room temperature for 16 h, after which it was concentrated under reduced pressure. The residue was dissolved in EtOAc. The organic phase was washed with H_2O (3×50 mL), dried over Na_2SO_4, filtered and concentrated under reduced pressure. Purification by flash column chromatography (hexanes/EtOAc 95:5) provided 1-(buta-1,3-dien-1-yl)-3-nitrobenzene **62** (548 mg, 3.13 mmol, 46%) as a yellow oil. A 1:1 mixture of *E*/*Z* isomers was obtained. ^{1}H-NMR (300 MHz, $CDCl_3$) δ 8.20 (dt, J=24.0, 2.0 Hz, 1H), 8.08 (dddd, J= 11.3, 8.1, 2.3, 1.1 Hz, 1H), 7.65 (ddt, J=18.6, 7.7, 1.5 Hz, 1H), 7.49 (dt, J=9.7, 7.9 Hz, 1H), 6.96–6.71 (m, 1H), 6.63–6.45 (m, 1H), 6.45–6.34 (m, 1H), 5.52–5.40 (m, 1H), 5.38–5.26 (m, 1H); ^{13}C-NMR (75 MHz, $CDCl_3$) δ 139.06, 139.02, 136.43, 134.97, 133.27, 132.61, 132.25, 132.03, 130.24, 129.62, 129.30, 127.69, 123.70, 122.14, 122.13, 121.91, 120.93, 120.19.

3-Butylaniline (63). To a solution of 1-(buta-1,3-dien-1-yl)-3-nitrobenzene **62** (567 mg, 3.24 mmol) in EtOAc (12 mL) was added Pd/C 10% (10 mg). The reaction vessel was evacuated under vacuum and filled back with hydrogen. The cycle was repeated twice and the suspension was stirred at room temperature for 16 h under H_2 atmosphere. The mixture was then filtered over a plug of celite, rinsed with DCM and concentrated under reduced pressure to give 3-butylaniline **63** (461 mg, 3.09 mmol, 95%) as an orange oil without any purification. ^{1}H-NMR (300 MHz, $CDCl_3$) δ 7.25–7.18 (m, 1H), 6.76 (d, J=7.5 Hz, 1H), 6.64–6.57 (m, 2H), 3.69 (s(br), 2H), 2.69 (t, J=9.0 Hz, 2H), 1.83–1.68 (m, 2H), 1.61–1.47 (sext, J=7.3 Hz, 2H), 1.12 (t, J=7.3 Hz, 3H); ^{13}C-NMR (75 MHz, $CDCl_3$) δ 146.32, 143.81, 128.84, 118.42, 115.06, 112.31, 35.48, 33.37, 22.24, 13.79.

2-((3-Butylphenyl)amino)benzoic acid (20). 2-Bromobenzoic acid (300 mg, 1.49 mmol) was reacted with 3-butylaniline **63** (298 mg, 2.00 mmol) according to general procedure F to afford product **20** (104 mg, 0.386 mmol, 26%) as a brown solid. ^{1}H-NMR (300 MHz, $CDCl_3$) δ 9.25 (s(br), 1H), 8.01 (dd, J=8.1, 1.6 Hz, 1H), 7.32 (ddd, J=8.6, 7.0, 1.7 Hz, 1H), 7.27–7.21 (m, 1H), 7.19 (dd, J=8.5, 0.7 Hz, 1H), 7.06 (dd, J=6.7, 1.0 Hz, 2H), 6.93 (d, J=7.6 Hz, 1H), 6.71 (ddd, J=8.1, 7.1, 1.0 Hz, 1H), 2.58 (t, J=9.0 Hz, 2H), 1.66–1.52 (m, 2H), 1.42–1.27(sext, J=7.3 Hz, 2H), 0.91 (t, J=7.3 Hz, 3H); ^{13}C-NMR (75 MHz, $CDCl_3$) δ 173.59, 149.28, 144.63, 140.33, 135.32, 132.73, 129.32, 124.51, 123.46, 120.58, 117.11, 114.26, 110.38, 35.73, 33.70, 22.53, 14.10; HRMS (ESI) $[M+H]^+$ calcd for $C_{17}H_{19}NO_2$: 270.1489, found 270.1493; HPLC purity: 97%..

1-Nitro-3-(pent-1-en-1-yl)benzene (64). To a solution of 3-nitrobenzaldehyde (1.22 g, 8.07 mmol) in dry THF (30 mL) was added *n*-butyltriphenylphosphonium iodide (4.31 g, 9.66 mmol) under argon atmosphere. Potassium *tert*-butoxide (1.09 g, 9.71 mmol) was added portionwise at 0 °C. The mixture was stirred at 0 °C for 15 min and then was allowed to warm up to room temperature over 16 h, after which it was concentrated under reduced pressure. The residue was dissolved in EtOAc. The organic phase was washed with H_2O (3×50 mL), dried over Na_2SO_4, filtered and concentrated under reduced pressure. Purification by flash column chromatography (hexanes/EtOAc 95:5) provided 1-nitro-3-(pent-1-en-1-yl)benzene **64** (651 mg, 3.40 mmol, 42%) as a yellow oil. ^{1}H NMR (300 MHz, $CDCl_3$) δ 8.10–7.91 (m, 2H), 7.55 (dd, J=11.8, 7.8 Hz, 1H), 7.47–7.34 (m, 1H), 6.36 (dd, J=13.4, 7.9 Hz, 1H), 5.78 (dt, J=11.7, 7.3 Hz, 1H), 2.25 (qd, J=7.4, 1.8 Hz, 2H), 1.45 (dd, J=14.7, 7.4 Hz, 2H), 0.90 (t, J=7.3 Hz, 3H); ^{13}C-NMR (75 MHz, $CDCl_3$) δ 148.07, 139.23, 135.70, 134.59, 128.92, 126.68, 123.18, 121.11, 30.47, 22.83, 13.62..

3-Pentylaniline (65). To a solution of 1-nitro-3-(pent-1-en-1-yl) benzene **64** (371 mg, 1.94 mmol) in EtOAc (10 mL) was added Pd/C 10% (6 mg). The reaction vessel was evacuated under vacuum and filled back with hydrogen. The cycle was repeated twice and the suspension was stirred at room temperature for 16 h under H_2 atmosphere. The mixture was filtered over a plug of celite, rinsed with DCM and concentrated under reduced pressure to give 3-pentylaniline **65** (268 mg, 1.64 mmol, 85%) as an orange oil without any purification. Spectral data are consistent with literature values[59] ^{1}H NMR (300 MHz, $CDCl_3$) δ 7.22–7.15 (m, 1H), 6.73 (d, J=7.6 Hz, 1H), 6.60 (dd, J=7.8, 1.4 Hz, 2H), 3.64 (s(br), 2H), 2.65 (t, J=9.0 Hz, 2H), 1.80–1.66 (m, 2H), 1.53–1.42 (m, 4H), 1.05 (t, J=6.9 Hz, 3H).

2-((3-Pentylphenyl)amino)benzoic acid (21). 3-Pentylaniline **65** (149 mg, 0.913 mmol) was reacted with methyl 2-bromobenzoate (304 mg, 1.41 mmol) according to general procedure C. The crude compound was used without any purification. Its saponification was performed according to general procedure D to afford **21** (186 mg, 0.656 mmol, 72%) was obtained as a yellow solid without the need of any purification. ^{1}H-NMR (300 MHz, $CDCl_3$) δ 9.42 (s(br), 1H), 8.16 (dd, J=8.0, 1.2 Hz, 1H), 7.45–7.37 (m, 1H), 7.33 (t, J=7.1 Hz, 2H), 7.21–7.15 (m, 2H), 7.05 (d, J=7.5 Hz, 1H), 6.82 (t, J=7.2 Hz, 1H), 2.70 (t, J=9.0 Hz, 2H), 1.74 (quint. J=6.0 Hz, 2H), 1.49–1.40 (m, 4H), 1.01 (t, J=6.8 Hz, 3H); ^{13}C-NMR (75 MHz, $CDCl_3$) δ 174.43, 149.23, 144.56, 140.27, 135.29, 132.75, 129.28, 124.43, 123.36, 120.50, 117.08, 114.20, 110.46, 35.98, 31.64, 31.21, 22.68, 14.18; HRMS (ESI) $[M+H]^+$ calcd for $C_{18}H_{21}NO_2$: 284.1645, found 284.1658; HPLC purity: >99%.

***n*-Pentyltriphenylphosphonium iodide (66)**. To a solution of triphenylphosphine (5.00 g, 19.1 mmol) in dry toluene (30 mL) was added 1-iodopentane (4.24 mL, 32.5 mmol). The reaction mixture was stirred at 110 °C for 48 h under argon atmosphere. After cooling down to room temperature, the precipitate was filtered and dried to yield to product **66** (8.78 g, 19.1 mmol, 99%) as a white powder. Spectral data are consistent with literature values[60] ^{1}H-NMR (300 MHz, $CDCl_3$) δ 7.85–7.75 (m, 9H), 7.74–7.66 (m, 6H), 3.69–3.56 (m, 2H), 1.70–1.54 (m, 4H), 1.30 (sext, J=7.3 Hz, 2H), 0.81 (t, J=7.3 Hz, 3H).

1-(Hex-1-en-1-yl)-3-nitrobenzene (67). To a solution of 3-nitrobenzaldehyde (2.46 g, 16.29 mmol) in dry THF (65 mL) was added **66** (9.00 g, 19.55 mmol) under argon atmosphere. Potassium *tert*-butoxide (2.19 g, 19.52 mmol) was added portionwise at 0 °C. The mixture was stirred at 0 °C for 15 min and then was allowed to warm up to room temperature for 16 h, after which it was concentrated under reduced pressure. The residue was dissolved in EtOAc. The organic phase was washed with H_2O (3×50 mL), dried over Na_2SO_4, filtered and concentrated under reduced pressure. Purification by flash column chromatography (hexanes/EtOAc 95:5) provided **67** (1.89 g, 9.21 mmol, 57%) as a yellow oil. Spectral data are consistent with literature values.[61] ^{1}H-NMR (300 MHz, $CDCl_3$) δ 8.15 (dt, J=17.2, 1.7 Hz, 1H), 8.09–8.00 (m, 1H), 7.64–7.54 (m, 1H), 7.52–7.41 (m, 1H), 6.43 (d, J=12.9 Hz, 1H), 5.83 (dt, J=11.7, 7.4 Hz, 1H), 2.36–2.26 (m 2H), 1.51–1.42 (m, 2H), 1.42–1.31 (m, 2H), 0.90 (t, J=7.2 Hz, 3H).

3-Hexylaniline (68). To a solution of **67** (563 mg, 2.74 mmol) in EtOAc (10 mL) was added Pd/C 10% (15 mg). The reaction vessel was evacuated under vacuum and filled with hydrogen. The cycle was repeated twice and the suspension was stirred at room temperature for 16 h under H_2 atmosphere. The mixture was then filtered over a plug of celite, rinsed with DCM and concentrated under reduced pressure to afford 3-hexylaniline **68** (429 mg, 2.42 mmol, 88%) as a yellow oil which was used directly in the next step. ^{1}H-NMR (300 MHz, $CDCl_3$) δ 7.08 (td, J=7.7, 1.0 Hz, 1H), 6.61 (d, J=7.7 Hz, 1H), 6.55–6.49 (m, 2H), 3.60 (s, 2H), 2.53 (t, J=7.6 Hz, 2H), 1.61 (quint, J=7.5 Hz, 2H), 1.40–1.29 (m, 6H), 0.90 (t, J=6.3 Hz, 3H); ^{13}C-NMR (75 MHz, $CDCl_3$) δ 146.34, 144.27, 129.15, 118.89, 115.35, 112.58, 36.06, 31.83, 31.42, 29.14, 22.69, 14.18.

2-((3-Hexylphenyl)amino)benzoic acid (22). 2-Bromobenzoic acid (109 mg, 0.54 mmol) was reacted with **68** (125 mg, 0.71 mmol) according to general procedure F to afford product **22** (24 mg, 0.081 mmol, 15%) as a yellow solid. ^{1}H-NMR (300 MHz, $CDCl_3$) δ 9.28 (s(br), 1H), 8.04 (dd, J=8.1, 1.5 Hz, 1H), 7.35 (ddd, J=8.6, 7.0, 1.6 Hz, 1H), 7.28 (d, J=8.7 Hz, 1H), 7.25–7.19 (m, 1H), 7.13–7.05 (m, 3H), 6.96 (d, J=7.6 Hz, 1H), 6.80–6.68 (m, 1H), 2.61 (t, J=9.0 Hz, 2H), 1.69–1.57 (m, 2H), 1.41–1.27 (m, 6H), 0.89 (t, J=6.7 Hz, 3H); ^{13}C-NMR (75 MHz, $CDCl_3$) δ 172.97, 149.26, 144.66, 140.32, 135.28, 132.69, 129.33, 124.49, 123.44, 120.56, 117.09, 114.24, 110.28, 36.05, 31.87, 31.53, 29.15, 22.77, 14.25; HRMS (ESI) $[M+H]^+$ calcd for $C_{19}H_{23}NO_2$: 298.1802, found 298.1796; HPLC purity: 96%.

1-(Hept-1-yn-1-yl)-3-nitrobenzene (69). To a solution of 1-iodo-3-nitrobenzene (500 mg, 2.0 mmol) in dry THF (5 mL) was added $PdCl_2(PPh_3)_2$ (14 mg, 0.02 mmol), CuI (8 mg, 0.04 mmol), DIPEA (1.1 mL, 6.3 mmol) and hept-1-yne (0.29 mL, 2.2 mmol). The reaction mixture was stirred at 50 °C for 16 h under argon atmosphere,

then cooled down to room temperature and diluted with EtOAc and H_2O. The aqueous phase was extracted with EtOAc (3×20 mL) and the combined organic phases were washed with brine (1× 60 mL), dried over Na_2SO_4, filtered and concentrated under reduced pressure. Purification by flash column chromatography (hexanes/EtOAc 99:1 to 90:10) provided **69** (436 mg, 2.0 mmol, >99%) as an orange oil. ^{1}H-NMR (300 MHz, $CDCl_3$) δ 8.23 (t, J=1.9 Hz, 1H), 8.10 (ddd, J=8.3, 2.3, 1.0 Hz, 1H), 7.68 (dt, J=7.7, 1.2 Hz, 1H), 7.45 (t, J= 8.0 Hz, 1H), 2.42 (t, J=7.1 Hz, 2H), 1.63 (quint, J=7.1 Hz, 2H), 1.48–1.30 (m, 4H), 0.93 (t, J=7.1 Hz, 3H); ^{13}C-NMR (151 MHz, $CDCl_3$) δ 148.21, 137.43, 129.25, 126.52, 126.10, 122.33, 93.78, 78.63, 31.24, 28.30, 22.34, 19.47, 14.10.

3-(Hept-1-yn-1-yl)aniline (70). The reduction of the nitro group in **69** (200 mg, 0.921 mmol) was performed according to general procedure A. Purification by flash column chromatography (hexanes/EtOAc 99:1 to 90:10) provided **70** (156 mg, 0.833 mmol, 90%) as an orange oil. ^{1}H-NMR (300 MHz, $CDCl_3$) δ 7.08 (t, J=7.8 Hz, 1H), 6.84 (d, J=7.6 Hz, 1H), 6.74 (s, 1H), 6.59 (dd, J=8.0, 2.5 Hz, 1H), 3.62 (s(br), 2H), 2.41 (t, J=7.1 Hz, 2H), 1.63 (quint.J=6.9 Hz, 2H), 1.51–1.34 (m, 4H), 0.96 (t, J=7.0 Hz, 3H); ^{13}C-NMR (75 MHz, $CDCl_3$) δ 146.27, 129.12, 124.77, 121.93, 117.91, 114.61, 89.88, 80.80, 31.15, 28.52, 22.28, 19.38, 14.04..

3-Heptylaniline (71). To a solution of **70** (189 mg, 1.0 mmol) in EtOAc (5 mL) was added Pd/C 10% (5 mg). The reaction vessel was evacuated under vacuum and filled back with hydrogen. The cycle was repeated twice and the suspension was stirred at room temperature for 16 h under H_2 atmosphere. The mixture was then filtered over a plug of celite, rinsed with DCM and concentrated under reduced pressure. Purification by flash column chromatography (hexanes/EtOAc 99:1 to 70/30) provided **71** (131 mg, 0.68 mmol, 68%) as a yellow oil. ^{1}H-NMR (300 MHz, $CDCl_3$) δ 7.11 (t, J=7.6 Hz, 1H), 6.64 (d, J=7.4 Hz, 1H), 6.59–6.50 (m, 2H), 3.62 (s(br), 2H), 2.56 (t, J=9.0 Hz, 2H), 1.70–1.56 (m, 2H), 1.41–1.29 (m, 8H), 0.94 (t, J=6.7 Hz, 3H); ^{13}C-NMR (75 MHz, $CDCl_3$) δ 146.38, 144.29, 129.16, 118.90, 115.35, 112.58, 36.07, 31.91, 31.48, 29.44, 29.29, 22.76, 14.19.

Methyl 2-((3-heptylphenyl)amino)benzoate (72). 3-Heptylaniline **71** (70 mg, 0.37 mmol) was reacted with methyl 2-bromobenzoate according to general procedure C. Purification by flash column chromatography (hexanes/EtOAc 99:1 to 90:10) provided product **72** (102 mg, 0.31 mmol, 84%) as a yellow oil. ^{1}H-NMR (300 MHz, $CDCl_3$) δ 9.45 (s(br), 1H), 7.97 (dd, J=8.0, 1.4 Hz, 1H), 7.35–7.26 (m, 2H), 7.24 (d, J=7.4 Hz, 1H), 7.11–7.05 (m, 2H), 6.92 (d, J=7.5 Hz, 1H), 6.78–6.67 (m, 1H), 3.91 (s, 3H), 2.60 (t, J=9.0 Hz, 2H), 1.69–1.55 (m, 2H), 1.36–1.26 (m, 8H), 0.89 (t, J=6.7 Hz, 3H); ^{13}C-NMR (75 MHz, $CDCl_3$) δ 169.08, 148.28, 144.53, 140.72, 134.20, 131.73, 129.24, 123.95, 122.83, 119.90, 117.00, 114.21, 111.87, 51.87, 36.05, 31.96, 31.54, 29.42, 29.32, 22.81, 14.24.

2-((3-Heptylphenyl)amino)benzoic acid (23). Methyl 2-((3-heptylphenyl)amino)benzoate **72** (102 mg, 0.31 mmol) was saponified according to general procedure D to afford **23** (93 mg, 0.30 mmol, 97%) as a yellow solid without the need of any purification. ^{1}H-NMR (300 MHz, Methanol-d_4) δ 7.96 (dd, J=8.0, 1.5 Hz, 1H), 7.27–7.21 (m, 1H), 7.20–7.13 (m, 2H), 7.03–6.94 (m, 2H), 6.83 (d, J=7.6 Hz, 1H), 6.67 (ddd, J=8.1, 6.9, 1.3 Hz, 1H), 2.51 (t, J=9.0 Hz, 2H), 1.55 (quint, J=7.1 Hz, 2H), 1.33–1.19 (m, 8H), 0.85 (t, J=6.8 Hz, 3H); ^{13}C-NMR (75 MHz, Methanol-d4) δ 171.84, 149.38, 145.39, 141.98, 134.99, 133.26, 130.18, 124.60, 123.15, 120.32, 117.89, 114.80, 113.26, 36.83, 32.97, 32.55, 30.27, 23.68, 14.48; HRMS (ESI) $[M+H]^+$ calcd for $C_{20}H_{25}NO_2$: 312.1958, found 312.1965; HPLC purity: >99%.

2-((3-Isopropylphenyl)amino)benzoic acid (24). 2-Bromobenzoic acid (210 mg, 1.04 mmol) was reacted with 3-isopropylaniline (198 mg, 1.46 mmol) according to general procedure F to afford product **24** (56 mg, 0.22 mmol, 21%) as a light yellow solid. ^{1}H-NMR (300 MHz, $CDCl_3$) δ 9.35 (s(br), 1H), 8.11 (dd, J=8.1, 1.5 Hz, 1H), 7.44–7.33 (m, 2H), 7.29 (t, J=8.8 Hz, 1H), 7.20–7.12 (m, 2H), 7.07 (d, J=7.6 Hz, 1H), 6.85–6.74 (m, 1H), 2.97 (sept, J=6.9 Hz, 1H), 1.33 (d, J=6.9 Hz, 6H); ^{13}C-NMR (75 MHz, $CDCl_3$) δ 174.25, 150.65, 149.32, 140.34, 135.36, 132.77, 129.40, 122.54, 121.62, 120.77, 117.11, 114.22, 110.41, 34.24, 29.85, 24.09; HRMS (ESI) $[M+H]^+$ calcd for $C_{16}H_{17}NO_2$: 256.1332, found 256.1339; HPLC purity: >99%.

Methyl 2-((3-(*tert*-butyl)phenyl)amino)benzoate (73). 3-(*Tert*-butyl) aniline (300 mg, 2.0 mmol) was reacted with methyl 2-bromobenzoate according to general procedure C. Purification by flash column chromatography (hexanes/EtOAc 99:1 to 95:5) provided product **73** (485 mg, 1.72 mmol, 86%) as a yellow oil. ^{1}H-NMR (300 MHz, $CDCl_3$) δ 9.48 (s(br), 1H), 7.97 (dd, J=8.1, 1.3 Hz, 1H), 7.35–7.23 (m, 4H), 7.19–7.06 (m, 2H), 6.76–6.67 (m, 1H), 3.91 (s, 3H), 1.33 (s, 9H); ^{13}C-NMR (75 MHz, $CDCl_3$) δ 169.12, 152.84, 148.39, 140.46, 134.23, 131.75, 129.00, 120.87, 120.30, 119.77, 116.93, 114.07, 111.76, 51.87, 34.86, 31.44.

2-((3-(*Tert*-butyl)phenyl)amino)benzoic acid (25). Methyl 2-((3-(*tert*-butyl)phenyl)amino)benzoate **73** (200 mg, 0.71 mmol) was saponified according to general procedure D to afford **25** (188 mg, 0.70 mmol, 99%) was obtained without the need of any purification as a brown solid. Spectral data are consistent with literature values.[62] ^{1}H-NMR (300 MHz, Methanol-d_4) δ 7.97 (dd, J=8.0, 1.5 Hz, 1H), 7.28 (ddd, J=8.6, 5.3, 1.6 Hz, 1H), 7.25–7.21 (m, 2H), 7.23–7.14 (m, 2H), 7.15–7.06 (m, 1H), 7.03 (ddd, J=7.9, 2.1, 0.9 Hz, 1H), 6.76–6.64 (m, 1H), 1.31 (s, 9H); HRMS (ESI) $[M+H]^+$ calcd for $C_{17}H_{19}NO_2$: 270.1489, found 270.15013; HPLC purity: >99%.

2-([1,1′-Biphenyl]-3-ylamino)benzoic acid (26). 2-Bromobenzoic acid (200 mg, 0.99 mmol) was reacted with 3-aminobiphenyl (235 mg, 1.39 mmol) according to general procedure F to afford product **26** (47 mg, 0.16 mmol, 16%) as a beige powder. ^{1}H-NMR (300 MHz, $CDCl_3$) δ 9.40 (s(br), 1H), 8.08 (dd, J=8.1, 1.4 Hz, 1H), 7.65–7.58 (m, 2H), 7.51 (t, J=1.7 Hz, 1H), 7.45 (td, J=7.5, 2.1 Hz, 3H), 7.42–7.33 (m, 3H), 7.35–7.26 (m, 2H), 6.84–6.73 (m, 1H); ^{13}C-NMR (75 MHz, $CDCl_3$) δ 173.62, 148.99, 142.84, 140.96, 140.85, 135.44, 132.81, 129.96, 128.95, 127.68, 127.28, 123.07, 121.96, 118.56, 117.49, 114.36, 110.67; HRMS (ESI) $[M+H]^+$ calcd for $C_{19}H_{15}NO_2$: 290.1176, found 290.1182; HPLC purity: 98%.

Methyl 2-bromo-3-fluorobenzoate (74). Esterification of 2-bromo-3-fluorobenzoic acid (300 mg, 1.37 mmol) was performed according to general procedure E to afford **74** (236 mg, 1.01 mmol, 74%) as a colorless oil without the need of any purification. ^{1}H-NMR (300 MHz, $CDCl_3$) δ 7.58–7.53 (m, 1H), 7.32 (td, J=8.0, 5.1 Hz, 1H), 7.23 (td, J= 8.3, 1.7 Hz, 1H), 3.93 (s, 3H); ^{19}F-NMR (282 MHz, $CDCl_3$) δ −102.88, −102.88, −102.90, −102.90, −102.91, −102.91, −102.93, −102.93; ^{13}C-NMR (75 MHz, $CDCl_3$) δ 165.93, 165.89, 161.25, 157.98, 134.39, 128.58, 128.47, 126.66, 126.61, 119.36, 119.05, 109.65, 109.35, 52.76.

Methyl 3-fluoro-2-((3-hexylphenyl)amino)benzoate (75). 3-Hexylaniline **68** (100 mg, 0.56 mmol) was reacted with **74** according to general procedure C. Purification by flash column chromatography (hexanes/EtOAc 99:1 to 90:10) provided product **75** (78 mg, 0.24 mmol, 42%) as a yellow oil. ^{1}H-NMR (300 MHz, $CDCl_3$) δ 8.87 (s(br), 1H), 7.83–7.78 (m, 1H), 7.29–7.23 (m, 1H), 7.19 (t, J=8.7 Hz, 1H), 6.91 (td, J=8.0, 4.6 Hz, 1H), 6.85 (d, J=7.6 Hz, 1H), 6.79 (dd, J= 8.0, 2.9 Hz, 2H), 3.91 (s, 3H), 2.59 (t, J=7.0 Hz, 2H), 1.69–1.59 (m, 2H), 1.38–1.29 (m, 6H), 0.92 (t, J=6.7 Hz, 3H); ^{13}C-NMR (75 MHz, $CDCl_3$) δ 182.37, 168.23, 151.98, 147.24, 143.76, 128.55, 126.94, 122.35, 121.00, 120.73, 119.66, 118.98, 116.06, 52.36, 36.11, 31.88, 31.49, 29.17, 22.76, 14.25; ^{19}F-NMR (282 MHz, $CDCl_3$) δ −115.20, −115.21, −115.22, −115.23, −115.24, −115.25.

3-Fluoro-2-((3-hexylphenyl)amino)benzoic acid (31). Methyl 3-fluoro-2-((3-hexylphenyl)amino)benzoate **75** (78 mg, 0.24 mmol)

was saponified according to general procedure D to afford **31** (60 mg, 0.19 mmol, 79%) as a brown oil without the need of any purification. ^{1}H-NMR (300 MHz, Methanol-d_4) δ 7.84 (dt, J=7.9, 1.0 Hz, 1H), 7.26 (ddd, J=12.1, 8.1, 1.5 Hz, 1H), 7.10 (td, J=7.7, 1.8 Hz, 1H), 6.95 (td, J=8.0, 4.7 Hz, 1H), 6.76 (d, J=7.6 Hz, 1H), 6.71–6.64 (m, 2H), 2.52 (t, J=9.0 Hz, 2H), 1.65–1.49 (m, 2H), 1.37–1.24 (m, 6H), 0.88 (t, J=6.6 Hz, 3H); ^{13}C-NMR (75 MHz, $CDCl_3$) δ 174.30, 156.45, 153.16, 143.80, 143.19, 133.45, 133.29, 128.59, 127.17, 124.07, 121.86, 120.51, 120.39, 119.98, 119.71, 118.26, 115.62, 36.04, 31.84, 31.46, 29.20, 22.76, 14.22; ^{19}F-NMR (282 MHz, Methanol-d_4) δ −118.95, −118.96, −118.98, −118.99, −119.00, −119.02, −119.03; HRMS (ESI) $[M+H]^+$ calcd for $C_{19}H_{22}FNO_2$: 316.1707, found 316.1720; HPLC purity: 99%.

Methyl 2-bromo-4-fluorobenzoate (76). Esterification of 2-bromo-4-fluorobenzoic acid (2.00 g, 9.13 mmol) was performed according to general procedure E to afford **76** (1.92 g, 8.25 mmol, 44%) as a colorless oil without the need of any purification. ^{1}H-NMR (300 MHz, $CDCl_3$) δ 7.89 (dd, J=8.7, 6.0 Hz, 1H), 7.43 (dd, J=8.3, 2.4 Hz, 1H), 7.09 (td, J=8.2, 2.5 Hz, 1H), 3.94 (s, 3H); ^{13}C-NMR (151 MHz, $CDCl_3$) δ 165.66, 164.80, 163.10, 133.52, 133.46, 128.11, 128.09, 123.28, 123.21, 122.09, 121.93, 114.71, 114.57, 52.63; ^{19}F-NMR (282 MHz, $CDCl_3$) δ −105.73, −105.75, −105.76, −105.78, −105.78, −105.81..

Methyl 4-fluoro-2-((3-hexylphenyl)amino)benzoate (77). 3-Hexylaniline **68** (121 mg, 0.68 mmol) was reacted with **76** according to general procedure C. Purification by flash column chromatography (hexanes/EtOAc 95:5) provided product **77** (211 mg, 0.64 mmol, 94%) as a yellow oil. ^{1}H-NMR (300 MHz, $CDCl_3$) δ 9.65 (s(br), 1H), 7.98 (dd, J=9.0, 6.8 Hz, 1H), 7.29 (td, J=7.4, 1.3 Hz, 1H), 7.11–7.06 (m, 2H), 6.99 (d, J=7.6 Hz, 1H), 6.87 (dd, J=12.2, 2.5 Hz, 1H), 6.45–6.37 (m, 1H), 3.91 (s, 3H), 2.67–2.59 (t, J=7.5 Hz, 2H), 1.71–1.58 (m, 2H), 1.41–1.30 (m, 6H), 0.96–0.88 (m, 3H); ^{13}C-NMR (75 MHz, $CDCl_3$) δ 168.61, 168.42, 165.28, 150.89, 150.73, 144.73, 139.85, 134.38, 134.23, 129.40, 124.84, 123.54, 120.62, 107.96, 104.73, 104.43, 100.07, 99.72, 51.84, 35.99, 31.85, 31.46, 29.10, 22.73, 14.21; ^{19}F-NMR (282 MHz, $CDCl_3$) δ −103.31, −103.32, −103.34, −103.34, −103.35, −103.36, −103.37, −103.38, −103.39, −103.41, −103.41.

4-Fluoro-2-((3-hexylphenyl)amino)benzoic acid (32). Saponification of methyl 4-fluoro-2-((3-hexylphenyl)amino)benzoate **77** (200 mg, 0.61 mmol) was performed according to general procedure D to afford **32** (95 mg, 0.30 mmol, 49%) as a yellow solid without the need of any purification. ^{1}H-NMR (300 MHz, $CDCl_3$) δ 9.43 (s(br), 1H), 8.04 (dd, J=8.7, 6.9 Hz, 1H), 7.30 (t, J=7.9 Hz, 1H), 7.12–7.05 (m, 2H), 7.01 (d, J=7.6 Hz, 1H), 6.80 (dd, J=12.1, 2.2 Hz, 1H), 6.48–6.38 (m, 1H), 2.68–2.56 (t, J=7.5 Hz, 2H), 1.71–1.55 (m, 2H), 1.41–1.24 (m, 6H), 0.89 (t, J=6.6 Hz, 3H); ^{13}C-NMR (75 MHz, $CDCl_3$) δ 172.87, 169.39, 166.04, 151.91, 151.75, 144.91, 139.47, 135.57, 135.41, 129.52, 125.38, 124.10, 121.23, 105.21, 104.90, 100.18, 99.83, 36.01, 31.86, 31.50, 29.13, 22.75, 14.24; ^{19}F-NMR (282 MHz, $CDCl_3$) δ −101.57, −101.59, −101.61, −101.63, −101.66; HRMS (ESI) $[M+H]^+$ calcd for $C_{19}H_{22}FNO_2$: 316.1707, found 316.1722; HPLC purity: >99%.

Methyl 2-bromo-5-fluorobenzoate (78). Esterification of 2-bromo-5-fluorobenzoic acid (300 mg, 1.37 mmol) was performed according to general procedure E to afford **78** (262 mg, 1.13 mmol, 82%) as a colorless oil without the need of any purification. ^{1}H-NMR (300 MHz, $CDCl_3$) δ 7.60 (dt, J=7.9, 2.5 Hz, 1H), 7.51 (dt, J=8.7, 2.9 Hz, 1H), 7.10–7.00 (m, 1H), 3.93 (s, 3H); ^{13}C-NMR (75 MHz, $CDCl_3$) δ 165.47, 163.06, 159.76, 135.97, 135.87, 133.56, 133.46, 120.23, 119.93, 118.79, 118.46, 116.19, 116.15, 52.82; ^{19}F-NMR (282 MHz, $CDCl_3$) δ −113.95, −113.96, −113.97, −113.98, −113.99, −113.99, −114.00, −114.02.

Methyl 5-fluoro-2-((3-hexylphenyl)amino)benzoate (79). 3-Hexylaniline **68** (100 mg, 0.56 mmol) was reacted with **78** according to general procedure C. Purification by flash column chromatography (hexanes/EtOAc 99:1 to 90:10) provided product **79** (93 mg, 0.28 mmol, 50%) as a yellow oil. ^{1}H-NMR (300 MHz, $CDCl_3$) δ 9.25 (s(br), 1H), 7.66 (dd, J=9.5, 3.1 Hz, 1H), 7.29–7.21 (m, 2H), 7.11–7.03 (m, 3H), 6.93 (d, J=7.6 Hz, 1H), 3.92 (s, 3H), 2.61 (t, J=9.0 Hz, 2H), 1.70–1.58 (m, 2H), 1.42–1.27 (m, 6H), 0.92 (t, J=6.7 Hz, 3H); ^{13}C-NMR (75 MHz, $CDCl_3$) δ 168.11, 168.08, 155.87, 152.74, 144.85, 144.83, 144.61, 140.91, 129.31, 123.88, 122.39, 122.01, 121.71, 119.43, 117.00, 116.69, 115.91, 115.82, 112.24, 112.16, 52.08, 36.03, 31.85, 31.48, 29.12, 22.74, 14.21; ^{19}F-NMR (282 MHz, $CDCl_3$) δ −126.87, −126.88, −126.89, −126.90, −126.91, −126.92, −126.93, −126.94.

5-Fluoro-2-((3-hexylphenyl)amino)benzoic acid (33). Saponification of methyl 5-fluoro-2-((3-hexylphenyl)amino)benzoate **79** (74 mg, 0.22 mmol) was performed according to general procedure D to afford **33** (66 mg, 0.21 mmol, 95%) as a yellow solid without the need of any purification. ^{1}H-NMR (300 MHz, Methanol-d_4) δ 7.62 (dd, J=9.6, 3.1 Hz, 1H), 7.25–7.17 (m, 1H), 7.17 (dd, J=2.6, 2.0 Hz, 1H), 7.08 (ddd, J=9.3, 7.7, 3.1 Hz, 1H), 7.00–6.95 (m, 2H), 6.86 (d, J=7.6 Hz, 1H), 2.55 (t, J=9.0 Hz, 2H), 1.64–1.52 (m, 2H), 1.33–1.26 (m, 6H), 0.88 (t, J=6.7 Hz, 3H); ^{13}C-NMR (75 MHz, Methanol-d_4) δ 170.68, 157.09, 153.98, 146.04, 145.59, 142.26, 130.29, 124.62, 122.88, 122.24, 120.02, 118.25, 116.75, 36.85, 32.86, 32.57, 30.03, 23.69, 14.43; ^{19}F-NMR (282 MHz, Methanol-d_4) δ −128.98, −129.00, −129.01, −129.01, −129.02, −129.03, −129.04, −129.06; HRMS (ESI) $[M+H]^+$ calcd for $C_{19}H_{22}FNO_2$: 316.1707, found 316.1718; HPLC purity: >99%.

Methyl 2-bromo-6-fluorobenzoate (80). Esterification of 2-bromo-6-fluorobenzoic acid (300 mg, 1.4 mmol) was performed according to general procedure E to afford **80** (140 mg, 0.6 mmol, 43%) as a colorless oil without the need of any purification. ^{1}H-NMR (300 MHz, $CDCl_3$) δ 7.38 (dd, J=8.1, 0.7 Hz, 1H), 7.30–7.20 (m, 1H), 7.11–7.02 (m, 1H), 3.96 (s, 3H); ^{13}C-NMR (75 MHz, $CDCl_3$) δ 164.43, 161.34, 157.97, 132.11, 131.99, 128.71, 128.67, 124.78, 124.51, 120.39, 120.34, 115.17, 114.89, 53.11; ^{19}F-NMR (282 MHz, $CDCl_3$) δ −111.50, −111.52, −111.54, −111.56.

Methyl 2-fluoro-6-((3-hexylphenyl)amino)benzoate (81). 3-Hexylaniline **68** (100 mg, 0.56 mmol) was reacted with **80** according to general procedure C. Purification by flash column chromatography (hexanes/EtOAc 99:1 to 90:10) provided product **81** (162 mg, 0.49 mmol, 88%) as a yellow oil. ^{1}H-NMR (300 MHz, $CDCl_3$) δ 9.09 (s(br), 1H), 7.28–7.14 (m, 2H), 7.06–7.01 (m, 2H), 6.98 (d, J=8.6 Hz, 1H), 6.93 (d, J=7.6 Hz, 1H), 6.46 (ddd, J=11.2, 8.1, 1.0 Hz, 1H), 3.94 (s, 3H), 2.59 (t, J=9.0 Hz, 2H), 1.65–1.58 (m, 2H), 1.37–1.27 (m, 6H), 0.93–0.86 (t, J=6.6 Hz, 3H); ^{13}C-NMR (75 MHz, $CDCl_3$) δ 167.86, 165.14, 161.75, 149.02, 144.64, 140.54, 133.87, 129.32, 124.27, 122.86, 119.96, 110.12, 105.22, 52.28, 36.02, 31.85, 31.48, 29.12, 22.75, 14.23; ^{19}F-NMR (282 MHz, $CDCl_3$) δ −105.83, −105.85, −105.87, −105.89.

2-Fluoro-6-((3-hexylphenyl)amino)benzoic acid (34=LM98). Methyl 2-fluoro-6-((3-hexylphenyl)amino)benzoate **81** (100 mg, 0.30 mmol) was saponified according to general procedure D to afford **34** (**LM98**) (57 mg, 0.18 mmol, 60%) as a brown solid without the need of any purification. ^{1}H-NMR (300 MHz, Methanol-d_4) δ 7.25–7.11 (m, 2H), 6.99–6.85 (m, 4H), 6.43 (ddd, J=11.2, 8.1, 0.7 Hz, 1H), 2.57–2.49 (t, J=7.5 Hz, 2H), 1.56 (quint, J=7.6 Hz, 2H), 1.33–1.23 (m, 6H), 0.86 (t, J=6.6 Hz, 3H); ^{13}C-NMR (75 MHz, Methanol-d_4) δ 169.79, 166.44, 163.06, 150.11, 150.05, 145.55, 141.87, 134.66, 134.51, 130.27, 124.98, 123.36, 120.56, 110.85, 110.81, 105.94, 105.62, 104.96, 104.77, 36.80, 32.83, 32.52, 30.00, 23.66, 14.44; ^{19}F-NMR (282 MHz, Methanol-d_4) δ −107.32, −107.34, −107.36, −107.38; HRMS (ESI) $[M+H]^+$ calcd for $C_{19}H_{22}FNO_2$: 316.1707, found 316.1722; HPLC purity: >99%.

ChemMedChem
Full Papers
doi.org/10.1002/cmdc.202100432
Chemistry Europe
European Chemical Societies Publishing

2-Iodo-6-methylbenzoic acid (82). To a solution of 2-methylbenzoic acid (500 mg, 3.67 mmol) in dry DMF (12 mL) was added *N*-iodosuccinimide (NIS) (826 mg, 3.67 mmol) and $Pd(OAc)_2$ (83 mg, 0.37 mmol). The reaction mixture was stirred at 100 °C for 2 h, cooled down to room temperature and concentrated under vacuum. The residue was dissolved in DCM, washed with saturated aqueous solution of brine (2×15 mL), dried over Na_2SO_3 and concentrated under reduced pressure. Purification by flash column chromatography (hexanes/EtOAc 98:2 to 85:15) provided product **82** (681 mg, 2.60 mmol, 71%) as a white solid. Spectral data are consistent with literature values.[63] ^{1}H-NMR (300 MHz, Chloroform-d) δ 7.70 (d, *J*=7.9 Hz, 1H), 7.22 (d, *J*=7.7 Hz, 1H), 7.03 (t, *J*=7.8 Hz, 1H), 2.45 (s, 3H).

2-((3-Hexylphenyl)amino)-6-methylbenzoic acid (35). 3-Hexylaniline **68** (100 mg, 0.56 mmol) was reacted with **82** according to general procedure B to afford product **35** (32 mg, 0.10 mmol, 18%) as a brown solid without any need for further purification. ^{1}H-NMR (500 MHz, DMSO-d_6) δ 7.95 (s(br), 1H), 7.18 (t, *J*=7.8 Hz, 1H), 7.12 (t, *J*=7.7 Hz, 1H), 7.06 (d, *J*=8.2 Hz, 1H), 6.87–6.83 (m, 2H), 6.77 (d, *J*=7.4 Hz, 1H), 6.71 (d, *J*=7.5 Hz, 1H), 2.35 (s, 3H), 1.53 (quint, *J*=7.3 Hz, 2H), 1.30–1.22 (m, 8H), 0.85 (t, *J*=6.7 Hz, 3H); ^{13}C-NMR (126 MHz, DMSO-d_6) δ 169.97, 143.43, 142.98, 142.44, 137.51, 130.36, 128.99, 122.93, 122.60, 120.91, 118.34, 115.70, 115.61, 35.19, 31.10, 30.80, 28.33, 22.06, 21.09, 13.95; HRMS (ESI) $[M+H]^+$ calcd for $C_{20}H_{25}NO_2$: 312.1958, found 312.1963; UPLC-MS purity: 93%.

Methyl 2-((4-hexylphenyl)amino)benzoate (83). 4-Hexylaniline (300 mg, 1.69 mmol) was reacted with methyl 2-bromobenzoate according to general procedure C. Purification by flash column chromatography (hexanes/EtOAc 99:1 to 90:10) provided product **83** (174 mg, 0.56 mmol, 33%) as a yellow oil. ^{1}H-NMR (300 MHz, $CDCl_3$) δ 9.47 (s(br), 1H), 8.02 (dd, *J*=8.1, 1.7 Hz, 1H), 7.38–7.28 (m, 2H), 7.24–7.21 (m, 4H), 6.79–6.72 (m, 1H), 3.96 (s, 3H), 2.66 (dd, *J*=8.7, 6.7 Hz, 2H), 1.68 (quint, *J*=7.5 Hz, 2H), 1.46–1.34 (m, 6H), 0.98 (t, *J*=6.0, 3H); ^{13}C-NMR (75 MHz, $CDCl_3$) δ 169.07, 148.71, 138.75, 138.28, 134.20, 131.69, 129.38, 129.16, 128.35, 123.23, 116.70, 113.91, 111.51, 51.81, 35.55, 31.88, 31.68, 29.14, 22.76, 14.24.

2-((4-Hexylphenyl)amino)benzoic acid (36). Saponification of **83** (75 mg, 0.24 mmol) was performed according to general procedure D to afford **36** (48 mg, 0.16 mmol, 67%) as a brown solid without the need of any purification. ^{1}H-NMR (300 MHz, Methanol-d_4) δ 7.95 (dd, *J*=8.0, 1.7 Hz, 1H), 7.29 (ddd, *J*=8.7, 7.0, 1.7 Hz, 1H), 7.19–7.09 (m, 5H), 6.73–6.64 (m, 1H), 2.58 (t, *J*=7.4 Hz, 2H), 1.61 (quint, *J*=7.5 Hz, 2H), 1.39–1.29 (m, 6H), 0.95–0.85 (t, *J*=6.8 Hz, 3H); ^{13}C-NMR (75 MHz, Methanol-d_4) δ 171.91, 149.89, 139.71, 139.57, 135.09, 133.23, 130.35, 123.68, 117.67, 114.57, 112.99, 36.36, 32.90, 32.78, 30.05, 23.69, 14.42; HRMS (ESI) $[M+H]^+$ calcd for $C_{19}H_{23}NO_2$: 298.1802, found 298.1815; HPLC purity: 99%.

Methyl 2-((4-(*tert*-butyl)phenyl)amino)benzoate (84). 4-*Tert*-butylaniline (0.32 mL, 2.01 mmol) was reacted with methyl 2-bromobenzoate according to general procedure C. Purification by flash column chromatography (hexanes/EtOAc 99:1 to 90:10) provided product **84** (422 mg, 1.49 mmol, 74%) as a yellow solid. ^{1}H-NMR (300 MHz, $CDCl_3$) δ 9.41 (s(br), 1H), 7.95 (dd, *J*=8.1, 1.6 Hz, 1H), 7.40–7.34 (m, 2H), 7.33–7.27 (m, 1H), 7.24–7.16 (m, 3H), 6.74–6.65 (m, 1H), 3.90 (s, 3H), 1.34 (s, 9H); ^{13}C-NMR (75 MHz, $CDCl_3$) δ 169.08, 148.60, 146.86, 138.12, 134.21, 131.71, 126.33, 122.76, 116.78, 114.04, 111.61, 51.86, 34.52, 31.58.

2-((4-(*Tert*-butyl)phenyl)amino)benzoic acid (37). Methyl 2-((4-(*tert*-butyl)phenyl)amino)benzoate **84** (100 mg, 0.35 mmol) was saponified according to general procedure D to afford **37** (82 mg, 0.30 mmol, 86%) as a yellow solid without the need of any purification. ^{1}H-NMR (300 MHz, $CDCl_3$) δ 8.02 (dd, *J*=8.1, 1.7 Hz, 1H), 7.42–7.30 (m, 3H), 7.23–7.15 (m, 3H), 6.77–6.69 (m, 1H), 1.34 (s, 9H); ^{13}C-NMR (75 MHz, $CDCl_3$) δ 173.63, 149.52, 147.40, 137.73, 135.29, 132.71, 126.42, 123.27, 116.92, 114.14, 110.20, 34.57, 31.57; HRMS (ESI) $[M+H]^+$ calcd for $C_{17}H_{19}NO_2$: 270.1489, found 270.1499; UPLC-MS purity: >99%.

Methyl 2-([1,1′-biphenyl]-4-ylamino)benzoate (85). 4-Aminobiphenyl (300 mg, 1.77 mmol) was reacted with methyl 2-bromobenzoate according to general procedure C. Purification by flash column chromatography (DCM 100%) provided product **85** (536 mg, 1.77 mmol, >99%) as an orange solid. ^{1}H-NMR (300 MHz, $CDCl_3$) δ 9.55 (s(br), 1H), 7.99 (dt, *J*=8.0, 1.1 Hz, 1H), 7.63–7.55 (m, 4H), 7.48–7.41 (m, 2H), 7.37–7.29 (m, 5H), 6.81–6.72 (m, 1H), 3.92 (s, 3H); ^{13}C-NMR (75 MHz, $CDCl_3$) δ 169.06, 147.79, 140.79, 140.27, 136.34, 134.26, 131.80, 128.91, 128.11, 127.08, 126.88, 122.50, 117.45, 114.42, 112.28, 51.95.

2-([1,1′-Biphenyl]-4-ylamino)benzoic acid (38). 85 (114 mg, 0.376 mmol) was saponified according to general procedure D to afford **38** (68 mg, 0.24 mmol, 64%) as a light yellow solid without the need of any purification. ^{1}H-NMR (500 MHz, DMSO-d_6) δ 9.75 (s(br), 1H), 7.92 (dd, *J*=8.1, 1.7 Hz, 1H), 7.68–7.64 (m, 4H), 7.48–7.40 (m, 3H), 7.36–7.30 (m, 4H), 6.81 (t, *J*=7.5 Hz, 1H); ^{13}C-NMR (126 MHz, DMSO-d_6) δ 169.93, 146.54, 140.12, 139.67, 134.48, 134.10, 131.90, 128.96, 128.91, 127.63, 126.94, 126.15, 121.21, 117.72, 114.20; HRMS (ESI) $[M+H]^+$ calcd for $C_{19}H_{15}NO_2$: 290.1176, found 290.1183; UPLC-MS purity: 95%.

N-(4-((3r,5r,7r)-adamantan-1-yl)phenyl)acetamide (86). To a solution of 1-bromoadamantane (250 mg, 1.16 mmol) in dichloroethane (10 mL) was added acetanilide (157 mg, 1.16 mmol). The reaction mixture was stirred for 5 min under argon atmosphere before $ZnCl_2$ (32 mg, 0.23 mmol) was added. The mixture was then heated at 75 °C for 16 h. EtOAc was added (100 mL) and the organic phase was washed with H_2O (50 mL) and a saturated aqueous solution of brine (50 mL). The organic phase was dried over Na_2SO_4 and evaporated. The crude material was purified by flash column chromatography (hexanes/EtOAc 95:5 to 40:60) to give **86** (199 mg, 0.739 mmol, 64%) as a white powder. Spectral data are consistent with literature values.[65] ^{1}H-NMR (300 MHz, $CDCl_3$) δ 7.42 (d, *J*=8.7 Hz, 2H), 7.31 (d, *J*=8.7 Hz, 2H), 7.07 (s(br), 1H), 2.16 (s, 3H), 2.12–2.06 (m, 3H), 1.90–1.86 (m, 6H), 1.83–1.69 (m, 6H).

4-((3r,5r,7r)-adamantan-1-yl)aniline hydrochloride (87). To a solution of **86** (70 mg, 0.26 mmol) in MeOH/H_2O (3:1) (4 mL) was added concentrated HCl (0.4 mL). The reaction mixture was stirred at 80 °C for 16 h, cooled back to room temperature and evaporated. The crude compound **87** (69 mg, 0.26 mmol, >99%) was used in the next step without further purification. Spectral data are consistent with literature values.[65] ^{1}H-NMR (300 MHz, Methanol-d_4) δ 7.52–7.45 (m, 2H), 7.26–7.20 (m, 2H), 2.13–2.06 (m, 3H), 1.95–1.91 (m, 6H), 1.90–1.75 (m, 6H).

Methyl 2-((4-((3r,5r,7r)-adamantan-1-yl)phenyl)amino)benzoate (88). 87 (100 mg, 0.379 mmol) was reacted with methyl 2-bromobenzoate according to general procedure C. Purification by flash column chromatography (hexanes/EtOAc 99:1 to 90:10) followed by prep-TLC (hexanes/EtOAc 95:5) provided product **88** (87 mg, 0.24 mmol, 63%) as a beige powder. ^{1}H-NMR (600 MHz, $CDCl_3$) δ 9.40 (s(br), 1H), 7.95 (d, *J*=8.1 Hz, 1H), 7.33 (d, *J*=6.8 Hz, 2H), 7.23–7.17 (m, 4H), 6.69 (s(br), 1H), 3.89 (s, 3H), 2.14–2.07 (m, 3H), 1.96–1.88 (m, 6H), 1.82–1.73 (m, 6H); ^{13}C-NMR (75 MHz, $CDCl_3$) δ 169.00, 148.53, 147.09, 138.11, 134.14, 131.67, 129.13, 128.32, 125.84, 122.70, 116.72, 114.00, 111.53, 51.77, 43.36, 36.90, 35.97, 29.08.

2-((4-((3r,5r,7r)-Adamantan-1-yl)phenyl)amino)benzoic acid (39). 88 (34 mg, 0.094 mmol) was saponified according to general procedure D to afford **39** (30 mg, 0.087 mmol, 93%) as a white powder without the need of any purification. ^{1}H-NMR (300 MHz,

Acetone-d_6) δ 8.45 (dd, J=8.0, 1.6 Hz, 1H), 7.86–7.79 (m, 3H), 7.70–7.63 (m, 3H), 7.20 (ddd, J=8.1, 7.1, 1.1 Hz, 1H), 2.58–2.53 (m, 3H), 2.42–2.37 (m, 6H), 2.29–2.21 (m, 6H); ^{13}C-NMR (75 MHz, DMSO-d_6) δ 170.07, 147.53, 146.01, 137.81, 134.13, 131.88, 129.49, 125.68, 121.54, 121.37, 116.93, 113.46, 112.10, 42.71, 36.21, 35.39, 28.37; HRMS (ESI) $[M+H]^+$ calcd for $C_{23}H_{25}NO_2$: 348.1958, found 348.1969; HPLC purity: 97%.

Methyl 2-((4-cyclohexylphenyl)amino)benzoate (89). 4-Cyclohexylaniline (300 mg, 1.71 mmol) was reacted with methyl 2-bromobenzoate according to general procedure C. Purification by flash column chromatography (hexanes/EtOAc 99:1 to 90:10) provided product **89** (402 mg, 1.30 mmol, 76%) as a yellow solid. ^{1}H-NMR (300 MHz, $CDCl_3$) δ 9.61 (s(br), 1H), 8.07 (d, J=8.0 Hz, 1H), 7.41–7.30 (m, 2H), 7.30–7.27 (m, 4H), 6.83–6.74 (m, 1H), 3.96 (s, 3H), 2.66–2.53 (m, 1H), 2.07–1.91 (m, 4H), 1.92–1.83 (m, 1H), 1.59–1.47 (m, 4H), 1.46–1.37 (m, 1H); ^{13}C-NMR (75 MHz, $CDCl_3$) δ 168.84, 148.50, 143.64, 138.28, 134.02, 131.56, 127.60, 122.93, 116.57, 113.76, 111.34, 51.55, 44.00, 34.57, 26.93, 26.17.

2-((4-Cyclohexylphenyl)amino)benzoic acid (40). **89** (200 mg, 0.646 mmol) was saponified according to general procedure D to afford **40** (93 mg, 0.31 mmol, 48%) as a light yellow solid without the need of any purification. ^{1}H-NMR (500 MHz, DMSO-d_6) δ 13.01 (s(br), 1H), 9.58 (s(br), 1H), 7.88 (dd, J=7.9, 1.7 Hz, 1H), 7.36 (ddd, J=8.7, 7.0, 1.7 Hz, 1H), 7.21 (d, J=8.5 Hz, 2H), 7.18–7.13 (m, 3H), 6.76–6.71 (m, 1H), 2.49–2.44 (m, 1H), 1.84–1.75 (m, 4H), 1.73–1.66 (m, 1H), 1.45–1.30 (m, 4H), 1.29–1.19 (m, 1H); ^{13}C-NMR (126 MHz, DMSO-d_6) δ 169.98, 147.55, 142.77, 138.09, 134.15, 131.83, 127.61, 121.90, 116.92, 113.44, 112.09, 43.16, 34.06, 26.38, 25.60; HRMS (ESI) $[M+H]^+$ calcd for $C_{19}H_{21}NO_2$: 296.1645, found 296.1652; UPLC-MS purity: >99%. Compound **40** has been recrystallized by the solvent diffusion technique. Coordinates for X-ray structure of **40** have been deposited in the Cambridge Crystallographic Date Centre (CCDC) under the number 2054155.

3-Nitrophenol (90). To (3-nitrophenyl)boronic acid (1.00 g, 5.99 mmol) and Cu_2O (26 mg, 0.18 mmol) was added a solution of hydrogen peroxide at 30% (3.6 mL). The reaction mixture was stirred at room temperature for 15 min, after which H_2O and Et_2O were added. The aqueous phase was extracted with Et_2O (3× 40 mL) and the combined organic phases were washed with 20% aqueous solution of NH_4OAc (1×60 mL), brine (1×60 mL), dried over Na_2SO_4, filtered and concentrated under reduced pressure. The product **90** (833 mg, 5.99 mmol, >99%) was obtained as a yellow solid and used without further purification. Spectral data are consistent with literature values.[66] ^{1}H-NMR (300 MHz, $CDCl_3$) δ 7.82 (ddd, J=8.2, 2.1, 0.8 Hz, 1H), 7.69 (t, J=2.3 Hz, 1H), 7.41 (t, J=8.2 Hz, 1H), 7.17 (ddd, J=8.2, 2.5, 0.8 Hz, 1H).

1-Nitro-3-(pentyloxy)benzene (91). To a solution of **90** (833 mg, 5.99 mmol) in dry DMF (30 mL) were added 1-iodopentane (0.86 mL, 6.6 mmol) and NaH dry 90% (175 mg, 6.59 mmol). The reaction mixture was stirred at 80 °C for 16 h under argon atmosphere, cooled down to room temperature, diluted with DCM and H_2O. The aqueous phase was extracted with DCM (3×50 mL) and the combined organic phases were washed with H_2O (3× 50 mL), brine (1×50 mL), dried over Na_2SO_4, filtered and concentrated under reduced pressure. Purification by flash column chromatography (DCM 100%) provided product **91** (545 mg, 2.60 mmol, 43%) was obtained as a yellow oil. ^{1}H-NMR (300 MHz, $CDCl_3$) δ 7.79 (ddd, J=8.1, 2.1, 0.8 Hz, 1H), 7.71 (t, J=2.3 Hz, 1H), 7.40 (t, J=8.2 Hz, 1H), 7.21 (ddd, J=8.3, 2.5, 0.8 Hz, 1H), 4.02 (t, J=6.5 Hz, 2H), 1.90–1.75 (m, 2H), 1.51–1.34 (m, 4H), 0.94 (t, J=7.1 Hz, 3H); ^{13}C-NMR (75 MHz, $CDCl_3$) δ 159.83, 149.34, 129.97, 121.82, 115.64, 108.81, 68.87, 28.83, 28.22, 22.53, 14.11.

3-(Pentyloxy)aniline (92). Nitro reduction of **91** (97 mg, 0.46 mmol) was performed according to general procedure A. Purification by flash column chromatography (DCM 100%) provided **92** (82 mg, 0.46 mmol, >99%) as a dark brown oil. ^{1}H-NMR (300 MHz, $CDCl_3$) δ 7.05 (t, J=8.0 Hz, 1H), 6.33 (ddd, J=8.2, 2.3, 0.7 Hz, 1H), 6.28 (ddd, J=7.8, 2.1, 0.8 Hz, 1H), 6.25 (t, J=2.2 Hz, 1H), 3.92 (t, J=6.6 Hz, 2H), 3.60 (s(br), 2H), 1.84–1.70 (m, 2H), 1.49–1.32 (m, 4H), 0.94 (t, J=7.0 Hz, 3H); ^{13}C-NMR (75 MHz, $CDCl_3$) δ 160.45, 147.85, 130.15, 107.85, 104.76, 101.81, 67.90, 29.13, 28.35, 22.59, 14.15.

Methyl 2-((3-(pentyloxy)phenyl)amino)benzoate (93). 3-(Pentyloxy)aniline **92** (82 mg, 0.46 mmol) was reacted with methyl 2-bromobenzoate according to general procedure C. Purification by flash column chromatography (hexanes/EtOAc 99:1 to 90:10) followed by preparative TLC (hexanes/EtOAc 95:5) provided product **93** (46 mg, 0.15 mmol, 32%) as a white powder. ^{1}H-NMR (300 MHz, $CDCl_3$) δ 9.45 (s(br), 1H), 7.96 (d, J=7.8 Hz, 1H), 7.31 (d, J=3.6 Hz, 2H), 7.23 (dd, J=13.9, 5.7 Hz, 1H), 6.85–6.77 (m, 2H), 6.77–6.70 (m, 1H), 6.64 (d, J=8.2 Hz, 1H), 3.94 (t, J=6.6 Hz, 2H), 3.90 (s, 3H), 1.78 (quint, J=6.0 Hz, 2H), 1.48–1.35 (m, 4H), 0.93 (t, J=6.9 Hz, 3H); ^{13}C-NMR (75 MHz, $CDCl_3$) δ 169.06, 160.32, 147.89, 142.15, 134.22, 131.73, 130.10, 117.32, 114.63, 114.59, 112.19, 109.88, 108.62, 68.19, 51.91, 29.12, 28.35, 22.61, 14.16.

2-((3-(Pentyloxy)phenyl)amino)benzoic acid (47). Methyl 2-((3-(pentyloxy)phenyl)amino)benzoate **93** (46 mg, 0.15 mmol) was saponified according to general procedure D to afford **47** (16 mg, 0.054 mmol, 36%) as a beige powder without the need of any purification. ^{1}H-NMR (300 MHz, Methanol-d_4) δ 7.97 (dd, J=8.0, 1.5 Hz, 1H), 7.36–7.25 (m, 2H), 7.20 (t, J=8.1 Hz, 1H), 6.80–6.70 (m, 3H), 6.61 (ddd, J=8.4, 2.4, 0.7 Hz, 1H), 3.94 (t, J=6.5 Hz, 2H), 1.76 (quint, J=6.0 Hz, 2H), 1.49–1.36 (m, 4H), 0.94 (t, J=7.1 Hz, 3H); ^{13}C-NMR (75 MHz, Methanol-d_4) δ 170.42, 160.24, 147.65, 142.08, 133.68, 131.87, 129.70, 116.89, 113.89, 113.57, 112.27, 109.03, 107.59, 67.61, 28.74, 28.00, 22.16, 12.99; HRMS (ESI) $[M+H]^+$ calcd for $C_{18}H_{21}NO_3$: 300.1594, found 300.1608; HPLC purity: 98%..

(3-Nitrophenyl)methanol (94). To a solution of 3-nitrobenzaldehyde (750 mg, 4.96 mmol) in EtOH (4 mL) at room temperature was added a suspension of $NaBH_4$ (124 mg, 3.27 mmol) in EtOH (4 mL). The reaction mixture was stirred at room temperature for 30 min, after which an aqueous solution of NaOH 10% was added (10 mL). After stirring the resulting mixture at room temperature for 5 min, it became limpid. EtOH was removed in vacuo and DCM was added. The aqueous phase was extracted with DCM (3×10 mL) and the combined organic phases were washed with saturated aqueous solution of $NaHCO_3$ (1×30 mL), brine (1×30 mL), dried over Na_2SO_4, filtered and concentrated under reduced pressure. Product **94** (694 mg, 4.53 mmol, 91%) was obtained as a yellow oil and used in the following step without further purification. Spectral data are consistent with literature values.[57] ^{1}H-NMR (300 MHz, $CDCl_3$) δ 8.22 (d, J=1.4 Hz, 1H), 8.11 (d, J=8.1 Hz, 1H), 7.68 (d, J=7.6 Hz, 1H), 7.52 (t, J=7.9 Hz, 1H), 4.80 (s, 2H).

1-(Butoxymethyl)-3-nitrobenzene (95). To a solution of **94** (350 mg, 2.29 mmol) in dry DMF (5 mL) were added 1-iodobutane (0.29 mL, 2.5 mmol) and NaH dry 90% (61 mg, 2.5 mmol). The reaction mixture was stirred at 80 °C for 16 h under argon atmosphere, cooled down to room temperature, diluted with DCM and quenched with H_2O. The aqueous phase was extracted with DCM (3×10 mL) and the combined organic phases were washed with H_2O (3×30 mL), brine (1×30 mL), dried over Na_2SO_4, filtered and concentrated under reduced pressure. Purification by flash column chromatography (DCM 100%) provided product **95** (205 mg, 0.980 mmol, 43%) was obtained as a yellow oil. ^{1}H-NMR (300 MHz, $CDCl_3$) δ 8.20 (s, 1H), 8.13 (d, J=8.1 Hz, 1H), 7.67 (d, J=7.6 Hz, 1H), 7.51 (t, J=7.9 Hz, 1H), 4.58 (s, 2H), 3.52 (t, J=6.5 Hz, 2H), 1.67–1.56 (m, 2H), 1.49–1.33 (m, 2H), 0.93 (t, J=7.3 Hz, 3H); ^{13}C-

NMR (75 MHz, $CDCl_3$) δ 148.47, 141.18, 133.38, 129.41, 122.56, 122.29, 71.70, 70.97, 31.88, 19.48, 14.02.

3-(Butoxymethyl)aniline (96). Nitro reduction of **95** (205 mg, 0.980 mmol) was performed according to general procedure A. Purification by flash column chromatography (hexanes/EtOAc 99:1 to 70:30) provided **96** (158 mg, 0.881 mmol, 90%) as a dark brown oil. ^{1}H-NMR (300 MHz, $CDCl_3$) δ 7.12 (t, J=7.7 Hz, 1H), 6.74–6.66 (m, 2H), 6.60 (dd, J=7.9, 1.7 Hz, 1H), 4.42 (s, 2H), 3.58 (s(br), 2H), 3.47 (t, J=6.6 Hz, 2H), 1.67–1.53 (m, 2H), 1.48–1.33 (m, 2H), 0.93 (t, J=7.3 Hz, 3H); ^{13}C-NMR (75 MHz, $CDCl_3$) δ 146.61, 140.08, 129.34, 117.93, 114.36, 114.31, 72.92, 70.27, 31.96, 19.48, 14.04.

Methyl 2-((3-(butoxymethyl)phenyl)amino)benzoate (97). 3-(Butoxymethyl)aniline **96** (158 mg, 0.881 mmol) was reacted with methyl 2-bromobenzoate according to general procedure C. Purification by flash column chromatography (hexanes/EtOAc 99:1 to 90:10) provided product **97** (203 mg, 0.648 mmol, 74%) as a yellow oil. ^{1}H-NMR (300 MHz, $CDCl_3$) δ 9.58 (s(br), 1H), 8.04–7.95 (m, 1H), 7.37–7.26 (m, 4H), 7.20 (d, J=7.9 Hz, 1H), 7.09 (d, J=7.5 Hz, 1H), 6.79–6.71 (m, 1H), 4.51 (s, 2H), 3.90 (s, 3H), 3.52 (t, J=6.5 Hz, 2H), 1.71–1.59 (m, 2H), 1.53–1.39 (m, 2H), 0.97 (t, J=7.3 Hz, 3H); ^{13}C-NMR (75 MHz, $CDCl_3$) δ 168.75, 147.76, 140.80, 140.22, 133.98, 131.55, 129.21, 122.53, 121.26, 121.18, 117.06, 114.01, 111.86, 72.53, 70.24, 51.60, 31.82, 19.37, 13.90.

2-((3-(Butoxymethyl)phenyl)amino)benzoic acid (48). Methyl 2-((3-(butoxymethyl)phenyl)amino)benzoate **97** (90 mg, 0.29 mmol) was saponified according to general procedure D to afford **48** (28 mg, 0.095 mmol, 33%) as a beige solid without the need of any purification. ^{1}H-NMR (500 MHz, DMSO-d_6) δ 9.67 (s(br), 1H), 7.90 (dd, J=7.9, 1.7 Hz, 1H), 7.39 (ddd, J=8.6, 7.1, 1.7 Hz, 1H), 7.32 (t, J=7.7 Hz, 1H), 7.23 (dd, J=8.5, 1.1 Hz, 1H), 7.20–7.12 (m, 2H), 7.01 (dt, J=7.7, 1.3 Hz, 1H), 6.78 (ddd, J=8.0, 7.1, 1.1 Hz, 1H), 4.44 (s, 2H), 3.43 (t, J=6.5 Hz, 2H), 1.57–1.48 (m, 2H), 1.40–1.29 (m, 2H), 0.87 (t, J=7.4 Hz, 3H); ^{13}C-NMR (126 MHz, DMSO-d_6) δ 169.91, 146.86, 140.52, 140.33, 134.05, 131.87, 129.34, 121.90, 120.04, 119.87, 117.47, 113.84, 112.79, 71.48, 69.32, 31.28, 18.89, 13.74; HRMS (ESI) $[M+H]^+$ calcd for $C_{18}H_{21}NO_3$: 300.1594, found 300.1603; UPLC-MS purity: >99%.

Methyl 2-((3-hexylphenyl)amino)nicotinate (98). 3-Hexylaniline **68** (200 mg, 1.13 mmol) was reacted with methyl 2-bromonicotinate according to general procedure C. Purification by flash column chromatography (hexanes/EtOAc 80:20) provided **98** (276 mg, 0.883 mmol, 79%) as a white solid. ^{1}H-NMR (300 MHz, $CDCl_3$) δ 10.23 (s(br), 1H), 8.40 (dd, J=4.8, 2.0 Hz, 1H), 8.21 (dd, J=7.8, 2.0 Hz, 1H), 7.74–7.68 (m, 1H), 7.50 (t, J=1.9 Hz, 1H), 7.30 (t, J=7.8 Hz, 1H), 6.93 (d, J=7.7 Hz, 1H), 6.68 (dd, J=7.8, 4.7 Hz, 1H), 3.91 (s, 3H), 2.67 (t, J=7.6 Hz, 2H), 1.70 (quint, J=7.6 Hz, 2H), 1.46–1.35 (m, 6H), 0.94 (t, J=6.5 Hz, 3H); ^{13}C-NMR (75 MHz, $CDCl_3$) δ 167.86, 156.16, 153.17, 143.54, 140.01, 139.61, 128.57, 122.99, 120.81, 118.18, 112.98, 106.71, 52.04, 36.05, 31.77, 31.40, 29.05, 22.63, 14.11.

2-((3-Hexylphenyl)amino)nicotinic acid (49). Methyl 2-((3-hexylphenyl)amino)nicotinate **98** (126 mg, 0.403 mmol) was saponified according to general procedure D to afford **49** (72 mg, 0.24 mmol, 60%) as a light yellow solid without the need of any purification. ^{1}H-NMR (300 MHz, $CDCl_3$) δ 9.98 (s(br), 1H), 8.40 (dd, J=4.7, 1.8 Hz, 1H), 8.29 (dd, J=7.8, 1.8 Hz, 1H), 7.51 (d, J=8.0 Hz, 1H), 7.38 (s, 1H), 7.30–7.22 (m, 1H), 6.92 (d, J=7.5 Hz, 1H), 6.74 (dd, J=7.8, 4.8 Hz, 1H), 6.17 (s(br), 1H), 2.61 (t, J=9.0 Hz, 2H), 1.68–1.54 (m, 2H), 1.40–1.27 (m, 6H), 0.88 (t, J=6.6 Hz, 3H); ^{13}C-NMR (75 MHz, $CDCl_3$) δ 171.81, 156.69, 153.70, 144.04, 141.77, 139.04, 128.89, 124.11, 122.14, 119.48, 113.37, 106.62, 36.16, 31.89, 31.55, 29.21, 22.77, 14.25; HRMS (ESI) $[M+H]^+$ calcd for $C_{18}H_{22}N_2O_2$: 299.1754, found 299.1752; HPLC purity: 97%.

Methyl 2-((3-(pentyloxy)phenyl)amino)nicotinate (99). 3-(Pentyloxy)aniline **92** (40 mg, 0.22 mmol) was reacted with methyl 2-bromonicotinate according to general procedure C. Purification by flash column chromatography (DCM 100%) provided product **99** (57 mg, 0.18 mmol, 82%) as a brown oil. ^{1}H-NMR (300 MHz, $CDCl_3$) δ 10.18 (s(br), 1H), 8.39 (dd, J=4.8, 2.0 Hz, 1H), 8.23 (dd, J=7.8, 2.0 Hz, 1H), 7.42 (t, J=1.6 Hz, 1H), 7.24–7.19 (m, 2H), 6.71 (dd, J=7.8, 4.8 Hz, 1H), 6.65–6.57 (m, 1H), 3.98 (t, J=6.6 Hz, 2H), 3.92 (s, 3H), 1.80 (quint, J=6.7 Hz, 2H), 1.53–1.32 (m, 4H), 0.94 (t, J=7.0 Hz, 3H); ^{13}C-NMR (75 MHz, $CDCl_3$) δ 168.03, 159.81, 156.20, 153.25, 140.92, 140.31, 129.53, 113.35, 113.27, 109.17, 107.42, 107.17, 68.08, 52.34, 29.14, 28.36, 22.61, 14.16.

2-((3-(Pentyloxy)phenyl)amino)nicotinic acid (50). Methyl 2-((3-(pentyloxy)phenyl)amino)nicotinate **99** (57 mg, 0.18 mmol) was saponified according to general procedure D to afford **50** (33 mg, 0.11 mmol, 61%) as a light yellow solid without the need of any purification. ^{1}H-NMR (300 MHz, Methanol-d_4) δ 8.31 (dd, J=7.7, 1.9 Hz, 1H), 8.26 (dd, J=4.9, 1.8 Hz, 1H), 7.40 (t, J=2.1 Hz, 1H), 7.18 (t, J=8.1 Hz, 1H), 7.05 (dd, J=8.0, 1.0 Hz, 1H), 6.78 (dd, J=7.7, 4.9 Hz, 1H), 6.59 (dd, J=8.1, 1.8 Hz, 1H), 3.94 (t, J=6.5 Hz, 2H), 1.75 (quint, J=6.0 Hz, 2H), 1.50–1.35 (m, 4H), 0.93 (t, J=7.1 Hz, 3H); ^{13}C-NMR (75 MHz, Methanol-d_4) δ 170.50, 161.13, 157.24, 152.60, 142.40, 141.84, 130.52, 114.47, 114.16, 110.14, 109.78, 108.37, 68.95, 30.14, 29.39, 23.54, 14.40; HRMS (ESI) $[M+H]^+$ calcd for $C_{17}H_{20}N_2O_3$: 301.1547, found 301.1557; HPLC purity: >99%.

Methyl 2-((4-((3r,5r,7r)-adamantan-1-yl)phenyl)amino)nicotinate (100). 87 (70 mg, 0.27 mmol) was reacted with methyl 2-bromonicotinate according to general procedure C. Purification by flash column chromatography (hexanes/EtOAc 99:1 to 95:15) provided product **100** (76 mg, 0.21 mmol, 78%) as a yellow oil. ^{1}H-NMR (300 MHz, $CDCl_3$) δ 10.10 (s(br), 1H), 8.37 (dd, J=4.7, 2.0 Hz, 1H), 8.22 (dd, J=7.8, 2.0 Hz, 1H), 7.68–7.57 (m, 2H), 7.41–7.30 (m, 2H), 6.68 (dd, J=7.8, 4.7 Hz, 1H), 3.92 (s, 3H), 2.16–2.07 (m, 3H), 1.97–1.89 (m, 6H), 1.86–1.72 (m, 6H); ^{13}C-NMR (75 MHz, $CDCl_3$) δ 168.01, 156.38, 153.42, 146.24, 140.22, 137.05, 128.90, 125.31, 121.04, 121.00, 112.98, 106.74, 52.22, 43.35, 36.93, 35.89, 29.09.

2-((4-((3r,5r,7r)-Adamantan-1-yl)phenyl)amino)nicotinic acid (51). Saponification of **100** (77 mg, 0.21 mmol) was performed according to general procedure D to afford **51** (11 mg, 0.032 mmol, 15%) as a white solid without the need of any purification. ^{1}H-NMR (500 MHz, DMSO-d_6) δ 10.54 (s(br), 1H), 8.33 (dd, J=4.8, 2.0 Hz, 1H), 8.22 (dd, J=7.7, 2.1 Hz, 1H), 7.61 (d, J=8.7 Hz, 2H), 7.29 (d, J=8.7 Hz, 2H), 6.81 (dd, J=7.7, 4.7 Hz, 1H), 2.09–2.04 (m, 3H), 1.87–1.83 (m, 6H), 1.75–1.72 (m, 6H); ^{13}C-NMR (151 MHz, DMSO-d_6) δ 169.34, 155.95, 152.78, 145.18, 140.67, 137.38, 125.09, 120.19, 113.79, 107.93, 42.93, 36.40, 35.48, 28.53; HRMS (ESI) $[M+H]^+$ calcd for $C_{22}H_{24}N_2O_2$: 349.1911, found 349.1911; UPLC-MS purity: 96%.

1-Nitro-4-(pentyloxy)benzene (101). To a solution of 4-nitrophenol (500 mg, 3.59 mmol) in MeCN (9 mL) were added K_2CO_3 (1.99 g, 14.4 mmol) and 1-iodopentane (0.52 mL, 4.0 mmol). The reaction mixture was stirred at 82 °C for 16 h, cooled down to room temperature, diluted with EtOAc and H_2O. The aqueous phase was extracted with EtOAc (3×30 mL) and the combined organic phases were washed with brine (1×50 mL), dried over Na_2SO_4, filtered and concentrated under reduced pressure. Product **101** (751 mg, 3.59 mmol, >99%) was obtained as a yellow oil and used without further purification. ^{1}H-NMR (300 MHz, $CDCl_3$) δ 8.22–8.14 (m, 2H), 6.96–6.89 (m, 2H), 4.04 (t, J=6.5 Hz, 2H), 1.82 (quint, J=6.0 Hz, 2H), 1.50–1.32 (m, 4H), 0.93 (t, J=7.1 Hz, 3H); ^{13}C-NMR (75 MHz, $CDCl_3$) δ 164.38, 141.43, 126.01, 114.51, 69.01, 28.78, 28.17, 22.50, 14.08.

4-(Pentyloxy)aniline (102). Nitro reduction of **101** (751 mg, 3.59 mmol) was performed according to general procedure A to afford product **102** (626 mg, 3.49 mmol, 97%) as a dark brown oil

which was used in the following step without further purification. ^{1}H-NMR (300 MHz, $CDCl_3$) δ 6.77–6.71 (m, 2H), 6.66–6.60 (m, 2H), 3.88 (t, J=6.6 Hz, 2H), 3.23 (s(br), 2H), 1.74 (quint, J=6.0 Hz, 2H), 1.47–1.32 (m, 4H), 0.92 (t, J=7.0 Hz, 3H); ^{13}C-NMR (75 MHz, $CDCl_3$) δ 152.47, 139.87, 116.55, 115.78, 68.81, 29.24, 28.34, 22.59, 14.1.

Methyl 2-((4-(pentyloxy)phenyl)amino)benzoate (103). 4-(Pentyloxy)aniline **102** (127 mg, 0.708 mmol) was reacted with methyl 2-bromobenzoate according to general procedure C. Purification by flash column chromatography (hexanes/EtOAc 95:5 to 90:10) provided product **103** (220 mg, 0.702 mmol, >99%) as a yellow solid. ^{1}H-NMR (300 MHz, $CDCl_3$) δ 9.31 (s(br), 1H), 7.96 (dd, J=8.1, 1.7 Hz, 1H), 7.27 (ddd, J=8.7, 7.0, 1.7 Hz, 1H), 7.21–7.15 (m, 2H), 7.00 (dd, J=8.6, 1.1 Hz, 1H), 6.96–6.88 (m, 2H), 6.67 (ddd, J=8.1, 7.0, 1.1 Hz, 1H), 3.97 (t, J=6.5 Hz, 2H), 3.91 (s, 3H), 1.82 (quint, J=6.7 Hz, 2H), 1.57–1.36 (m, 4H), 0.97 (t, J=7.1 Hz, 3H); ^{13}C-NMR (75 MHz, $CDCl_3$) δ 169.49, 156.81, 150.14, 134.64, 133.66, 132.01, 126.42, 116.58, 115.75, 113.81, 111.23, 68.75, 52.11, 29.54, 28.74, 22.99, 14.54..

2-((4-(Pentyloxy)phenyl)amino)benzoic acid (52). 103 (215 mg, 0.686 mmol) was saponified according to general procedure D to afford **52** (143 mg, 0.478 mmol, 70%) as a light yellow solid without the need of any purification. ^{1}H-NMR (300 MHz, $CDCl_3$) δ 8.02 (dd, J=8.1, 1.7 Hz, 1H), 7.34–7.23 (m, 1H), 7.18 (d, J=8.7 Hz, 2H), 7.00–6.85 (m, 3H), 6.69 (t, J=7.5 Hz, 1H), 3.97 (t, J=6.6 Hz, 2H), 1.81 (quint, J=6.7 Hz, 2H), 1.56–1.33 (m, 4H), 0.95 (t, J=7.0 Hz, 3H); ^{13}C-NMR (75 MHz, $CDCl_3$) δ 173.61, 150.53, 135.25, 132.76, 132.52, 129.39, 126.41, 116.28, 115.35, 113.55, 103.20, 68.34, 29.03, 28.24, 22.50, 14.06; HRMS (ESI) $[M+H]^+$ calcd for $C_{18}H_{21}NO_3$: 300.1594, found 300.1603; HPLC purity: >99%.

Methyl 2-((4-(pentyloxy)phenyl)amino)nicotinate (104). 4-(Pentyloxy)aniline **102** (40 mg, 0.22 mmol) was reacted with methyl 2-bromonicotinate according to general procedure C. Purification by flash column chromatography (DCM 100%) provided product **104** (58 mg, 0.18 mmol, 84%) as a yellow oil. ^{1}H-NMR (300 MHz, $CDCl_3$) δ 9.93 (s(br), 1H), 8.32 (dd, J=4.8, 2.0 Hz, 1H), 8.20 (dd, J=7.8, 2.0 Hz, 1H), 7.55–7.47 (m, 2H), 6.93–6.85 (m, 2H), 6.65 (dd, J=7.8, 4.8 Hz, 1H), 3.95 (t, J=6.6 Hz, 2H), 3.91 (s, 3H), 1.79 (quint, J=6.0 Hz, 2H), 1.49–1.36 (m, 4H), 0.94 (t, J=7.1 Hz, 3H); ^{13}C-NMR (75 MHz, $CDCl_3$) δ 168.04, 156.69, 155.60, 153.40, 140.33, 132.45, 123.52, 114.92, 112.71, 106.55, 68.39, 52.22, 29.15, 28.33, 22.58, 14.14.

2-((4-(Pentyloxy)phenyl)amino)nicotinic acid (53). 104 (58 mg, 0.19 mmol) was saponified according to general procedure D to afford **53** (51 mg, 0.17 mmol, 89%) as a beige solid without the need of any purification. ^{1}H-NMR (300 MHz, Methanol-d_4) δ 8.41 (dd, J=7.7, 1.9 Hz, 1H), 8.11 (dd, J=5.3, 1.9 Hz, 1H), 7.45–7.38 (m, 2H), 6.97–6.91 (m, 2H), 6.81 (dd, J=7.7, 5.3 Hz, 1H), 3.98 (t, J=6.5 Hz, 2H), 1.78 (quint, J=6.0 Hz, 2H), 1.50–1.39 (m, 4H), 0.96 (t, J=7.1 Hz, 3H); ^{13}C-NMR (75 MHz, Methanol-d_4) δ 169.93, 158.06, 156.81, 149.57, 143.95, 131.84, 125.67, 116.27, 113.80, 111.30, 69.31, 30.12, 29.37, 23.52, 14.40; HRMS (ESI) $[M+H]^+$ calcd for $C_{17}H_{20}N_2O_3$: 301.1547, found 301.1544; HPLC purity: >99%.

Ethyl 3-((3-(pentyloxy)phenyl)amino)benzoate (105). 3-(Pentyloxy) aniline **92** (40 mg, 0.22 mmol) was reacted with ethyl 3-iodobenzoate according to general procedure C. Purification by flash column chromatography (hexanes/EtOAc 99:1 to 85:15) provided product **105** (50 mg, 0.15 mmol, 69%) as a yellow oil. ^{1}H-NMR (300 MHz, $CDCl_3$) δ 7.74–7.70 (m, 1H), 7.59 (dt, J=7.1, 1.7 Hz, 1H), 7.34–7.27 (m, 2H), 7.17 (ddd, J=8.3, 7.3, 1.0 Hz, 1H), 6.67–6.62 (m, 2H), 6.51 (ddd, J=8.2, 2.2, 1.1 Hz, 1H), 5.82 (s, 1H), 4.36 (q, J=7.1 Hz, 2H), 3.92 (t, J=6.6 Hz, 2H), 1.77 (quint, J=6.7 Hz, 2H), 1.45–1.32 (m, 7H), 0.92 (t, J=7.0 Hz, 3H); ^{13}C-NMR (75 MHz, $CDCl_3$) δ 166.71, 160.43, 143.95, 143.40, 131.81, 130.27, 129.39, 122.06, 121.93, 118.88, 110.58, 107.69, 104.56, 68.08, 61.10, 29.10, 28.34, 22.59, 14.45, 14.15.

3-((3-(Pentyloxy)phenyl)amino)benzoic acid (54). 105 (50 mg, 0.15 mmol) was saponified according to general procedure D to afford **54** (43 mg, 0.14 mmol, 96%) as a brown oil without the need of any purification. ^{1}H-NMR (300 MHz, Methanol-d_4) δ 7.75 (s(br), 1H), 7.51–7.45 (m, 1H), 7.29–7.24 (m, 2H), 7.10 (t, J=8.1 Hz, 1H), 6.70–6.65 (m, 1H), 6.64 (t, J=2.1 Hz, 1H), 6.42 (dd, J=8.1, 2.1 Hz, 1H), 3.89 (t, J=6.5 Hz, 2H), 1.77–1.67 (m, 2H), 1.43–1.33 (m, 4H), 0.92 (t, J=7.0 Hz, 3H); ^{13}C-NMR (75 MHz, Methanol-d_4) δ 170.81, 161.51, 145.77, 145.41, 133.54, 130.89, 130.07, 122.26, 122.12, 118.99, 111.08, 107.88, 104.99, 68.85, 30.10, 29.35, 23.50, 14.39; HRMS (ESI) $[M+H]^+$ calcd for $C_{18}H_{21}NO_3$: 300.1594, found 300.1587; HPLC purity: 95%.

Methyl 2-((3-(trifluoromethyl)phenyl)amino)nicotinate (106). 3-(Trifluoromethyl)aniline (0.15 mL, 1.2 mmol) was reacted with methyl 2-bromonicotinate according to general procedure C. Purification by flash column chromatography (hexanes/EtOAc 99:1 to 90:10) provided product **106** (350 mg, 1.18 mmol, 98%) as a transparent oil. ^{1}H-NMR (300 MHz, $CDCl_3$) δ 10.40 (s(br), 1H), 8.41 (dd, J=4.8, 2.0 Hz, 1H), 8.24 (dd, J=7.8, 2.0 Hz, 1H), 8.15 (s, 1H), 7.90 (d, J=8.1 Hz, 1H), 7.44 (t, J=7.9 Hz, 1H), 7.30 (d, J=8.3 Hz, 1H), 6.77 (dd, J=7.8, 4.8 Hz, 1H), 3.94 (s, 3H); ^{13}C-NMR (75 MHz, $CDCl_3$) δ 167.96, 155.75, 153.08, 140.50, 140.27, 131.80, 131.37, 130.95, 130.53, 129.26, 126.15, 123.44, 122.54, 119.03, 118.98, 118.92, 118.87, 117.12, 117.06, 117.01, 116.96, 114.13, 107.48, 52.39; ^{19}F-NMR (282 MHz, $CDCl_3$) δ −62.62.

2-((3-(Trifluoromethyl)phenyl)amino)nicotinic acid (2) (Niflumic acid; NA). 106 (350 mg, 1.18 mmol) was saponified according to general procedure D to afford niflumic acid **2** (274 mg, 0.971 mmol, 82%) as a beige solid without the need of any purification. ^{1}H-NMR (300 MHz, DMSO-d_6) δ 11.71 (s(br), 1H), 8.41–8.28 (m, 2H), 8.26 (dd, J=7.6, 2.1 Hz, 1H), 7.84 (dd, J=8.1, 2.1 Hz, 1H), 7.51 (t, J=8.0 Hz, 1H), 7.27 (d, J=7.6 Hz, 1H), 6.88 (dd, J=7.6, 4.8 Hz, 1H); ^{13}C-NMR (151 MHz, DMSO-d_6) δ 206.39, 155.38, 150.78, 141.22, 140.20, 129.69, 129.58, 129.37, 125.21, 123.41, 122.70, 117.29, 117.28, 114.82, 114.80, 114.79, 114.48, 30.64; ^{19}F-NMR (282 MHz, DMSO-d_6) δ −61.12; HRMS (ESI) $[M+H]^+$ calcd for $C_{13}H_9F_3N_2O_2$: 283.0689, found 283.0683; HPLC purity: 97%.

Acknowledgements

A.G. and S.L. would like to thank the réseau Québécois de recherche sur les médicaments (RQRM) for a research grant. L.M. would like to thank the Centre d'excellence de recherche sur les maladies orphelines – Fondation Courtois (CERMO-FC) for a post-graduate scholarship. A.F. would like to thank Pharmaqam for a post-graduate scholarship. We are also grateful for support by the SGC, a registered charity (Number 1097737) that receives funds from AbbVie, Bayer Pharma AG, Boehringer Ingelheim, Canada Foundation for Innovation, Eshelman Institute for Innovation, Genome Canada through Ontario Genomics Institute [OGI-055], Innovative Medicines Initiative (EU/EFPIA) [ULTRA-DD Grant No. 115766], Janssen, Merck KGaA, Darmstadt, Germany, MSD, Novartis Pharma AG, Ontario Ministry of Research, Innovation and Science (MRIS), Pfizer, São Paulo Research Foundation-FAPESP, Takeda and Wellcome [106169/ZZ14/Z]. A.G. is the holder of an institutional chair in epigenetics and medicinal chemistry at UQAM. B.A. holds an Institutional Research Chair in Cancer Prevention and Treatment at UQAM. This work was supported by

NSERC CREATE Grant (432008-2013). We thank Pr. Xavier Ottenwaelder from the department of chemistry and biochemistry of Concordia University for the X-ray analysis of compound ***40****. Crystallography work is based upon research conducted at the Northeastern Collaborative Access Team beamlines, which are funded by the National Institute of General Medical Sciences from the National Institutes of Health (P30GM124165). The Eiger 16 M detector on 24-ID-E beam line is funded by a NIH-ORIP HEI grant (S10OD021527). This research used resources of the Advanced Photon Source, a U.S. Department of Energy (DOE) Office of Science User Facility operated for the DOE Office of Science by Argonne National Laboratory under Contract No. DE-AC02-06CH11357.*

Conflict of Interest

The authors declare no conflict of interest.

Keywords: Hippo pathway · TEAD · Flufenamic acid · palmitic acid · SAR

[1] K. Harvey, N. Tapon, *Nat. Rev. Cancer* **2007**, *7*, 182–191.
[2] L. Cairns, T. Tran, J. M. Kavran, *ACS Chem. Biol.* **2017**, *12*, 601–610.
[3] S. Piccolo, S. Dupont, M. Cordenonsi, *Physiol. Rev.* **2014**, *94*, 1287–1312.
[4] M. K. Kim, J. W. Jang, S. C. Bae, *BMB Rep.* **2018**, *51*, 126–133.
[5] S. Strano, E. Munarriz, M. Rossi, L. Castagnoli, Y. Shaul, A. Sacchi, M. Oren, M. Sudol, G. Cesareni, G. Blandino, *J. Biol. Chem.* **2001**, *276*, 15164–15173.
[6] H. Zhang, H. A. Pasolli, E. Fuchs, *Proc. Natl. Acad. Sci. USA* **2011**, *108*, 2270–2275.
[7] B. Zhao, L. Li, Q. Lei, K. L. Guan, *Genes Dev.* **2010**, *24*, 862–874.
[8] A. V. Pobbati, W. Hong, *Cancer Biol. Ther.* **2013**, *14*, 390–398.
[9] M. Z. Xu, S. W. Chan, A. M. Liu, K. F. Wong, S. T. Fan, J. Chen, R. T. Poon, L. Zender, S. W. Lowe, W. Hong, J. M. Luk, *Oncogene* **2011**, *30*, 1229–1240.
[10] D. Pan, *Dev. Cell.* **2010**, *19*, 491–505.
[11] A. A. Ahmed, A. D. Mohamed, M. Gener, W. Li, E. Taboada, *Mol. Cell. Oncol.* **2017**, *4*, e1295127.
[12] M. Corvaisier, M. Bauzone, F. Corfiotti, F. Renaud, M. El Amrani, D. Monté, S. Truant, E. Leteurtre, P. Formstecher, I. Van Seuningen, C. Gespach, G. Huet, *Oncotarget* **2016**, *7*, 56699–56712.
[13] L. Guo, L. Teng, *Int. J. Oncol.* **2015**, *46*, 1444–1452.
[14] J. F. Knight, C. J. Shepherd, S. Rizzo, D. Brewer, S. Jhavar, A. R. Dodson, C. S. Cooper, R. Eeles, A. Falconer, G. Kovacs, M. D. Garrett, A. R. Norman, J. Shipley, D. L. Hudson, *Br. J. Cancer.* **2008**, *99*, 1849–1858.
[15] T. Hucl, J. R. Brody, E. Gallmeier, C. A. Iacobuzio-Donahue, I. K. Farrance, S. E. Kern, *Cancer Res.* **2007**, *67*, 9055–9065.
[16] Y. Liu, G. Wang, Y. Yang, Z. Mei, Z. Liang, A. Cui, T. Wu, C. Y. Liu, L. Cui, *Oncogene* **2016**, *35*, 2789–2800.
[17] B. Lim, J. L. Park, H. J. Kim, Y. K. Park, J. H. Kim, H. A. Sohn, S. M. Noh, K. S. Song, W. H. Kim, Y. S. Kim, S. Y. Kim, *Carcinogenesis* **2014**, *35*, 1020–1027.
[18] R. Johnson, G. Halder, *Nat. Rev. Drug Discovery* **2014**, *13*, 63–79.
[19] B. Zhao, X. Ye, J. Yu, L. Li, W. Li, S. Li, J. Yu, J. D. Lin, C. Y. Wang, A. M. Chinnaiyan, Z. C. Lai, K. L. Guan *Genes Dev.* **2008**, *22*, 1962–1971.
[20] B. Zhao, J. Kim, X. Ye, Z. C. Lai, K. L. Guan, *Cancer Res.* **2009**, *69*, 1089–1098.
[21] J. Dong, G. Feldmann, J. Huang, S. Wu, N. Zhang, S. A. Comerford, M. F. Gayyed, R. A. Anders, A. Maitra, D. Pan, *Cell.* **2007**, *130*, 1120–1133.
[22] F. Zanconato, M. Cordenonsi, S. Piccolo, *Cancer Cell* **2016**, *29*, 783–803.
[23] J. S. A. Warren, Y. Xiao, J. M. Lamar, *Cancers* **2018**, *10*, 115–151.
[24] Y. Liu-Chittenden, B. Huang, J. Sup Shim, Q. Chen, S.-J. Lee, R. A. Anders, J. O. Liu, D. Pan, *Genes Dev.* **2012**, *26*, 1300–1305.
[25] Z. Li, B. Zhao, P. Wang, F. Chen, Z. Dong, H. Yang, K. L. Guan, Y. Xu, *Genes Dev.* **2010**, *24*, 235–240.
[26] Z. Zhou, T. Hu, Z. Xu, Z. Lin, Z. Zhang, T. Feng, L. Zhu, Y. Rong, H. Shen, J. M. Luk, X. Zhang, N. Qin, *FASEB J.* **2015**, *29*, 724–732.
[27] Z. Zhang, Z. Lin, Z. Zhou, H. C. Shen, S. F. Yan, A. V. Mayweg, Z. Xu, N. Qin, J. C. Wong, Z. Zhang, Y. Rong, D. C. Fry, T. Hu, *ACS Med. Chem. Lett.* **2014**, *5*, 993–998.
[28] P. Furet, B. Salem, Y. Mesrouze, T. Schmelzle, I. Lewis, J. Kallen, P. Chène, *Bioorg. Med. Chem. Lett.* **2019**, *29*, 2316–2319.
[29] Z. R. Crook, G. P. Sevilla, D. Friend, M. Y. Brusniak, A. D. Bandaranayake, M. Clarke, M. Gewe, A. J. Mhyre, D. Baker, R. K. Strong, P. Bradley, J. M. Olson, *Nat. Commun.* **2017**, *8*, 2244–2258.
[30] S. Jiao, H. Wang, Z. Shi, A. Dong, W. Zhang, X. Song, F. He, Y. Wang, Z. Zhang, W. Wang, X. Wang, T. Guo, P. Li, Y. Zhao, H. Ji, L. Zhang, Z. Zhou, *Cancer Cell* **2014**, *25*, 166–180.
[31] F. Gibault, M. Coevoet, M. Sturbaut, A. Farce, N. Renault, F. Allemand, J.-F. Guichou, A.-S. Drucbert, C. Foulon, R. Magnez, X. Thuru, M. Corvaisier, G. Huet, P. Chavatte, P. Melnyk, F. Bailly, P. Cotelle, *Cancers* **2018**, *10*, 140–153.
[32] S. A. Smith, R. B. Sessions, D. K. Shoemark, C. Williams, R. Ebrahimighaei, M. C. McNeill, M. P. Crump, T. R. McKay, G. Harris, A. C. Newby, M. Bond, *J. Med. Chem.* **2019**, *62*, 1291–1305.
[33] A. V. Pobbati, B. P. Rubin, *Molecules* **2020**, *25*, 6001–6017.
[34] Y. Li, S. Liu, E. Y. Ng, R. Li, A. Poulsen, J. Hill, A. V. Pobbati, A. W. Hung, W. Hong, T. H. Keller, C. Kang, *Biochem. J.* **2018**, *475*, 2043–2055.
[35] P. Chan, X. Han, B. Zheng, M. DeRan, J. Yu, G. K. Jarugumilli, H. Deng, D. Pan, X. Luo, X. Wu, *Nat. Chem. Biol.* **2016**, *12*, 282–289.
[36] C. L. Noland, S. Gierke, P. D. Schnier, J. Murray, W. N. Sandoval, M. Sagolla, A. Dey, R. N. Hannoush, W. J. Fairbrother, C. N. Cunningham, *Structure* **2016**, *24*, 179–186.
[37] Y. Mesrouze, M. Meyerhofer, F. Bokhovchuk, P. Fontana, C. Zimmermann, T. Martin, C. Delaunay, A. Izaac, J. Kallen, T. Schmelzle, D. Erdmann, P. Chène, *Protein Sci.* **2017**, *26*, 2399–2409.
[38] X. Wu, International Patent WO 2017/053706 A1, **2017**.
[39] N. G. Kim, B. M. Gumbiner, *Proc. Natl. Acad. Sci. USA* **2019**, *116*, 9877–9882.
[40] A. V. Pobbati, X. Han, A. W. Hung, S. Weiguang, N. Huda, G. Y. Chen, C. Kang, C. S. B. Chia, X. Luo, W. Hong, A. Poulsen, *Structure* **2015**, *23*, 2076–2086.
[41] M. Barth, S. Contal, J. L. Junien, C. Massardier, C. Montalbetti, A. Soude, International Patent WO 2020/070181 A1, **2020**.
[42] J. K. Holden, J. J. Crawford, C. L. Noland, S. Schmidt, J. R. Zbieg, J. A. Lacap, R. Zang, G. M. Miller, Y. Zhang, P. Beroza, R. Reja, W. Lee, J. Y. W. K. Tom, R. Fong, M. Steffek, S. Clausen, T. J. Hagenbeek, T. Hu, Z. Zhou, H. C. Shen, C. N. Cunningham, *Cell Rep.* **2020**, *31*, 107809.
[43] V. B. K. Kunig, M. Potowski, M. Akbarzadeh, M. K. Škopić, D. Dos Santos Smith, L. Arendt, I. Dormuth, H. Adihou, B. Andlovic, H. Karatas, S. Shaabani, T. Zarganes-Tzitzikas, C. G. Neochoritis, R. Zhang, M. Groves, S. M. Guéret, C. Ottmann, J. Rahnenführer, R. Fried, A. Dömling, A. Brunschweiger, *Angew. Chem. Int. Ed. Engl.* **2020**, *59*, 20338–20342.
[44] W. Lu, J. Wang, Y. Li, H. Tao, H. Xiong, F. Lian, J. Gao, H. Ma, T. Lu, D. Zhang, X. Ye, H. Ding, L. Yue, Y. Zhang, H. Tang, N. Zhang, Y. Yang, H. Jiang, K. Chen, B. Zhou, C. Luo, *Eur. J. Med. Chem.* **2019**, *184*, 111767.
[45] K. Bum-Erdene, D. Zhou, H. Gonzalez-Gutierrez, M. K. Ghozayel, Y. Si, D. Xu, H. E. Shannon, B. J. Bailey, T. W. Corson, K. E. Pollok, C. D. Wells, S. O. Meroueh, *Cell Chem. Biol.* **2019**, *26*, 378–389.
[46] A. V. Pobbati, T. Mejuch, S. Chakraborty, H. Karatas, S. R. Bharath, S. M. Guéret, P. A. Goy, G. Hahne, A. Pahl, S. Sievers, E. Guccione, H. Song, H. Waldmann, W. Hong, *ACS Chem. Biol.* **2019**, *14*, 2909–2921.
[47] F. H. Niesen, H. Berglund, M. Vedadi, *Nat. Protoc.* **2007**, *2*, 2212–2221.
[48] M. Vedadi, F. H. Niesen, A. Allali-Hassani, O. Y. Fedorov, P. J. Finerty Jr, G. A. Wasney, R. Yeung, C. Arrowsmith, L. J. Ball, H. Berglund, R. Hui, B. D. Marsden, P. Nordlund, M. Sundstrom, J. Weigelt, A. M. Edwards, *Proc. Natl. Acad. Sci. USA* **2006**, *103*, 15835–15840.
[49] N. Igoe, E. D. Bayle, C. Tallant, O. Fedorov, J. C. Meier, P. Savitsky, C. Rogers, Y. Morias, S. Scholze, H. Boyd, D. Cunoosamy, D. M. Andrews, A. Cheasty, P. E. Brennan, S. Müller, S. Knapp, P. V. Fish, *J. Med. Chem.* **2017**, *60*, 6998–7011.
[50] A. N. Bullock, J. E. Debreczeni, O. Y. Fedorov, A. Nelson, B. D. Marsden, S. Knapp, *J. Med. Chem.* **2005**, *48*, 7604–7614.
[51] A. M. Omar, M. A. Elfaky, S. T. Arold, S. H. Soror, M. T. Khayat, H. Z. Asfour, F. H. Bamane, M. E. El-Araby, *Biomolecules* **2020**, *10*, 479–501.
[52] U. S. Hameed, I. Haider, M. Jamil, B. A. Kountche, X. Guo, R. A. Zarban, D. Kim, A. Al-Babili, S. T. Arold, *EMBO Rep.* **2018**, *19*, e45619.
[53] T. Sugiki, K. Furuita, T. Fujiwara, C. Kojima, *Molecules* **2018**, *23*, 148-174.
[54] C. Dalvit, A. Vulpetti, *J. Med. Chem.* **2019**, *62*, 2218–2244.
[55] S. Akoka, L. Barantin, M. Trierweiler, *Anal. Chem.* **1999**, *71*, 2554–2557.

ChemMedChem | Full Papers doi.org/10.1002/cmdc.202100432 | Chemistry Europe European Chemical Societies Publishing

[56] T. Machleidt, C. C. Woodroofe, M. K. Schwinn, J. Méndez, M. B. Robers, K. Zimmerman, P. Otto, D. L. Daniels, T. A. Kirkland, K. V. Wood, *ACS Chem. Biol.* **2015**, *10*, 1797–1804.
[57] S. Dupont, L. Morsut, M. Aragona, E. Enzo, S. Giulitti, M. Cordenonsi, F. Zanconato, J. Le Digabel, M. Forcato, S. Bicciato, N. Elvassore, S. Piccolo, *Nature* **2011**, *474*, 179–183.
[58] H. Andersson, H. Demaegdt, G. Vauquelin, G. Lindeberg, A. Karlén, M. Hallberg, *Bioorg. Med. Chem.* **2008**, *16*, 6924–6935.
[59] G. Ortar, M. Grazia Cascio, L. De Petrocellis, E. Morera, F. Rossi, A. Schiano-Moriello, M. Nalli, V. de Novellis, D. F. Woodward, S. Maione, V. Di Marzo, *J. Med. Chem.* **2007**, *50*, 6554–6569.
[60] B. Ringstrand, M. Oltmanns, J. A. Batt, A. Jankowiak, R. P. Denicola, P. Kaszynski, *Beilstein J. Org. Chem.* **2011**, *7*, 386–393.
[61] V. P. Prasad, S. Wagner, P. Keul, S. Hermann, B. Levkau, M. Schäfers, G. Haufe, *Bioorg. Med. Chem.* **2014**, *22*, 5168–5181.
[62] C. Féau, L. A. Arnold, A. Kosinski, F. Zhu, M. Connelly, R. K. Guy, *ACS Chem. Biol.* **2009**, *4*, 834–843.
[63] T. S. Mei, R. Giri, N. Maugel, J. Q. Yu, *Angew. Chem. Int. Ed. Engl.* **2008**, *47*, 5215–5219.
[64] D. S. Zurabishvili, M. O. Lomidze, S. A. Samsoniya, A. Wesquet, U. Kazmaier, *Chem. Heterocycl. Compd.* **2008**, *44*, 941–949.
[65] A. Koperniku, A. S. Foscolos, I. Papanastasiou, G. B. Foscolos, A. Tsotinis, D. Schols, *Lett. Org. Chem.* **2016**, *13*, 171–176.
[66] C. M. Rudzinski, A. M. Young, D. G. Nocera, *J. Am. Chem. Soc.* **2002**, *124*, 1723–1727.

Manuscript received: June 15, 2021
Accepted manuscript online: June 23, 2021
Version of record online: ■■, ■■

FULL PAPERS

2.3 Informations supplémentaires

Les informations supplémentaires concernant les protocoles expérimentaux ainsi que les spectres RMN des composés synthétisés sont présentés dans l'annexe A.

2.4 Conclusion

La mise en place d'une voie de synthèse efficace a permis un accès rapide à de nombreux dérivés de l'acide flufénamique. Grâce à une conception mélangeant apports des structures co-cristallines, modifications systématiques et emploi d'amarrage moléculaire, différents inhibiteurs de TEAD ont pu être obtenus, incluant **LM98**. Avec un ΔT_{agg} de 6.4 °C, **LM98** se lie dans la poche palmitique de TEAD, comme le démontrent des études par RMN-^{19}F et l'obtention de co-cristaux en présence de hTEAD2-YBD. Bien que **LM98** n'empêche pas la formation du complexe YAP-TEAD, le composé agit en inhibant la palmitoylation de TEAD, réduisant ainsi de 30% l'activité de TEAD par dosage de luciférase tout en diminuant de 61% et 40% l'expression de *CTGF* et *Cyr61*, deux gènes normalement activés par YAP-TEAD. Pour finir, le potentiel thérapeutique de **LM98** s'illustre par une inhibition de la migration de cellules cancéreuses, arrêtant notamment les cellules en phase S du cycle cellulaire.

2.5 Contributions des auteurs à l'article

L'auteure principale a accompli la synthèse et la caractérisation de l'acide niflumique (**2**), de MGH-CP1 (**3**), de la moitié des dérivés de la table 2 ainsi que de l'ensemble des composés des tables 3, 4 et 5 (à l'exception de **52**). Elle a également effectué les études d'amarrage moléculaire, a orienté le SAR et la conception des analogues tout en participant activement à la coordination des différents contributeurs tout au long du

projet. Par la suite, l'auteure a réalisé la recherche bibliographique et a été la rédactrice principale de l'article. Finalement, la présente auteure a rédigé la partie expérimentale (à l'exception des protocoles portant sur l'évaluation biologique) et s'est occupée du traitement de l'ensemble des spectres RMN.

Shuay Abdullayev a effectué la synthèse et la caractérisation des dérivés de la table 1 et de la moitié de la table 2.

Ahmed Fnaiche a réalisé la synthèse et la caractérisation du composé **52**.

Victoria Vu a contribué au développement du test de dosage par luciférase ainsi qu'au test nanoBRET.

Narjara González Suárez a réalisé les expériences de RT-qPCR, migration cellulaire, cicatrisation des plaies et cytométrie de flux.

Hong Zheng, Magdalena M. Szewczyk, Fengling Li, Guillermo Senisterra, Abdellah Allali Hassani, Irene Chau et Aiping Dong ont testé les composés par DSF, DSLS, SPR, ITC et ont effectué les tests de palmitoylation par MS.

Simon Woo a effectué les expériences RMN-^{19}F en présence de la protéine.

Borhane Annabi, Levon Halabelian, Steven LaPlante, Masoud Vedadi, Dalia Barsyte-Lovejoy et Vijayaratnam Santhakumar ont supervisé l'ensemble des travaux réalisés au sein de leurs équipes respectives. Ils ont également participé aux phases de relecture de l'article.

Pour finir, l'auteur de correspondance Alexandre Gagnon a supervisé l'ensemble du projet (tout particulièrement les travaux de l'auteure principale, de Shuay Abdullayev

et d'Ahmed Fnaiche), a guidé la coordination des différentes équipes de recherche, a participé à la relecture de l'article et s'est chargé du processus de soumission.

CHAPITRE III

LA CHIMIE COMPUTATIONNELLE AU SERVICE DU DÉVELOPPEMENT D'INHIBITEURS DE TEAD

La chimie computationnelle peut fournir une aide précieuse lors de la conception d'inhibiteurs, autant pour la découverte de nouveaux *hits* que lors de la phase de SAR *hit to lead*.[263,264] Ce chapitre portera donc sur l'utilisation de divers outils informatiques afin soit de guider l'optimisation de la série présentée au chapitre précédant, soit d'identifier de nouveaux inhibiteurs de TEAD.

3.1 Conception assistée par ordinateur d'analogues de l'acide flufénamique

S'il est indéniable qu'il est peu probable de prédire avec exactitude la réalité, la chimie computationnelle n'en reste pas moins un outil précieux lors des phases d'optimisation de pharmacophores en chimie médicinale. Les différentes structures co-cristallines de TEAD-YBD en présence de ligands variés (acide palmitique et acide flufénamique, notamment) et, par la suite, l'obtention de notre propre co-cristal en présence de l'un de nos dérivés, permettent la conception de médicaments basée sur la structure.

3.1.1 Modélisations moléculaires dans TEAD2

L'ensemble des dérivés imaginés ou synthétisés ont donc été modélisés afin d'envisager leurs probables interactions avec les acides aminés de la poche palmitique de TEAD. Une fois validée, cette approche peut permettre à la fois d'aider à rationaliser

certains résultats biophysiques obtenus mais aussi d'assister la conception de nouveaux dérivés, notamment en prédisant l'absence d'affinité de certains analogues ou en enrichissant la structure de composés actifs connus. Comme chaque programme de modélisation possède ses avantages et ses inconvénients,[265] plusieurs d'entre eux ont été adoptés afin d'obtenir une image plus proche de la réalité.

3.1.1.1 Modélisation par édition de ligand dans ICM-pro

Pour commencer, différentes modélisations par édition de ligand (en l'occurrence, l'acide flufénamique) ont été réalisées sous ICM-pro (Molsoft). Dans ICM-pro,[266] les calculs d'énergie sont basés sur les paramètres de champ de force des peptides ECEPP/3 (*empirical conformational energy program for peptides 3*) tout en prenant en compte les charges partielles MMFF[267] ainsi que différents termes de correction associés à l'énergie libre de solvatation et à la contribution entropique.[268] La poche du récepteur est exprimée par cinq cartes d'interactions potentielles : électrostatiques, hydrophobiques, liaisons hydrogène et deux termes représentants différents potentiels de van der Waals. Par la suite, le ligand est modélisé de façon flexible dans la protéine rigide suivant la procédure suivante : (1) sélection aléatoire d'une conformation basée sur l'algorithme de Monte Carlo à probabilité biaisée (BPMC)[269] ainsi que sur les angles de torsion et de rotation du ligand, (2) minimisation énergétique locale, (3) calcul de l'énergie complète, (4) acceptation ou rejet de l'énergie totale selon les critères de Metropolis,[270] (5) sauvegarde des conformations favorables afin de créer un historique de recherches des meilleurs minima, (6) retour à l'étape (1) avec une nouvelle conformation aléatoire indépendante de la précédente mais résultant quand même d'une distribution de probabilité continue.[268,271] Basé essentiellement sur la méthode de simulation de Monte-Carlo, l'une des forces de ICM-pro réside dans l'obtention de poses d'amarrage fiables.[272,273] En revanche, le score d'amarrage n'est généralement pas estimé avec une précision suffisante pour permettre de classer les ligands en fonction de leurs énergies libres de liaison prédites. Pour ces raisons, des

études complémentaires par arrimage dans Glide (Schrödinger) ont également été réalisées.

3.1.1.2 Modélisation par arrimages dans Glide

De par sa prise en compte de la flexibilité des chaînes latérales, Glide s'avère l'un des programmes les plus efficaces en termes de prédiction des affinités de liaison entre ligands et protéines.[265] L'algorithme de Glide[274,275] met en place des grilles basées sur des techniques de recherche systématique des positions, orientations et conformations du ligand au niveau de la poche de liaison par l'intermédiaire d'une série de filtres hiérarchiques. Les grilles sont initialement générées à partir du centre de gravité du ligand présent dans la structure co-cristalline. Par la suite, un ensemble de conformations de ligands est généré par une recherche systématique des minima de torsions, formant ainsi plusieurs groupes caractérisés par une conformation commune du noyau et des chaînes latérales variables. Chaque groupe de conformères est ensuite placé dans la poche de liaison, puis les poses sélectionnées sont minimisées en utilisant les grilles précalculées pour la protéine. Ces grilles sont basées sur le champ de force OPLS-AA50[276] avec une constante diélectrique dépendant de la distance d'une valeur définie à 2 par défaut. Pour finir, les poses les plus basses en énergie sont soumises à une procédure de Monte Carlo qui permet d'examiner les minima de torsion et d'affiner l'orientation des chaînes latérales du ligand.[271,272] L'affinité des ligands peut alors être classée en utilisant la fonction Glide_Score, une version avancée de ChemScore51[277] qui incorpore la solvatation, les gènes stériques, les interactions répulsives, etc. Malgré le nombre considérable de termes pris en compte par le Glide_Score, il est à noter que les énergies de liaison rapportées permettent principalement de distinguer les ligands actifs versus inactifs. Une différence de quelques kcal/mol ne doit pas être considérée significative et ne peut donc pas servir à faire un classement absolu des activités relatives des ligands. Chez Glide, plus le score négatif obtenu est bas, plus la probabilité que le ligand se lie à la protéine est élevée. La meilleure pose est quant à elle isolée en

utilisant la fonction Emodel qui combine plusieurs scores énergétiques, dont le Glide_Score et la tension propre au ligand par exemple. Glide propose plusieurs types d'amarrage : criblage virtuel à haut débit (HTVS), amarrage de précision standard (SP) et amarrage extra-précis (XP). SP est la procédure standard expliquée ci-dessus. HTVS réduit considérablement le nombre de conformations testées, permettant ainsi d'augmenter la vitesse de calcul et de passer plus rapidement à travers le criblage d'une large base de données. L'amarrage XP est réalisé quant à lui à partir des résultats obtenus lors de l'amarrage SP. Ce type d'amarrage demande davantage de temps et ne s'effectue généralement que sur une population limitée de ligands. La précision obtenue ne réside pas uniquement sur une meilleure prédiction de la position et conformation du ligand dans le site de liaison mais aussi sur un score prenant en compte davantage de paramètres que le Glide_score, par exemple les pénalités de désolvatation ou l'enceinte hydrophobe.[278]

L'ensemble des données générées sous ICM et Glide coïncide avec les données expérimentales (ligands actifs ou inactifs) et confirme l'importance de l'acide carboxylique de l'acide flufénamique en raison des multiples interactions qu'il réalise : liaison hydrogène intramoléculaire avec l'amine centrale du ligand permettant potentiellement de le stabiliser dans sa conformation active, formation d'un pont salin avec l'amine de la chaîne latérale de la lysine 357 et présence de liaisons hydrogène avec le soufre et l'amine du squelette peptidique de la cystéine 380. Les résultats obtenus ont été intégrés dans le processus de conception de divers analogues, permettant notamment le développement de dérivés substitués en *para* de l'amine tels que présentés dans le chapitre précédent. Afin d'obtenir des données plus précises pour valider la synthèse de nouveaux analogues ou non, des études de perturbation d'énergie libre (FEP) ont également été effectuées.

3.1.2 Études de perturbation d'énergie libre

À ce jour, prédire avec précision l'affinité d'un ligand pour une protéine demeure un défi important. Les méthodes de calcul d'énergie libre de liaisons ligand-protéine basées sur des principes de la thermodynamique statistique sont considérées comme étant les plus efficaces dans ce domaine, tout particulièrement celles faisant appel à la dynamique moléculaire telle que les études FEP. En échange de calculs intensifs, cette approche prend en compte non seulement l'aspect énergétique (d'une façon similaire aux fonctions de score présentées précédemment) mais également différents paramètres entropiques. Cette méthode de calcul, appuyée ici par la fonction FEP implémentée dans le programme Desmond de Schrödinger, permet généralement d'obtenir des valeurs d'énergies libres de liaisons relatives présentant d'excellentes corrélations avec les affinités de liaisons expérimentales.[279] Cet outil se retrouve donc de plus en plus utilisé dans l'industrie pharmaceutique afin d'accélérer le processus *hit to lead*.[280]

Les études FEP emploient des techniques de calcul d'énergie libre alchimique, c'est-à-dire faisant intervenir des intermédiaires fictifs. En effet, s'il est extrêmement difficile de simuler avec précision l'évènement de liaison d'un ligand à une protéine (étapes 1 et 2 sur la Figure 3.1), il est possible de contourner ce problème en modélisant à la place le processus de transformation d'un ligand à un autre (étapes A et B sur la Figure 3.1). Puisque la différence d'énergie libre entre les états finaux est indépendante du chemin emprunté pour la calculer, $\Delta\Delta G_{liaison} = \Delta G_2 - \Delta G_1 = \Delta G_B - \Delta G_A$.[281] Cette différence d'énergie libre entre le ligand à tester (LT) et le ligand de référence (LR) (ΔG_A ou ΔG_B que nous nommerons ΔG_{FEP}) est évaluée avec l'équation de Zwanzig :[282]

$$\Delta G_{FEP} = G_{LT} - G_{LR} = -k_B T \ln \langle e^{\frac{-(V_{LT} - V_{LR})}{k_B T}} \rangle_{LR} = k_B T \ln \langle e^{\frac{-(V_{LR} - V_{LT})}{k_B T}} \rangle_{LT}$$

Où V_{LT} et V_{LR} sont des fonctions d'énergies potentielles de LT et LR et les crochets triangulaires indiquent la moyenne d'ensemble pondérée de Boltzmann générée lors de la modélisation pour le ligand correspondant. En simulant l'évolution entre le ligand à tester et le ligand de référence à travers de nombreux intermédiaires non physiques proches les uns des autres, il est possible de faire des approximations qui permettent de calculer la différence entre l'état initial et l'état final avec précision.

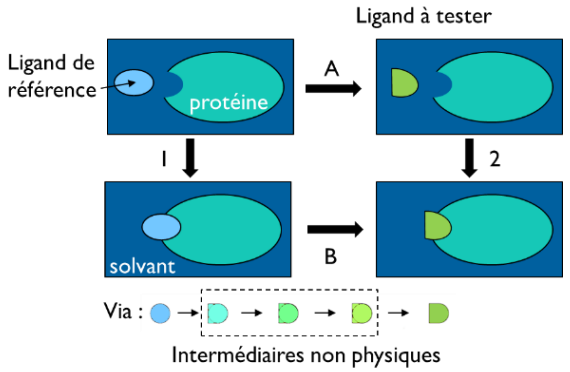

Figure 3.1 Principe du FEP

Le modèle a tout d'abord été testé sur des ligands dont les affinités apparentes avaient déjà été évaluées par DSLS. En temps normal, la comparaison du $\Delta\Delta G_{FEP}$ avec le $\Delta\Delta G_{expérimental}$ permet de déterminer un facteur de correction à appliquer lors des futures modélisations. En l'occurrence, le manque de données sur les constantes de dissociation des analogues synthétisés n'a pas permis la déduction d'un tel facteur. Il a malgré tout été confirmé que tous les composés actifs avaient bien un $\Delta\Delta G_{FEP}$ négatif par rapport à l'acide flufénamique et, à l'inverse, un $\Delta\Delta G_{FEP}$ positif pour les composés inactifs. Il est admis que plus le $\Delta\Delta G_{FEP}$ est bas, plus le ligand étudié à de chances d'interagir fortement avec la poche de liaison. Le meilleur dérivé apparent avec une substitution en *méta* de l'amine centrale au niveau du cycle aromatique de gauche correspond à celui avec une chaîne heptyle, ce qui est en harmonie avec les résultats DSLS présentés dans le tableau 2 du chapitre précédent. En se basant sur les différents résultats obtenus, il semblerait que des isostères de l'acide carboxylique soient

également favorables à la formation d'interactions avec TEAD, sans pour autant permettre de gagner nettement en activité. Différents analogues plus polaires, notamment certains portant une amine libre en *méta* de l'acide carboxylique sur le phényle de droite ou un groupement 4-propylpipéridine en *méta* de l'amine centrale sur le cycle aromatique de gauche, sont également ressortis comme des options d'apparences favorables pour le maintien de l'affinité tout en améliorant la solubilité (Figure 3.2).

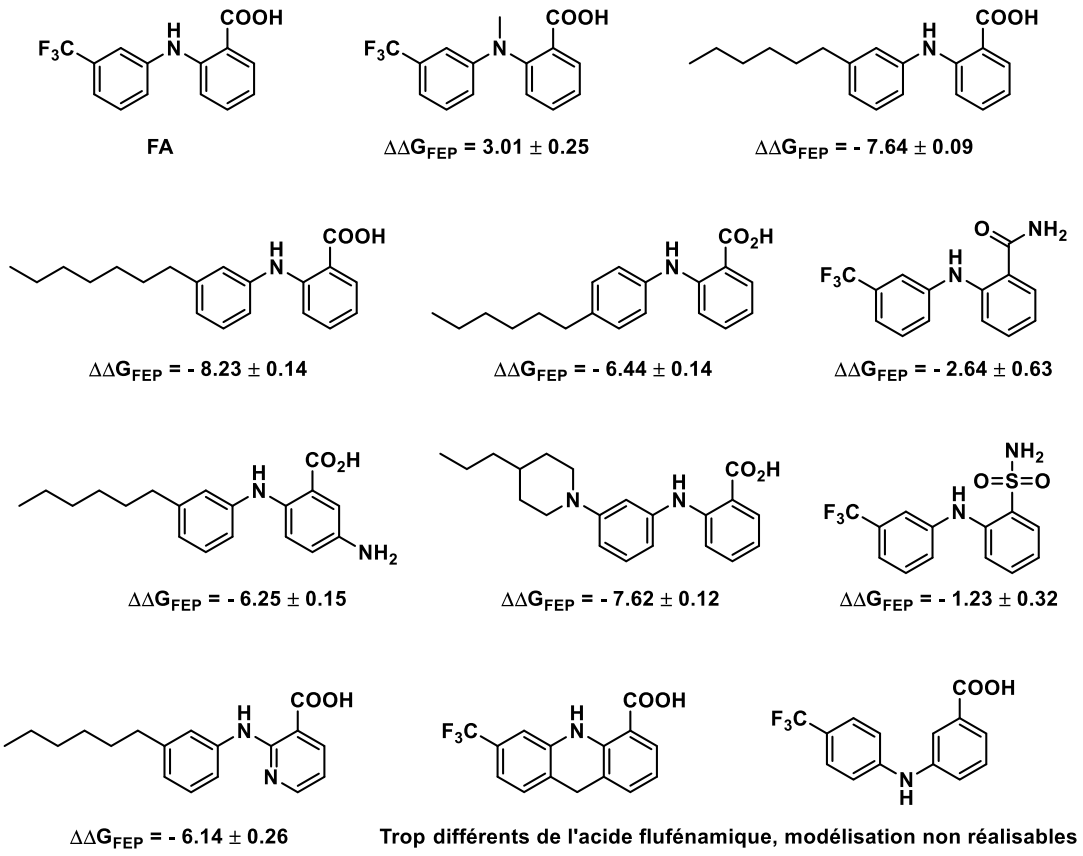

Figure 3.2 Exemples d'analogues testés par FEP

En raison de la méthode de calcul utilisée, le programme Desmond simule les dynamiques moléculaires dans le temps. Il est ainsi possible d'accéder à de multiples données telles que l'écart quadratique moyen (root mean square deviation, RMSD) de

la protéine et du ligand, la fluctuation moyenne pondérée (root mean square fluctuation, RMSF) de la protéine et du ligand, les contacts protéine/ligand ou encore le profil de torsion du ligand dans le temps. Ces informations permettent un design beaucoup plus pointu et rationnel des divers analogues. Il a ainsi pu être établi qu'en plus des liaisons observées lors des modélisations entre nos analogues et la lysine 357 ainsi que la cystéine 380, l'acide carboxylique permet également l'interaction avec la proline 378 via un pont-eau. Il a aussi pu être confirmé que les dérivés inactifs présentant des modifications au niveau du connecteur central maintiennent ces interactions principales mais perdent la liaison hydrogène intramoléculaire, validant l'hypothèse que cette dernière participe à la stabilisation de la conformation active (Figure 3.3.a et Figure 3.3.c). De même, il a été illustré que les analogues contenant d'imposants groupements alkyles favorisent les interactions hydrophobiques avec davantage de résidus que l'acide flufénamique de départ (Figure 3.3.b). Il est à noter que le diagramme en barre (Figure 3.3.b) représentant les contacts protéine/ligand est normalisé au cours de la simulation. Ainsi, une valeur de 0.8 suggère que pendant 80% de la durée de la modélisation, un certain type d'interaction a eu lieu entre le résidu en question et le ligand. Des valeurs supérieures à 1 sont donc possibles puisqu'un même acide aminé peut interagir de plusieurs façons ou à plusieurs endroits avec le ligand (Figure 3.3.a).

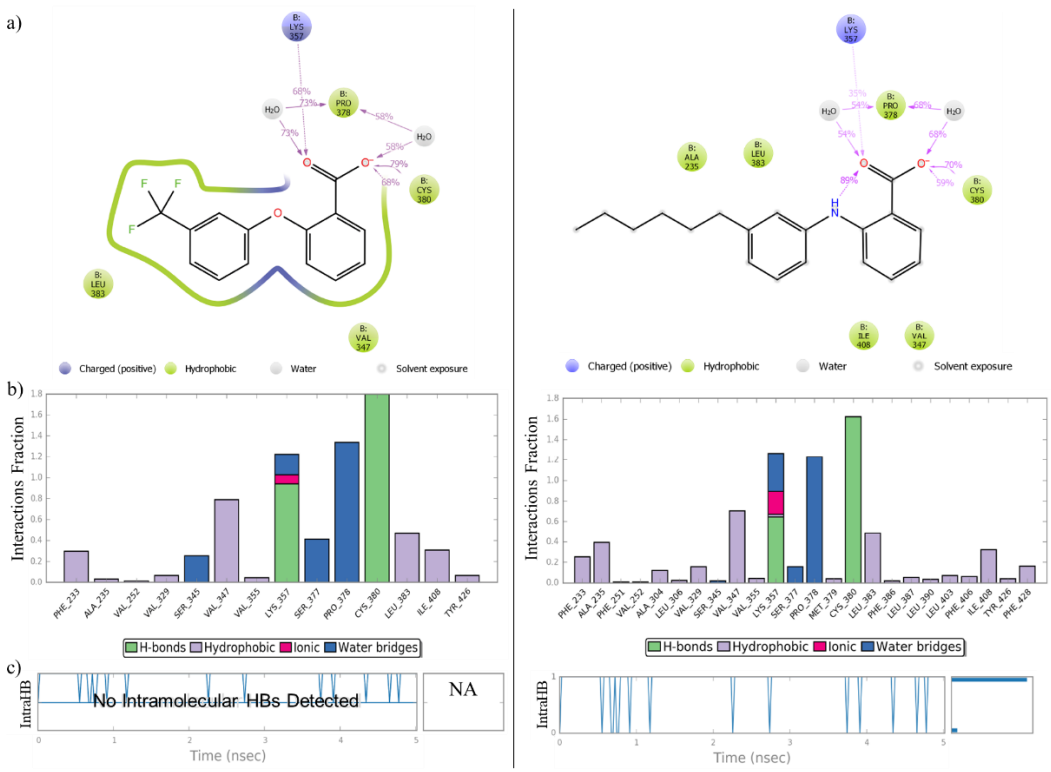

Figure 3.3 Analyses des dynamiques moléculaires de deux analogues par : a) visualisation schématique des contacts protéine/ligand au cours du temps (seuls les contacts qui occurent plus de 30% du temps sont représentés), b) visualisation graphique des contacts protéine/ligand au cours du temps, c) nombre de liaisons H intramoléculaires au cours du temps

Sachant que les données RMSF du ligand sont utiles pour déterminer les changements de position des atomes au sein de la molécule, il a également été possible de corroborer les conclusions obtenues par amarrage afin de comprendre comment les dérivés avec des groupements en *para* de l'amine centrale au niveau du cycle aromatique de gauche s'insèrent dans la cavité hydrophobe. Le RMSF pour un atome i est calculé selon la formule suivante :

$$RMSF_i = \sqrt{\frac{1}{T}\sum_{t=1}^{T}\left(r_i'(t) - r_i(t_{ref})\right)^2}$$

Où T correspond à la durée de la simulation, t_{ref} est le temps de référence (en l'occurrence zéro), r est la position de l'atome i au moment initial t_{ref} tandis que r' s'apparente à la position de l'atome i au moment t. Tandis que le dérivé hexyle en *méta* présente des fluctuations principalement en bout de chaîne alkyle et au niveau des deux atomes d'oxygène de l'acide carboxylique, le dérivé hexyle en *para* montre également des mouvements importants au niveau des différents atomes formant le cycle aromatique de gauche (Figure 3.4.a). En adéquation avec les modélisations présentées dans l'article du chapitre II, les profils de torsion du ligand illustrent la rotation du phényle afin d'accommoder la chaîne latérale dans la poche palmitique (Figure 3.4.b).

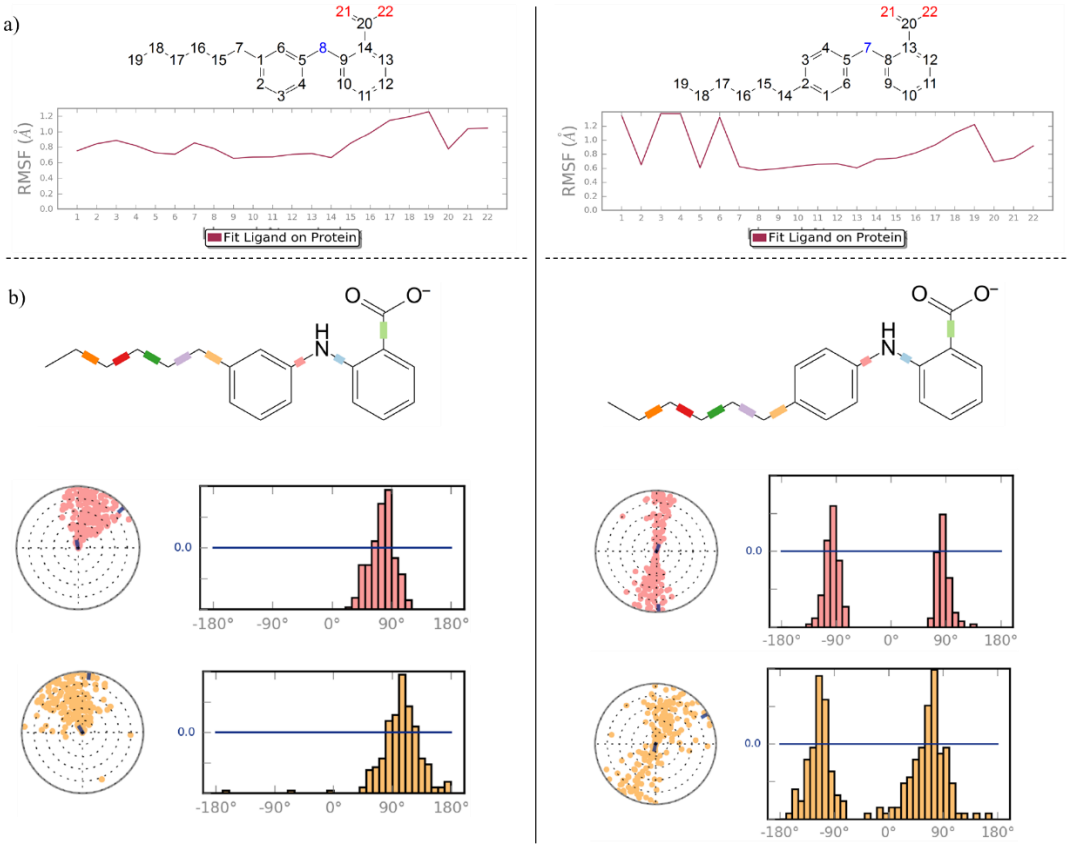

Figure 3.4 Analyses des dynamiques moléculaires de deux analogues par : a) RMSF du ligand au cours du temps, b) profil de torsion du ligand au cours du temps

De façon surprenante, les données de modélisation par dynamique moléculaire pour les dérivés de l'acide niflumique indiquent la formation d'une nouvelle liaison hydrogène entre l'amine de la pyridine et la sérine 345. Néanmoins, les résultats obtenus par mesures DSLS et par modélisation FEP indiquent tous deux que les dérivés NA sont généralement moins actifs que leurs parents FA, peut-être en raison de plus faibles interactions avec la proline 378 au cours du temps. Malgré tout, les données générées demeurent intéressantes et permettent d'envisager l'obtention de nouvelles interactions au sein de la poche de liaison (Figure 3.5).

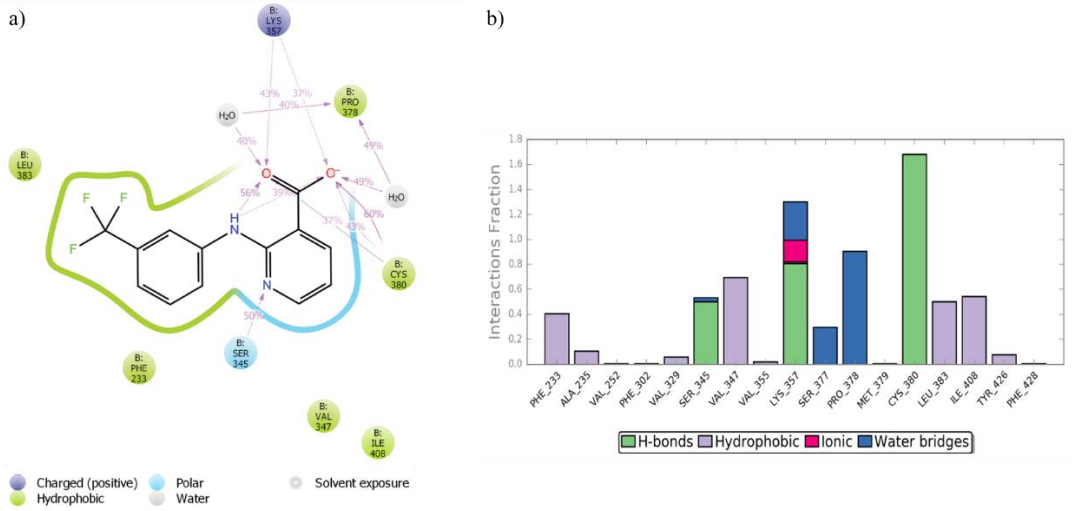

Figure 3.5 Analyses des dynamiques moléculaires de l'acide niflumique par : a) visualisation schématique des contacts protéine/ligand au cours du temps (seuls les contacts qui occurent plus de 30% du temps sont représentés), b) visualisation graphique des contacts protéine/ligand au cours du temps

L'ensemble des modélisations présentées jusqu'alors se restreignent à l'acide flufénamique et ses dérivés. Afin d'augmenter nos chances de développer un inhibiteur puissant de TEAD, effectuer un criblage virtuel plus large pourrait permettre de découvrir de nouveaux *hits*, donnant ainsi lieu au lancement potentiel de nouvelles campagnes de SAR et d'optimisation, tout en améliorant la conception des dérivés de l'acide flufénamique.

3.2 Criblage virtuel à haut débit (HTVS)

En se basant sur les modélisations précédentes et les analyses qui en ont découlé, il semble raisonnable d'assumer que le pharmacophore minimal de l'acide flufénamique soit l'acide 2-aminobenzoïque. Pour cette raison, il a été décidé de construire une librairie virtuelle de composés contenant ce motif.

3.2.1 Librairie combinatoire d'acides 2-aminobenzoïques

La création de cette librairie virtuelle repose sur la combinaison de l'acide 2-bromobenzoïque avec une librairie d'amines primaires créée spécifiquement pour cette utilisation. En se basant sur la banque de données d'Emolecules composée d'approximativement 8 millions de blocs de construction (*building blocks*) commerciaux, une recherche de sous-structure a été effectuée. En appliquant le langage SMARTS, n'importe quelle amine primaire n'étant pas sous forme d'ion ammonium et se liant via une liaison simple à un atome de carbone (n'étant pas un amide, ni un cyanimide, ni un thioamide, ni quaternaire) a ainsi été extraite afin de former un fichier contenant 845 963 molécules. Un premier filtre a ensuite été appliqué afin de ne conserver que des fragments potentiellement utilisables en chimie médicinale. Seules les molécules contenant (1) uniquement des atomes H, C, O, N, F, Cl, Br, I, S, (2) entre 5 et 25 atomes au total, (3) de 0 à 2 centres chiraux, (4) de 0 à 6 accepteurs de liaisons hydrogène et (5) de 0 à 6 donneurs de liaisons hydrogène ont été conservées, réduisant ainsi la quantité d'amines primaires à 708 569. Ce nombre étant encore considérable, un deuxième filtre aux conditions plus restreintes a été appliqué, ne gardant que les blocs possédant (1) entre 5 et 20 atomes au total, (2) de 0 à 5 accepteurs de liaisons hydrogène et (3) de 0 à 5 donneurs de liaisons hydrogène. Les 526 141 blocs isolés ont ensuite été soumis à un filtre appliquant les règles de chimie médicinale de Lilly (*Lilly MedChem Rules*). Ce filtre permet de ne garder que les composés présentant des propriétés désirables en chimie médicinale, rejetant ainsi toute molécule

potentiellement covalente (comprenant par exemple des halogénures d'acyle), instable (présence d'aldéhydes latents), pouvant interférer avec les mesures biophysiques (en termes de fluorescence ou d'absorbance notamment) ou présentant des risques pour l'intégrité de la protéine (oxydants ou détergents). Après suppression des duplicatas, 396 495 amines primaires ont été identifiées comme adaptées à une utilisation en chimie thérapeutique. Cette librairie virtuelle fut ensuite combinée avec l'acide 2-bromobenzoïque à l'aide de Reactor (JChem suite, ChemAxon) afin de générer 399 853 dérivés 2D de l'acide 2-aminobenzoïque (Figure 3.6).

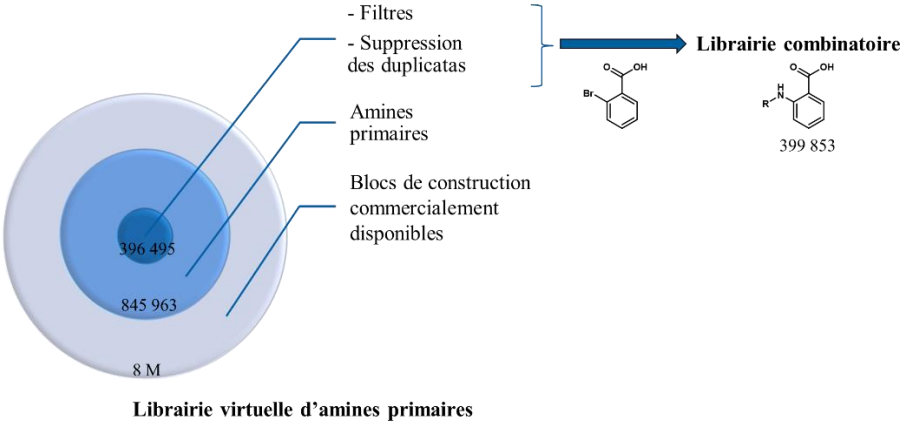

Figure 3.6 Flux d'élaboration de la librairie combinatoire d'acides 2-aminobenzoïques

Une fois la librairie combinatoire en main, un criblage virtuel contre TEAD2 a été lancé afin de déterminer de potentiels nouveaux inhibiteurs.

3.2.2 Criblage virtuel basé sur la librairie combinatoire d'acides 2-aminobenzoïques

Dans un premier temps, l'ensemble des molécules contenues dans la librairie combinatoire furent converties en 3D (LigPrep, Schrödinger) afin de permettre le criblage virtuel dans la poche centrale hydrophobe de TEAD2 (code pdb : 5dq8). Par la suite, plusieurs séries successives d'amarrage moléculaire (HTVS, SP puis XP de Glide) combinées à des paliers de réussite permirent d'obtenir 15 000 molécules interagissant virtuellement avec TEAD2. Il est à noter que les paliers appliqués

correspondent soit à l'affinité supposée du ligand, via le calcul du Glide_Score, soit à l'efficacité du ligand. En utilisant l'affinité comme critère principal, le risque est d'obtenir des molécules de taille déjà considérable, laissant peu de place à l'introduction de nouveaux groupements lors de l'optimisation. L'ajout du paramètre d'efficacité du ligand (LE), qui se définit par le ratio entre l'énergie libre de Gibbs ΔG et le nombre d'atomes n'étant pas des hydrogènes dans la molécule, permet de ne pas manquer les ligands qui utilisent leurs atomes efficacement. Après application d'un filtre permettant de reconnaître la présence de nouvelles liaisons avec les résidus de la poche palmitique, 32 molécules ont finalement été extraites et analysées (Annexe B) (Figure 3.7).

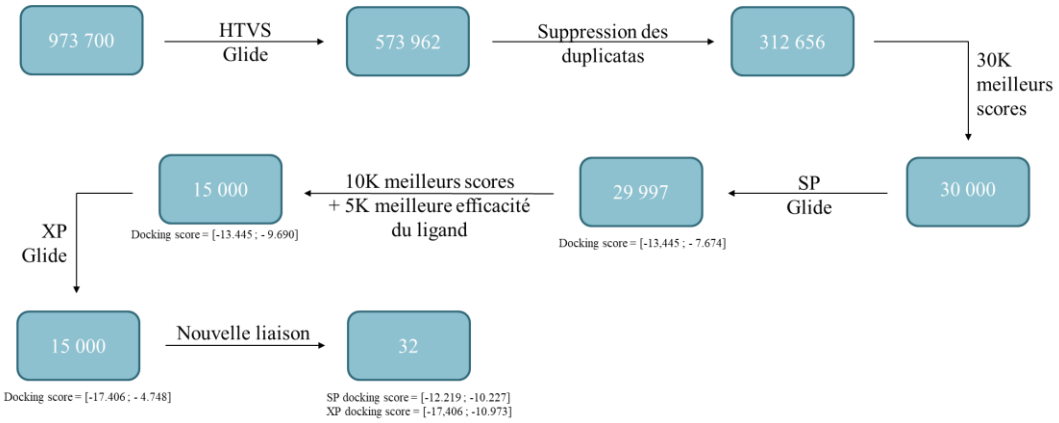

Figure 3.7 Flux du criblage virtuel basé sur la librairie combinatoire d'acides 2-aminobenzoïques

Parmi ces 32 molécules, toutes présentent l'un des quatre types de squelettes présentés dans la Figure 3.8.

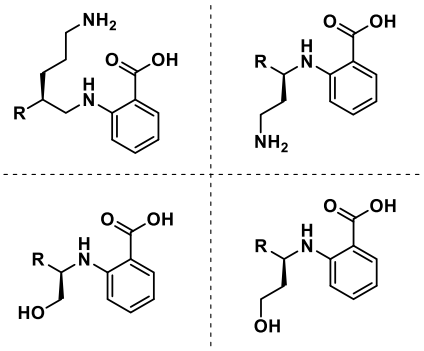

Figure 3.8 Type de squelettes retrouvés chez l'ensemble des 32 candidats finaux

Les amines forment un pont salin et des liaisons hydrogène avec l'acide glutamique 359, et parfois certains ponts-eau avec la sérine 345 ou avec l'acide carboxylique du squelette peptidique de la leucine 374 et celui de la cystéine 343 (Figure 3.9.a). De leur côté, les alcools créent préférentiellement un pont-H avec la sérine 345 (Figure 3.9.b). En fonction des structures, certaines interactions de type π sont également observées avec la tyrosine 426, la phénylalanine 428, la phénylalanine 386 ou la phénylalanine 233 (Figure 3.9.c).

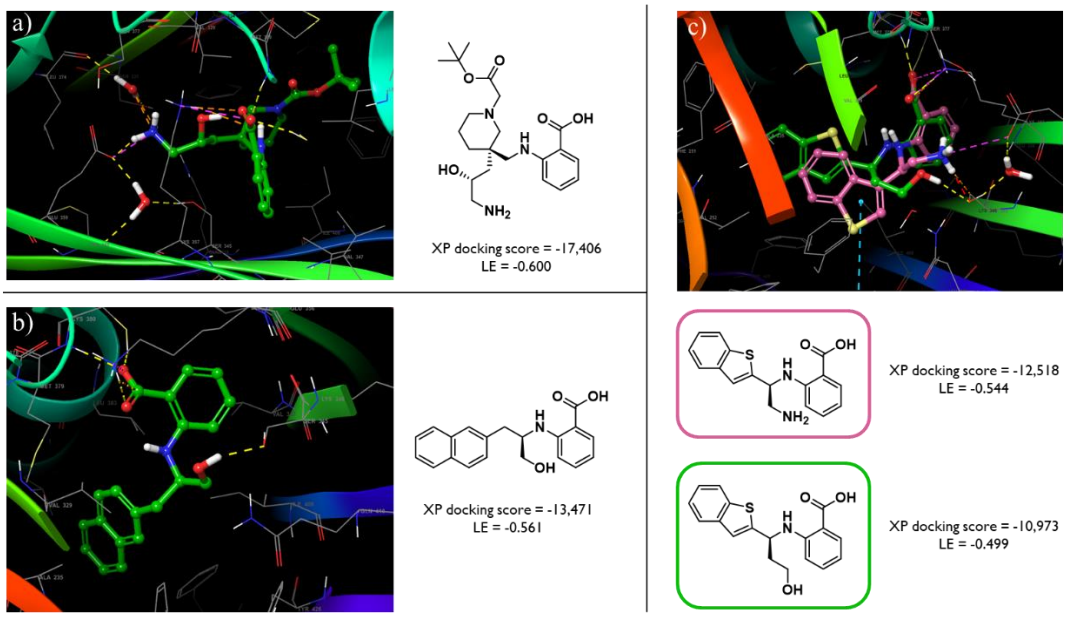

Figure 3.9 Exemples de molécules issues du criblage virtuel illustrant les interactions caractéristiques obtenues au sein de la poche palmitique de TEAD2

Parmi l'ensemble des candidats obtenus, deux retiennent tout particulièrement notre attention en raison de leurs scores de modélisation et leurs excellents résultats d'efficacité de ligand, laissant présager que si leur activité est confirmée, ils feront des *hits* de départ sur lesquels il sera facile de rajouter des groupements pour l'optimisation (Figure 3.10). Il est à envisager que la série avec l'amine primaire devienne problématique pour une utilisation *in vivo* en raison d'une faible diffusion passive et d'un risque élevé de métabolisation rapide. Si le *hit* s'avérait prometteur, le développement de pro-drogues pourrait être mis en place.[283] À défaut, commencer l'optimisation sur un dérivé avec l'alcool primaire semble une stratégie davantage viable.

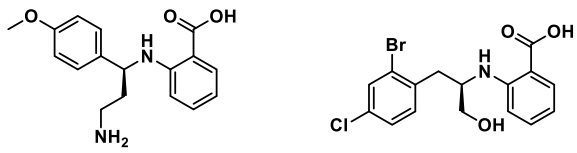

Figure 3.10 Potentiels nouveaux hits comme inhibiteurs de TEAD

Bien que certaines des molécules obtenues soit un peu éloigné de l'acide flufénamique, il est fort probable que les enseignements du SAR mené jusqu'alors puissent être transposés aux nouvelles séries. Inversement, des études de superposition entre les molécules finales et le *lead* dérivé de l'acide flufénamique permettraient d'exploiter le criblage pour diriger la synthèse de nouveaux analogues de la série déjà en cours, comme l'illustre la Figure 3.11.

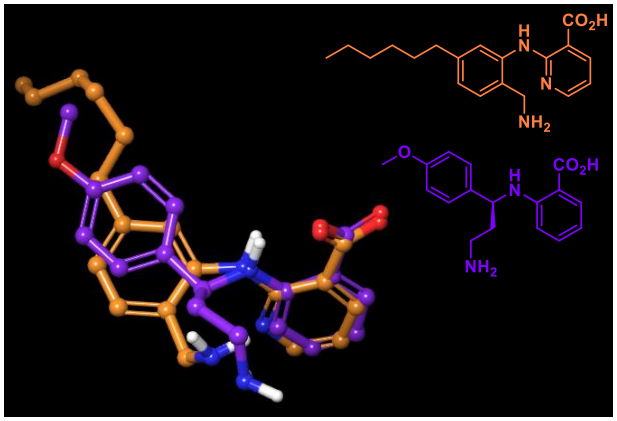

Figure 3.11 Superposition d'un *hit* issu du criblage virtuel à haut débit (violet) et d'une molécule dérivée de l'acide flufénamique (orange)

Finalement, un deuxième criblage virtuel, cette fois basé non pas sur une librairie combinatoire mais simplement sur une recherche de sous-structures de type acide 2-aminobenzoïque a aussi été réalisé.

3.2.3 Criblage virtuel basé sur les sous-structures de type acide 2-aminobenzoïque

Dans un premier temps, la base de données Emolecules a été filtrée afin d'isoler tous les composés comprenant un squelette de type acide 2-aminobenzoïque, où les atomes non substitués du cycle aromatique peuvent correspondre à n'importe quel atome. Les 12 847 blocs de construction obtenus ont ensuite été transposés en coordonnées 3D via LigPrep puis soumis à des criblages successifs dans Glide (HTVS, SP puis XP). Parmi les 7 270 candidats restants, seuls ceux ayant un score de modélisation inférieur à 10 ou réalisant des liaisons hydrogène avec l'un des acides aminés polaires de la poche (acide glutamique 359, sérine 345 ou glutamine 410) ont été conservés. Un rapide survol des 1 323 structures permet le constat que celles capables de créer de nouvelles interactions hydrogène possèdent soit des amines, soit des alcools primaires, d'une façon similaire à celles obtenues lors du criblage précédent, tandis que les autres présentent des squelettes semblables aux dérivés développés dans le chapitre II. Avant de se lancer dans la synthèse de certains de ces dérivés, il a été décidé de prioriser le test de composés commerciaux afin de valider la stratégie. Les 124 composés disponibles à l'achat ont ensuite été groupés en fonction de leurs structures, permettant d'isoler 23 potentielles classes d'inhibiteurs commerciaux de TEAD2 (Annexe B) (Figure 3.12).

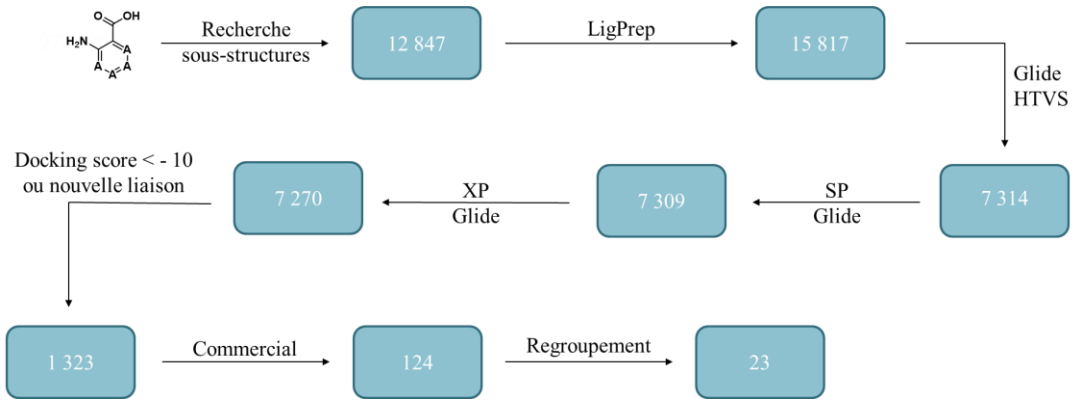

Figure 3.12 Flux du criblage virtuel basé sur les sous-structures de type acide 2-aminobenzoïque

Parmi ces 23 candidats, ceux avec le meilleur score d'amarrage exploitent la partie gauche de la cavité, certains étant même hautement similaires aux analogues développés dans le chapitre II (Figure 3.13a et Figure 3.13.b). Les seuls fragments créant de nouvelles liaisons hydrogène avec les résidus de la poche ressemblent quant à eux aux *hits* issus du criblage virtuel présenté dans la partie 3.2.2 (Figure 3.13.c et Figure 3.13.d). Il serait intéressant de tester ces composés par DSLS afin de les comparer aux dérivés déjà développés et de valider l'effort de synthèse associé aux composés de la Figure 3.10.

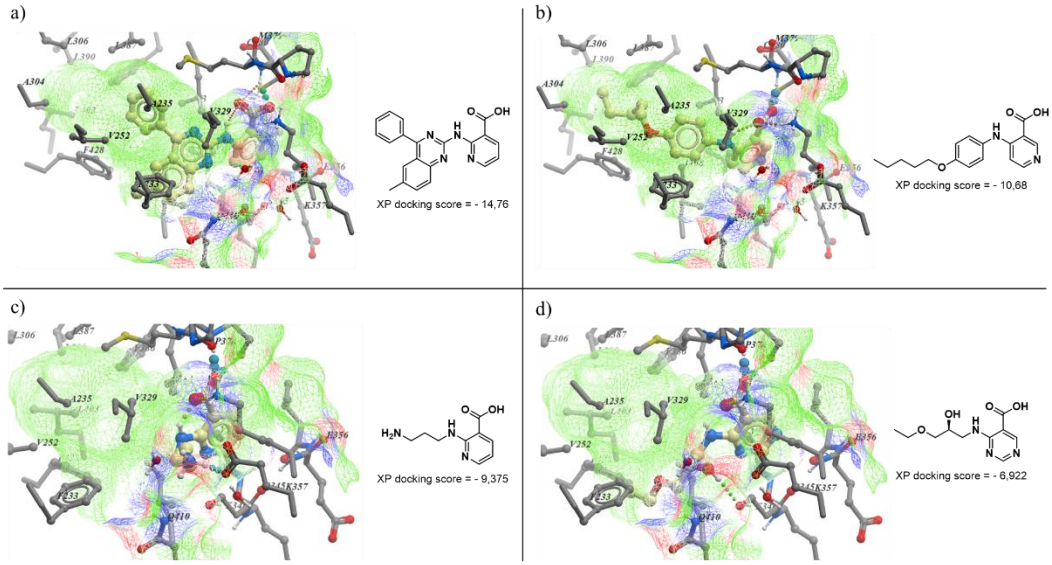

Figure 3.13 Exemples représentatifs de *hits* potentiels obtenus lors du criblage virtuel basé sur les sous-structures de type acide 2-aminobenzoïque

Pour conclure, l'utilisation de divers outils informatiques a non seulement permis de guider l'optimisation de la série présentée au chapitre précédent mais aussi d'identifier de potentiels nouveaux inhibiteurs de TEAD. Si les *hits* sont confirmés, des techniques informatiques de saut de squelette (scaffold-hopping) pourraient être employées afin de diversifier davantage la structure.

CHAPITRE IV

DÉVELOPPEMENT D'INHIBITEURS DE PB1 PRÉSENTANT UNE SÉLECTIVITÉ ACCRUE CONTRE SMARCA2

4.1 Introduction

PB1 est une protéine contenant des domaines bromés qui agit comme lecteur épigénétique pour le compte du remodeleur de chromatine PBAF. Malgré les nombreuses études démontrant l'implication de PBAF et PB1 dans divers cancers, le rôle exact de PB1 n'a pas encore pu être élucidé en raison d'une absence d'inhibiteur efficace sélectif des domaines bromés de PB1 par rapport aux autres membres de la sous-famille VIII. Les travaux rapportés dans cet article feront donc état du développement et de la caractérisation d'inhibiteurs puissants présentant une sélectivité jusqu'alors non atteinte pour les domaines bromés clefs de PB1 par rapport à SMARCA2.

4.2 Article issu de ces travaux

ACS OMEGA

http://pubs.acs.org/journal/acsodf

Article

Design and Synthesis of LM146, a Potent Inhibitor of PB1 with an Improved Selectivity Profile over SMARCA2

Léa Mélin, Emily Gesner, Sarah Attwell, Olesya A. Kharenko, Edward H. van der Horst, Henrik C. Hansen, and Alexandre Gagnon*

Cite This: *ACS Omega* 2021, 6, 21327−21338

Read Online

ACCESS | Metrics & More | Article Recommendations | Supporting Information

ABSTRACT: PB1 is a bromodomain-containing protein hypothesized to act as the nucleosome-recognition subunit of the PBAF complex. Although PB1 is a key component of the PBAF chromatin remodeling complex, its exact role has not been elucidated due to the lack of potent and selective inhibitors. Chemical probes that target specific bromodomains within the complex would constitute highly valuable tools to characterize the function and therapeutic pertinence of PB1 and of each of its bromodomains. Here, we report the design and synthesis of lead compound **LM146**, which displays strong stabilization of the second and fifth bromodomains of PB1 as shown by DSF. **LM146** does not interact with bromodomains outside of sub-family VIII and binds to PB1(2), PB1(5), and SMARCA2B with K_D values of 110, 61, and 2100 nM, respectively, providing a ∼34-fold selectivity profile for PB1(5) over SMARCA2.

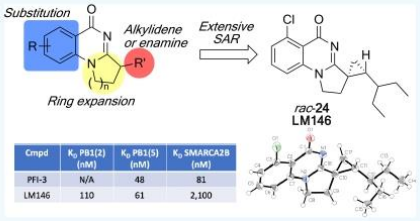

INTRODUCTION

ε-N-Acetylation of lysine residues on histone tails is one of the most fundamental and dynamic epigenetic transformations that controls changes in chromatin accessibility.[1] This post-translational modification plays a key role in regulating gene expression and is often associated with transcriptional activation.[2] Bromodomains are selective protein motifs that act as epigenetic readers by mediating the interaction with acetylated lysine of histones and transcriptional regulators.[3−5] They are defined by four α helices linked by two flexible loops forming a hydrophobic pocket and are usually composed of about 110 amino acids.[6] The human proteome expresses 61 bromodomains distributed across 46 proteins, which can be clustered into eight sub-families based on both their structure similarities and their sequence homology.[7]

Bromodomain-containing proteins (BCPs) are often part of multivalent complexes, and many possess other chromatin recognition domains such as PHD fingers, PWWP domains, or multiple bromodomains.[8] Polybromo-1 protein (PB1, also referred to as PBRM1 or BAF180) is a component of the BRG1/BRM-associated factor (PBAF) complex, a human analog of the yeast switch/sucrose non-fermenting (SWI/SNF) complex. PB1 is a unique epigenetic reader that contains six distinct bromodomains, while other known bromodomain-containing proteins possess at most two bromodomains. The multi-subunit PBAF complex contains three BCPs: BRD7, a member of the sub-family IV, and SMARCA4 (also known as BRG1) and PB1, two members of the sub-family VIII. While it is known that PBAF acts as a chromatin remodeling complex by repositioning nucleosomes through ATP hydrolysis,[9] the exact role of each component remains ambiguous. However, it has been established that the BCPs are necessary components for the complex's cellular function.[10]

Intensive research has been dedicated to the SWI/SNF family complexes as their components are recurrently mutated in many cancers.[11−15] In light of the biological importance of PBAF, chemical probes that target different bromodomains within the complex would constitute highly valuable tools to elucidate the exact function and therapeutic pertinence of each member.

Molecular probes targeting sub-family IV have been reported, including I-BRD9, a BRD9 selective inhibitor with a pIC_{50} of 7.3, and more than 70-fold selectivity over a panel of other bromodomains,[16] as well as numerous BRD9/BRD7 dual inhibitors such as LP99,[17] BI-9564,[18] TP-472,[19] or GSK6776.[20] However, chemical probes targeting sub-family VIII are fewer and lack selectivity within the group. PFI-3 potently targets the bromodomains of SMARCA2A/B (two isoforms derived from alternative splicing: a long transcript, named SMARCA2A, and a short transcript, SMARCA2B), SMARCA4, as well as the fifth bromodomain of PB1 (PB1(5)) with K_D values of 81, 86, 97, and 54 nM, respectively (Figure 1).[21] Compound **1**, an analog of PFI-3, was also described as

Received: March 24, 2021
Accepted: July 27, 2021
Published: August 9, 2021

https://doi.org/10.1021/acsomega.1c01555
ACS Omega 2021, 6, 21327−21338

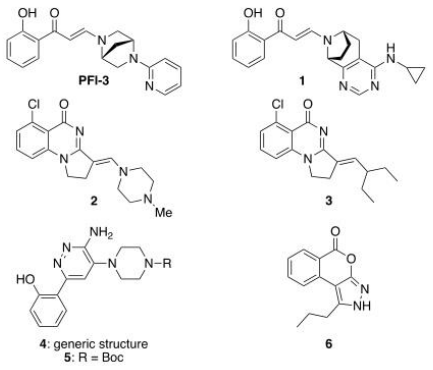

Figure 1. Reported sub-family VIII bromodomain inhibitors.

targeting simultaneously SMARCA2, SMARCA4, and PB1(5) as well as the second bromodomain of PB1 (PB1(2)) with K_D values of 37, 53, 30, and 190 nM, respectively.[22] In 2016, Sutherell *et al.* reported compound **2** that binds to PB1(5), SMARCA2B, and SMARCA4 with K_D values of 124, 262, and 417 nM, respectively, and analog **3** that showed stronger interaction with PB1 than SMARCAs.[23] The same year, pyridazine derivatives of generic structure **4** were reported by Constellation Pharmaceuticals and Genentech as pan-inhibitors of SMARCA2/4 and PB1(5).[24] In 2020, some of these patented molecules were fully characterized by the SGC, revealing K_D values of 35, 36, and 13 nM against SMARCA2, SMARCA4, and PB1(5), respectively, for compound **5**.[25] The only inhibitor showing some degree of selectivity within the sub-family VIII for PB1(5) is the tricyclic compound **6**. However, with a K_D value of 3.3 μM, **6** lacks potency for PB1(5).[26] To the best of our knowledge, there are currently no potent inhibitors of PB1 with selectivity toward specific bromodomains.

Given that PB1 is predicted to act as the nucleosome-recognition subunit of the PBAF complex and that somatic PB1 mutations occur in many cancers, including up to 50% of clear cell renal cell carcinomas (ccRCC),[27,28] we aimed to develop potent and selective PB1 inhibitors as tool compounds for *in vitro* functional characterization. Because it has been recently demonstrated that bromodomains 2, 4, and 5 are critical for PB1 activity by mediating the binding to acetylated histone peptides as well as to modified recombinant and cellular nucleosomes[29] and since their collaboration is key for PB1 tumor suppressor functions,[30] we elected to focus on the development of chemical probes targeting PB1(2), PB1(4), and PB1(5). Herein, we report the synthesis and biological evaluation of a new potent derivative of compound **3** that binds to PB1 with significant selectivity over SMARCA2 and with preference for distinct bromodomains of PB1.

RESULTS AND DISCUSSION

We began by resynthesizing compound **3** for use as a reference in our assays. Since the binding pocket around the aromatic ring of **3** is slightly larger in PB1(5) than in SMARCA2A, we then prepared a small ensemble of derivatives where substituents are introduced on the aromatic ring, as shown in Table 1. These compounds were easily accessed using the synthetic route reported by Sutherell *et al.* (see Experimental Section for details).[23] The stereochemistry of the double bond was previously demonstrated to be *E* for these types of compounds.[23] The proton NMR spectrum of resynthesized known compound **3** was identical to the data from the literature.[23] Other new compounds had similar proton NMR spectra and were assumed to have the *E* stereochemistry. Differential scanning fluorimetry (DSF) was used to quickly evaluate the binding of our compounds against PB1(2), PB1(4), PB1(5), and SMARCA2A. This thermal shift assay was previously reported to be suitable for rapid determination of apparent potency and selectivity for bromodomains.[22,23] However, since proteins can behave differently, the extent of thermal stabilization should not be interpreted as an absolute scale of compound affinity.[31] In agreement with the literature results, resynthesized **3** showed strong binding to PB1(2) and PB1(5), thus validating our thermal shift biophysical assay. The presence of the chloride *ortho* to the carbonyl moiety in **3** was previously shown to be beneficial for PB1(5) protein

Table 1. Structure Activity Relationship (SAR) of Left-Hand Side (LHS) Substituted Derivatives of 3 against Sub-Family VIII Bromodomains by the DSF Assay

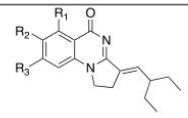

ΔT_m (°C): < 0 | 0 – 2 | 2 – 4 | 4 – 6 | 6 – 9 | > 9

Compound	R_1	R_2	R_3	ΔT_m (°C)[a] PB1(2)	PB1(4)	PB1(5)	SMARCA2A
3	Cl	H	H	6.78	2.13	10.33	5.33
7	H	Cl	H	0.47	–0.14	0.9	–0.49
8	H	H	Cl	2.07	–0.18	0.87	–2.09
9	Cl	Cl	H	–1.6	–0.21	2.23	2.86
10	H	OMe	H	0.56	–1.4	–0.56	0.14
11	H	H	OMe	–1.53	–0.7	–0.49	0
12	H	OH	H	2.52	–0.21	–0.56	–0.28
13	H	H	OH	3.49	0.21	–0.42	–0.07

[a]Values shown are the average of at least two replicates with a compound concentration of 100 μM.

https://doi.org/10.1021/acsomega.1c01555
ACS Omega 2021, 6, 21327−21338

Table 2. Structure Activity Relationship (SAR) of Right-Hand Side (RHS) Substituted Derivatives of 3 against Sub-Family VIII Bromodomains by the DSF Assay

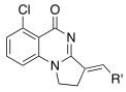

ΔT_m (°C):	< 0	0 – 2	2 – 4	4 – 6	6 – 9	> 9

Compound	R'	ΔT_m (°C)[a] PB1(2)	PB1(4)	PB1(5)	SMARCA2A
3	3-Pentyl	6.78	2.13	10.33	5.33
14	*sec*-Butyl	2.24	0.4	7.96	3.77
15	*n*-Propyl	3.03	0.28	11	4.61
16	Et	–0.23	–0.56	5.03	–1.47
17	*tert*-Butyl	2.33	0.79	6.71	–0.14
18	*iso*-Butyl	1.98	0.56	9.14	2.38
19	Neopentyl	4.96	0.77	7.06	1.61
20	Phenyl	–6.11	–4.8	0.07	2.14

[a]Values shown are the average of at least two replicates with a compound concentration of 100 μM.

Table 3. Structure Activity Relationship (SAR) of Ring Expanded, Saturated, and Cyclopropanated Substituted Derivatives of 3 against Sub-Family VIII Bromodomains by the DSF Assay

ΔT_m (°C):	< 0	0 – 2	2 – 4	4 – 6	6 – 9	> 9

Compound	Structure	ΔT_m (°C)[a] PB1(2)	PB1(4)	PB1(5)	SMARCA2A
3	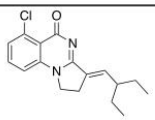	6.78	2.13	10.33	5.33
21	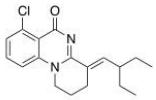	3.23	0.51	5.82	0.48
22	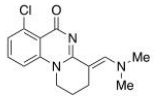	1.44	0.49	4.79	0.49
rac-**23**	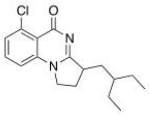	2.66	–2.24	1.54	1.33
rac-**24** (**LM146**)	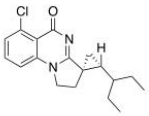	14.11	2.52	10.06	1.40

[a]Values shown are the average of at least two replicates with a compound concentration of 100 μM.

stabilization due to a halogen bond interaction with the carbonyl of Met731.[23] However, this chloride also led to good affinity with SMARCA2A, probably as a result of a similar halogen bond interaction with the carbonyl of Leu1456. We therefore studied the impact of moving or replacing the chloride in **3** on the stabilization of PB1 and SMARCA2A. Compounds **3**, **7**, and **8** confirmed that the optimal position for the chlorine is in R_1, that is, adjacent to the carbonyl. Indeed, complete loss of affinity to all domains of PB1 as well as to SMARCA2A was observed when the chloride was moved to the R_2 position, as shown by compound **7**. Interestingly, marginal but specific stabilization of PB1(2) was retained when the chloride was moved to R_3, as indicated by compound **8**. Conversely, dichloride **9** showed a reversal of apparent selectivity by weakly binding to PB1(5) and SMARCA2A, suggesting that the negative effect of the chloride at R_2 is

https://doi.org/10.1021/acsomega.1c01555
ACS Omega 2021, 6, 21327−21338

compensated by the chloride at R_1. Sutherell *et al.* reported that a methoxy in R_1 leads to complete loss of stabilization of PB1(5) in the related enamine series.[23] Similarly, we observed that compounds **10** and **11** that contain a methoxy at R_2 or R_3 do not bind to PB1 nor to SMARCA2A. However, polar hydroxy groups were tolerated by PB1(2), as indicated by compounds **12** and **13**, leading to inhibitors with first known apparent selectivity over the other sub-family VIII bromodomains.

As gaining selectivity over SMARCA2A while keeping high binding affinity with PB1 proved to be challenging when the aromatic ring was not substituted with a chloride in R_1, we decided to move our efforts to the right-hand side R′ alkylidene chain (Table 2). Although it is solvent-exposed, the olefinic R′ chain was previously shown to play a major role in orienting the core inside the pocket.[23] Replacing the 3-pentyl group in compound **3** by a *sec*-butyl (compound **14**) resulted in erosion of apparent affinity for all targets. Compound **15** that possesses a linear *n*-propyl chain showed reduced stabilization of PB1(2) compared to **3** but retained the stabilization of PB1(5). Shortening the chain length provided compound **16**, which showed exclusive binding to PB1(5). The stabilization of PB1(2) and PB1(5) could be increased by building on steric hindrance with the introduction of a *tert*-butyl group in compound **17**. We also found that the *iso*-butyl and neopentyl derivatives **18** and **19** have high apparent affinity for PB1(5), with **19** also showing strong stabilization of the second domain of PB1.

Sutherell *et al.* reported that replacement of the alkyl chain by an aromatic ring in the *des*-chloro version of **3** leads to retention of affinity against PB1(5).[23] Surprisingly, in the chloro series, we observed no stabilization of PB1(5), weak binding to SMARCA2A, and even a drastic destabilization of PB1(2) and PB1(4) for the phenyl derivative **20**. Compounds **14** to **20** provide valuable information on the structural elements that are required for optimal stabilization of PB1 domains and SMARCA while also offering diversified binding profiles.

As the entrance of the pocket appears to be a key region to selectively inhibit PB1 over SMARCA2A, we decided to expand the lower right-hand side cycle size as illustrated in Table 3 with the hypothesis that these compounds would not fit in the narrower entrance of SMARCA2. This modification could also help deviate from planarity by introducing extra tetrahedral carbons while also increasing the overall solubility of the compounds. To evaluate the impact of this ring expansion, we prepared the tricyclic compound **21** in the olefinic series and compound **22** in the enamine series using routes from the literature (see Experimental Section for details).[32] As anticipated, the expansion of the lower ring completely canceled the affinity for SMARCA2A. In addition, this modification also abrogated the binding to PB1(4), considerably reduced the binding to PB1(2), but retained good affinity to PB1(5).

Motivated by the impact of geometrical features on the apparent selectivity profile, we then synthesized the saturated analog **23** using the sequence illustrated in Scheme 1. For initial assessment and for ease of synthesis, the racemic version was targeted. Intermediate **28** was first prepared according to Sutherell *et al.* by hydrolysis of the cyano group in **25** followed by amide formation between **26** and 4-chlorobutyryl chloride and cyclization of **27**.[23] Condensation of **28** with 2-ethylbutanal afforded derivative **3**. At this stage, we were

Scheme 1. Synthesis Route for 23

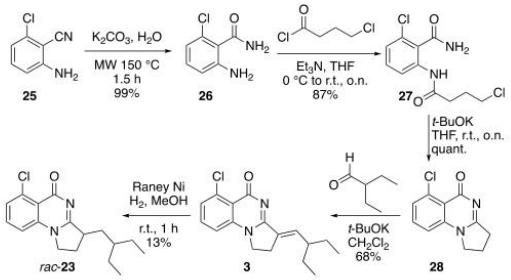

faced with the challenge of chemoselectively saturating the olefin in the presence of the aryl chloride. After testing various conditions, we found that reacting **3** with Raney nickel under a hydrogen atmosphere provided the desired saturated product **23** in low yield, albeit with the chlorine still in place.

DSF results indicate that **23** binds weakly to PB1(2) but none of the other bromodomains nor to SMARCA2A. Since the alkene seemed to be the key for maintaining binding, cyclopropyl derivative **24** (**LM146**) was designed in order to keep the orientation and conformational rigidity of the olefin. Considered a common alkene replacement in medicinal chemistry, the cyclopropane would also add some steric hindrance at the entrance of the cavity, which was previously hypothesized to be essential for gaining selectivity over SMARCA2. Therefore, we synthesized the cyclopropyl derivative **LM146** as a racemic mixture by engaging compound **3** in a Johnson−Corey−Chaykovsky cyclopropanation reaction (Scheme 2). The relative stereochemistry of **LM146** was

Scheme 2. Synthesis and X-ray Structure of Cyclopropyl Derivative LM146 (*rac*-24) CCDC No.: 2070470

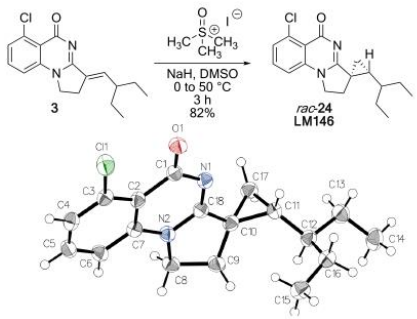

confirmed by X-ray analysis, with the obtention of a structure in a centrosymmetric space group ($P2_1/c$) typical of racemic mixtures. DSF results indicate that **LM146** provides a clear increase in ΔT_m for PB1(2) compared to **3** while keeping the stabilization of PB1(4) and PB1(5). Moreover, **LM146** showed very minor apparent interaction with SMARCA2A.

In order to confirm its utility as a potential tool compound for biological studies of PB1, **LM146** was tested against a panel of 32 bromodomains, including BET bromodomains, in a bromoMAX assay performed at Eurofins (see the Supporting Information). Results show that at 10 μM, **LM146** only binds to bromodomains within the sub-family VIII, with less affinity

https://doi.org/10.1021/acsomega.1c01555
ACS Omega 2021, 6, 21327−21338

for SMARCA4, as illustrated by the interaction map in Figure 2. These results are in agreement with the binding mode of the

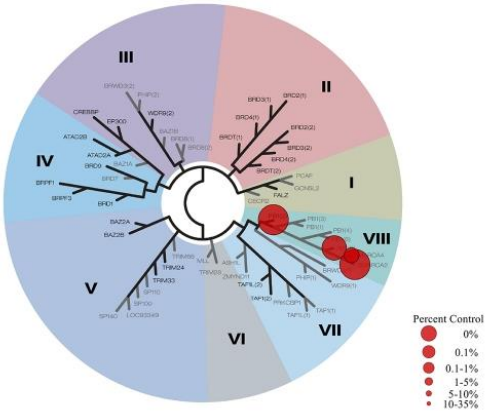

Figure 2. Selectivity profile for **LM146** screened at 10 μM against 32 selected bromodomains in a bromoMAX assay.

parent compounds **2** and **3** (and presumably our derivatives), which displace conserved water molecules within the acetylated lysine pocket. These water molecules were previously reported to have stronger binding in other bromodomain sub-families, partly explaining the selectivity observed for sub-family VIII.[33]

Key compounds were then selected for dissociation constant determination using a bromoSCAN assay performed at Eurofins (see the Supporting Information) in order to accurately evaluate the binding affinity of our compounds against PB1(2), PB1(5) and SMARCA2B. Compound **18** was selected for its apparent selectivity profile, which favors binding to PB1(5), while compounds **21** and **24** were chosen for their structural features that diverge from existing literature compounds combined with the absence of apparent interaction with SMARCA2A. As shown in Table 4, compound **18** is a moderate inhibitor of PB1(5) with a K_D value of 490 nM, a ~3-fold selectivity over PB1(2), and ~10-fold selectivity over SMARCA2B. Analog **21**, even if less potent, shows high selectivity for the PB1 bromodomains with an unprecedented ~24-fold selectivity for PB1(5) over SMARCA2B. Finally, cyclopropyl derivative **LM146** is as potent as PFI-3 and its analog **1** but shows increased selectivity toward PB1 over SMARCA2B with a ~34-fold selectivity profile in favor of PB1(5) and a ~19-fold selectivity profile in favor of PB1(2). To our knowledge, **LM146** constitutes the first potent modulator of PB1 bromodomains with a high selectivity profile over SMARCA2. Representative full inhibition curves for **LM146** against PB1(5) and SMARCA2B show a gradual dose–response with increasing compound concentration (Figure 3).

Table 4. K_D Values for Key Compounds

	K_D (nM)		
cmpd	PB1(2)	PB1(5)	SMARCA2B
PFI-3[a]	N/A[d]	48	81
1[a]	190	30	37
2[b]	N/A[d]	124	262
3[c]	190	47	290
18[c]	1600	490	4800
21[c]	5400	1100	26,000
LM146[c]	110	61	2100

[a]Values were assessed by ITC and reported in ref 21. [b]Values were assessed by ITC and reported in ref 23. [c]Values were assessed by bromoSCAN (see the Supporting Information). [d]N/A = not applicable.

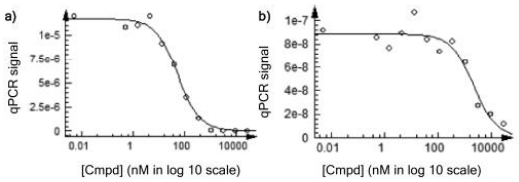

Figure 3. Representative bromoSCAN traces for K_D determination of **LM146** against (a) PB1(5) and (b) SMARCA2B.

CONCLUSIONS

In summary, we described the optimization of reported compound **3** with the aim of developing potent and selective PB1 inhibitors. DSF biophysical characterization allowed the assessment of SAR and led to the discovery of compounds with various apparent selectivity profiles that should allow further *in vitro* functional characterization of PB1 subdomains. Lead compound **LM146** showed no binding to any bromodomains outside the sub-family VIII at 10 μM and displayed K_D values of 110, 61, and 2100 nM against PB1(2), PB1(5), and SMARCA2B, respectively. **LM146** is a PB1-pan inhibitor with a ~34-fold selectivity profile for PB1(5) over SMARCA2B and a ~19-fold selectivity profile for PB1(2) over SMARCA2B. The inhibitors reported herein should contribute to expanding the toolbox for studying the role of PB1 in chromatin remodeling and disease development.

EXPERIMENTAL SECTION

General Information. Unless otherwise stated, reactions were performed in non-flame dried glassware, and commercial reagents were used without further purification. Anhydrous solvents were obtained using an encapsulated solvent purification system and were further dried over 4 Å molecular sieves. The evolution of reactions was monitored by analytical thin-layer chromatography (TLC) using silica gel 60 F254 precoated plates visualized by ultraviolet radiation (254 nm). Flash chromatography was performed employing 230–400 mesh silica using the indicated solvent system according to standard techniques. Nuclear magnetic resonance ^{1}H spectra were recorded on a Bruker Avance-III 300 or 600 MHz, and ^{13}C spectra were recorded on a Bruker Avance-III 75 or 151 MHz spectrometer. Chemical shifts for ^{1}H NMR spectra were recorded in parts per million from tetramethylsilane with the solvent resonance as the internal standard (chloroform-*d*, δ 7.26 ppm; methanol-d_4, δ 3.31 ppm; and dimethyl sulfoxide-d_6, δ 2.50 ppm). Data is reported as follows: chemical shift, multiplicity (s = singlet, s(br) = broad singlet, d = doublet, t = triplet, q = quartet, quint = quintet, sext = sextet, m = multiplet, dd = doublet of doublet, dt = doublet of triplet, ddd = doublet of doublet of doublet, dtd = doublet of triplet of

https://doi.org/10.1021/acsomega.1c01555
ACS Omega 2021, 6, 21327–21338

doublet), coupling constant J in Hz, and integration. Chemical shifts for ^{13}C NMR spectra are recorded in parts per million from tetramethylsilane using the solvent resonance as the internal standard (chloroform-*d*, δ 77.16 ppm; methanol-d_4, δ 49.00 ppm; and dimethysulfoxide-d_6, δ 39.52 ppm). Purity was assessed on an Agilent 1260 infinity HPLC system equipped with an Agilent Eclipse Plus C18 (3.5 μM and 4.6 × 100 mm) column using a 20 min gradient method (0 to 100% MeCN + 0.06% TFA in water + 0.06% TFA; the absorbance was measured at 254 nm). HRMS was performed on a TOF LCMS analyzer using the electrospray (ESI) mode.

General Procedure A. The appropriate 2-aminobenzonitrile (1.0 equiv) and K_2CO_3 (0.2 equiv) were added to a microwave tube in nanopure water. After irradiation under microwave at 150 °C for 1 h 30 min, the reaction mixture was cooled and extracted with EtOAc. The combined organic phases were dried over Na_2SO_4, filtered, and evaporated under vacuum. When indicated, the crude residue was purified by flash column chromatography to give the title compound.

General Procedure B. A solution of the appropriate substituted 2-aminobenzamide (1.0 equiv) in THF (2.5 mL per mmol of substrate) was cooled to 0 °C. Triethylamine (2.0 equiv) followed by the appropriate acid chloride (1.2 equiv) in THF (2 mL per mmol substrate) was added to the stirred solution. The reaction was stirred at room temperature overnight. The mixture was then diluted with EtOAc and washed with a saturated aqueous solution of $NaHCO_3$. The aqueous phase was back extracted with EtOAc, and the combined organic phases were dried over Na_2SO_4, filtered, and evaporated under vacuum. The crude residue was purified by flash column chromatography to give the desired compound.

General Procedure C. To a solution of the appropriate benzamide (1.0 equiv) in THF (10 mL per mmol of substrate) was added *t*-BuOK (2.0 equiv). The reaction was stirred at room temperature overnight, and then the solvent was removed in vacuo. The resulting residue was dissolved in CH_2Cl_2, and the resulting solution was washed with a saturated aqueous solution of $NaHCO_3$. The aqueous layer was back extracted with CH_2Cl_2, and the combined organic phases were dried over Na_2SO_4, filtered, and evaporated under vacuum. The crude residue was purified by flash column chromatography to give the title compound.

General Procedure D. *t*-BuOK (1.2 equiv) was added to a solution of the appropriate cyclized substrate (1.0 equiv) in CH_2Cl_2 (0.4 M). The mixture was vigorously stirred for 5 min, and then the appropriate aldehyde (1.1 equiv) was added. After 1 h, a saturated aqueous solution of $NaHCO_3$ and CH_2Cl_2 was added. The phases were separated, and the aqueous layer was extracted with CH_2Cl_2. The combined organic layers were dried over Na_2SO_4, filtered, and evaporated under vacuum. The crude residue was purified by flash column chromatography to give the title compound.

*2-Amino-6-chlorobenzamide (**26**).* 2-Amino-6-chlorobenzonitrile (2.00 g and 13.1 mmol) was hydrolyzed in 18 mL of nanopure water according to general procedure A to afford 2-amino-6-chlorobenzamide **26** (2.22 g, 13.0 mmol, and 99%) as a white powder. The crude compound was taken directly in the next step. Spectral data are consistent with literature values.[23] ^1H NMR (300 MHz, $CDCl_3$) δ 7.06 (t, J = 8.0 Hz, 1H), 6.73 (dd, J = 7.9, 1.0 Hz, 1H), 6.60 (dd, J = 8.2, 1.0 Hz, 1H), 6.19 (s(br), 1H), 5.97 (s(br), 1H), 4.84 (s(br), 2H).

*2-Chloro-6-(4-chlorobutanamido)benzamide (**27**).* 2-Amino-6-chlorobenzamide **26** (2.22 g and 13.0 mmol) and 4-chlorobutanoyl chloride (1.75 mL and 15.6 mmol) were reacted according to general procedure B. Purification by flash column chromatography (SiO_2, hexanes/EtOAc 60/40 to 30/70) afforded 2-chloro-6-(4-chlorobutanamido)benzamide **27** (3.11 g, 11.3 mmol, and 87%) as a white solid. Spectral data are consistent with literature values.[23] ^1H NMR (300 MHz, $CDCl_3$) δ 9.26 (s(br), 1H), 8.11 (d, J = 8.3 Hz, 1H), 7.31 (t, J = 8.2 Hz, 1H), 7.15 (dd, J = 8.1, 1.1 Hz, 1H), 6.44 (s(br), 2H), 3.62 (t, J = 6.3 Hz, 2H), 2.55 (t, J = 7.2 Hz, 2H), 2.15 (quint, J = 6.6 Hz, 2H).

*6-Chloro-2,3-dihydropyrrolo[1,2-a]quinazolin-5(1H)-one (**28**).* 2-Chloro-6-(4-chlorobutanamido)benzamide **27** (220 mg and 0.800 mmol) was cyclized according to general procedure C. Purification by flash column chromatography (SiO_2, CH_2Cl_2/MeOH 95:5) provided 6-chloro-2,3-dihydropyrrolo-[1,2-*a*]quinazolin-5(1*H*)-one **28** (175 mg, 0.793 mmol, and 99%) as a white solid. Spectral data are consistent with literature values.[23] ^1H NMR (300 MHz, $CDCl_3$) δ 7.52 (t, J = 8.1 Hz, 1H), 7.39 (dd, J = 8.0, 1.1 Hz, 1H), 7.07 (dd, J = 8.2, 1.1 Hz, 1H), 4.19 (t, J = 7.4 Hz, 2H), 3.15 (t, J = 8.1 Hz, 2H), 2.40 (quint, J = 7.6 Hz, 2H).

*(E)-6-Chloro-3-(2-ethylbutylidene)-2,3-dihydropyrrolo-[1,2-a]quinazolin-5(1H)-one (**3**).* 6-Chloro-2,3-dihydropyrrolo[1,2-*a*]quinazolin-5(1*H*)-one **28** (156 mg and 0.707 mmol) and 2-ethylbutanal (96 μL and 0.78 mmol) were reacted according to general procedure D. Purification by flash column chromatography (SiO_2, CH_2Cl_2/MeOH 96:4) provided **3** (146 mg, 0.482 mmol, and 68%) as a white solid. Spectral data are consistent with literature values.[23] ^1H NMR (300 MHz, $CDCl_3$) δ 7.45 (t, J = 8.1 Hz, 1H), 7.30 (dd, J = 7.9, 1.1 Hz, 1H), 7.04 (dd, J = 8.3, 1.1 Hz, 1H), 6.85 (dt, J = 10.8, 2.7 Hz, 1H), 4.20−4.09 (m, 2H), 2.99 (ddd, J = 7.9, 6.6, 2.7 Hz, 2H), 2.22−2.07 (m, 1H), 1.63−1.47 (m, 2H), 1.45−1.28 (m, 2H), 0.85 (t, J = 7.4 Hz, 6H); HRMS (ESI) calcd for $[C_{17}H_{19}ClN_2O + H]^+$: 303.12587, found 303.12554, calcd for $[C_{17}H_{19}ClN_2O + Na]^+$: 325.10781, found 325.10795; HPLC purity: >99%.

*2-Amino-5-chlorobenzamide (**29**).* 2-Amino-5-chlorobenzonitrile (500 mg and 3.28 mmol) was hydrolyzed in 6 mL of nanopure water according to general procedure A. Purification by flash column chromatography (SiO_2, hexanes/EtOAc 50:50 to 0:100) provided 2-amino-5-chlorobenzamide **29** (421 g, 2.47 mmol, and 75%) as a white solid. Spectral data are consistent with literature values.[32] ^1H NMR (300 MHz, methanol-d_4) δ 7.53 (d, J = 2.4 Hz, 1H), 7.14 (dd, J = 8.8, 2.5 Hz, 1H), 6.72 (d, J = 8.8 Hz, 1H).

*5-Chloro-2-(4-chlorobutanamido)benzamide (**30**).* 2-Amino-5-chlorobenzamide **29** (421 mg and 2.47 mmol) and 4-chlorobutanoyl chloride (0.331 mL and 2.96 mmol) were reacted according to general procedure B. Purification by flash column chromatography (SiO_2, hexanes/EtOAc 60/40 to 30/70) provided 5-chloro-2-(4-chlorobutanamido)benzamide **30** (463 mg, 1.68 mmol, and 68%) as a yellow solid. Spectral data are consistent with literature values.[32] ^1H NMR (300 MHz, $CDCl_3$) δ 11.08 (s(br), 1H), 8.61 (d, J = 8.9 Hz, 1H), 7.51−7.43 (m, 2H), 6.14 (s, 1H), 5.75 (s, 1H), 3.65 (t, J = 6.3 Hz, 2H), 2.60 (t, J = 7.2 Hz, 2H), 2.19 (quint, J = 6.6 Hz, 2H).

*7-Chloro-2,3-dihydropyrrolo[1,2-a]quinazolin-5(1H)-one (**31**).* 5-Chloro-2-(4-chlorobutanamido)benzamide **30** (463 mg and 1.68 mmol) was cyclized according to general procedure C. Purification by flash column chromatography (SiO_2, CH_2Cl_2/MeOH 95:5) provided 7-chloro-2,3-dihydropyrrolo-[1,2-*a*]quinazolin-5(1*H*)-one **31** (73 mg, 0.33 mmol, and

https://doi.org/10.1021/acsomega.1c01555
ACS Omega 2021, 6, 21327−21338

20%) as a beige solid. Spectral data are consistent with literature values.[32] ^{1}H NMR (300 MHz, $CDCl_3$) δ 8.19 (d, J = 2.4 Hz, 1H), 7.63 (dd, J = 8.7, 2.4 Hz, 1H), 7.15 (d, J = 8.8 Hz, 1H), 4.24 (t, J = 7.4 Hz, 2H), 3.20 (t, J = 8.1 Hz, 2H), 2.42 (quint, J = 7.8 Hz, 2H).

(E)-7-Chloro-3-(2-ethylbutylidene)-2,3-dihydropyrrolo-[1,2-a]quinazolin-5(1H)-one (7). 7-Chloro-2,3-dihydropyrrolo[1,2-*a*]quinazolin-5(1*H*)-one **31** (73 mg and 0.33 mmol) and 2-ethylbutanal (45 μL and 0.36 mmol) were reacted according to general procedure D. Purification by flash column chromatography (SiO_2, CH_2Cl_2/MeOH 96:4) provided **7** (61 mg, 0.20 mmol, and 61%) as a beige solid. Spectral data are consistent with literature values.[32] ^{1}H NMR (300 MHz, $CDCl_3$) δ 8.19 (d, J = 2.4 Hz, 1H), 7.56 (dd, J = 8.7, 2.4 Hz, 1H), 7.13 (d, J = 8.7 Hz, 1H), 6.89 (dt, J = 10.8, 2.7 Hz, 1H), 4.19 (dd, J = 7.9, 6.7 Hz, 2H), 3.02 (ddd, J = 8.0, 6.6, 2.8 Hz, 2H), 2.25−2.08 (m, 1H), 1.63−1.47 (m, 2H), 1.45−1.28 (m, 2H), 0.85 (t, J = 7.4 Hz, 6H); ^{13}C NMR (75 MHz, $CDCl_3$) δ 169.32, 160.40, 143.08, 137.32, 133.86, 131.82, 131.03, 128.25, 120.73, 116.17, 45.99, 44.27, 27.58, 23.06, 12.05; HRMS (ESI) calcd for $[C_{17}H_{19}ClN_2O + H]^+$: 303.12587, found 303.12598; HPLC purity: >99%.

2-Amino-4-chlorobenzamide (32). 2-Amino-4-chlorobenzonitrile (500 mg and 3.28 mmol) was hydrolyzed in 6 mL of nanopure water according to general procedure A. Purification by flash column chromatography (SiO_2, hexanes/EtOAc 50:50 to 0:100) provided 2-amino-4-chlorobenzamide **32** (400 mg, 2.34 mmol, and 71%) as a beige solid. ^{1}H NMR (300 MHz, methanol-d_4) δ 7.47 (d, J = 8.5 Hz, 1H), 6.74 (d, J = 2.1 Hz, 1H), 6.54 (dd, J = 8.5, 2.1 Hz, 1H); ^{13}C NMR (75 MHz, DMSO-d_6) δ 169.91, 140.83, 136.62, 130.30, 122.11, 119.43, 117.96.

4-Chloro-2-(4-chlorobutanamido)benzamide (33). 2-Amino-4-chlorobenzamide **32** (400 mg and 2.35 mmol) and 4-chlorobutanoyl chloride (0.316 mL and 2.82 mmol) were reacted according to general procedure B. Purification by flash column chromatography (SiO_2, hexanes/EtOAc 60/40 to 30/70) provided 4-chloro-2-(4-chlorobutanamido)benzamide **33** (357 mg, 1.30 mmol, and 55%) as a beige solid. ^{1}H NMR (300 MHz, $CDCl_3$) δ 11.36 (s(br), 1H), 8.76 (d, J = 2.1 Hz, 1H), 7.44 (d, J = 8.5 Hz, 1H), 7.06 (dd, J = 8.4, 2.1 Hz, 1H), 6.06 (s(br), 1H), 5.77 (s(br), 1H), 3.65 (t, J = 6.3 Hz, 2H), 2.61 (t, J = 7.2 Hz, 2H), 2.20 (quint, J = 6.7 Hz, 2H); ^{13}C NMR (151 MHz, $CDCl_3$) δ 171.01, 170.58, 141.41, 139.83, 128.38, 122.93, 121.54, 116.43, 44.35, 35.08, 27.98.

8-Chloro-2,3-dihydropyrrolo[1,2-a]quinazolin-5(1H)-one (34). 4-Chloro-2-(4-chlorobutanamido)benzamide **33** (346 mg and 1.26 mmol) was cyclized according to general procedure C. Purification by flash column chromatography (SiO_2, CH_2Cl_2/MeOH 95:5) provided 8-chloro-2,3-dihydropyrrolo-[1,2-*a*]quinazolin-5(1*H*)-one **34** (80 mg, 0.36 mmol, and 29%) as a beige solid. ^{1}H NMR (300 MHz, $CDCl_3$) δ 8.06 (d, J = 8.5 Hz, 1H), 7.28 (dd, J = 8.5, 1.9 Hz, 1H), 7.11 (d, J = 1.9 Hz, 1H), 4.17 (t, J = 7.4 Hz, 2H), 3.14 (t, J = 8.1 Hz, 2H), 2.39 (quint, J = 7.8 Hz, 2H); ^{13}C NMR (75 MHz, $CDCl_3$) δ 169.36, 167.26, 140.02, 139.43, 130.35, 126.38, 116.94, 114.70, 48.95, 32.87, 18.70.

(E)-8-Chloro-3-(2-ethylbutylidene)-2,3-dihydropyrrolo-[1,2-a]quinazolin-5(1H)-one (8). 8-Chloro-2,3-dihydropyrrolo[1,2-*a*]quinazolin-5(1*H*)-one **34** (80 mg and 0.36 mmol) and 2-ethylbutanal (49 μL and 0.40 mmol) were reacted according to general procedure D. Purification by flash column chromatography (SiO_2, CH_2Cl_2/MeOH 96:4) provided **8** (107 mg, 0.353 mmol, and 98%) as a beige solid. ^{1}H NMR (300 MHz, $CDCl_3$) δ 8.29 (d, J = 8.5 Hz, 1H), 7.41 (dd, J = 8.5, 1.9 Hz, 1H), 7.22 (d, J = 1.9 Hz, 1H), 7.00 (dt, J = 10.8, 2.7 Hz, 1H), 4.19 (dd, J = 8.0, 6.8 Hz, 2H), 3.06 (ddd, J = 9.6, 6.8, 2.8 Hz, 2H), 2.27−2.12 (m, 1H), 1.65−1.51 (m, 2H), 1.49−1.32 (m, 2H), 0.89 (t, J = 7.4 Hz, 6H); ^{13}C NMR (75 MHz, CDCl3) δ 169.76, 160.79, 143.46, 140.03, 139.84, 130.96, 130.69, 126.64, 118.20, 114.37, 45.96, 44.41, 27.65, 23.15, 12.11; HRMS (ESI) calcd for $[C_{17}H_{19}ClN_2O + H]^+$: 303.12587, found 303.12559, calcd for $[C_{17}H_{19}ClN_2O + Na]^+$: 325.10781, found 325.10818; HPLC purity: >99%.

6-Amino-2,3-dichlorobenzamide (35). 6-Amino-2,3-dichlorobenzonitrile (500 mg and 2.67 mmol) was hydrolyzed in 4.5 mL of nanopure water according to general procedure A to afford 6-amino-2,3-dichlorobenzamide **35** (547 mg, 2.67 mmol, quant.) as a beige powder. Compound was used in the next step without further purification. ^{1}H NMR (300 MHz, DMSO-d_6) δ 7.92 (s(br), 1H), 7.66 (s(br), 1H), 7.23 (d, J = 8.8 Hz, 1H), 6.66 (d, J = 8.8 Hz, 1H), 5.30 (s, 2H); ^{13}C NMR (75 MHz, DMSO-d_6) δ 166.83, 145.51, 129.96, 127.74, 123.50, 117.25, 115.00.

2,3-Dichloro-6-(4-chlorobutanamido)benzamide (36). 6-Amino-2,3-dichlorobenzamide **35** (499 mg and 2.43 mmol) and 4-chlorobutanoyl chloride (0.327 mL and 2.92 mmol) were reacted according to general procedure B. Purification by flash column chromatography (SiO_2, hexanes/EtOAc 60/40 to 30/70) provided 2,3-dichloro-6-(4-chlorobutanamido)-benzamide **36** (269 mg, 0.869 mmol, and 36%) as a white solid. ^{1}H NMR (300 MHz, $CDCl_3$) δ 8.88 (s(br), 1H), 8.13 (d, J = 9.0 Hz, 1H), 7.50 (d, J = 9.0 Hz, 1H), 6.21 (s(br), 1H), 6.14 (s(br), 1H), 3.64 (t, J = 6.2 Hz, 2H), 2.56 (t, J = 7.2 Hz, 2H), 2.17 (quint, J = 6.6 Hz, 2H); ^{13}C NMR (75 MHz, DMSO-d_6) δ 171.34, 165.66, 134.51, 134.03, 129.92, 128.12, 127.98, 125.84, 44.94, 33.08, 28.25.

6,7-Dichloro-2,3-dihydropyrrolo[1,2-a]quinazolin-5(1H)-one (37). 2,3-Dichloro-6-(4-chlorobutanamido)benzamide **36** (94 mg and 0.30 mmol) was cyclized according to general procedure C. Purification by flash column chromatography (SiO_2, CH_2Cl_2/MeOH 95:5) provided 6,7-dichloro-2,3-dihydropyrrolo[1,2-*a*]quinazolin-5(1*H*)-one **37** (21 mg, 0.082 mmol, and 27%) as a beige solid. ^{1}H NMR (300 MHz, DMSO-d_6) δ 7.96 (d, J = 9.0 Hz, 1H), 7.45 (d, J = 9.0 Hz, 1H), 4.19 (t, J = 7.3 Hz, 2H), 3.00 (t, J = 8.0 Hz, 2H), 2.24 (quint, J = 7.7 Hz, 2H); ^{13}C NMR (75 MHz, DMSO-d_6) δ 166.69, 166.60, 140.26, 134.50, 132.00, 130.10, 116.86, 116.73, 49.92, 32.47, 18.51.

(E)-6,7-Dichloro-3-(2-ethylbutylidene)-2,3-dihydropyrrolo-[1,2-a]quinazolin-5(1H)-one (9). 6,7-Dichloro-2,3-dihydropyrrolo[1,2-*a*]qui]]nazolin-5(1*H*)-one **37** (21 mg and 0.082 mmol) and 2-ethylbutanal (11 μL and 0.089 mmol) were reacted according to general procedure D. Purification by flash column chromatography (SiO_2, CH_2Cl_2/MeOH 96:4) provided **9** (14 mg, 0.042 mmol, and 51%) as a beige solid. ^{1}H NMR (300 MHz, $CDCl_3$) δ 7.66 (d, J = 8.9 Hz, 1H), 7.04 (d, J = 8.9 Hz, 1H), 6.90 (dt, J = 10.8, 2.7 Hz, 1H), 4.18 (dd, J = 8.0, 6.8 Hz, 2H), 3.03 (ddd, J = 8.0, 6.7, 2.8 Hz, 2H), 2.26−2.11 (m, 1H), 1.66−1.50 (m, 2H), 1.48−1.31 (m, 2H), 0.88 (t, J = 7.4 Hz, 6H); ^{13}C NMR (75 MHz, $CDCl_3$) δ 159.35, 146.35, 143.42, 139.53, 134.20, 134.05, 131.88, 130.62, 117.89, 113.87, 46.51, 44.47, 27.66, 23.01, 12.16; HRMS (ESI) calcd for $[C_{17}H_{18}Cl_2N_2O + H]^+$: 337.08690, found 337.08631, calcd for $[C_{17}H_{18}Cl_2N_2O + Na]^+$: 359.06884, found 359.06781; HPLC purity: >99%.

https://doi.org/10.1021/acsomega.1c01555
ACS Omega 2021, 6, 21327−21338

*2-Amino-5-methoxybenzamide (**38**).* 2-Amino-5-methoxybenzonitrile (500 mg and 3.37 mmol) was hydrolyzed in 6 mL of nanopure water according to general procedure A. Purification by flash column chromatography (SiO_2, hexanes/EtOAc 50:50 to 0:100) provided 2-amino-5-methoxybenzamide **38** (385 mg, 2.32 mmol, and 69%) as a beige solid. Spectral data are consistent with literature values.[32] ^{1}H NMR (300 MHz, methanol-d_4) δ 7.09 (d, J = 2.9 Hz, 1H), 6.89 (dd, J = 8.9, 2.9 Hz, 1H), 6.73 (d, J = 8.9 Hz, 1H), 3.74 (s, 3H).

*2-(4-Chlorobutanamido)-5-methoxybenzamide (**39**).* 2-Amino-5-methoxybenzamide **38** (245 mg and 1.47 mmol) and 4-chlorobutanoyl chloride (0.197 mL and 1.76 mmol) were reacted according to general procedure B. Purification by flash column chromatography (SiO_2, hexanes/EtOAc 60/40 to 30/70) provided 2-(4-chlorobutanamido)-5-methoxybenzamide **39** (396 mg, 1.46 mmol, and 99%) as a beige solid. Spectral data are consistent with literature values.[32] ^{1}H NMR (300 MHz, $CDCl_3$) δ 10.76 (s(br), 1H), 8.50 (d, J = 9.0 Hz, 1H), 7.08−7.01 (m, 2H), 6.17 (s(br), 1H), 5.72 (s(br), 1H), 3.82 (s, 3H), 3.65 (t, J = 6.3 Hz, 2H), 2.57 (t, J = 7.2 Hz, 2H), 2.19 (quint, J = 6.7 Hz, 2H).

*7-Methoxy-2,3-dihydropyrrolo[1,2-a]quinazolin-5(1H)-one (**40**).* 2-(4-Chlorobutanamido)-5-methoxybenzamide **39** (396 mg and 1.46 mmol) was cyclized according to general procedure C. Purification by flash column chromatography (SiO_2, CH_2Cl_2/MeOH 95:5) provided 7-methoxy-2,3-dihydropyrrolo[1,2-*a*]quinazolin-5(1*H*)-one **40** (217 mg, 1.00 mmol, and 68%) as a beige solid. Spectral data are consistent with literature values.[32] ^{1}H NMR (300 MHz, $CDCl_3$) δ 7.57 (d, J = 2.9 Hz, 1H), 7.21 (dd, J = 9.0, 2.9 Hz, 1H), 7.09 (d, J = 9.0 Hz, 1H), 4.20 (t, J = 7.3 Hz, 2H), 3.83 (s, 3H), 3.12 (t, J = 8.0 Hz, 2H), 2.36 (quint, J = 8.1 Hz, 2H).

*(E)-3-(2-Ethylbutylidene)-7-methoxy-2,3-dihydropyrrolo-[1,2-a]quinazolin-5(1H)-one (**10**).* 7-Methoxy-2,3-dihydropyrrolo[1,2-*a*]quinazolin-5(1*H*)-one **40** (111 mg and 0.513 mmol) and 2-ethylbutanal (69 μL and 0.56 mmol) were reacted according to general procedure D. Purification by flash column chromatography (SiO_2, CH_2Cl_2/MeOH 96:4) provided **10** (123 mg, 0.412 mmol, and 80%) as a beige solid. ^{1}H NMR (300 MHz, $CDCl_3$) δ 7.60 (d, J = 2.8 Hz, 1H), 7.13 (dd, J = 8.9, 2.8 Hz, 1H), 7.06 (d, J = 8.9 Hz, 1H), 6.78 (dt, J = 10.8, 2.7 Hz, 1H), 4.12 (dd, J = 7.8, 6.6 Hz, 2H), 3.77 (s, 3H), 2.93 (ddd, J = 8.0, 6.6, 2.7 Hz, 2H), 2.17−2.02 (m, 1H), 1.57−1.37 (m, 2H), 1.37−1.19 (m, 2H), 0.78 (t, J = 7.4 Hz, 6H); ^{13}C NMR (75 MHz, CDCl3) δ 170.32, 158.90, 157.75, 141.14, 132.94, 131.27, 123.16, 120.82, 115.96, 108.65, 55.74, 45.84, 43.93, 27.46, 22.94, 11.85; HRMS (ESI) calcd for $[C_{18}H_{22}N_2O_2 + H]^+$: 299.17540, found 299.17538; HPLC purity: >99%.

*2-Amino-4-methoxybenzamide (**41**).* 2-Amino-4-methoxybenzonitrile (500 mg and 3.37 mmol) was hydrolyzed in 6 mL of nanopure water according to general procedure A. Purification by flash column chromatography (SiO_2, hexanes/EtOAc 50:50 to 0:100) provided 2-amino-4-methoxybenzamide **41** (133 mg, 0.800 mmol, and 24%) as a beige solid. ^{1}H NMR (300 MHz, DMSO-d_6) δ 7.48 (d, J = 8.8 Hz, 1H), 6.73 (s, 2H), 6.19 (d, J = 2.6 Hz, 1H), 6.06 (dd, J = 8.8, 2.6 Hz, 1H), 3.69 (s, 3H); ^{13}C NMR (75 MHz, DMSO-d_6) δ 170.99, 162.18, 152.42, 130.47, 106.85, 102.11, 99.28, 54.77.

*2-(4-Chlorobutanamido)-4-methoxybenzamide (**42**).* 2-Amino-4-methoxybenzamide **41** (133 mg and 0.800 mmol) and 4-chlorobutanoyl chloride (0.11 mL and 0.98 mmol) were reacted according to general procedure B. Purification by flash column chromatography (SiO_2, hexanes/EtOAc 60/40 to 30/70) provided 2-(4-chlorobutanamido)-4-methoxybenzamide **42** (180 mg, 0.665 mmol, and 83%) as a beige solid. ^{1}H NMR (300 MHz, $CDCl_3$) δ 11.71 (s(br), 1H), 8.35 (d, J = 2.6 Hz, 1H), 7.44 (d, J = 8.8 Hz, 1H), 6.59 (dd, J = 8.8, 2.6 Hz, 1H), 6.02 (s(br), 2H), 3.85 (s, 3H), 3.65 (t, J = 6.3 Hz, 2H), 2.61 (t, J = 7.2 Hz, 2H), 2.20 (quint, J = 6.7 Hz, 3H); ^{13}C NMR (75 MHz, $CDCl_3$) δ 171.50, 171.18, 163.70, 142.85, 128.96, 110.21, 109.98, 105.10, 55.67, 44.39, 35.29, 28.08.

*8-Methoxy-2,3-dihydropyrrolo[1,2-a]quinazolin-5(1H)-one (**43**).* 2-(4-Chlorobutanamido)-4-methoxybenzamide **42** (180 mg and 0.665 mmol) was cyclized according to general procedure C. Purification by flash column chromatography (SiO_2, CH_2Cl_2/MeOH 95:5) provided 8-methoxy-2,3-dihydropyrrolo[1,2-*a*]quinazolin-5(1*H*)-one **43** (64 mg, 0.30 mmol, and 45%) as a beige solid. ^{1}H NMR (600 MHz, $CDCl_3$) δ 8.04 (d, J = 8.8 Hz, 1H), 6.85 (dd, J = 8.9, 2.3 Hz, 1H), 6.40 (d, J = 2.3 Hz, 1H), 4.09 (t, J = 7.4 Hz, 2H), 3.85 (s, 3H), 3.10−3.04 (m, 2H), 2.33 (quint, J = 7.8 Hz, 2H); ^{13}C NMR (151 MHz, $CDCl_3$) δ 169.86, 166.44, 163.82, 140.35, 130.40, 113.67, 112.21, 97.85, 55.83, 48.79, 32.74, 18.57.

*(E)-3-(2-Ethylbutylidene)-8-methoxy-2,3-dihydropyrrolo-[1,2-a]quinazolin-5(1H)-one (**11**).* 8-Methoxy-2,3-dihydropyrrolo[1,2-*a*]quinazolin-5(1*H*)-one **43** (64 mg and 0.30 mmol) and 2-ethylbutanal (39 μL and 0.32 mmol) were reacted according to general procedure D. Purification by flash column chromatography (SiO_2, CH_2Cl_2/MeOH 96:4) provided **11** (43 mg, 0.14 mmol, and 47%) as a beige solid. ^{1}H NMR (300 MHz, $CDCl_3$) δ 8.14 (d, J = 8.9 Hz, 1H), 6.91−6.81 (m, 2H), 6.45 (d, J = 2.3 Hz, 1H), 4.08 (dd, J = 8.0, 6.7 Hz, 2H), 3.86 (s, 3H), 2.97 (ddd, J = 8.0, 6.6, 2.7 Hz, 2H), 2.22−2.07 (m, 1H), 1.60−1.45 (m, 2H), 1.43−1.26 (m, 2H), 0.84 (t, J = 7.4 Hz, 6H); ^{13}C NMR (75 MHz, $CDCl_3$) δ 170.23, 163.82, 160.15, 141.94, 140.59, 131.29, 130.49, 113.66, 113.32, 97.60, 55.85, 45.76, 44.11, 27.56, 23.02, 11.99; HRMS (ESI) calcd for $[C_{18}H_{22}N_2O_2 + H]^+$: 299.17540, found 299.17565; HPLC purity: >99%.

*(E)-3-(2-Ethylbutylidene)-7-hydroxy-2,3-dihydropyrrolo-[1,2-a]quinazolin-5(1H)-one (**12**).* A solution of the methoxy substrate **10** (40 mg, 0.13 mmol, and 1 equiv) in dry CH_2Cl_2 (2.7 mL) was cooled to 0 °C. Boron tribromide 1 M in CH_2Cl_2 (1.3 mL, 1.3 mmol, and 10 equiv) was added dropwise to the stirred reaction mixture. The reaction was stirred at room temperature for 24 h. The mixture was then diluted with CH_2Cl_2 and a saturated aqueous solution of $NaHCO_3$. The aqueous phase was extracted with CH_2Cl_2, and the combined organic phases were dried over Na_2SO_4, filtered, and evaporated under vacuum. The crude residue was purified by flash column chromatography (SiO_2, CH_2Cl_2/MeOH 95:5) to give the title compound **12** (36 mg, 0.13 mmol, quant.) as a yellow solid. ^{1}H NMR (300 MHz, methanol-d_4) δ 7.57 (d, J = 1.5 Hz, 1H), 7.55 (d, J = 4.5 Hz, 1H), 7.38 (dd, J = 9.0, 2.7 Hz, 1H), 6.84 (dt, J = 10.6, 2.6 Hz, 1H), 4.53−4.43 (m, 2H), 3.15 (td, J = 7.5, 7.0, 2.7 Hz, 2H), 2.41−2.23 (m, 1H), 1.72−1.58 (m, 2H), 1.54−1.37 (m, 2H), 0.95 (t, J = 7.4 Hz, 6H); ^{13}C NMR (75 MHz, methanol-d_4) δ 165.95, 159.20, 157.80, 145.40, 132.41, 132.04, 125.48, 122.23, 119.85, 112.72, 45.57, 28.54, 24.37, 12.24; HRMS (ESI) calcd for $[C_{17}H_{20}N_2O_2 + H]^+$: 285.15975, found 285.16012, calcd for $[C_{17}H_{20}N_2O_2 + Na]^+$: 307.1417, found 307.1417; HPLC purity: >99%.

*(E)-3-(2-Ethylbutylidene)-8-hydroxy-2,3-dihydropyrrolo-[1,2-a]quinazolin-5(1H)-one (**13**).* A solution of the methoxy substrate **11** (38 mg, 0.13 mmol, and 1 equiv) in dry CH_2Cl_2

https://doi.org/10.1021/acsomega.1c01555
ACS Omega 2021, 6, 21327−21338

(2.7 mL) was cooled to 0 °C. Boron tribromide 1 M in CH_2Cl_2 (1.3 mL, 1.3 mmol, and 10 equiv) was added dropwise to the stirred reaction mixture. The reaction was stirred at room temperature for 24 h. The mixture was then diluted with CH_2Cl_2 and a saturated aqueous solution of $NaHCO_3$. The aqueous phase was extracted with CH_2Cl_2, and the combined organic phases were dried over Na_2SO_4, filtered, and evaporated under vacuum. The crude residue was purified by flash column chromatography (SiO_2, CH_2Cl_2/MeOH 95:5) to give the title compound **13** (7.8 mg, 0.027 mmol, and 21%) as a yellow solid. ^{1}H NMR (300 MHz, methanol-d_4) δ 8.06 (d, J = 8.8 Hz, 1H), 6.99 (dd, J = 8.8, 2.2 Hz, 1H), 6.80−6.73 (m, 2H), 4.33−4.25 (m, 2H), 3.09 (td, J = 7.5, 2.8 Hz, 2H), 2.39−2.20 (m, 1H), 1.70−1.56 (m, 2H), 1.51−1.35 (m, 2H), 0.94 (t, J = 7.4 Hz, 6H); ^{13}C NMR (151 MHz, methanol-d_4) δ 172.95, 164.81, 161.92, 142.63, 142.56, 133.95, 131.04, 116.97, 112.99, 101.04, 47.53, 45.21, 28.71, 24.17, 12.29; HRMS (ESI) calcd for $[C_{17}H_{20}N_2O_2 + H]^+$: 285.15975, found 285.15902, calcd for $[C_{17}H_{20}N_2O_2 + Na]^+$: 307.1417, found 307.14081; HPLC purity: 98%.

*(E)-6-Chloro-3-(2-methylbutylidene)-2,3-dihydropyrrolo-[1,2-a]quinazolin-5(1H)-one (**14**).* 6-Chloro-2,3-dihydropyrrolo[1,2-*a*]quinazolin-5(1*H*)-one **28** (66 mg and 0.30 mmol) and 2-methylbutanal (35 μL and 0.33 mmol) were reacted according to general procedure D. Purification by flash column chromatography (SiO_2, CH_2Cl_2/MeOH 96:4) provided **14** (50 mg, 0.17 mmol, 57%) as a white solid. ^{1}H NMR (300 MHz, $CDCl_3$) δ 7.42 (t, J = 8.1 Hz, 1H), 7.27−7.23 (dd, J = 7.9, 0.7 HZ, 1H), 7.02 (dd, J = 8.2 Hz, 0.7 Hz, 1H), 6.84 (dt, J = 10.3, 2.7 Hz, 1H), 4.12 (t, J = 7.3 Hz, 2H), 3.02−2.92 (m, 2H), 2.39−2.26 (m, 1H), 1.50−1.33 (m, 2H), 1.04 (d, J = 6.7 Hz, 3H), 0.86 (t, J = 7.4 Hz, 3H); ^{13}C NMR (75 MHz, $CDCl_3$) δ 168.01, 159.43, 143.42, 141.00, 135.77, 132.92, 129.66, 128.59, 116.35, 113.45, 46.46, 36.68, 29.52, 22.56, 19.48, 12.04; HRMS (ESI) calcd for $[C_{16}H_{17}ClN_2O + H]^+$: 289.11022, found 289.1108; HPLC purity: >99%.

*(E)-3-Butylidene-6-chloro-2,3-dihydropyrrolo[1,2-a]-quinazolin-5(1H)-one (**15**).* 6-Chloro-2,3-dihydropyrrolo[1,2-*a*]quinazolin-5(1*H*)-one **28** (75 mg and 0.34 mmol) and butyraldehyde (33 μL and 0.37 mmol) were reacted according to general procedure D. Purification by flash column chromatography (SiO_2, CH_2Cl_2/MeOH 96:4) provided **15** (11 mg, 0.040 mmol, and 12%) as a white solid. ^{1}H NMR (300 MHz, $CDCl_3$) δ 7.46 (t, J = 8.1 Hz, 1H), 7.29 (dd, J = 7.9, 0.7 Hz, 1H), 7.06 (dd, J = 8.2, 0.7 Hz, 1H), 7.03−6.96 (m, 1H), 4.20−4.13 (m, 2H), 2.99 (t, J = 6.1 Hz, 2H), 2.21 (q, J = 7.4 Hz, 2H), 1.53 (sext, J = 7.3 Hz, 2H), 0.96 (t, J = 7.4 Hz, 3H); ^{13}C NMR (75 MHz, $CDCl_3$) δ 168.19, 159.42, 141.06, 138.39, 136.08, 133.10, 130.95, 128.87, 116.41, 113.56, 46.65, 32.09, 22.72, 21.78, 14.07; HRMS (ESI) calcd for $[C_{15}H_{15}ClN_2O + H]^+$: 275.09457, found 275.09405, calcd for $[C_{15}H_{15}ClN_2O + Na]^+$: 297.07651, found 297.07538; HPLC purity: >99%.

*(E)-6-Chloro-3-propylidene-2,3-dihydropyrrolo[1,2-a]-quinazolin-5(1H)-one (**16**).* 6-Chloro-2,3-dihydropyrrolo[1,2-*a*]quinazolin-5(1*H*)-one **28** (75 mg and 0.34 mmol) and propionaldehyde (28 μL and 0.37 mmol) were reacted according to general procedure D. Purification by flash column chromatography (SiO_2, CH_2Cl_2/MeOH 96:4) provided **16** (0.6 mg, 0.002 mmol, and 1%) as a white solid. ^{1}H NMR (300 MHz, $CDCl_3$) δ 7.55 (t, J = 8.1 Hz, 1H), 7.44 (d, J = 7.5 Hz, 1H), 7.22−7.15 (m, 1H), 7.11 (d, J = 7.3 Hz, 1H), 4.20 (t, J = 6.8 Hz, 2H), 3.09−2.96 (m, 2H), 2.37−2.21 (m, 2H), 1.13 (t, J = 7.5 Hz, 3H); HRMS (ESI) calcd for $[C_{14}H_{13}ClN_2O + H]^+$: 261.07892, found 261.07797; HPLC purity: 98%.

*(E)-6-Chloro-3-(2,2-dimethylpropylidene)-2,3-dihydropyrrolo[1,2-a]quinazolin-5(1H)-one (**17**).* 6-Chloro-2,3-dihydropyrrolo[1,2-*a*]quinazolin-5(1*H*)-one **28** (75 mg and 0.34 mmol) and pivalaldehyde (40 μL and 0.37 mmol) were reacted according to general procedure D. Purification by flash column chromatography (SiO_2, CH_2Cl_2/MeOH 96:4) provided **17** (17 mg, 0.059 mmol, and 17%) as a beige solid. ^{1}H NMR (300 MHz, $CDCl_3$) δ 7.46 (t, J = 8.1 Hz, 1H), 7.33 (dd, J = 7.9, 1.0 Hz, 1H), 7.12 (t, J = 2.7 Hz, 1H), 7.05 (dd, J = 8.2, 1.0 Hz, 1H), 4.17−4.07 (m, 2H), 3.16 (td, J = 7.4, 7.0, 2.8 Hz, 2H), 1.21 (s, 9H); ^{13}C NMR (75 MHz, $CDCl_3$) δ 168.05, 160.72, 147.36, 141.06, 136.09, 132.93, 128.79, 127.18, 116.64, 113.40, 46.70, 34.30, 29.65, 23.19; HRMS (ESI) calcd for $[C_{16}H_{17}ClN_2O + H]^+$: 289.11022, found 289.10894, calcd for $[C_{16}H_{17}ClN_2O + Na]^+$: 311.09216, found 311.09099; HPLC purity: >99%.

*(E)-6-Chloro-3-(2,2-dimethylpropylidene)-2,3-dihydropyrrolo[1,2-a]quinazolin-5(1H)-one (**18**).* 6-Chloro-2,3-dihydropyrrolo[1,2-*a*]quinazolin-5(1*H*)-one **28** (75 mg and 0.34 mmol) and 3-methylbutanal (40 μL and 0.37 mmol) were reacted according to general procedure D. Purification by flash column chromatography (SiO_2, CH_2Cl_2/MeOH 96:4) provided **18** (5 mg, 0.02 mmol, and 5%) as a beige solid. ^{1}H NMR (300 MHz, $CDCl_3$) δ 7.50 (t, J = 8.1 Hz, 1H), 7.37 (d, J = 7.8 Hz, 1H), 7.12 (dt, J = 8.3, 2.5 Hz, 2H), 7.07 (d, J = 8.1 Hz, 1H), 4.21−4.11 (m, 2H), 2.99 (t, J = 6.2 Hz, 2H), 2.14 (t, J = 7.2 Hz, 2H), 1.94 − 1.75 (m, 1H), 0.97 (d, J = 6.6 Hz, 6H); HRMS (ESI) calcd for $[C_{16}H_{17}ClN_2O + H]^+$: 289.11022, found 289.10879, calcd for $[C_{16}H_{17}ClN_2O + Na]^+$: 311.09216, found 311.09085; HPLC purity: 97%.

*(E)-6-Chloro-3-(3,3-dimethylbutylidene)-2,3-dihydropyrrolo[1,2-a]quinazolin-5(1H)-one (**19**).* 6-Chloro-2,3-dihydropyrrolo[1,2-*a*]quinazolin-5(1*H*)-one **28** (70 mg and 0.32 mmol) and 3,3-dimethylbutanal (44 μL and 0.35 mmol) were reacted according to general procedure D. Purification by flash column chromatography (SiO_2, CH_2Cl_2/MeOH 96:4) provided **19** (10 mg, 0.033 mmol, and 10%) as a beige solid. ^{1}H NMR (300 MHz, $CDCl_3$) δ 7.51 (t, J = 8.1 Hz, 1H), 7.39 (dd, J = 7.9, 1.0 Hz, 1H), 7.23−7.14 (m, 1H), 7.08 (dd, J = 8.2, 1.0 Hz, 1H), 4.21−4.11 (m, 2H), 3.00 (t, J = 6.0 Hz, 2H), 2.15 (d, J = 7.9 Hz, 2H), 0.99 (s, 9H); ^{13}C NMR (75 MHz, $CDCl_3$) δ 168.16, 159.14, 141.02, 135.84, 132.96, 132.22, 128.64, 116.34, 113.49, 113.42, 46.44, 44.30, 32.31, 29.57, 22.86; HRMS (ESI) calcd for $[C_{17}H_{19}ClN_2O + H]^+$: 303.12587, found 303.12722, calcd for $[C_{17}H_{19}ClN_2O + Na]^+$: 325.10781, found 325.10619; HPLC purity: >99%.

*(E)-3-Benzylidene-6-chloro-2,3-dihydropyrrolo[1,2-a]-quinazolin-5(1H)-one (**20**).* 6-Chloro-2,3-dihydropyrrolo[1,2-*a*]quinazolin-5(1*H*)-one **28** (75 mg and 0.34 mmol) and benzaldehyde (38 μL and 0.37 mmol) were reacted according to general procedure D. Purification by flash column chromatography (SiO_2, CH_2Cl_2/MeOH 96:4) provided **20** (2 mg, 0.006 mmol, and 2%) as a white solid. ^{1}H NMR (300 MHz, $CDCl_3$) δ 8.02 (t, J = 2.6 Hz, 1H), 7.58−7.51 (m, 3H), 7.48−7.37 (m, 4H), 7.14 (dd, J = 8.2, 0.9 Hz, 1H), 4.34−4.26 (m, 2H), 3.42 (td, J = 7.7, 2.7 Hz, 2H); HRMS (ESI) calcd for $[C_{18}H_{13}ClN_2O + H]^+$: 309.07892, found 309.07753, calcd for $[C_{18}H_{13}ClN_2O + Na]^+$: 331.06086, found 331.05951; HPLC purity: 97%.

*2-Chloro-6-(5-chloropentanamido)benzamide (**44**).* 2-Amino-6-chlorobenzamide **26** (2.18 g and 12.8 mmol) and

https://doi.org/10.1021/acsomega.1c01555
ACS Omega 2021, 6, 21327−21338

5-chloropentanoyl chloride (1.97 mL and 15.3 mmol) were reacted according to general procedure B. Purification by flash column chromatography (SiO_2, hexanes/EtOAc 60/40 to 30/70) provided 2-chloro-6-(5-chloropentanamido)benzamide **44** (2.70 g, 9.3 mmol, and 73%) as a beige solid. Spectral data are consistent with literature values.[32] ^{1}H NMR (300 MHz, $CDCl_3$) δ 9.32 (s(br), 1H), 8.23 (dd, J = 8.4, 1.1 Hz, 1H), 7.34 (t, J = 8.2 Hz, 1H), 7.16 (dd, J = 8.1, 1.1 Hz, 1H), 6.31 (s(br), 1H), 6.12 (s(br), 1H), 3.57 (td, J = 5.6, 4.9, 2.8 Hz, 2H), 2.41 (td, J = 6.5, 5.4, 3.1 Hz, 2H), 1.90−1.83 (m, 4H).

*7-Chloro-1,2,3,4-tetrahydro-6H-pyrido[1,2-a]quinazolin-6-one (**45**).* 2-Chloro-6-(5-chloropentanamido)benzamide **44** (655 mg and 2.27 mmol) was cyclized according to general procedure C. Purification by flash column chromatography (SiO_2, CH_2Cl_2/MeOH 95:5) provided 7-chloro-1,2,3,4-tetrahydro-6*H*-pyrido[1,2-*a*]quinazolin-6-one **45** (237 mg, 1.01 mmol, and 44%) as a beige solid. Spectral data are consistent with literature values.[32] ^{1}H NMR (300 MHz, $CDCl_3$) δ 7.25 (dd, J = 8.6, 7.8 Hz, 1H), 7.12 (dd, J = 8.7, 1.1 Hz, 1H), 7.04 (dd, J = 7.8, 1.0 Hz, 1H), 3.80 (t, J = 6.2 Hz, 2H), 2.74 (t, J = 6.6 Hz, 2H), 2.03−1.93 (m, 2H), 1.82−1.72 (m, 2H). ^{13}C NMR (75 MHz, $CDCl_3$) δ 165.59, 160.33, 142.81, 134.39, 132.25, 128.12, 116.50, 112.96, 47.06, 32.38, 22.17, 18.55.

*(E)-7-Chloro-4-(2-ethylbutylidene)-1,2,3,4-tetrahydro-6H-pyrido[1,2-a]quinazolin-6-one (**21**).* 7-Chloro-1,2,3,4-tetrahydro-6*H*-pyrido[1,2-*a*]quinazolin-6-one **45** (70 mg and 0.30 mmol) and 2-ethylbutanal (41 μL and 0.33 mmol) were reacted according to general procedure D. Purification by flash column chromatography (SiO_2, CH_2Cl_2/MeOH 96:4) provided **21** (43 mg, 0.14 mmol, and 45%) as a yellow solid. ^{1}H NMR (300 MHz, $CDCl_3$) δ 7.53−7.44 (m, 1H), 7.38−7.29 (m, 3H), 4.04−3.96 (m, 2H), 2.61 (ddd, J = 7.9, 4.3, 1.6 Hz, 2H), 2.32−2.18 (m, 1H), 2.13 (quint, J = 6.2 Hz, 2H), 1.62−1.44 (m, 2H), 1.44−1.26 (m, 2H), 0.82 (t, J = 7.4 Hz, 6H); ^{13}C NMR (75 MHz, $CDCl_3$) δ 166.56, 155.71, 147.53, 143.62, 135.35, 132.51, 128.36, 127.54, 117.89, 113.00, 47.64, 42.85, 27.74, 23.55, 22.04, 12.20; HRMS (ESI) calcd for $[C_{18}H_{21}ClN_2O + H]^+$: 317.14152, found 317.14249; HPLC purity: >99%.

*(E)-7-Chloro-4-((dimethylamino)methylene)-1,2,3,4-tetrahydro-6H-pyrido[1,2-a]quinazolin-6-one (**22**).* To a solution of 7-chloro-1,2,3,4-tetrahydro-6*H*-pyrido[1,2-*a*]quinazolin-6-one **45** (70 mg, 0.30 mmol, and 1.0 equiv) in DMF was added phosphoryl trichloride (56 μL, 0.60 mmol, and 2.0 equiv). The reaction was heated to 70 °C for 16 h, and then the solution was cooled to room temperature, diluted with CH_2Cl_2, and slowly quenched using a saturated aqueous solution of $NaHCO_3$. The aqueous layer was extracted twice with CH_2Cl_2, and the combined organic phases were dried over Na_2SO_4, filtered, and evaporated under vacuum. Purification by flash column chromatography (SiO_2, CH_2Cl_2/MeOH 98:2 to 94:6) provided **22** (46 mg, 0.16 mmol, and 53%) as a yellow solid. ^{1}H NMR (300 MHz, $CDCl_3$) δ 8.17 (s, 1H), 7.30 (t, J = 8.2 Hz, 1H), 7.17 (d, J = 7.7 Hz, 1H), 7.07 (d, J = 8.4 Hz, 1H), 3.82−3.73 (m, 2H), 3.06 (s, 6H), 2.69−2.60 (m, 2H), 1.99 (quint, J = 6.1 Hz, 2H); ^{13}C NMR (75 MHz, $CDCl_3$) δ 165.61, 158.40, 150.89, 144.18, 134.62, 131.58, 126.64, 117.36, 111.84, 94.06, 46.81, 43.67, 23.10, 22.28; HRMS (ESI) calcd for $[C_{15}H_{16}ClN_3O + H]^+$: 290.10547, found 290.10590, calcd for $[C_{15}H_{16}ClN_3O + Na]^+$: 312.08741, found 312.08816; HPLC purity: 97%.

*6-Chloro-3-(2-ethylbutyl)-2,3-dihydropyrrolo[1,2-a]-quinazolin-5(1H)-one (**23**).* A solution of substrate **3** (59 mg, 0.19 mmol, and 1.0 equiv) in MeOH was purged with argon for 30 min at room temperature before treatment with Raney nickel (41 mg, 0.70 mmol, 3.5 equiv, and pre-washed 3 times with MeOH). The reaction mixture was then purged with hydrogen before being stirred under a hydrogen atmosphere for 1 h at room temperature. The mixture was then filtered through a pad of celite, washed with MeOH, and concentrated under pressure. Purification by flash column chromatography (SiO_2, CH_2Cl_2/MeOH 98:2 to 96:4) provided **23** (8 mg, 0.03 mmol, 13%) as a white solid. ^{1}H NMR (300 MHz, $CDCl_3$) δ 7.52 (t, J = 8.1 Hz, 1H), 7.39 (dd, J = 7.9, 0.8 Hz, 1H), 7.07 (dd, J = 8.2, 0.7 Hz, 1H), 4.17 (td, J = 9.7, 9.2, 3.9 Hz, 1H), 4.04 (dt, J = 10.3, 8.0 Hz, 1H), 3.25 (dtd, J = 12.0, 8.4, 3.8 Hz, 1H), 2.55 (dtd, J = 12.5, 8.3, 3.9 Hz, 1H), 2.18−2.07 (m, 1H), 2.06−1.92 (m, 1H), 1.53−1.39 (m, 3H), 1.37−1.27 (m, 4H), 0.88 (td, J = 7.2, 5.4 Hz, 6H); ^{13}C NMR (151 MHz, $CDCl_3$) δ 168.24, 141.12, 136.64, 132.99, 128.72, 116.30, 113.29, 47.73, 41.95, 38.27, 35.97, 26.05, 26.00, 24.35, 11.10, 10.52; HRMS (ESI) calcd for $[C_{17}H_{21}ClN_2O + H]^+$: 305.14152, found 305.14167; HPLC purity: >99%.

*6′-Chloro-2-(pentan-3-yl)-1′,2′-dihydro-5′H-spiro-[cyclopropane-1,3′-pyrrolo[1,2-a]quinazolin]-5′-one (**24** = **LM146**).* A solution of trimethylsulfoxonium iodide (40 mg, 0.18 mmol, and 1.5 equiv) in dry DMSO (0.7 mL) was cooled to 0 °C. Sodium hydride 95% (5.0 mg, 0.18 mmol, and 1.5 equiv) was added to the stirred solution. The mixture was allowed to warm-up to room temperature over 1 h. A solution of substrate **3** (37 mg, 0.12 mmol, and 1.0 equiv) in dry DMSO (0.8 mL) was added dropwise to the reaction mixture, which was then stirred at 50 °C for 1 h 30 min under an argon atmosphere. The mixture was diluted with CH_2Cl_2 and quenched with a saturated aqueous solution of NH_4Cl. The aqueous phase was extracted with CH_2Cl_2 (three times). Combined organic phases were washed with brine, dried over Na_2SO_4, filtered, and evaporated under vacuum. Purification by flash column chromatography (SiO_2, CH_2Cl_2/MeOH 97:3) provided racemic **24** (**LM146**) (31 mg, 0.098 mmol, and 82%) as a white solid. ^{1}H NMR (300 MHz, $CDCl_3$) δ 7.49 (t, J = 8.1 Hz, 1H), 7.34 (dd, J = 7.9, 0.9 Hz, 1H), 7.04 (dd, J = 8.0, 0.9 Hz, 1H), 4.19 (dtd, J = 19.6, 10.2, 5.7 Hz, 2H), 2.49−2.25 (m, 2H), 1.74−1.63 (m, 2H), 1.62−1.47 (m, 2H), 1.46−1.33 (m, 2H), 0.90 (dt, J = 23.4, 7.5 Hz, 7H), 0.79 (dd, J = 6.7, 3.7 Hz, 1H); ^{13}C NMR (75 MHz, $CDCl_3$) δ 168.79, 168.36, 141.29, 136.41, 132.84, 128.32, 116.40, 112.89, 47.05, 41.48, 32.80, 28.89, 26.58, 26.10, 23.50, 22.75, 11.16, 10.96; HRMS (ESI) calcd for $[C_{18}H_{21}ClN_2O + H]^+$: 317.14152, found 317.14255, calcd for $[C_{18}H_{21}ClN_2O + Na]^+$: 339.12346, found 339.1219; HPLC purity: 93%. ^{1}H NMR analysis indicates that the material purified by flash chromatography contains traces of the starting material **3**. LM-MS analysis confirmed the presence of the starting material **3** (m/z = 303.3) and also showed traces of a compound with a m/z ratio of 317.0 that is most likely the diasteromeric product of **24**. These impurities could only be removed by reversed phase preparative HPLC using a Sunfire C18 column (19 × 100 mm, 5 um) and 25 to 55% MeCN in water (+0.01% formic acid) as the eluent (21.6 mL/min) to afford small amounts sufficient for ^{1}H NMR. **LM146** was crystallized by the solvent diffusion technique using chloroform. The X-ray structure has been deposited into the Cambridge Crystallographic Data Centre CCDC (no. 2070470).

https://doi.org/10.1021/acsomega.1c01555
ACS Omega 2021, 6, 21327−21338

■ ASSOCIATED CONTENT

Supporting Information

The Supporting Information is available free of charge at https://pubs.acs.org/doi/10.1021/acsomega.1c01555.

Experimental procedures, NMR spectra of all final analogs, X-ray analysis report of **24** (**LM146**), additional bromoSCAN traces, and bromoMAX data (PDF)

■ AUTHOR INFORMATION

Corresponding Author

Alexandre Gagnon − *Département de Chimie, Université du Québec à Montréal, Montréal, Québec H3C 3P8, Canada;* orcid.org/0000-0002-0242-0936; Phone: (514) 987-3000; Email: gagnon.alexandre@uqam.ca

Authors

Léa Mélin − *Département de Chimie, Université du Québec à Montréal, Montréal, Québec H3C 3P8, Canada*

Emily Gesner − *Zenith Epigenetics Ltd., Calgary, Alberta T3E 6L1, Canada*

Sarah Attwell − *Zenith Epigenetics Ltd., Calgary, Alberta T3E 6L1, Canada*

Olesya A. Kharenko − *Zenith Epigenetics Ltd., Calgary, Alberta T3E 6L1, Canada;* orcid.org/0000-0003-4710-3886

Edward H. van der Horst − *Zenith Epigenetics Ltd., Calgary, Alberta T3E 6L1, Canada*

Henrik C. Hansen − *Zenith Epigenetics Ltd., Calgary, Alberta T3E 6L1, Canada*

Complete contact information is available at: https://pubs.acs.org/10.1021/acsomega.1c01555

Notes

The authors declare no competing financial interest.

■ ACKNOWLEDGMENTS

We thank the Natural Sciences and Engineering Research Council of Canada (NSERC) for a Collaborative Research and Development Grant (CRD).

■ REFERENCES

(1) Shahbazian, M. D.; Grunstein, M. Functions of Site-Specific Histone Acetylation and Deacetylation. *Annu. Rev. Biochem.* **2007**, *76*, 75−100.

(2) Choudhary, C.; Kumar, C.; Gnad, F.; Nielsen, M. L.; Rehman, M.; Walther, T. C.; Olsen, J. V.; Mann, M. Lysine Acetylation Targets Protein Complexes and Co-Regulates Major Cellular Functions. *Science* **2009**, *325*, 834−840.

(3) Filippakopoulos, P.; Knapp, S. Targeting Bromodomains: Epigenetic Readers of Lysine Acetylation. *Nat. Rev. Drug Disc.* **2014**, *13*, 337−356.

(4) Zeng, L.; Zhou, M.-M. Bromodomain: An Acetyl-Lysine Binding Domain. *FEBS Lett.* **2002**, *513*, 124−128.

(5) Schiedel, M.; Moroglu, M.; Ascough, D. M. H.; Chamberlain, A. E. R.; Kamps, J. J. A. G.; Sekirnik, A. R.; Conway, S. J. Chemical Epigenetics: The Impact of Chemical and Chemical Biology Techniques on Bromodomain Target Validation. *Angew. Chem., Int. Ed.* **2019**, *58*, 17930−17952.

(6) Zhang, G.; Smith, S. G.; Zhou, M.-M. Discovery of Chemical Inhibitors of Human Bromodomains. *Chem. Rev.* **2015**, *115*, 11625−11668.

(7) Filippakopoulos, P.; Picaud, S.; Mangos, M.; Keates, T.; Lambert, J.-P.; Barsyte-Lovejoy, D.; Felletar, I.; Volkmer, R.; Müller, S.; Pawson, T.; Gingras, A.-C.; Arrowsmith, C. H.; Knapp, S. Histone Recognition and Large-Scale Structural Analysis of the Human Bromodomain Family. *Cell* **2012**, *149*, 214−231.

(8) Ruthenburg, A. J.; Li, H.; Patel, D. J.; Allis, C. D. Multivalent Engagement of Chromatin Modifications by Linked Binding Modules. *Nat. Rev. Mol. Cell Biol.* **2007**, *8*, 983−994.

(9) Wilson, B. G.; Roberts, C. W. M. SWI/SNF Nucleosome Re-Modellers and Cancer. *Nat. Rev. Cancer* **2011**, *11*, 481−492.

(10) Thompson, M. Polybromo-1: the Chromatin Targeting Subunit of the PBAF Complex. *Biochimie* **2009**, *91*, 309−319.

(11) Shain, A. H.; Pollack, J. R. The Spectrum of SWI/SNF Mutations, Ubiquitous in Human Cancers. *PLoS One* **2013**, *8*, No. e55119.

(12) Masliah-Planchon, J.; Bièche, I.; Guinebretière, J.-M.; Bourdeaut, F.; Delattre, O. SWI/SNF Chromatin Remodeling and Human Malignancies. *Annu. Rev. Pathol.* **2015**, *10*, 145−171.

(13) Hodges, C.; Kirkland, J. G.; Crabtree, G. R. The Many Roles of BAF (mSWI/SNF) and PBAF Complexes in Cancer. *Cold Spring Harb. Perspect. Med.* **2016**, *6*, a026930.

(14) Kadoch, C.; Crabtree, G. R. Mammalian SWI/SNF Chromatin Remodeling Complexes and Cancer: Mechanistic Insights Gained from Human Genomics. *Sci. Adv.* **2015**, *1*, No. e1500447.

(15) St Pierre, R.; Kadoch, C. Mammalian SWI/SNF Complexes in Cancer: Emerging Therapeutic Opportunities. *Curr. Opin. Genet. Dev.* **2017**, *42*, 56−67.

(16) Theodoulou, N. H.; Bamborough, P.; Bannister, A. J.; Becher, I.; Bit, R. A.; Che, K. H.; Chung, C.-w.; Dittmann, A.; Drewes, G.; Drewry, D. H.; Gordon, L.; Grandi, P.; Leveridge, M.; Lindon, M.; Michon, A.-M.; Molnar, J.; Robson, S. C.; Tomkinson, N. C. O.; Kouzarides, T.; Prinjha, R. K.; Humphreys, P. G. Discovery of I-BRD9, a Selective Cell Active Chemical Probe for Bromodomain Containing Protein 9 Inhibition. *J. Med. Chem.* **2016**, *59*, 1425−1439.

(17) Clark, P. G. K.; Vieira, L. C. C.; Tallant, C.; Fedorov, O.; Singleton, D. C.; Rogers, C. M.; Monteiro, O. P.; Bennett, J. M.; Baronio, R.; Müller, S.; Daniels, D. L.; Méndez, J.; Knapp, S.; Brennan, P. E.; Dixon, D. J. LP99: Discovery and Synthesis of the First Selective BRD7/9 Bromodomain Inhibitor. *Angew. Chem., Int. Ed.* **2015**, *54*, 6217−6221.

(18) Martin, L. J.; Koegl, M.; Bader, G.; Cockcroft, X.-L.; Fedorov, O.; Fiegen, D.; Gerstberger, T.; Hofmann, M. H.; Hohmann, A. F.; Kessler, D.; Knapp, S.; Knesl, P.; Kornigg, S.; Müller, S.; Nar, H.; Rogers, C.; Rumpel, K.; Schaaf, O.; Steurer, S.; Tallant, C.; Vakoc, C. R.; Zeeb, M.; Zoephel, A.; Pearson, M.; Boehmelt, G.; McConnell, D. Structure-Based Design of an in Vivo Active Selective BRD9 Inhibitor. *J. Med. Chem.* **2016**, *59*, 4462−4475.

(19) Moustakim, M.; Clark, P. G. K.; Hay, D. A.; Dixon, D. J.; Brennan, P. E. Chemical Probes and Inhibitors of Bromodomains Outside the BET Family. *Med. Chem. Commun.* **2016**, *7*, 2246−2264.

(20) Clegg, M. A.; Bamborough, P.; Chung, C.-w.; Craggs, P. D.; Gordon, L.; Grandi, P.; Leveridge, M.; Lindon, M.; Liwicki, G. M.; Michon, A.-M.; Molnar, J.; Rioja, I.; Soden, P. E.; Theodoulou, N. H.; Werner, T.; Tomkinson, N. C. O.; Prinjha, R. K.; Humphreys, P. G. Application of Atypical Acetyl-Lysine Methyl Mimetics in the Development of Selective Inhibitors of the Bromodomain-Containing Protein 7 (BRD7)/Bromodomain-Containing Protein 9 (BRD9) Bromodomains. *J. Med. Chem.* **2020**, *63*, 5816−5840.

(21) Fedorov, O.; Castex, J.; Tallant, C.; Owen, D. R.; Martin, S.; Aldeghi, M.; Monteiro, O.; Filippakopoulos, P.; Picaud, S.; Trzupek, J. D.; Gerstenberger, B. S.; Bountra, C.; Willmann, D.; Wells, C.; Philpott, M.; Rogers, C.; Biggin, P. C.; Brennan, P. E.; Bunnage, M. E.; Schüle, R.; Günther, T.; Knapp, S.; Müller, S. Selective Targeting of the BRG/PB1 Bromodomains Impairs Embryonic and Trophoblast Stem Cell Maintenance. *Sci. Adv.* **2015**, *1*, No. e1500723.

(22) Gerstenberger, B. S.; Trzupek, J. D.; Tallant, C.; Fedorov, O.; Filippakopoulos, P.; Brennan, P. E.; Fedele, V.; Martin, S.; Picaud, S.; Rogers, C.; Parikh, M.; Taylor, A.; Samas, B.; O'Mahony, A.; Berg, E.; Pallares, G.; Torrey, A. D.; Treiber, D. K.; Samardjiev, I. J.; Nasipak, B. T.; Padilla-Benavides, T.; Wu, Q.; Imbalzano, A. N.; Nickerson, J. A.; Bunnage, M. E.; Müller, S.; Knapp, S.; Owen, D. R. Identification

of a Chemical Probe for Family VIII Bromodomains through Optimization of a Fragment Hit. *J. Med. Chem.* **2016**, *59*, 4800−4811.
(23) Sutherell, C. L.; Tallant, C.; Monteiro, O. P.; Yapp, C.; Fuchs, J. E.; Fedorov, O.; Siejka, P.; Müller, S.; Knapp, S.; Brenton, J. D.; Brennan, P. E.; Ley, S. V. Identification and Development of 2,3-dihydropyrrolo[1,2-*a*]quinazolin-5(1*H*)-one Inhibitors Targeting Bromodomains within the Switch/Sucrose Non-Fermenting Complex. *J. Med. Chem.* **2016**, *59*, 5095−5101.
(24) Albrecht, B. K.; Côté, A.; Crawford, T.; Duplessis, M.; Good, A. C.; Leblanc, Y.; Magnuson, S. R.; Nasveschuk, C. G.; Romero, F. A.; Tang, Y.; Taylor, A. M. Therapeutic Pyridazine Compounds and Uses Thereof. International Patent WO 2016/138114 A1, 2016.
(25) Wanior, M.; Preuss, F.; Ni, X.; Krämer, A.; Mathea, S.; Göbel, T.; Heidenreich, D.; Simonyi, S.; Kahnt, A. S.; Joerger, A. C.; Knapp, S. Pan-SMARCA/PB1 Bromodomain Inhibitors and Their Role in Regulating Adipogenesis. *J. Med. Chem.* **2020**, *63*, 14680−14699.
(26) Myrianthopoulos, V.; Gaboriaud-Kolar, N.; Tallant, C.; Hall, M.-L.; Grigoriou, S.; Brownlee, P. M.; Fedorov, O.; Rogers, C.; Heidenreich, D.; Wanior, M.; Drosos, N.; Mexia, N.; Savitsky, P.; Bagratuni, T.; Kastritis, E.; Terpos, E.; Filippakopoulos, P.; Müller, S.; Skaltsounis, A.-L.; Downs, J. A.; Knapp, S.; Mikros, E. Discovery and Optimization of a Selective Ligand for the Switch/Sucrose Non-fermenting-Related Bromodomains of Polybromo Protein-1 by the Use of Virtual Screening and Hydration Analysis. *J. Med. Chem.* **2016**, *59*, 8787−8803.
(27) Varela, I.; Tarpey, P.; Raine, K.; Huang, D.; Ong, C. K.; Stephens, P.; Davies, H.; Jones, D.; Lin, M.-L.; Teague, J.; Bignell, G.; Butler, A.; Cho, J.; Dalgliesh, G. L.; Galappaththige, D.; Greenman, C.; Hardy, C.; Jia, M.; Latimer, C.; Lau, K. W.; Marshall, J.; McLaren, S.; Menzies, A.; Mudie, L.; Stebbings, L.; Largaespada, D. A.; Wessels, L. F.; Richard, S.; Kahnoski, R. J.; Anema, J.; Tuveson, D. A.; Perez-Mancera, P. A.; Mustonen, V.; Fischer, A.; Adams, D. J.; Rust, A.; Chan-on, W.; Subimerb, C.; Dykema, K.; Furge, K.; Campbell, P. J.; Teh, B. T.; Stratton, M. R.; Futreal, P. A. Exome Sequencing Identifies Frequent Mutation of the SWI/SNF Complex Gene PBRM1 in Renal Carcinoma. *Nature* **2011**, *469*, 539−542.
(28) The Cancer Genome Atlas Research Network. Comprehensive Molecular Characterization of Clear Cell Renal Cell Carcinoma. *Nature* **2013**, *499*, 43−49.
(29) Slaughter, M. J.; Shanle, E. K.; McFadden, A. W.; Hollis, E. S.; Suttle, L. E.; Strahl, B. D.; Davis, I. J. PBRM1 Bromodomains Variably Influence Nucleosome Interactions and Cellular Function. *J. Biol. Chem.* **2018**, *293*, 13592−13603.
(30) Liao, L.; Alicea-Velázquez, N. L.; Langbein, L.; Niu, X.; Cai, W.; Cho, E.-A.; Zhang, M.; Greer, C. B.; Yan, Q.; Cosgrove, M. S.; Yang, H. High Affinity Binding of H3K14ac through Collaboration of Bromodomains 2, 4 and 5 is Critical for the Molecular and Tumor Suppressor Functions of PBRM1. *Mol. Oncol.* **2019**, *13*, 811−828.
(31) Kemp, M. M.; Weïwer, M.; Koehler, A. N. Unbiased Binding Assays for Discovering Small-Molecule Probes and Drugs. *Bioorg. Med. Chem.* **2012**, *20*, 1979−1989.
(32) Sutherell, C. L.; Ley, S. V. On the Synthesis and Reactivity of 2,3-Dihydropyrrolo[1,2-a]quinazolin-5(1H)-ones. *Synthesis* **2017**, *49*, 135−144.
(33) Aldeghi, M.; Ross, G. A.; Bodkin, M. J.; Essex, J. W.; Knapp, S.; Biggin, P. C. Large-Scale Analysis of Water Stability in Bromodomain Binding Pockets with Grand Canonical Monte Carlo. *Commun. Chem.* **2018**, *1*, 10.1038.

https://doi.org/10.1021/acsomega.1c01555
ACS Omega 2021, 6, 21327−21338

4.3 Informations supplémentaires

Les informations supplémentaires concernant les protocoles expérimentaux, les caractérisations ainsi que les spectres RMN des composés synthétisés sont présentés dans l'annexe C.

4.4 Conclusion

Le SAR réalisé autour du composé **3**, rapporté par Sutherell *et al.*, a permis d'en optimiser l'activité et la sélectivité jusqu'à obtention de **LM146**. À 10 μM, **LM146** interagit uniquement avec des domaines bromés appartenant à la sous-famille VIII. Avec des ΔT_m de 14.11 °C, 10.06 °C et 1.40 °C contre PB1(2), PB1(5) et SMARCA2A respectivement, la sélectivité apparente de **LM146** pour PB1 a pu être confirmée par bromoSCAN, révélant ainsi des valeurs de K_d de 110 nM, 61 nM et 2100 nM contre PB1(2), PB1(5) et SMARCA2B. Le développement d'un tel inhibiteur sélectif de PB1 permettra sans nul doute d'explorer avec davantage de précision le rôle exact de PB1 au sein de PBAF tout en testant le potentiel thérapeutique de la protéine.

4.5 Contributions des auteurs à l'article

La présente auteure a effectué la conception, la synthèse et la caractérisation de l'ensemble des composés présents dans l'article. Elle a réalisé la recherche bibliographique et a été la rédactrice principale de l'article et du SI.

Emily Gesner a réalisé l'ensemble des tests DSF.

Sarah Attwell et Olesya A. Kharenko ont validé la cible biologique initiale et ont contribué au projet par l'intermédiaire de tests biologiques non mentionnés dans l'article.

Edward H. van der Horst et Henrik C. Hansen ont supervisés les travaux réalisés au sein de Zenith Epigenetics, Ltd.

Finalement, l'auteur de correspondance Alexandre Gagnon a supervisé l'ensemble du projet, tout particulièrement les travaux de l'auteure principale, a guidé la coordination des différentes équipes de recherche et s'est chargé du processus de soumission.

L'ensemble des auteurs a contribué à la relecture de l'article.

CHAPITRE V

SYNTHÈSE DE NVS-BPTF-1, INHIBITEUR DE BPTF, ET ÉVALUATION DE SON IMPACT SUR L'IMMUNOPROTÉASOME

5.1 Introduction

BPTF est une protéine multidomaines qui agit comme sous-unité principale du remodeleur de chromatine NURF. S'il ne fait aucun doute que NVS-BPTF-1 demeure à ce jour la sonde chimique la plus efficace et sélective pour le domaine bromé de BPTF, sa synthèse n'a encore jamais été rapportée. Cet article présente donc la première voie de synthèse divulguée, permettant ainsi un accès rapide à cet inhibiteur et potentiellement différents dérivés. Afin d'évaluer le potentiel en immunothérapie de BPTFBrD, des études concernant l'impact de son inhibition sélective grâce à NVS-BPTF-1 seront également rapportées.

5.2 Article issu de ces travaux

Bioorg. Med. Chem. Lett. 47 (2021) 128208

Contents lists available at ScienceDirect

Bioorganic & Medicinal Chemistry Letters

journal homepage: www.elsevier.com/locate/bmcl

Synthesis of NVS-BPTF-1 and evaluation of its biological activity

Léa Mélin [a], Cyrus Calosing [b], Olesya A. Kharenko [b], Henrik C. Hansen [b], Alexandre Gagnon [a,*]

[a] Département de chimie, Université du Québec à Montréal, C.P. 8888, Succ. Centre-Ville, Montréal, Québec H3C 3P8, Canada
[b] Zenith Epigenetics Ltd, Suite 300, 4820 Richard Road SW, Calgary, AB T3E 6L1, Canada

ARTICLE INFO

Keywords:
NVS-BPTF-1
BPTF
NURF
Synthesis

ABSTRACT

BPTF (bromodomain and PHD finger containing transcription factor) is a multidomain protein that plays essential roles in transcriptional regulation, *T*-cell homeostasis and stem cell pluripotency. As part of the chromatin remodeling complex hNURF (nucleosome remodeling factor), BPTF epigenetic reader subunits are particularly important for BPTF cellular function. Here we report the synthesis of NVS-BPTF-1, a previously reported highly potent and selective BPTF-bromodomain inhibitor. Evaluation of the impact of the inhibition of BPTF-bromodomain using NVS-BPTF-1 on selected proteins involved in the antigen processing pathway revealed that exclusively targeting BPTF-bromodomain is insufficient to observe an increase of PSMB8, PSMB9, TAP1 and TAP2 proteins.

Gene expression is highly regulated by chromatin topology. Even in the euchromatin state, transcription factors can hardly access the *cis*-sequences of DNA and usually require the combined action of both epigenetic enzymes and chromatin remodelers beforehand. Covalent modifications of histone tails, increased exposition of naked DNA or alteration of nucleosomes organization in a promoter region can strongly impact gene expression and, ultimately, cell phenotypes.[1]

NURF (nucleosome remodeling factor) is one of the conserved ATP-dependent chromatin remodeling factors belonging to the ISWI family. Rather than binding to naked DNA or histones, NURF preferentially interacts with nucleosomes through the positively charged *N*-terminal histone tails[2] and catalyzes nucleosome sliding.[3] By doing so, NURF is able to assist the binding of transcription factors and is therefore key for gene activation initiation.[4] Human NURF (hNURF) is composed of three subunits: the conserved ISWI ATPase core SNF2L, BPTF (bromodomain and PHD finger containing transcription factor, also known as FALZ for fetal alzheimer antigen) and RbAP48/46 (retinoblastoma associated proteins 46 and 48), two mammalian orthologs of Drosophila NURF301 and NURF55, respectively.[5]

BPTF, the largest and most essential component of the hNURF complex, is critical for transcriptional regulation during embryogenesis.[6,7] Outside of this specific developmental stage, BPTF maintains chromatin accessibility, allowing stem cell pluripotency,[8] *T*-cell homeostasis and function,[9] and transcriptional regulation.[10] In order to do so, BPTF harbors multiple motifs characteristic of transcriptional coactivators: one non-BET (bromodomain and extra-terminal domain) bromodomain, two PHD domains and a glutamine-rich acidic domain.[11] These epigenetic readers are particularly important for BPTF cellular function as they serve as recognition units for acetylated or methylated lysine residues. It has therefore been demonstrated that BPTF binds to acetylated H3 and H4 histone tails via its bromodomain and to H3K4Me3 via its second PHD finger.[12]

As lysine acetylation of histone tails is one of the most dynamic post-translation modification associated with chromatin accessibility and increased gene expression,[13] mutation and overexpression of bromodomain containing proteins (BCPs) have been associated with many diseases, such as cancer, inflammation or neurological disorders.[14] In particular, aberrant expression of BPTF has been implicated in the development and progression of multiple types of cancer, including colorectal cancer,[15] lung adenocarcinomas,[16] melanoma,[17] and neuroblastomas.[18] Slowly emerging as a potential target for novel anti-cancer drugs because of its required recruitment for c-MYC activation,[19,20] it is interesting to note that BPTF knockdowns enhance $CD8^+$ *T*-cell and NK-cells mediated antitumor immunity,[21,22] therefore also highlighting BPTF as a potential target for the development of immunotherapies.

Despite BPTF biological pertinence in cancer and the fact that inhibiting the bromodomain of BCPs has been successful in the past for treating BCPs-related diseases (as illustrated by the numerous BET inhibitors currently in clinical trials), only few chemical probes targeting BPTF-bromodomain have been developed (Fig. 1). AU1, the first small molecule showing some selectivity for BPTF, was reported in 2015.[23] Discovered during an ^{19}F NMR dual screening against BPTF and BRD4,

* Corresponding author.
E-mail address: gagnon.alexandre@uqam.ca (A. Gagnon).

https://doi.org/10.1016/j.bmcl.2021.128208
Received 29 April 2021; Received in revised form 9 June 2021; Accepted 13 June 2021
Available online 16 June 2021

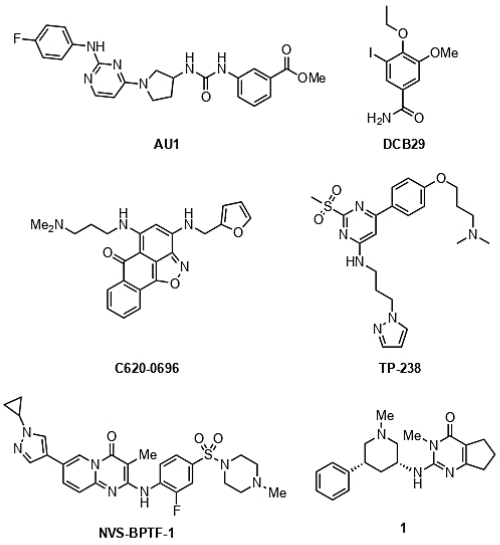

Fig. 1. Reported BPTF inhibitors.

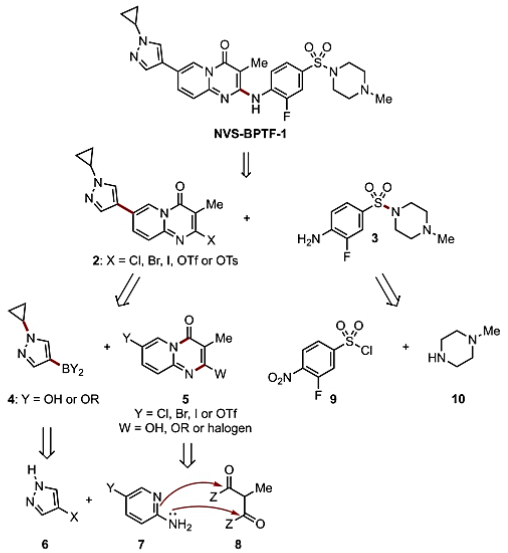

Scheme 1. Retrosynthetic analysis of NVS-BPTF-1.

AU1 displays a K_d value of 2.8 μM for BPTF as determined by isothermal titration calorimetry (ITC), while no binding against BRD4 was observed. In 2019, DCB29, a dialkoxy iodo benzamide derivative, was developed through structure-based virtual screening as a selective BPTF-bromodomain inhibitor with an IC_{50} value of 13.2 μM, obtained by homogenous time-resolved fluorescence resonance energy transfer (HTRF) assays.[24] The same year, compound C620-0696 was reported with a K_d value of 35.5 μM against BPTF as assessed by a biolayer interferometry (BLI) assay. C620-0696 exhibits cytotoxicity to BPTF overexpression in non-small-cell lung cancer (NSCLC) cell lines and also inhibits the binding between the BPTF bromodomain and H4K16Ac, which leads to repression of c-MYC transcription activation.[25]

Finally, the SGC, in collaboration with Takeda, reported on their website TP-238, the first chemical probe with low nanomolar potency against BPTF bromodomain. However, TP-238 inhibited both CECR2 and BPTF in an AlphaScreen assay with IC_{50} values of 30 nM and 350 nM, respectively.[26] This lack of selectivity was countered with the release of NVS-BPTF-1. Produced through a collaboration between the SGC and Novartis, NVS-BPTF-1 is the first highly potent, selective and cell active chemical probe for BPTF-bromodomain. NVS-BPTF-1 gave an IC_{50} value of 56 nM in an AlphaScreen assay and a K_d value of 71 nM in a BLI assay.[27] A DSF screen and a BROMOscan revealed no significant interaction with a panel of other human bromodomains. In HEK293 cells, NVS-BPTF-1 showed on-target activity with an IC_{50} of 16 nM, as measured by a nanoBRET assay. While writing this manuscript, compound **1** was published as a new BPTF-bromodomain inhibitor with a K_d value of 428 nM for BPTF as determined by ITC. Compound **1** down-regulated both c-MYC and BPTF expression in A549 cells.[28]

Even though NVS-BPTF-1 is currently the most potent and selective chemical probe against BPTF, to the best of our knowledge, its synthesis has not been reported yet. We would like to disclose herein a rapid and modular chemical route to access this tool compound. Preliminary evaluation of the biological activity of NVS-BPTF-1 is also described.

The retrosynthetic analysis of NVS-BPTF-1 invited a disconnection on the central aniline function, leading to the left-hand side pyridopyrimidinone synthon **2** and the right-hand side 1-((3-fluoro-4-aminophenyl)sulfonyl)-4-methylpiperazine fragment **3** (Scheme 1). We envisioned that the presence of a suitable leaving group X on **2** such as an halide, a triflate or a tosylate could allow an S_NAr transformation or a metal-catalyzed *N*-arylation reaction with **3**. Although complications could arise from the anticipated low nucleophilicity of aniline **3**, we hypothesized that this approach would have a higher chance of success than the complementary C—N disconnection that would require the preparation of an intriguing and poorly-characterized amino-pyrimidinone version of **2** (i.e. X = NH_2). Left-hand side fragment **2** could then be prepared by a palladium-catalyzed cross-coupling reaction between an *N*-cyclopropylboron species **4**, either in the form of a boronic acid or ester, and a halo or triflyl pyridopyrimidinone core of type **5**. Should this cross-coupling be challenging, we assumed that the role of the partners could be inverted, that is, the boron function would be installed on **5**. The installation of the cyclopropyl unit on the pyrazole's NH would be performed through a copper-catalyzed *N*-cyclopropylation reaction on **6** via one of the numerous conditions involving boron or bismuth reagents. The boron would be installed on **6** via a lithium–halogen exchange reaction or a metal-catalyzed cross-coupling process. A search of the literature revealed a paucity of methods to form the densely functionalized central core **5**. It was our hope that this scaffold could be obtained by a condensation reaction between **7** and a properly activated malonic system **8**. Finally, the aniline portion **3** would be prepared from **9** and **10** through conventional sulfonamide bond construction and nitro reduction.

We first prepared aniline **3** by reacting 3-fluoro-4-nitrobenzenesulfonyl chloride **9** with 1-methylpiperazine **10**, followed by reduction of the nitro group in **11** under Béchamp's conditions (Scheme 2). Quick attempt at improving the yield of this transformation, for example by increasing the reaction time or the temperature, or pre-forming the sodium amide of **10** proved unsuccessful and therefore, we continued with the synthesis of the western portion of our target molecule.

Thus, we prepared the *N*-cyclopropyl-4-borylpyrazolyl synthon **4** (c.f. Scheme 1) by first installing the cyclopropyl moiety onto 1-cyclopropyl-4-iodo-1*H*-pyrazole **12** via a copper-catalyzed *N*-cyclopropylation reaction (Scheme 3). After testing various conditions, we found that this transformation could be efficiently accomplished using 2.0 equivalents of cyclopropylboronic acid in the presence of a stoichiometric amount of cupric acetate and a mixture of dimethylaminopyridine and pyridine in refluxing dioxane under an oxygen atmosphere.

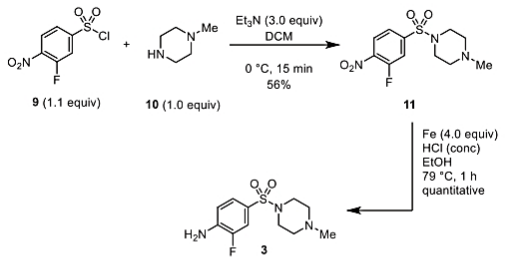

Scheme 2. Synthesis of aniline **3**.

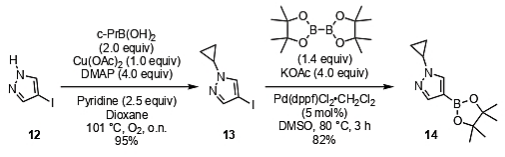

Scheme 3. Synthesis of 1-cyclopropyl-4-(4,4,5,5-tetramethyl-1,3,2-dioxaborolan-2-yl)-1*H*-pyrazole **14**.

Attempts at transforming the iodide in **13** into a boron functionality through a lithium–halogen exchange process followed by reaction with trimethylborate proved difficult. Consequently, iodide **13** was converted into the corresponding 1-cyclopropyl-4-(4,4,5,5-tetramethyl-1,3,2-dioxaborolan-2-yl)-1*H*-pyrazole **14** via a palladium-catalyzed cross-coupling reaction with bis(pinacolato)diboron. Rapid optimization of the reaction conditions led us to use [1,1′-bis(diphenyl-phosphino) ferrocene]-dichloropalladium(II) as the catalyst in combination with potassium acetate as the base and DMSO as the solvent.

We next turned our attention to the preparation of the pyridopyrimidinone scaffold **5** (c.f. Scheme 1). A quick search of the literature indicated a lack of methods to prepare compounds of this type with a methyl group in position 3. Attempts at directly coupling 5-bromoaminopyridine **15** with 2-methylmalonic dimethylester **16** under smooth or forcing conditions failed to deliver the desired condensation product **17**, but provided instead a mixture of the mono-condensation adduct **18** and its corresponding decarboxylation product **19** (Scheme 4a).

We hypothesized that a more reactive malonic system could potentially facilitate this apparently difficult condensation reaction. Thus, 2-methylmalonic acid **20** was preactivated with HATU in the presence of Hünig's base and then reacted with **15** (Scheme 4b). Again, product **17** could not be isolated using this approach, even when conducted under drastic conditions. Ultimately, the cyclization problem was solved by transforming 2-methylmalonic acid **21** into its corresponding bis (2,4,6-trichlorophenyl)ester derivative **23** through reaction with 2,4,6-trichlorophenol **22** in neat phosphorus oxychloride (Scheme 4c). Reacting **23** with 5-bromo-2-aminopyridine **15** in hot toluene over 2 h finally afforded the desired cyclized product **17** in 83% yield (Scheme 4c).

Direct reaction of *N*-cyclopropylpyrazolylboronic pinacol ester **14** with bromopyrimidinone **17** was then attempted with the aim of generating **24** (Scheme 5). After testing numerous conditions, we could not obtain the desired product and we thus opted to convert the OH (which might also exist in the tautomeric keto-form) into the corresponding chloride. This chloride would serve as a valuable handle for a subsequent S_NAr reaction with aniline **3**. In the event, **17** was converted into **25** through heating in a mixture of phosphoryl chloride and phosphorus pentachloride. Unfortunately, all attempts to realize the S_NAr reaction between **25** and **3** failed, even under harsh conditions. Thus, **25** was engaged in a cross-coupling reaction with **14** with the hope that this

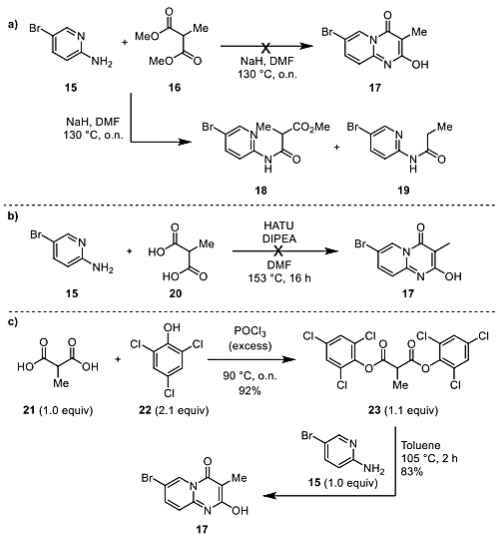

Scheme 4. Synthesis of the 7-bromo-2-hydroxy-3-methyl-4*H*-pyrido[1,2-*a*] pyrimidin-4-one core **17**.

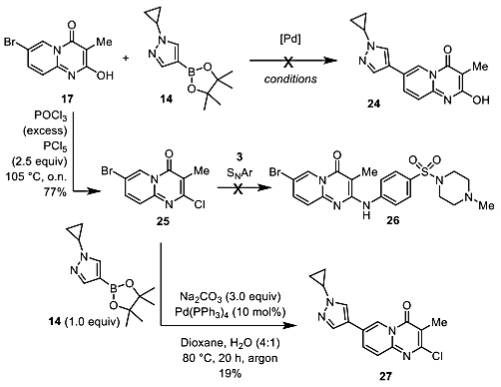

Scheme 5. Synthesis of pyridopyrimidinone **27**.

transformation would occur with some level of selectivity on the bromide over the chloride. Happily, this strategy delivered **27**, albeit in a moderate 19% yield. Since other catalysts or conditions failed to improve the efficiency of the process, we decided to continue with the union of **27** with **3**.

Attempts at coupling **3** and **27** through a S_NAr reaction under various conditions failed to provide the desired product NVS-BPTF-1. We assumed that the deactivation of the aniline **3** by the combined electron-withdrawing effects of the fluoride in *ortho* position and the sulfonamide in *para* were responsible (at least partially) for this lack of reactivity. Therefore, we turned our attention to a metal-catalyzed approach and found that key intermediates **3** and **27** could be coupled under Buchwald-Hartwig conditions using palladium(II) acetate, racemic BINAP in refluxing toluene in the presence of cesium carbonate, affording NVS-BPTF-1 in 56% yield with greater than 99% purity (Scheme 6).

The structure of synthetic NVS-BPTF-1 was confirmed through X-ray

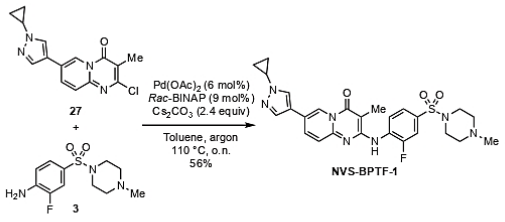

Scheme 6. Synthesis of NVS-BPTF-1 through Buchwald-Hartwig coupling between **27** and **3**.

diffraction analysis on crystals obtained from methylene chloride via the solvent diffusion technique (Fig. 2).

Mayes and collaborators have shown that depletion of BPTF in B16F10 models leads to upregulation of PSMB8 and PSMB9 which are part of the immunoproteasome, as well as TAP1 and TAP2 which belong to the transporter associated with antigen-processing complex.[21] They observed that this upregulation results in enhanced antigenicity and improved *T*-cell antitumor activity. With our resynthesized NVS-BPTF-1 in hand, we thus aimed to evaluate if inhibition of BPTF would result in a similar upregulation of these four specific proteins as in the knockdown model, thus allowing us to determine the potential therapeutic pertinence of BPTF-bromodomain in the context of immunotherapies for the treatment of cancer.

First, we confirmed the activity and the selective profile of NVS-BPTF-1 using both an AlphaScreen assay and a DSF thermal shift assay (differential scanning fluorimetry) against BPTF and BRD4(BD1) (Fig. 3). In the event, an IC_{50} of 30 nM and a ΔT_m of 5.7 °C were obtained, which are in good agreement with values presented online by the SGC (i.e. IC_{50} of 56 nM against BPTF in an AlphaScreen assay and ΔT_m of 6.16 °C).[27]

Since the selectivity of the probe was already assessed by the SGC via a DSF screen and a BROMOscan assay,[27] we then evaluated the effect of our compound on proliferation in various cancer cell lines. Contrary to AU1 and C620-0696, NVS-BPTF-1 did not affect the proliferation of B16F10 mouse melanoma cell lines (Fig. 4). While AU1 and C620-0696 are low micromolar inhibitors of the BPTF bromodomain, this difference could be attributed to off-target effects, previously reported in the literature.[29] In a similar fashion, NVS-BPTF-1 did not inhibit the proliferation of multiple human cancer cell lines (Fig. S1), while siRNA knockdowns of BPTF were previously reported as reducing proliferation of various cancer cell lines.[16,30,31]

Previous reports revealed that interferon gamma (IFNγ)[32] and shRNA knockdown of BPTF[21] can increase the amount of immunoproteasome proteins PSMB8 and PSMB9 and antigen transport proteins TAP1 and TAP2. Our results also indicate that BPTF siRNA knockdown

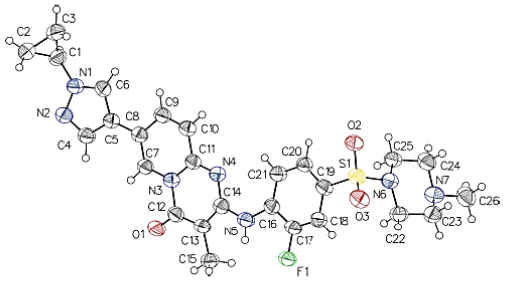

Fig. 2. Thermal atomic displacement ORTEP ellipsoid plot for NVS-BPTF-1 (CCDC number: 2080173). Ellipsoids are drawn at the 50% probability level and hydrogen atoms are shown as spheres of arbitrary size.

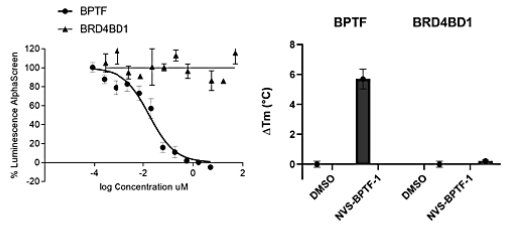

Fig. 3. a) AlphaScreen (IC_{50} = 30 nM; n = 4) and b) DSF (ΔT_m = 5.7 °C) assays using resynthesized NVS-BPTF-1 against BPTF and BRD4(BD1).

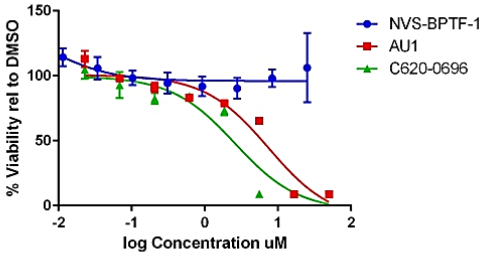

Fig. 4. Proliferation assay in B16F10 model.

can enhance the proteasome subunit beta type-9 protein (PSMB9) in B16F10 cells (Fig. S2). However, when NVS-BPTF-1 was used, this activation was not detected in B16F10 mouse melanoma cell lines (Fig. 5), nor in A549 (lung) or BT549 (breast) human cancer cell lines (Fig. S3).

Since NVS-BPTF-1 did not affect the level of PSMB8 and PSMB9 or TAP1 and TAP2, we hypothesized that targeting BPTF-bromodomain alone is not sufficient to observe any impact on the expression of these proteins.

In conclusion, a modular synthetic route was developed for NVS-BPTF-1, the first potent and selective inhibitor of BPTF bromodomain. Binding of resynthesized NVS-BPTF-1 to BPTF was confirmed using a DSF assay while inhibition was demonstrated using an AlphaScreen assay. No impact on B16F10 cell proliferation was observed upon exposure to NVS-BPTF-1. Contrary to BPTF knockdown models, inhibition of BPTF with NVS-BPTF-1 did not lead to increased levels of TAP1, TAP2, PSMB8 or PSMB9. These results suggest that only targeting BPTF-bromodomain might not be a viable strategy for the development of immunotherapies.

Declaration of Competing Interest

The authors declare that they have no known competing financial interests or personal relationships that could have appeared to influence

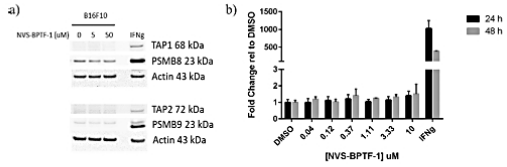

Fig. 5. Effects of NVS-BPTF-1 on PSMB8, PSMB9, TAP1 and TAP2. a) Western blot of B16F10 mouse melanoma cell lines treated with NVS-BPTF-1 or 20 ng/mL IFNg for 72 h; b) effects on PSMB9 mRNA in B16F10 mouse melanoma cell lines.

the work reported in this paper.

Acknowledgments

We would like to thank the Natural Sciences and Engineering Research Council of Canada (NSERC) and Zenith Epigenetics Ltd for a Collaborative Research and Development Grant. C.C., O.K., and H.H. are salaried employees of Zenith Epigenetics Ltd.

Appendix A. Supplementary data

Supplementary data to this article can be found online at https://doi.org/10.1016/j.bmcl.2021.128208.

References

1 Li B, Carey M, Workman JL. The role of chromatin during transcription. *Cell*. 2007;128(4):707–719. https://doi.org/10.1016/j.cell.2007.01.015.
2 Georgel PT, Tsukiyama T, Wu C. Role of histone tails in nucleosome remodeling by drosophila NURF. *EMBO J*. 1997;16(15):4717–4726. https://doi.org/10.1093/emboj/16.15.4717.
3 Hamiche A, Sandaltzopoulos R, Gdula DA, Wu C. ATP-dependent histone octamer sliding mediated by the chromatin remodeling complex NURF. *Cell*. 1999;97(7):833–842. https://doi.org/10.1016/s0092-8674(00)80796-5.
4 Mizuguchi G, Tsukiyama T, Wisniewski J, Wu C. Role of nucleosome remodeling factor NURF in transcriptional activation of chromatin. *Mol Cell*. 1997;1(1):141–150. https://doi.org/10.1016/S1097-2765(00)80015-5.
5 Barak O, Lazzaro MA, Lane WS, Speicher DW, Picketts DJ, Shiekhattar R. Isolation of Human NURF: a regulator of engrailed gene expression. *EMBO J*. 2003;22(22):6089–6100. https://doi.org/10.1093/emboj/cdg582.
6 Landry J, Sharov AA, Piao Y, et al. Essential role of chromatin remodeling protein Bptf in early mouse embryos and embryonic stem cells. *PLoS Genet*. 2008;4(10):e1000241. https://doi.org/10.1371/journal.pgen.1000241.
7 Goller T, Vauti F, Ramasamy S, Arnold H-H. Transcriptional regulator BPTF/FAC1 is essential for trophoblast differentiation during early mouse development. *Mol Cell Biol*. 2008;28(22):6819–6827. https://doi.org/10.1128/MCB.01058-08.
8 Frey WD, Chaudhry A, Slepicka PF, et al. BPTF maintains chromatin accessibility and the self-renewal capacity of mammary gland stem cells. *Stem Cell Rep*. 2017;9(1):23–31. https://doi.org/10.1016/j.stemcr.2017.04.031.
9 Wu B, Wang Y, Wang C, Wang GG, Wu J, Wan YY. BPTF is essential for T cell homeostasis and function. *J Immunol*. 2016;197(11):4325–4333. https://doi.org/10.4049/jimmunol.1600642.
10 Jordan-Sciutto KL, Dragich JM, Bowser R. DNA binding activity of the fetal Alz-50 clone 1 (FAC1) protein is enhanced by phosphorylation. *Biochem Biophys Res Commun*. 1999;260(3):785–789. https://doi.org/10.1006/bbrc.1999.0986.
11 Jones MH, Hamana N, Shimane M. Identification and characterization of BPTF, a novel bromodomain transcription factor. *Genomics*. 2000;63(1):35–39. https://doi.org/10.1006/geno.1999.6070.
12 Wysocka J, Swigut T, Xiao H, et al. A PHD finger of NURF couples histone H3 lysine 4 trimethylation with chromatin remodelling. *Nature*. 2006;442(7098):86–90. https://doi.org/10.1038/nature04815.
13 Shahbazian MD, Grunstein M. Functions of site-specific histone acetylation and deacetylation. *Annu Rev Biochem*. 2007;76(1):75–100. https://doi.org/10.1146/annurev.biochem.76.052705.162114.
14 Muller S, Filippakopoulos P, Knapp S. Bromodomains as therapeutic targets. *Expert Rev Mol Med*. 2011;13. https://doi.org/10.1017/S1462399411001992.
15 Xiao S, Liu L, Lu X, Long J, Zhou X, Fang M. The prognostic significance of bromodomain PHD-finger transcription factor in colorectal carcinoma and association with vimentin and E-cadherin. *J Cancer Res Clin Oncol*. 2015;141(8):1465–1474. https://doi.org/10.1007/s00432-015-1937-y.
16 Dai M, Lu J-J, Guo W, et al. BPTF promotes tumor growth and predicts poor prognosis in lung adenocarcinomas. *Oncotarget*. 2015;6(32):33878–33892.
17 Dar AA, Majid S, Bezrookove V, et al. BPTF transduces MITF-driven prosurvival signals in melanoma cells. *PNAS*. 2016;113(22):6254–6258. https://doi.org/10.1073/pnas.1606027113.
18 Buganim Y, Goldstein I, Lipson D, et al. A novel translocation breakpoint within the BPTF gene is associated with a pre-malignant phenotype. *PLoS ONE*. 2010;5(3):e9657. https://doi.org/10.1371/journal.pone.0009657.
19 Richart L, Carrillo-de Santa Pau E, Río-Machín A, et al. BPTF is required for C-MYC transcriptional activity and in vivo tumorigenesis. *Nat Commun*. 2016;7(1). https://doi.org/10.1038/ncomms10153.
20 Richart L, Real FX, Sanchez-Arevalo Lobo VJ. C-MYC partners with BPTF in human cancer. *Mol Cell Oncol*. 2016;3(3):e1152346. https://doi.org/10.1080/23723556.2016.1152346.
21 Mayes K, Alkhatib SG, Peterson K, et al. BPTF depletion enhances T-cell-mediated antitumor immunity. *Cancer Res*. 2016;76(21):6183–6192. https://doi.org/10.1158/0008-5472.CAN-15-3125.
22 Mayes K, Elsayed Z, Alhazmi A, et al. BPTF inhibits NK cell activity and the abundance of natural cytotoxicity receptor co-ligands. *Oncotarget*. 2017;8(38):64344–64357.
23 Urick AK, Hawk LML, Cassel MK, et al. Dual screening of BPTF and Brd4 using protein-observed fluorine NMR uncovers new bromodomain probe molecules. *ACS Chem Biol*. 2015;10(10):2246–2256. https://doi.org/10.1021/acschembio.5b00483.
24 Zhang D, Han J, Lu W, et al. Discovery of alkoxy benzamide derivatives as novel BPTF bromodomain inhibitors via structure-based virtual screening. *Bioorg Chem*. 2019;86:494–500. https://doi.org/10.1016/j.bioorg.2019.01.035.
25 Xu J, Wang Q, Leung ELH, et al. Compound C620–0696, a new potent inhibitor targeting BPTF, the chromatin-remodeling factor in non-small-cell lung cancer. *Front Med*. 2020;14(1):60–67. https://doi.org/10.1007/s11684-019-0694-8.
26 TP-238 https://www.thesgc.org/chemical-probes/TP-238 (accessed 2021 -03 -29).
27 NVS-BPTF-1 https://www.thesgc.org/chemical-probes/NVS-BPTF-1 (accessed 2021 -03 -12).
28 Xiong L, Mao X, Guo Y, et al. Discovery of selective BPTF bromodomain inhibitors by screening and structure-based optimization. *Biochem Biophys Res Commun*. 2021;545:125–131. https://doi.org/10.1016/j.bbrc.2021.01.067.
29 Kirberger SE, Ycas PD, Johnson JA, et al. Selectivity, ligand deconstruction, and cellular activity analysis of a BPTF bromodomain inhibitor. *Org. Biomol. Chem*. 2019;17(7):2020–2027. https://doi.org/10.1039/C8OB02599A.
30 Zhao X, Zheng F, Li Y, et al. BPTF promotes hepatocellular carcinoma growth by modulating HTERT signaling and cancer stem cell traits. *Redox Biol*. 2019;20:427–441. https://doi.org/10.1016/j.redox.2018.10.018.
31 Green AL, DeSisto J, Flannery P, et al. bptf regulates growth of adult and pediatric high-grade glioma through the MYC pathway. *Oncogene*. 2020;39(11):2305–2327. https://doi.org/10.1038/s41388-019-1125-7.
32 Heink S, Ludwig D, Kloetzel P-M, Krüger E. IFN-γ-induced immune adaptation of the proteasome system is an accelerated and transient response. *PNAS*. 2005;102(26):9241–9246. https://doi.org/10.1073/pnas.0501711102.

5.3 Informations supplémentaires

Les informations supplémentaires concernant les protocoles expérimentaux, les caractérisations ainsi que les spectres RMN des composés synthétisés sont présentés dans l'annexe D.

5.4 Conclusion

Une voie de synthèse contenant 9 étapes a pu être développée afin d'obtenir rapidement NVS-BPTF-1. Basée sur l'assemblage de différentes sous-parties de la molécule, cette méthode est modulable et peut s'adapter facilement en cas d'études SAR sur NVS-BPTF-1. Bien que NVS-BPTF-1 soit un inhibiteur puissant et sélectif du domaine bromé de BPTF, la sonde chimique n'impacte pas la prolifération de cellules cancéreuses ni l'immunoprotéasome. Ces études permettent de conclure que l'engagement sélectif du domaine bromé de BPTF semble insuffisant pour le développement de nouvelles immunothérapies.

5.5 Contribution des auteurs à l'article

La présente auteure a conçu la voie de synthèse de NVS-BPTF-1 et a réalisé les caractérisations de l'ensemble des intermédiaires et du produit final. Elle a réalisé la recherche bibliographique et a été la rédactrice principale de l'article et du SI.

Cyrus Calosing a effectué tous les tests portant sur la prolifération cellulaire et le protéasome.

Olesya A. Kharenko a réalisé le test alphascreen ainsi que le DSF.

Henrik C. Hansen a supervisé l'ensemble des travaux effectués à Zenith Epigenetics, Ltd.

Finalement, l'auteur de correspondance Alexandre Gagnon a supervisé l'ensemble du projet, tout particulièrement les travaux de l'auteure principale, a guidé la coordination des différentes équipes de recherche et s'est chargé du processus de soumission.

L'ensemble des auteurs a contribué à la relecture de l'article.

CONCLUSION

Les travaux réalisés au cours de cette thèse de doctorat ont contribué au développement d'inhibiteurs de TEAD, PB1 et BPTF, trois régulateurs de l'expression génique souvent mutés chez les patients atteints de cancer.

La première phase de ce doctorat a porté sur des inhibiteurs de la poche palmitique de TEAD. La mise en place d'une voie de synthèse efficace passant par un couplage de Buchwald-Hartwig a permis un accès rapide à de nombreux dérivés de l'acide flufénamique. Grâce à une conception mélangeant apports des structures co-cristallines, modifications systématiques et emploi d'amarrage moléculaire, différents inhibiteurs de TEAD ont pu être obtenus, incluant **LM98**. Avec un ΔT_{agg} de 6.4 °C, **LM98** interagit avec TEAD, conclusion corroborée par des études RMN-^{19}F en présence de TEAD4. L'obtention de co-cristaux en présence de hTEAD2-YBD (code pdb : 6VAH) a permis de confirmer que **LM98** se lie dans la poche palmitique, formant notamment une liaison hydrogène entre son acide carboxylique et l'azote de l'amide présent sur le squelette peptidique de la cystéine 380. D'autres interactions, de type hydrophobes ou encore l'empilement pi en T entre le phényl de gauche et la phénylalanine 233, permettent d'ancrer davantage la molécule dans la poche. Bien que **LM98** n'empêche pas la formation du complexe YAP-TEAD, le composé agit en inhibant la palmitoylation de TEAD, réduisant ainsi de 30% l'activité de TEAD par dosage de luciférase tout en diminuant de 61% et 40% l'expression de *CTGF* et *Cyr61*, deux gènes normalement activés par YAP-TEAD. Finalement, le potentiel thérapeutique de **LM98** s'illustre par une inhibition de la migration de cellules cancéreuses, arrêtant notamment les cellules en phase S du cycle cellulaire.

Il est à noter que d'autres dérivés présentant des ΔT_{agg} élevés s'illustrent également par leurs impacts importants sur l'activité de TEAD et sur l'expression des gènes associés au complexe. Par exemple, le composé **40**, avec un ΔT_{agg} de 10 °C, présente une inhibition presque complète de TEAD à 30 µM tandis que l'analogue **51**, avec un ΔT_{agg} de 8.4 °C, diminue de 80% et 71% l'expression de *CTGF* et *Cyr61*, respectivement, à 10 µM.

Dans le futur, il pourrait être intéressant de déterminer les propriétés pharmacocinétiques des meilleurs dérivés pour, si possible, tester l'impact de ces dits dérivés dans des modèles de souris xénogreffes. Sachant la solubilité limitée de certains composés issus de cette série, il est cependant à envisager que d'autres inhibiteurs de TEAD puissent s'avérer davantage adaptés à une utilisation comme sonde chimique.

Avec le désir de pallier ces inconvénients, plusieurs criblages virtuels à haut débit ont été réalisés. Les *hits* potentiels retenus présentent tous un squelette contenant un acide benzoïque afin de maintenir les interactions hydrogènes connues avec la poche palmitique de TEAD, un ou plusieurs groupements polaires censés faire de nouvelles interactions, et une lipophilie réduite. Bien qu'il n'ait pas été possible d'effectuer les synthèses de ces *hits* dans le cadre de cette thèse, ces travaux seront poursuivis au sein du laboratoire du professeur Alexandre Gagnon.

Dans un second temps, des inhibiteurs sélectifs des domaines bromés de PB1 ont été développés. Basées sur les travaux rapportés par Sutherell *et al.*, des études de SAR ont permis d'obtenir **LM146**. À 10 µM, **LM146** interagit uniquement avec des domaines bromés appartenant à la sous-famille VIII. Avec des ΔT_m de 14.11 °C, 10.06 °C et 1.40 °C contre PB1(2), PB1(5) et SMARCA2A respectivement, la sélectivité apparente de **LM146** pour PB1 a pu être confirmée par bromoSCAN, révélant ainsi des valeurs de K_d de 110 nM, 61 nM et 2100 nM contre PB1(2), PB1(5) et SMARCA2B. Approximativement 34 fois plus actif vis-à-vis de PB1(5) par rapport

à SMARCA2B et environ 19 fois plus actif vis-à-vis de PB1(2) par rapport à SMARCA2B, **LM146** peut être considéré comme une sonde chimique puissante avec une sélectivité accrue contre les autres domaines bromés existants, y compris SMARCA2. Dans le futur, la séparation des deux énantiomères de **LM146** pourrait permettre d'améliorer davantage la sélectivité et l'activité du composé s'il s'avère qu'un seul des isomères est responsable des résultats rapportés. Alors que des études d'amarrage moléculaire n'ont pas permis d'expliquer la sélectivité obtenue, il serait également intéressant d'obtenir des co-cristaux de **LM146** en présence des différents domaines bromés, notamment PB1(5), afin de vérifier si un décalage accentué de la boucle ZA est à l'origine du profil sélectif de **LM146** par rapport au *hit* de départ.

D'autres analogues synthétisés au cours de ce projet présentent quant à eux des profils de sélectivités apparentes pour divers domaines bromés clefs de PB1. Après confirmation future de l'affinité par bromoSCAN, nul doute que l'ensemble de ces inhibiteurs se compléteront afin de permettre des études plus précises sur le rôle exact de PB1 et ses divers domaines bromés.

Pour finir, les travaux de cette thèse de doctorat se sont portés sur **NVS-BPTF-1**. S'il ne fait aucun doute que **NVS-BPTF-1** demeure à ce jour la sonde chimique la plus efficace et sélective pour le domaine bromé de BPTF, sa synthèse n'avait encore jamais été rapportée. Une voie de synthèse contenant 9 étapes, incluant 5 étapes linéaires au maximum, a pu être développée afin d'obtenir rapidement cette sonde chimique. Basée sur l'assemblage de différentes sous-parties de la molécule, cette méthode est modulable et peut s'adapter facilement en cas d'études SAR sur **NVS-BPTF-1**. Bien que **NVS-BPTF-1** soit un inhibiteur puissant et sélectif du domaine bromé de BPTF, il a été démontré au cours de cette thèse que la sonde chimique n'impacte pas la prolifération de cellules cancéreuses ni l'immunoprotéasome. Ces études permettent de conclure que l'engagement sélectif du domaine bromé de BPTF semble insuffisant pour le développement de nouvelles immunothérapies.

ANNEXE A

« DEVELOPMENT OF SMALL-MOLECULE TEAD INHIBITORS DERIVED FROM FLUFENAMIC ACID. » - PARTIE EXPÉRIMENTALE

ChemMedChem

Supporting Information

Development of LM98, a Small-Molecule TEAD Inhibitor Derived from Flufenamic Acid

Léa Mélin, Shuay Abdullayev, Ahmed Fnaiche, Victoria Vu, Narjara González Suárez, Hong Zeng, Magdalena M. Szewczyk, Fengling Li, Guillermo Senisterra, Abdellah Allali-Hassani, Irene Chau, Aiping Dong, Simon Woo, Borhane Annabi, Levon Halabelian, Steven R. LaPlante, Masoud Vedadi, Dalia Barsyte-Lovejoy, Vijayaratnam Santhakumar, and Alexandre Gagnon*

Table of content

1. Biological evaluation

a) Surface Plasmon Resonance (SPR)

Biotinylated TEAD4 was captured onto one flow cell of a streptavidin-conjugated SA chip at approximately 6,000 response units (RU) according to the manufacturer's protocol, while another flow cell was left empty for reference subtraction. Compounds were tested at 50 μM as the highest concentration, and dilution factor of 0.33 was used to yield 5 concentrations in HBS–EP buffer (20 mM HEPES pH 7.4, 150 mM NaCl, 3 mM EDTA, 0.05% Tween-20). Experiments were performed at 20 °C using the same buffer with 3% DMSO in single cycle kinetic with 90s contact time and a dissociation time of 60 s at a flow rate of 75 μL/min. A 1:1 binding model was used for curve fitting (Biacore T200 Evaluation software, GE Health Sciences Inc.).

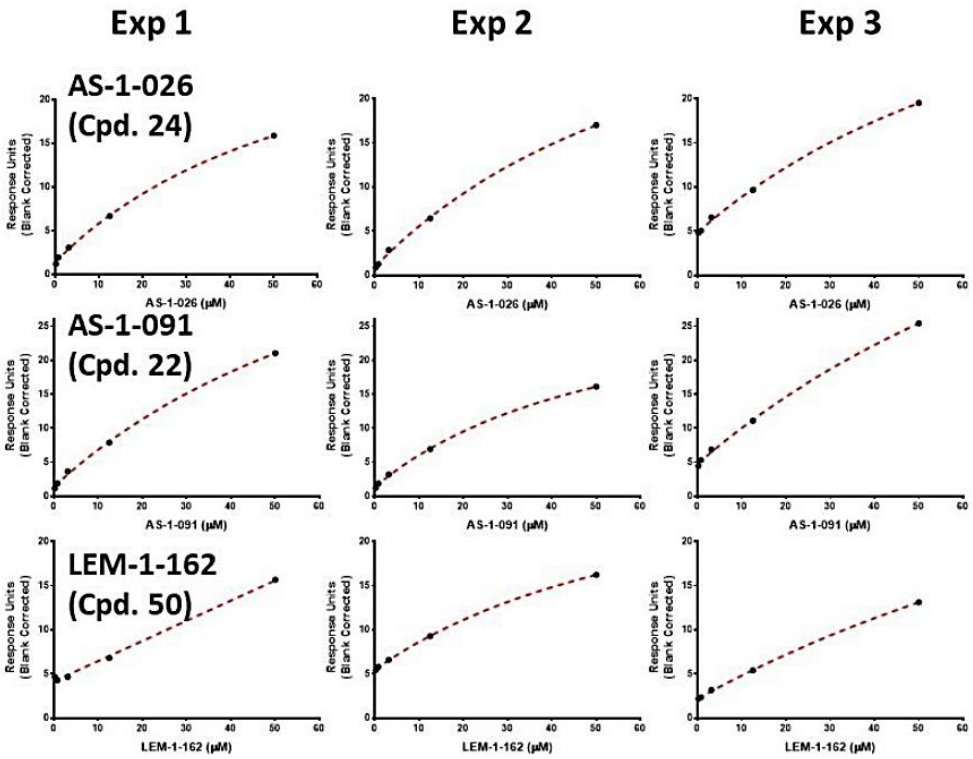
Exp 1
Exp 2
Exp 3
AS-1-026
(Cpd. 24)
AS-1-091
(Cpd. 22)
LEM-1-162
(Cpd. 50)
Response Units
(Blank Corrected)
AS-1-026 (μM)
AS-1-091 (μM)
LEM-1-162 (μM)

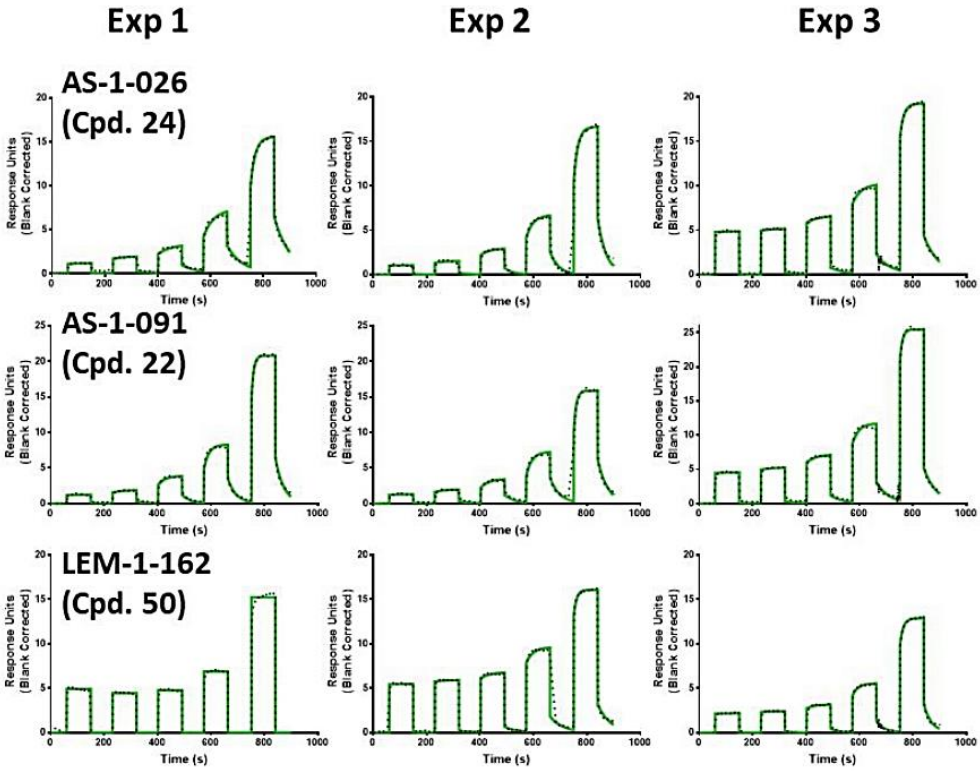
Exp 1
Exp 2
Exp 3
AS-1-026
(Cpd. 24)
AS-1-091
(Cpd. 22)
LEM-1-162
(Cpd. 50)
Response Units
(Blank Corrected)
Time (s)

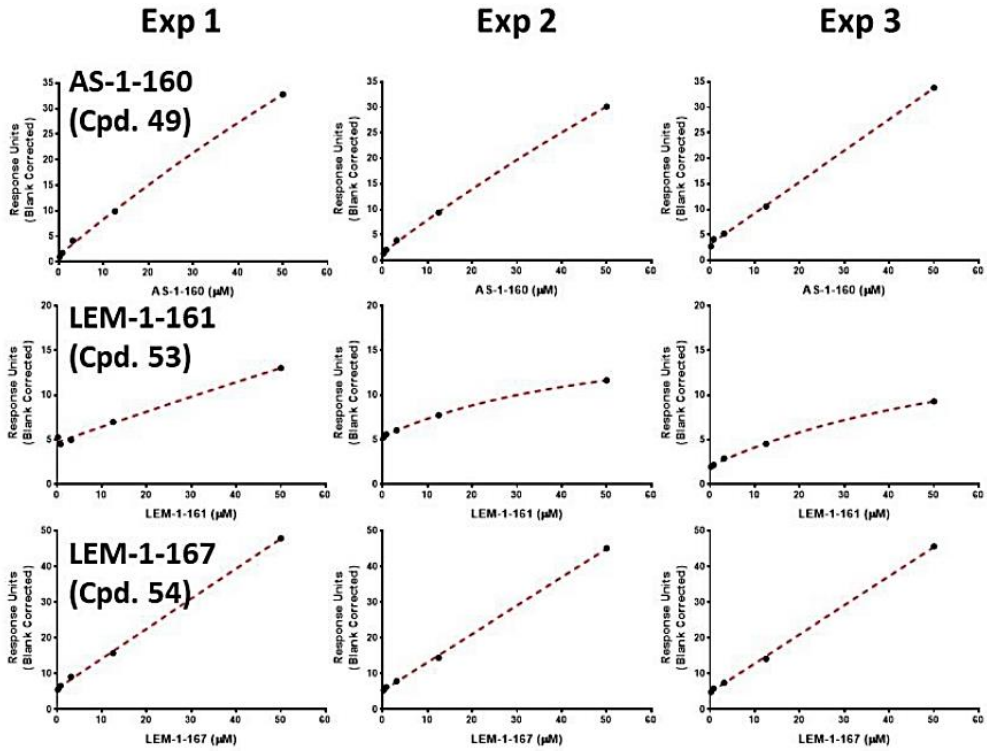
Exp 1
Exp 2
Exp 3
AS-1-160
(Cpd. 49)
LEM-1-161
(Cpd. 53)
LEM-1-167
(Cpd. 54)
Response Units
(Blank Corrected)
AS-1-160 (μM)
LEM-1-161 (μM)
LEM-1-167 (μM)

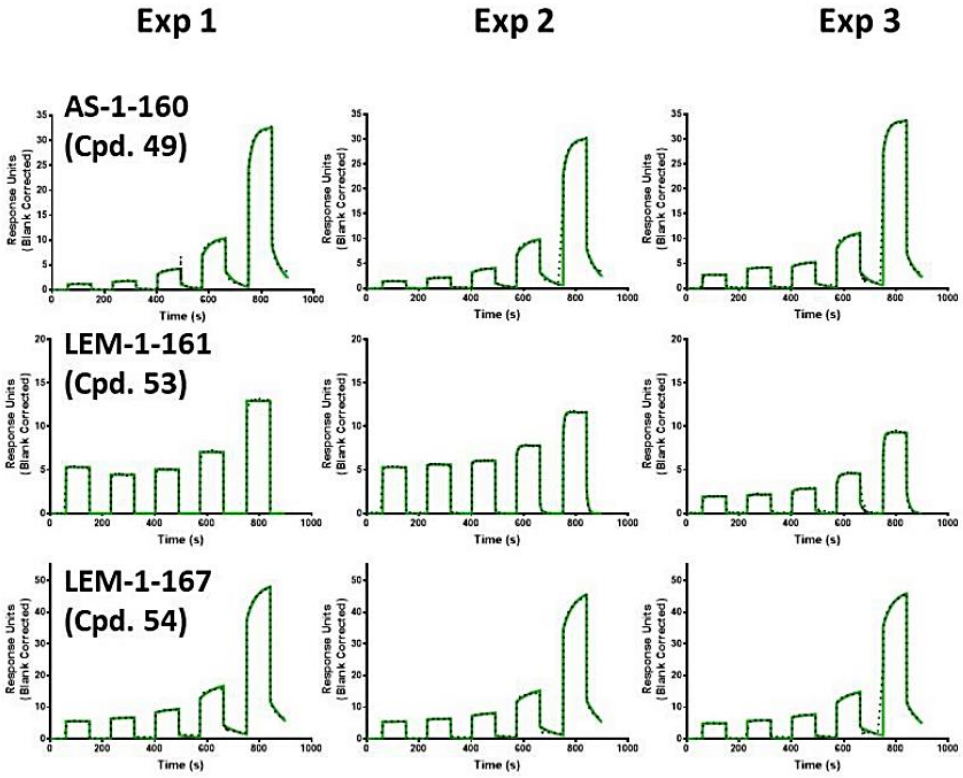
Exp 1
Exp 2
Exp 3
AS-1-160
(Cpd. 49)
LEM-1-161
(Cpd. 53)
LEM-1-167
(Cpd. 54)
Response Units
(Blank Corrected)
Time (s)

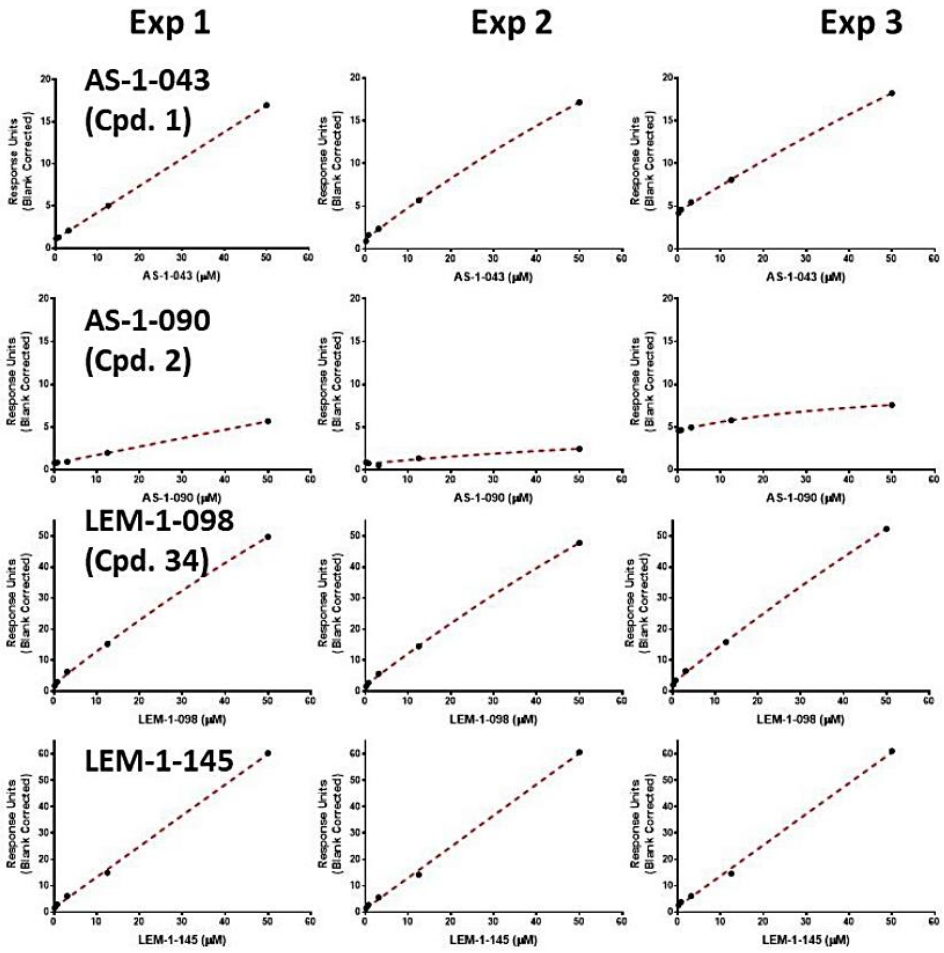
Exp 1
Exp 2
Exp 3
AS-1-043
(Cpd. 1)
AS-1-090
(Cpd. 2)
LEM-1-098
(Cpd. 34)
LEM-1-145
Response Units
(Blank Corrected)
AS-1-043 (μM)
AS-1-090 (μM)
LEM-1-098 (μM)
LEM-1-145 (μM)

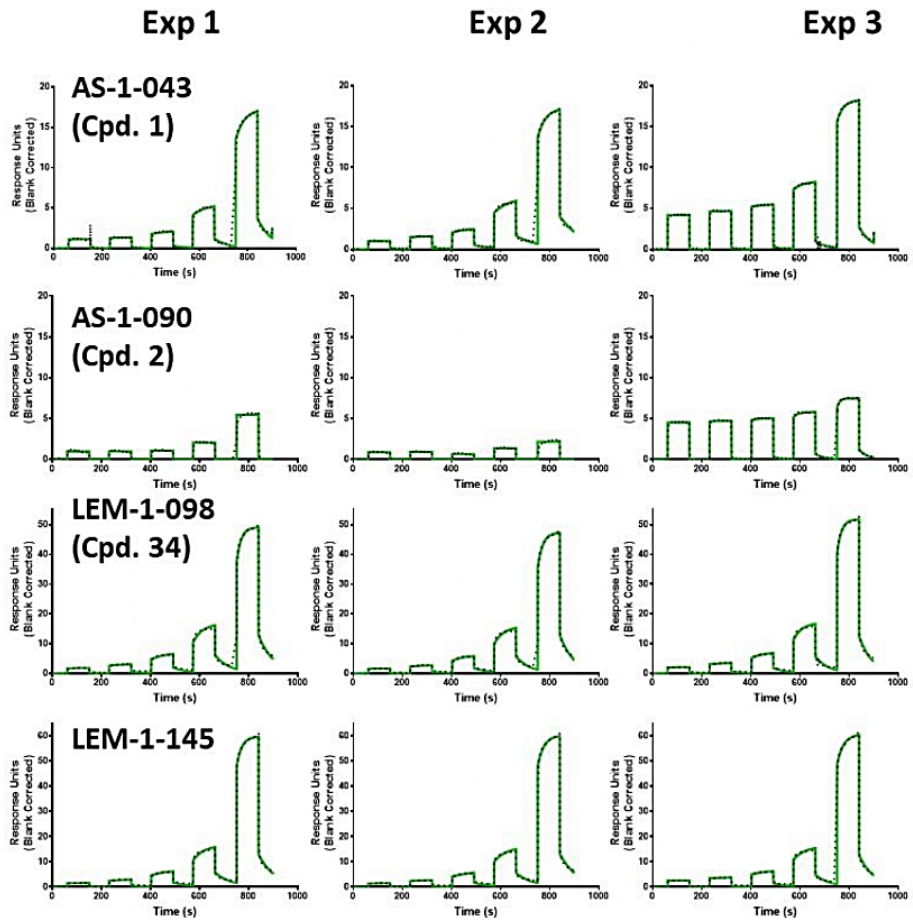

Figure S1. Evaluating the binding of compounds to TEAD4 by surface plasmon resonance (SPR). All compounds were tested as described on page S3. For each compound, sensorgrams (solid green) with the kinetic fit (black dots) are shown for 3 replicates. The steady state response (black circles) with 1:1 binding model fitting (red dashed line) are also shown for each corresponding sensorgram. Name of each tested compound is indicated on the first replicate. These data are not used for rank-ordering compounds and are solely presented to describe why we did not rely on them (see the results section for more information).

b) Isothermal Titration Calorimetry (ITC)

Binding of each compound to TEAD4 was tested by MicroCal Auto-iTC200 (Malvern Panalytical Ltd. Malvern, UK) using the reverse titrations due to poor solubility of compounds. The TEAD4 was dialyzed against the buffer (20 mM Tris pH 8.0, 150 mM NaCl), and used (120 µL) at 180 µM. A 20 µM solution of compound was loaded into the sample well (400 µL) in the 96-well tray. Data were fitted with a one binding site model using the Instrument Origin® software.

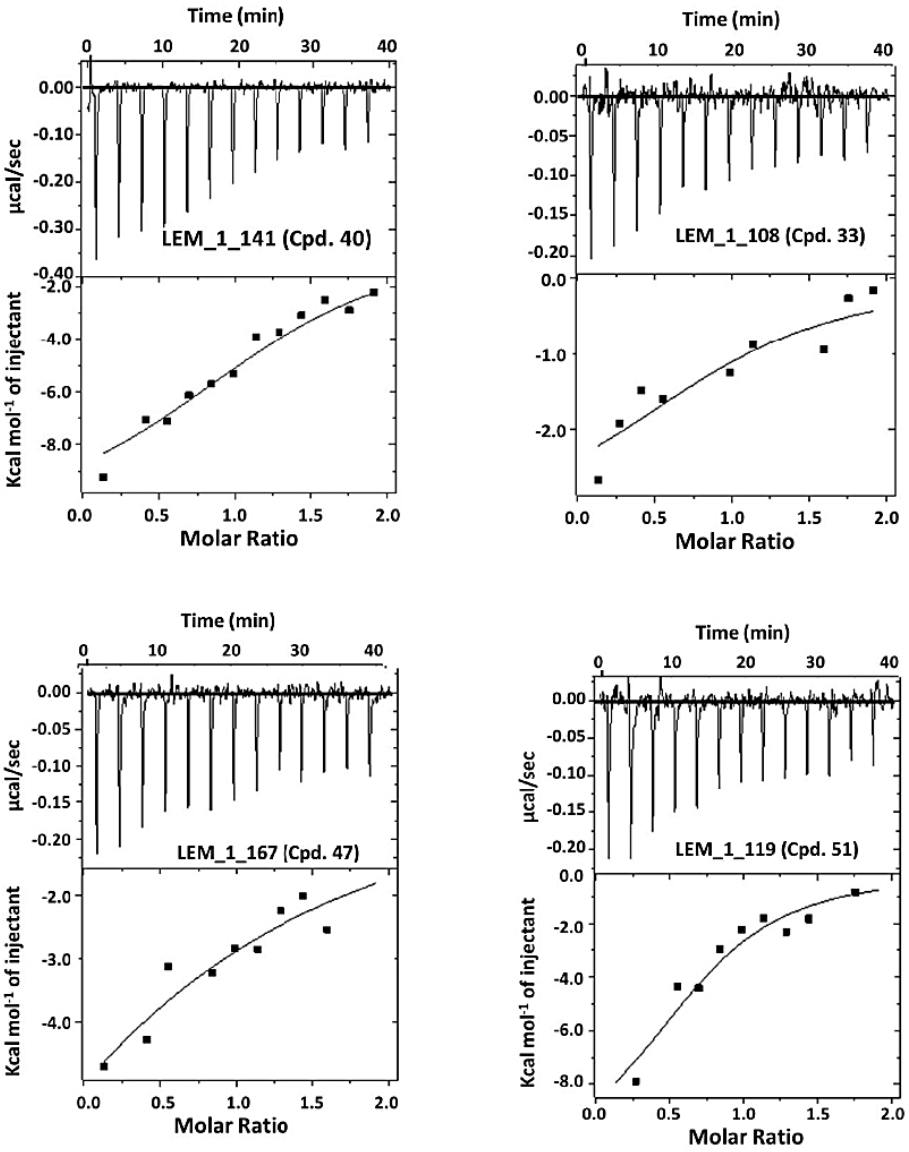

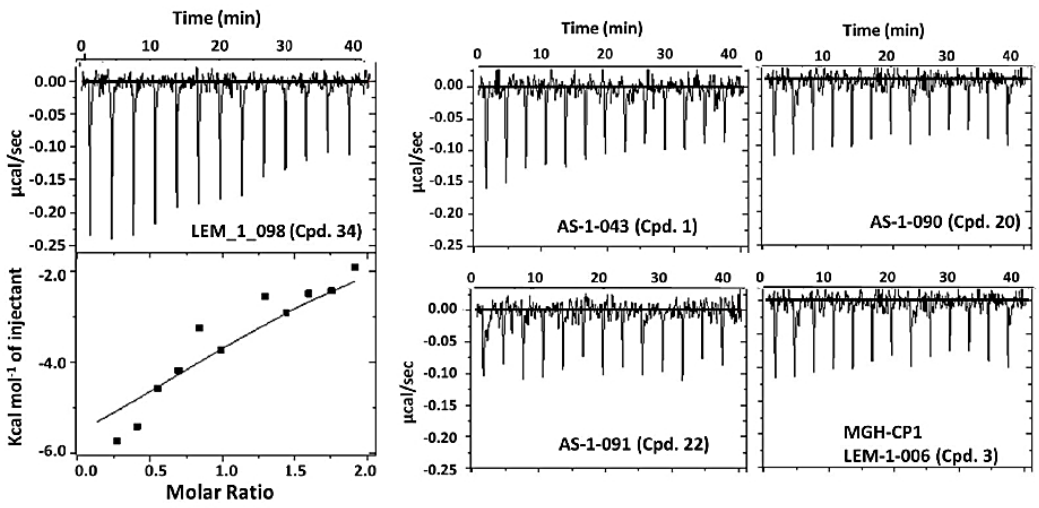

Figure S2. Evaluating the binding of compounds to TEAD4 by isothermal titration calorimetry (ITC). All experiments were performed as described on page S8.

c) Differential static light scattering (DSLS)

Binding of the compounds to TEAD4 was evaluated by monitoring the effect of compounds on the thermal stability of the protein using differential static light scattering (DSLS, StarGazer, Harbinger).[1] TEAD4 was used at final concentration of 0.2 mg/mL in a buffer consisting of 0.1 M HEPES pH 7.5 and 150 mM NaCl. This method assesses ligand binding through ligand induced stability where protein aggregation due to denaturation is measured while heating the sample from 25 to 85 °C at 1 °C/min in a 50 µL volume (covered with 50 µL of mineral oil to prevent evaporation) in a clear-bottom 384-well plate (from Nunc). Aggregation was monitored by the increase of scattered light using CCD camera detection. Pixel intensities were integrated using image analysis software, plotted against temperature and data were then fitted to a Boltzmann sigmoid function to obtain the aggregation temperature (T_{agg}) from the midpoint of the transition.

d) NMR studies to monitor free-state behavior and protein binding

The ^{1}H NMR data for the compound free-state behavior experiments and ^{19}F NMR data for the compound-binding studies were collected using 3 mm NMR tubes on a 600 MHz Bruker Avance III NMR spectrometer equipped with a helium cryoprobe and a SampleJet sample changer.

Samples for the compound free-state behavior studies were prepared by diluting DMSO-d_6 stocks of compounds (5 mM) with aqueous buffer (10 mM HEPES-d_{18}, 150 mM NaCl, 0.5 mM TCEP-d_{15}:DCl, 10% D_2O, pH 7.4) to give a final nominal compound concentration of 50 μM containing 1% DMSO-d_6. The standard Bruker 1D ^1H sequence with excitation sculpting (zgesgp) was used with a relaxation delay of 10 s and 64 scans. Spectra were processed using Bruker Topspin, and compound concentrations were determined using the ERETIC method as implemented in Bruker Topspin. Maleic acid was used for calibration of the ERETIC peak.

For the compound binding studies, the free state (SF) samples were prepared by diluting DMSO-d_6 stocks of compounds (5 mM) with aqueous buffer (100 mM HEPES, 150 mM NaCl, 10% D_2O, pH 7.5) to give a final nominal compound concentration of 50 μM containing 1% DMSO-d_6. To prepare the samples containing protein (SP), a 15.2 μM protein stock solution was prepared by diluting thawed samples of protein in storage buffer (272 μM TEAD4 in 20 mM Tris, 150 mM NaCl, 10 mM 2-mercaptoethanol, pH 8.0) with aqueous buffer (100 mM HEPES, 150 mM NaCl, 10% D_2O, pH 7.5). This 15.2 μM protein stock solution was then used to dilute DMSO-d_6 stocks of compounds (5 mM) to give samples with a final nominal compound concentration of 50 μM, TEAD4 concentration of 15 μM, and 1% DMSO-d_6 content. All protein containing solutions were kept on ice. ^{19}F NMR data were acquired using the ^1H-decoupled 1D ^{19}F Bruker experiment (zgfhigqn.2) with a relaxation delay of 5 s and 256 scans. Spectra were processed using Bruker Topspin.

e) Mass spectrometry analysis for the covalent palmitoylation of TEAD4

TEAD4 (final concentration of 15 μM) in the absence and presence (30 μM) of Palmitoyl-CoA (Palm-CoA, P9716, Sigma) was mixed with various concentrations of each compound and incubated for 2 hr at RT before being quenched by adding 0.1% trifluoroacetic acid. The resulting samples were separated on a HPLC column with 5-95% acetonitrile in water as eluent. The MS data were analyzed using an Agilent LC/MSD Time-of-Flight Mass Spectrometer equipped with an electrospray ionization source.

A: Compound 34

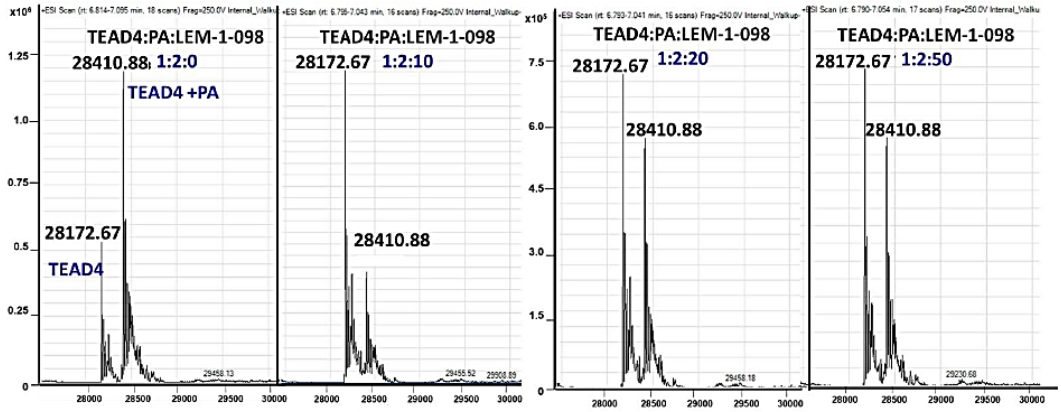

B: Compound 40

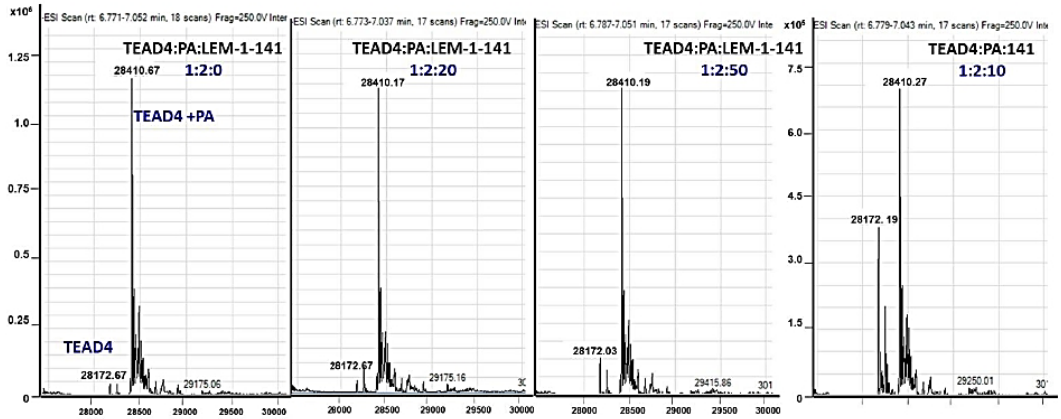

C: Compound 32

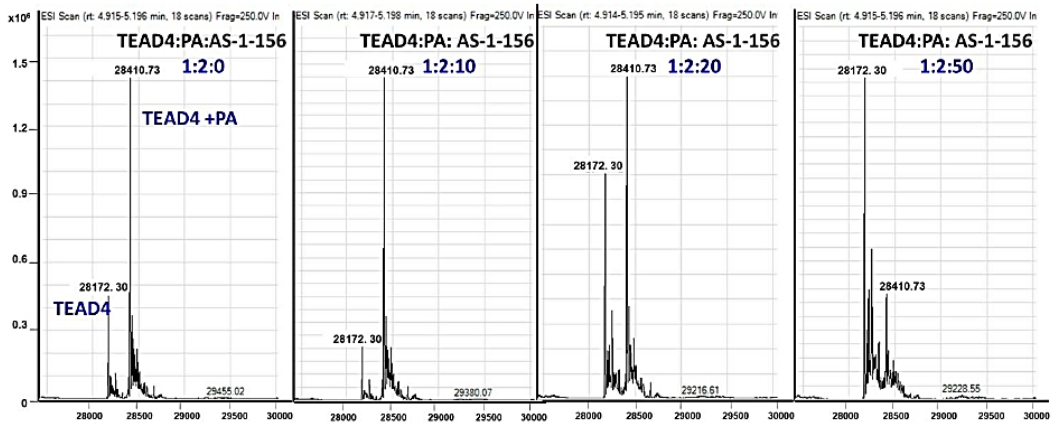

D: Compound 49

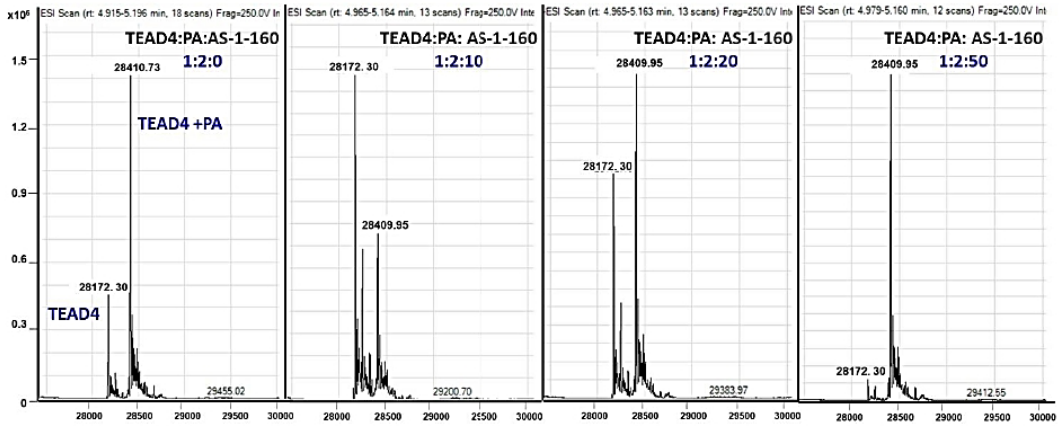

E: Compound 50

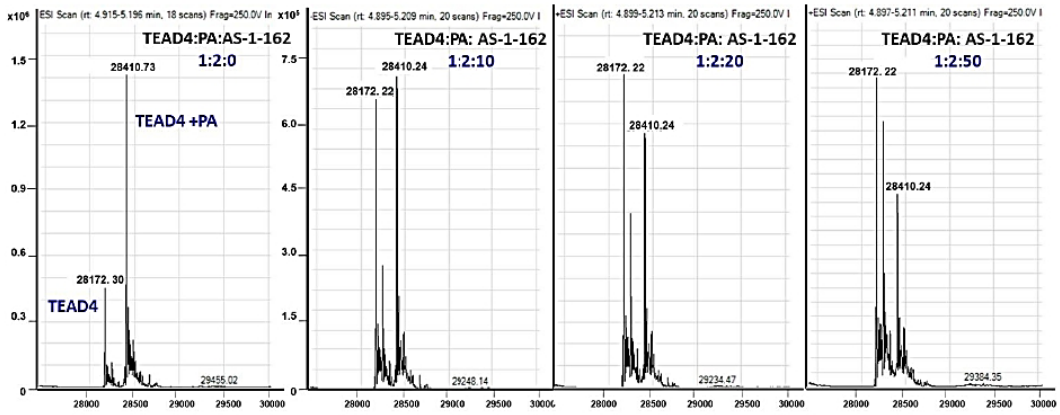

F: Compound 1

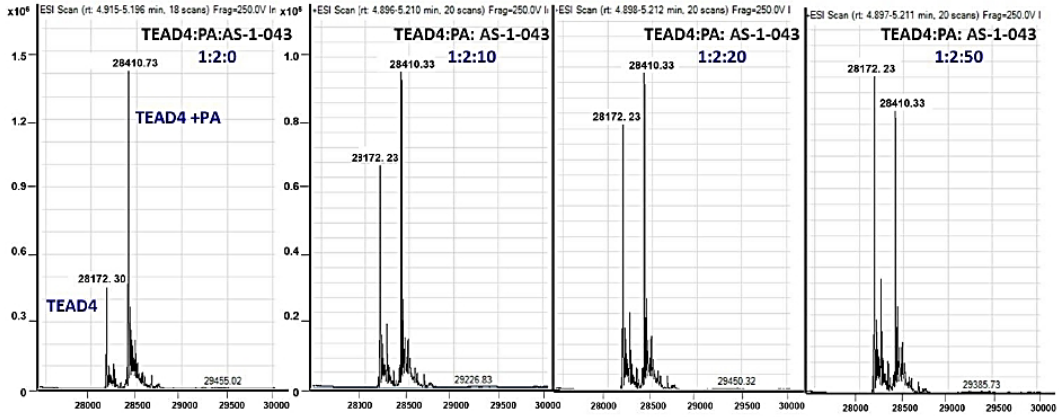

G: Compound 22

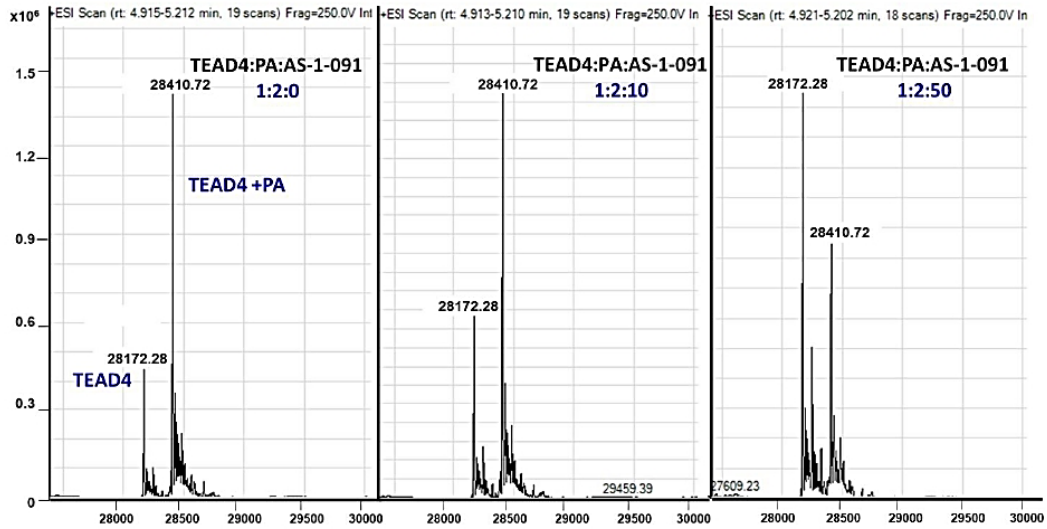

H: Compound 47

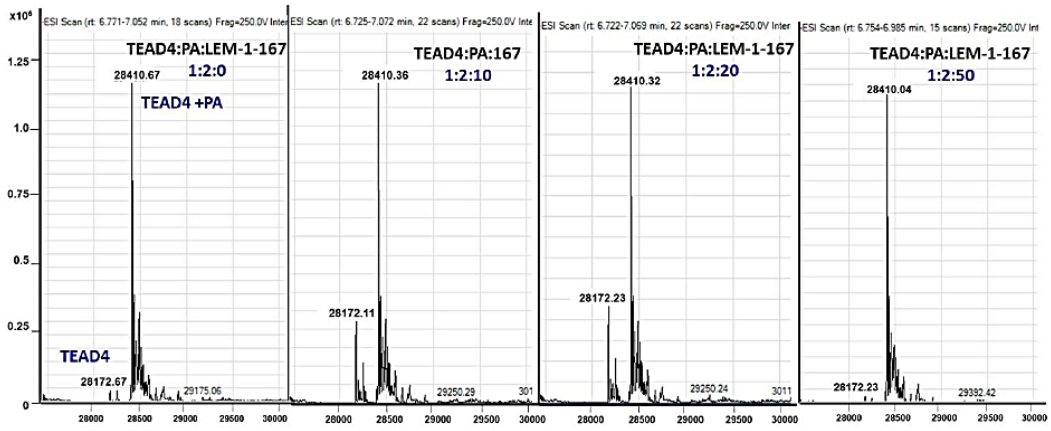

Figure S3. Monitoring the effect of small molecules on the covalent palmitoylation of TEAD4 by mass spectrometry. In each case, TEAD4 (15 μM) was incubated with Palmitoyl-CoA (30 μM) in a 1 to 2 ratio in the presence of 0-, 10-, 20- and 50-times TEAD4 molar ratio of each compound. The spectra show the peak for TEAD4 with no treatment at molecular weight of 28172 Da, and after 2h incubation with Palmitoyl-CoA at 28410 Da. The change in the spectra for different ratio of TEAD4- Palmitoyl-CoA- Compound (highlighted in blue) are presented for (A) compound **34**, (B), compound **40** (C) compound **32** (D) compound **49** (E) compound **50** (F) compound **1** (G) compound **22** (H) compound **47**.

f) Cell culture

HEK293T cells (ATCC® CRL-3216™) were grown in DMEM (Wisent) supplemented with 10% FBS (Wisent), penicillin (100 U/mL) and streptomycin (100 µg/mL).

g) TEAD Dual-luciferase reporter assay

HEK293T cells were seeded in 6-well plates ($8x10^5$/well in 2 mL) and were transfected with total 2 µg of plasmid constructs (empty pCDNA3 vector for control and 8x-GTIIC vector otherwise) per well using X-tremeGENE HP DNA Transfection Reagent (Sigma) following manufacturer instructions with a 2:1 ratio of transfection reagent:DNA 4 hours after seeding. After 20 hours, transfected cells were re-plated in white-bottom (white, 6555098, Greiner Bio One) 96-well plates (2×10^4/well in 100 µL). 4 hours after re-plating, 20 µL of compound is added at 6x final desired concentration. Matched DMSO controls with the same DMSO concentrations as compound dilutions are also included. 20 hours later, media was removed and Promega Dual-Luciferase® Reporter Assay kit was used to prepare samples for Firefly and Renilla signal measurement. In brief, 15 µL of 1X Passive Lysis Buffer was added to each well and the plate was gently shaken at room temperature for 15 minutes to lyse cells. After cell lysis, plates are put through a freeze-thaw cycle at -80 °C. Once plate temperatures have warmed to room temperature, 75 µL of Luciferase Assay Reagent II (LARII) is added to each well. Immediately after, cells were shaken for 30 seconds and Firefly emission at 580 nm was measured using CLARIOstar microplate reader (Mandel). Then 75 µL of 1X Stop & Glo® Reagent was added to each well, cells were shaken for 30 seconds and Renilla emission at 480 nm was measured.

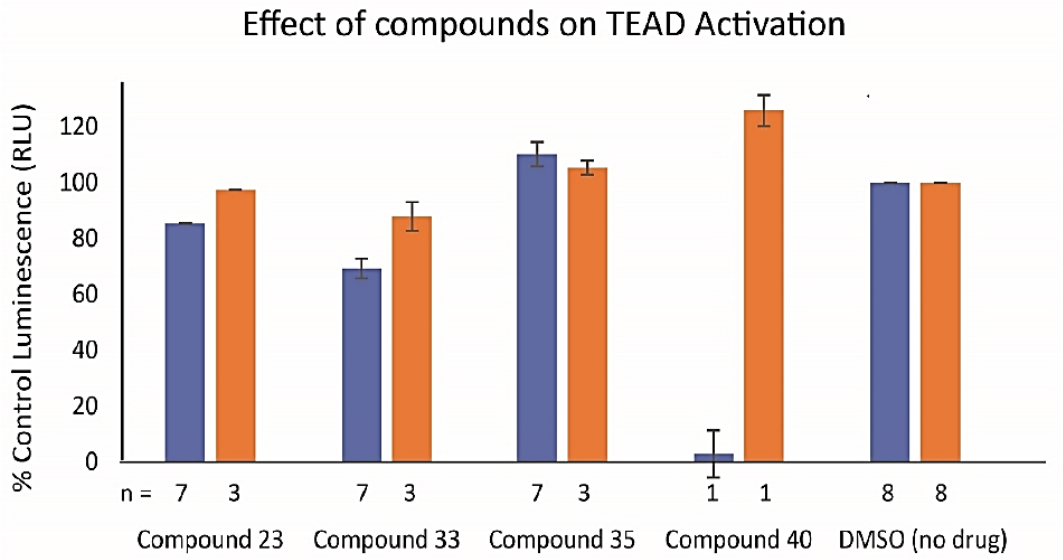

Figure S4. Effect of compounds **23, 33, 35 and 40** on TEAD activation in cells measured by dual-luciferase reporter assay (compound concentration of ~31.6 μM for blue bars and of ~10 μM for orange bars)

h) NanoBRET assay

HEK293T (ATCC® CRL-3216™) cells were grown in DMEM (Wisent) supplemented with 10% FBS (Wisent), penicillin (100 U/mL) and streptomycin (100 μg/mL) and seeded in white 96-well white plates (4 x 10^5 cells/mL). 4 h later cells were transfected with C-terminally Halotag-tagged YAP1 (0.03 μg/well), C-terminally NanoLuc-tagged TEAD1 or NL alone (0.001 μg/well) and 0.07 μg of empty vector, using Extreme gene HP transfection reagent, following manufacturer instructions. The following day media was removed and replaced with 40 μl DMEM F12 (no phenol red, 4% FBS) +/- 618 fluorescent ligand (Promega, 0.5 μL/mL) and +/- indicated inhibitors concentrations. 4 h later 10 μL of Nanoglo substrate was added (Promega 8 μL/mL) and 460 nm donor and 618 nm acceptor signals were read. Mean corrected NanoBRET ratios (mBU) were determined by subtracting mean of 618/460 signal from cells without NanoBRET™ 618 Ligand x 1000 from mean of 618/460 signal from cells with NanoBRET™ 618 Ligand x 1000.

i) Total RNA isolation, cDNA synthesis and real-time quantitative PCR

Total RNA was extracted from treated MDA-MB-231 cell monolayers using TriZol reagent (Life Technologies, Gaithersburg, MD). For cDNA synthesis, 2 μg of total RNA were reverse-transcribed using a high-capacity cDNA reverse transcription kit (Applied Biosystems, Foster

City, CA). cDNA was stored at -80 °C prior to PCR. Gene expression was quantified by real-time quantitative PCR using iQ SYBR Green Supermix (Bio-Rad, Hercules, CA). DNA amplification was carried out using an Icycler iQ5 (Bio-Rad, Hercules, CA) and product detection was performed by measuring binding of the fluorescent dye SYBR Green I to double-stranded DNA. The QuantiTect primer sets were provided by Qiagen (Valencia, CA): CTGF (Hs_CTGF_1_SG, QT00052899), Cyr61 (Hs_CYR61_1_SG, QT00003451), PPIA (Hs_PPIA_4_SG, QT01866137), and GAPDH (Hs_GAPDH_1_SG, QT00079247). The relative quantities of target gene mRNA compared against two internal controls, GAPDH and PPIA mRNA, were measured by following a ΔC_T method employing an amplification plot (fluorescence signal *vs*. cycle number). The difference (ΔC_T) between the mean values in the triplicate samples of target gene and those of GAPDH and PPIA mRNAs were calculated by CFX Manager™ (Bio-Rad, Hercules, CA) and the relative quantified value (RQV) was expressed as $2^{-\Delta C_T}$.

j) Real-time cell migration assay

Cell migration assays were carried out using the Real-Time Cell Analyzer (RTCA) Dual-Plate (DP) Instrument of the xCELLigence system (Roche Diagnostics). Adherent MDA-MD-231 breast cancer cells were treated with vehicle (1% DMSO) or 10 μM compound **34** (**LM98**) for 48 hours in serum-free media. Cells were then trypsinized and seeded (20,000 cells/well) onto CIM-Plates 16 (Roche Diagnostics). These migration plates are similar to conventional Transwells (8 μm pore size) but have gold electrode arrays on the bottom side of the membrane to provide real-time measurement of cell migration. Prior to cell seeding, the underside of the wells from the upper chamber were coated with 25 μL of 0.15% gelatin in PBS and incubated for 1 hour at 37 °C. Cell migration was monitored for 3 hours, and the impedance values were measured by the RTCA DP Instrument software and expressed in arbitrary units. Each experiment was performed in triplicate.

2. TEAD2 purification, crystallization, and structural determination

The human TEAD2 gene (residue range 221-451) was subcloned into a pNIC-CH vector encoding a C-terminal His6 tag and expressed in pET28-DE3 E.coli cells. The recombinant TEAD2 YAP-binding domain was first affinity purified with Nickel-NTA resin followed by size-exclusion chromatography using S200 column pre-equilibrated with 20 mM Tris-HCl [pH 8.0] and 150 mM NaCl. Prior to setting crystal trays, TEAD2 at 10 mg/mL was mixed with 3-fold molar excess of compound **34** (**LM98**) and incubated on ice for 30 minutes. Co-crystals of

TEAD2-**LM98** were obtained in vapour-diffusion sitting drops by mixing the protein at 1:1 ratio with precipitant solution containing 3.5 M sodium formate, and 0.1 M Bis-Tris Propane pH [7.0]. Crystals were then cryo-protected using reservoir solution supplemented with 2 mM Compound **34** (**LM98**) and 20% (v/v) glycerol, and cryo-cooled in liquid nitrogen. X-ray diffraction data for TEAD2-LM98 were collected at the beamline 24ID-E at the Advanced Photon Source (APS). Data were processed with HKL3000[1]. Initial phases were obtained by using TEAD2-flufenamic acid structure (PDB ID: 5DQ8) as initial model in Fourier transform with Refmac[2]. Model building was performed in COOT[3] and refined with Refmac. Molprobity[4] was used for structural validation. Compound **34** (**LM98**) restraints were generated using Grade Web Server (http://grade.globalphasing.org). Images were prepared with PyMol (www.pymol.org). Data collection and refinement statistics for TEAD2-LM98 are summarized in the **Table S1**.

Table S1. X-ray crystallography data collection and refinement statistics

	TEAD2_LM98 (PDB ID:6VAH)
Data collection	
Space group	C2
Cell dimensions	
a, *b*, *c* (Å)	120.79, 61.30, 79.86
α, β, γ (°)	90.00, 118.10, 90.00
Resolution (Å) (highest resolution shell)	50.0 - 2.1 (2.14-2.1)
R_{merge}	0.09 (0.55)
$I / \sigma I$	9.2 (1.85)
Completeness (%)	97.0 (88.2)
Redundancy	4.1 (2.9)
Refinement	
Resolution (Å))	39.07 - 2.11
No. reflections	27256
R_{work} / R_{free}	20.3/24.2
No. atoms	
Protein	3163
Ligand	46
Water	28
B-factors	
Protein	57.3
Ligand	55.1
Water	50.3
R.m.s. deviations	
Bond lengths (Å)	0.009
Bond angles (°)	1.383

*Values in parentheses are for highest-resolution shell.

3. References

1. Vedadi, M.; Niesen, F.H.; Allali-Hassani, A.; Fedorov, O.Y.; Finerty, P.J. Jr.; Wasney, G.A.; Yeung, R.; Arrowsmith, C.; Ball, L.J.; Berglund, H.; Hui, R.; Marsden, B.D.; Nordlund, P.; Sundstrom, M.; Weigelt, J.; Edwards, A.M. Chemical Screening Methods to Identify Ligands that Promote Protein Stability, Protein Crystallization, and Structure Determination. *Proc Natl Acad Sci USA* **2006**, *103*,15835–15840.

2. Minor, W.; Cymborowski, M.; Otwinowski, Z.; Chruszcz, M. HKL -3000: the Integration of Data Reduction and Structure Solution – from Diffraction Images to an Initial Model in Minutes. *Acta Crystallographica* Section D Biological Crystallography **2006,** *62*, 859–866.

3. Evans, P.R.; Murshudov, G.N. How Good are my Data and What Is the Resolution? *Acta Crystallographica* Section D Biological Crystallography **2013**, *69*, 1204–1214.

4. Emsley, P.; Lohkamp, B.; Scott, W.G.; Cowtan, K. Features and Development of Coot. *Acta Crystallographica* Section D Biological Crystallography **2010**, *66*, 486–501.

5. Williams, C.J.; Headd, J.J.; Moriarty, N.W.; Prisant, M.G.; Videau, L.L.; Deis, L.N.; Verma, V.; Keedy, D.A.; Hintze, B.J.; Chen, V.B.; Jain, S.; Lewis, S.M.; Arendall, W.B. 3rd; Snoeyink, J.; Adams, P.D.; Lovell, S.C.; Richardson, J.S.; Richardson, D.C. MolProbity: More and Better Reference Data for Improved All-Atom Structure Validation. *Protein Science* **2018**, 27, 293–315.

4. NMR spectra

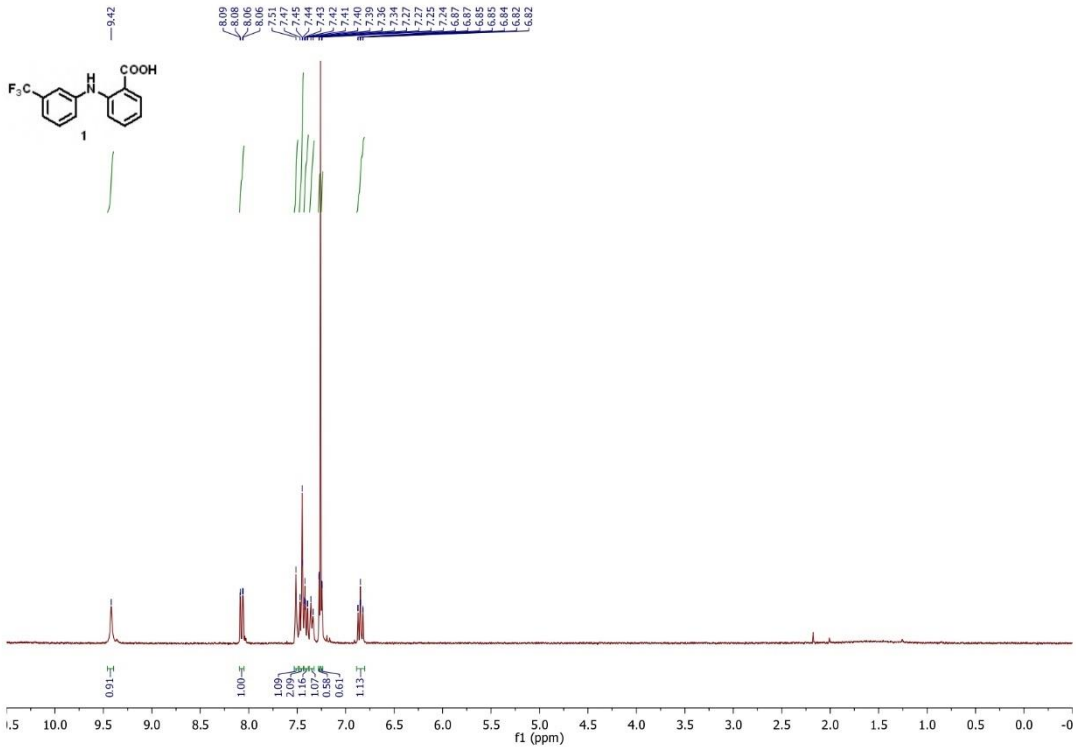
9.42
8.09
8.08
8.06
8.06
7.51
7.47
7.45
7.44
7.43
7.42
7.41
7.40
7.39
7.36
7.34
7.27
7.27
7.25
7.24
6.87
6.87
6.85
6.85
6.84
6.82
6.82
COOH
F3C
H
N
1
0.91
1.00
1.09
2.09
1.16
1.07
0.97
0.61
1.13
f1 (ppm)

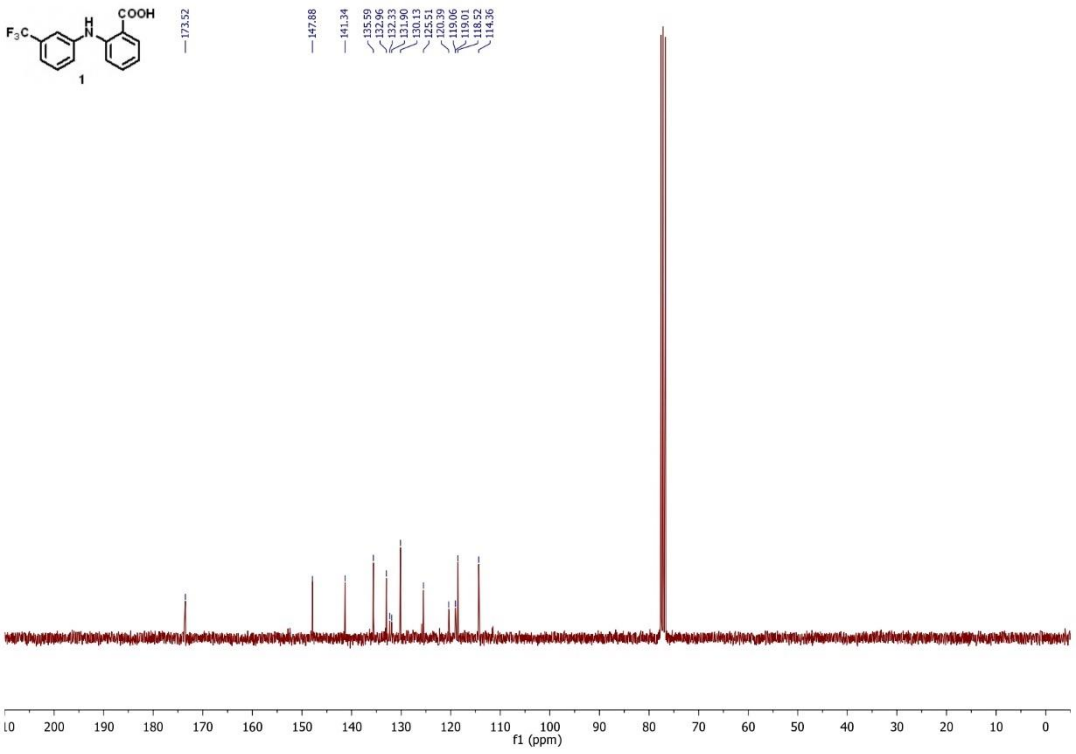
COOH
F3C
H
N
1
173.52
147.88
141.34
135.59
132.96
132.33
131.90
130.13
125.51
120.39
119.06
119.01
118.52
114.36
f1 (ppm)

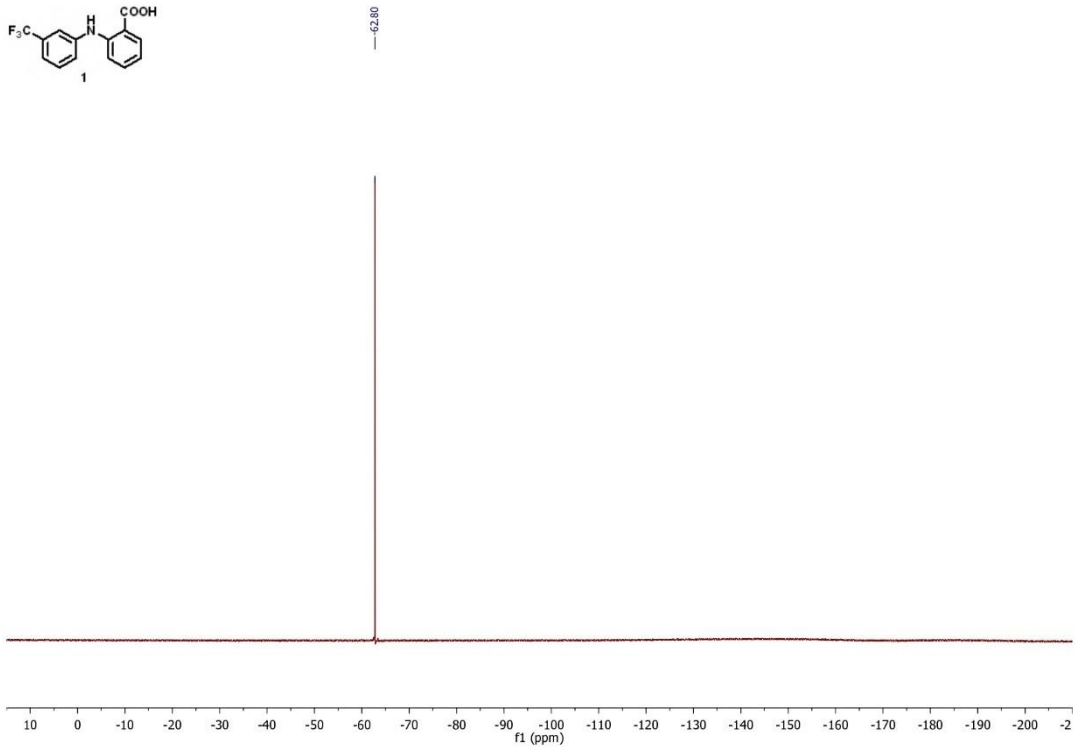
COOH
F3C
H
N
1
-62.80
10 0 -10 -20 -30 -40 -50 -60 -70 -80 -90 -100 -110 -120 -130 -140 -150 -160 -170 -180 -190 -200 -2
f1 (ppm)

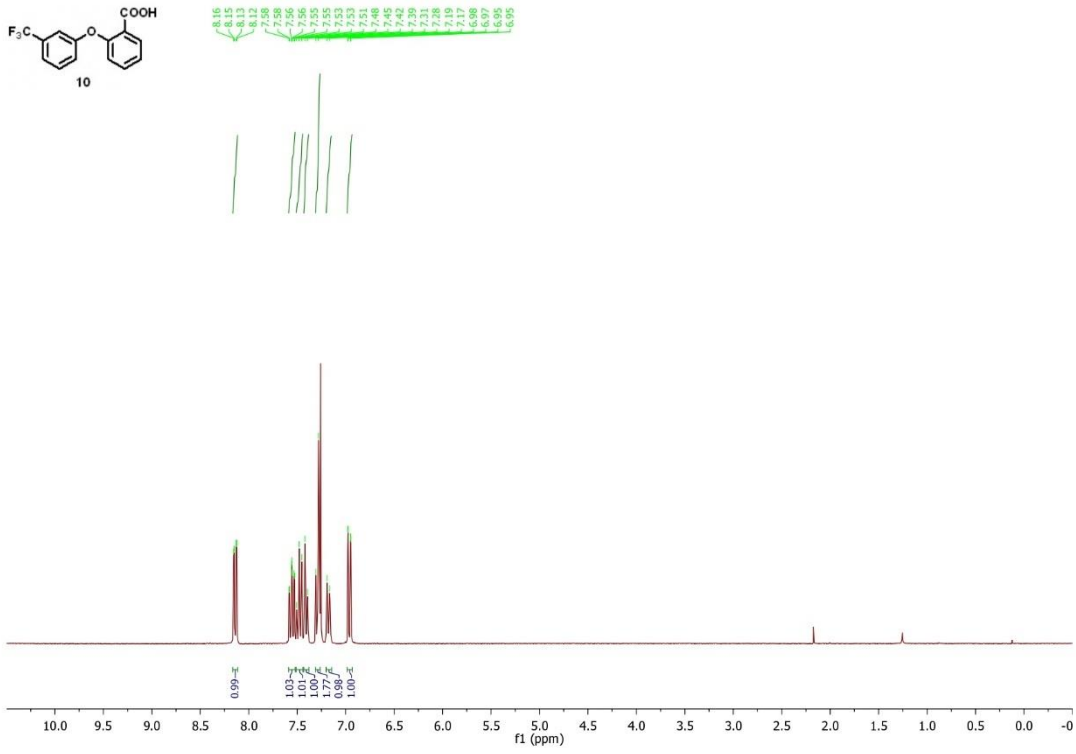
COOH
F3C
O
10
8.16
8.15
8.13
8.12
7.58
7.56
7.55
7.53
7.51
7.48
7.45
7.43
7.39
7.31
7.28
7.19
7.17
6.98
6.97
6.96
6.95
0.99
1.03
1.01
1.00
1.77
0.98
1.00
10.0 9.5 9.0 8.5 8.0 7.5 7.0 6.5 6.0 5.5 5.0 4.5 4.0 3.5 3.0 2.5 2.0 1.5 1.0 0.5 0.0 -0
f1 (ppm)

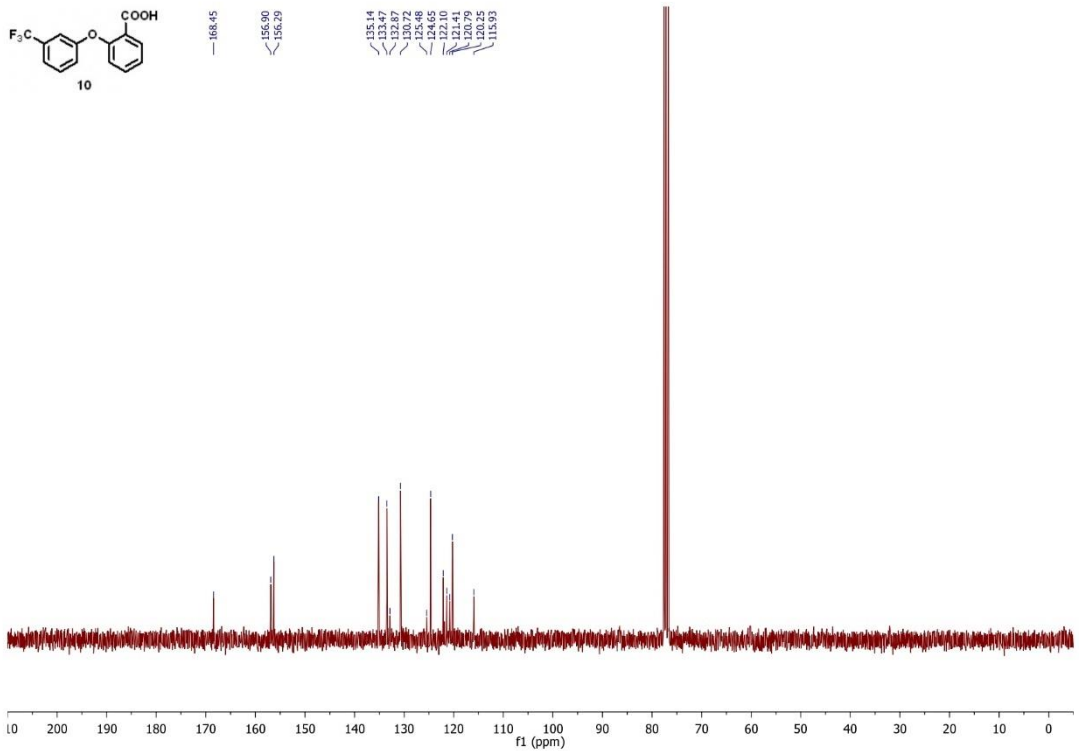
COOH
F3C
O
10
168.45
156.90
156.29
135.14
133.47
132.87
130.72
125.48
124.65
122.10
121.41
120.79
120.25
115.93
f1 (ppm)

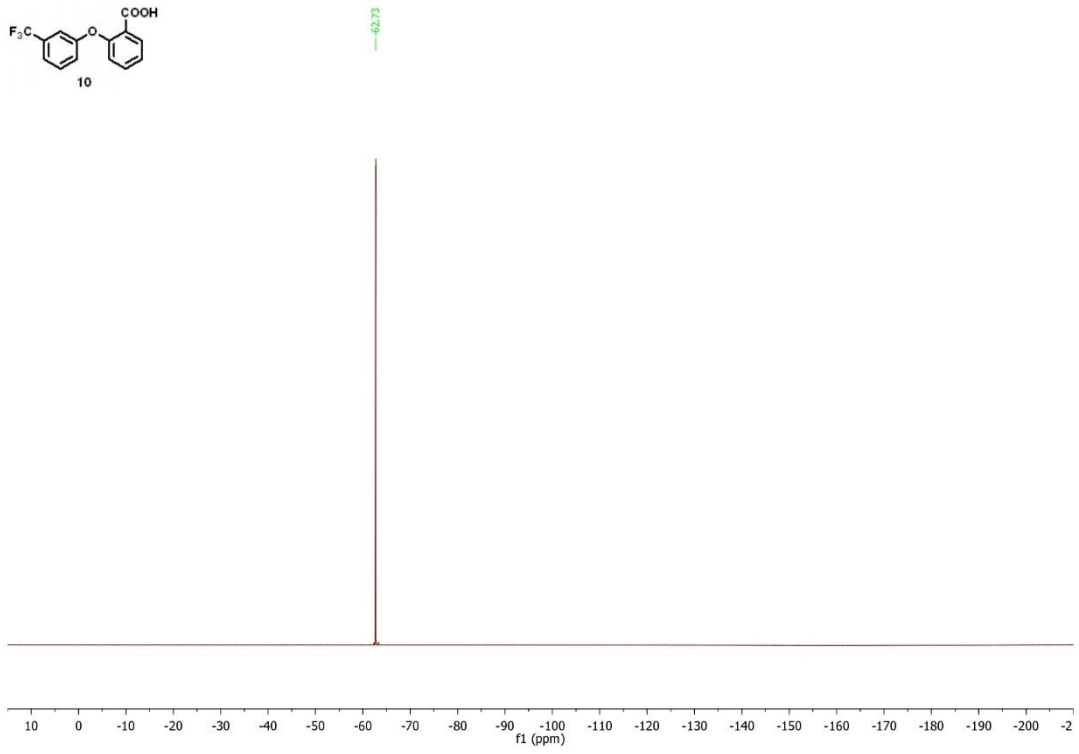
COOH
F3C
O
10
-62.73
f1 (ppm)

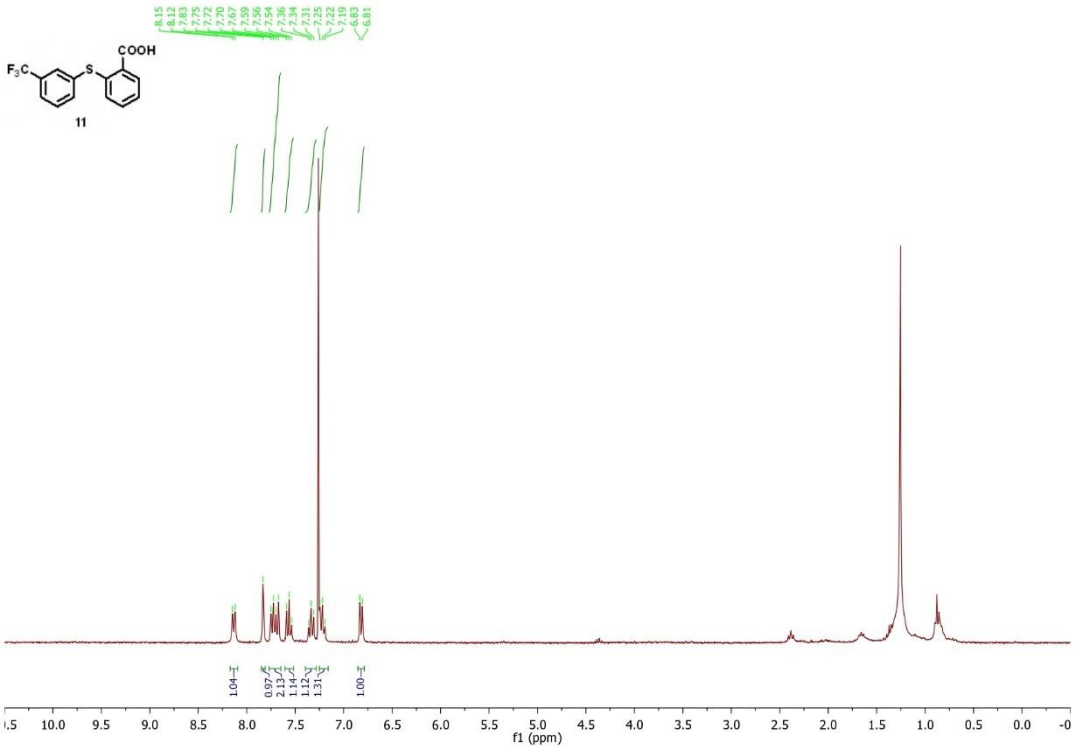
COOH
F3C
S
11
f1 (ppm)

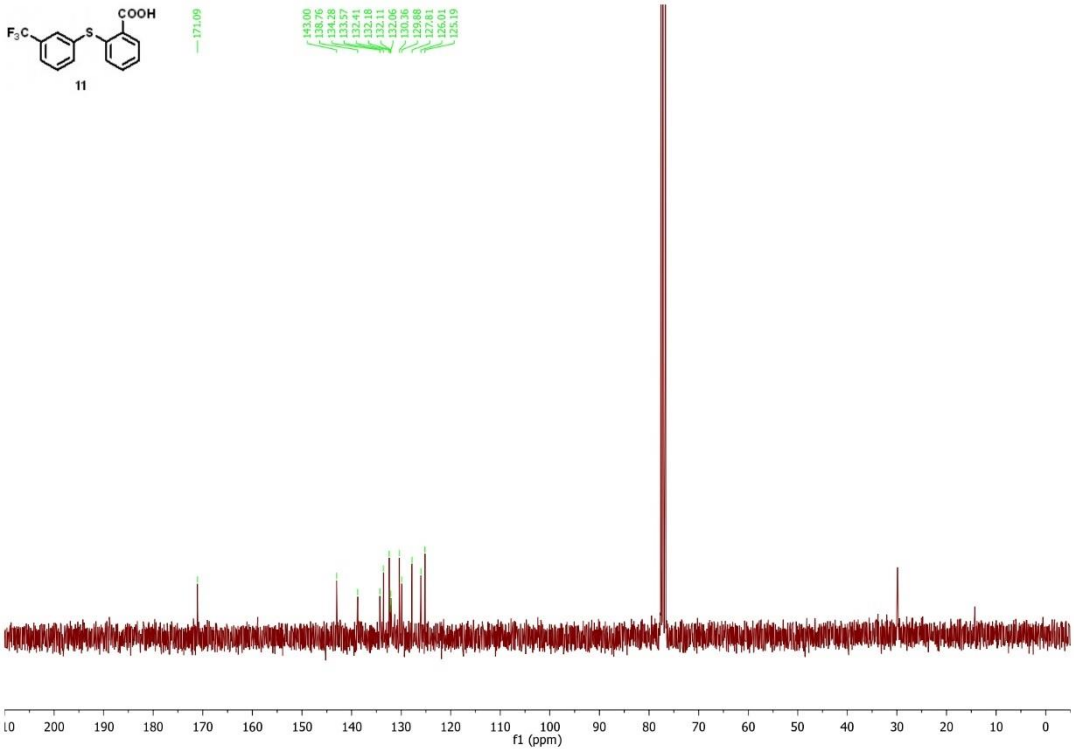
COOH
F3C
S
11
f1 (ppm)

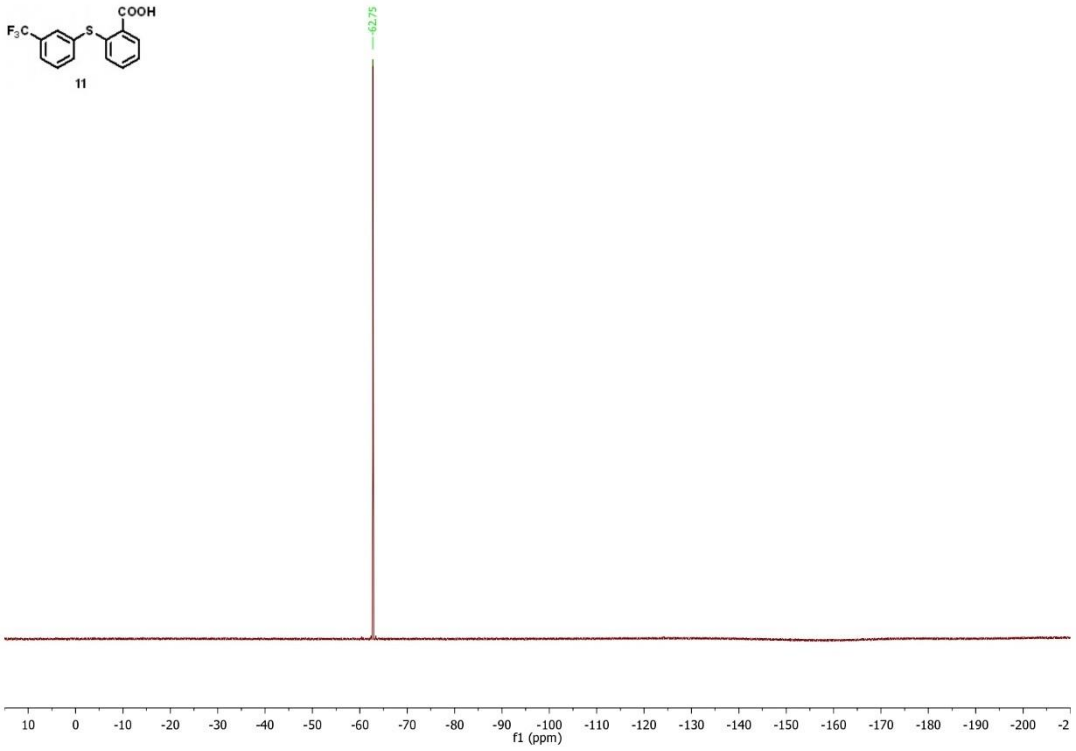
COOH
F3C
S
11
-62.75
10 0 -10 -20 -30 -40 -50 -60 -70 -80 -90 -100 -110 -120 -130 -140 -150 -160 -170 -180 -190 -200 -2
f1 (ppm)

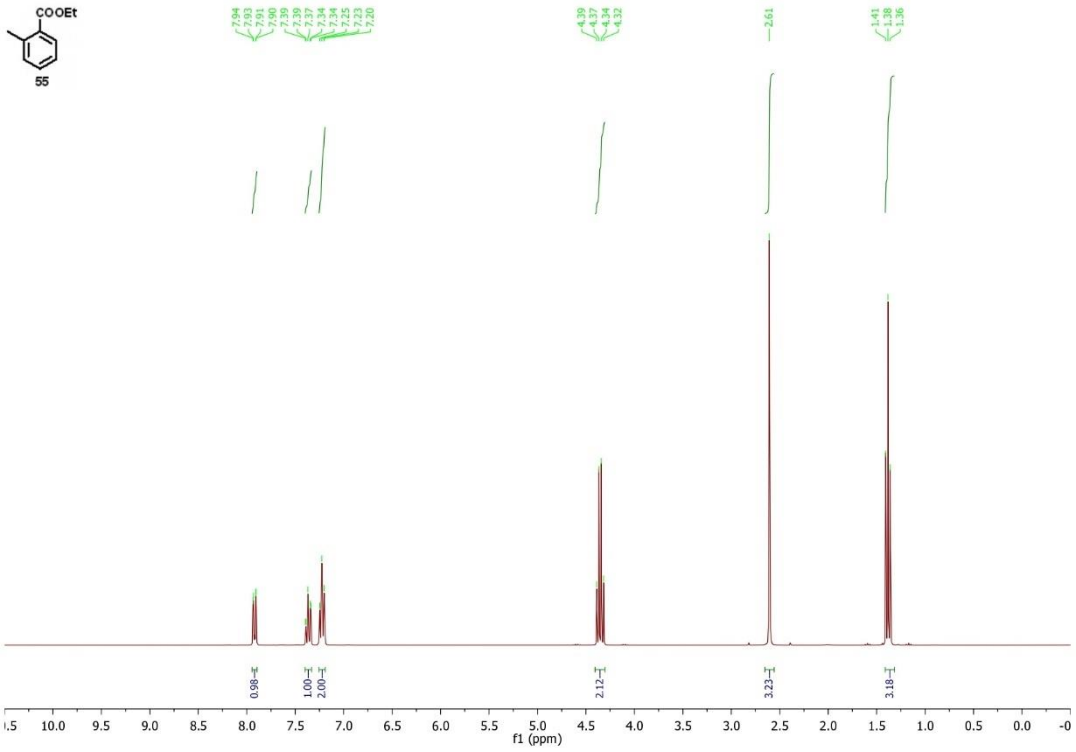
COOEt
55
7.94
7.93
7.91
7.90
7.39
7.39
7.37
7.34
7.34
7.25
7.23
7.20
4.39
4.37
4.34
4.32
2.61
1.41
1.38
1.36
0.98
1.00
2.00
2.12
3.23
3.18
f1 (ppm)

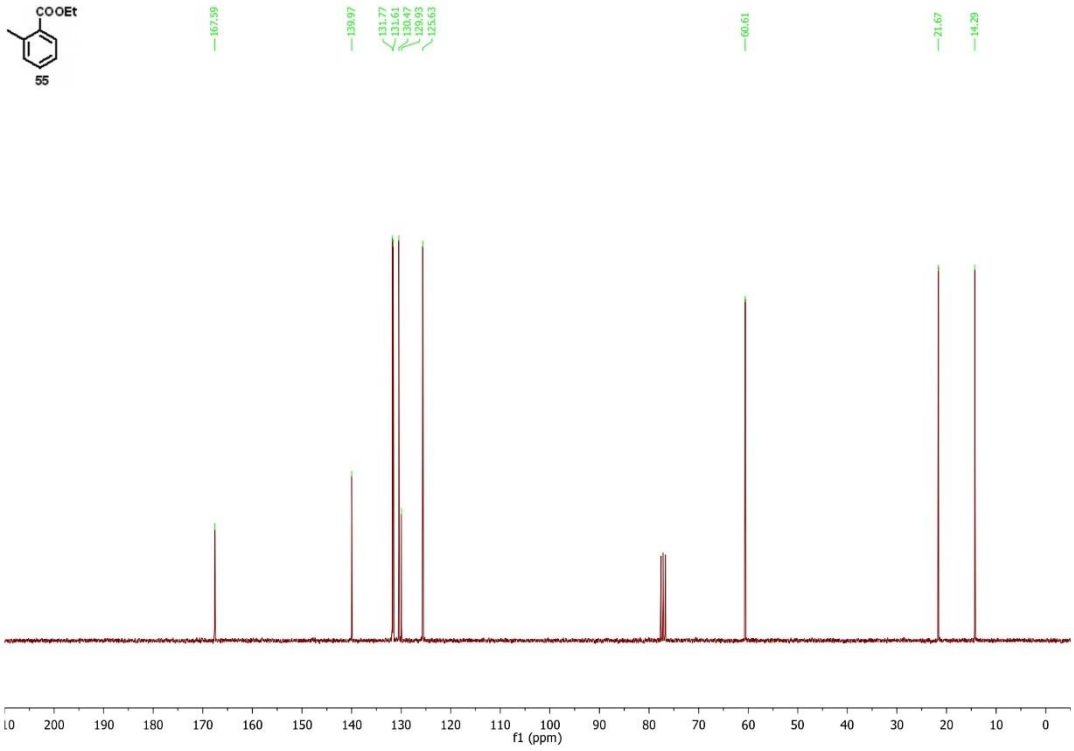
COOEt
55
167.59
139.97
131.77
131.61
130.47
129.93
125.63
60.61
21.67
14.29
f1 (ppm)

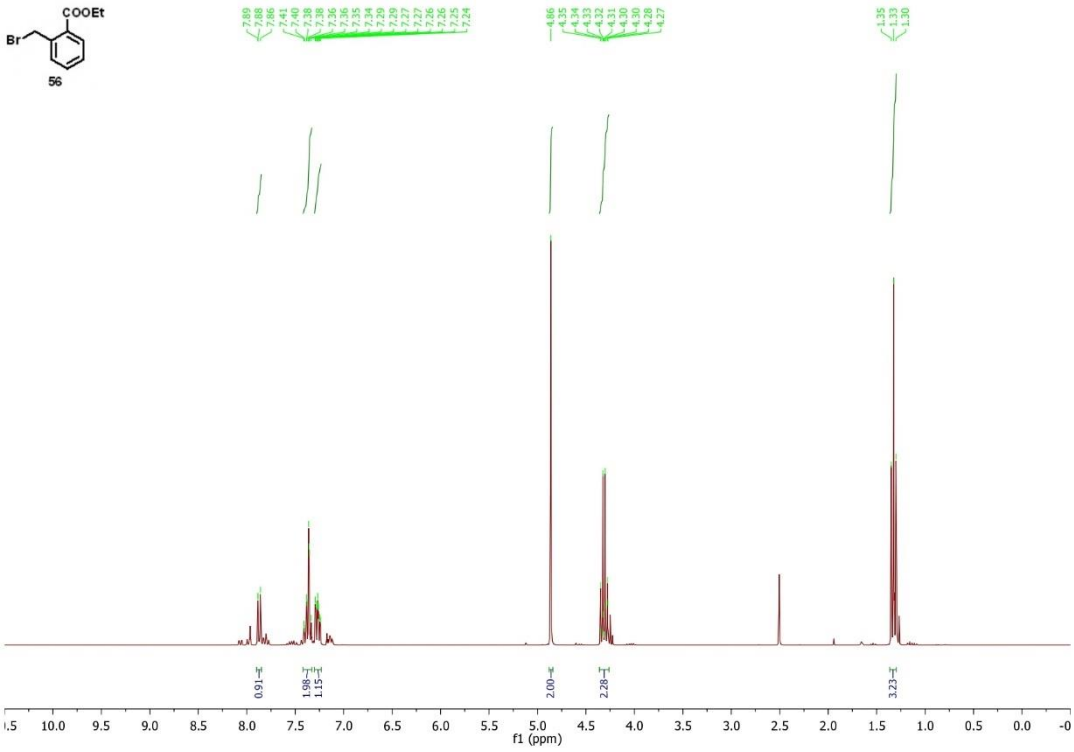
COOEt
Br
56
7.89
7.88
7.86
7.41
7.40
7.38
7.36
7.35
7.34
7.29
7.27
7.26
7.25
7.24
4.36
4.35
4.34
4.33
4.32
4.31
4.30
4.28
4.27
1.35
1.33
1.30
0.91
1.98
1.15
2.00
2.28
3.23
f1 (ppm)

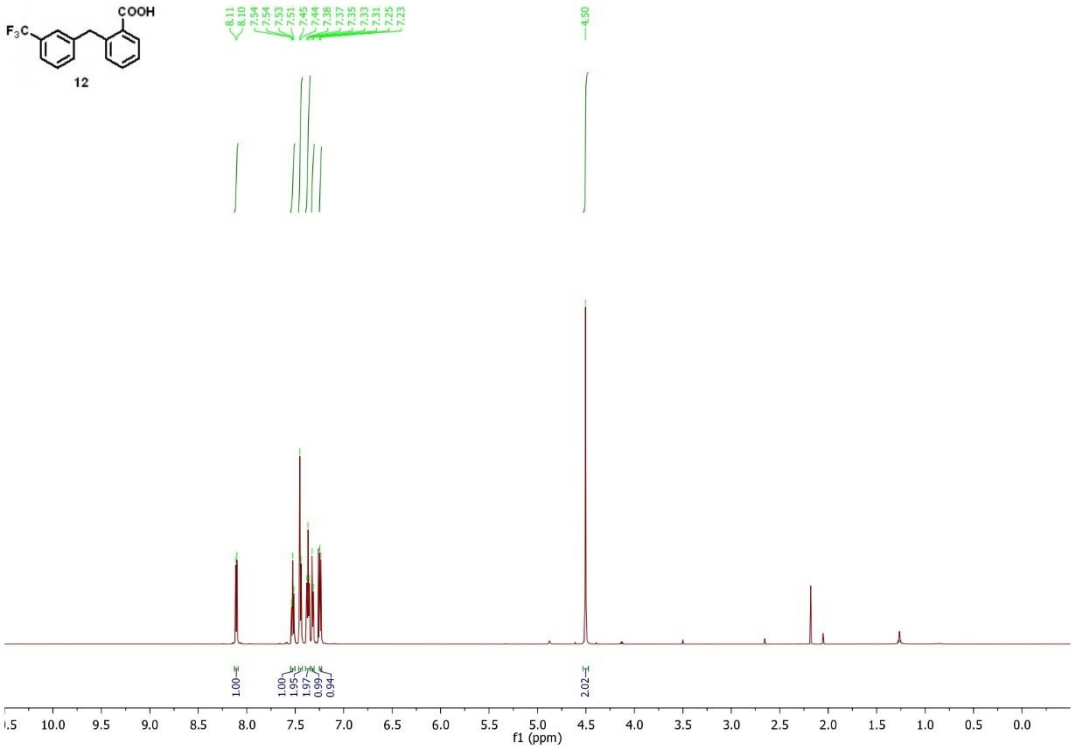
COOH
F3C
12
8.11
8.10
7.54
7.54
7.53
7.51
7.45
7.44
7.38
7.37
7.35
7.33
7.31
7.25
7.23
4.50
1.00
1.00
1.95
1.97
0.99
0.94
2.02
f1 (ppm)

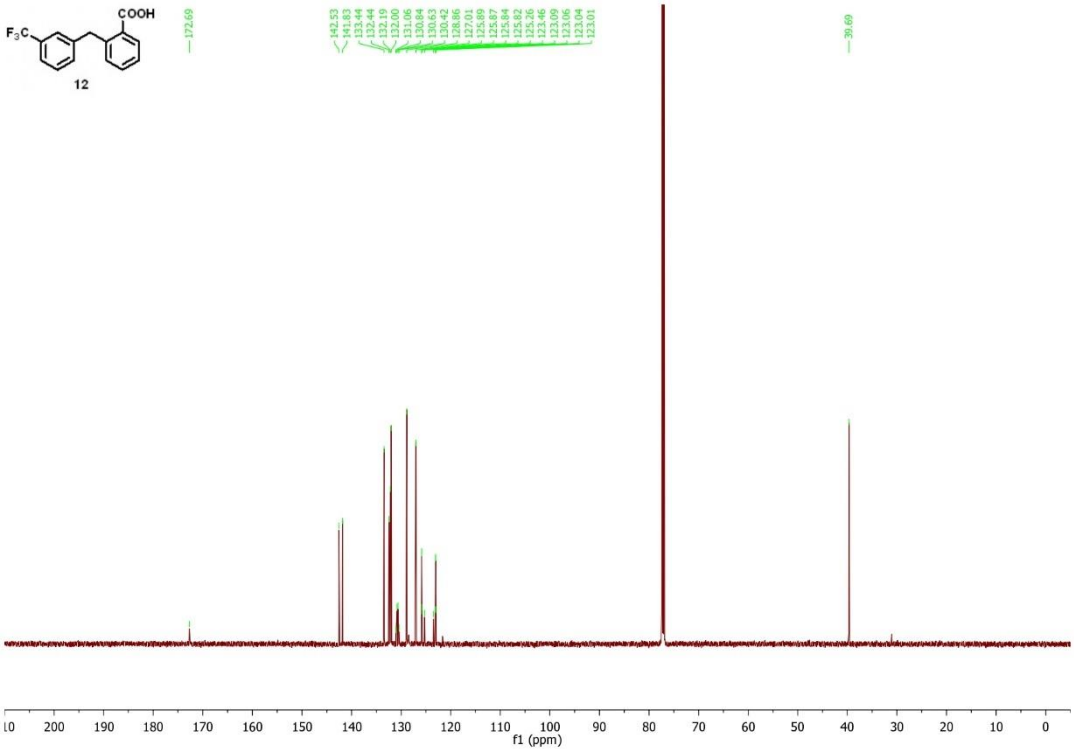
COOH
F3C
12
172.69
142.53
141.83
133.44
132.44
132.19
132.00
131.06
130.84
130.63
130.42
128.86
127.01
126.89
125.87
125.84
125.82
125.26
123.46
123.09
123.06
123.04
123.01
39.69
f1 (ppm)

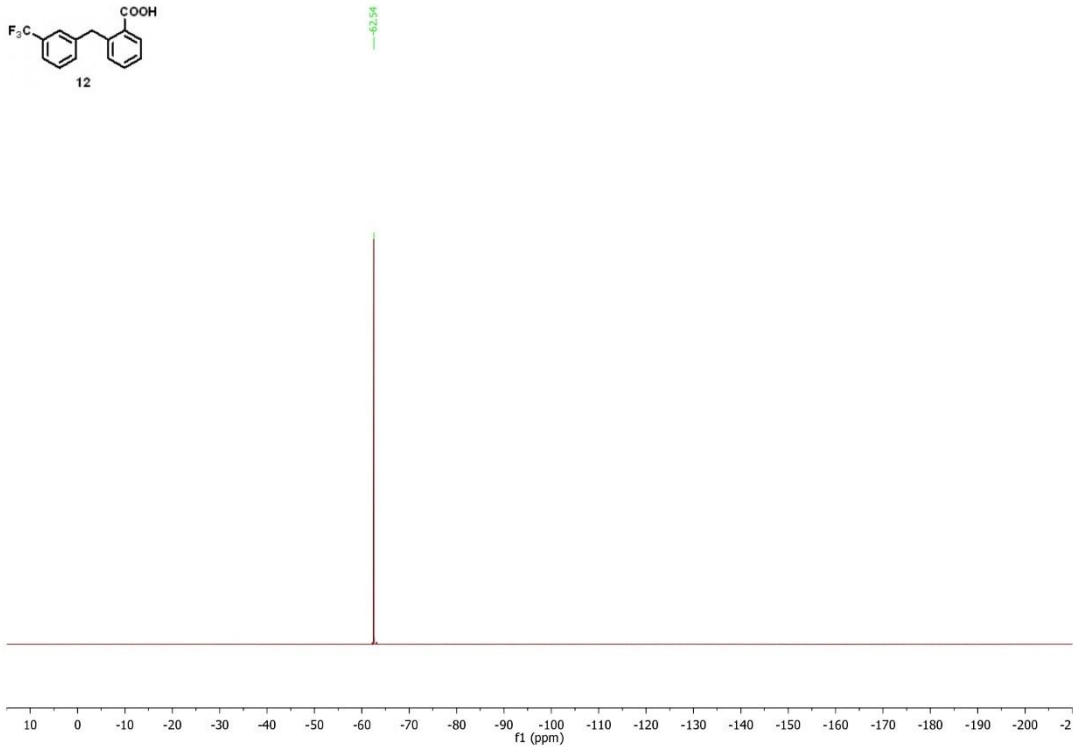
COOH
F3C
12
-62.54
10 0 -10 -20 -30 -40 -50 -60 -70 -80 -90 -100 -110 -120 -130 -140 -150 -160 -170 -180 -190 -200 -2
f1 (ppm)

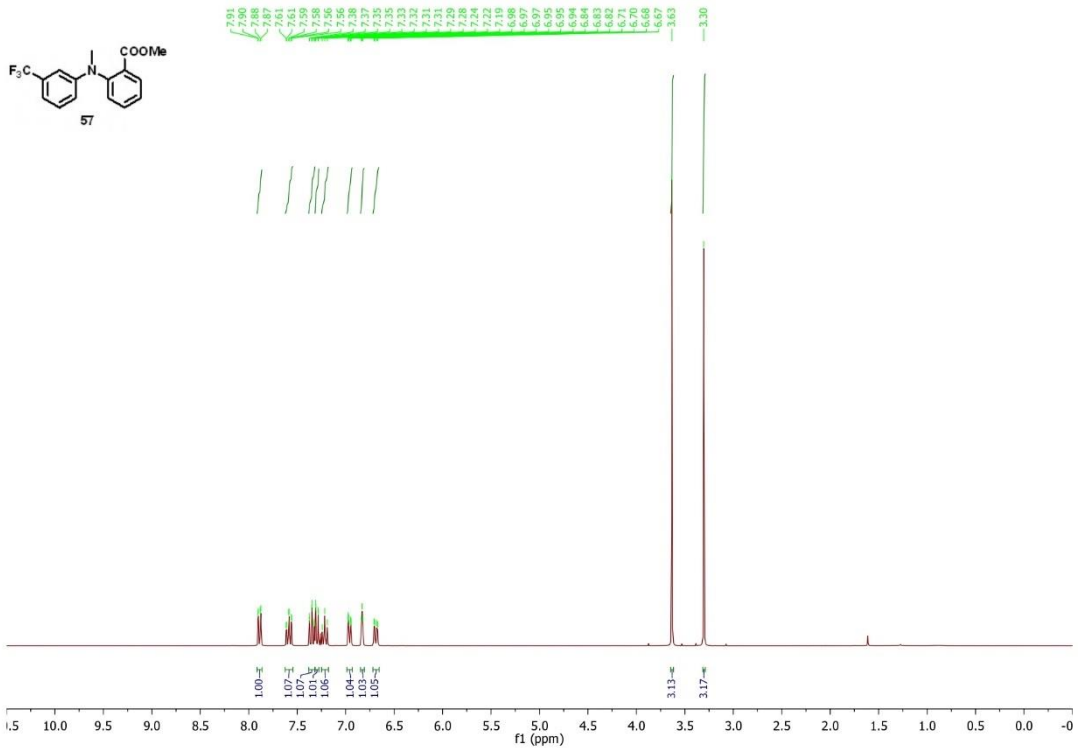
COOMe
F3C
N
57
7.91 7.90 7.88 7.87 7.61 7.61 7.59 7.58 7.56 7.56 7.38 7.37 7.35 7.35 7.33 7.32 7.31 7.31 7.29 7.28 7.24 7.22 7.19 6.98 6.97 6.97 6.95 6.95 6.94 6.84 6.83 6.82 6.71 6.70 6.68 6.67
3.63
3.30
1.00 1.07 1.07 1.01 1.06 1.04 1.03 1.05
3.13 3.17
f1 (ppm)

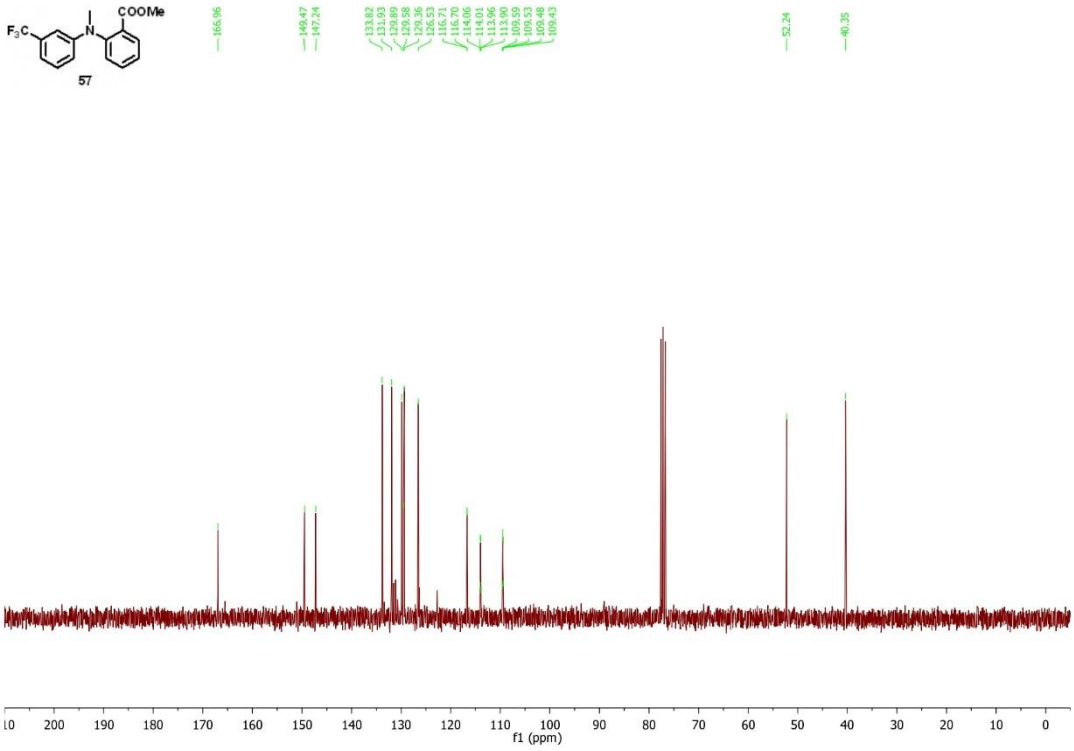
COOMe
F3C
N
57
166.96
149.47
147.24
133.82
131.93
129.89
129.58
129.36
126.53
116.71
116.70
114.06
114.01
113.96
113.90
109.59
109.53
109.48
109.43
52.24
40.35
f1 (ppm)

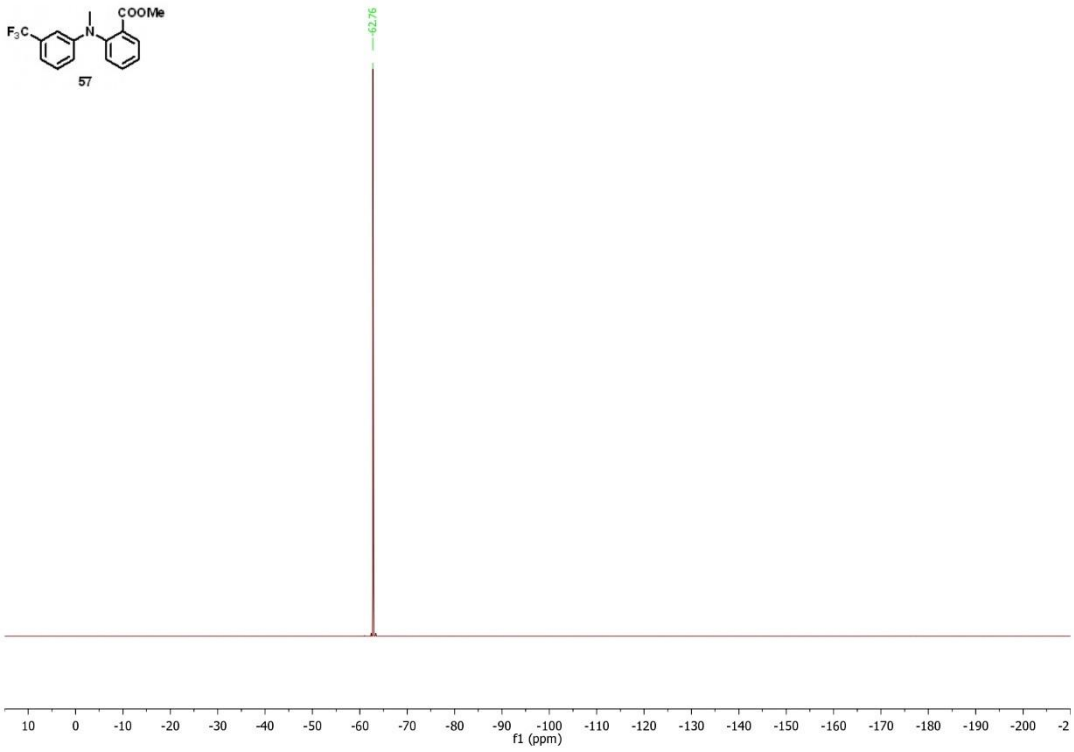
COOMe
F3C
N
57
62.76
f1 (ppm)

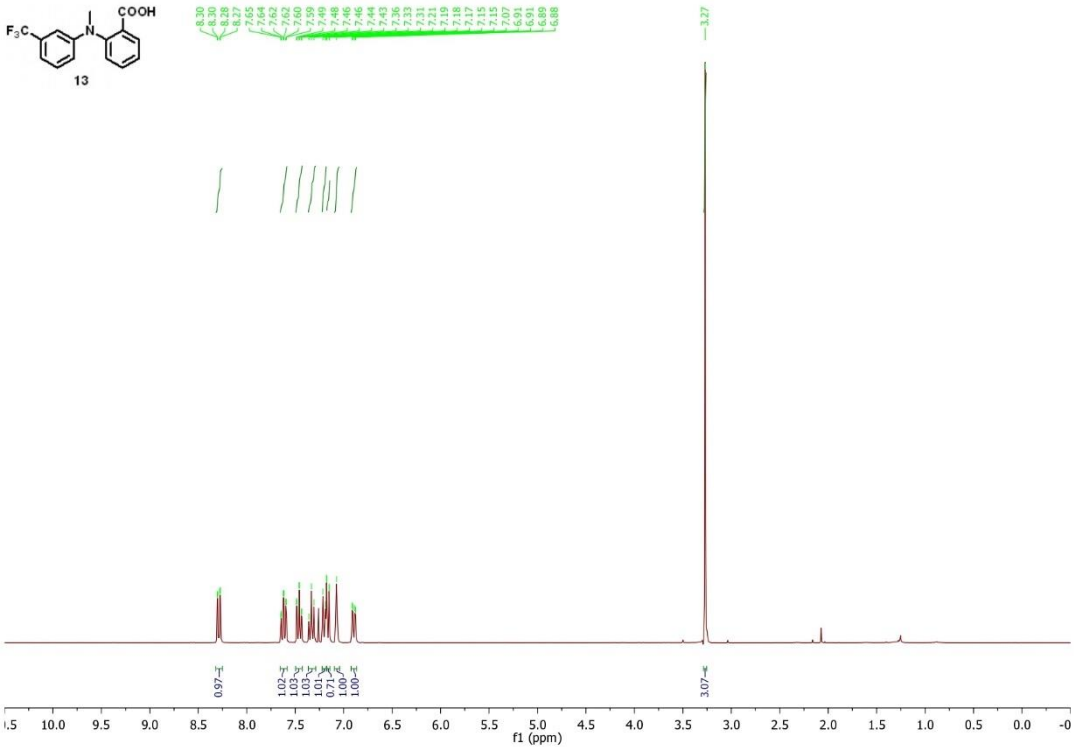
COOH
F3C
N
13
8.30
8.30
8.28
8.27
7.65
7.64
7.62
7.62
7.60
7.59
7.49
7.48
7.46
7.46
7.44
7.43
7.36
7.33
7.31
7.21
7.19
7.18
7.17
7.15
7.15
7.07
6.91
6.89
6.88
3.27
0.97
1.02
1.03
1.03
1.01
0.71
1.00
1.00
3.07
f1 (ppm)

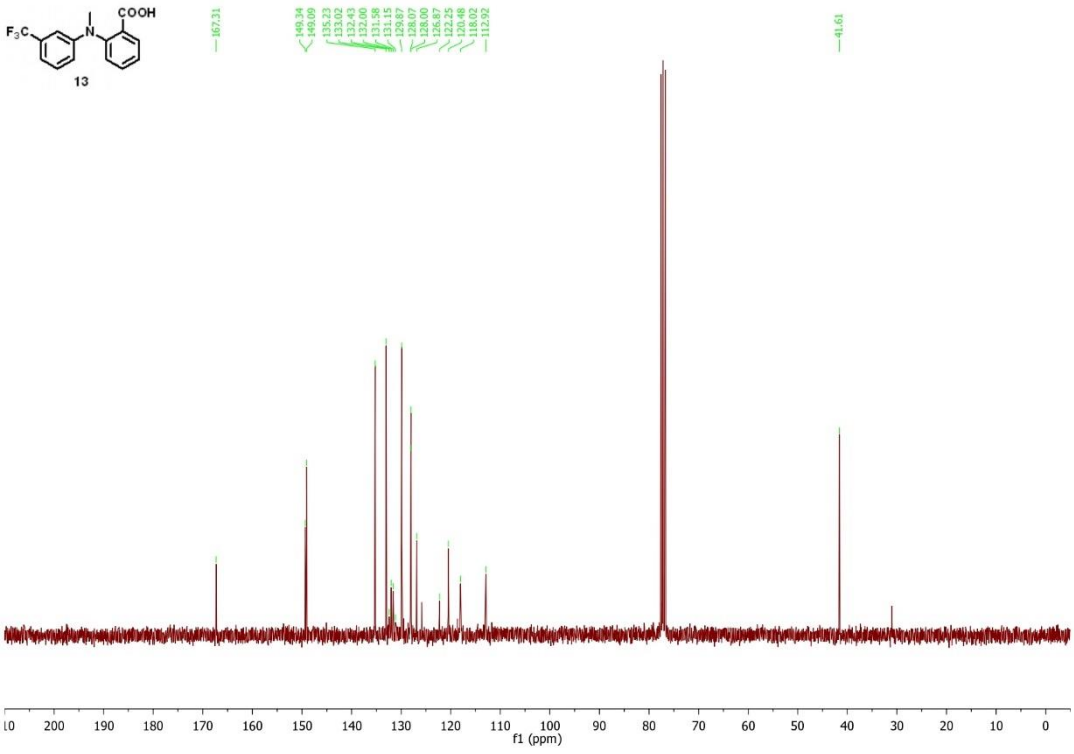
COOH
F3C
N
13
167.31
149.34
149.09
135.23
133.02
132.43
132.00
131.58
131.15
129.87
128.07
128.00
126.87
122.25
120.48
118.02
112.92
41.61
f1 (ppm)

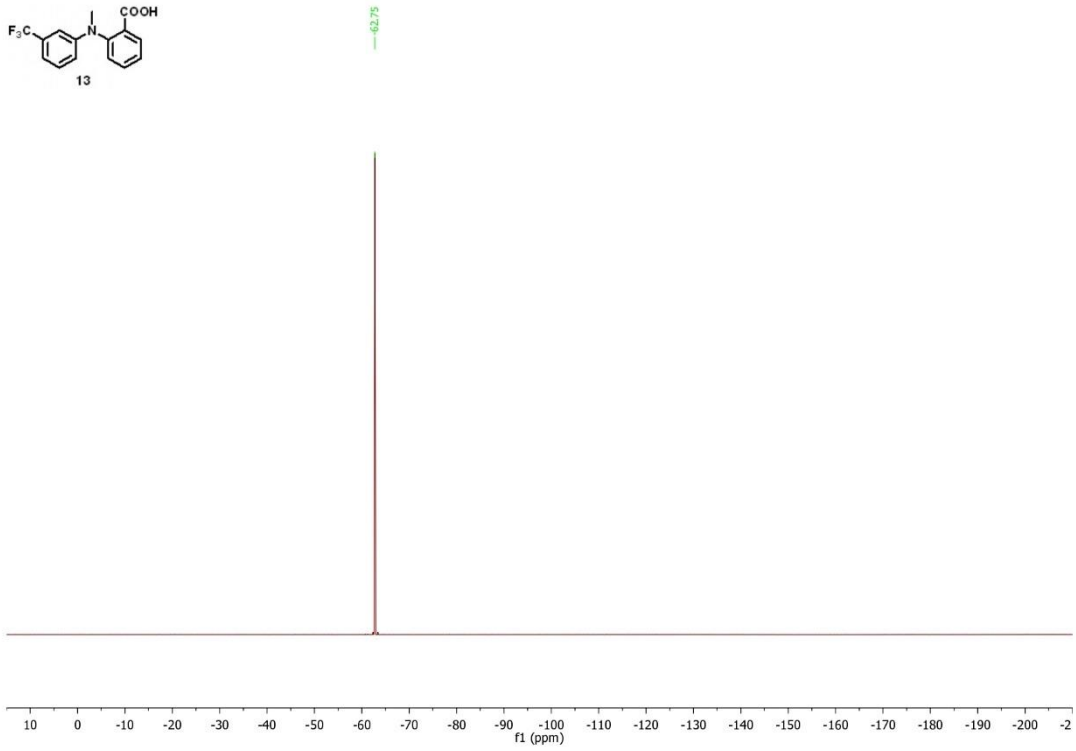
COOH
F3C
N
13
-62.75
10 0 -10 -20 -30 -40 -50 -60 -70 -80 -90 -100 -110 -120 -130 -140 -150 -160 -170 -180 -190 -200
f1 (ppm)

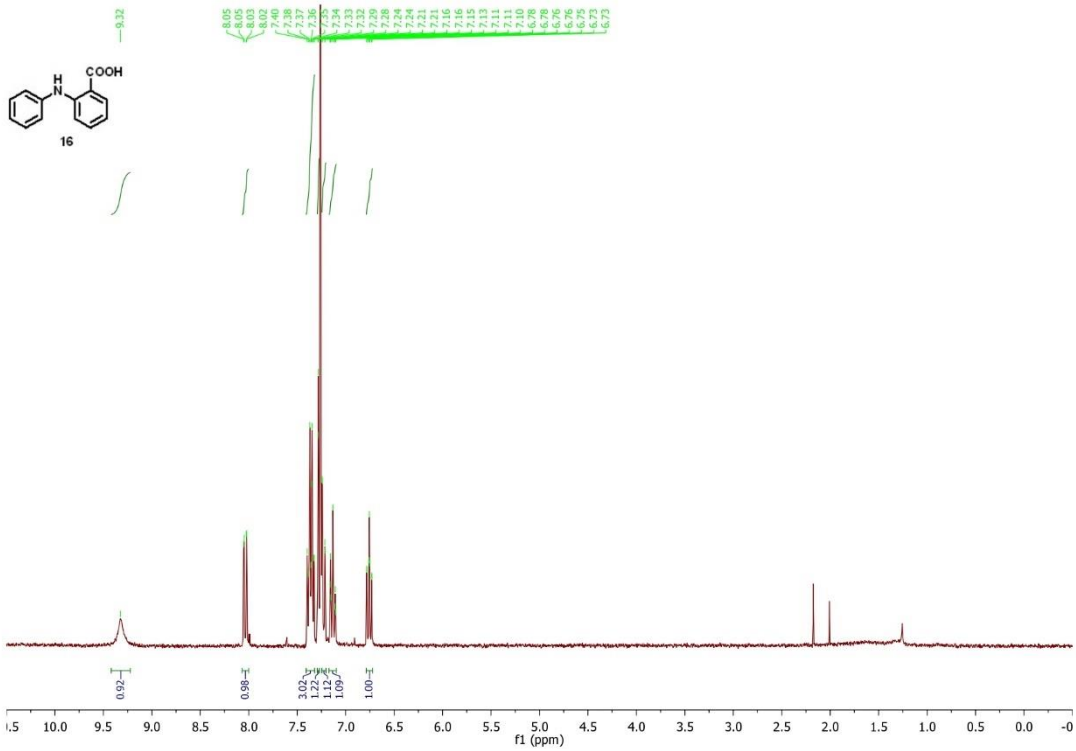
COOH
H
N
16
9.32
8.05 8.05 8.03 8.02 7.40 7.38 7.37 7.36 7.35 7.34 7.33 7.32 7.29 7.28 7.24 7.24 7.21 7.21 7.16 7.16 7.15 7.13 7.11 7.11 7.10 6.78 6.78 6.76 6.76 6.75 6.73 6.73
0.92 0.98 3.02 1.22 1.12 1.09 1.00
10.0 9.5 9.0 8.5 8.0 7.5 7.0 6.5 6.0 5.5 5.0 4.5 4.0 3.5 3.0 2.5 2.0 1.5 1.0 0.5 0.0
f1 (ppm)

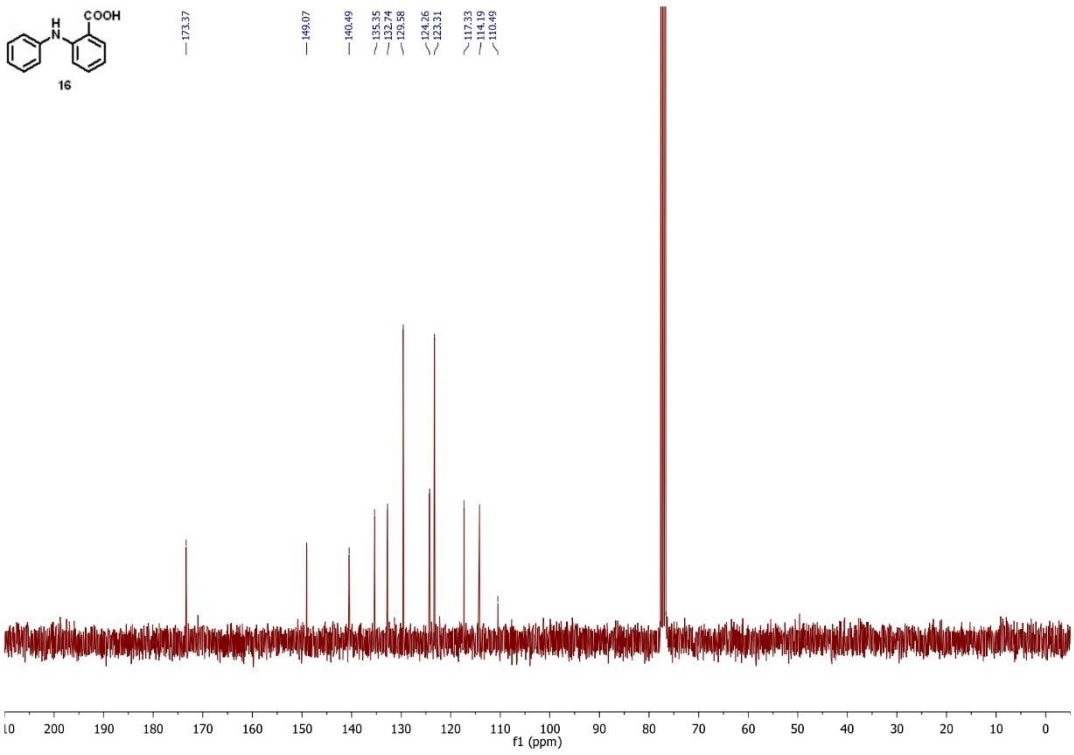
COOH
H
N
16
173.37
149.07
140.49
135.35
132.74
129.58
124.26
123.31
117.33
114.19
110.49
f1 (ppm)

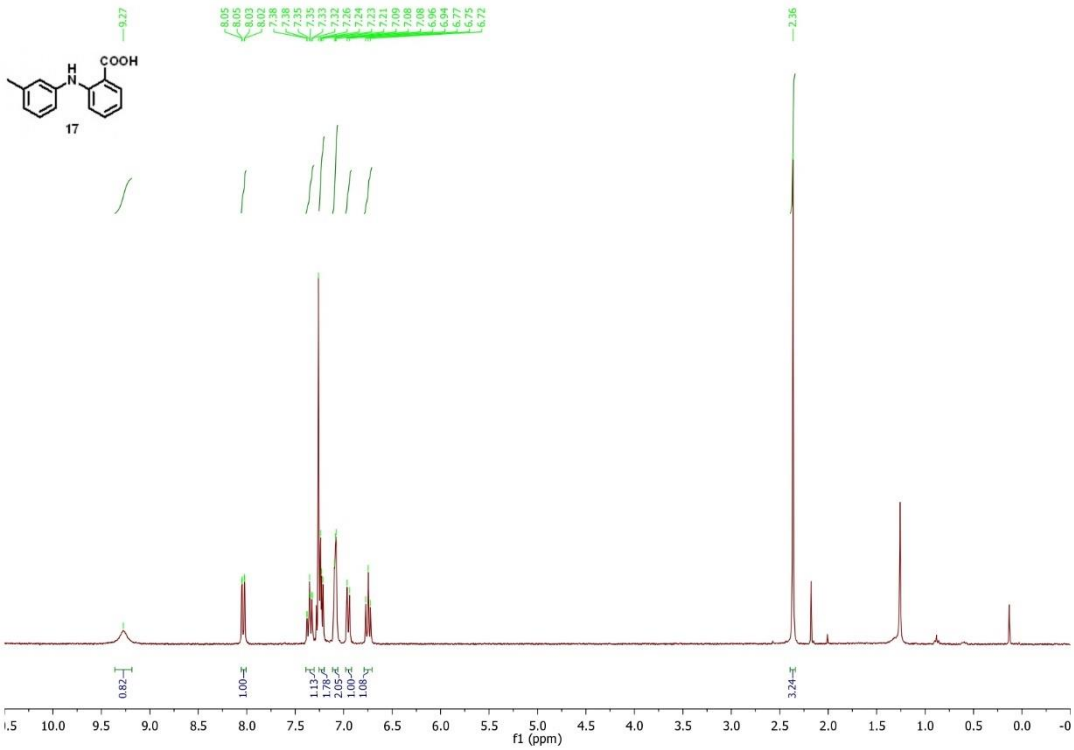
COOH
H
N
17
9.27
8.05
8.05
8.03
8.02
7.38
7.36
7.35
7.33
7.32
7.26
7.24
7.23
7.21
7.09
7.08
7.08
6.96
6.94
6.77
6.75
6.72
2.36
0.82
1.00
1.13
1.78
2.05
1.00
1.08
3.24
f1 (ppm)

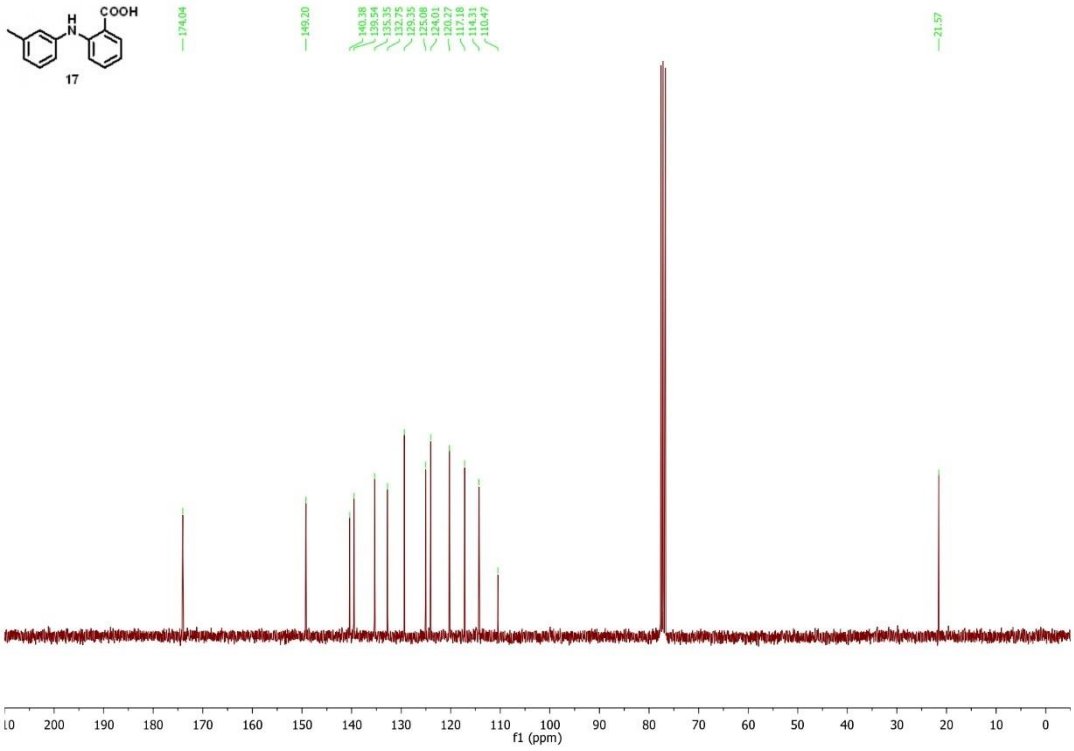
COOH
H
N
17
174.04
149.20
140.38
139.54
135.35
132.75
130.35
125.08
124.01
120.27
117.18
114.31
110.47
21.57
f1 (ppm)

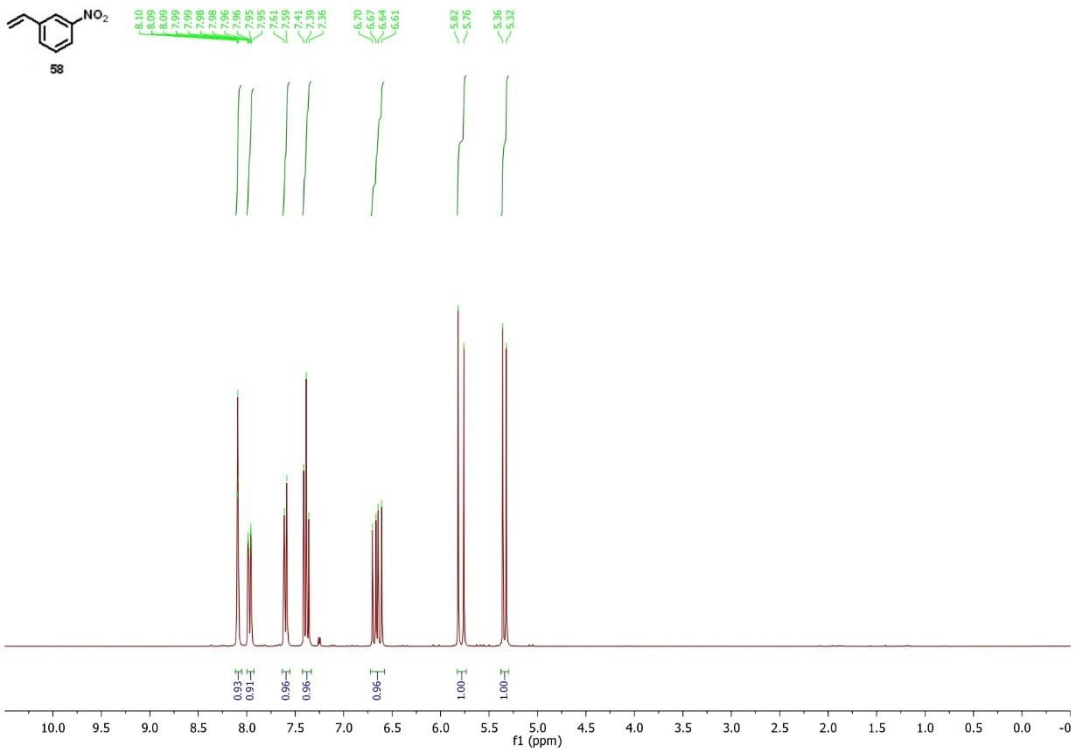
NO2
58
8.10
8.09
8.09
7.99
7.99
7.98
7.98
7.96
7.96
7.95
7.95
7.61
7.59
7.41
7.39
7.36
6.70
6.67
6.64
6.61
5.82
5.76
5.36
5.32
0.93
0.91
0.96
0.96
0.96
1.00
1.00
f1 (ppm)

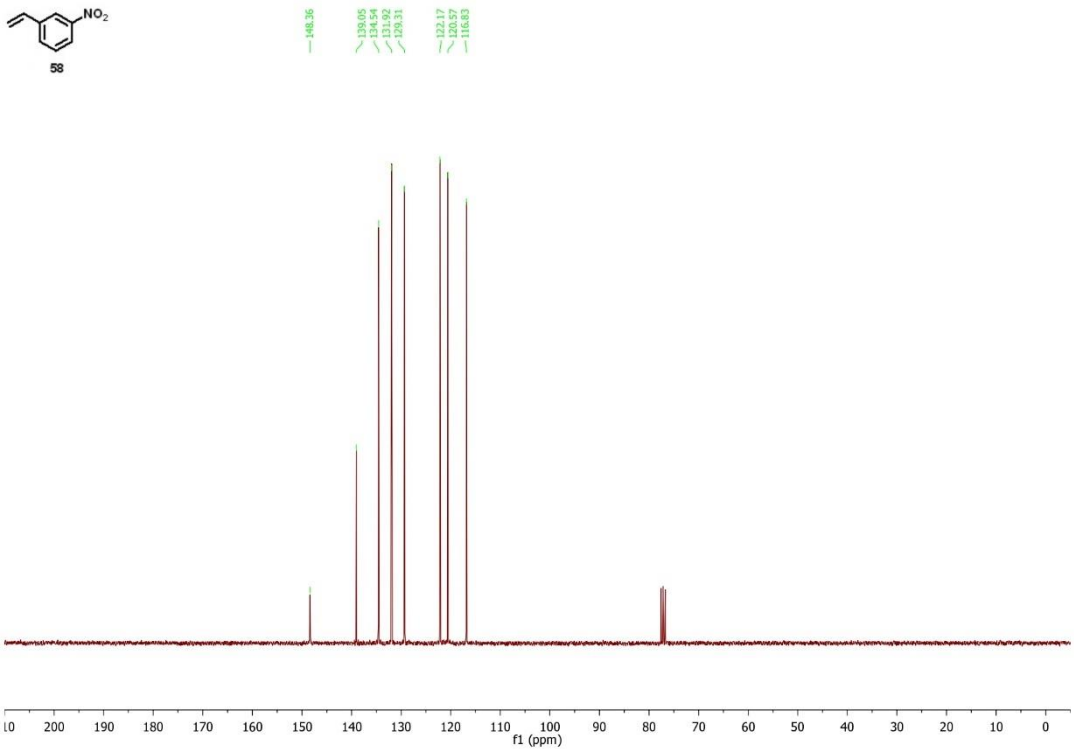
58
148.36
139.05
134.54
131.92
129.31
122.17
120.57
116.83
f1 (ppm)

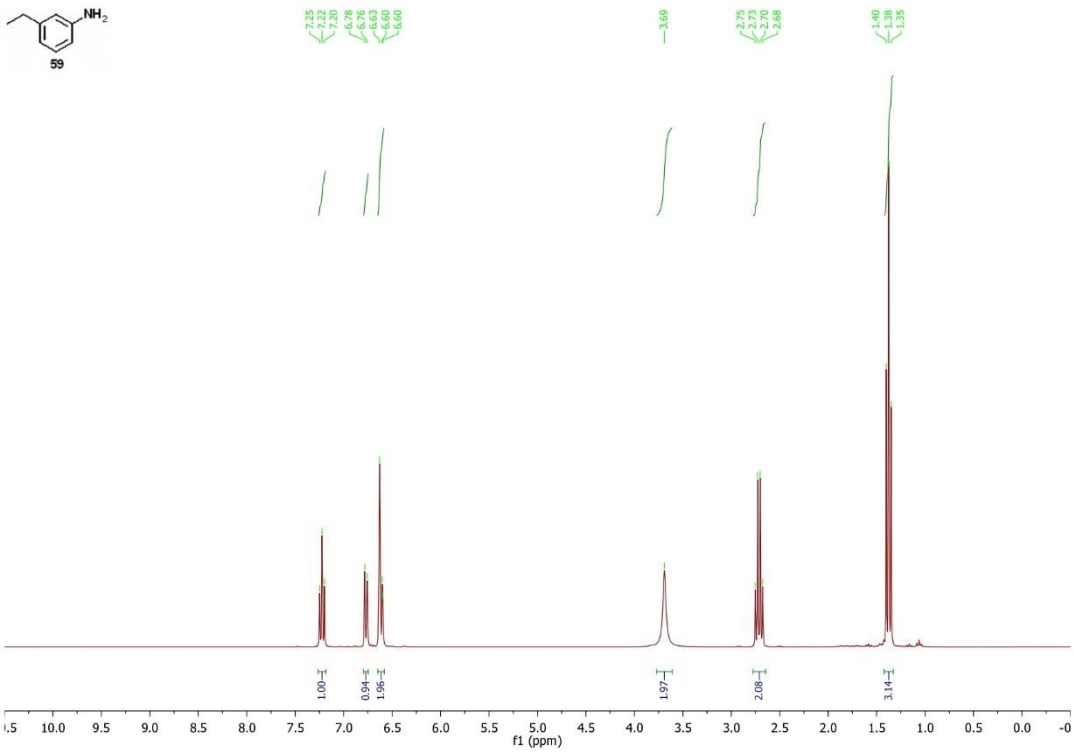
59
7.25
7.22
7.20
6.78
6.76
6.63
6.60
6.60
3.69
2.75
2.73
2.70
2.68
1.40
1.38
1.35
1.00
0.94
1.96
1.97
2.08
3.14
f1 (ppm)

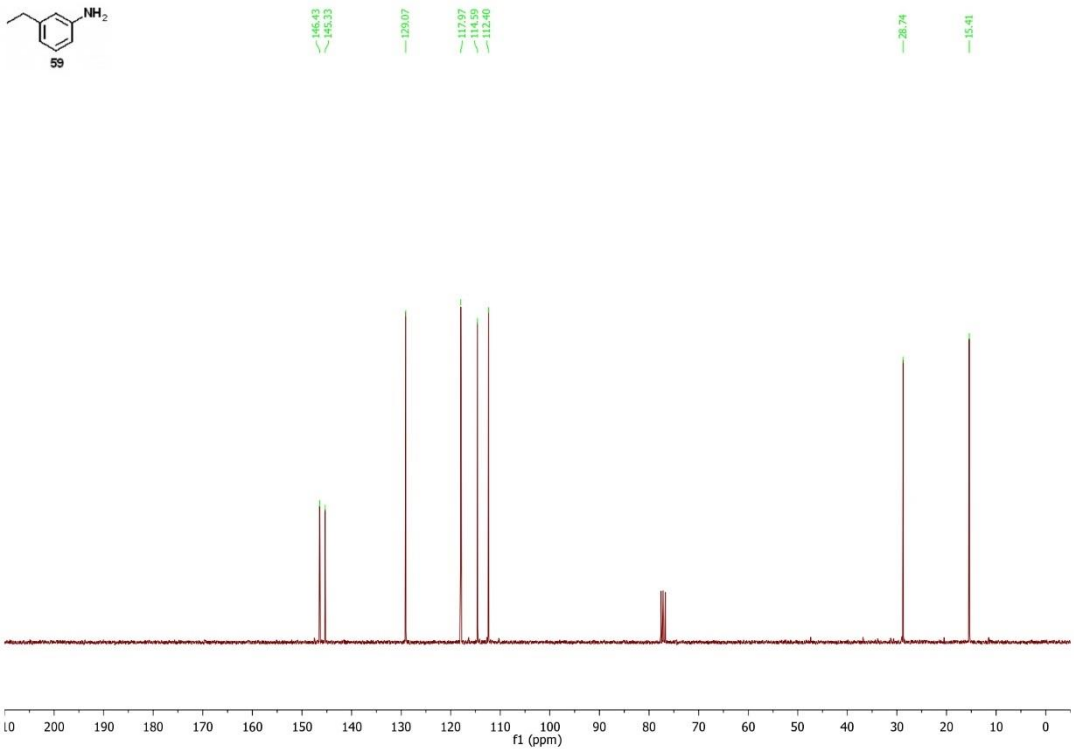
NH2
59
146.43
145.33
129.07
117.97
114.59
112.40
28.74
15.41
f1 (ppm)

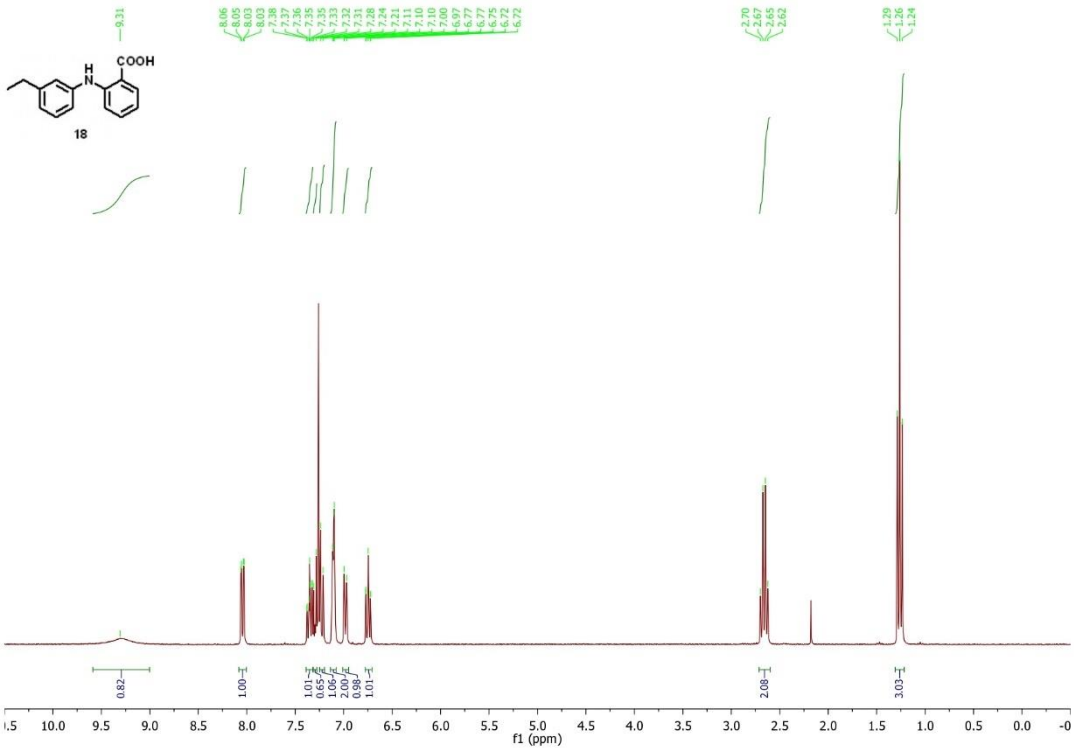
9.31
8.06
8.05
8.03
8.03
7.38
7.37
7.36
7.35
7.35
7.33
7.32
7.31
7.28
7.24
7.21
7.11
7.10
7.10
7.00
6.97
6.77
6.75
6.72
6.72
2.70
2.67
2.65
2.62
1.29
1.26
1.24
COOH
H
N
18
0.82
1.00
1.01
0.65
1.06
2.00
0.98
1.01
2.08
3.03
f1 (ppm)

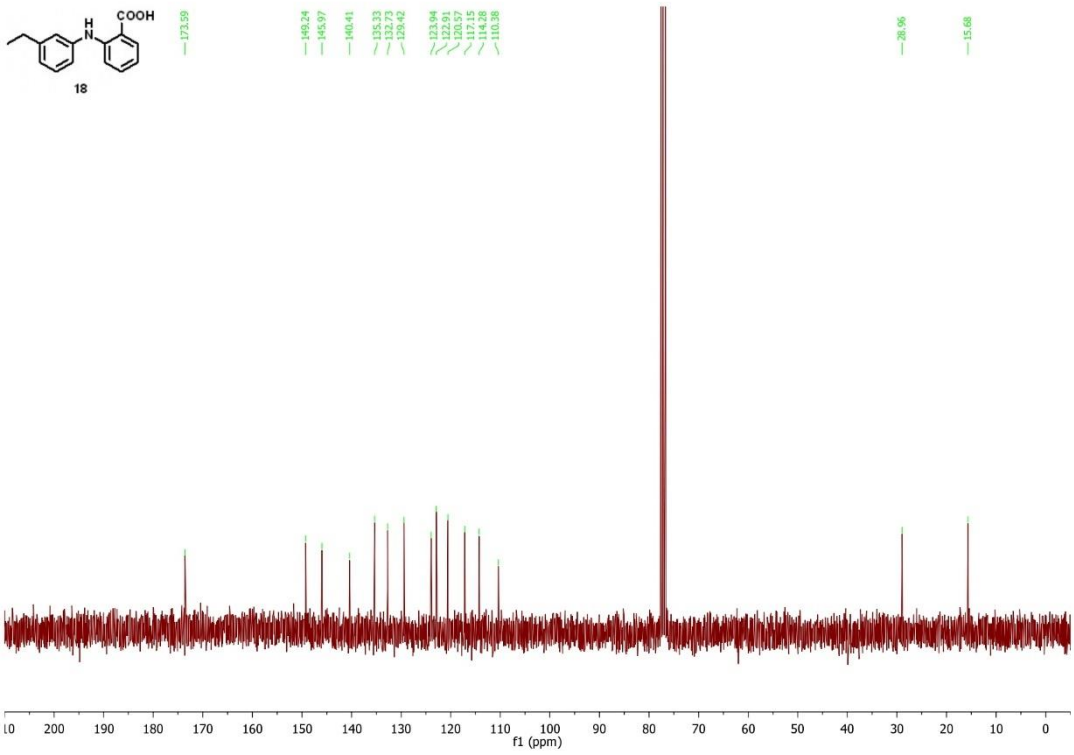
COOH
H
N
18
173.59
149.24
145.97
140.41
135.33
132.73
129.42
123.94
122.91
120.57
117.15
114.28
110.38
28.96
15.68
f1 (ppm)

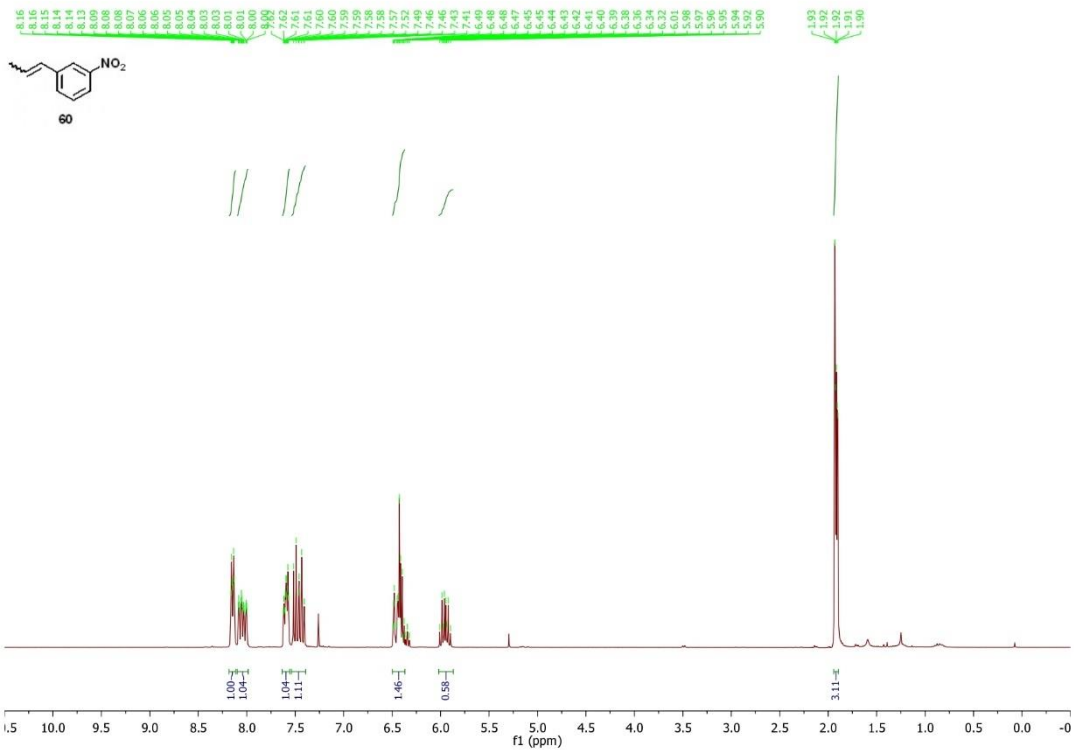
NO2
60
1.00
1.04
1.04
1.11
1.46
0.58
3.11
f1 (ppm)

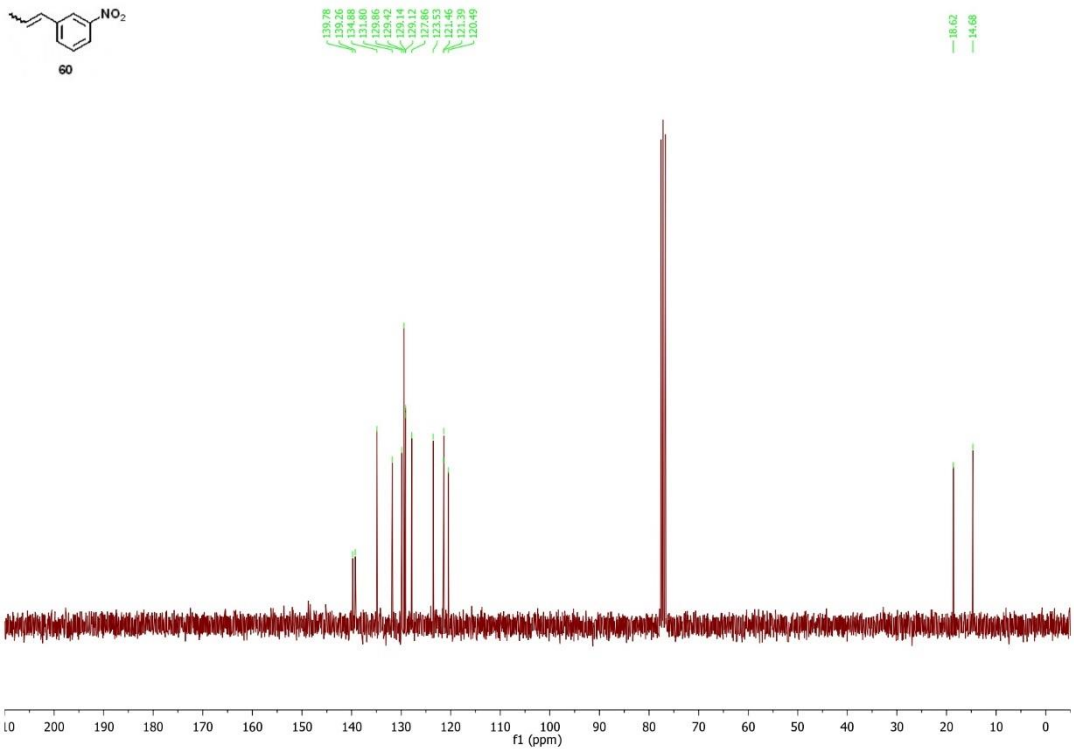
NO2
60
139.78
139.26
134.88
131.80
129.86
129.42
129.14
128.12
127.66
123.53
121.46
121.39
120.49
18.62
14.68
f1 (ppm)

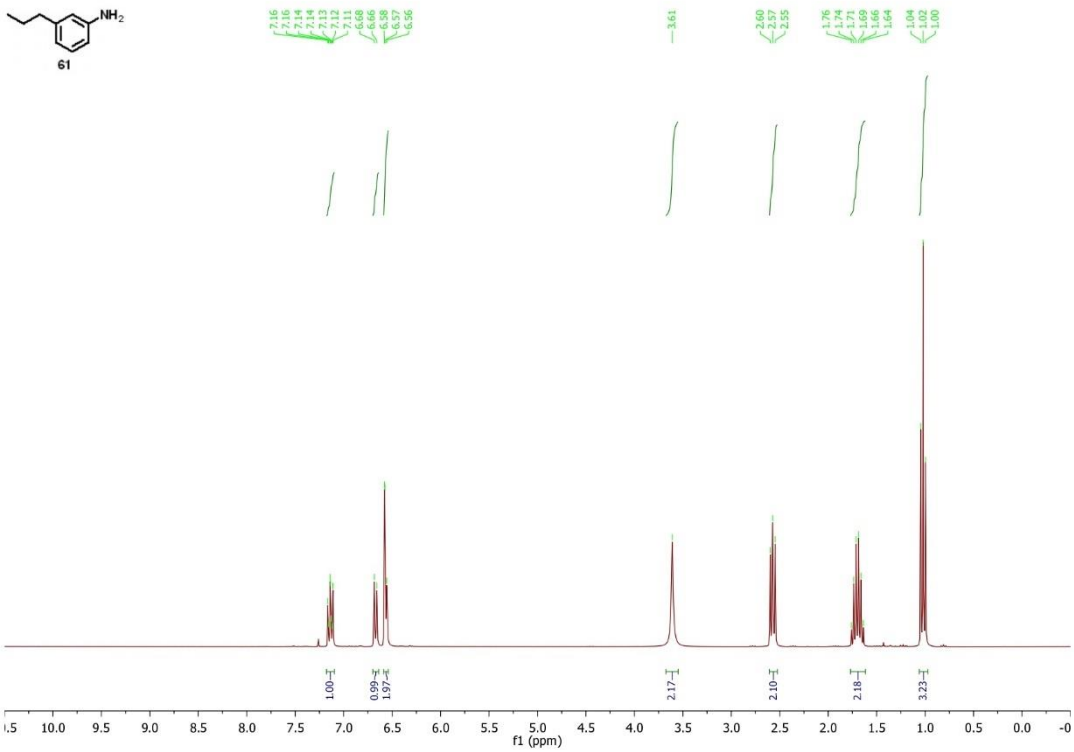
NH2
61
7.16
7.15
7.14
7.13
7.12
7.11
6.68
6.66
6.58
6.57
6.56
3.61
2.60
2.57
2.55
1.76
1.74
1.71
1.69
1.66
1.64
1.04
1.02
1.00
1.00
0.99
1.97
2.17
2.10
2.18
3.23
f1 (ppm)

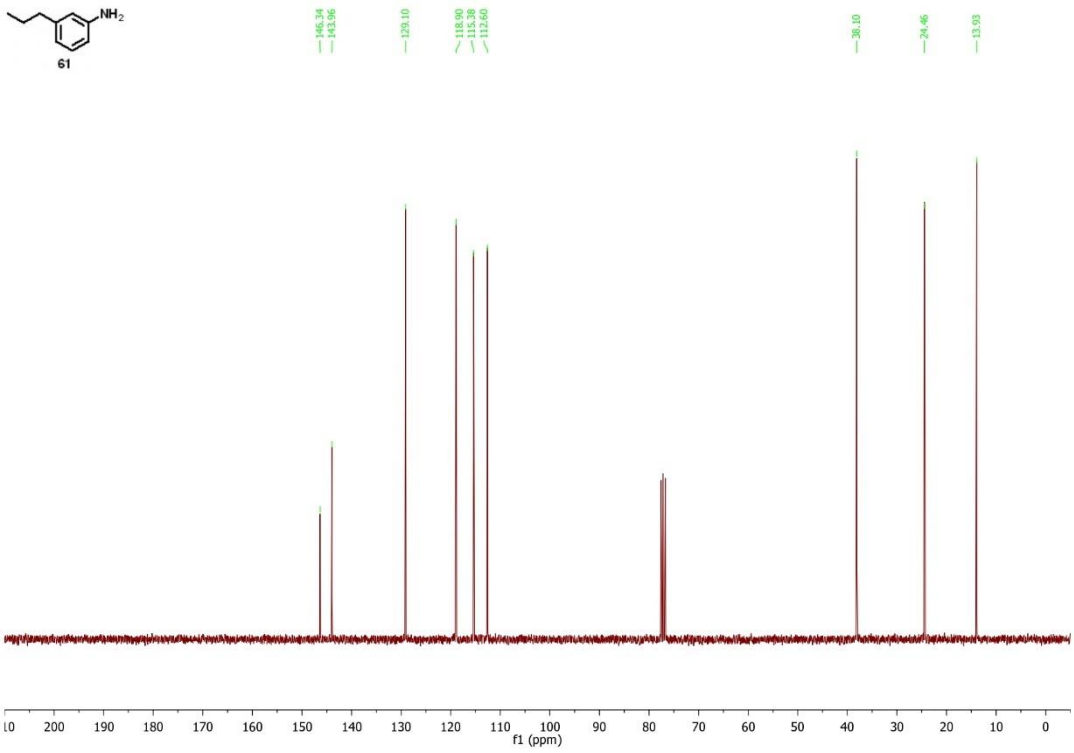
NH2
61
146.34
143.96
129.10
118.90
115.38
112.60
38.10
24.46
13.93
f1 (ppm)

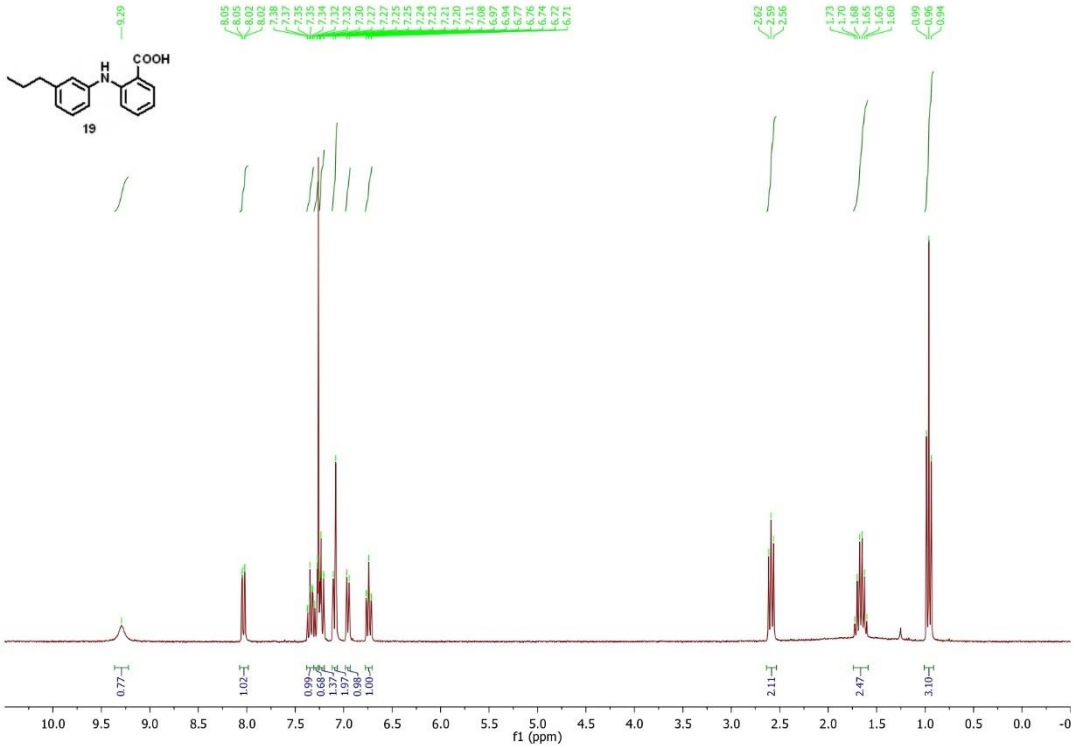
COOH
H
N
19
9.29
8.05
8.02
7.38
7.37
7.35
7.34
7.32
7.30
7.27
7.25
7.24
7.23
7.21
7.20
7.11
7.08
6.97
6.94
6.77
6.76
6.74
6.72
6.71
2.62
2.59
2.56
1.73
1.70
1.68
1.65
1.63
1.60
0.99
0.96
0.94
0.77
1.02
0.99
0.68
1.37
1.97
0.98
1.00
2.11
2.47
3.10
f1 (ppm)

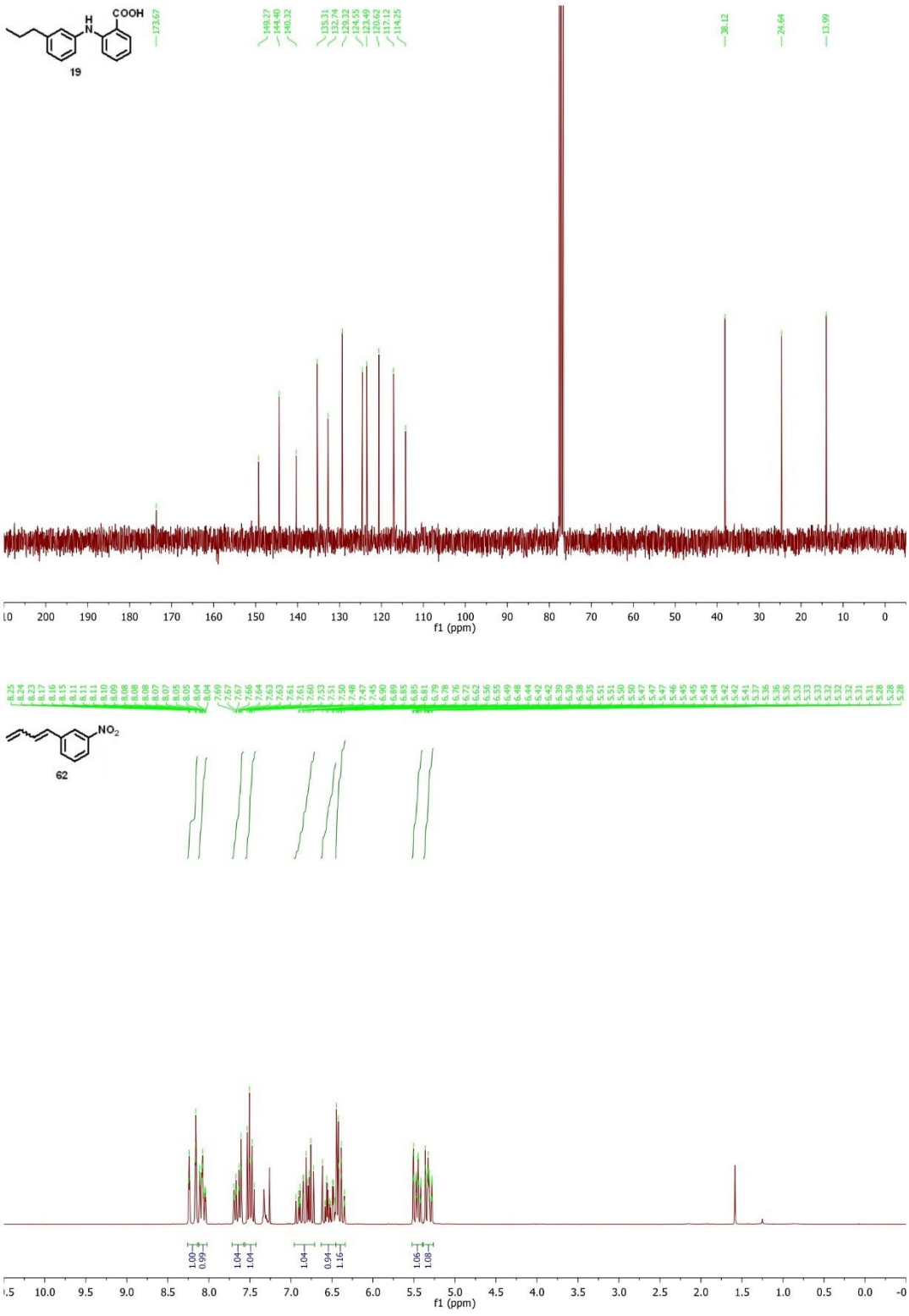
COOH
19
f1 (ppm)
NO2
62
f1 (ppm)

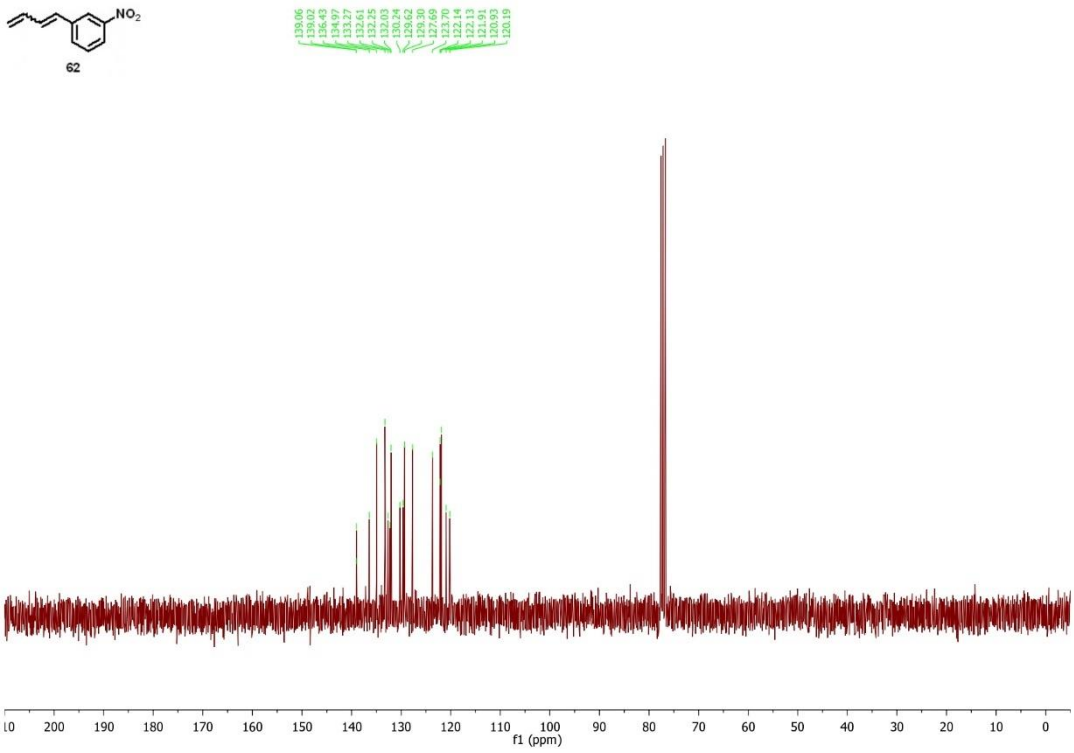
NO2
62
139.06
139.02
136.43
134.97
133.27
132.61
132.25
130.03
130.24
129.62
129.30
127.69
123.70
122.14
122.13
121.91
120.93
120.19
f1 (ppm)

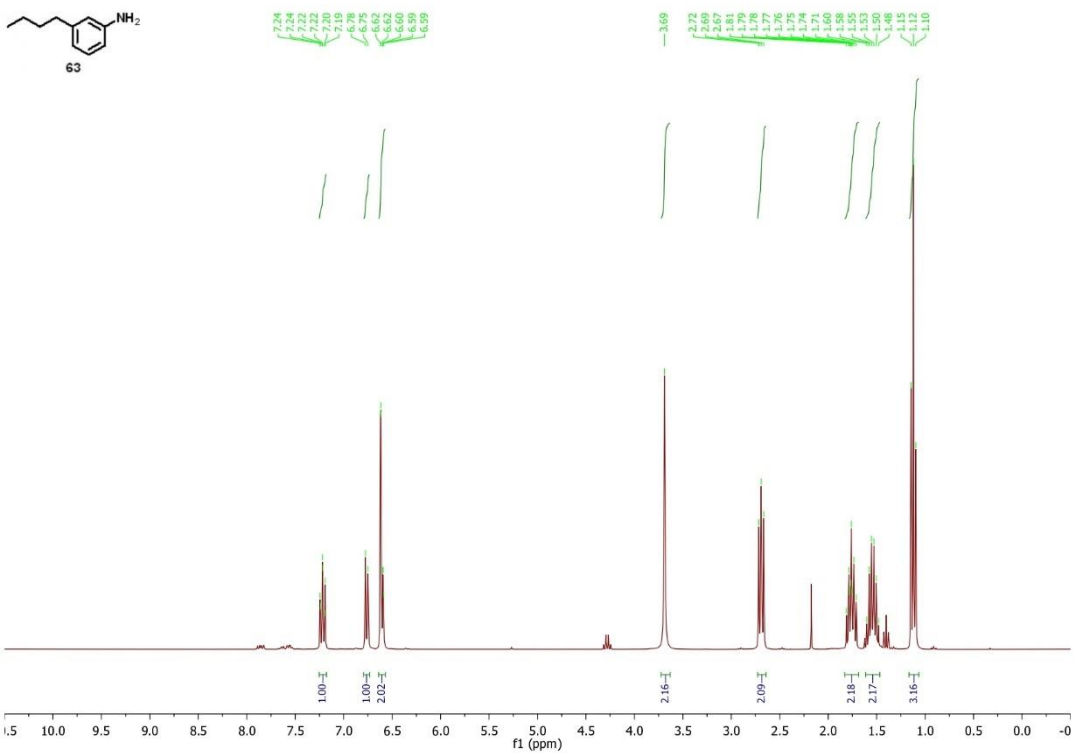
NH2
63
7.24
7.24
7.22
7.22
7.20
7.19
6.78
6.75
6.62
6.62
6.60
6.60
6.59
6.59
3.69
2.72
2.69
2.67
1.81
1.79
1.78
1.77
1.76
1.75
1.74
1.71
1.60
1.58
1.55
1.53
1.50
1.48
1.15
1.12
1.10
1.00
1.00
2.02
2.16
2.09
2.18
2.17
3.16
f1 (ppm)

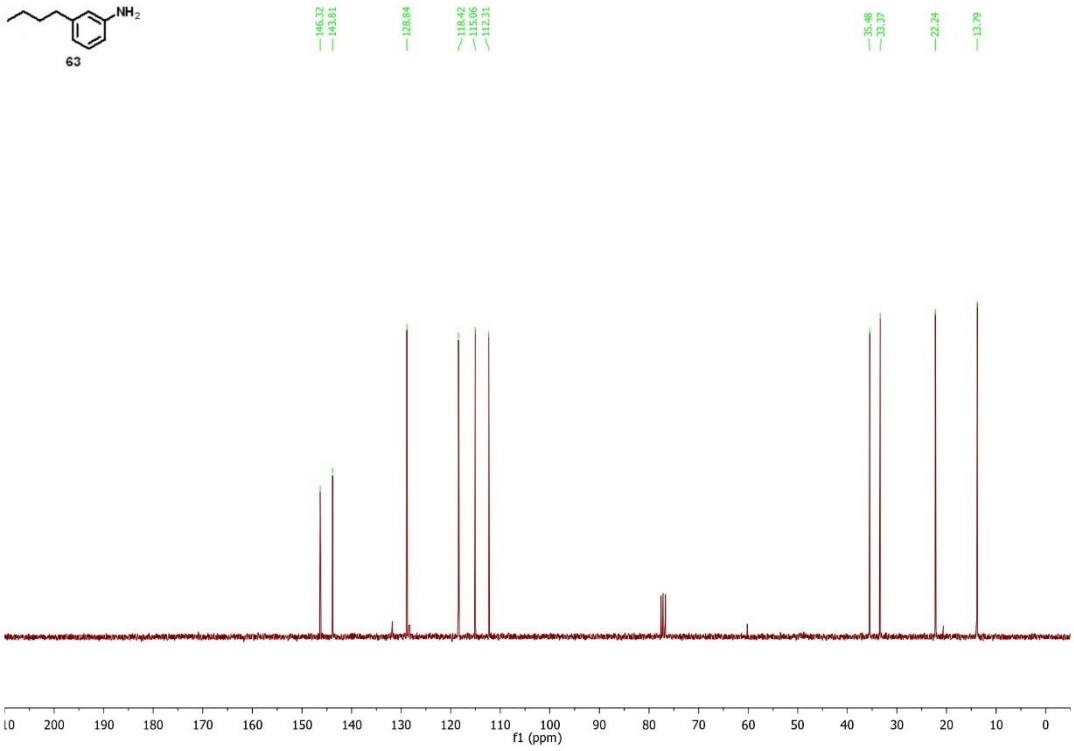
NH2
63
146.32
143.81
128.84
118.42
115.06
112.31
35.48
33.37
22.24
13.79
f1 (ppm)

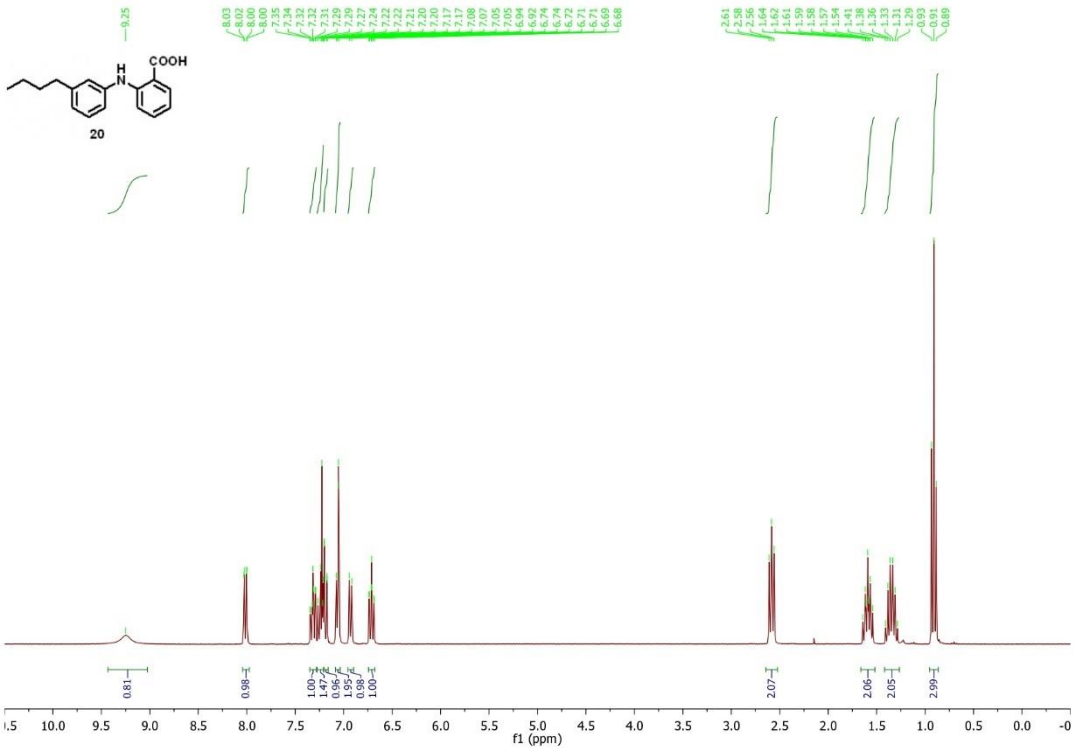
COOH
H
N
20
9.25
f1 (ppm)

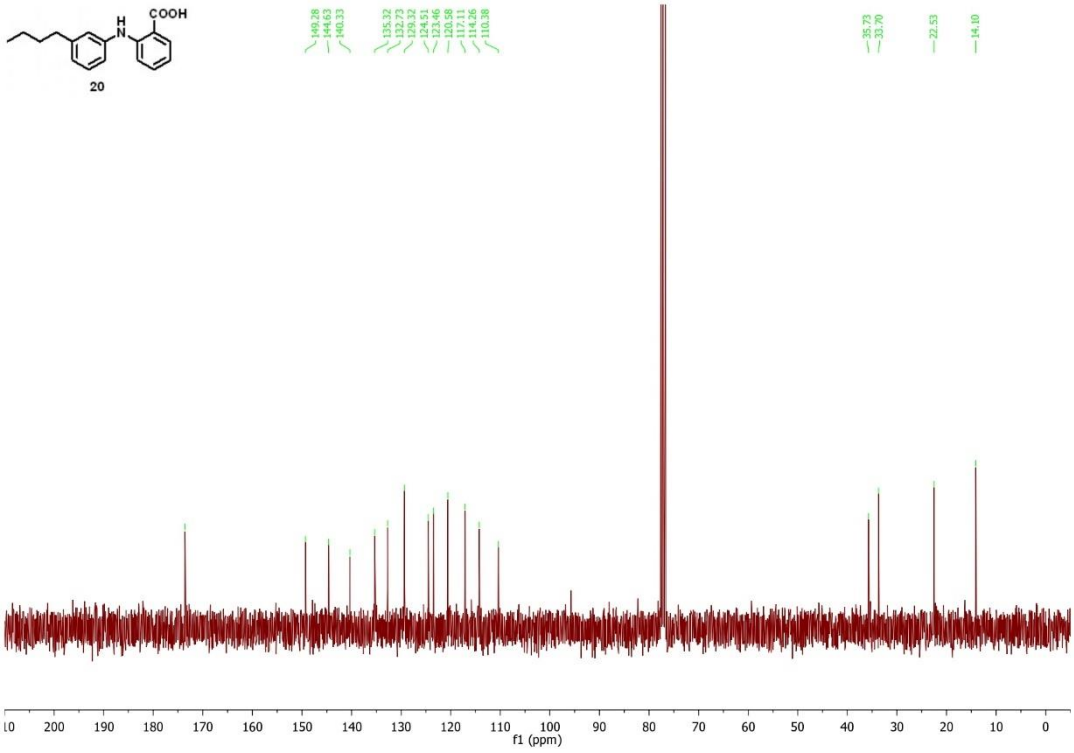
COOH
H
N
20
140.28
144.63
140.33
135.32
132.73
130.32
124.51
123.46
120.58
117.11
114.26
110.38
35.73
33.70
22.53
14.10
f1 (ppm)

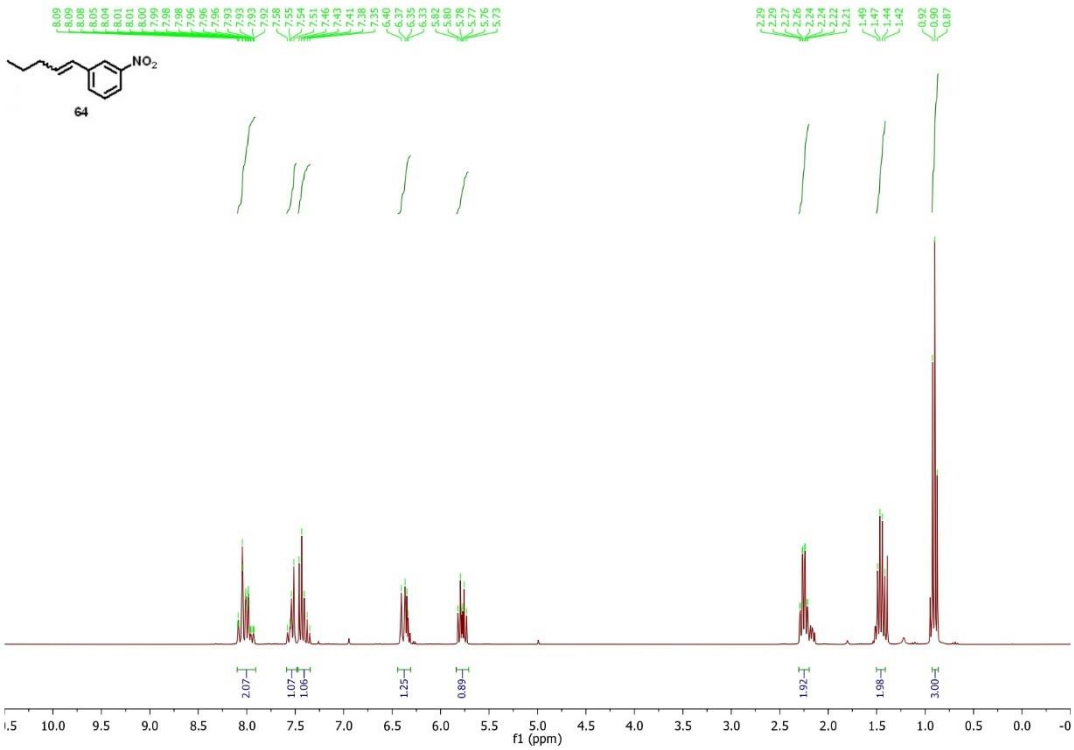
NO2
64
f1 (ppm)

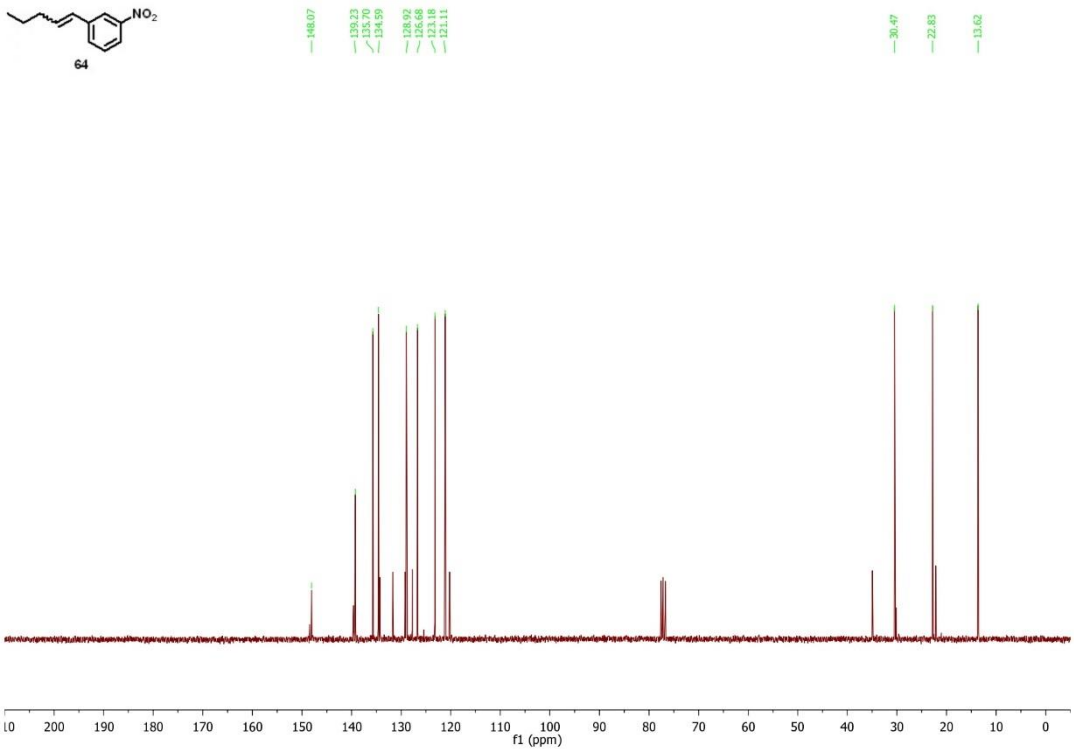
NO2
64
148.07
139.23
135.70
134.59
128.92
126.68
123.18
121.11
30.47
22.83
13.62
f1 (ppm)

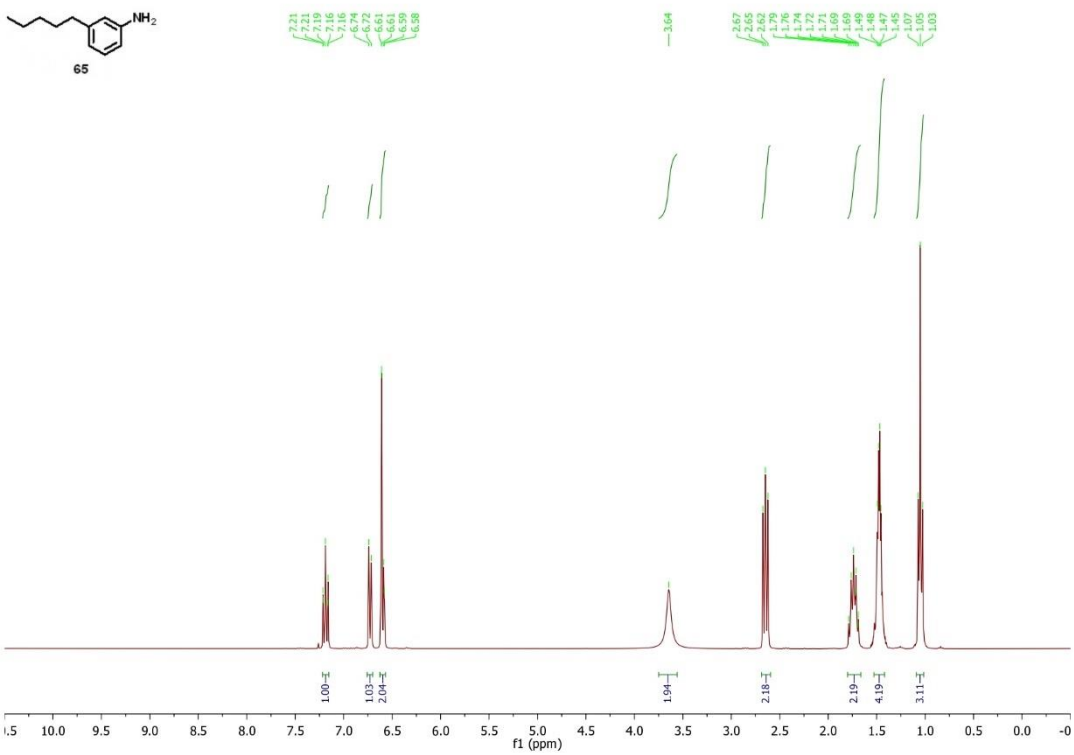
NH2
65
7.21
7.21
7.19
7.16
7.16
6.74
6.72
6.61
6.61
6.59
6.58
3.64
2.67
2.65
2.62
1.79
1.76
1.74
1.72
1.71
1.69
1.69
1.49
1.48
1.47
1.45
1.07
1.05
1.03
1.00
1.03
2.04
1.94
2.18
2.19
4.19
3.11
f1 (ppm)

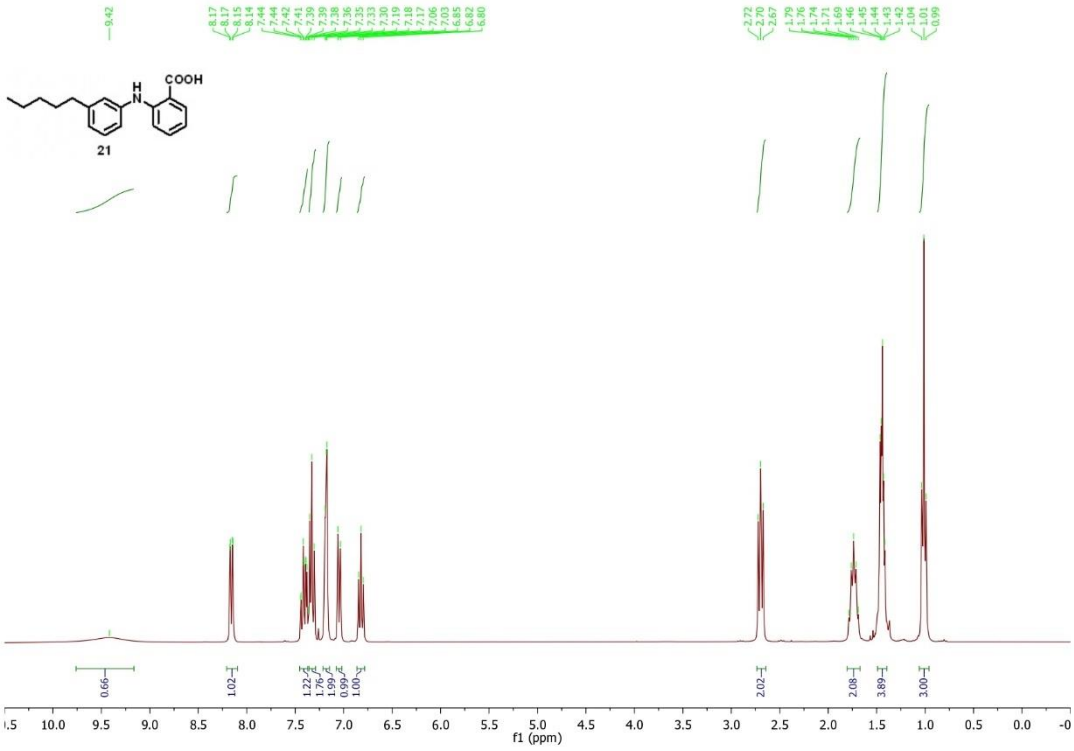
9.42
8.17
8.17
8.15
8.14
7.44
7.44
7.42
7.41
7.39
7.39
7.38
7.36
7.35
7.33
7.20
7.19
7.18
7.17
7.06
7.03
6.85
6.82
6.80
2.72
2.70
2.67
1.79
1.76
1.74
1.71
1.69
1.46
1.45
1.44
1.43
1.42
1.04
1.01
0.99
COOH
H
N
21
0.66
1.02
1.22
1.76
1.99
0.99
1.00
2.02
2.08
3.89
3.00
f1 (ppm)

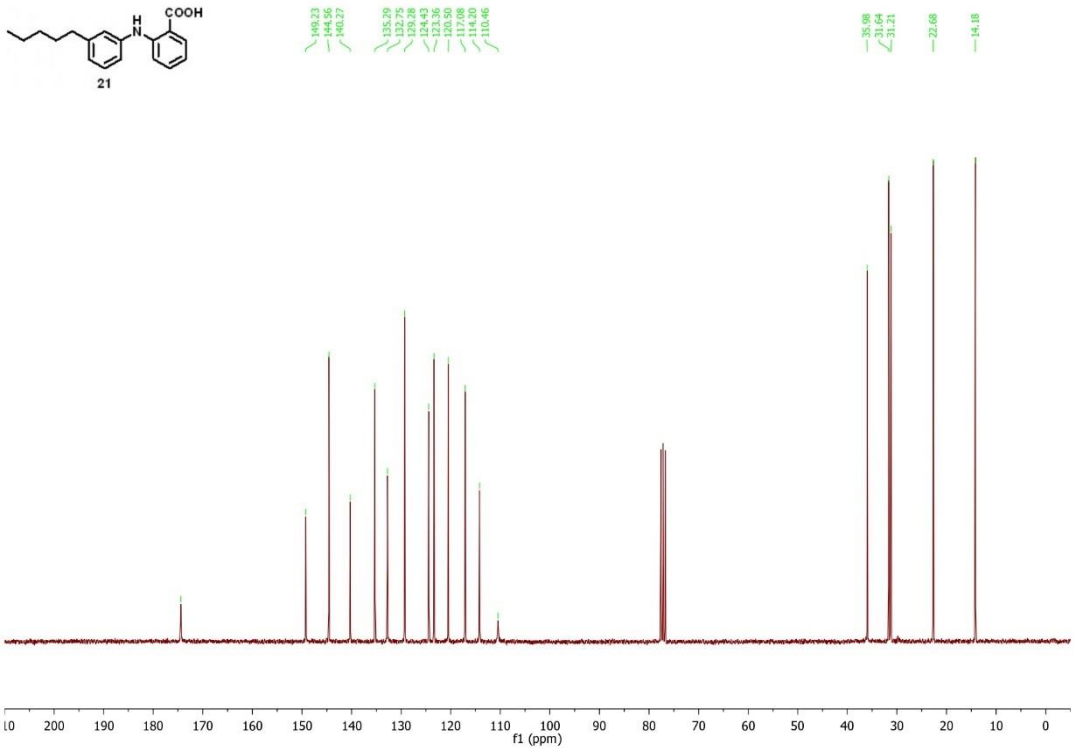
149.23
144.55
140.27
135.29
132.75
129.28
124.43
123.36
120.50
117.08
114.20
110.46
35.98
31.64
31.21
22.68
14.18
COOH
H
N
21
f1 (ppm)

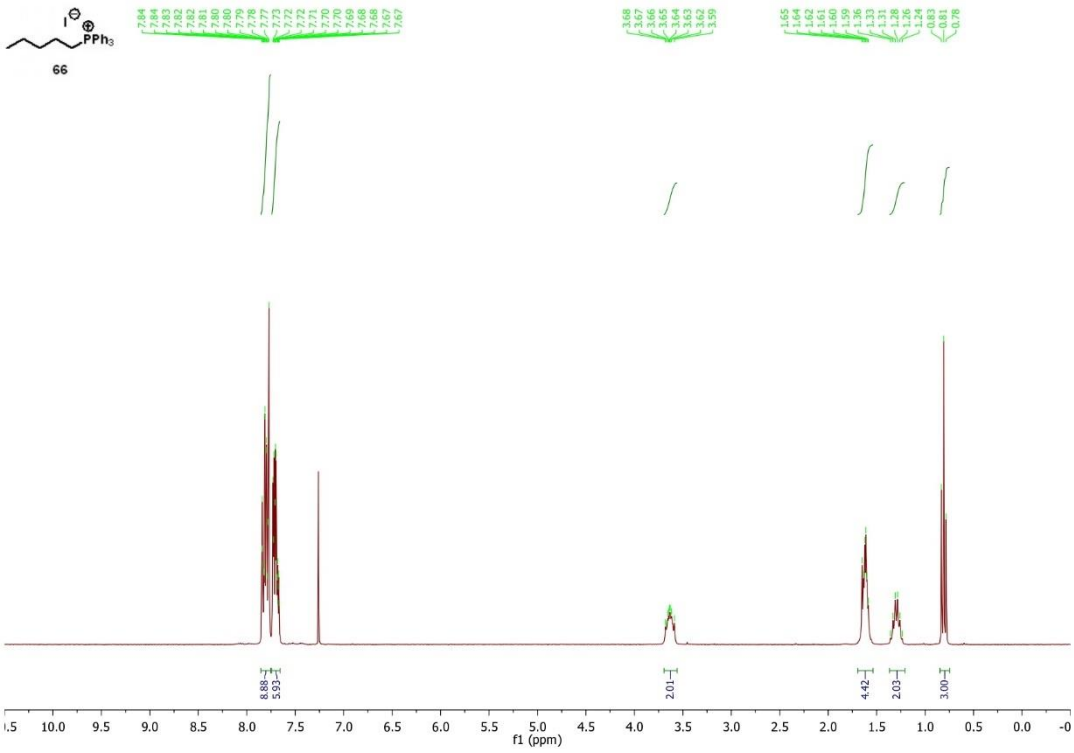
66
f1 (ppm)

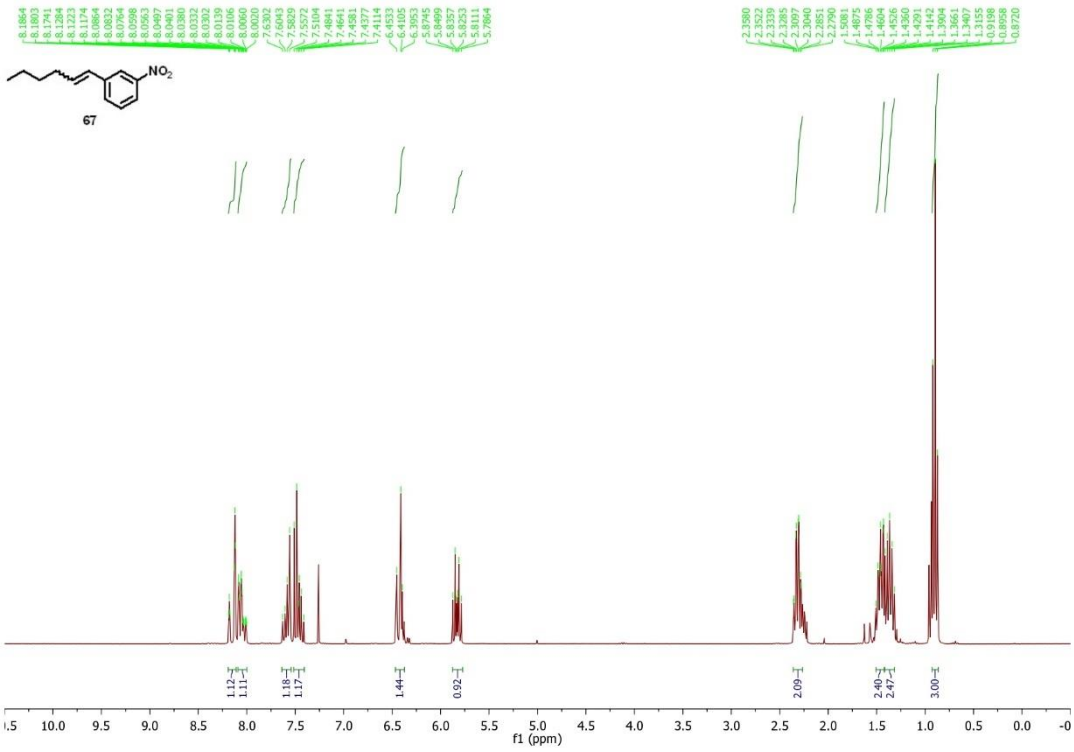
67
f1 (ppm)

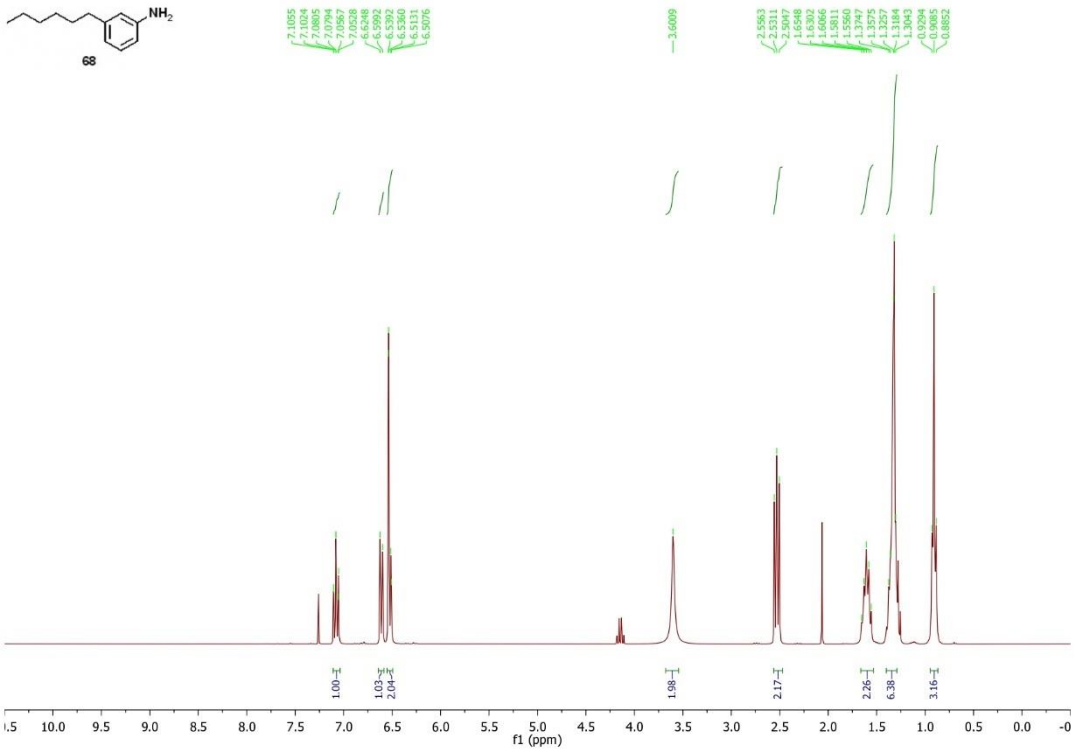
NH2
68
7.1055
7.1024
7.0805
7.0794
7.0597
7.0528
6.6248
6.5992
6.5392
6.5360
6.5131
6.5076
3.6009
2.5583
2.5311
2.5047
1.6548
1.6302
1.6066
1.5811
1.5560
1.5347
1.3575
1.3257
1.3184
1.3043
0.9294
0.9085
0.8852
1.00
1.03
2.04
1.98
2.17
2.26
6.38
3.16
f1 (ppm)

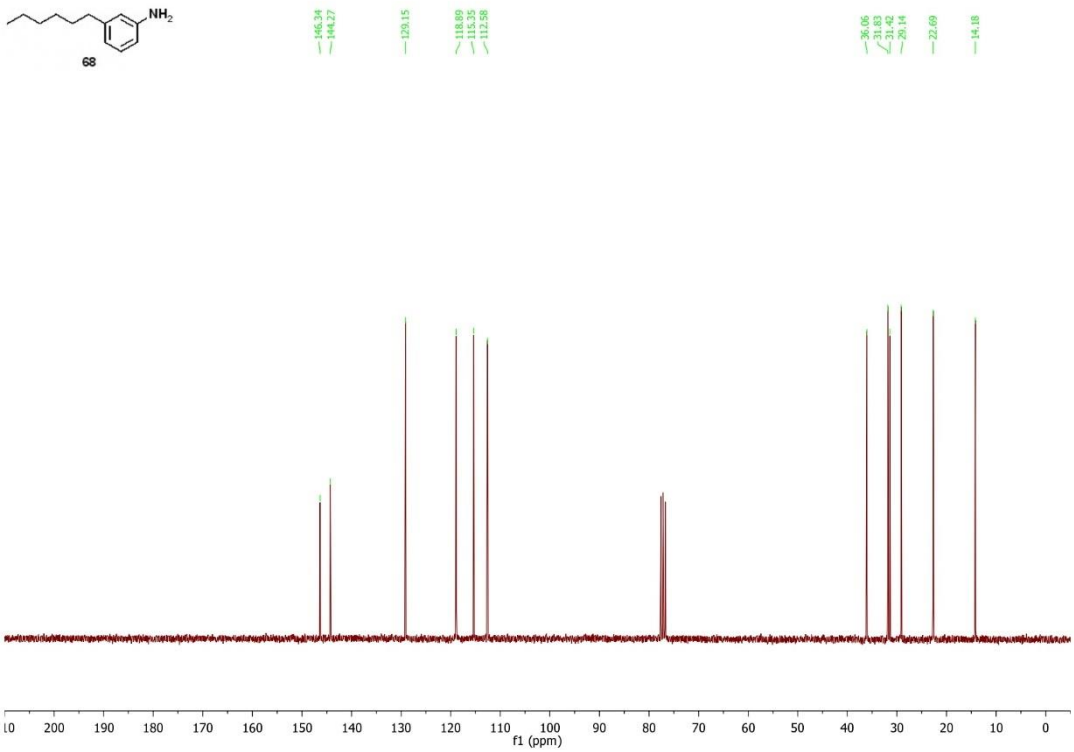
NH2
68
146.34
144.27
129.15
118.89
115.35
112.58
36.06
31.83
31.42
29.14
22.69
14.18
f1 (ppm)

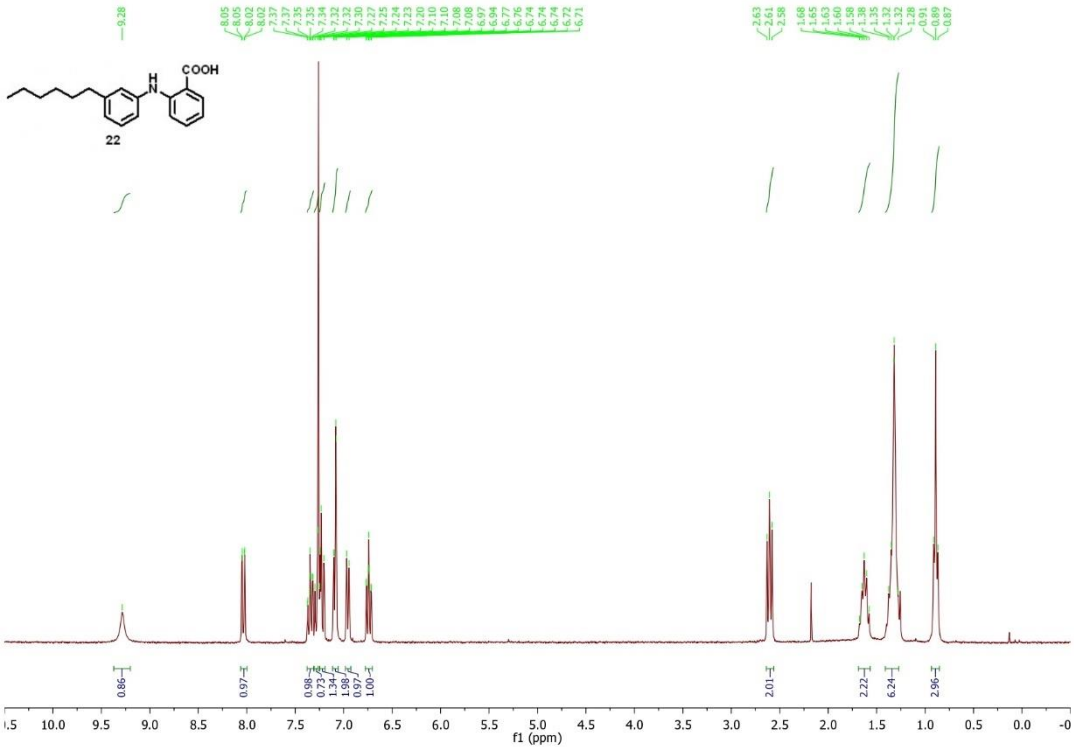
22
f1 (ppm)

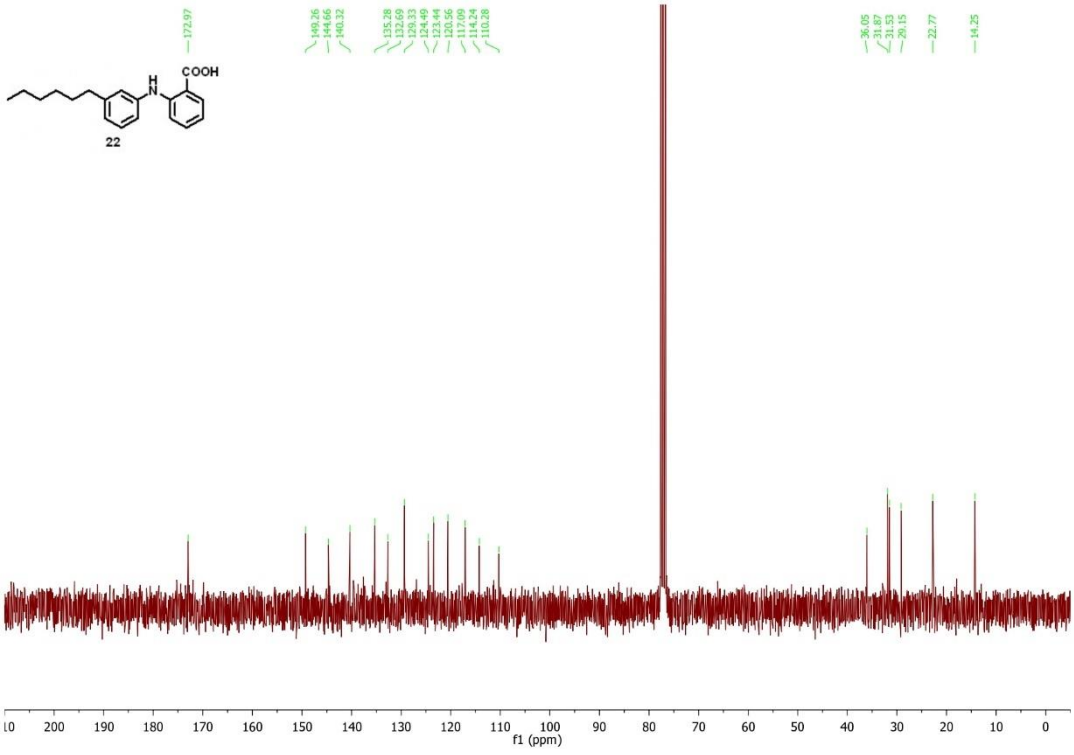
22
f1 (ppm)

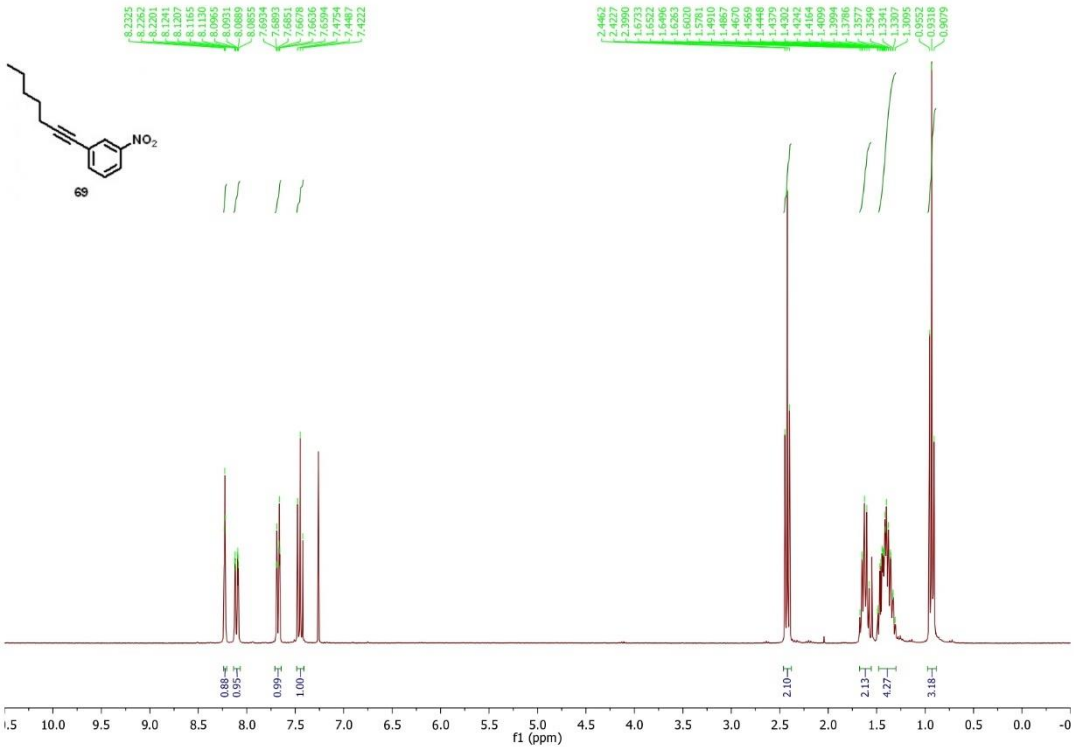
69
f1 (ppm)

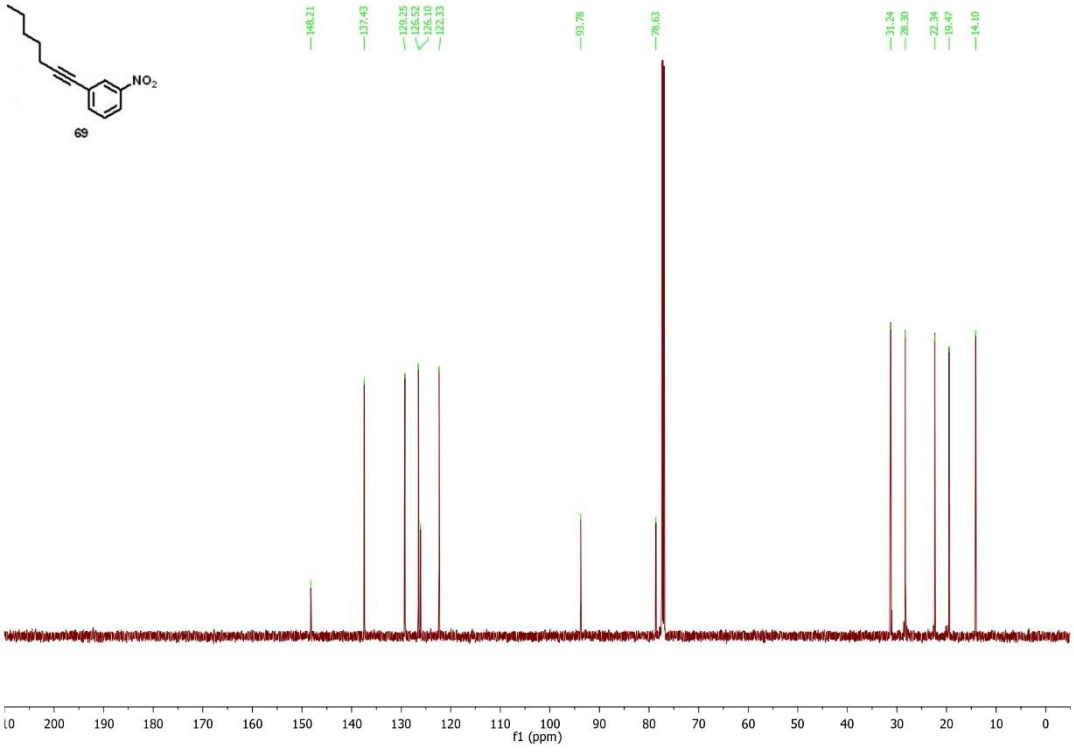
69
f1 (ppm)

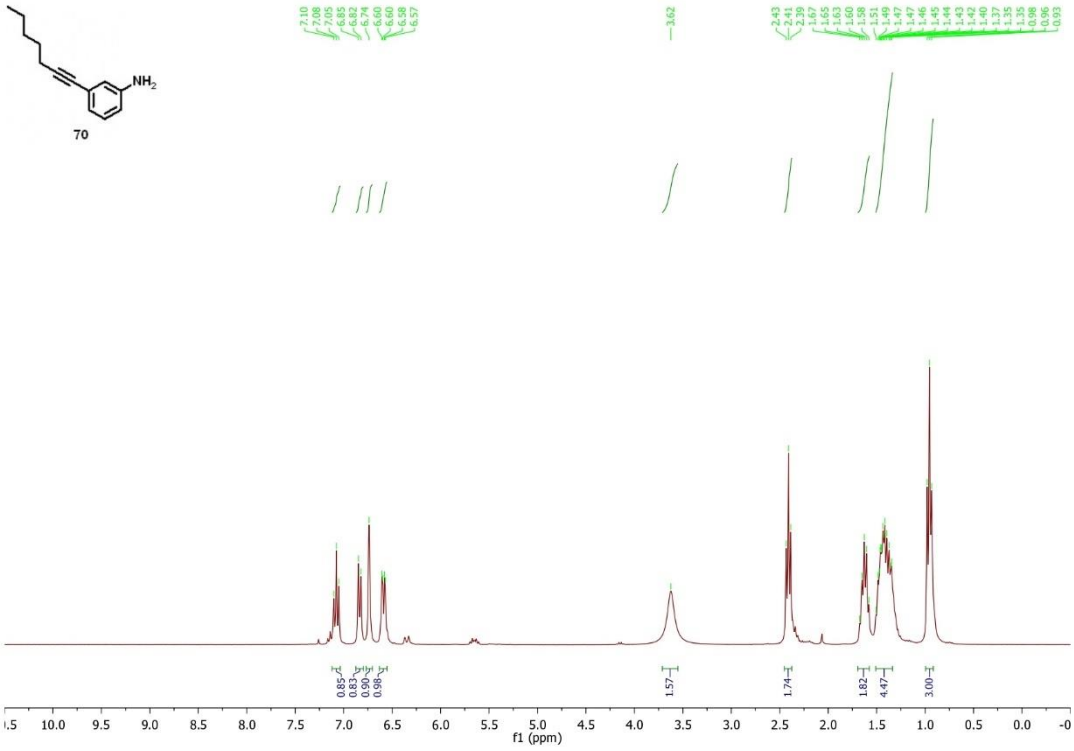
NH2
70
7.10
7.08
7.05
6.85
6.82
6.74
6.60
6.60
6.58
6.57
3.62
2.43
2.41
2.39
1.67
1.65
1.63
1.60
1.58
1.51
1.49
1.47
1.47
1.46
1.45
1.44
1.43
1.42
1.40
1.37
1.35
1.35
0.98
0.96
0.93
0.85
0.83
0.90
0.98
1.57
1.74
1.82
4.47
3.00
f1 (ppm)

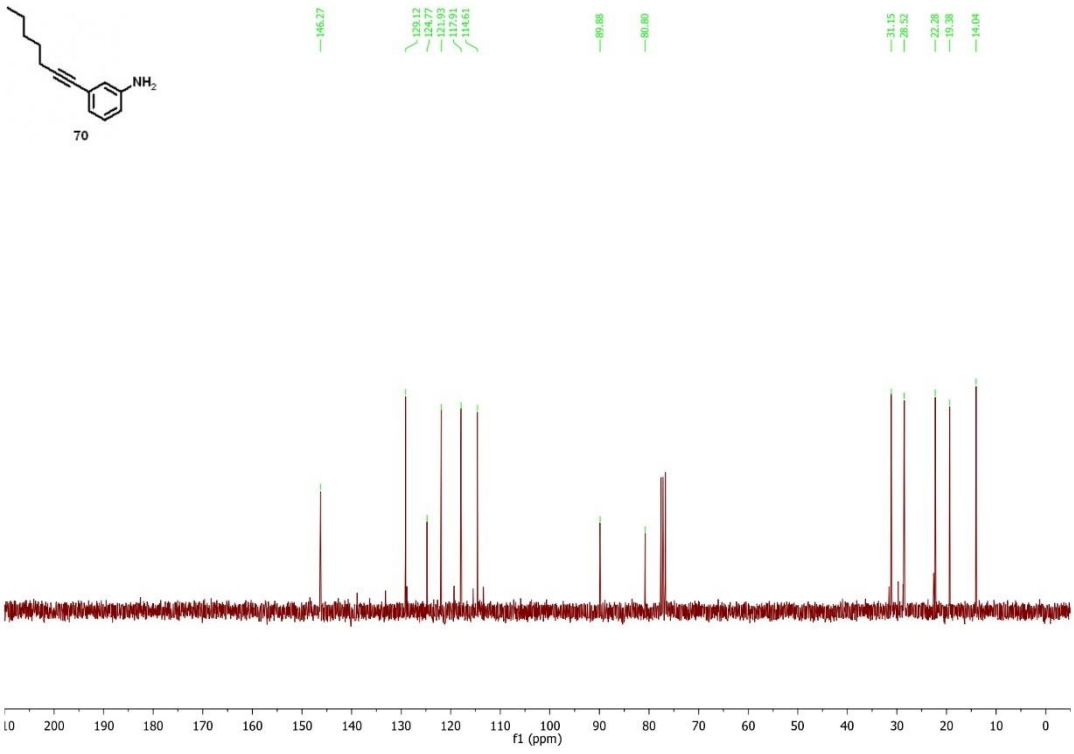
NH2
70
146.27
129.12
124.77
121.93
117.91
114.61
89.88
80.80
31.15
28.52
22.28
19.38
14.04
f1 (ppm)

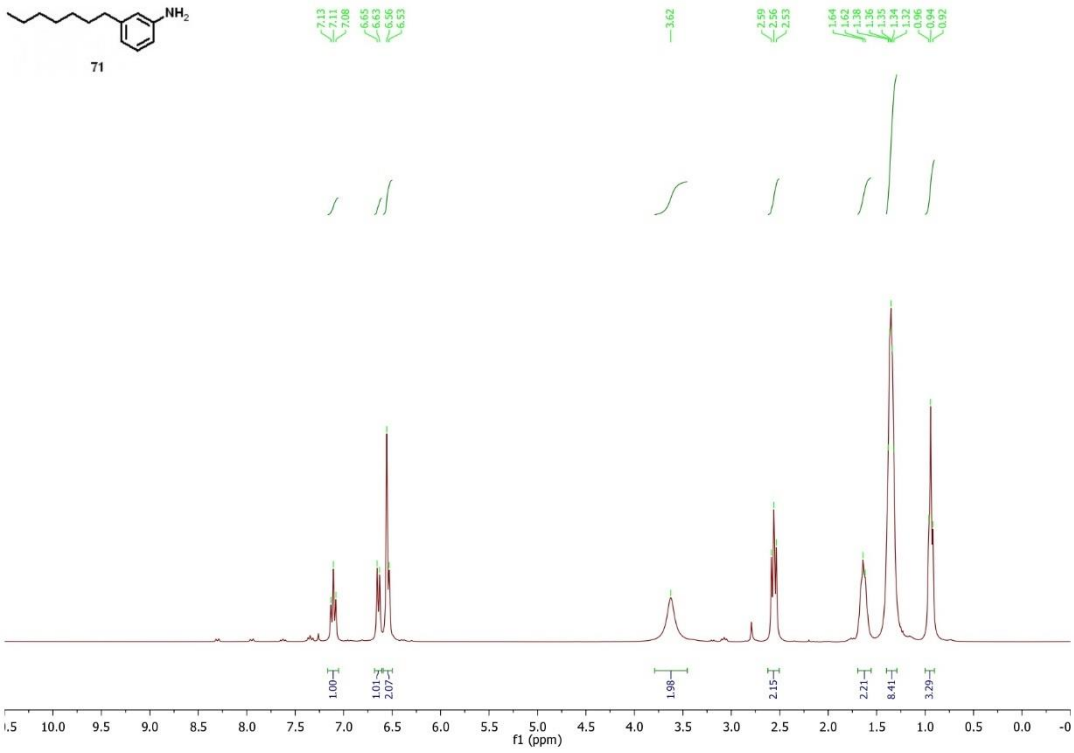
NH2
71
7.13
7.11
7.08
6.65
6.63
6.56
6.53
3.62
2.59
2.56
2.53
1.64
1.62
1.38
1.36
1.35
1.34
1.32
0.96
0.94
0.92
1.00
1.01
2.07
1.98
2.15
2.21
8.41
3.29
f1 (ppm)

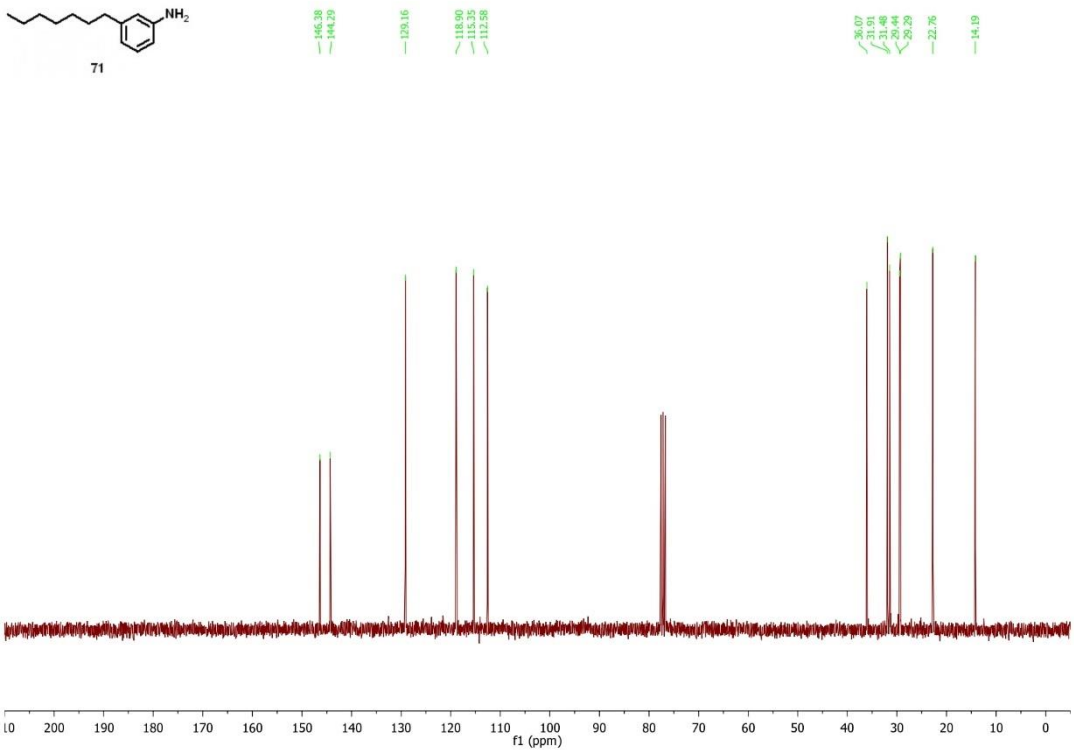
NH2
71
146.38
144.29
129.16
118.90
115.35
112.58
36.07
31.91
31.48
29.44
29.29
22.76
14.19
f1 (ppm)

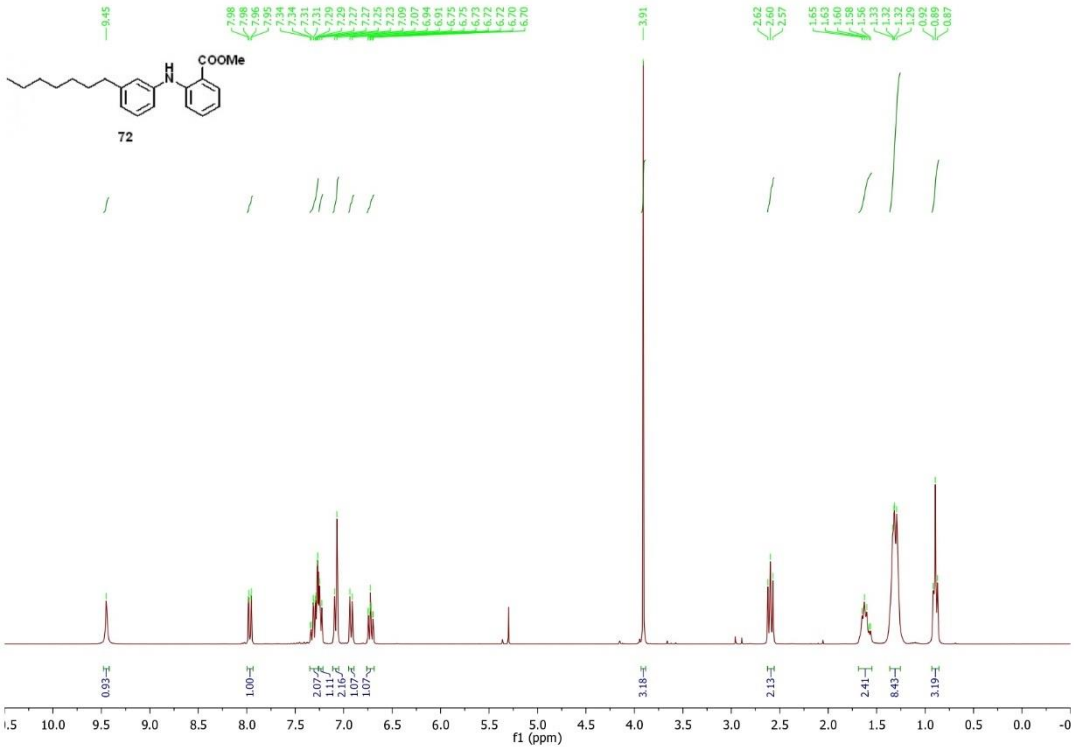
COOMe
H
N
72
f1 (ppm)

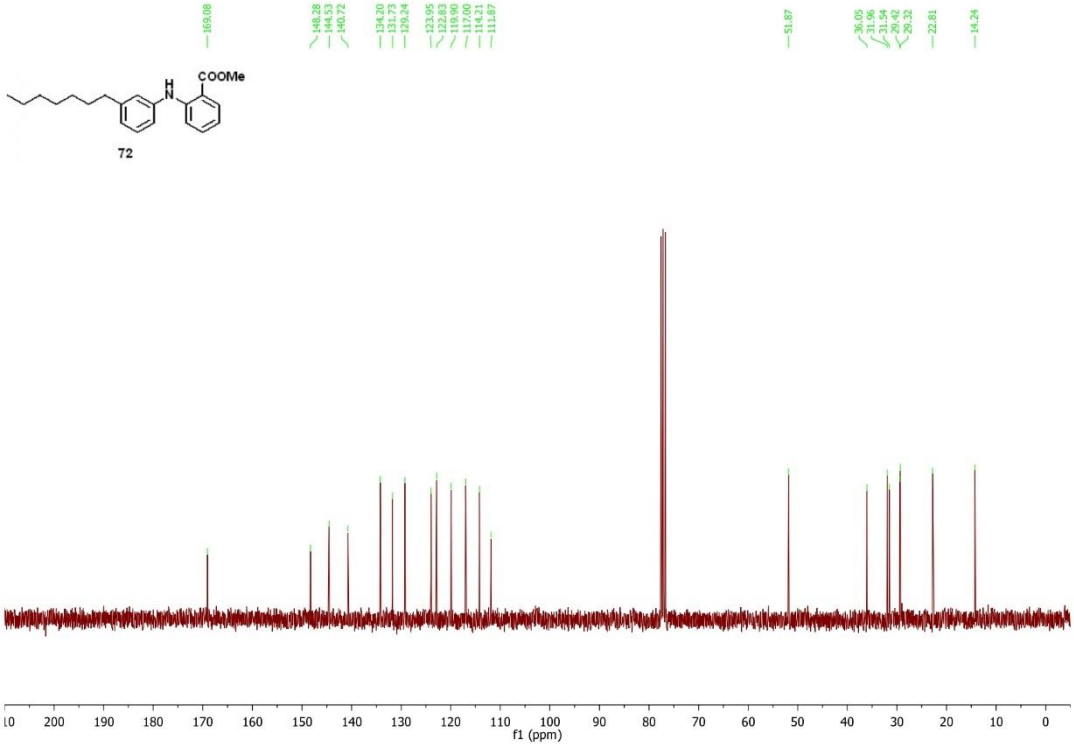
COOMe
H
N
72
f1 (ppm)

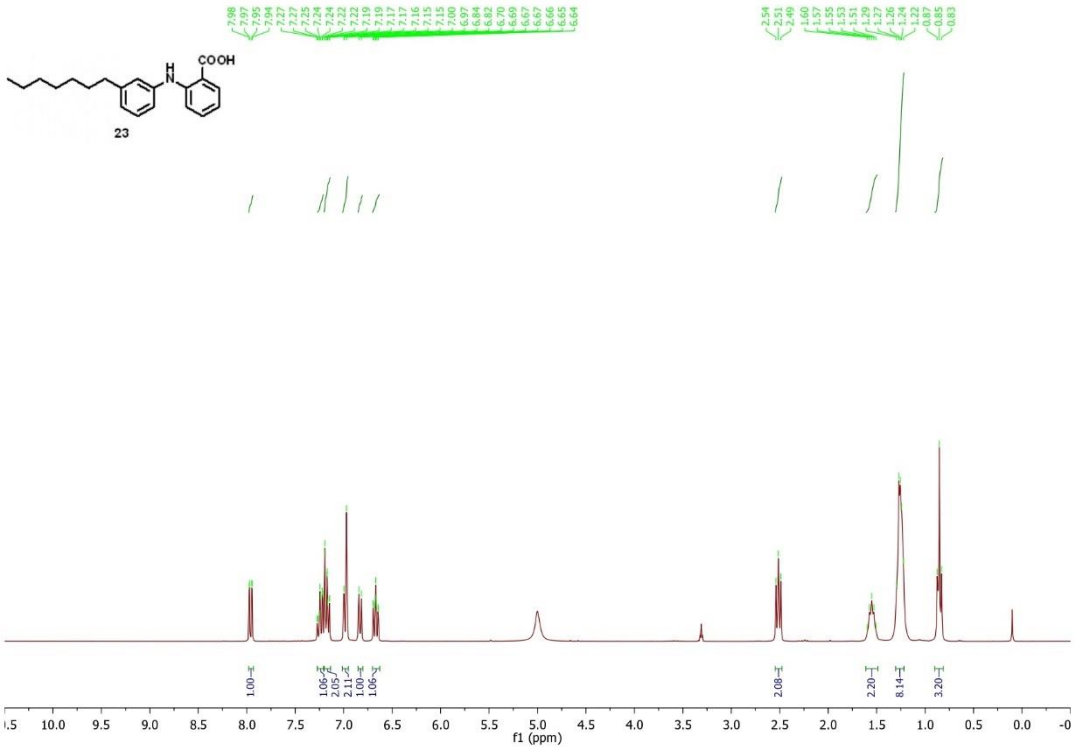
COOH
H
N
23
f1 (ppm)

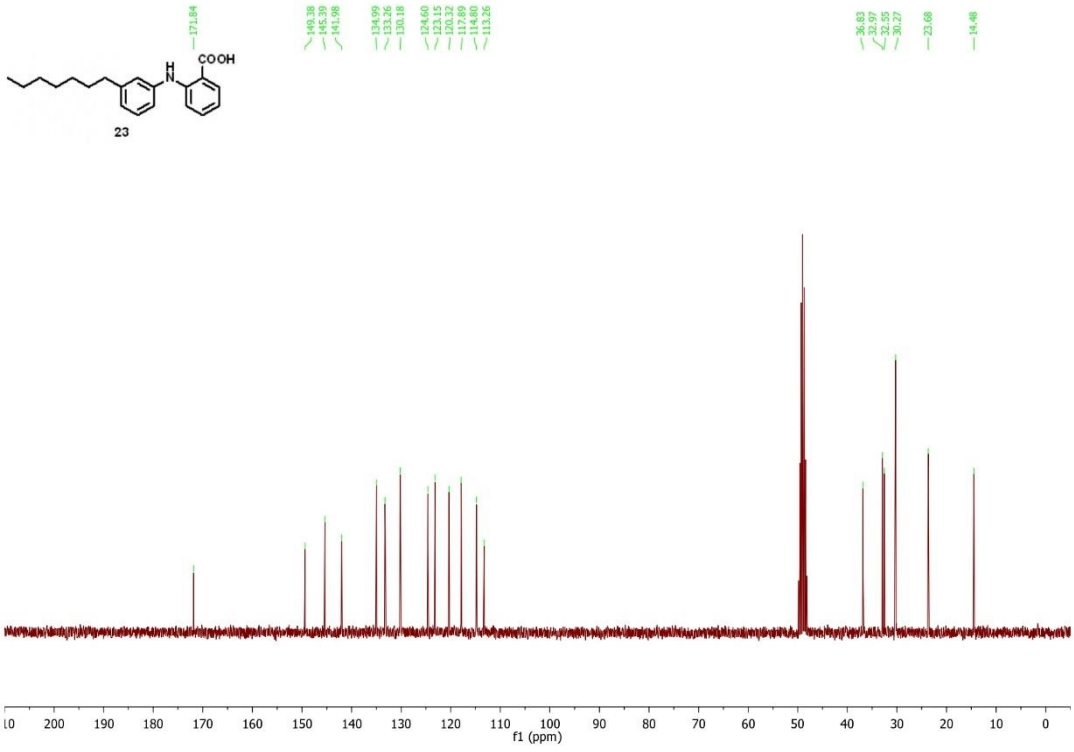
COOH
H
N
23
f1 (ppm)

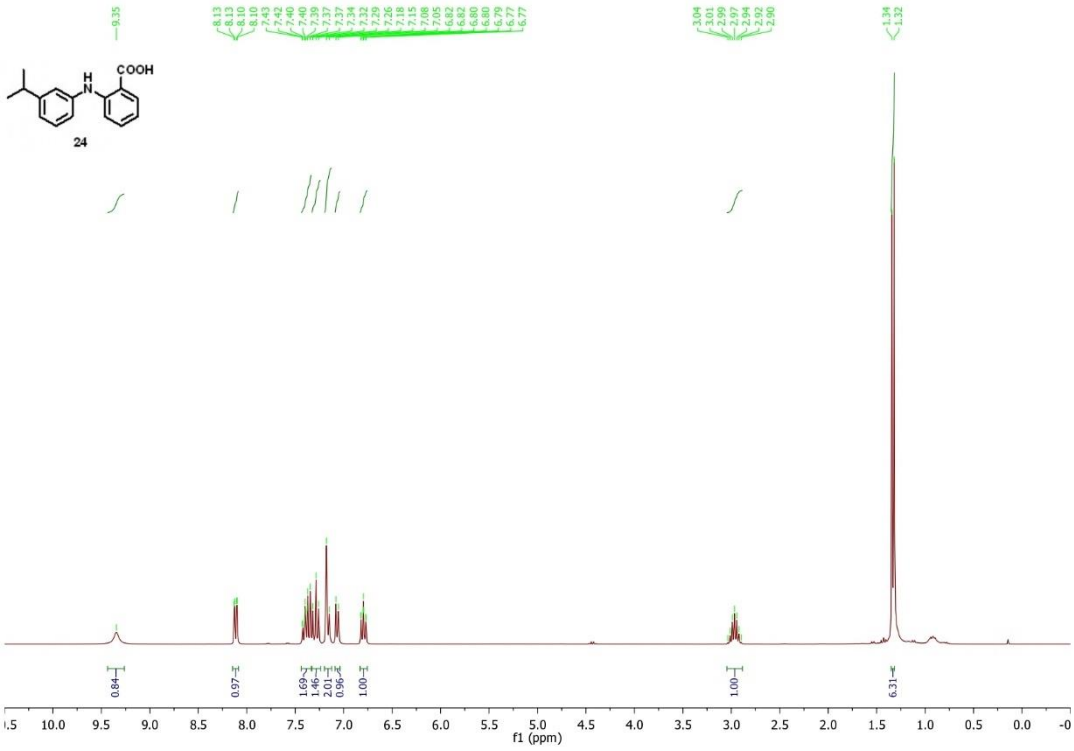
9.35
8.13
8.13
8.10
8.10
7.43
7.42
7.40
7.40
7.39
7.39
7.37
7.37
7.34
7.32
7.29
7.26
7.18
7.15
7.08
7.05
6.82
6.82
6.80
6.80
6.79
6.77
6.77
3.04
3.01
2.99
2.97
2.94
2.92
2.90
1.34
1.32
COOH
H
N
24
0.84
0.97
1.69
1.46
2.01
0.96
1.00
1.00
6.31
f1 (ppm)

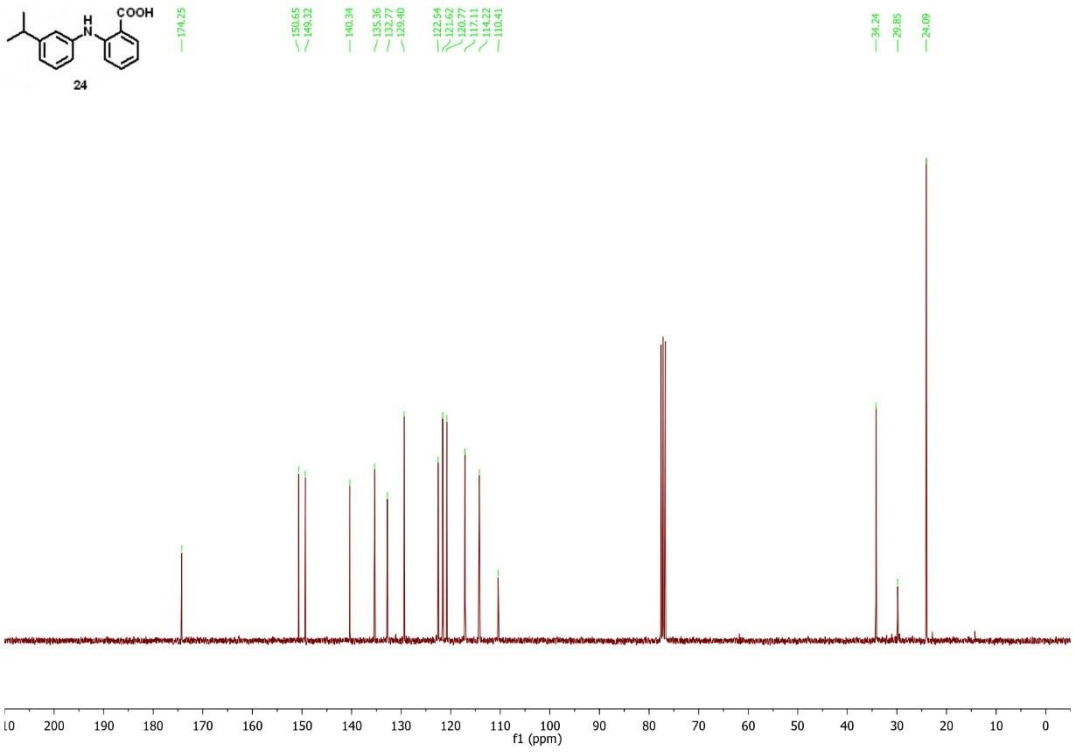
174.25
150.65
149.32
140.34
135.36
132.77
129.40
122.54
121.62
120.77
117.11
114.22
110.41
34.24
29.85
24.09
COOH
H
N
24
f1 (ppm)

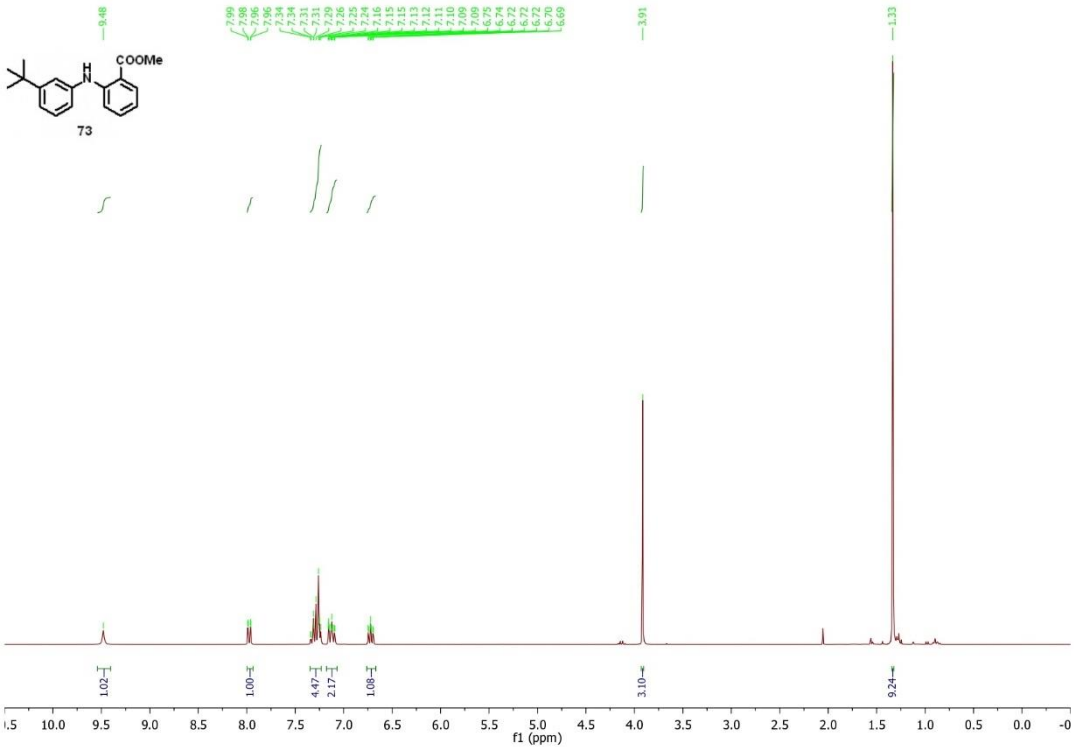
COOMe
73
9.48
7.99
7.98
7.96
7.96
7.34
7.34
7.31
7.31
7.29
7.26
7.25
7.24
7.16
7.15
7.15
7.13
7.12
7.11
7.10
7.09
7.09
6.75
6.74
6.72
6.72
6.72
6.70
6.69
3.91
1.33
1.02
1.00
4.47
2.17
1.08
3.10
9.24
f1 (ppm)

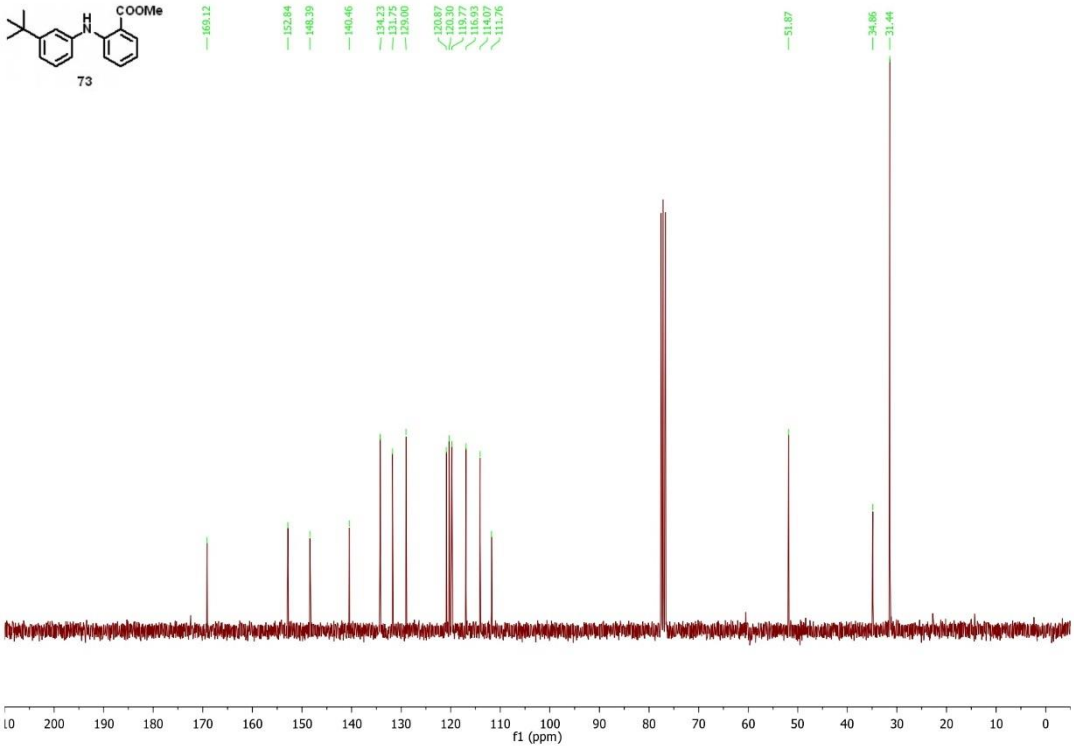
COOMe
73
169.12
152.84
148.39
140.46
134.23
131.75
129.00
120.87
120.30
119.77
116.93
114.07
111.76
51.87
34.86
31.44
f1 (ppm)

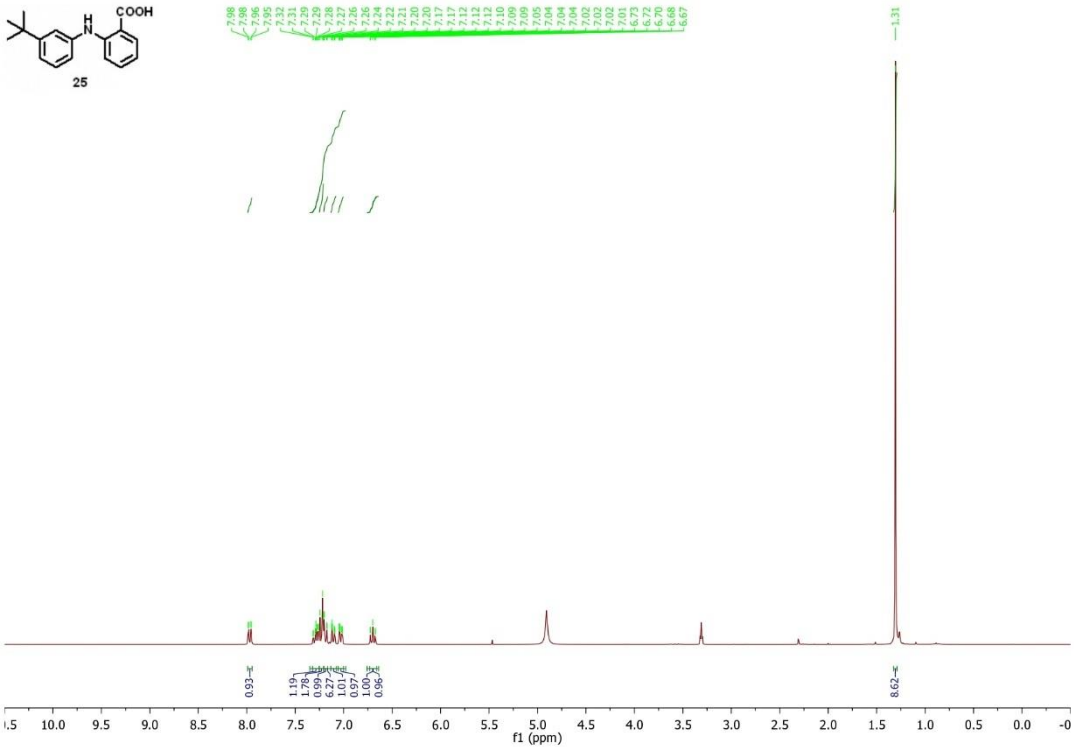
COOH
H
N
25
f1 (ppm)

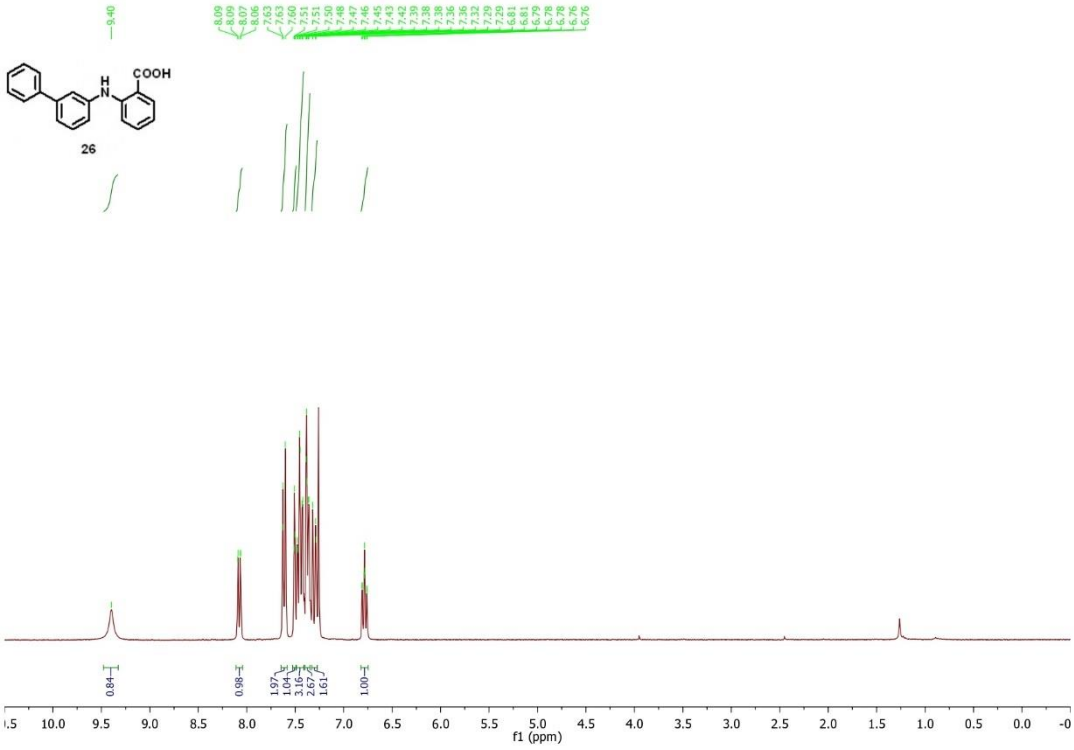
COOH
H
N
26
f1 (ppm)

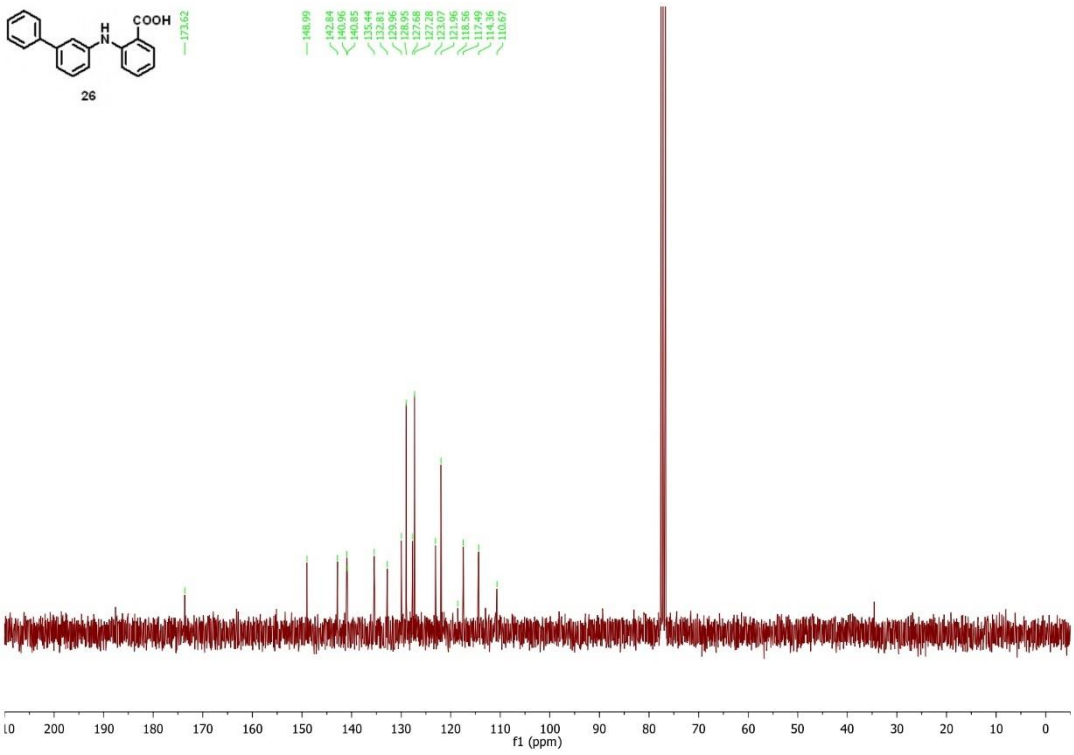
COOH
H
N
26
173.62
148.99
142.84
140.86
140.85
135.44
132.81
129.96
128.95
127.68
127.28
123.07
121.96
118.56
117.49
114.36
110.67
f1 (ppm)

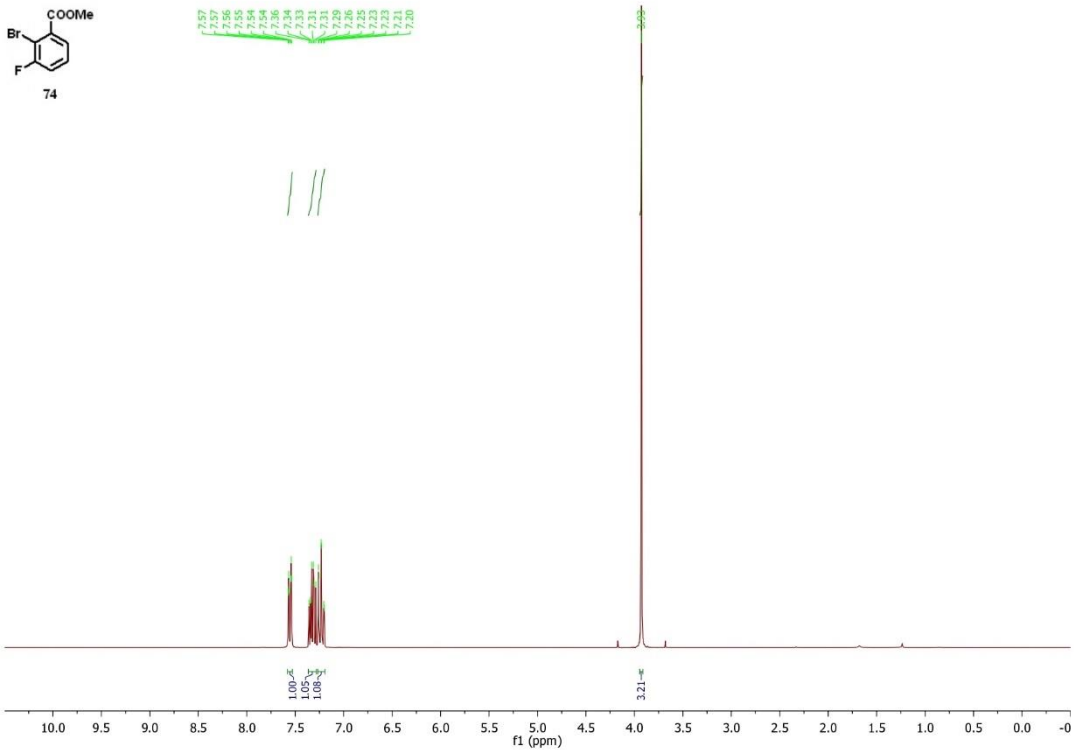
COOMe
Br
F
74
7.57
7.57
7.56
7.55
7.54
7.54
7.36
7.34
7.33
7.31
7.31
7.29
7.26
7.25
7.23
7.23
7.21
7.20
3.93
1.00
1.05
1.08
3.21
f1 (ppm)

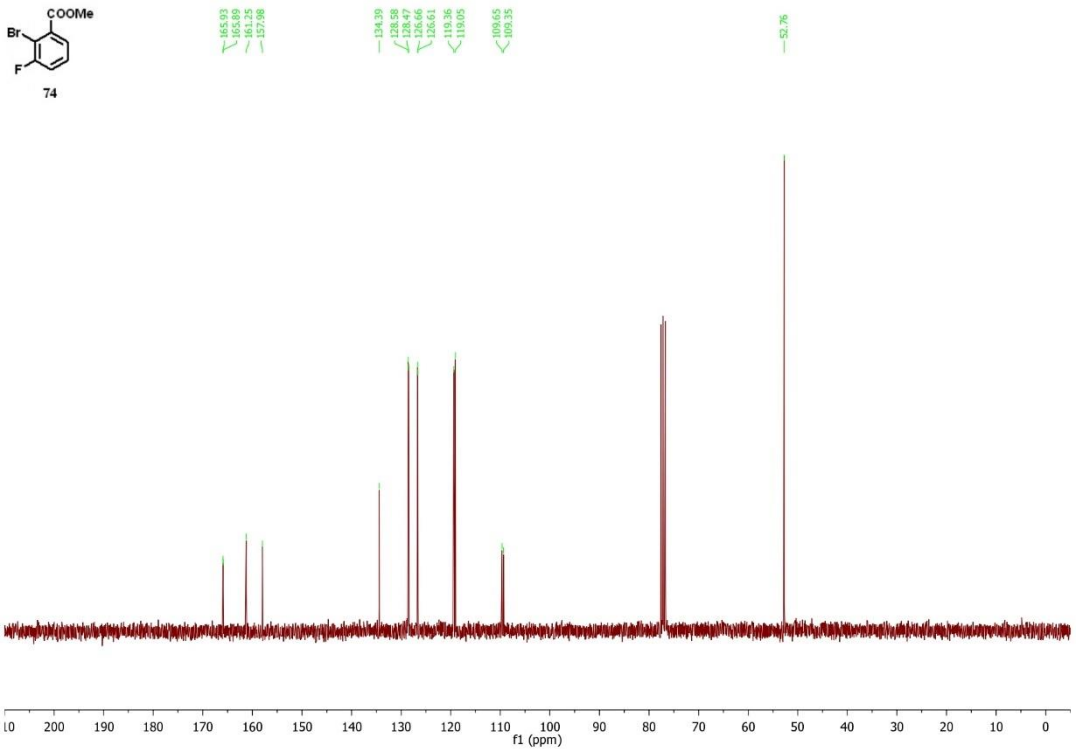
COOMe
Br
F
74
165.93
165.89
161.25
157.98
134.39
128.58
128.47
126.66
126.61
119.36
119.05
109.65
109.35
52.76
f1 (ppm)

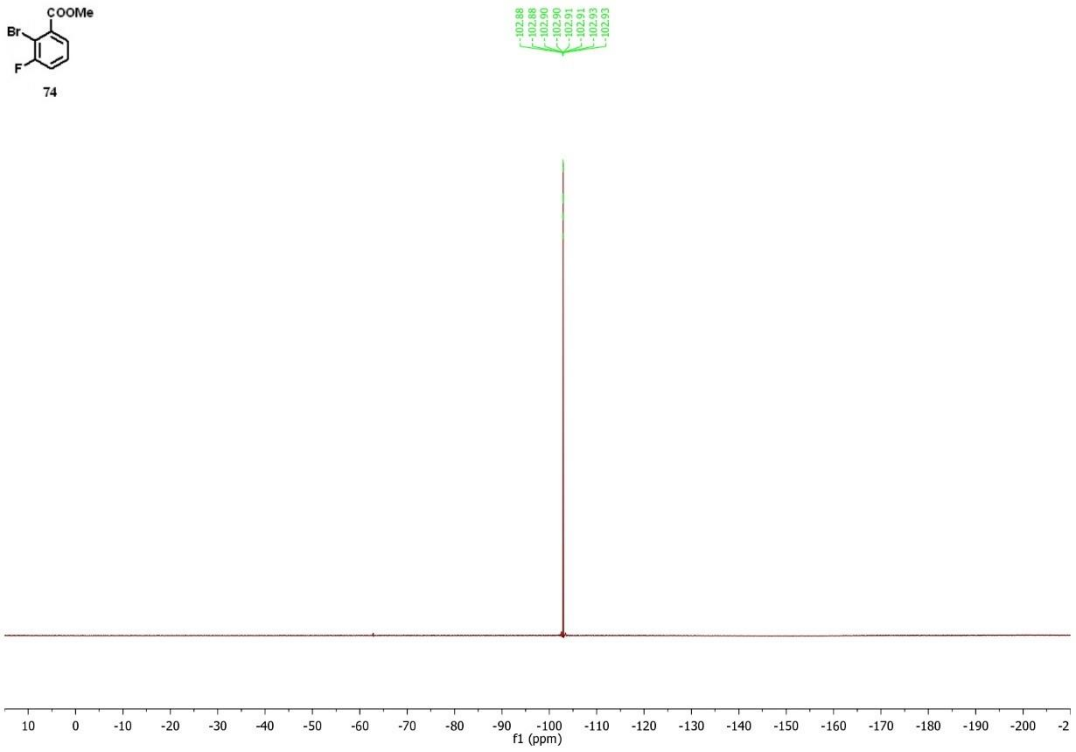
COOMe
Br
F
74
-102.88
-102.88
-102.90
-102.90
-102.91
-102.91
-102.93
-102.93
f1 (ppm)

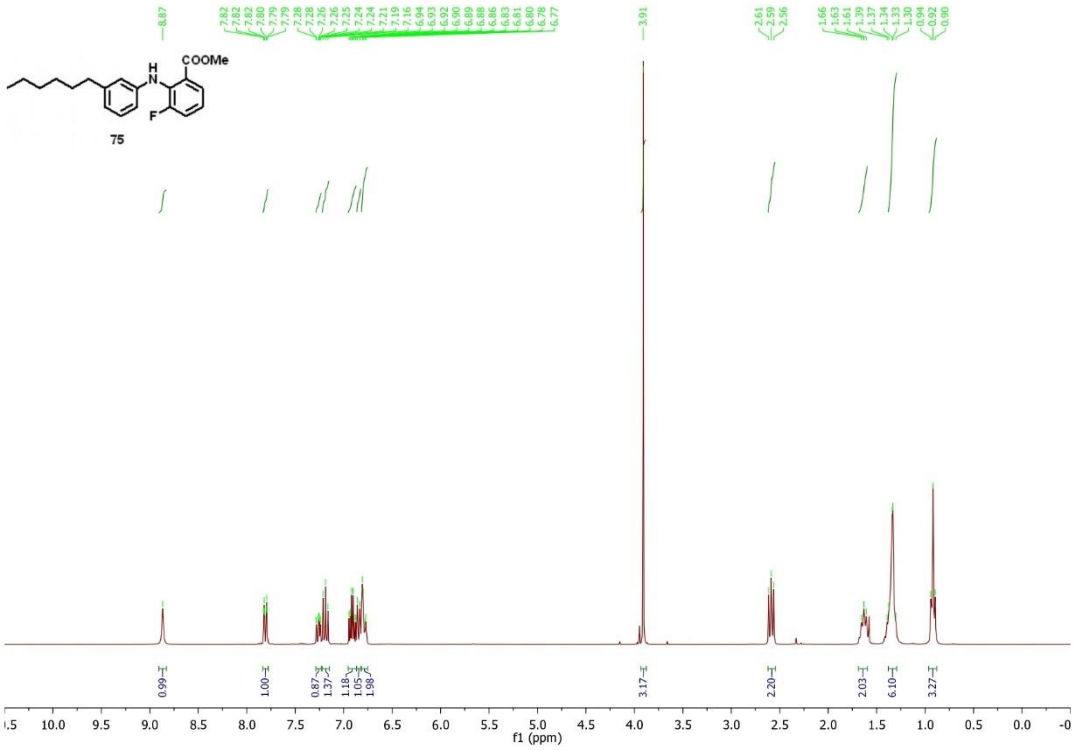
COOMe
H
N
F
75
f1 (ppm)

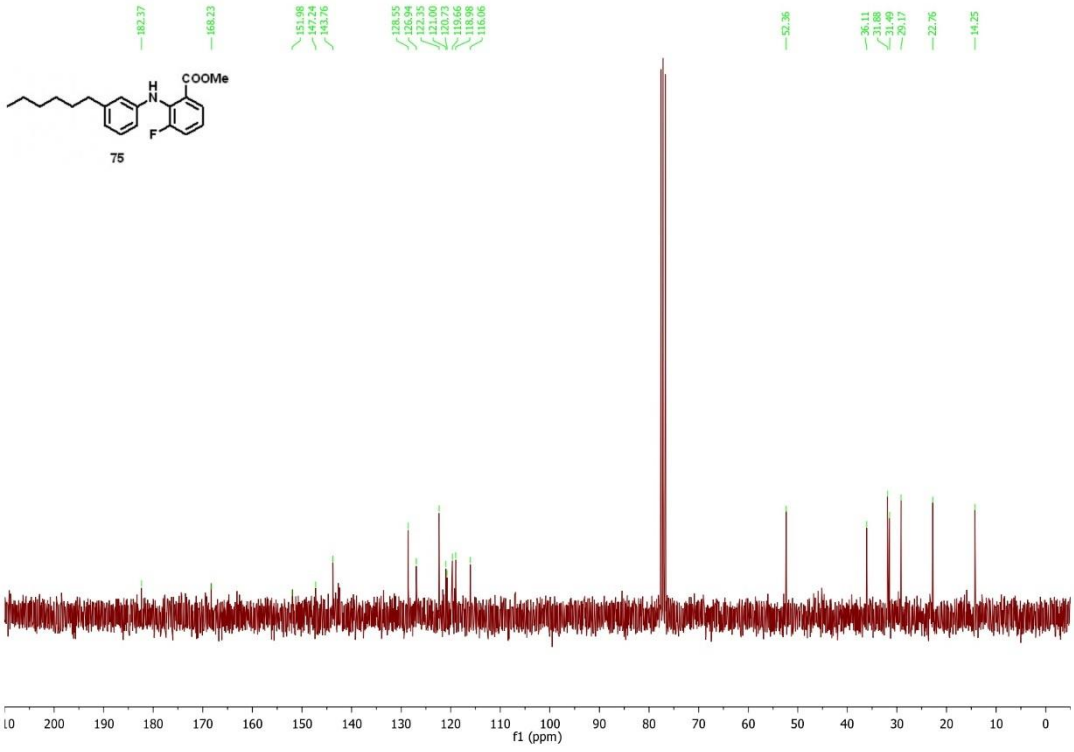
COOMe
H
N
F
75
f1 (ppm)

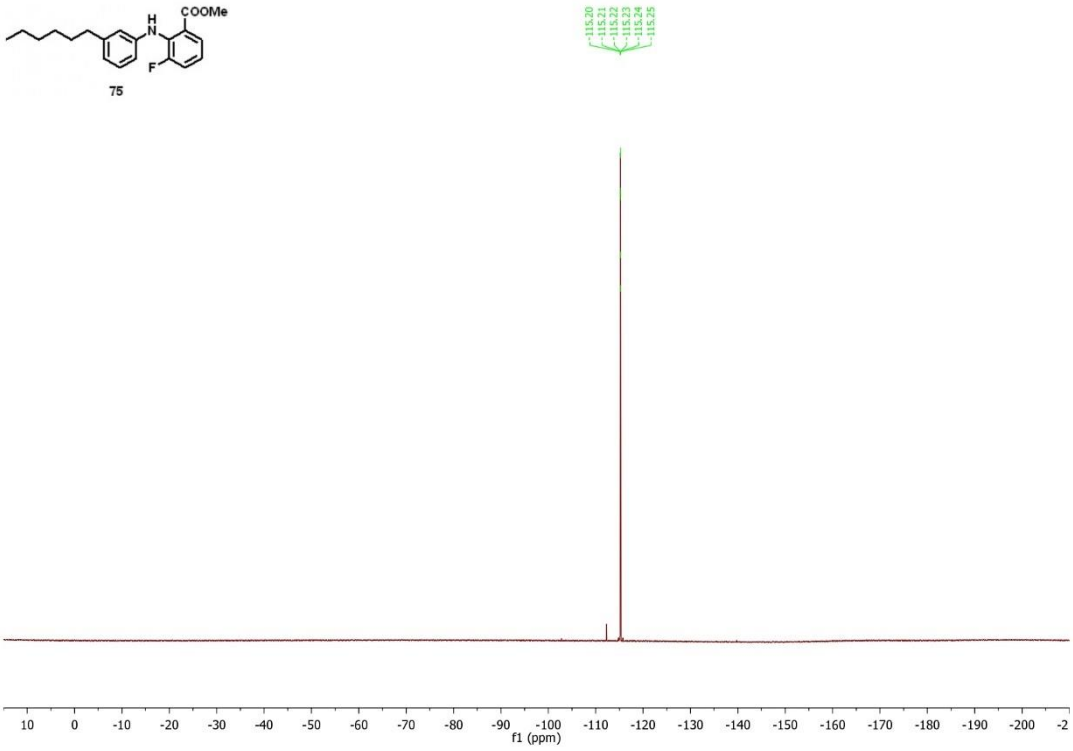
COOMe
H
N
F
75
-115.20
-115.21
-115.22
-115.23
-115.24
-115.25
10 0 -10 -20 -30 -40 -50 -60 -70 -80 -90 -100 -110 -120 -130 -140 -150 -160 -170 -180 -190 -200 -2
f1 (ppm)

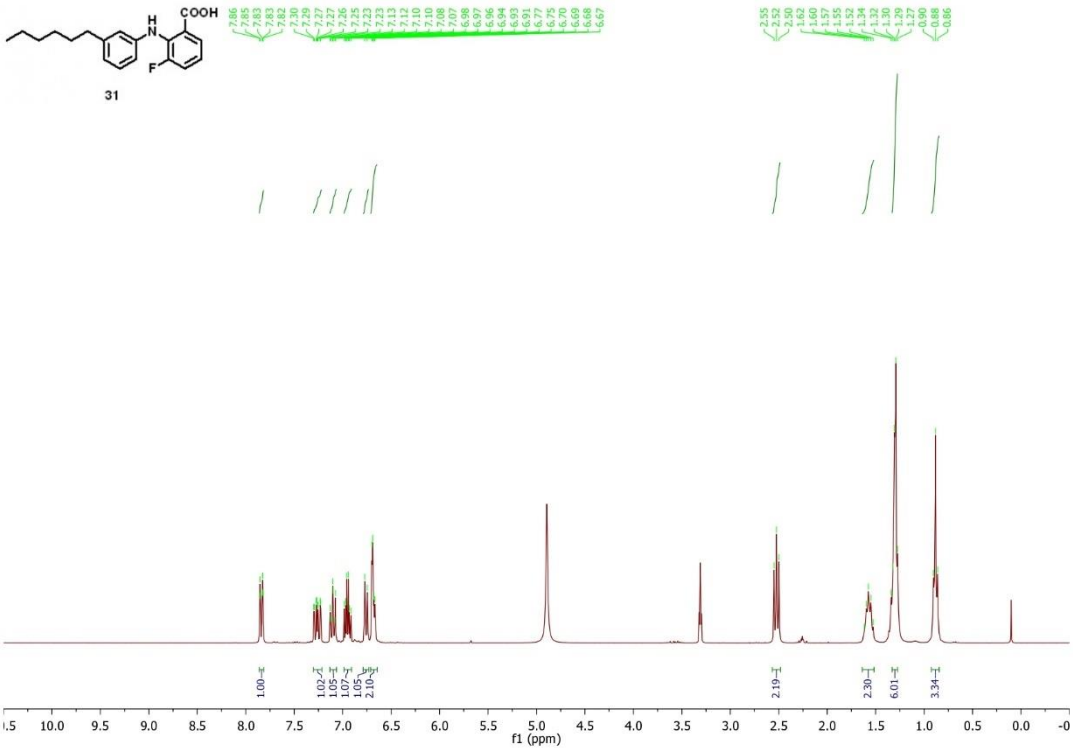
COOH
H
N
F
31
1.00
1.02
1.05
1.07
1.05
2.10
2.19
2.30
6.01
3.34
10.0 9.5 9.0 8.5 8.0 7.5 7.0 6.5 6.0 5.5 5.0 4.5 4.0 3.5 3.0 2.5 2.0 1.5 1.0 0.5 0.0
f1 (ppm)

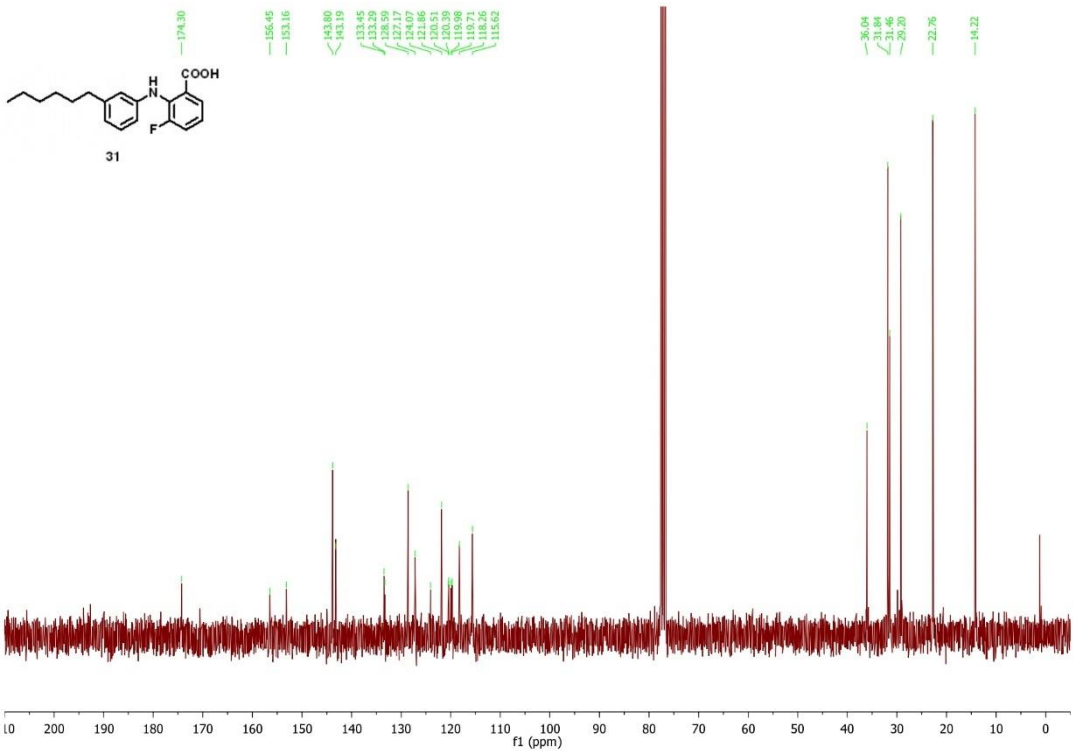
174.30
156.45
153.16
143.80
143.19
133.45
133.29
128.59
127.77
124.07
121.86
120.51
120.39
119.98
119.71
118.26
115.62
36.04
31.84
31.46
29.20
22.76
14.22
COOH
H
N
F
31
f1 (ppm)

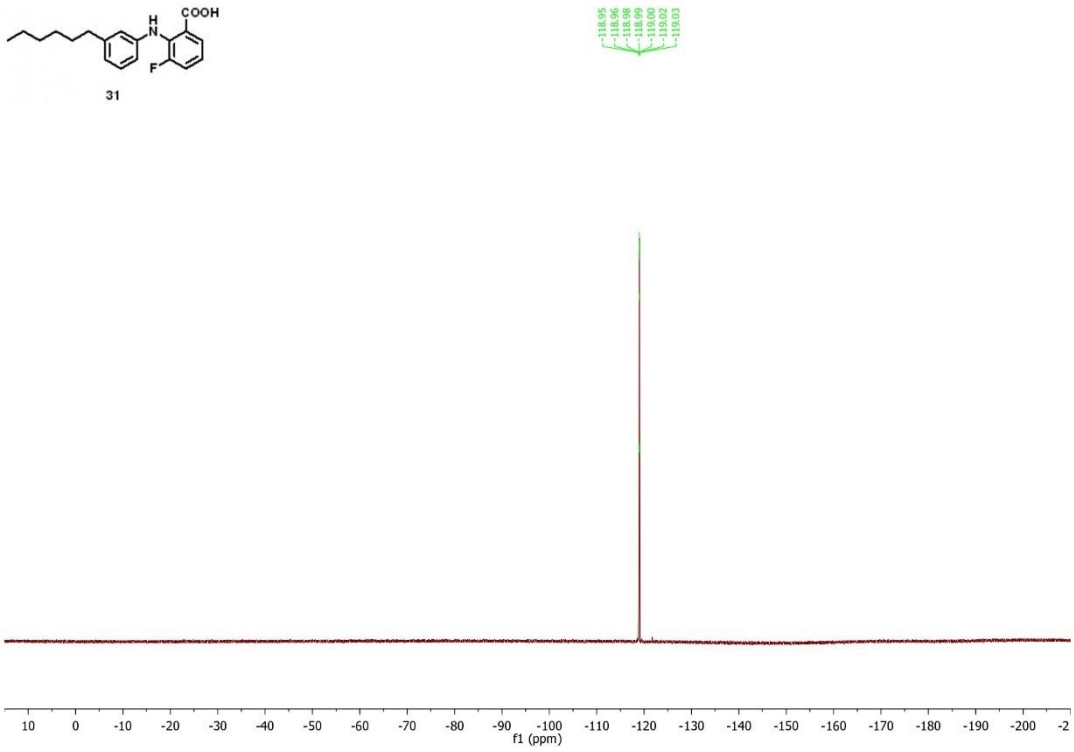
118.95
118.96
118.98
118.99
119.00
119.02
119.03
COOH
H
N
F
31
f1 (ppm)

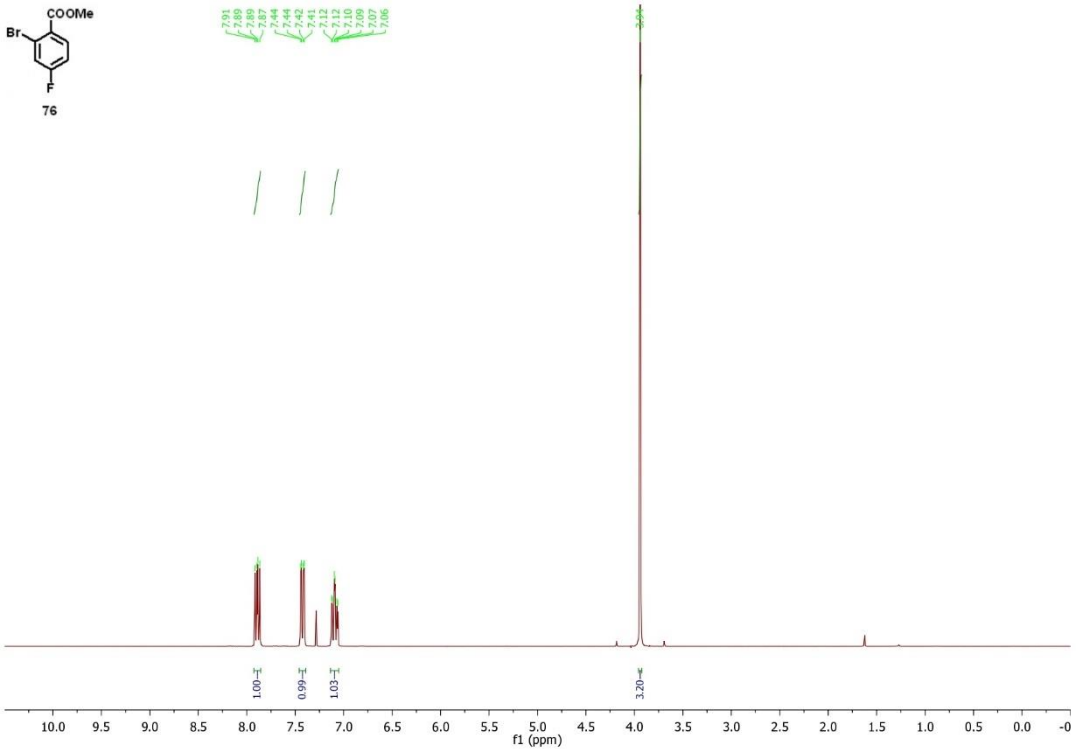
COOMe
Br
F
76
7.91
7.89
7.89
7.87
7.44
7.44
7.42
7.41
7.12
7.10
7.09
7.07
7.06
3.94
1.00
0.99
1.03
3.20
10.0 9.5 9.0 8.5 8.0 7.5 7.0 6.5 6.0 5.5 5.0 4.5 4.0 3.5 3.0 2.5 2.0 1.5 1.0 0.5 0.0 -0
f1 (ppm)

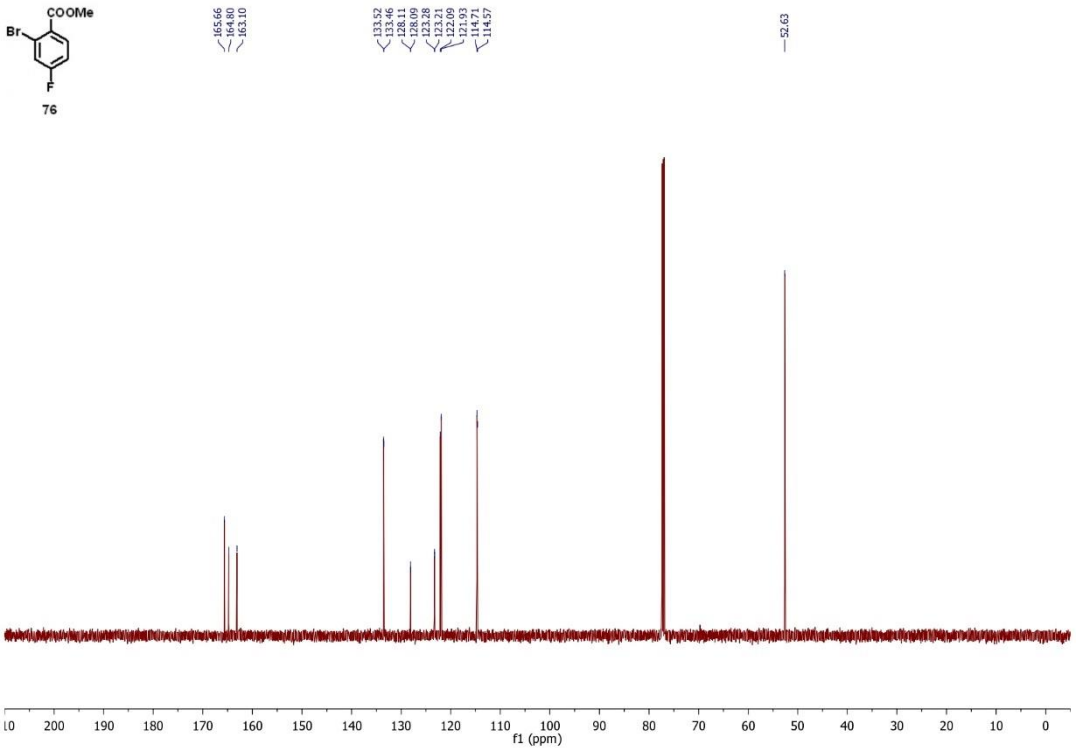
COOMe
Br
F
76
165.66
164.80
163.10
133.52
133.46
128.11
128.09
123.38
123.21
122.09
121.93
114.71
114.57
52.63
200 190 180 170 160 150 140 130 120 110 100 90 80 70 60 50 40 30 20 10 0
f1 (ppm)

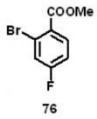
COOMe
Br
F

76

-105.73
-105.75
-105.76
-105.78
-105.78
-105.81
10 0 -10 -20 -30 -40 -50 -60 -70 -80 -90 -100 -110 -120 -130 -140 -150 -160 -170 -180 -190 -200 -2
f1 (ppm)

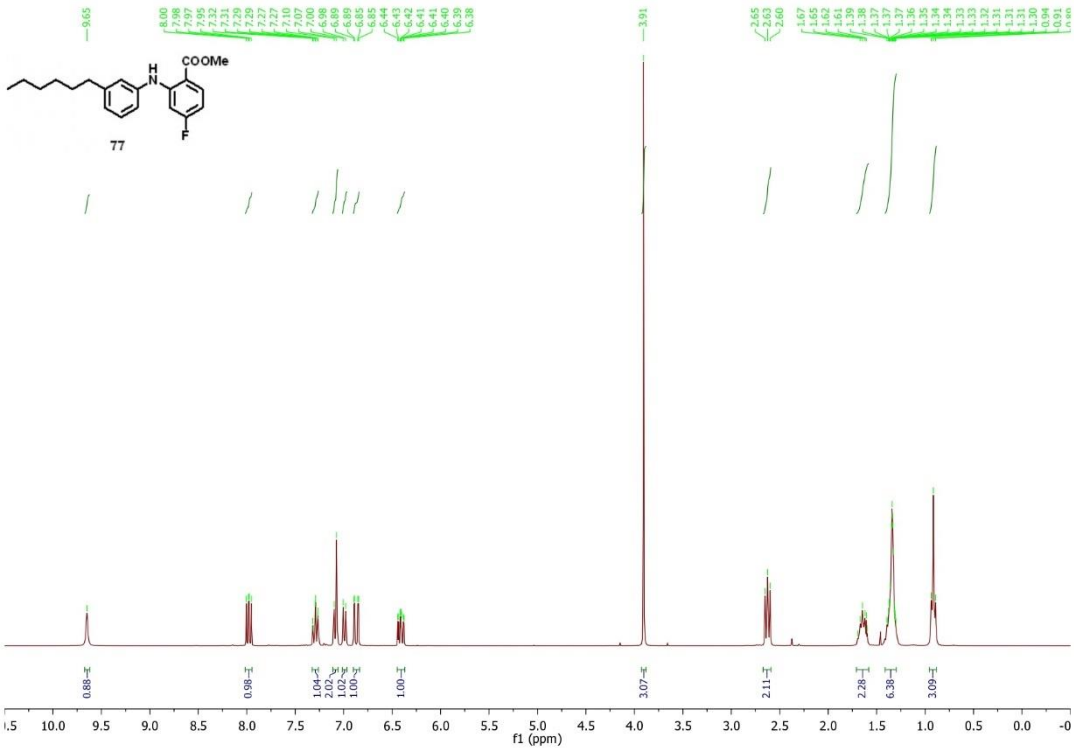
9.65
8.00
7.98
7.97
7.95
7.32
7.31
7.29
7.29
7.27
7.27
7.10
7.07
7.00
6.98
6.89
6.89
6.85
6.85
6.44
6.43
6.42
6.41
6.41
6.40
6.39
6.38
3.91
2.65
2.63
2.60
1.67
1.65
1.62
1.61
1.39
1.38
1.37
1.37
1.37
1.36
1.35
1.34
1.34
1.33
1.33
1.32
1.32
1.31
1.31
1.31
1.30
1.30
1.30
0.94
0.91
0.88
0.98
1.04
2.02
1.02
1.00
1.00
3.07
2.11
2.28
6.38
3.09
f1 (ppm)

77

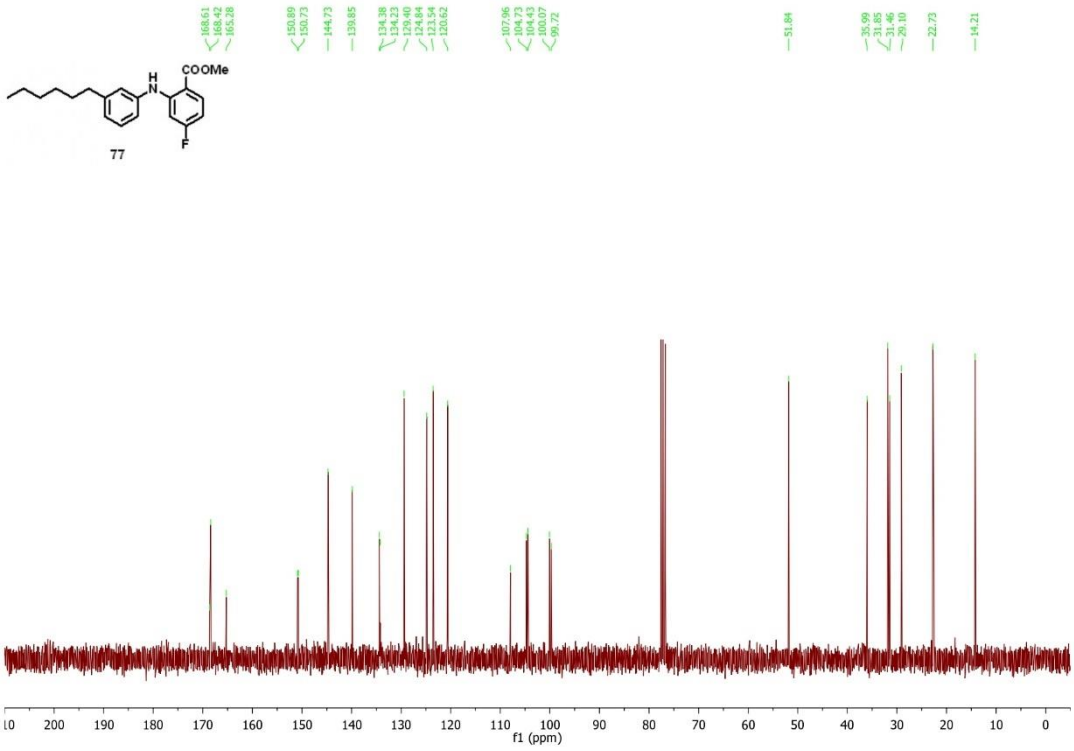
168.61
168.42
165.28
150.89
150.73
144.73
139.85
134.38
134.23
129.40
124.84
123.54
120.62
107.96
104.73
104.43
100.07
96.72
51.84
35.99
31.85
31.46
29.10
22.73
14.21
COOMe
H
N
F
77
f1 (ppm)

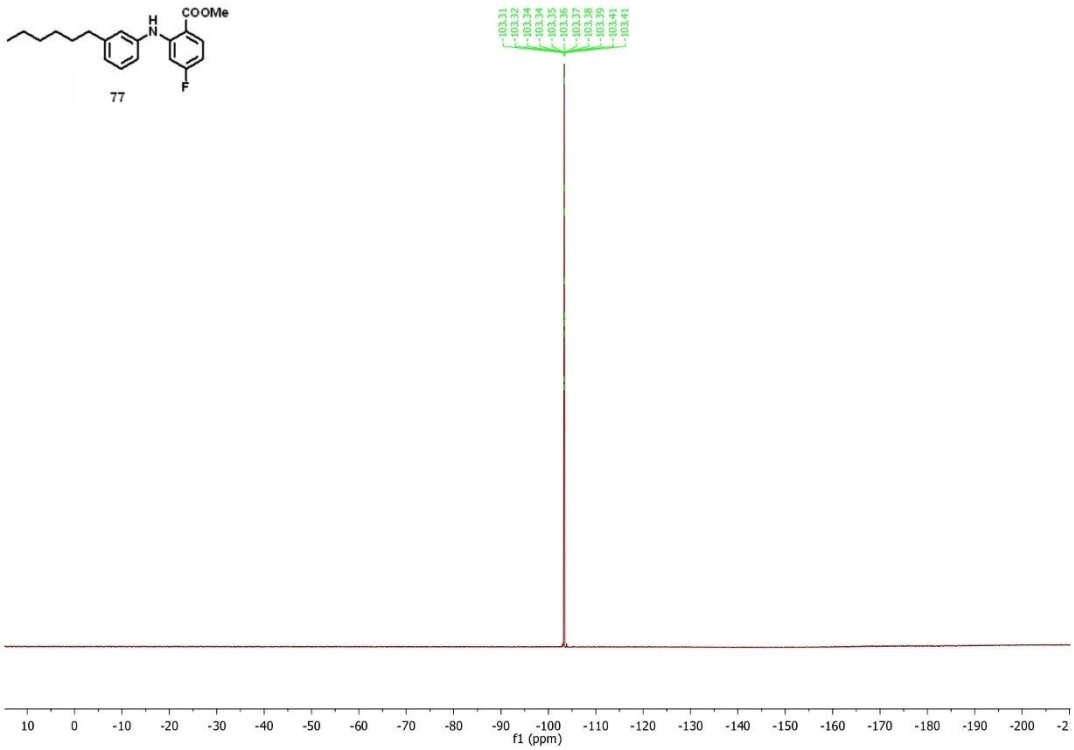
-103.31
-103.32
-103.34
-103.34
-103.35
-103.36
-103.37
-103.38
-103.39
-103.41
-103.41
COOMe
H
N
F
77
f1 (ppm)

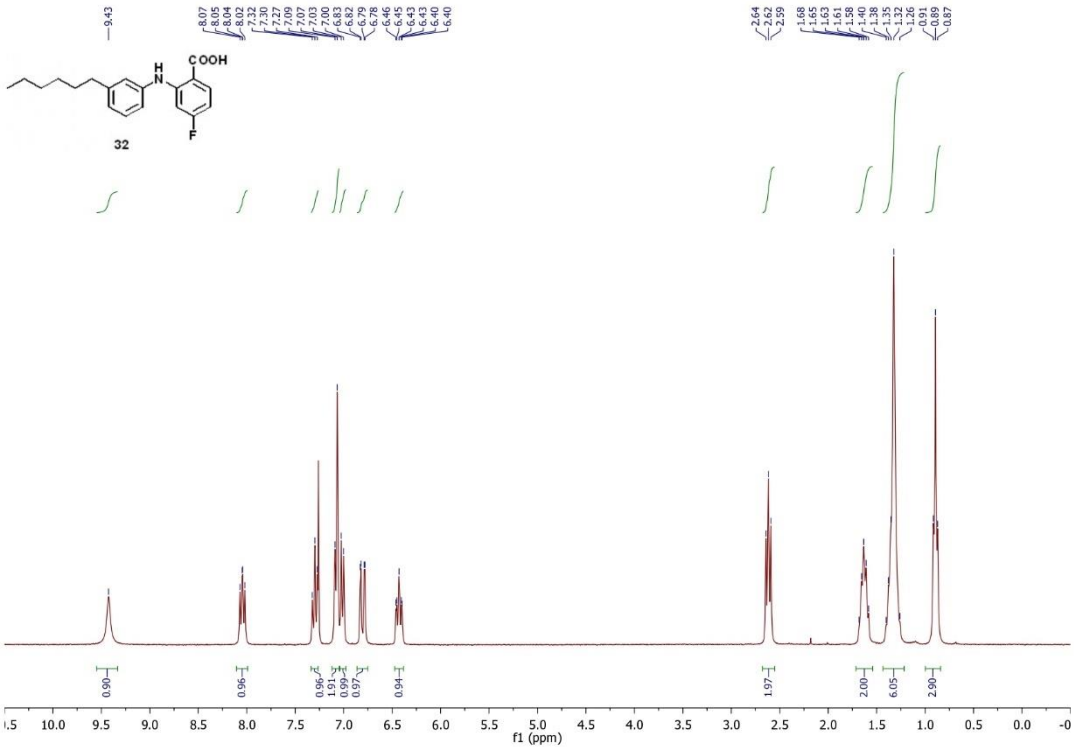
9.43
8.07
8.05
8.04
8.02
7.32
7.30
7.27
7.09
7.07
7.03
7.00
6.83
6.82
6.79
6.78
6.46
6.45
6.43
6.40
6.40
2.64
2.62
2.59
1.68
1.65
1.63
1.61
1.58
1.40
1.38
1.35
1.32
1.26
0.91
0.89
0.87
COOH
H
N
F
32
0.90
0.96
0.96
1.91
0.99
0.97
0.94
1.97
2.00
6.05
2.90
f1 (ppm)

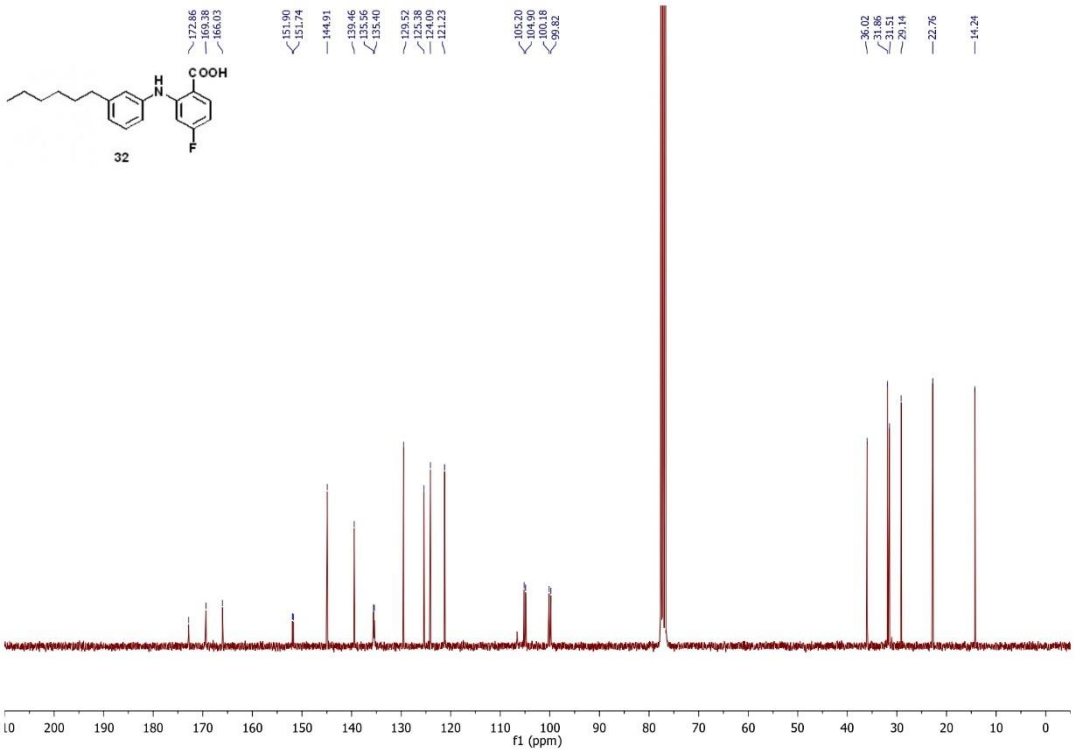
172.86
169.38
166.03
151.90
151.74
144.91
139.46
135.56
135.40
129.52
125.38
124.09
121.23
105.20
104.90
100.18
99.82
36.02
31.86
31.51
29.14
22.76
14.24
COOH
H
N
F
32
f1 (ppm)

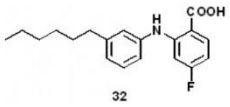
COOH
H
N
F

32


-101.57
-101.60
-101.62
-101.64
-101.67

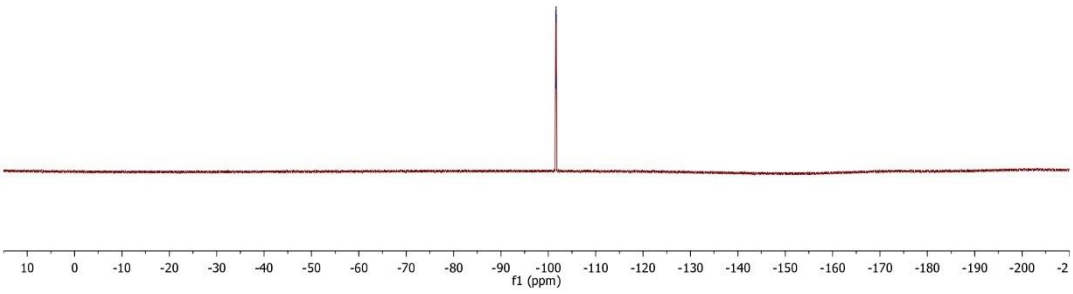
10 0 -10 -20 -30 -40 -50 -60 -70 -80 -90 -100 -110 -120 -130 -140 -150 -160 -170 -180 -190 -200 -2
f1 (ppm)


COOMe
Br
F

78

7.63
7.62
7.62
7.60
7.59
7.59
7.58
7.53
7.52
7.51
7.50
7.49
7.48
7.09
7.08
7.07
7.07
7.06
7.06
7.05
7.04
7.04
7.03
7.02
3.93
1.00
1.04
1.07
3.26
10.0 9.5 9.0 8.5 8.0 7.5 7.0 6.5 6.0 5.5 5.0 4.5 4.0 3.5 3.0 2.5 2.0 1.5 1.0 0.5 0.0 -0
f1 (ppm)

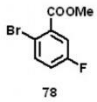
COOMe
Br
F

78

165.47
163.06
159.76
135.97
135.87
133.56
133.46
120.23
119.93
118.79
118.46
116.19
116.15
52.82
f1 (ppm)

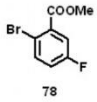
COOMe
Br
F

78

113.95
113.96
113.97
113.98
113.98
113.99
114.00
114.02
f1 (ppm)

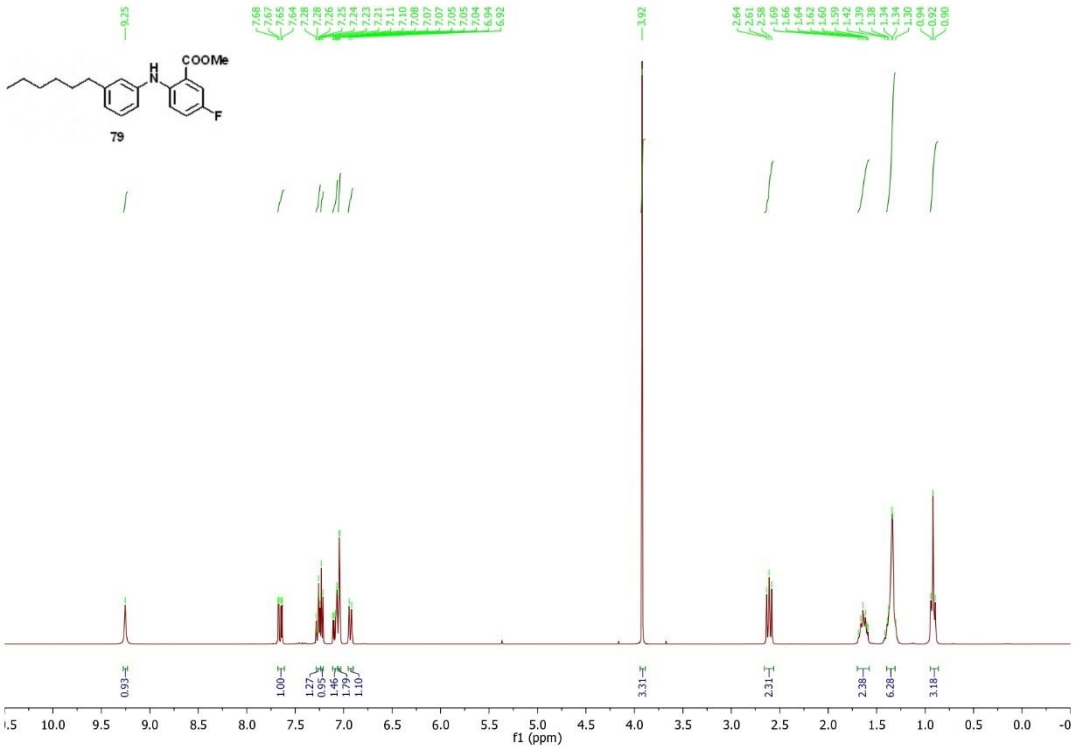
COOMe
H
N
F
79
f1 (ppm)

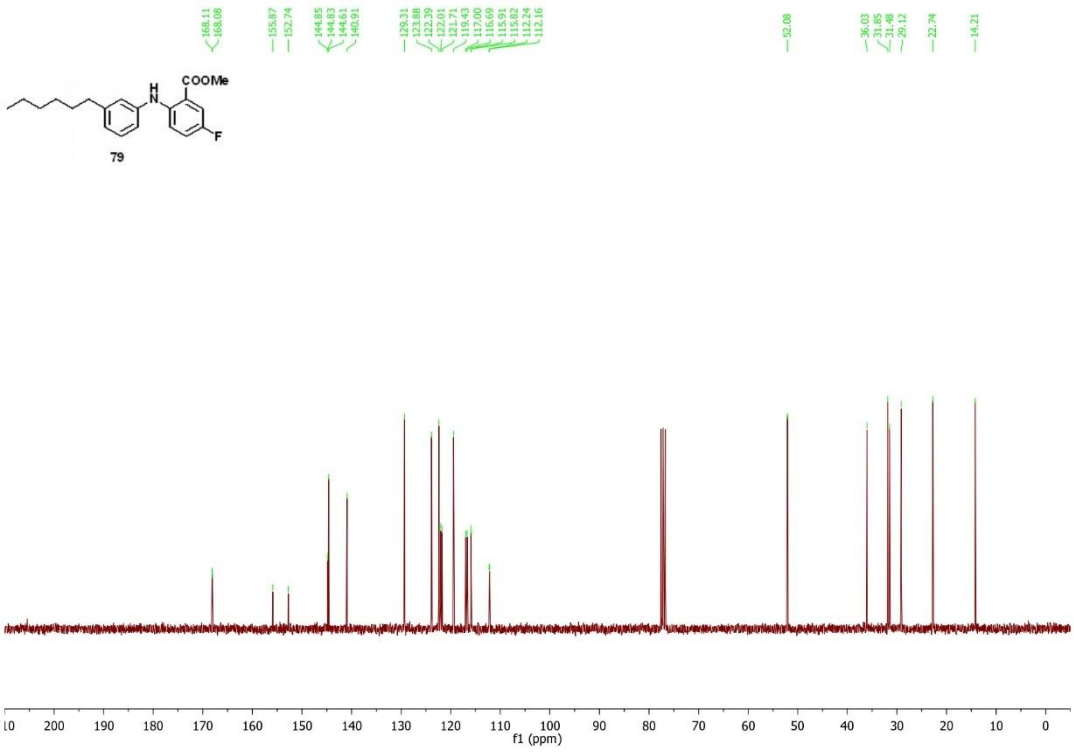
COOMe
H
N
F
79
f1 (ppm)

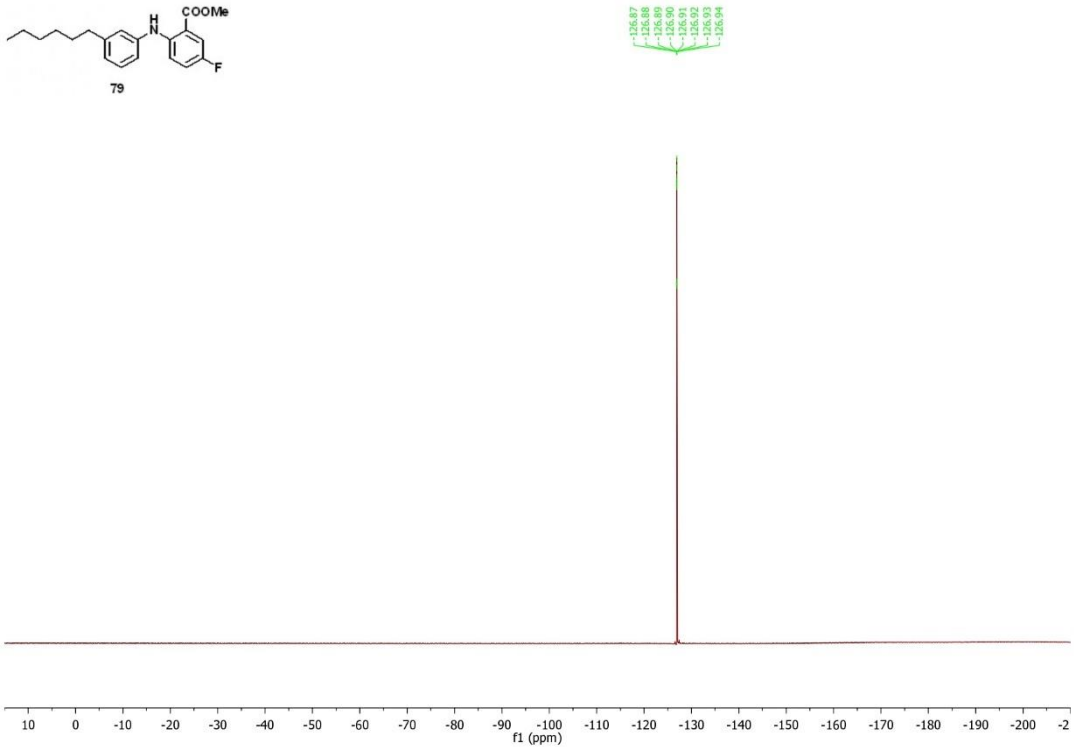
COOMe
H
N
F
79
-126.87
-126.88
-126.89
-126.90
-126.91
-126.92
-126.93
-126.94
10 0 -10 -20 -30 -40 -50 -60 -70 -80 -90 -100 -110 -120 -130 -140 -150 -160 -170 -180 -190 -200 -2
f1 (ppm)

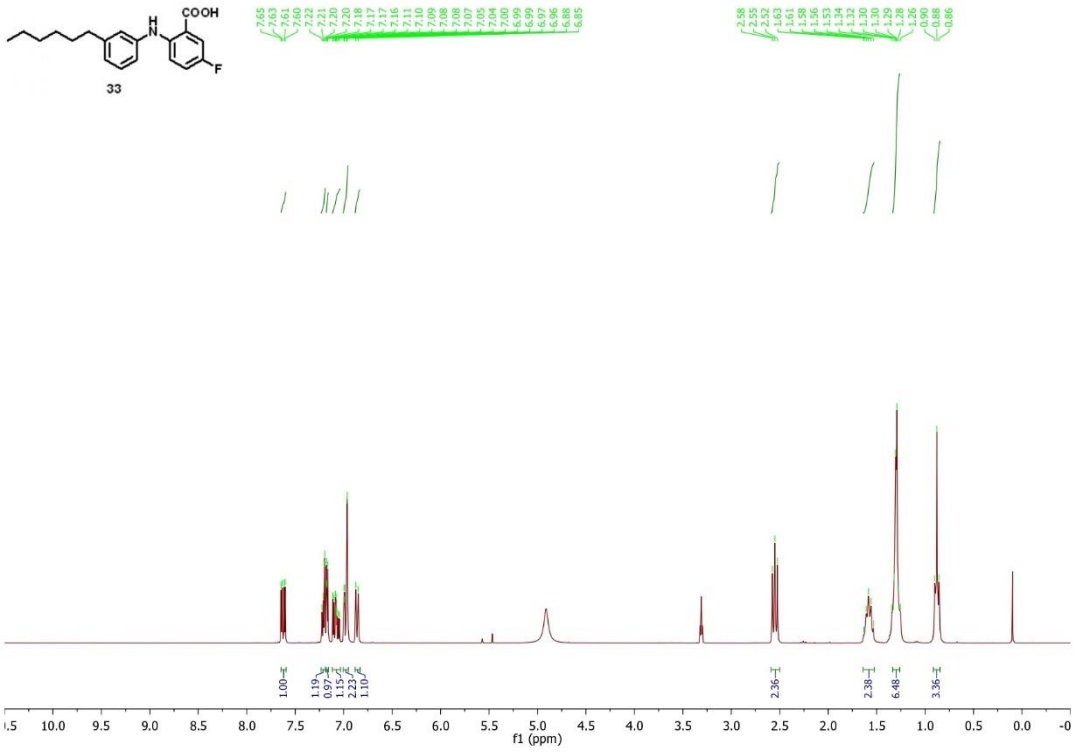
COOH
H
N
F
33
7.65
7.63
7.61
7.60
7.22
7.21
7.20
7.20
7.18
7.17
7.17
7.16
7.11
7.10
7.09
7.08
7.08
7.07
7.05
7.04
7.00
6.99
6.99
6.97
6.96
6.88
6.85
2.58
2.55
2.52
1.63
1.61
1.58
1.56
1.53
1.34
1.32
1.30
1.30
1.29
1.28
1.26
0.90
0.88
0.86
1.00
1.19
0.97
1.15
2.23
1.10
2.36
2.38
6.48
3.36
.5 10.0 9.5 9.0 8.5 8.0 7.5 7.0 6.5 6.0 5.5 5.0 4.5 4.0 3.5 3.0 2.5 2.0 1.5 1.0 0.5 0.0 -0
f1 (ppm)

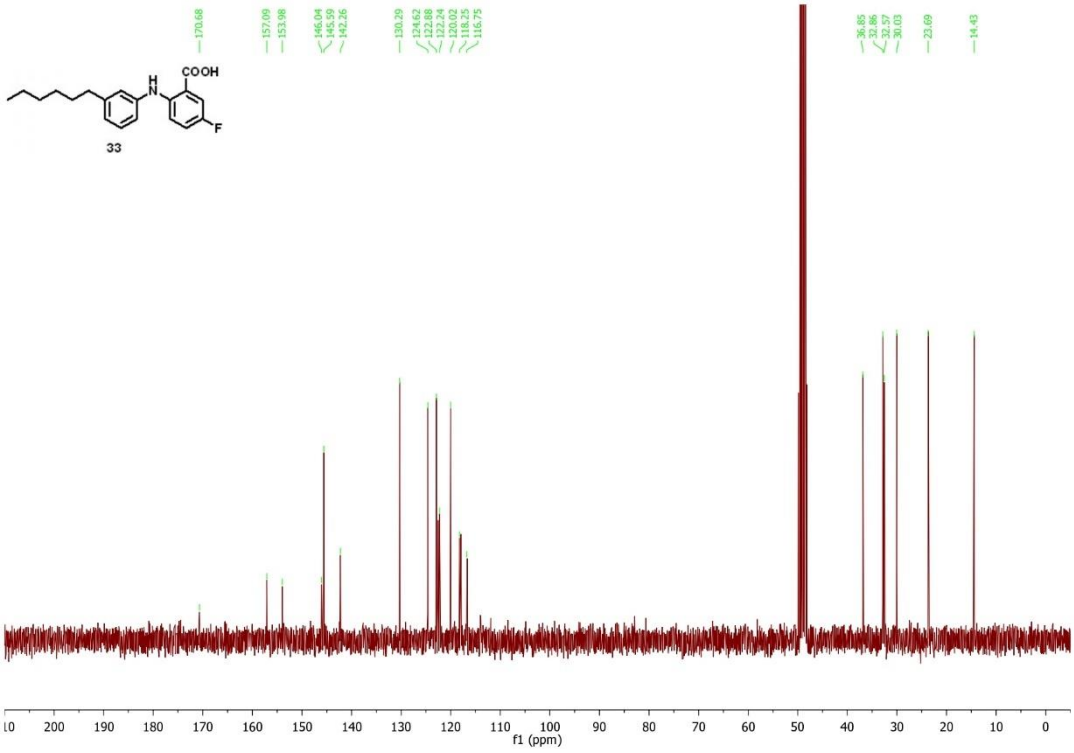
170.68
157.09
153.98
146.04
145.59
142.26
130.29
124.62
122.88
122.24
120.02
118.25
116.75
36.85
30.86
29.57
30.03
23.69
14.43
COOH
H
N
F
33
f1 (ppm)

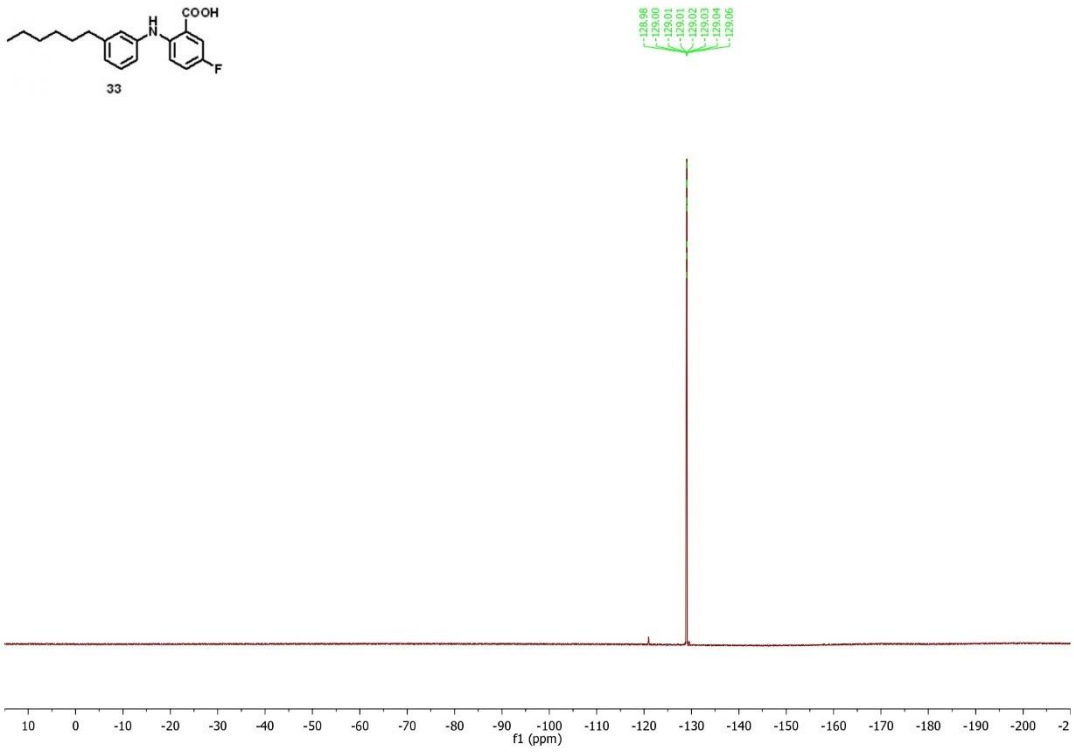
128.98
129.00
129.01
129.01
129.02
129.03
129.04
129.06
COOH
H
N
F
33
f1 (ppm)

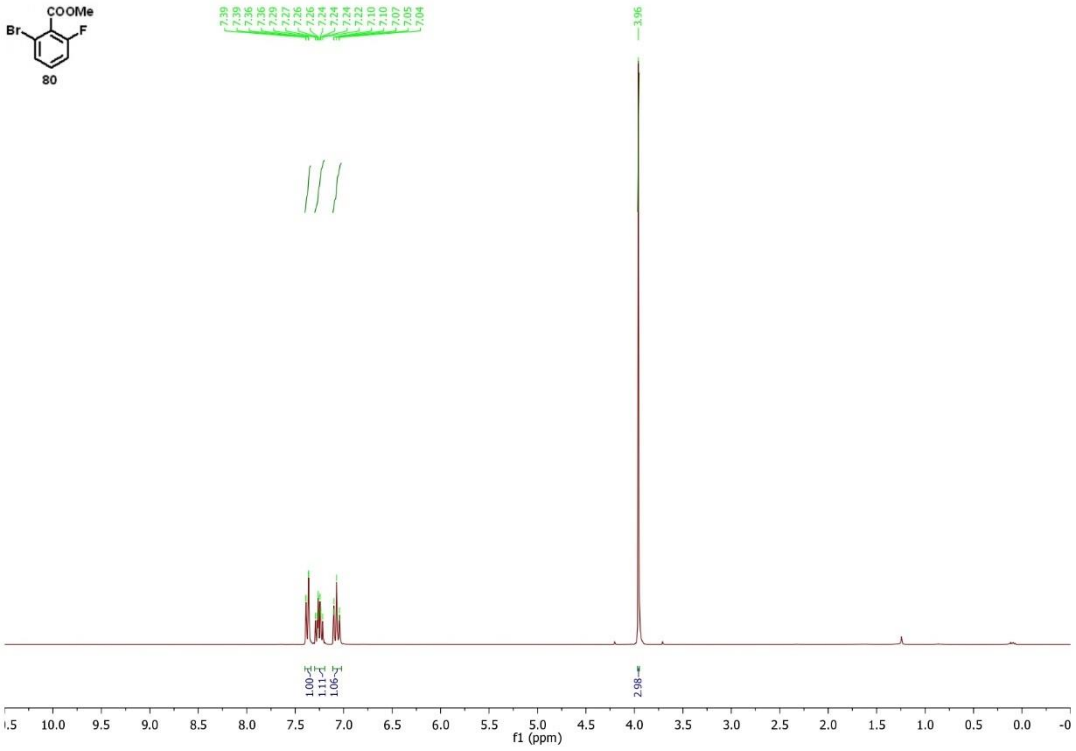
COOMe
Br
F
80
7.39
7.39
7.36
7.36
7.29
7.27
7.26
7.26
7.24
7.24
7.24
7.22
7.10
7.10
7.07
7.05
7.04
3.96
1.00
1.11
1.06
2.98
f1 (ppm)

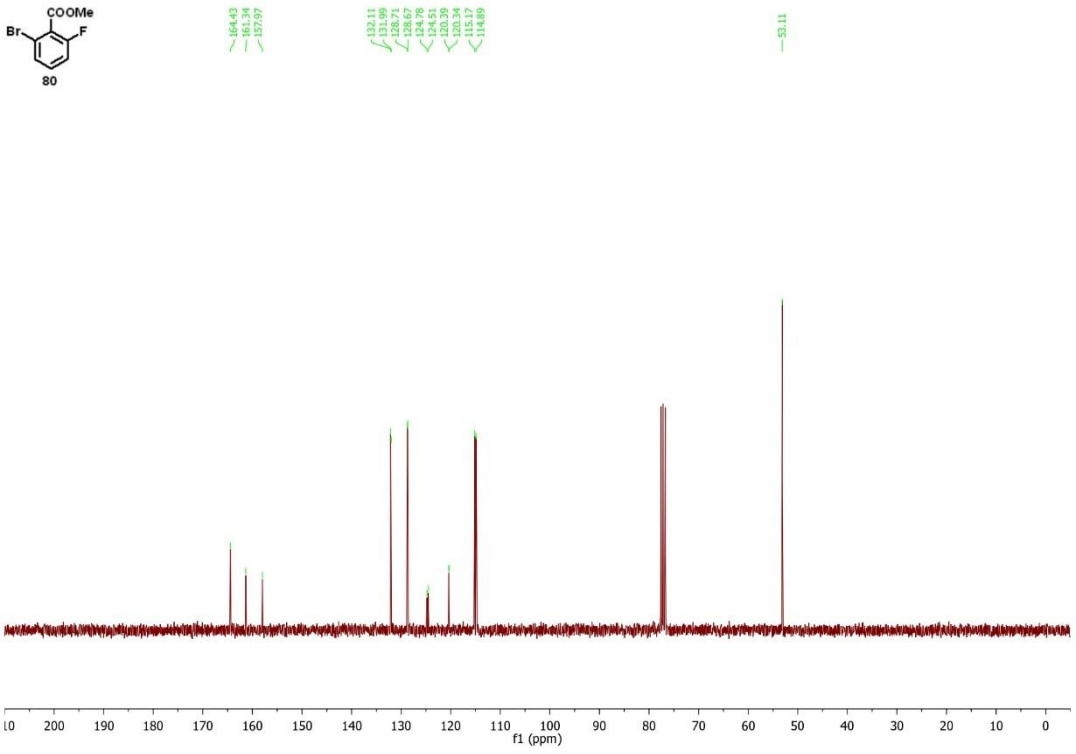
COOMe
Br
F
80
164.43
161.34
157.97
132.11
131.99
128.71
128.67
124.78
124.51
120.39
120.34
115.17
114.89
53.11
f1 (ppm)


COOMe
Br
F

80

-111.50
-111.52
-111.54
-111.56
10 0 -10 -20 -30 -40 -50 -60 -70 -80 -90 -100 -110 -120 -130 -140 -150 -160 -170 -180 -190 -200 -2
f1 (ppm)

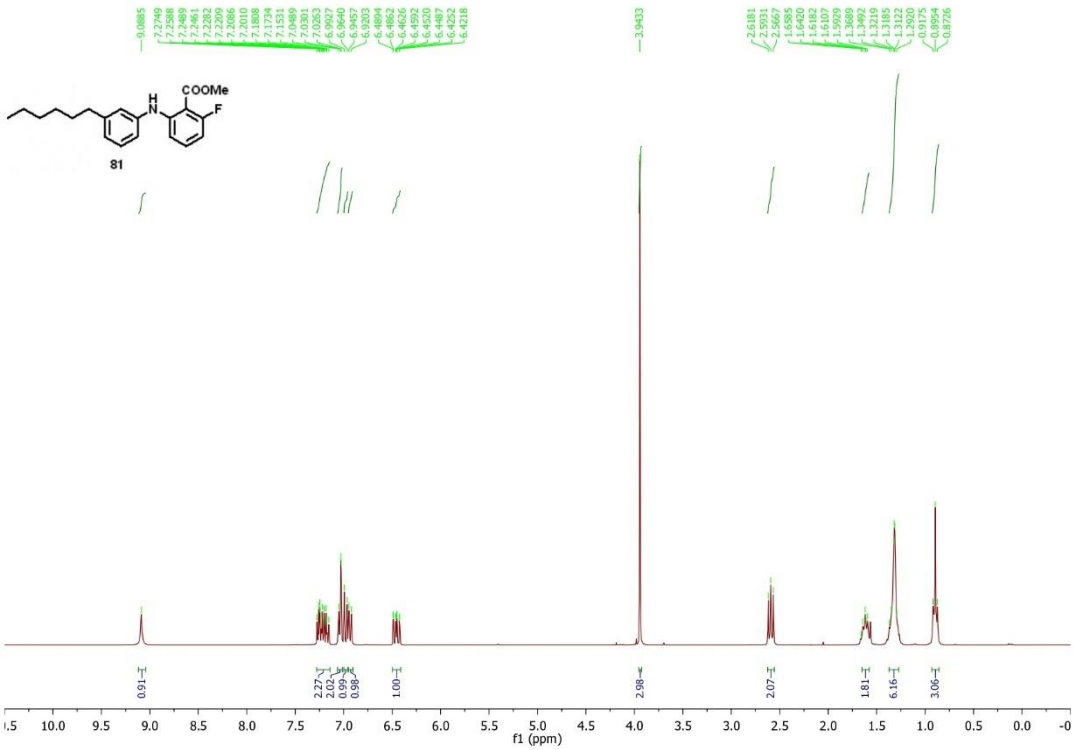
9.0885
7.2749
7.2588
7.2489
7.2461
7.2282
7.2209
7.2086
7.2010
7.1808
7.1734
7.1531
7.0489
7.0301
7.0263
6.9947
6.9749
6.9457
6.9203
6.4894
6.4862
6.4626
6.4592
6.4520
6.4487
6.4252
6.4218
3.9433
2.6181
2.5931
2.5677
1.6585
1.6420
1.6182
1.6107
1.5929
1.3689
1.3492
1.3219
1.3185
1.3122
1.2920
0.9175
0.8954
0.8726
COOMe
F
H
N
0.91
2.27
2.02
0.99
0.99
1.00
2.98
2.07
1.81
6.16
3.06
f1 (ppm)

81

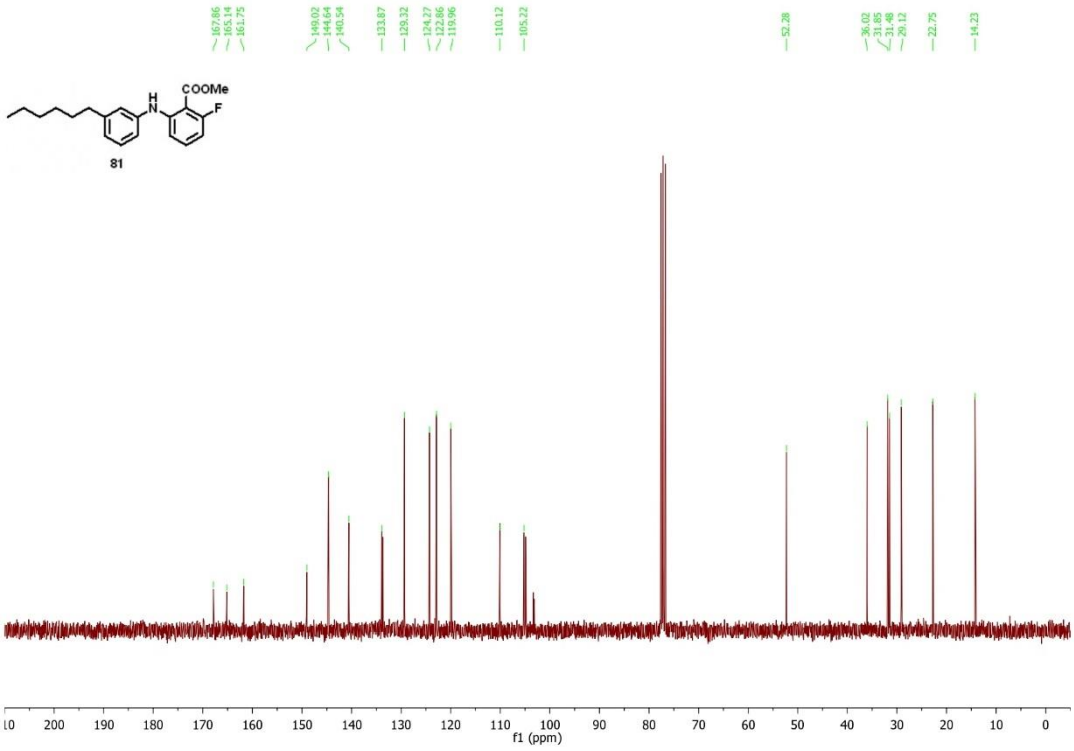
167.86
165.14
161.75
140.02
144.64
140.54
133.67
129.32
124.27
122.86
119.96
110.12
105.22
52.28
36.02
31.85
31.48
29.12
22.75
14.23
COOMe
F
H
N
81
f1 (ppm)

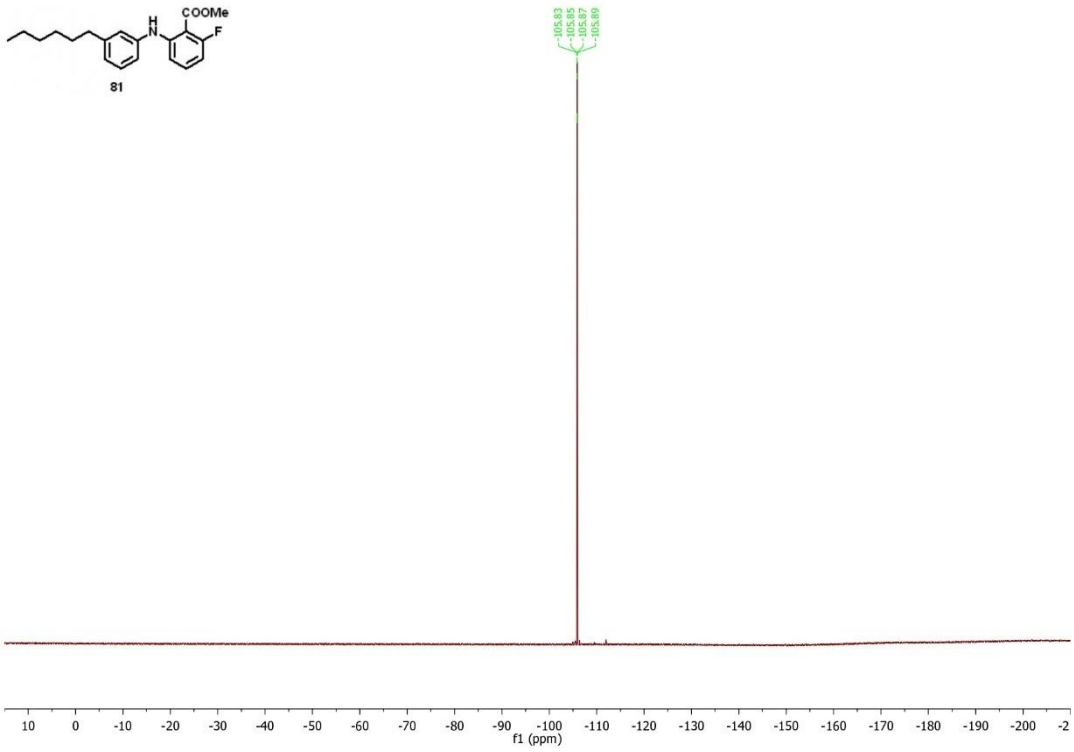
105.83
105.85
105.87
105.89
COOMe
F
H
N
81
f1 (ppm)

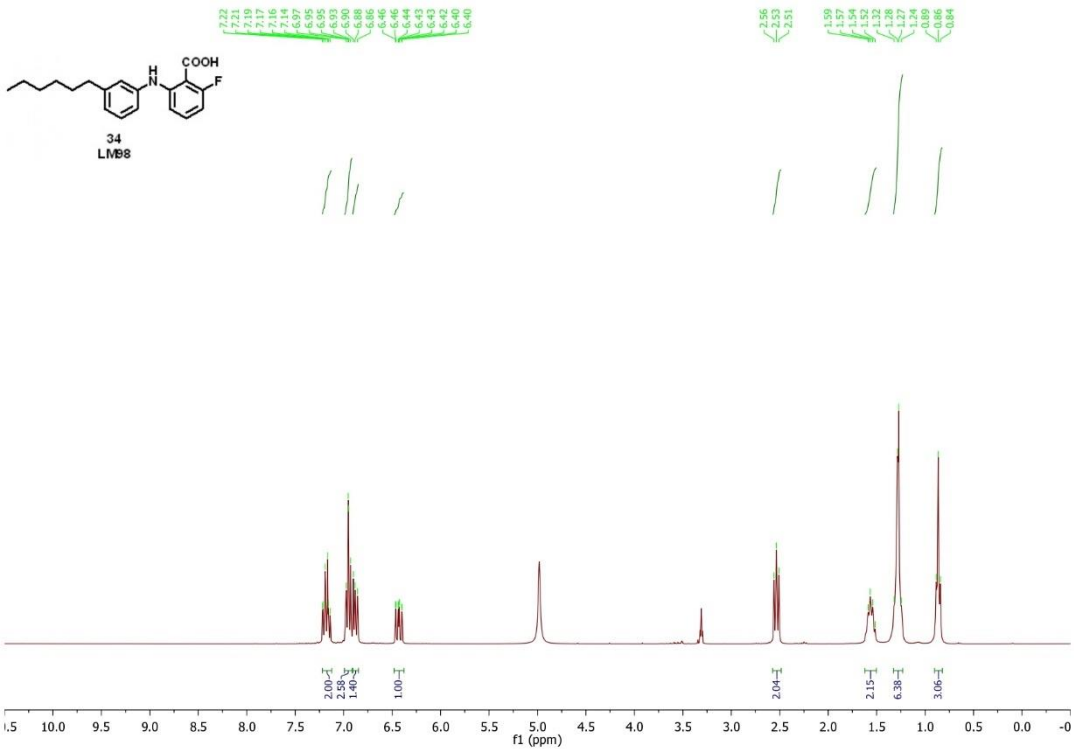
34
LMB8
f1 (ppm)

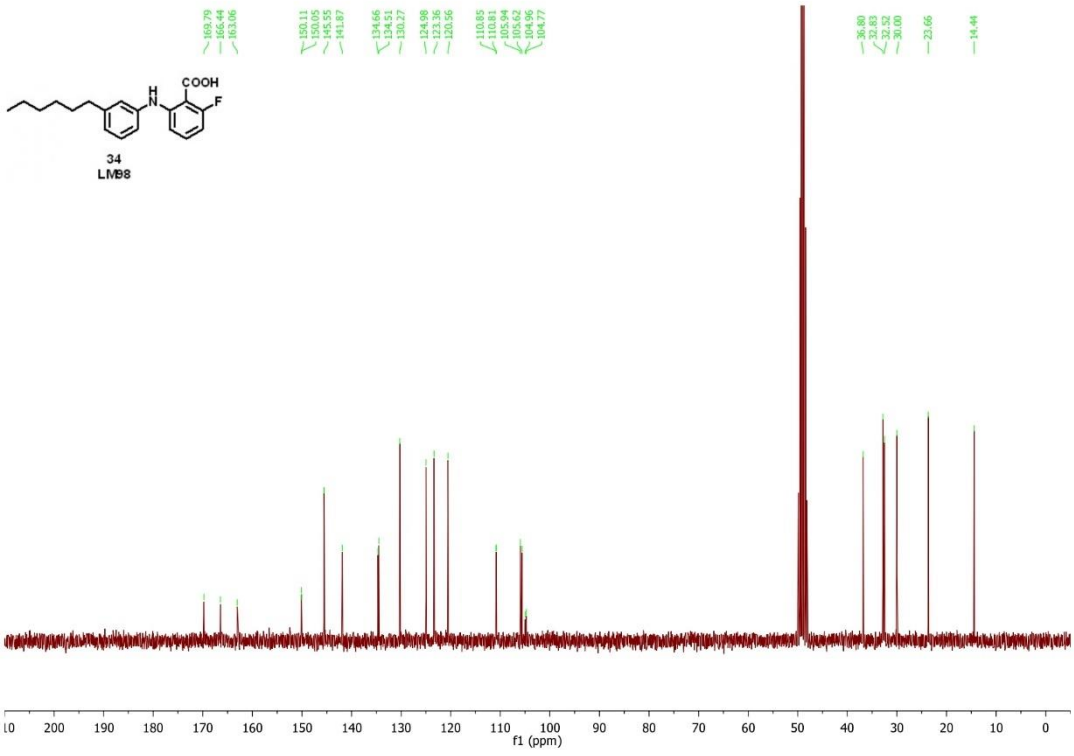
34
LMB8
f1 (ppm)

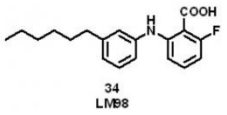
COOH
H
N
F

34
LMB8


-107.32
-107.34
-107.36
-107.38

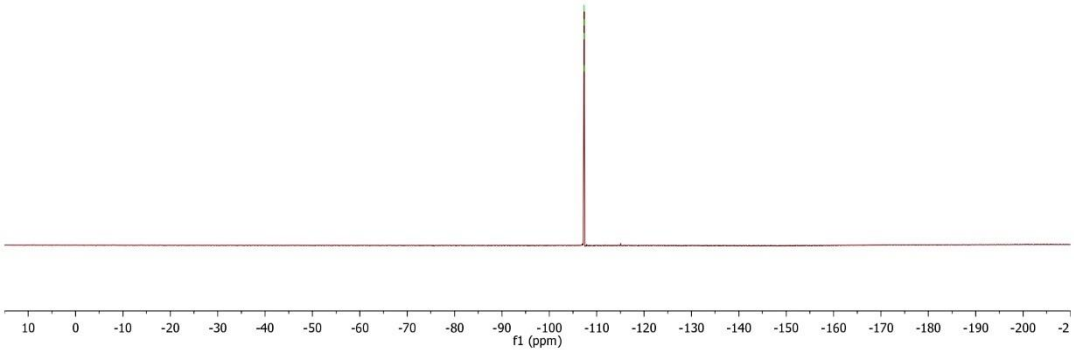
10 0 -10 -20 -30 -40 -50 -60 -70 -80 -90 -100 -110 -120 -130 -140 -150 -160 -170 -180 -190 -200 -2
f1 (ppm)


COOH

82

7.71
7.68
7.23
7.20
7.05
7.03
7.00
2.45
1.00
1.11
1.09
3.38
10.0 9.5 9.0 8.5 8.0 7.5 7.0 6.5 6.0 5.5 5.0 4.5 4.0 3.5 3.0 2.5 2.0 1.5 1.0 0.5 0.0 -0
f1 (ppm)

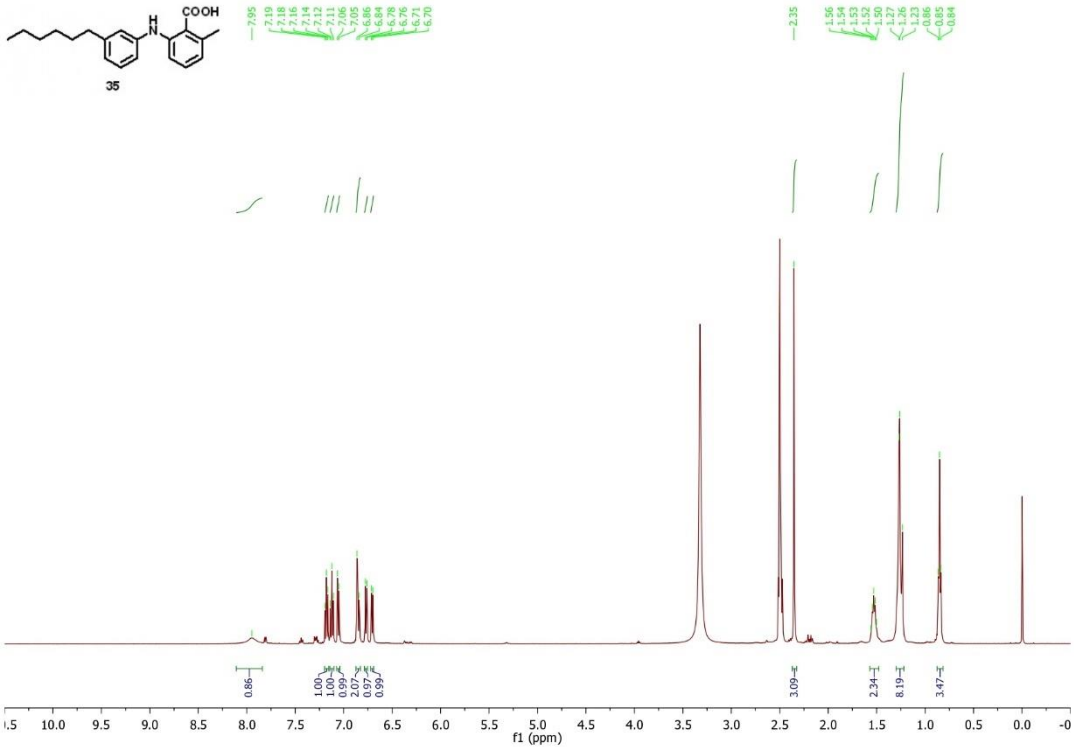
COOH
H
N
35
f1 (ppm)

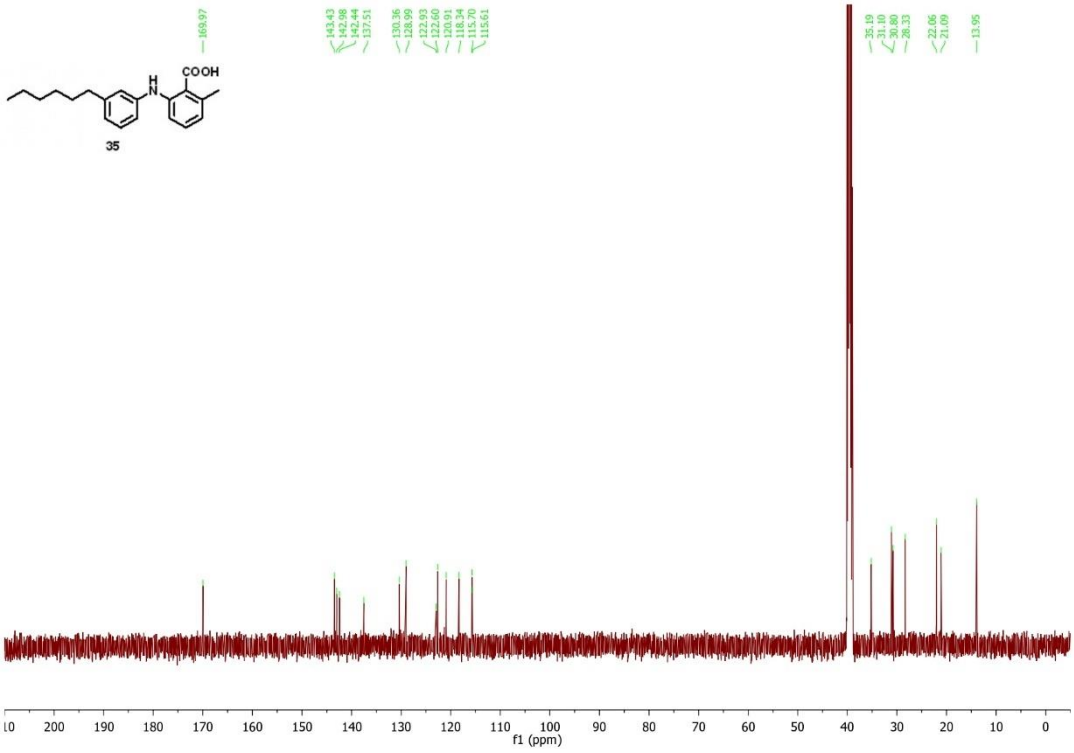
COOH
H
N
35
f1 (ppm)

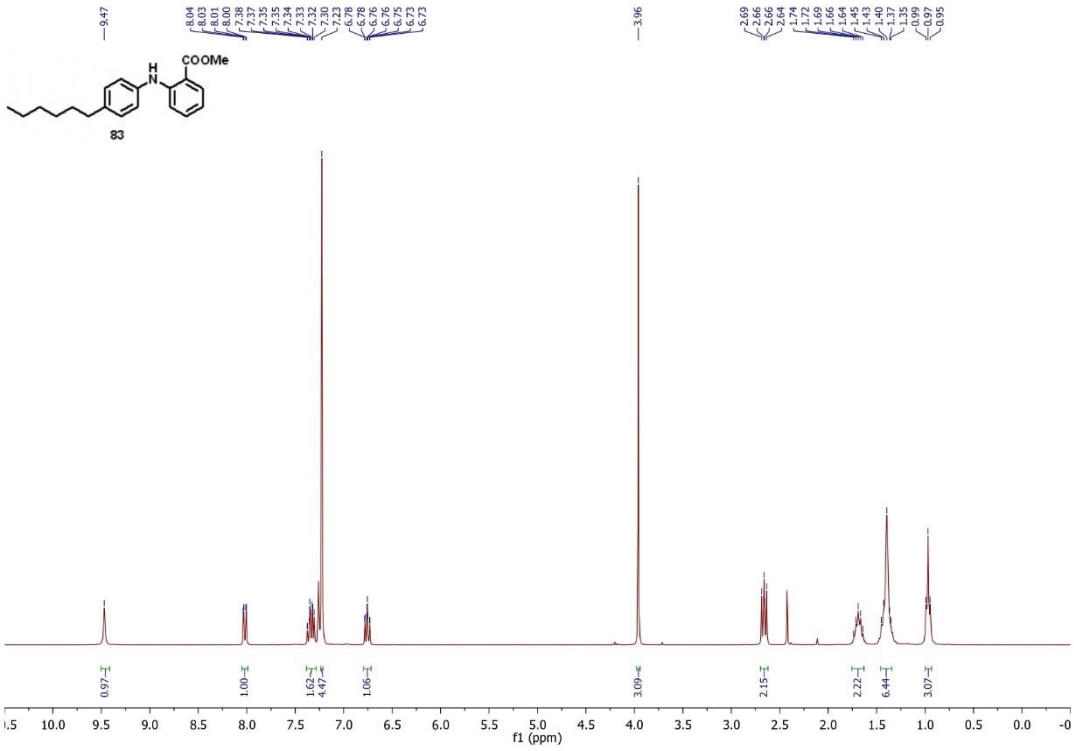
9.47
8.04
8.03
8.01
8.00
7.38
7.37
7.35
7.35
7.34
7.33
7.32
7.30
7.23
6.78
6.76
6.76
6.75
6.73
6.73
3.96
2.69
2.66
2.66
2.64
1.74
1.72
1.69
1.66
1.64
1.45
1.43
1.40
1.37
1.35
0.99
0.97
0.95
COOMe
H
N
83
0.97
1.00
1.62
4.47
1.06
3.09
2.15
2.22
6.44
3.07
f1 (ppm)

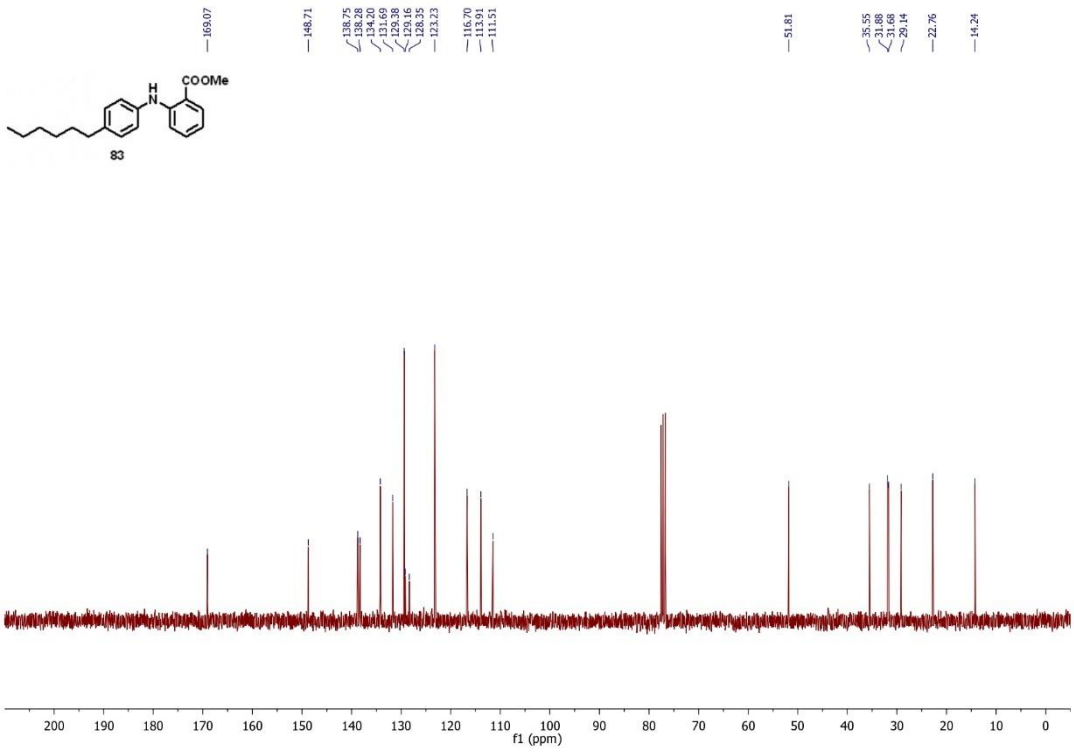
169.07
148.71
138.75
138.28
134.20
131.69
129.38
129.16
128.35
123.23
116.70
113.91
111.51
51.81
35.55
31.88
31.68
29.14
22.76
14.24
COOMe
H
N
83
f1 (ppm)

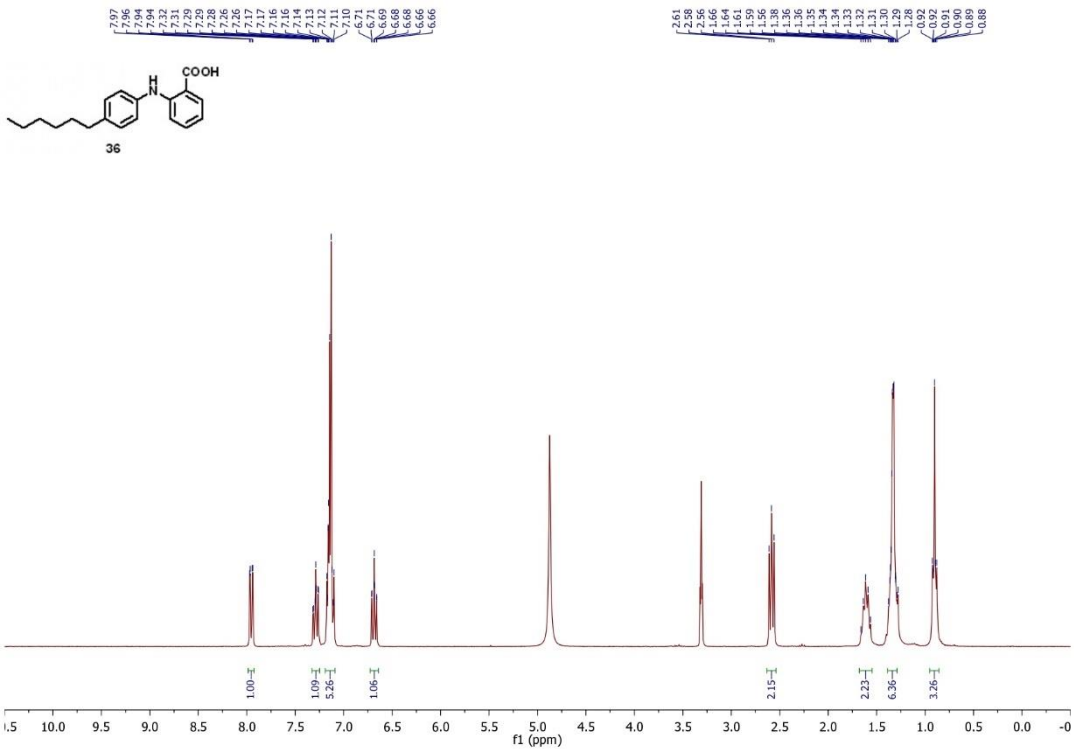
7.97
7.96
7.94
7.94
7.32
7.31
7.29
7.29
7.28
7.26
7.26
7.17
7.17
7.16
7.16
7.14
7.13
7.12
7.11
7.10
6.71
6.69
6.68
6.68
6.66
6.66
2.61
2.58
2.56
1.66
1.64
1.61
1.59
1.56
1.38
1.36
1.36
1.35
1.34
1.34
1.33
1.32
1.31
1.30
1.29
1.28
0.92
0.92
0.91
0.90
0.89
0.88
COOH
H
N
36
1.00
1.09
5.26
1.06
2.15
2.23
6.36
3.26
f1 (ppm)

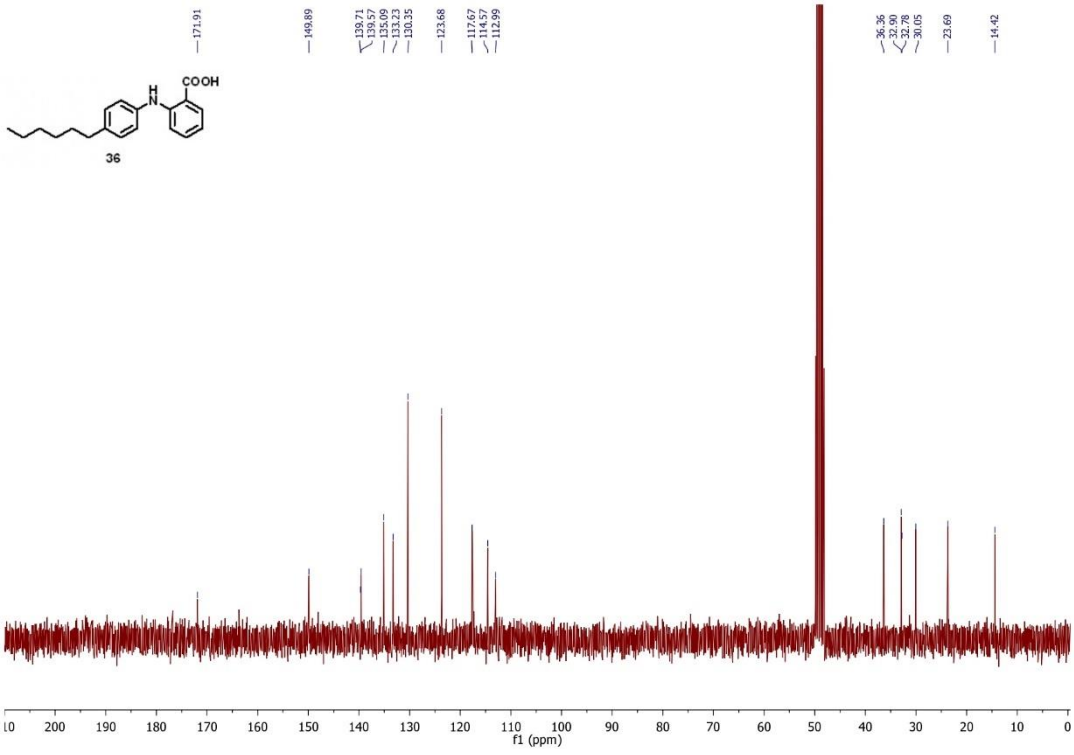
171.91
149.89
139.71
139.57
135.09
133.23
130.35
123.68
117.67
114.57
112.99
36.36
32.90
32.78
30.05
23.69
14.42
COOH
H
N
36
f1 (ppm)

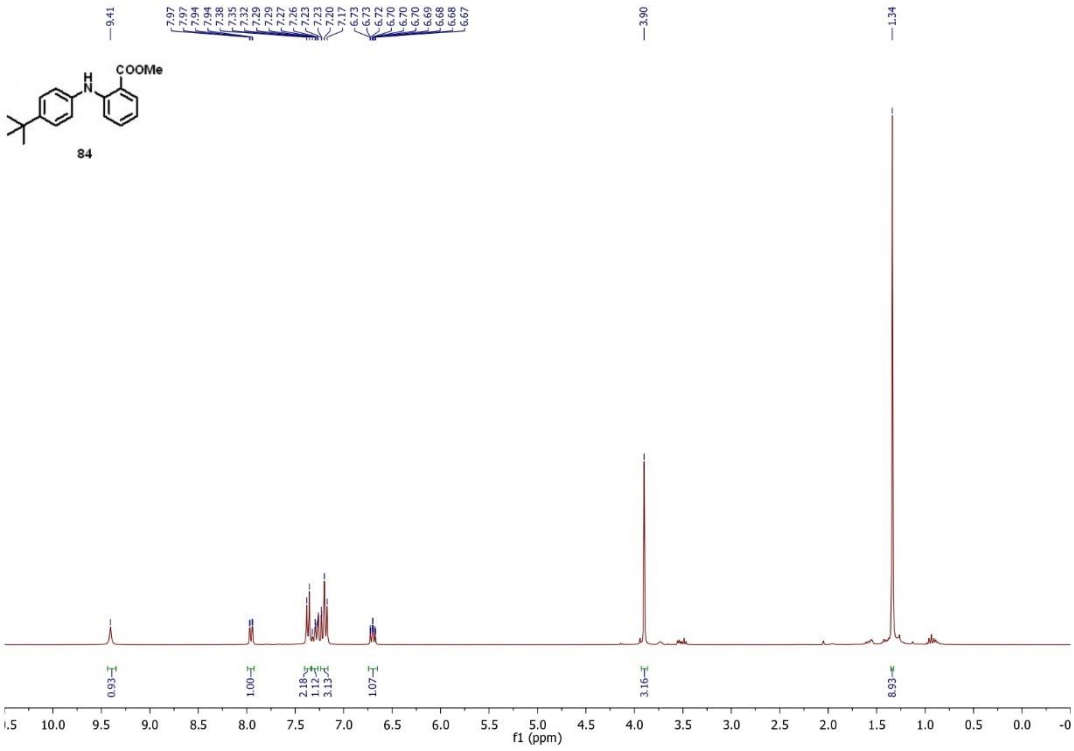
9.41
7.97
7.97
7.94
7.94
7.38
7.35
7.32
7.29
7.29
7.27
7.26
7.23
7.23
7.20
7.17
6.73
6.73
6.72
6.70
6.70
6.70
6.69
6.68
6.68
6.67
3.90
1.34
COOMe
H
N
84
0.93
1.00
2.18
1.12
3.13
1.07
3.16
8.93
f1 (ppm)

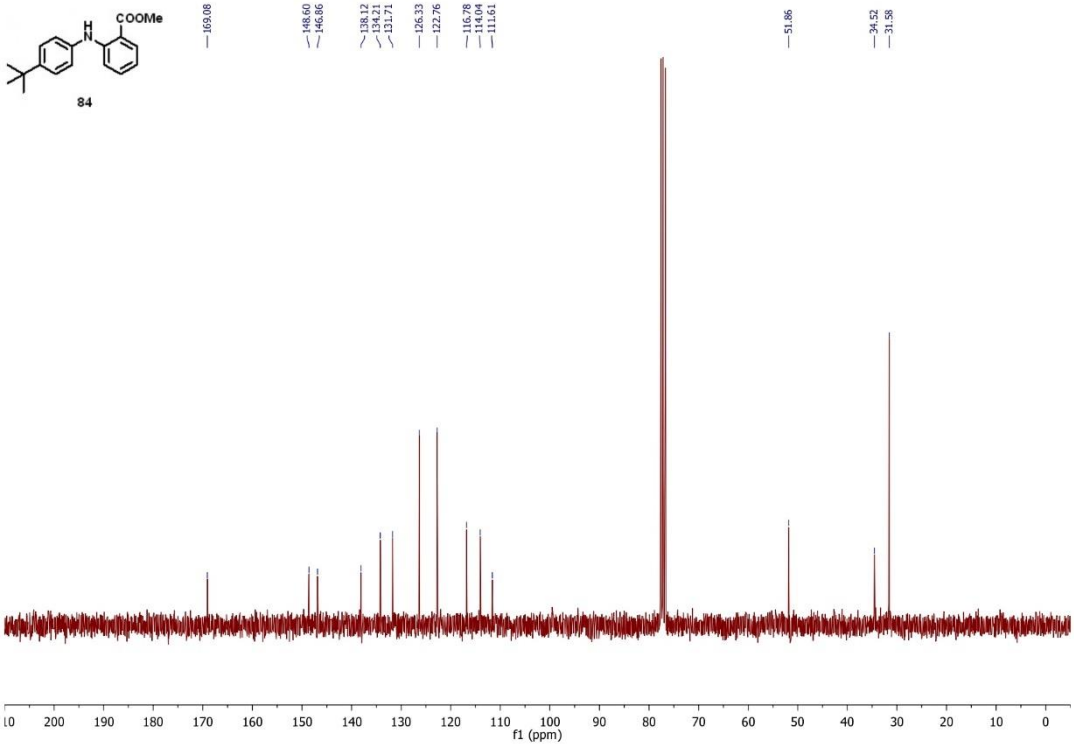
169.08
148.60
146.86
138.12
134.21
131.71
126.33
122.76
116.78
114.04
111.61
51.86
34.52
31.58
COOMe
H
N
84
f1 (ppm)

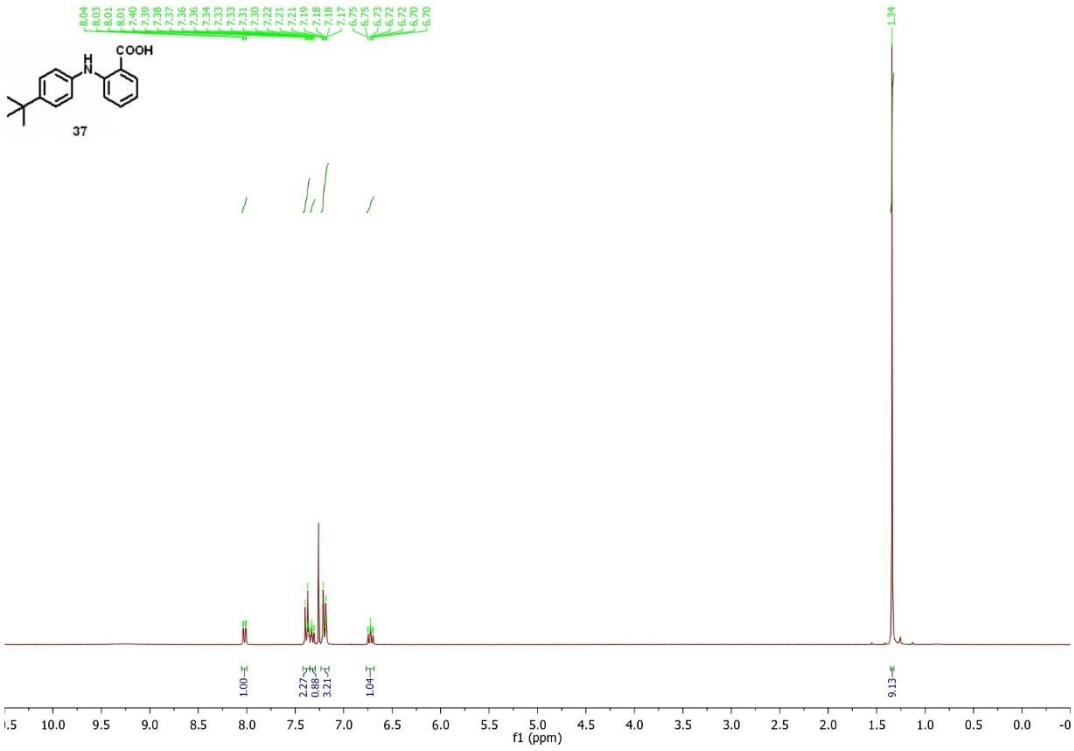
COOH
37
f1 (ppm)

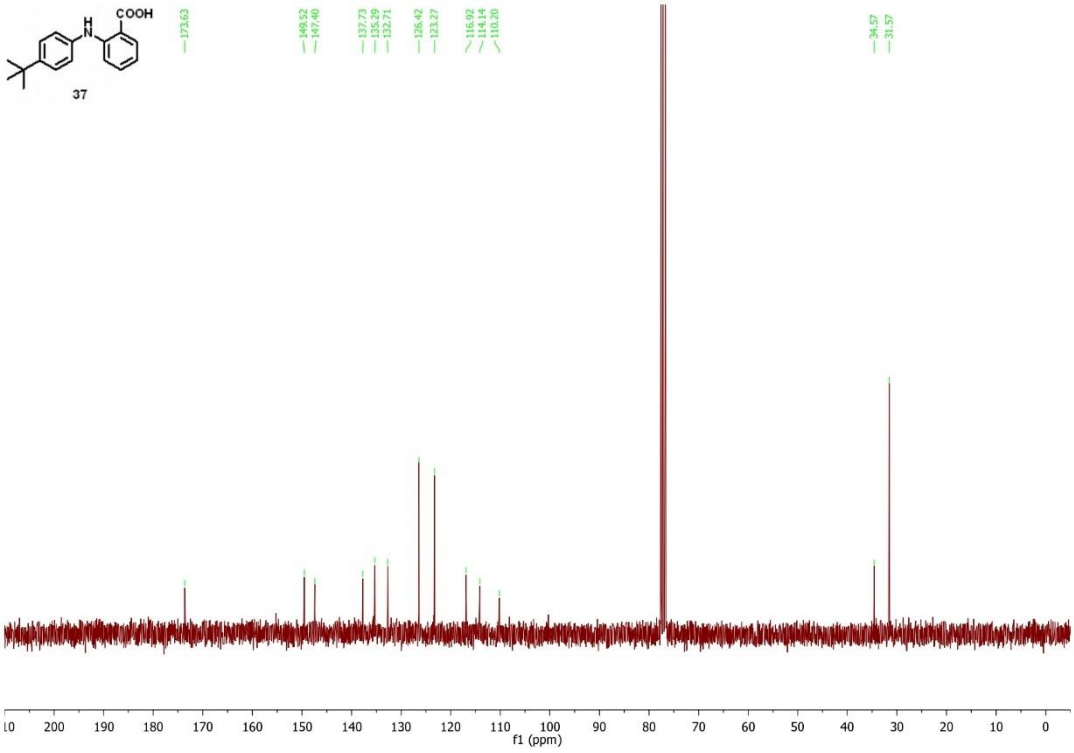
COOH
37
f1 (ppm)

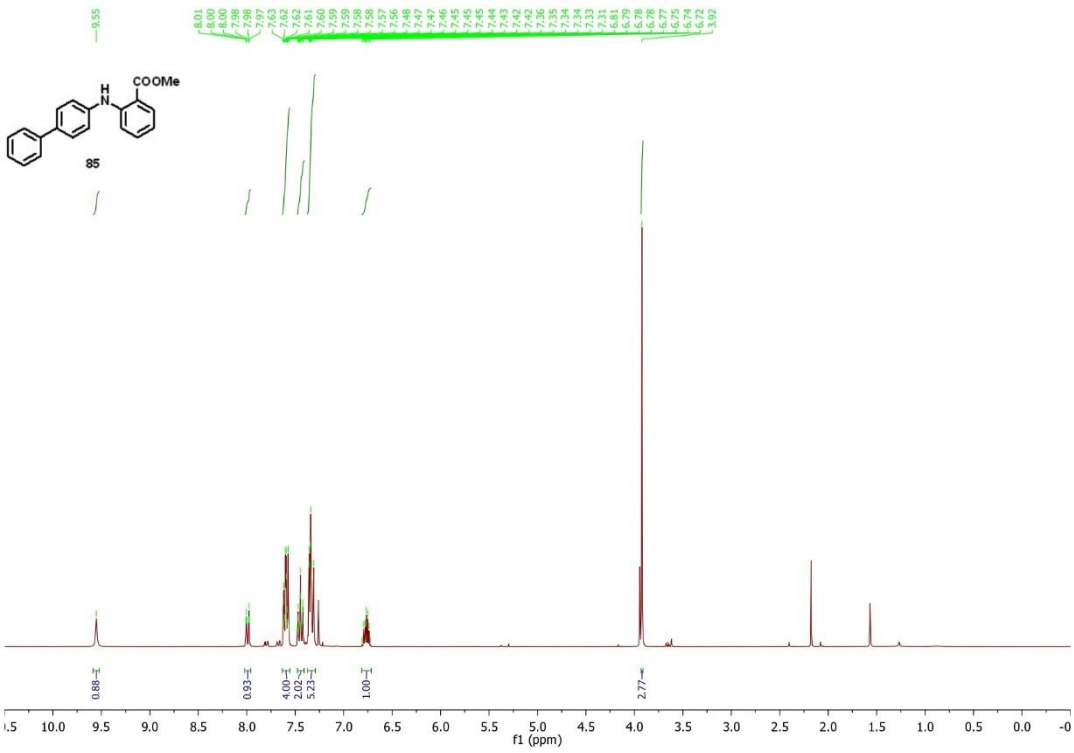
COOMe
H
N
85
f1 (ppm)

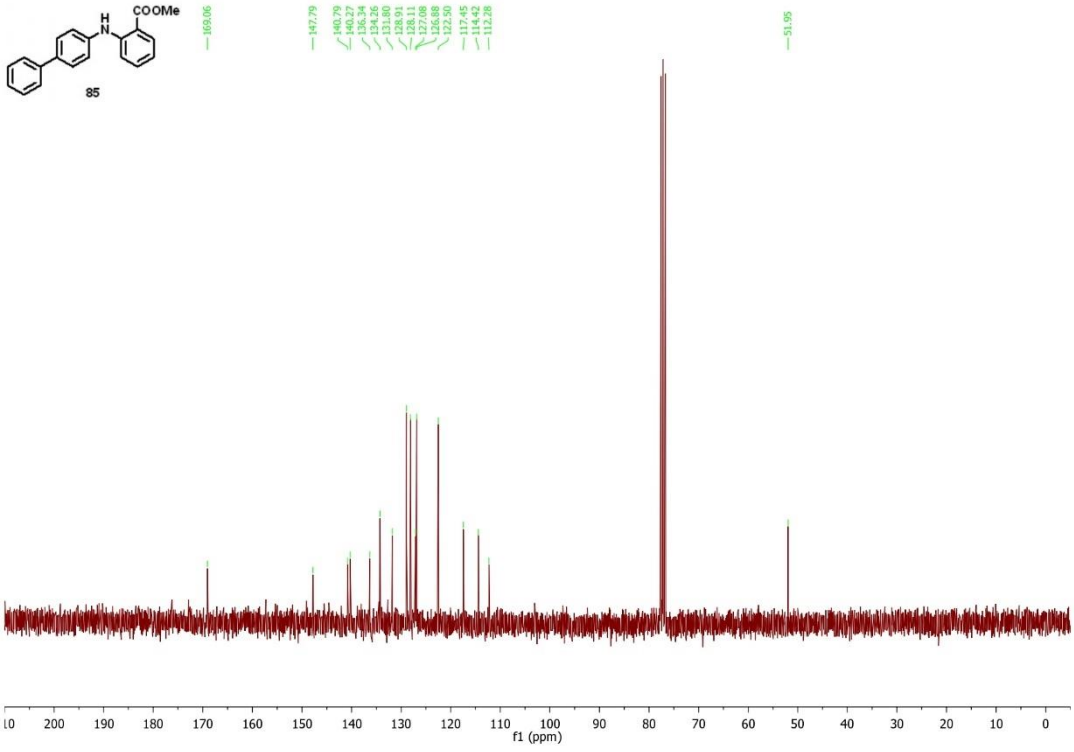
COOMe
H
N
85
f1 (ppm)

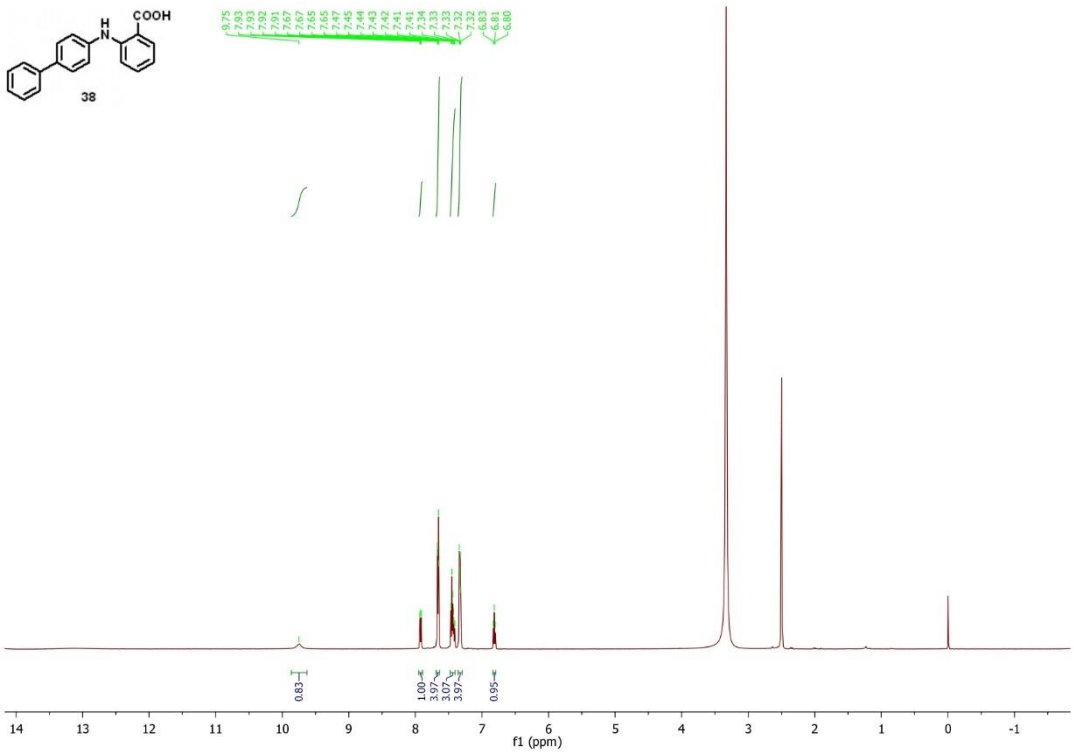
COOH
H
N
38
9.75
7.93
7.93
7.92
7.91
7.67
7.67
7.65
7.65
7.47
7.45
7.44
7.43
7.42
7.41
7.41
7.34
7.33
7.32
7.32
6.83
6.81
6.80
0.83
1.00
3.97
3.07
3.97
0.95
14 13 12 11 10 9 8 7 6 5 4 3 2 1 0 -1
f1 (ppm)

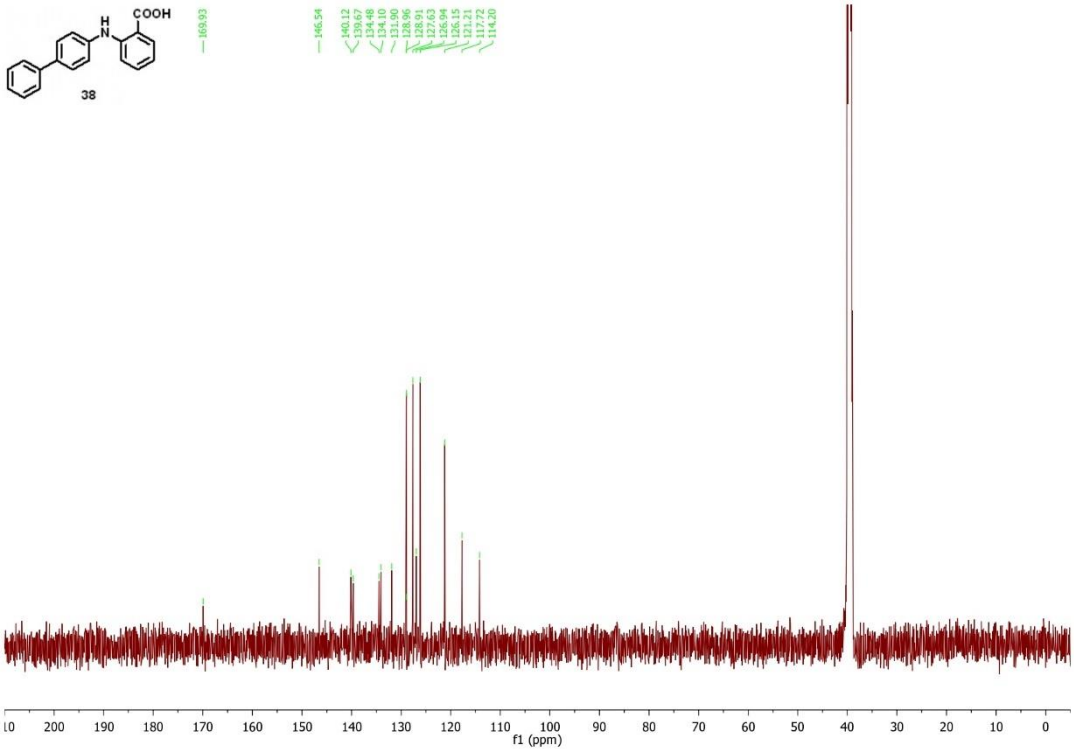
COOH
H
N
38
169.93
146.54
140.12
139.67
134.48
134.10
131.90
128.96
128.91
127.63
126.94
126.15
121.11
117.72
114.20
200 190 180 170 160 150 140 130 120 110 100 90 80 70 60 50 40 30 20 10 0
f1 (ppm)

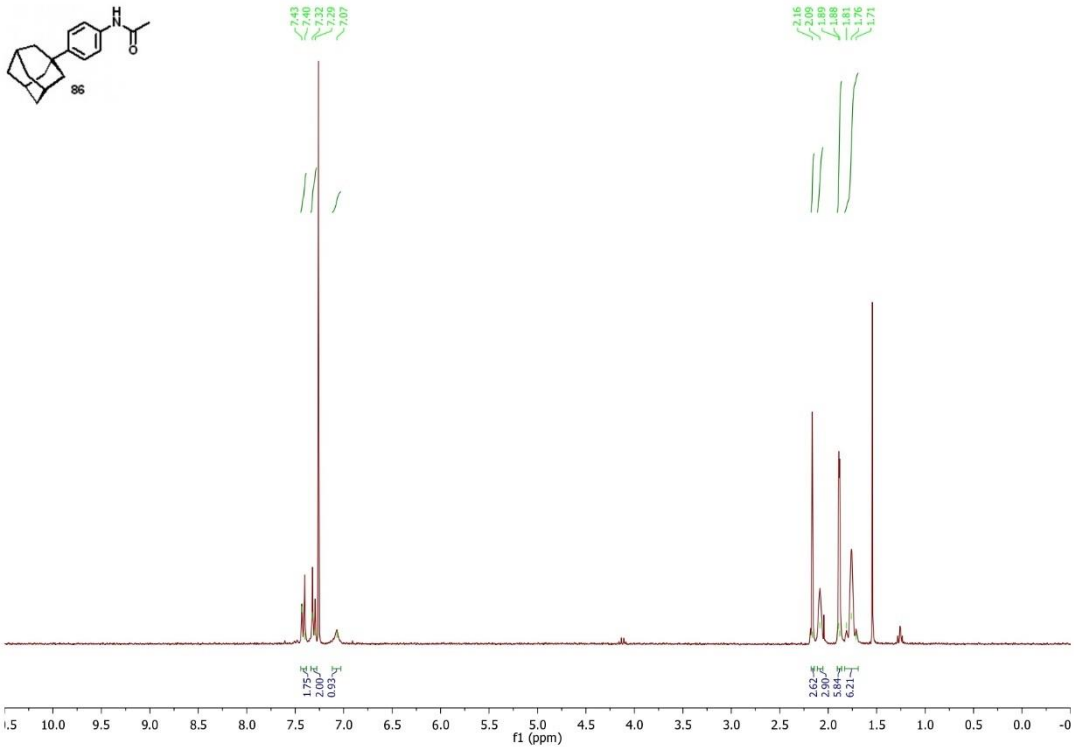
86
7.43
7.40
7.32
7.29
7.07
2.16
2.09
1.89
1.88
1.81
1.76
1.71
1.75
2.00
0.93
2.62
2.90
5.84
6.21
f1 (ppm)

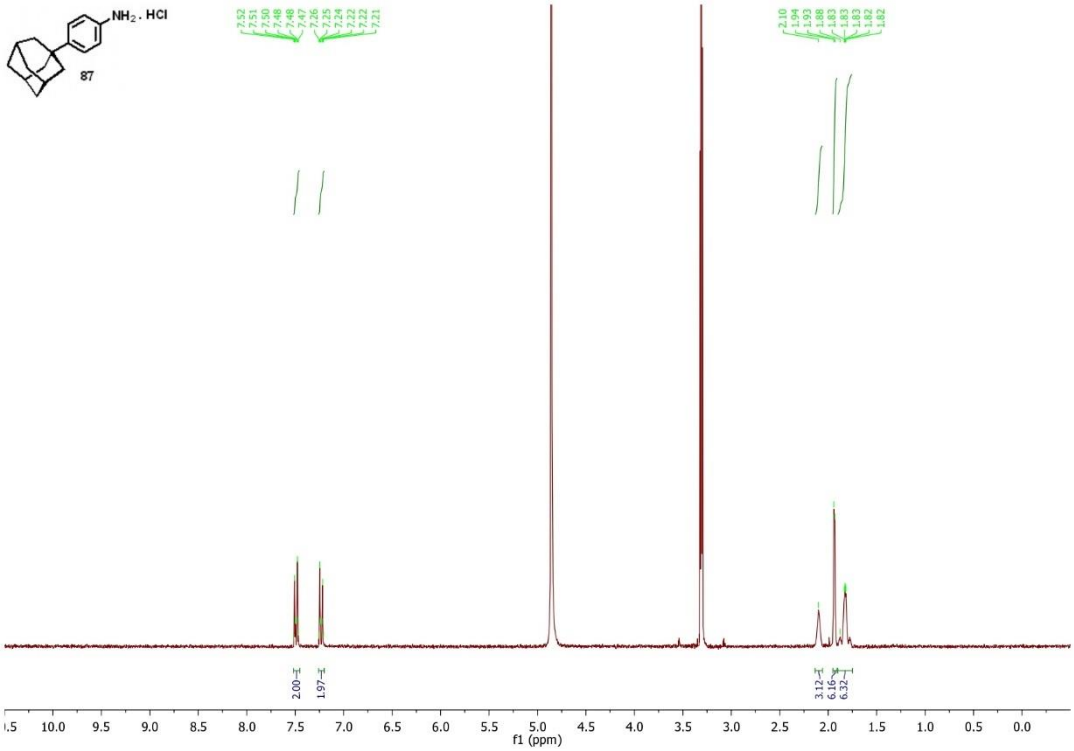
NH2 . HCl
87
7.52
7.51
7.50
7.48
7.47
7.26
7.25
7.24
7.22
7.22
7.21
2.10
1.94
1.93
1.88
1.83
1.83
1.83
1.82
1.82
2.00
1.97
3.12
6.16
6.32
f1 (ppm)

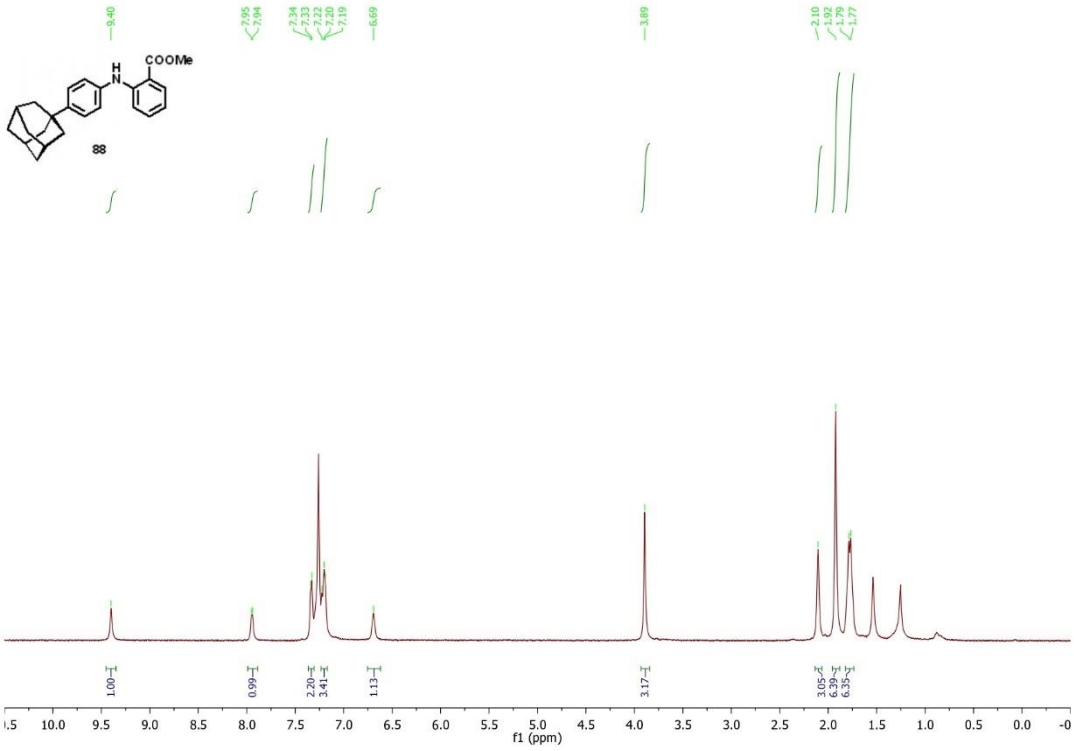
9.40
7.95
7.94
7.34
7.33
7.22
7.20
7.19
6.69
3.89
2.10
1.92
1.79
1.77
COOMe
H
N
88
1.00
0.99
2.20
3.41
1.13
3.17
3.05
6.39
6.35
f1 (ppm)

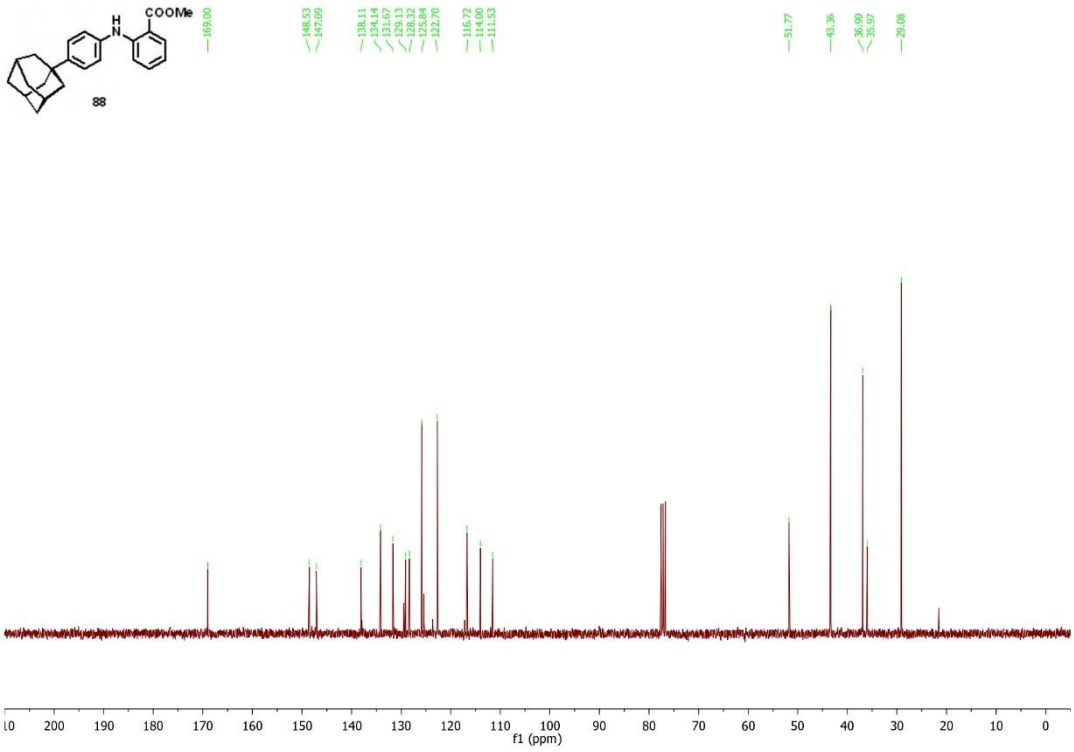
169.00
148.53
147.09
138.11
134.14
131.67
129.13
128.32
125.84
122.70
116.72
114.00
111.53
51.77
43.36
36.90
35.97
29.08
COOMe
H
N
88
f1 (ppm)

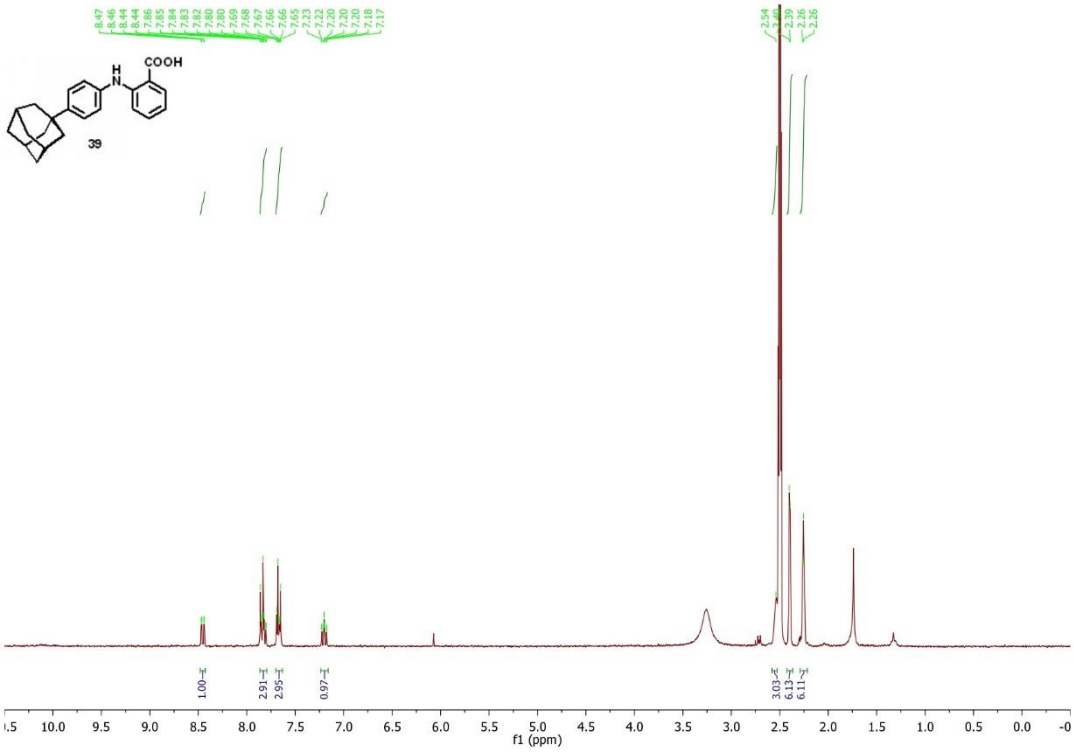
COOH
H
N
39
f1 (ppm)

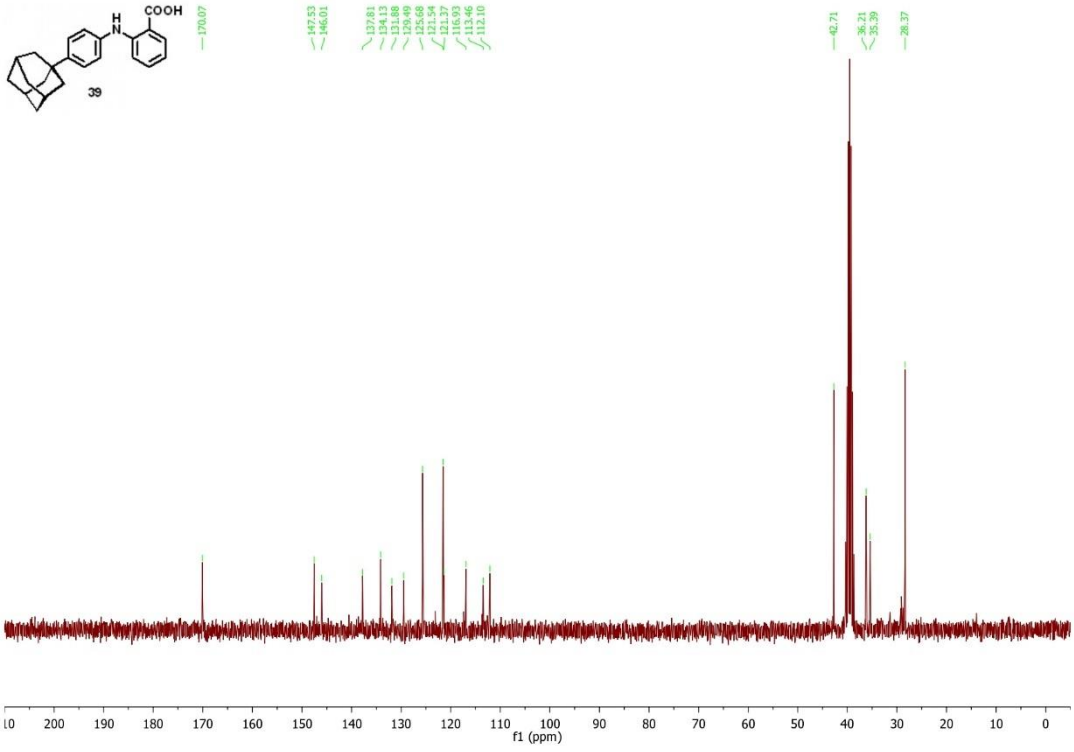
COOH
H
N
39
f1 (ppm)

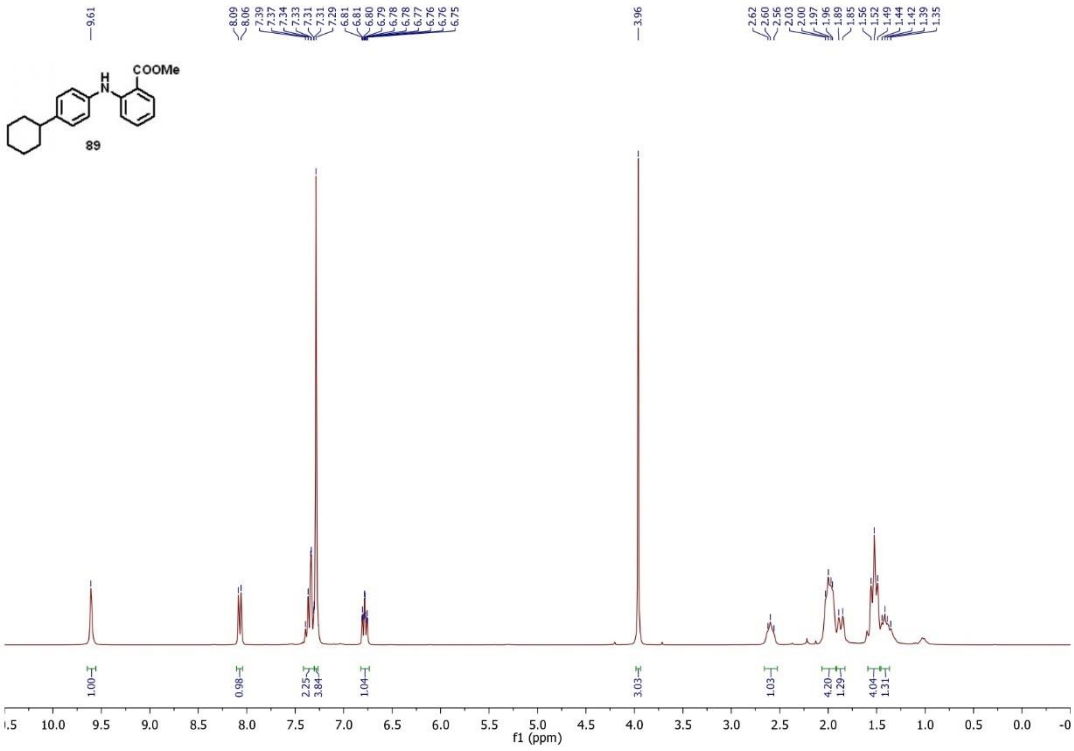
9.61
8.09
8.06
7.39
7.37
7.34
7.33
7.31
7.31
7.29
6.81
6.81
6.80
6.79
6.78
6.78
6.77
6.76
6.76
6.75
3.96
2.62
2.60
2.56
2.03
2.00
1.97
1.96
1.89
1.85
1.56
1.52
1.49
1.44
1.42
1.39
1.35
COOMe
89
1.00
0.98
2.25
3.84
1.04
3.03
1.03
4.20
1.29
4.04
1.31
f1 (ppm)

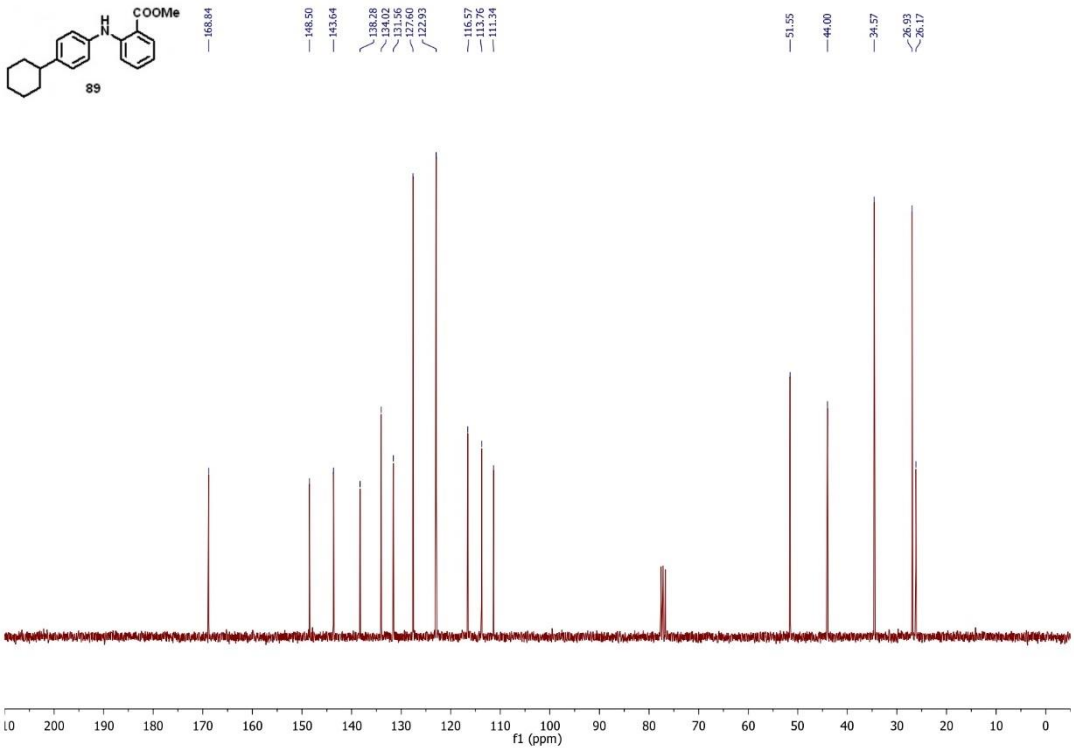
168.84
148.50
143.64
138.28
134.02
131.56
127.60
122.93
116.57
113.76
111.34
51.55
44.00
34.57
26.93
26.17
COOMe
89
f1 (ppm)

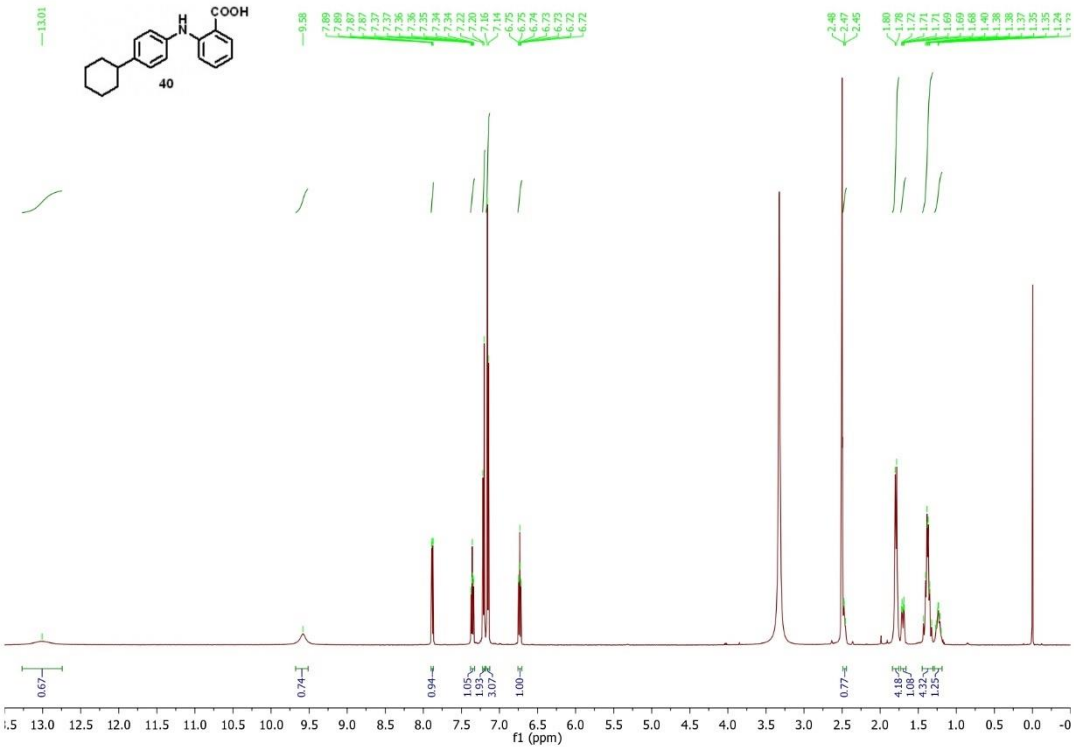
COOH
H
N
40
13.01
9.58
7.89
7.87
7.37
7.36
7.35
7.34
7.22
7.20
7.16
7.14
6.75
6.74
6.73
6.72
2.48
2.47
2.45
1.80
1.78
1.72
1.71
1.69
1.66
1.40
1.38
1.37
1.35
1.24
0.67
0.74
0.94
1.05
1.93
3.07
1.00
0.77
4.18
1.08
4.32
1.25
f1 (ppm)

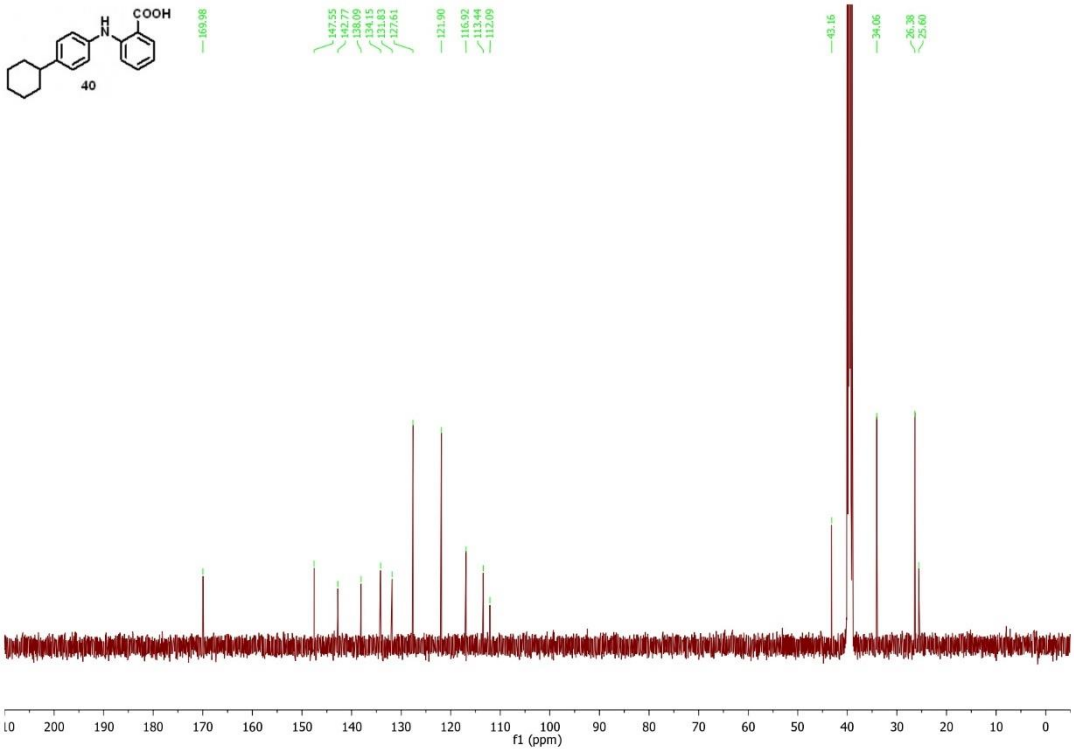
COOH
H
N
40
169.98
147.55
142.77
138.09
134.15
131.83
127.61
121.90
116.92
113.44
112.09
43.16
34.06
26.38
25.60
f1 (ppm)

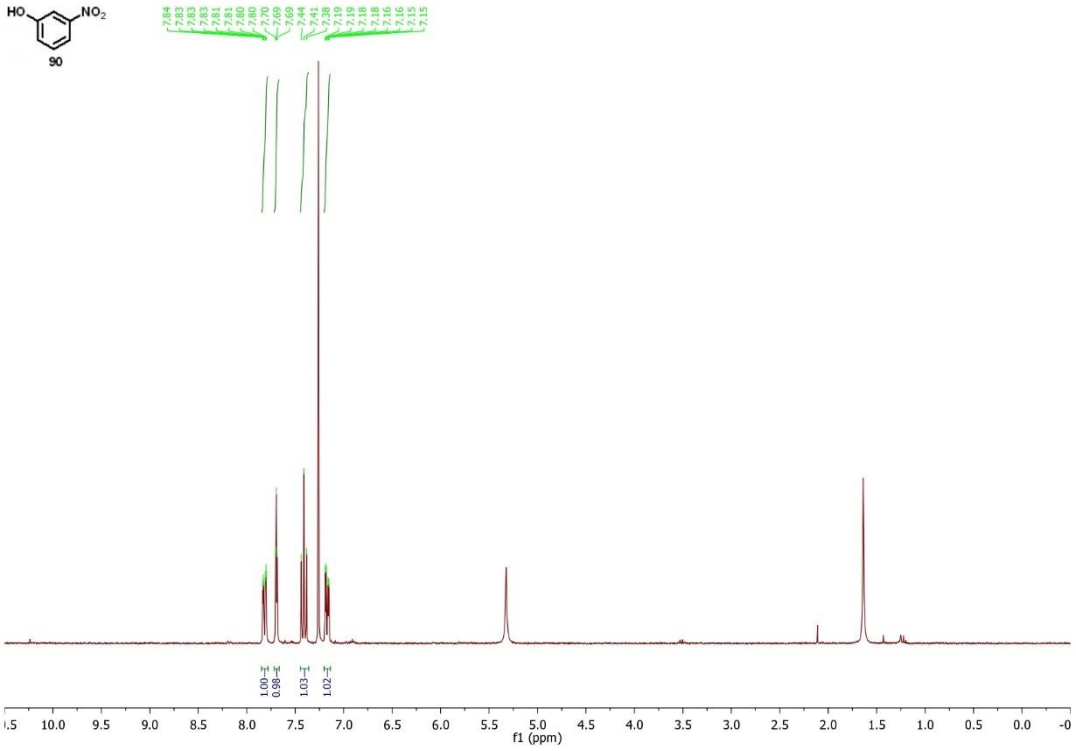
HO
NO2
90
f1 (ppm)

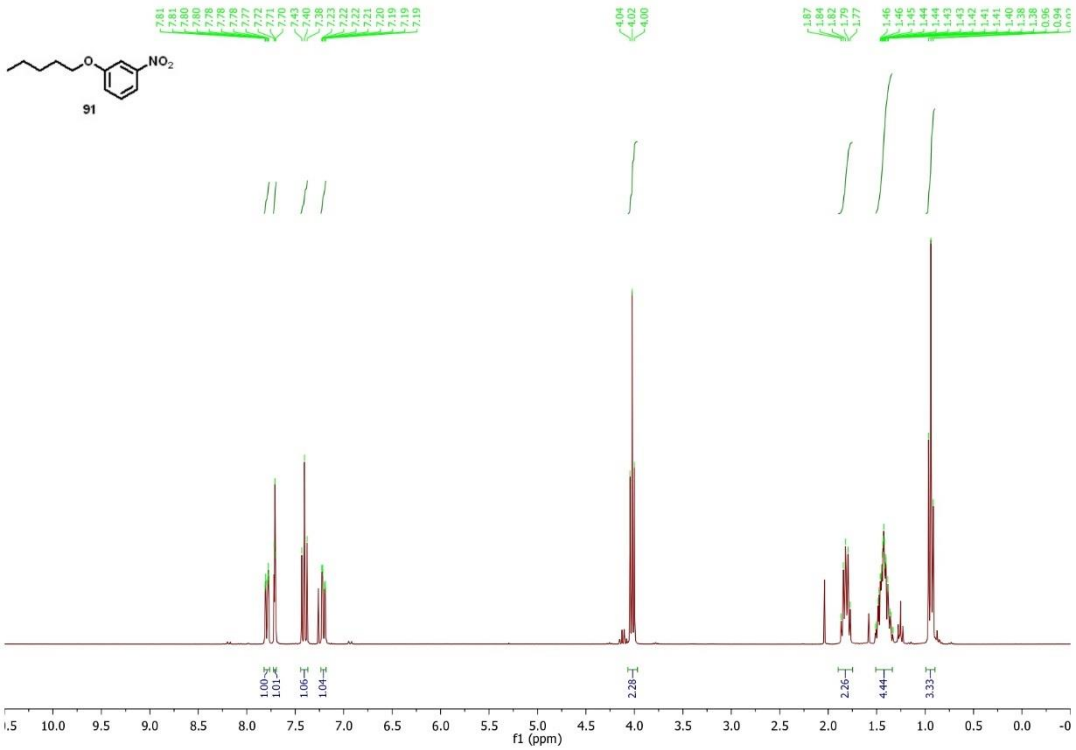
O
NO2
91
f1 (ppm)

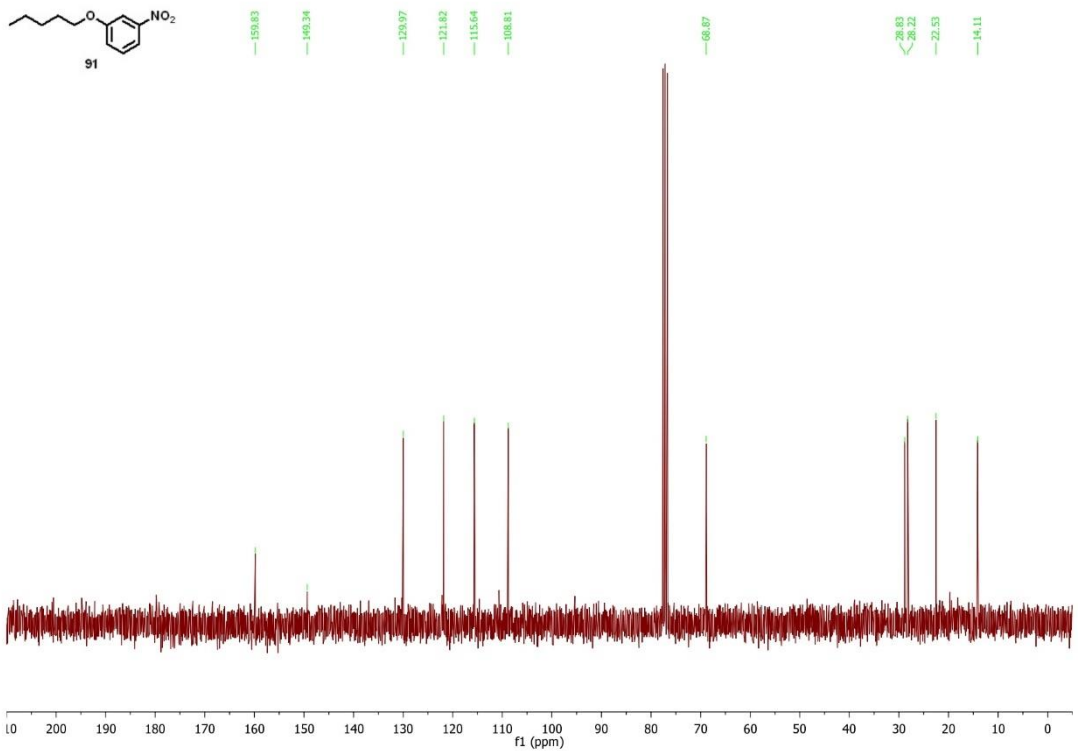
91
159.83
149.34
129.97
121.62
115.64
108.81
68.87
28.83
28.22
22.53
14.11
f1 (ppm)
92
7.08
7.05
7.02
6.35
6.34
6.34
6.34
6.32
6.31
6.31
6.30
6.30
6.29
6.29
6.27
6.27
6.26
6.26
6.26
6.25
6.24
3.94
3.92
3.89
3.60
1.82
1.79
1.77
1.75
1.72
1.46
1.45
1.44
1.44
1.43
1.41
1.40
1.40
1.38
1.37
1.36
1.35
0.96
0.94
0.91
1.00
0.99
0.98
0.97
2.19
1.79
2.13
4.25
3.15
f1 (ppm)

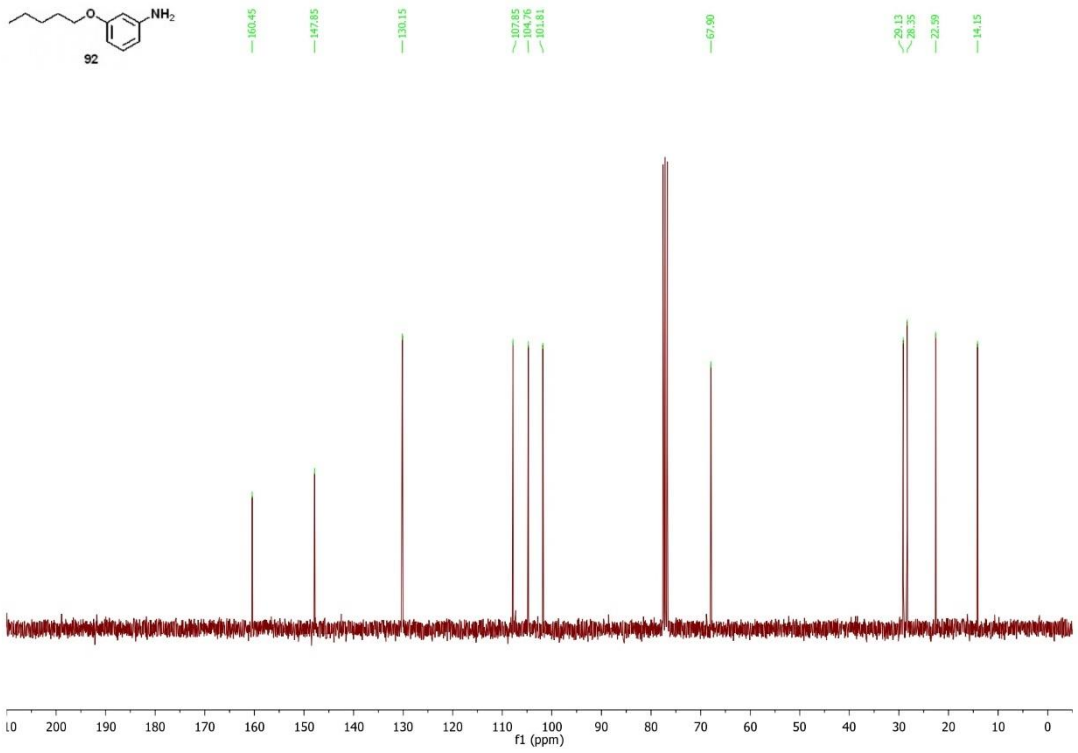
92
160.45
147.85
130.15
107.85
104.76
101.81
67.90
29.13
28.35
22.59
14.15
f1 (ppm)

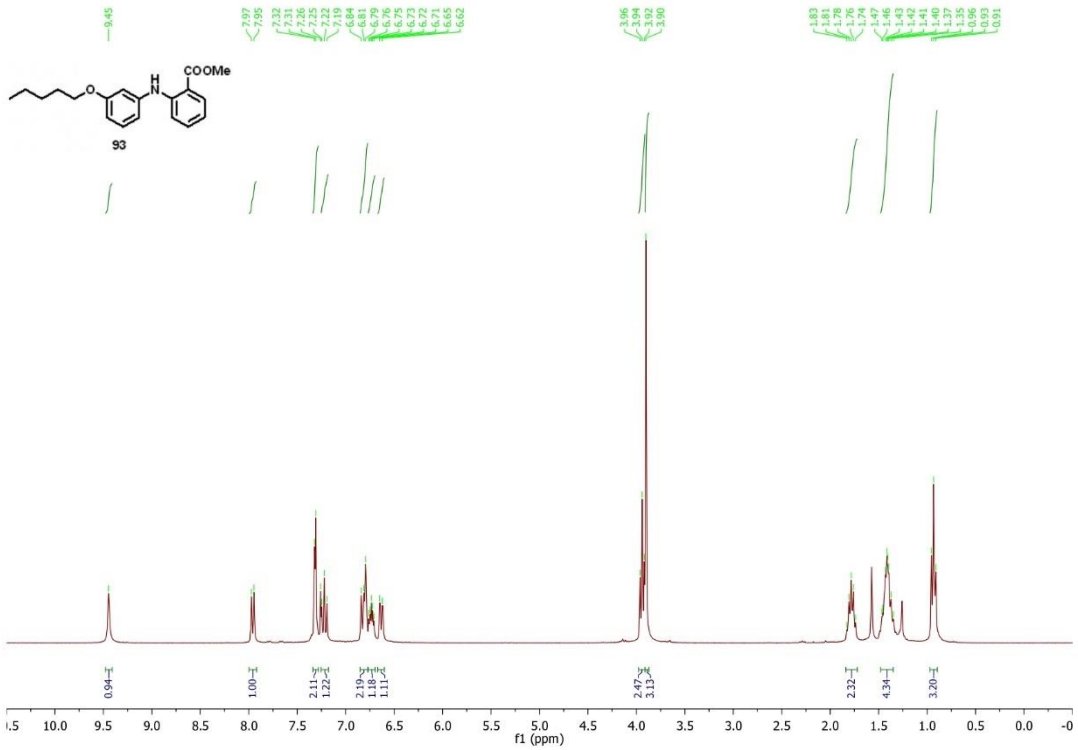
93
COOMe
9.45
7.97
7.95
7.32
7.31
7.26
7.25
7.22
7.19
6.84
6.81
6.79
6.76
6.75
6.73
6.72
6.71
6.65
6.62
3.96
3.94
3.92
3.90
1.83
1.81
1.78
1.76
1.74
1.47
1.46
1.43
1.42
1.41
1.40
1.37
1.35
0.96
0.93
0.91
0.94
1.00
2.11
1.22
2.19
1.14
1.11
2.47
3.13
2.32
4.34
3.20
f1 (ppm)

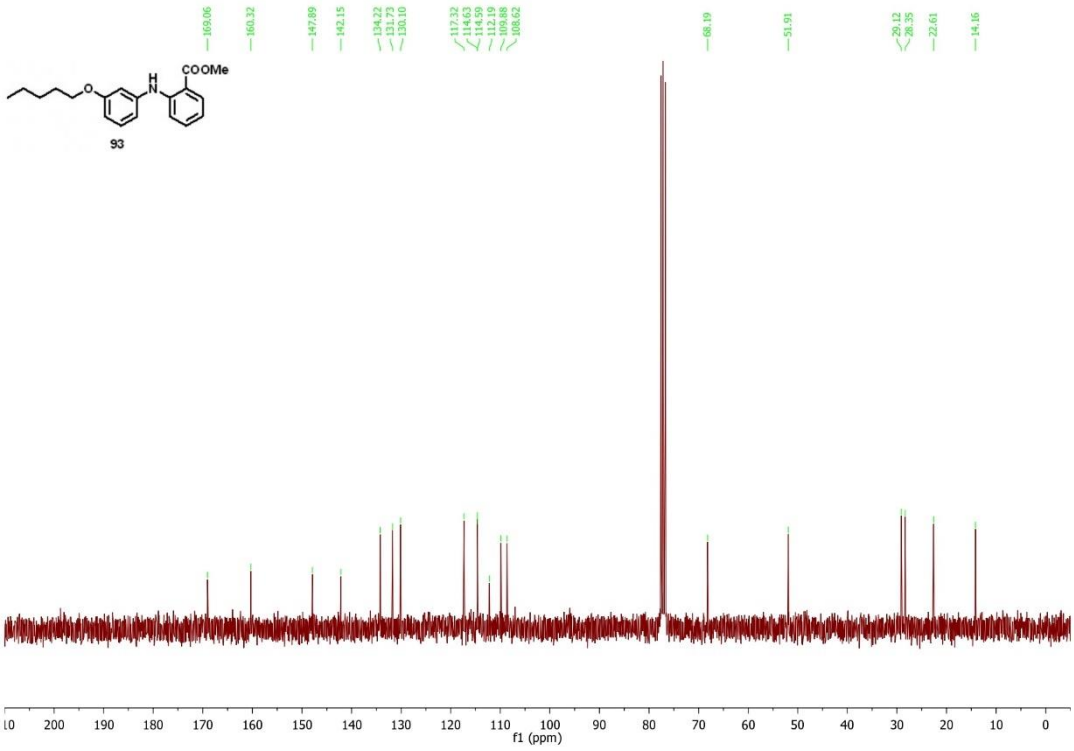
169.06
160.32
147.89
142.15
134.22
131.73
130.10
117.32
114.63
114.59
112.19
109.88
108.62
68.19
51.91
29.12
28.35
22.61
14.16
COOMe
93
f1 (ppm)

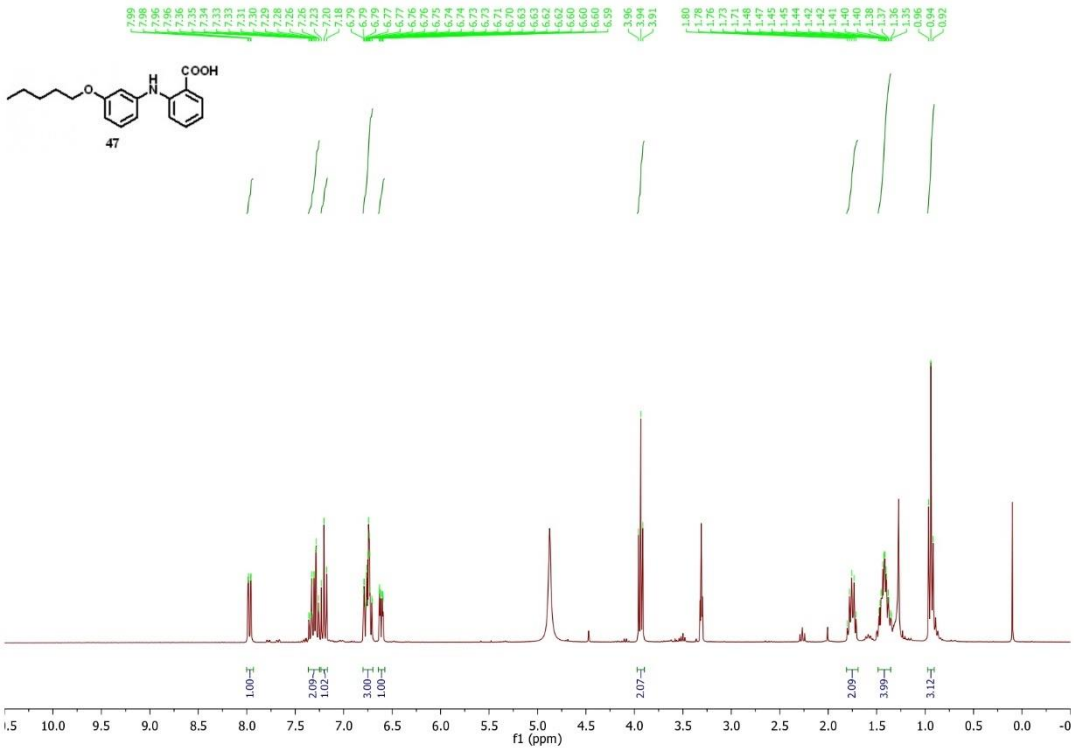
COOH
47
1.00
2.09
1.02
3.00
1.00
2.07
2.09
3.99
3.12
f1 (ppm)

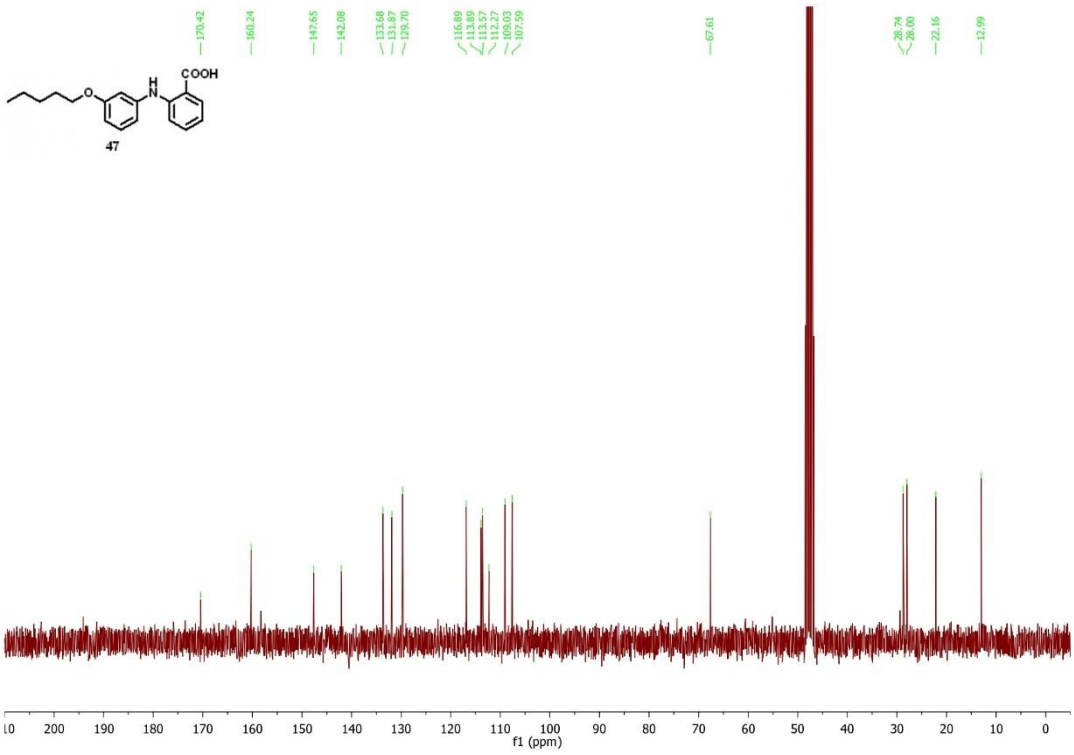
170.42
160.24
147.65
142.08
133.68
131.87
129.70
116.89
113.89
113.57
112.27
109.03
107.59
67.61
28.74
28.00
22.16
12.99
COOH
H
N
O
47
f1 (ppm)

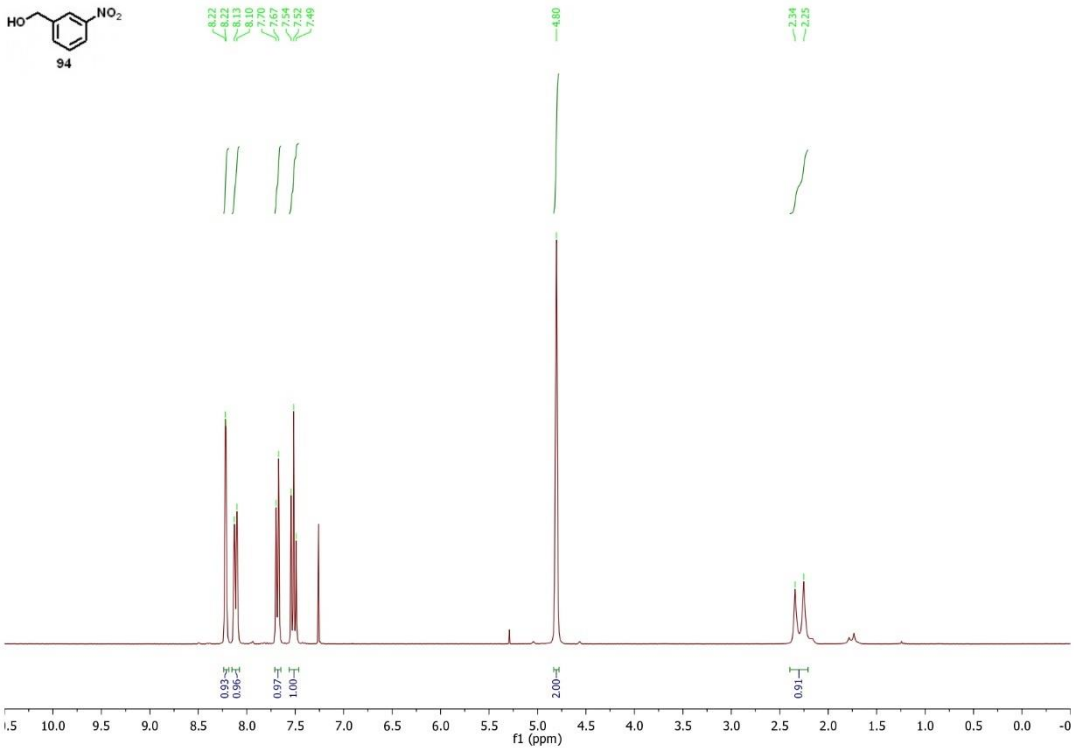
8.22
8.22
8.13
8.10
7.70
7.67
7.54
7.52
7.49
4.80
2.34
2.25
HO
NO2
94
0.93
0.96
0.97
1.00
2.00
0.91
f1 (ppm)

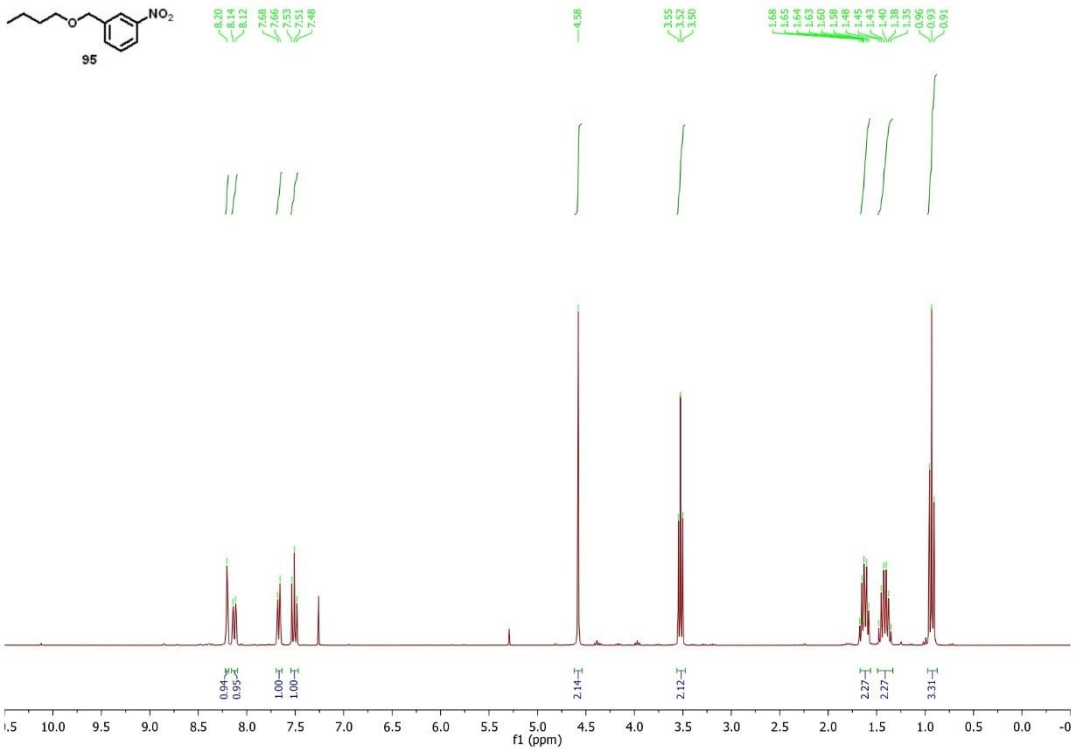
95
8.20
8.14
8.12
7.68
7.66
7.53
7.51
7.48
4.58
3.55
3.52
3.50
1.68
1.65
1.64
1.63
1.60
1.58
1.48
1.45
1.43
1.40
1.38
1.35
0.96
0.93
0.91
0.94
0.95
1.00
1.00
2.14
2.12
2.27
2.27
3.31
f1 (ppm)

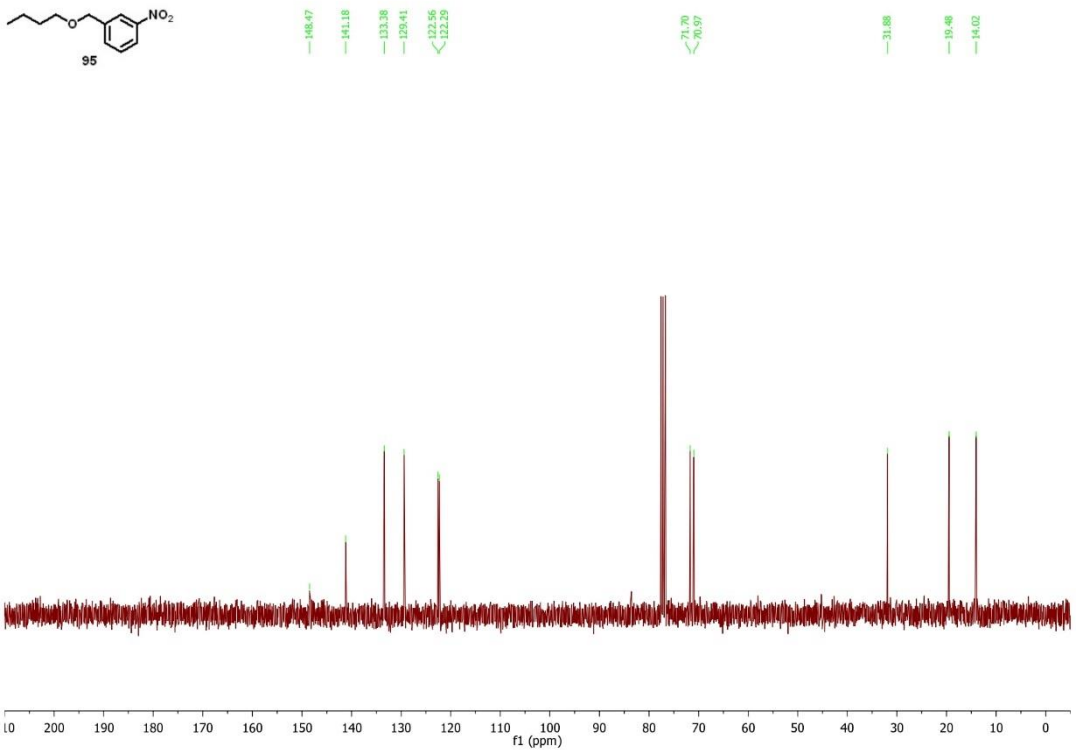
95
148.47
141.18
133.38
129.41
122.56
122.29
71.70
70.97
31.88
19.48
14.02
f1 (ppm)

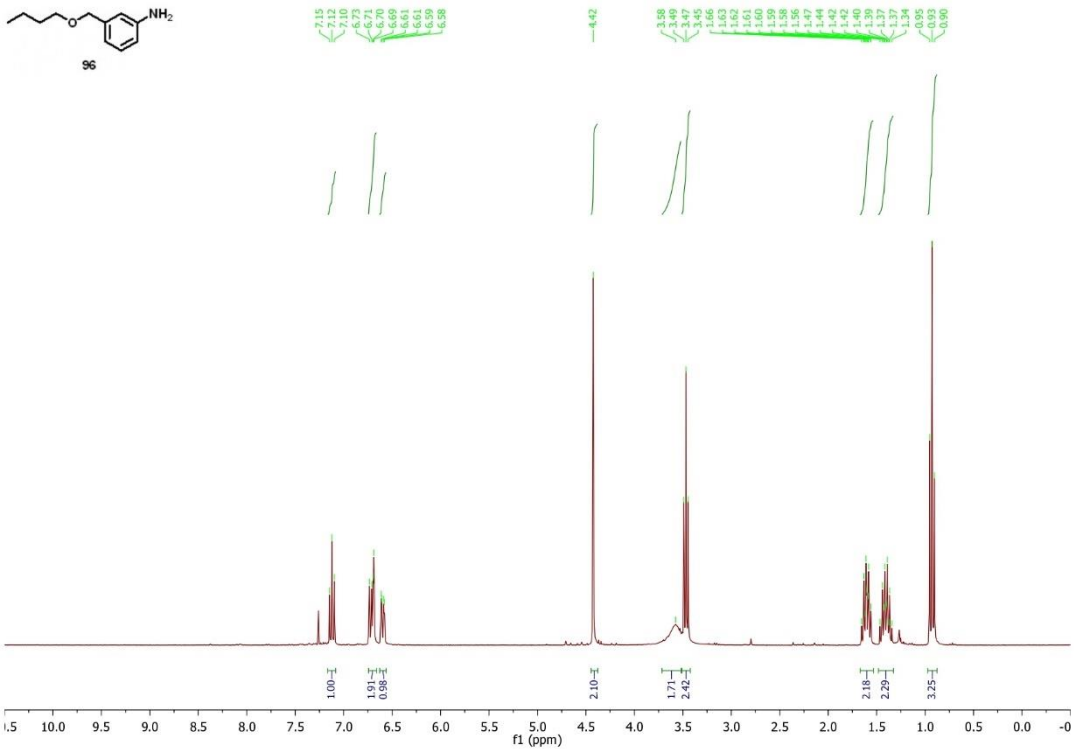
NH2
O
96
7.15
7.12
7.10
6.73
6.71
6.70
6.69
6.61
6.61
6.59
6.58
4.42
3.58
3.49
3.47
3.45
1.66
1.63
1.62
1.61
1.60
1.59
1.58
1.56
1.47
1.44
1.43
1.42
1.40
1.39
1.37
1.37
1.34
0.95
0.93
0.90
1.00
1.91
0.98
2.10
1.71
2.42
2.18
2.29
3.25
f1 (ppm)

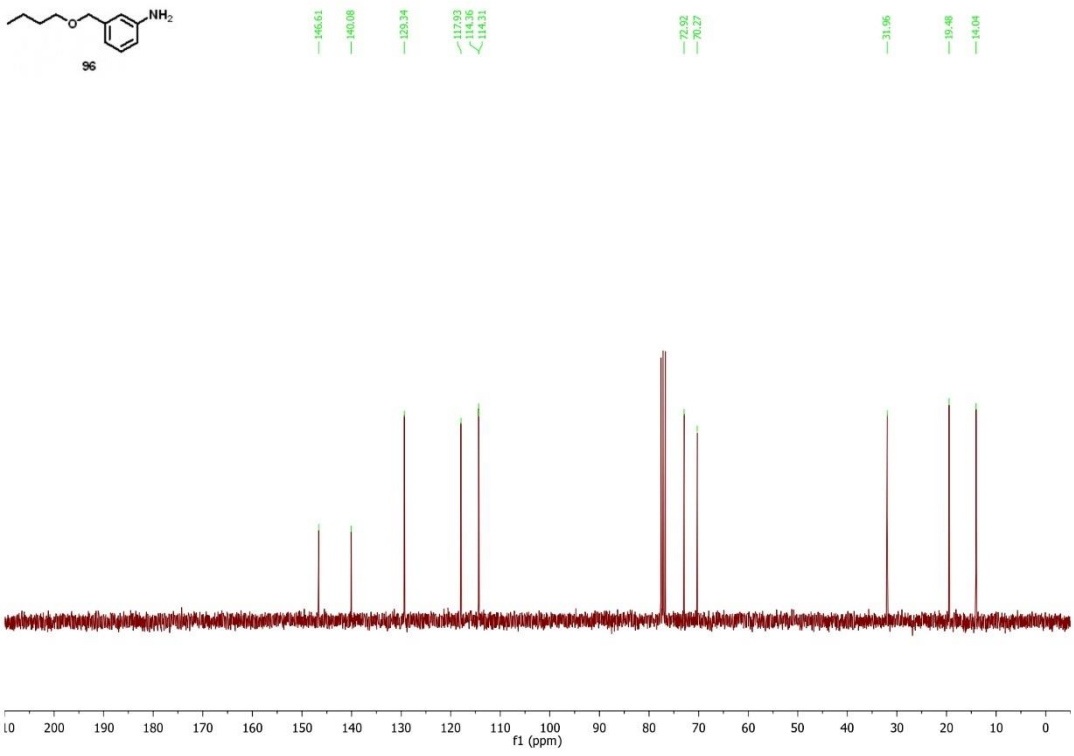
NH2
O
96
146.61
140.08
129.34
117.93
114.36
114.31
72.92
70.27
31.96
19.48
14.04
f1 (ppm)

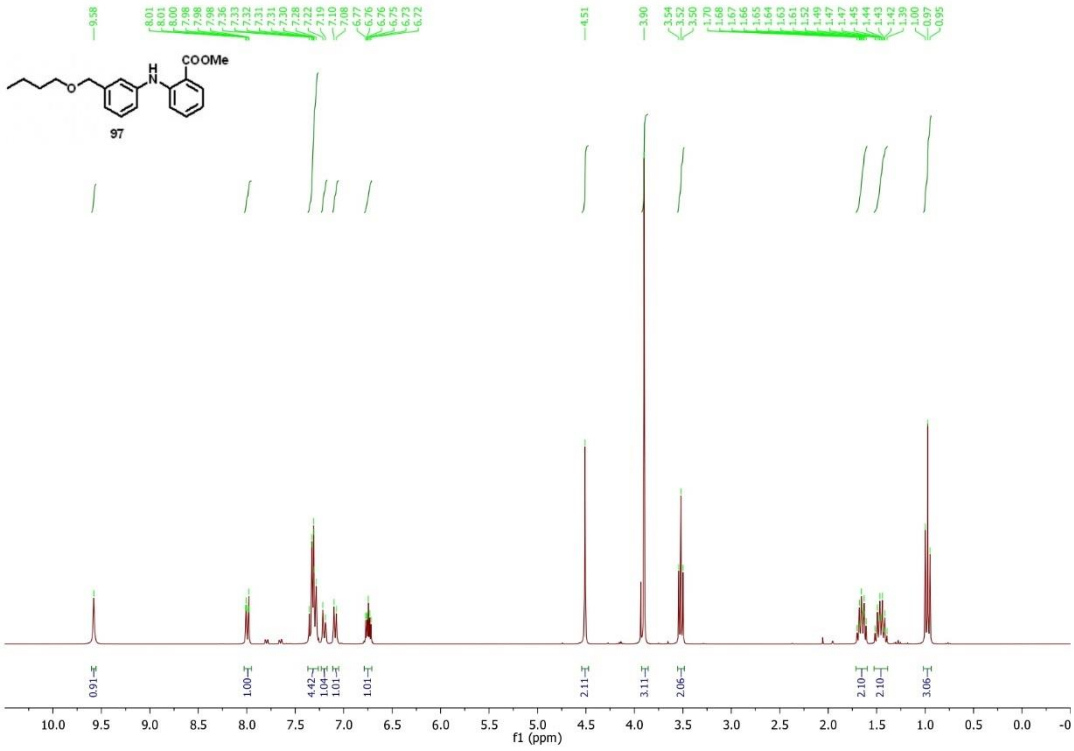
COOMe
97
f1 (ppm)

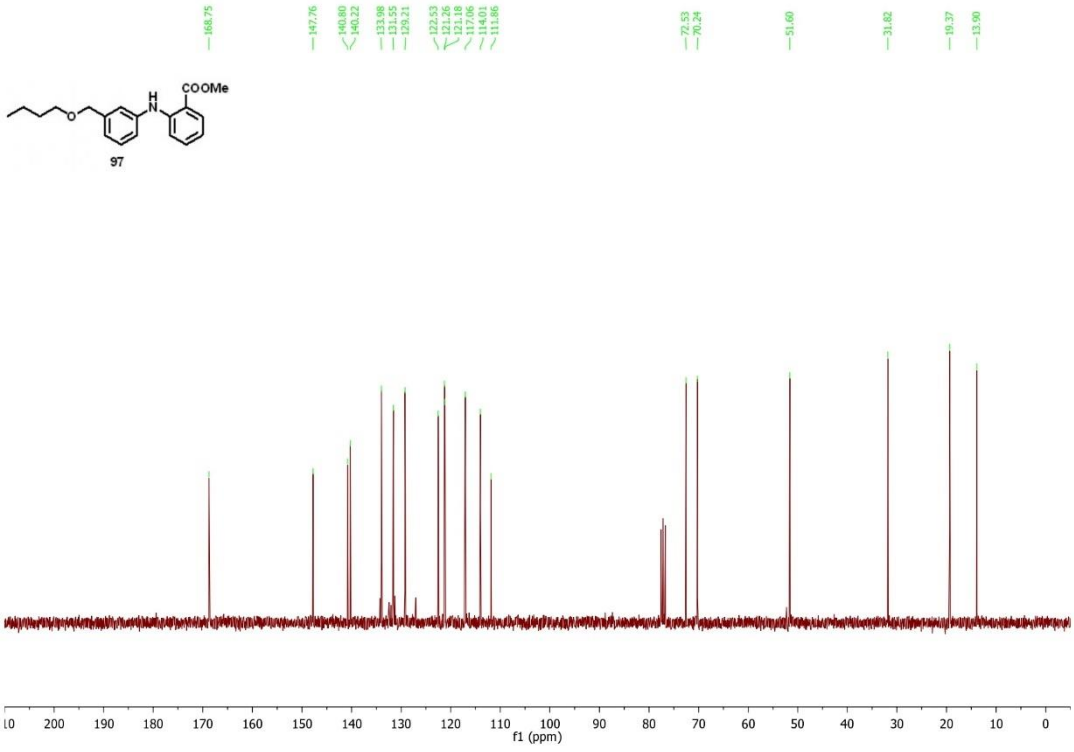
COOMe
97
f1 (ppm)

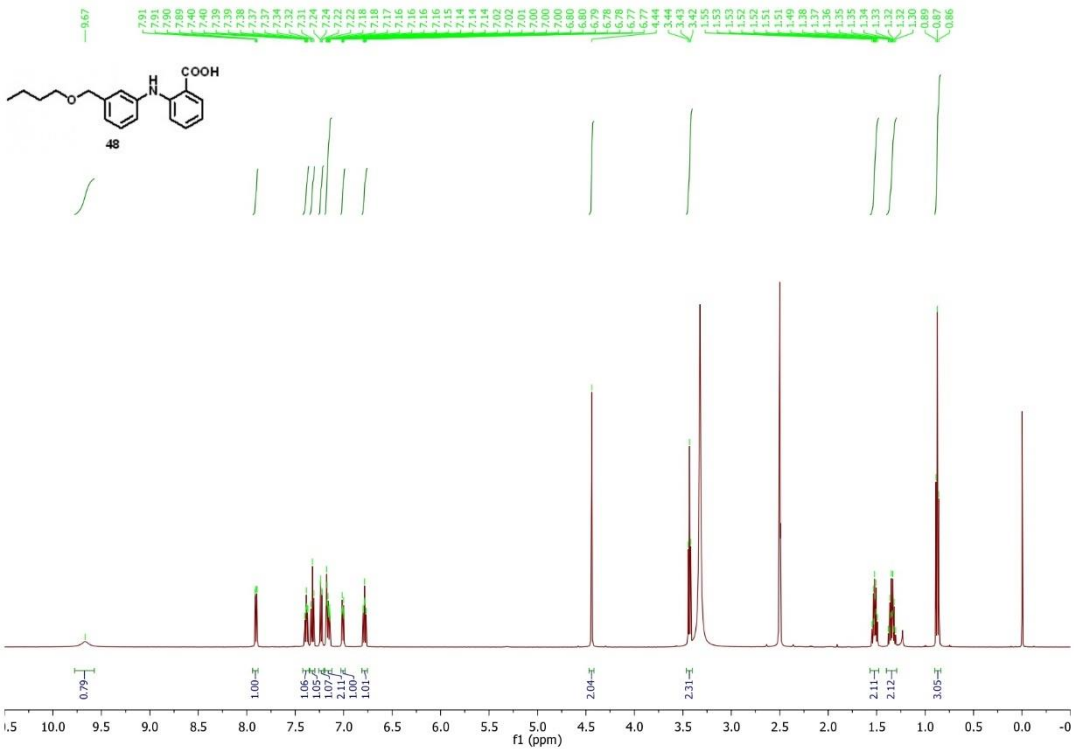
COOH
H
N
O
48
f1 (ppm)

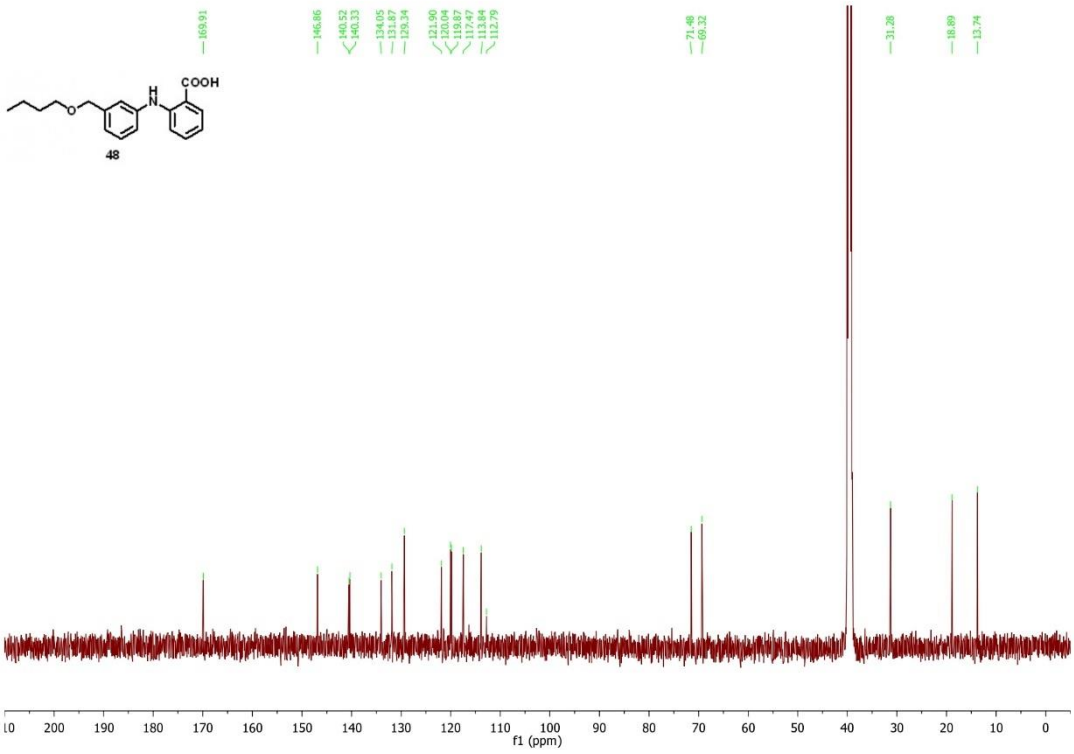
COOH
H
N
O
48
f1 (ppm)

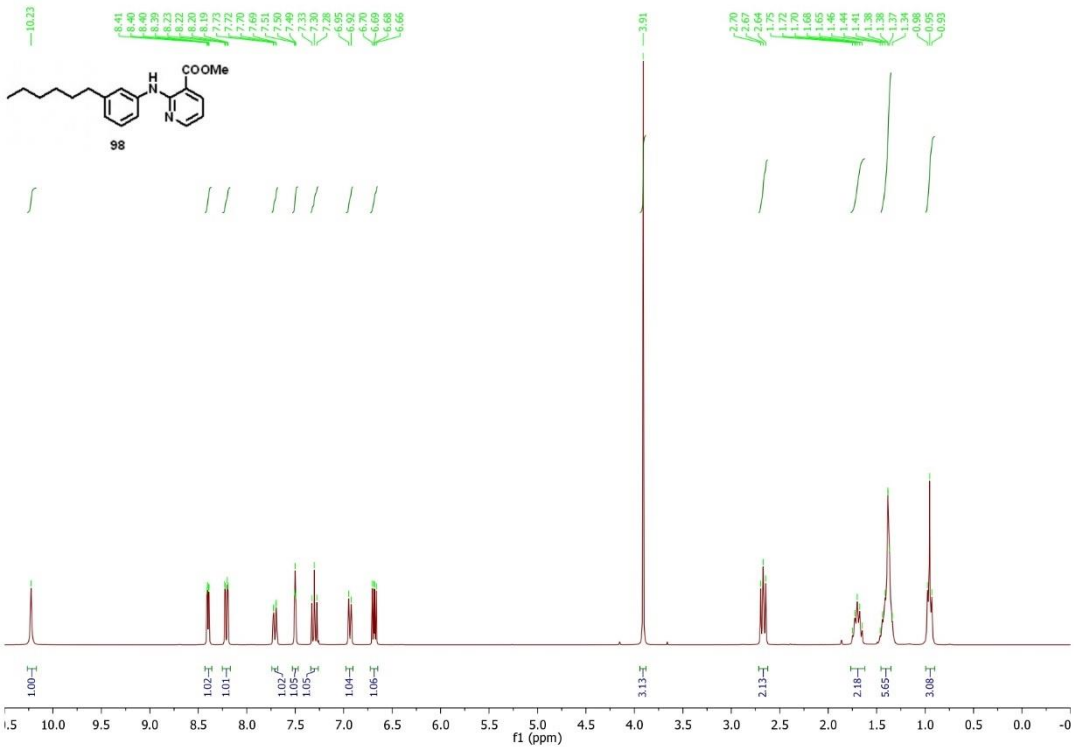
10.23
8.41
8.40
8.40
8.39
8.23
8.22
8.20
8.19
7.73
7.72
7.70
7.69
7.51
7.50
7.49
7.33
7.30
7.28
6.95
6.92
6.70
6.69
6.68
6.66
3.91
2.70
2.67
2.64
1.75
1.72
1.70
1.68
1.65
1.46
1.44
1.41
1.38
1.38
1.37
1.34
0.98
0.95
0.93
COOMe
H
N
N
98
1.00
1.02
1.01
1.02
1.05
1.05
1.04
1.06
3.13
2.13
2.18
5.65
3.08
f1 (ppm)

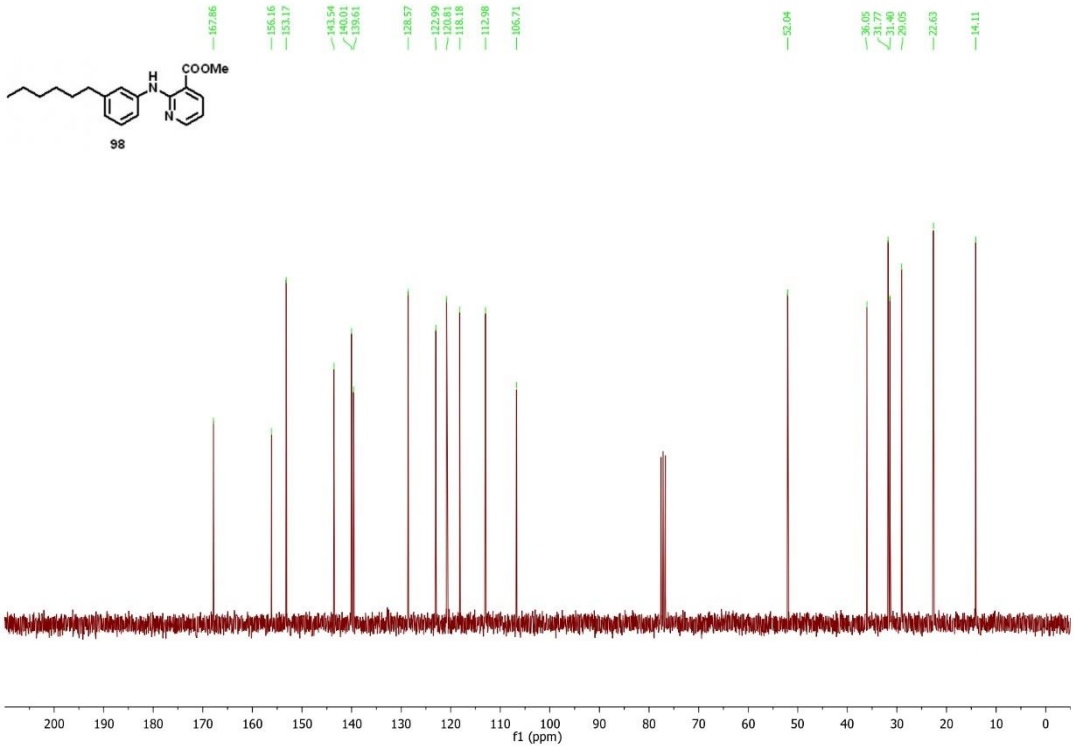
167.86
156.16
153.17
143.54
140.01
139.61
128.57
122.99
120.81
118.18
112.98
106.71
52.04
36.05
31.77
31.40
29.05
22.63
14.11
COOMe
H
N
N
98
f1 (ppm)

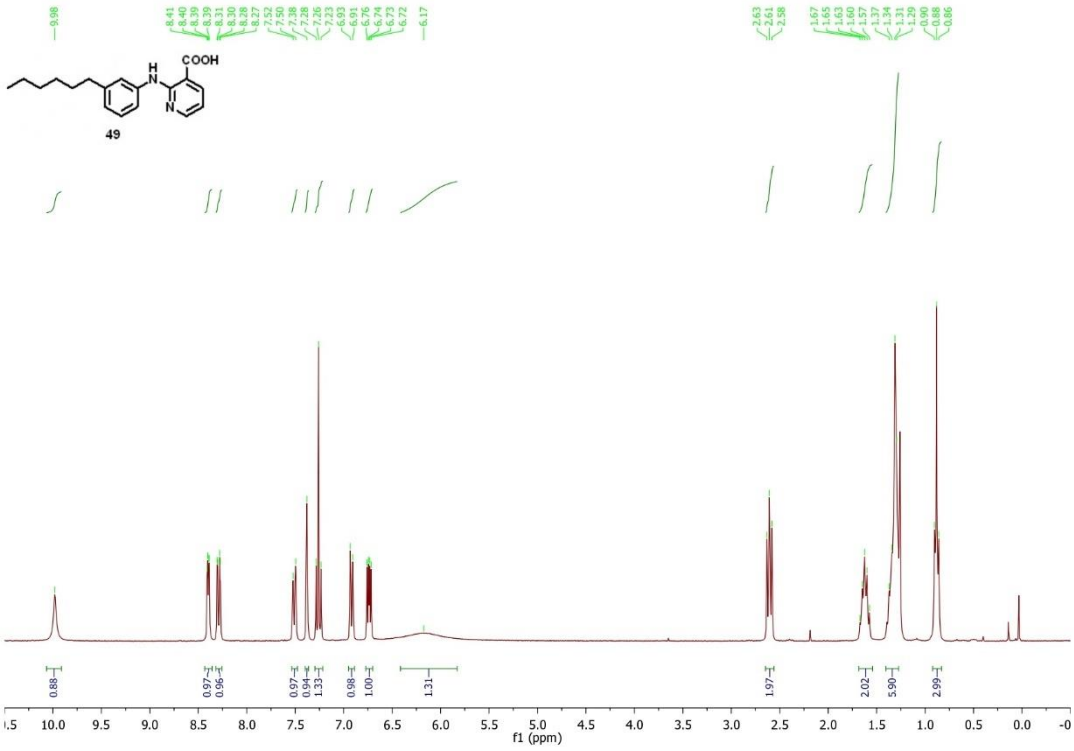
9.98
8.41
8.40
8.39
8.39
8.31
8.30
8.28
8.27
7.52
7.50
7.38
7.28
7.26
7.23
6.93
6.91
6.76
6.74
6.73
6.72
6.17
2.63
2.61
2.58
1.67
1.65
1.63
1.60
1.57
1.37
1.34
1.31
1.29
0.90
0.88
0.86
COOH
H
N
N
49
0.88
0.97
0.96
0.97
0.94
1.33
0.98
1.00
1.31
1.97
2.02
5.90
2.99
f1 (ppm)

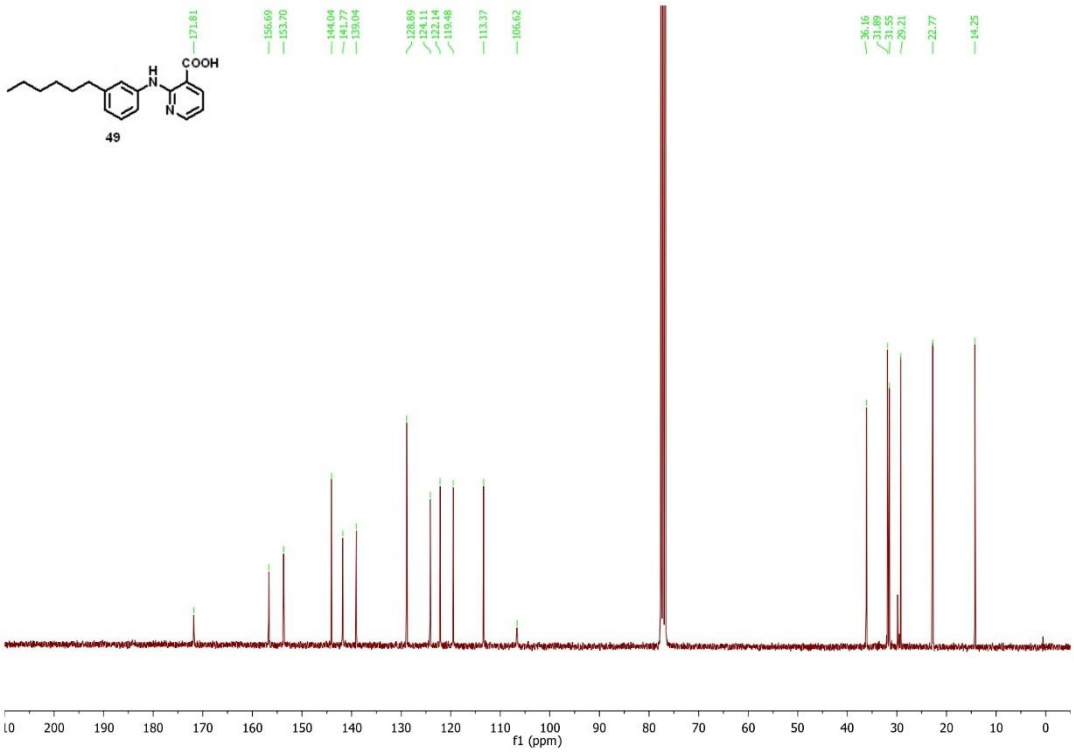
171.81
156.69
153.70
144.04
141.77
139.04
128.89
124.11
122.14
119.48
113.37
106.62
36.16
31.89
31.55
29.21
22.77
14.25
COOH
H
N
N
49
f1 (ppm)

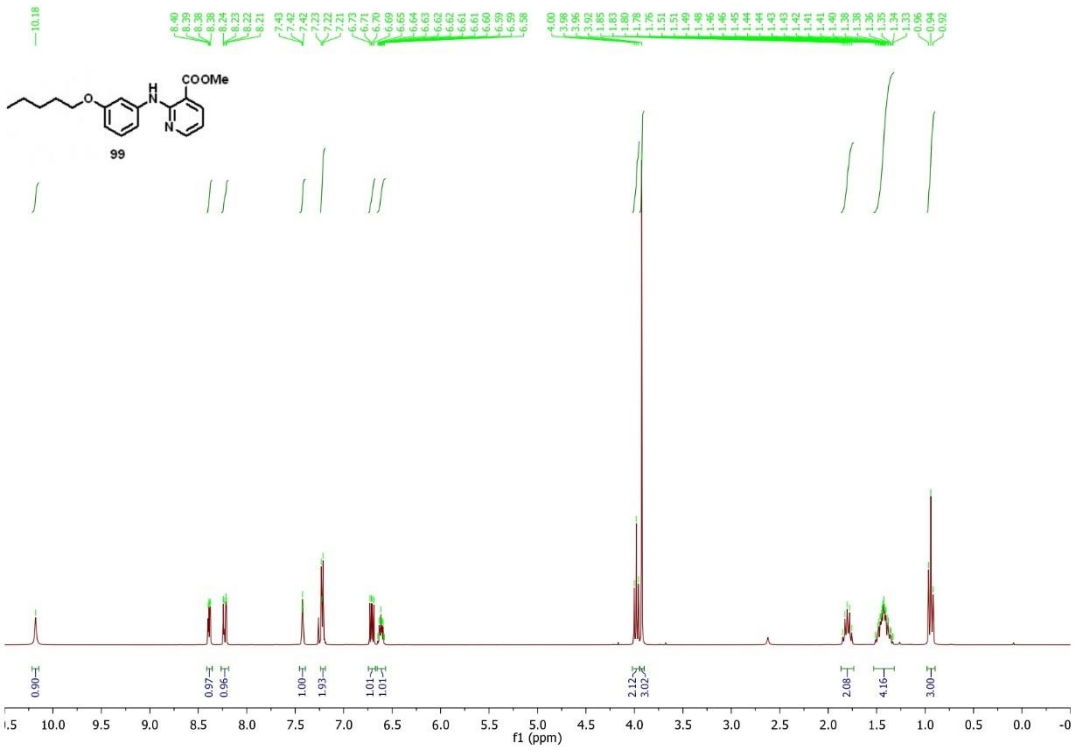
COOMe
99
f1 (ppm)

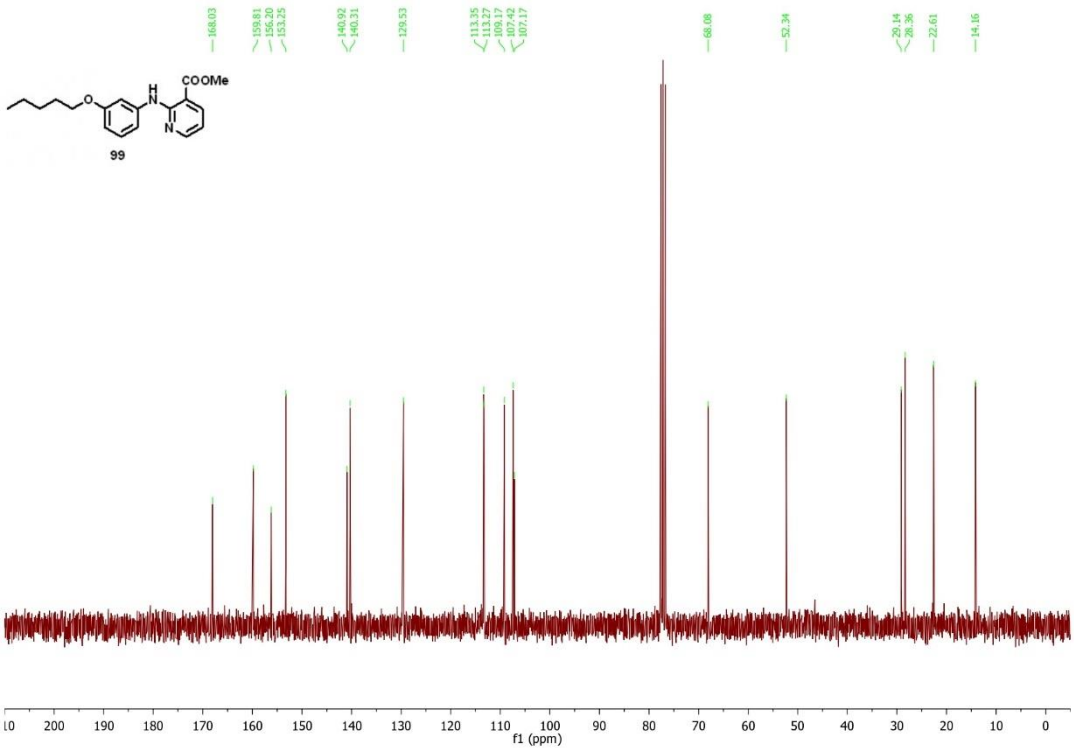
COOMe
99
f1 (ppm)

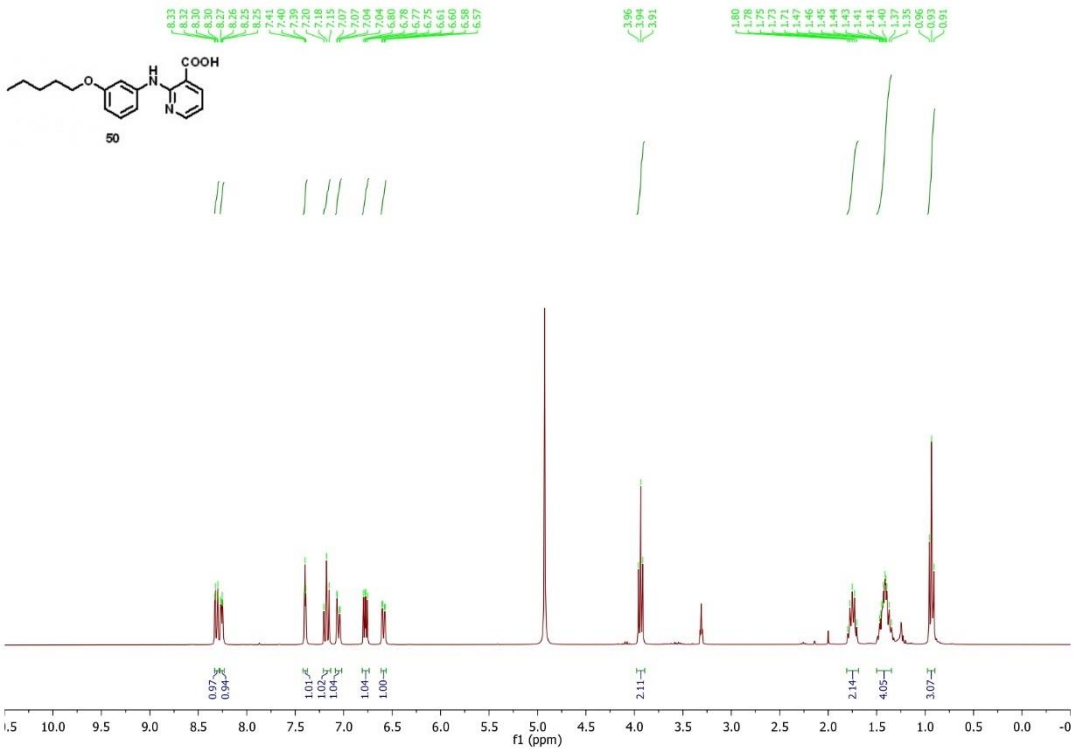
COOH
H
N
O
N
50
f1 (ppm)

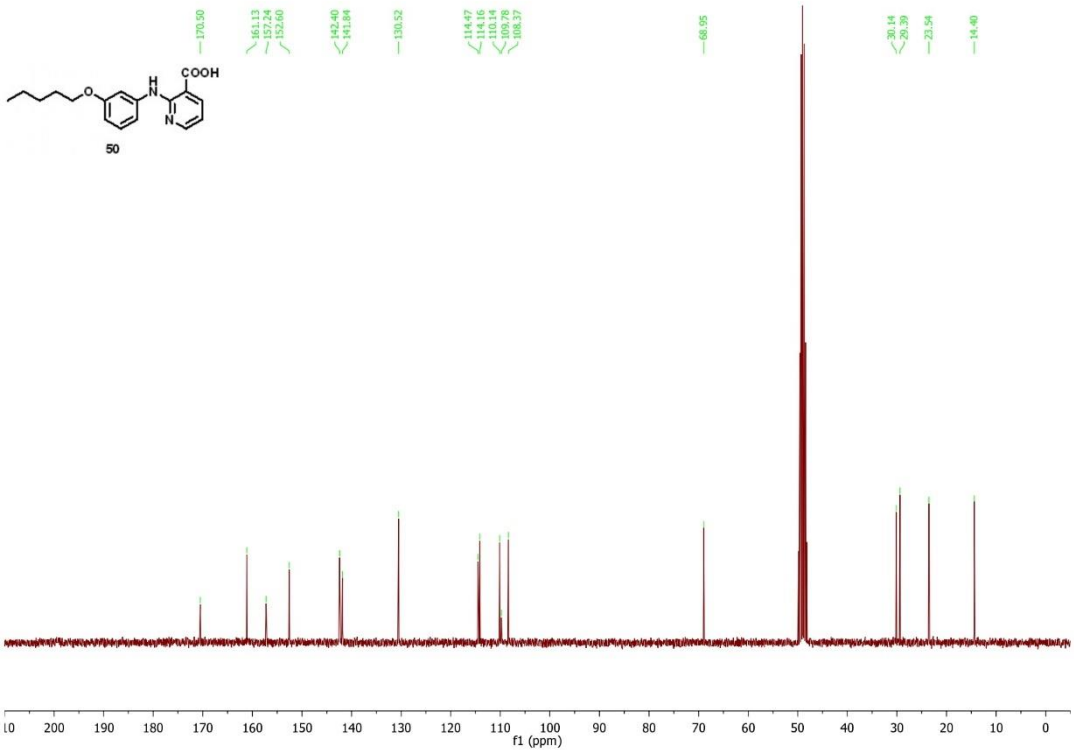
COOH
H
N
O
N
50
f1 (ppm)

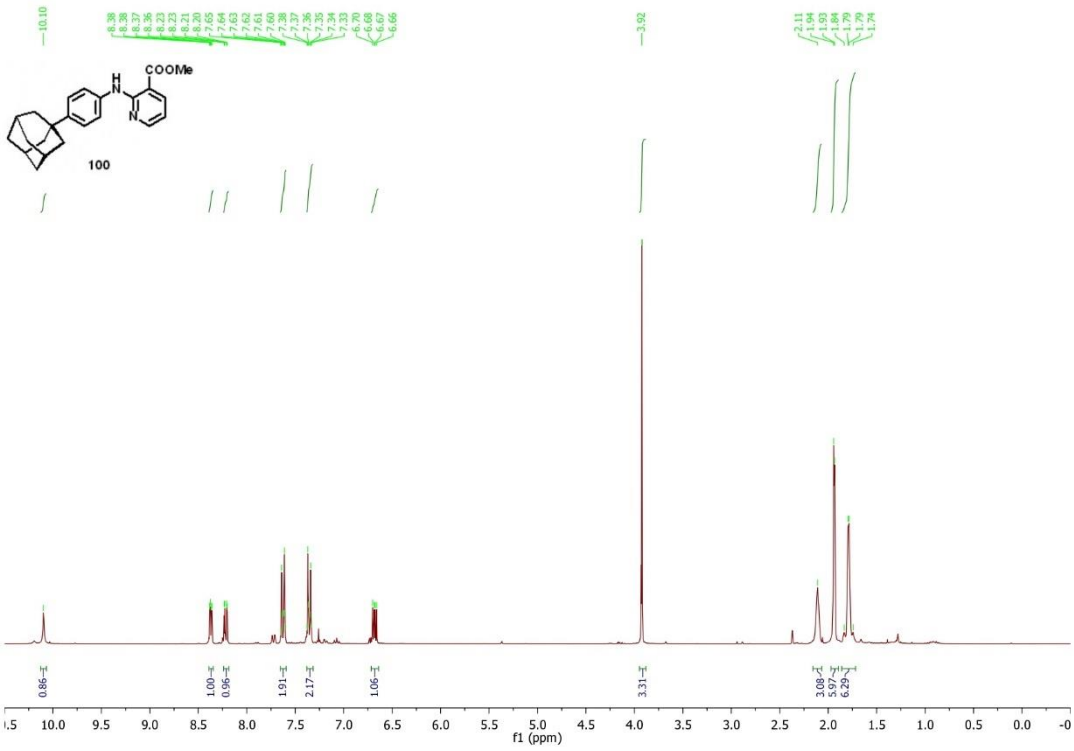
COOMe
100
f1 (ppm)

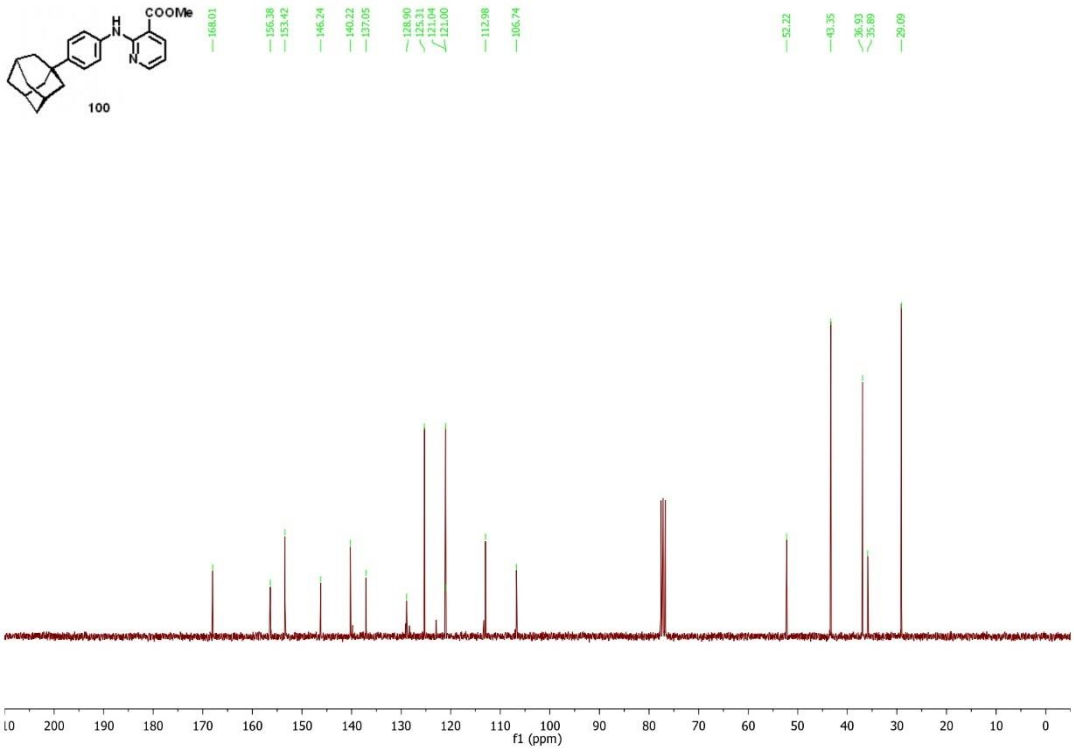
COOMe
100
f1 (ppm)

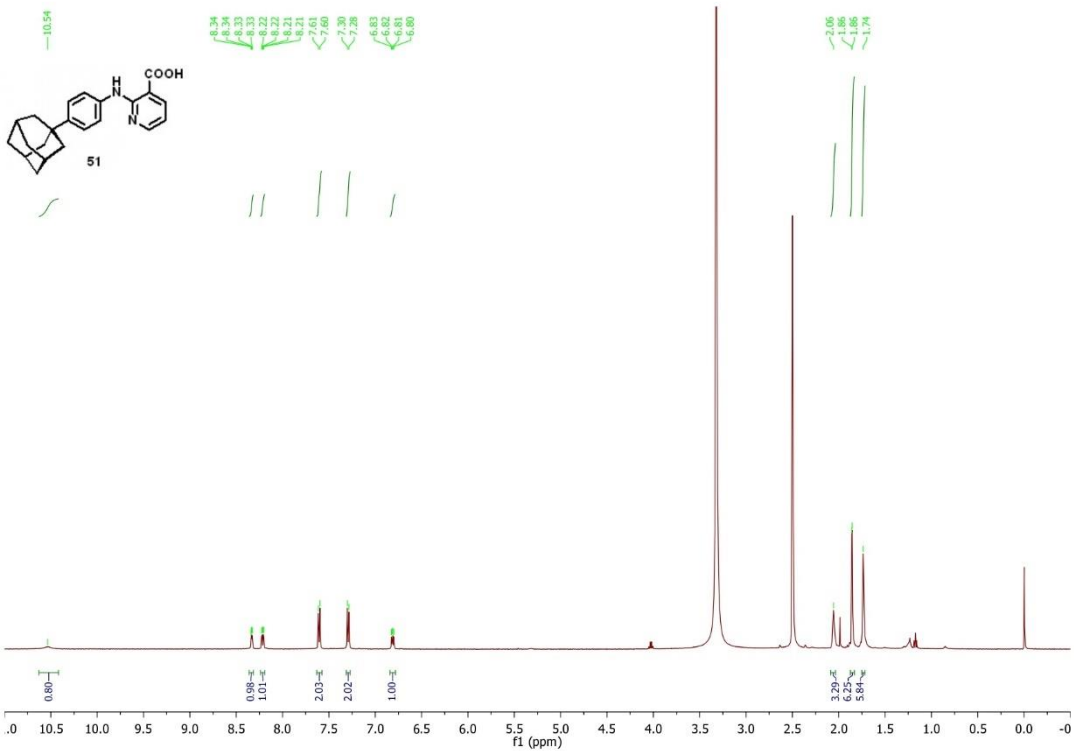
10.54
8.34
8.34
8.33
8.33
8.22
8.22
8.21
8.21
7.61
7.60
7.30
7.28
6.83
6.82
6.81
6.80
2.06
1.86
1.86
1.74
COOH
N
H
51
0.89
0.98
1.01
2.03
2.02
1.00
3.29
6.25
5.84
f1 (ppm)

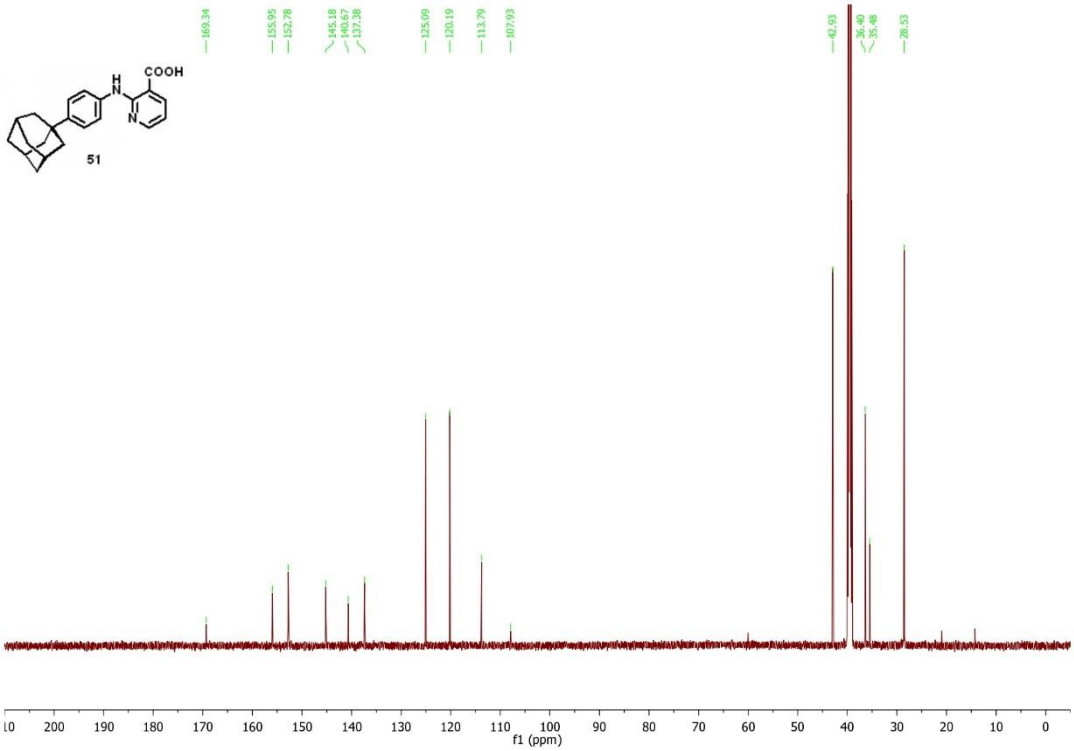
169.34
155.95
152.78
145.18
140.67
137.38
125.09
120.19
113.79
107.93
42.93
36.40
35.48
28.53
COOH
N
H
51
f1 (ppm)

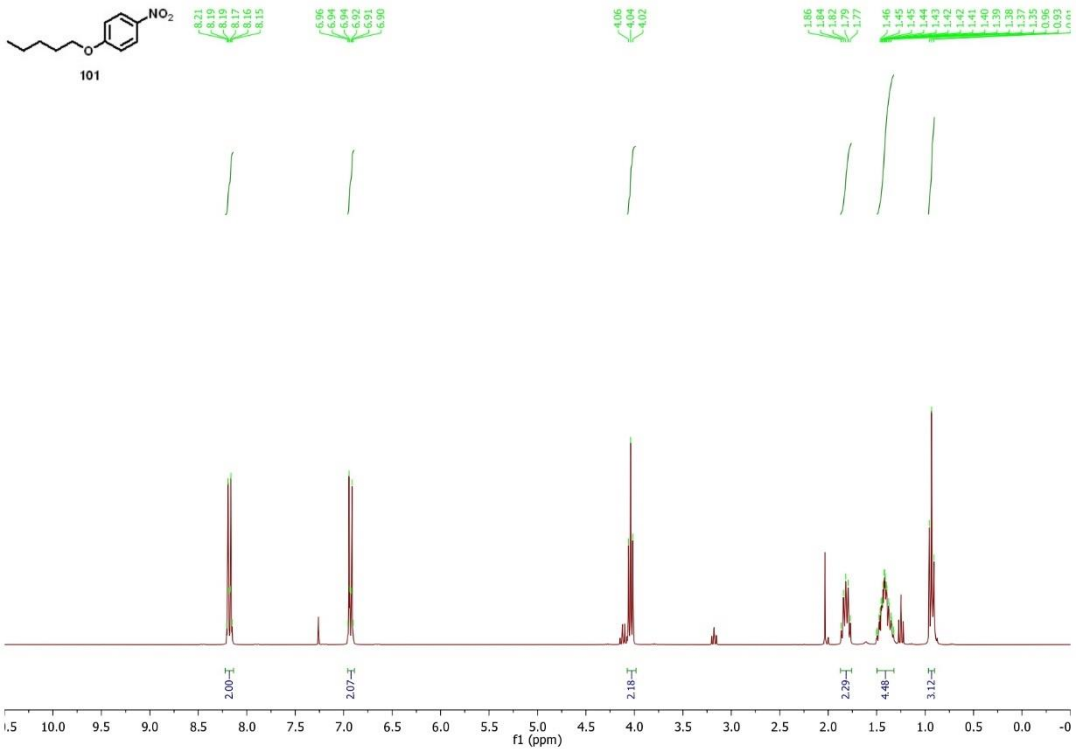
101
f1 (ppm)

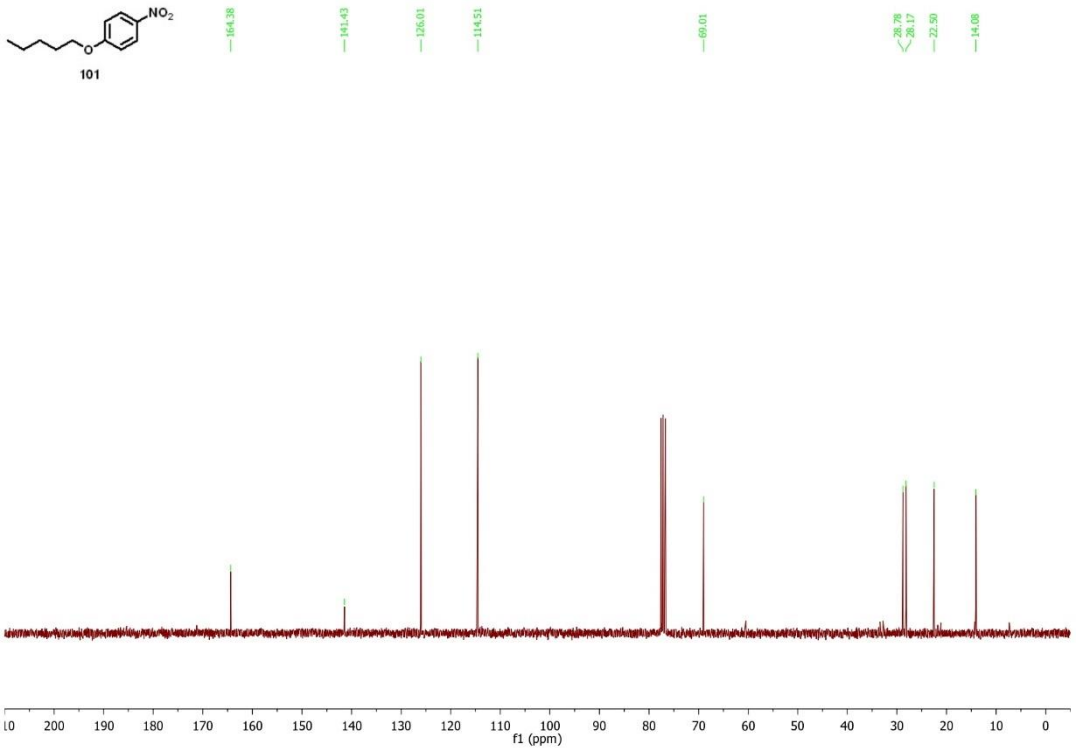
101
f1 (ppm)

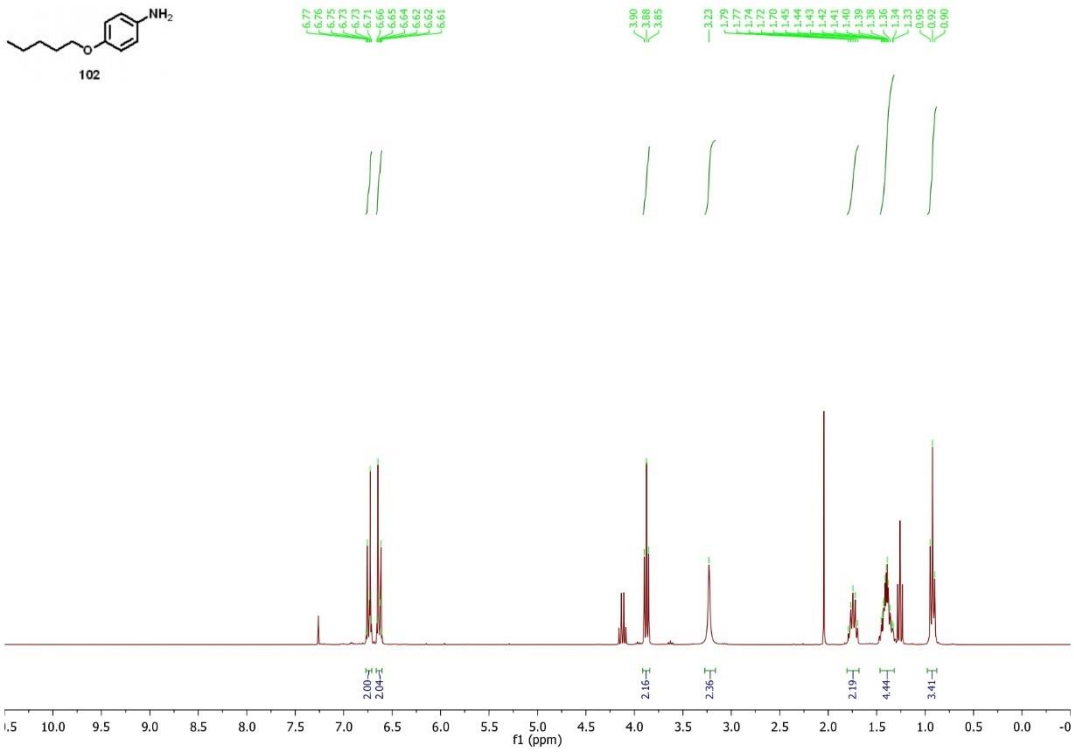
NH2
O
102
6.77
6.76
6.75
6.73
6.73
6.71
6.66
6.65
6.64
6.62
6.62
6.61
3.90
3.88
3.85
3.23
1.79
1.77
1.74
1.72
1.70
1.45
1.44
1.43
1.42
1.41
1.40
1.39
1.38
1.36
1.34
1.33
0.95
0.92
0.90
2.00
2.04
2.16
2.36
2.19
4.44
3.41
f1 (ppm)

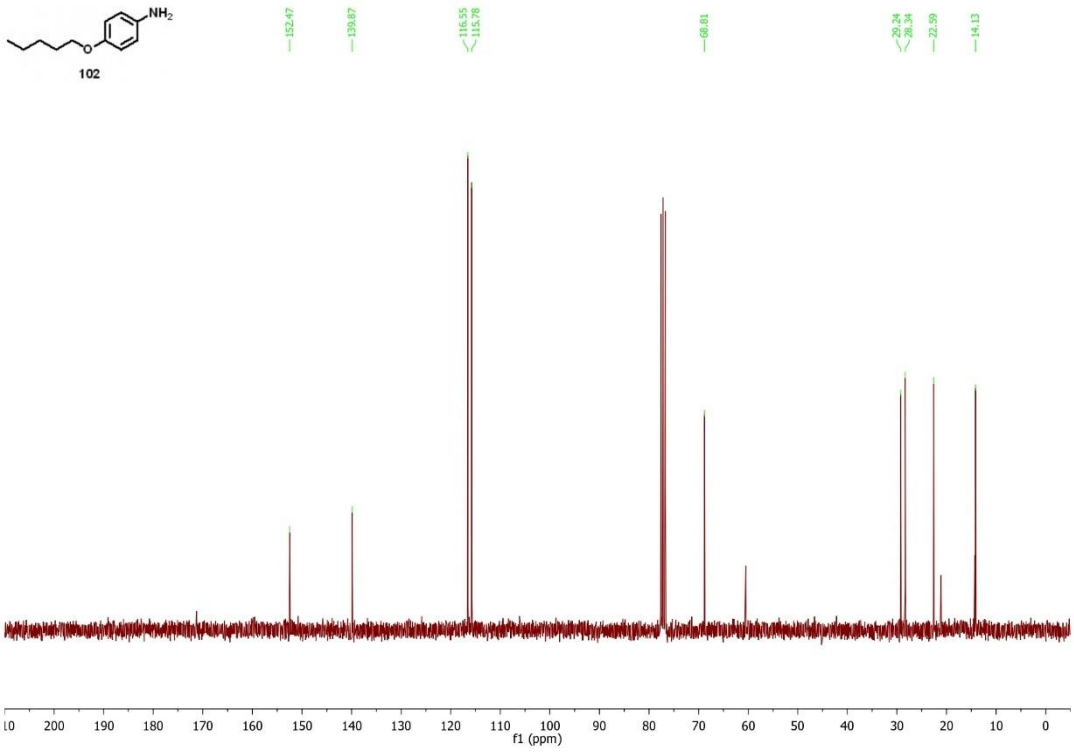
NH2
O
102
152.47
139.87
116.55
115.78
68.81
29.24
28.34
22.59
14.13
f1 (ppm)

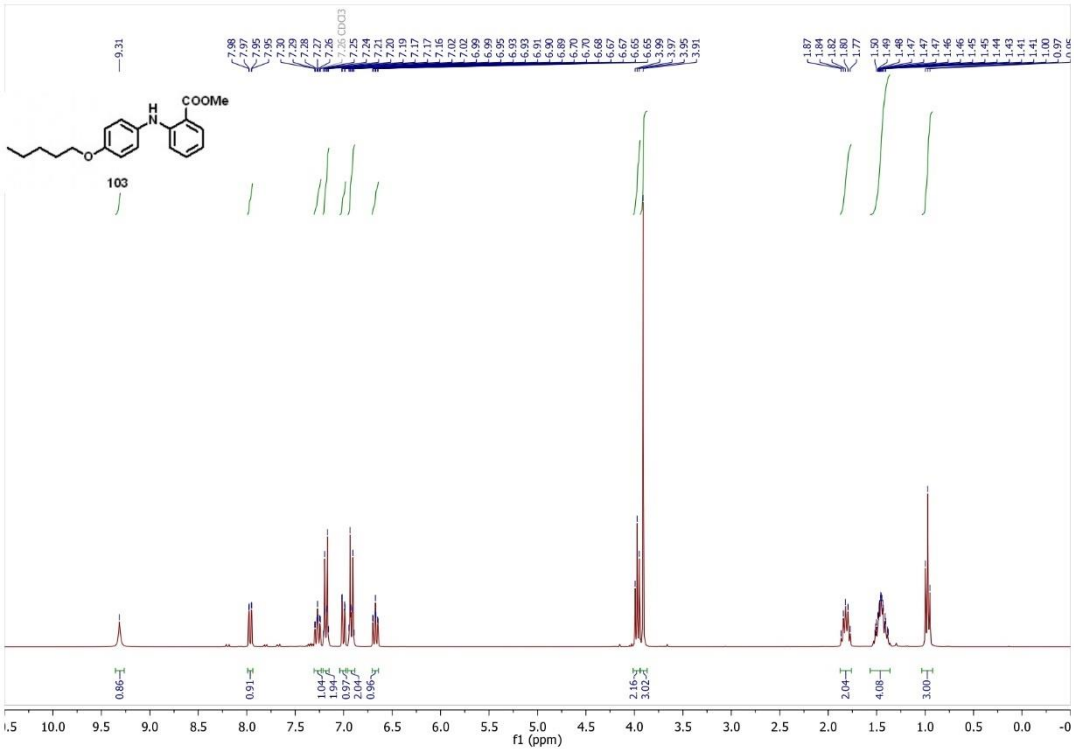
COOMe
H
N
O
103
f1 (ppm)

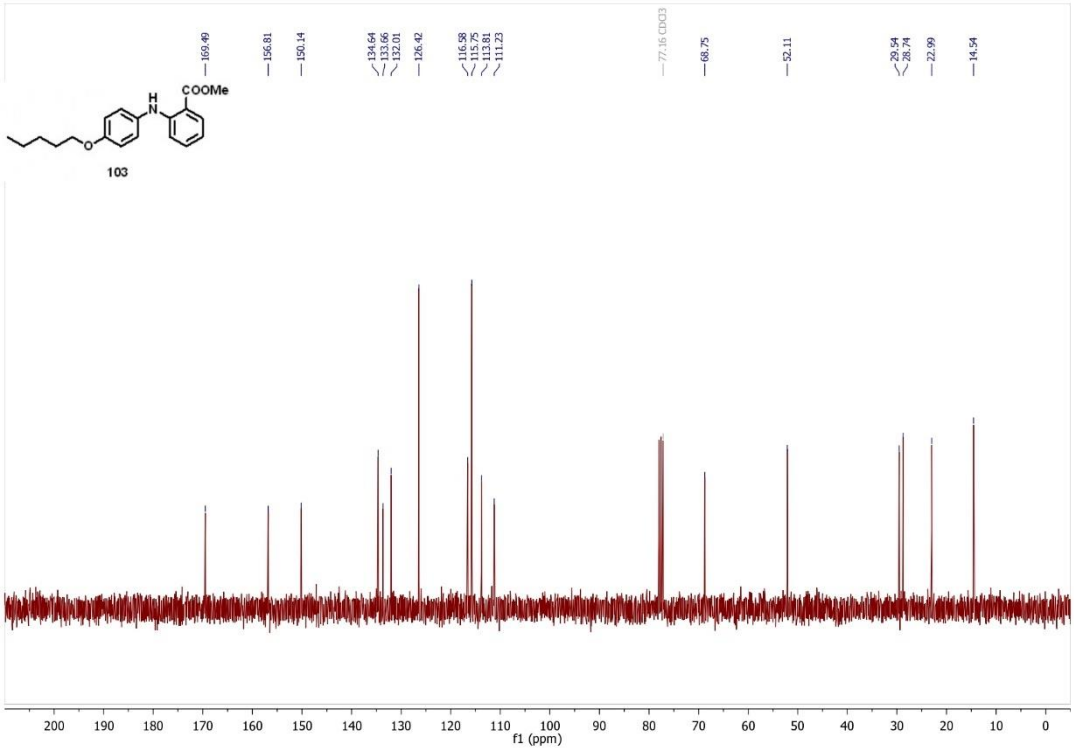
COOMe
H
N
O
103
f1 (ppm)

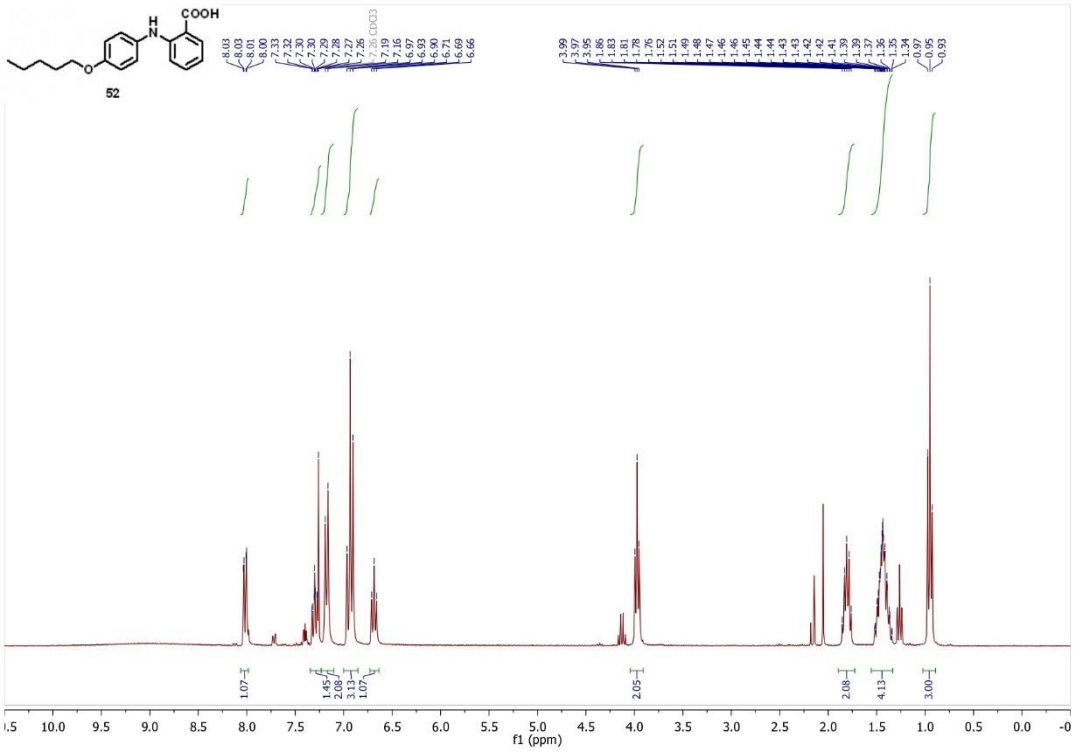
COOH
H
N
O
52
8.03
8.03
8.01
8.00
7.33
7.32
7.30
7.30
7.29
7.28
7.27
7.26
7.19
7.15
6.97
6.93
6.90
6.71
6.69
6.66
3.99
3.97
3.95
1.86
1.83
1.81
1.78
1.76
1.52
1.51
1.49
1.48
1.47
1.46
1.46
1.45
1.44
1.44
1.43
1.43
1.42
1.42
1.41
1.39
1.39
1.37
1.36
1.35
1.34
0.97
0.95
0.93
1.07
1.45
2.08
3.13
1.07
2.05
2.08
4.13
3.00
f1 (ppm)

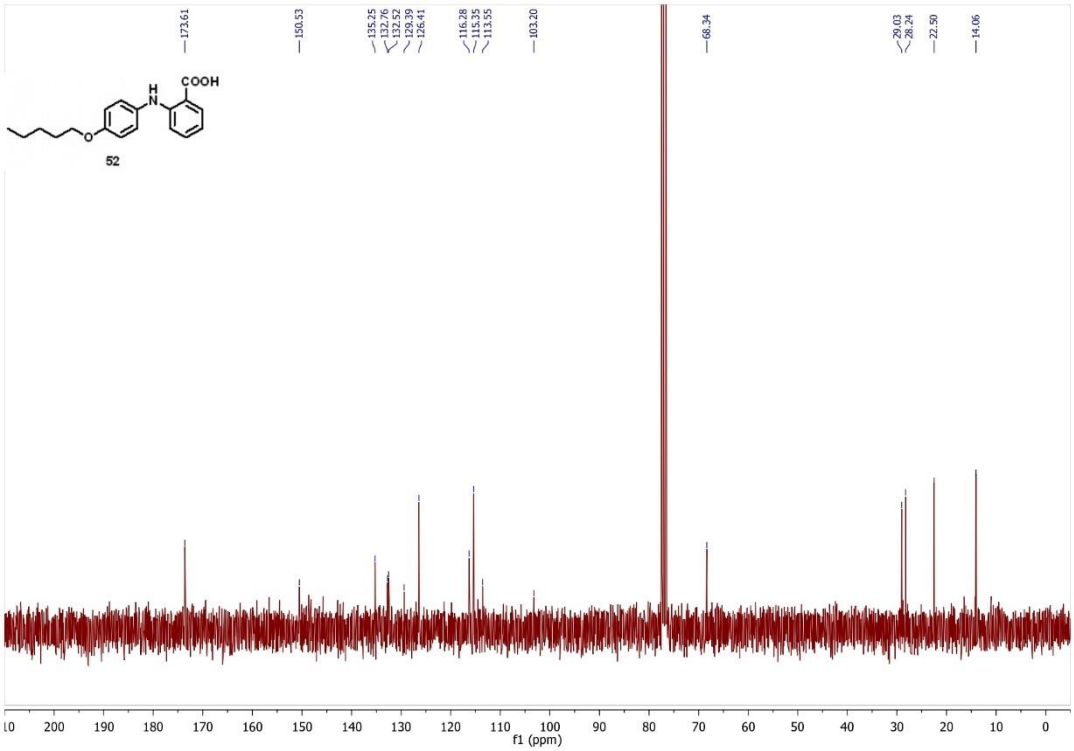
173.61
150.53
135.25
133.76
132.52
129.39
126.41
116.28
115.35
113.55
103.20
68.34
29.03
28.24
22.50
14.06
COOH
H
N
O
52
f1 (ppm)

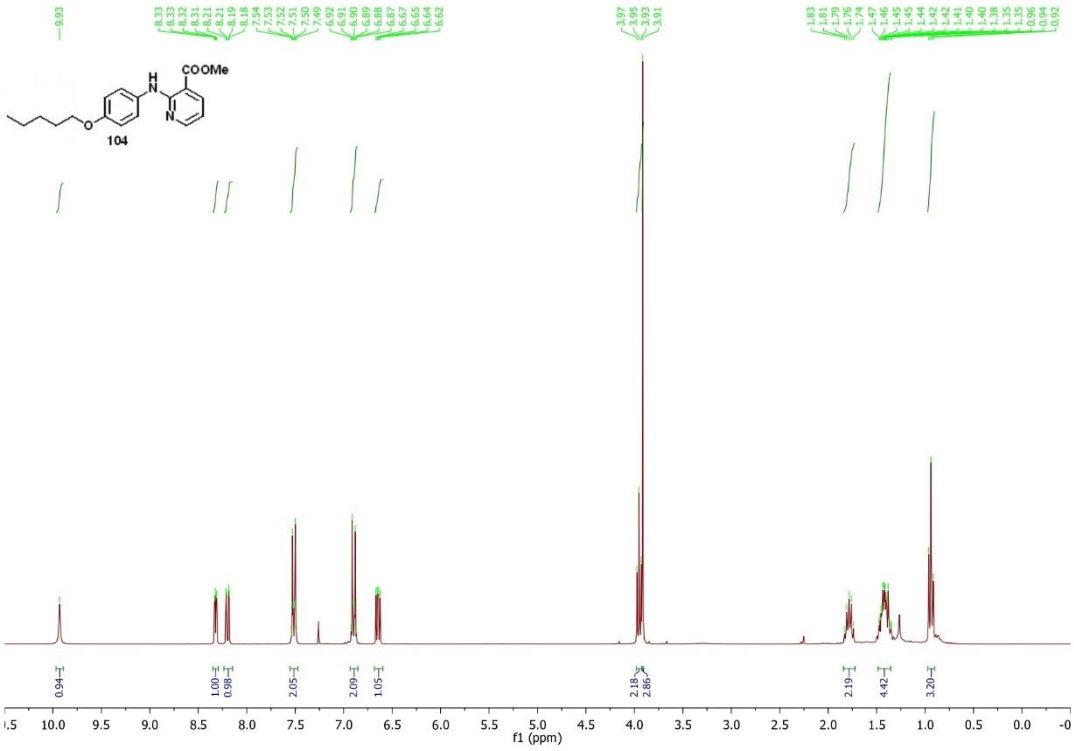
COOMe
104
f1 (ppm)

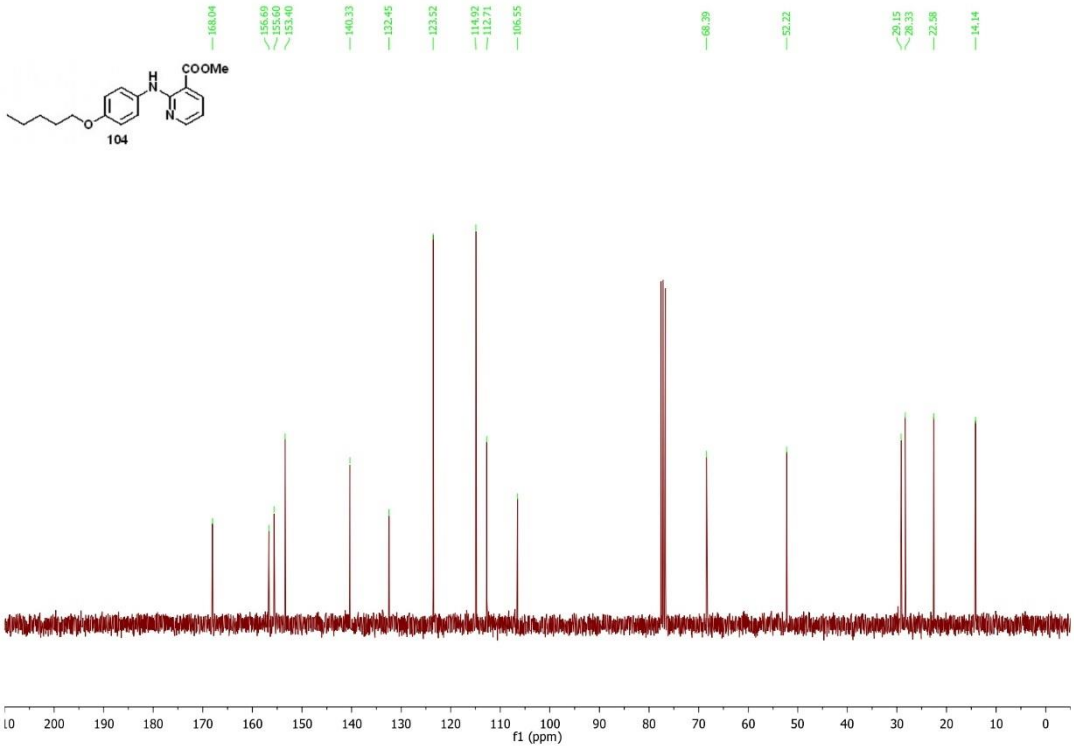
COOMe
104
f1 (ppm)

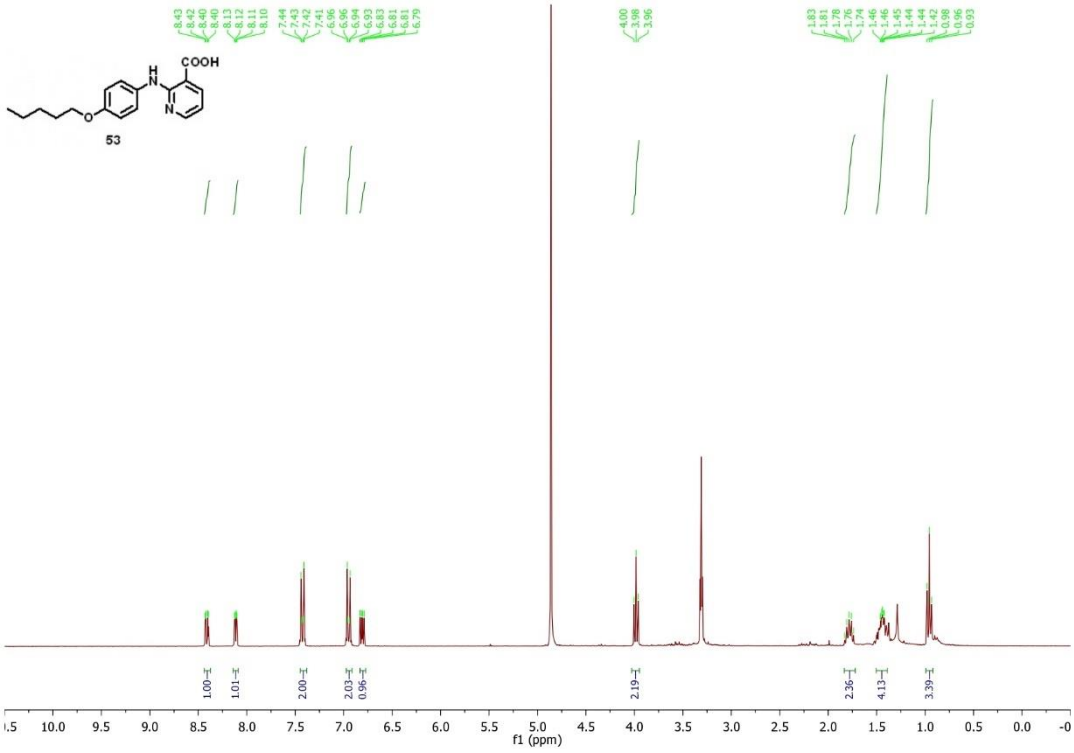
COOH
H
N
O
N
53
f1 (ppm)

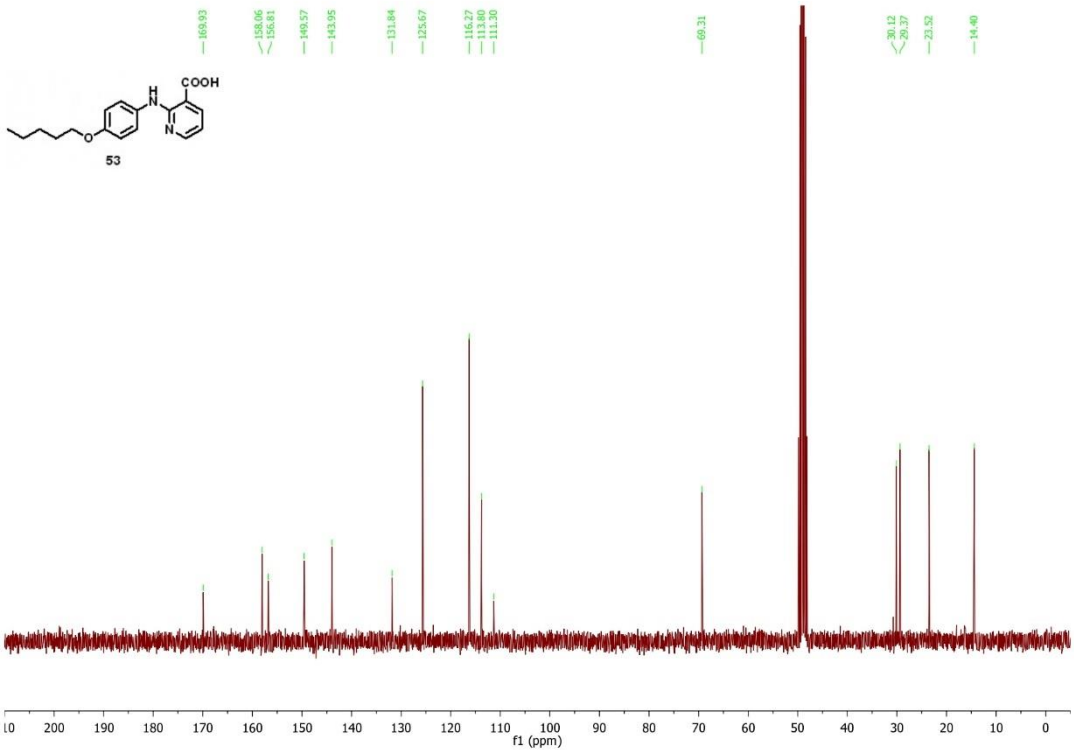
COOH
H
N
O
N
53
f1 (ppm)

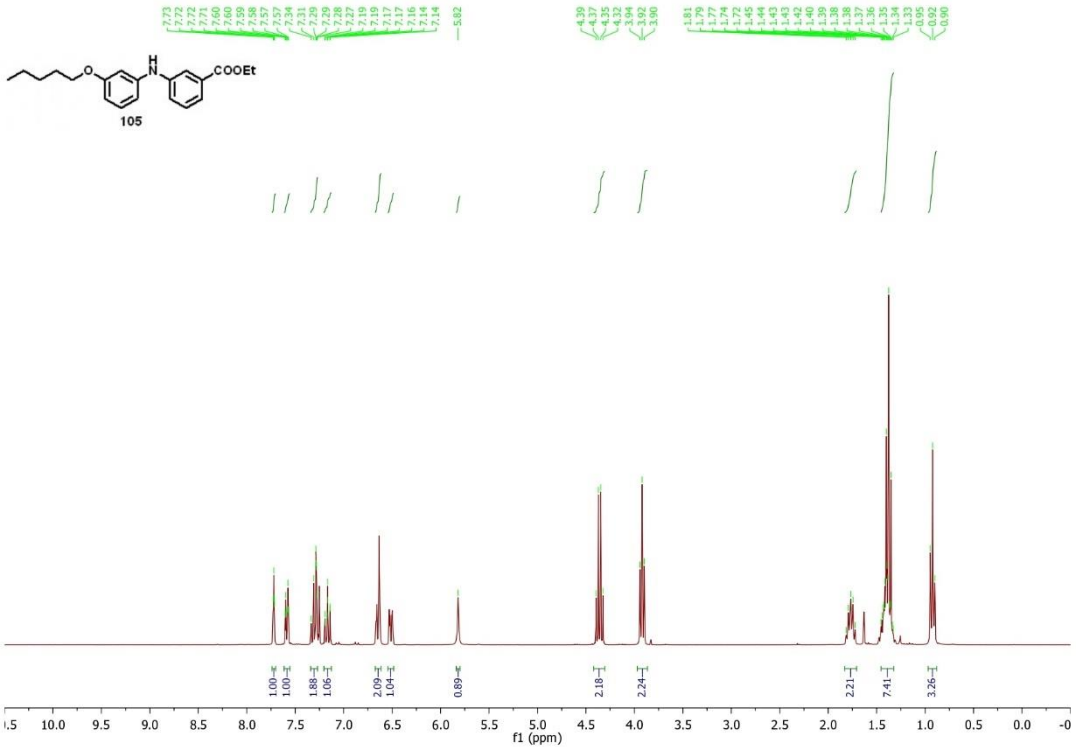
COOEt
105
f1 (ppm)

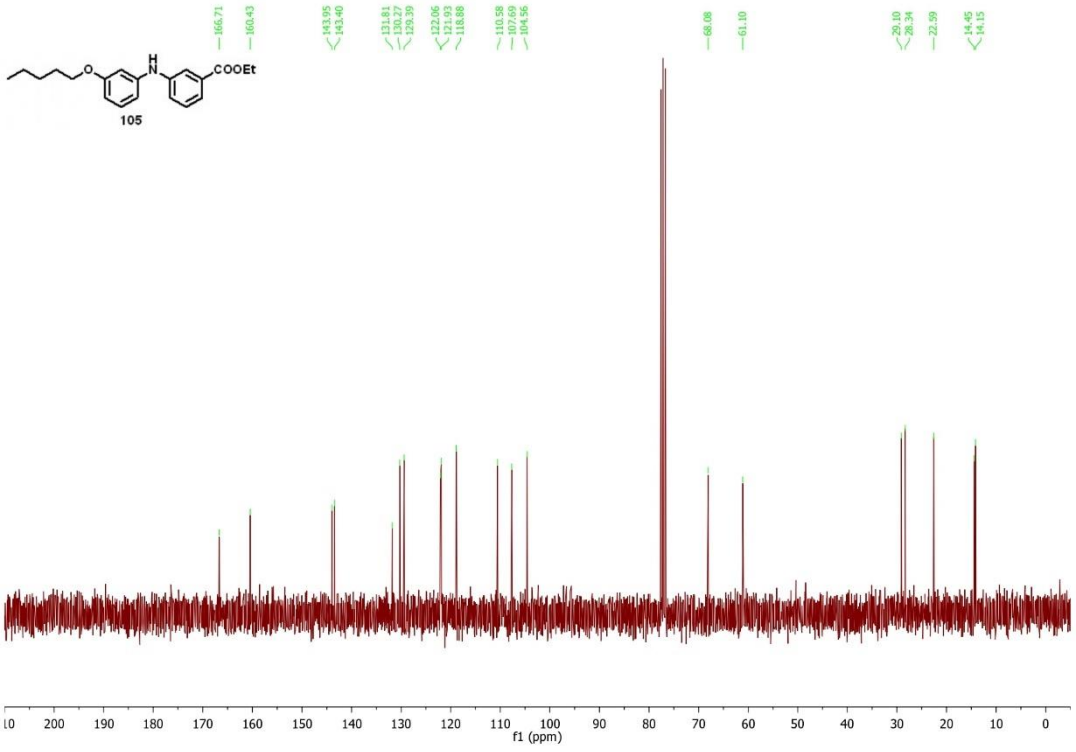
COOEt
105
f1 (ppm)

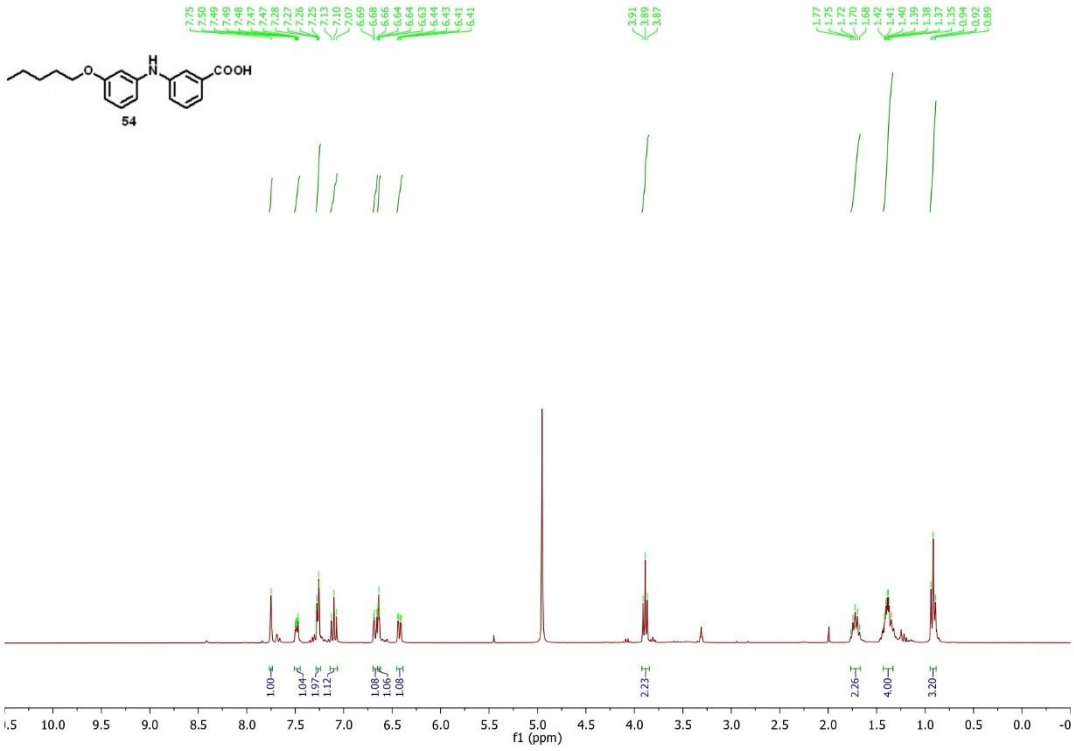
54
COOH
f1 (ppm)

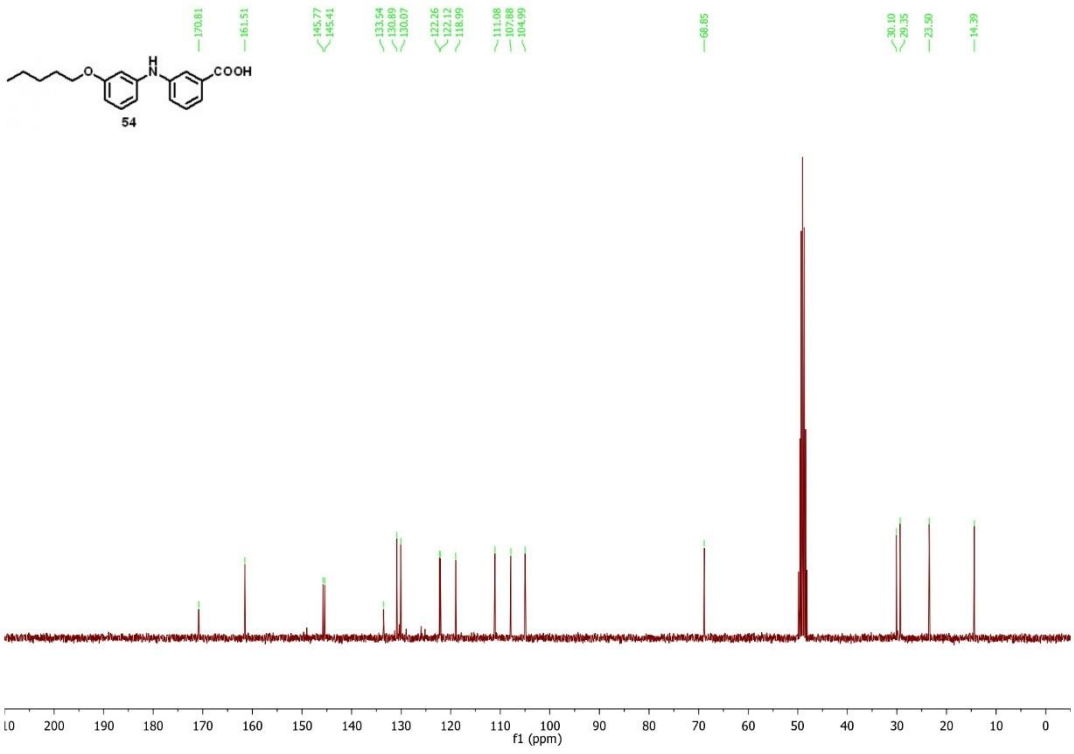
54
COOH
f1 (ppm)

ANNEXE B

RÉSULTATS DES CAMPAGNES DE CRIBLAGE VIRTUEL À HAUT DÉBIT

1. Résultats du criblage virtuel basé sur la librairie combinatoire d'acides 2-aminobenzoïques

Les scores de modélisations et les efficacités de ligand (LE) rapportés sont issus de l'arrimage SP de Glide.

Molécules	Docking score	LE
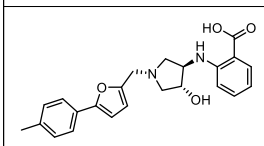	-12,65	-0,4363
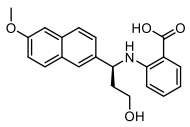	-12,61	-0,4852
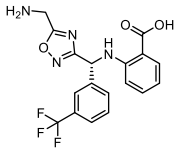	-12,22	-0,4364
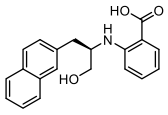	-12,21	-0,5088
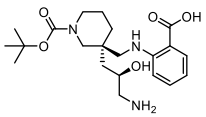	-12,19	-0,4203
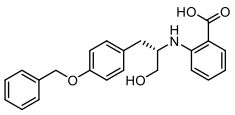	-12,05	-0,4303
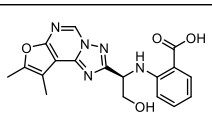	-11,76	-0,4357
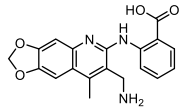	-11,76	-0,4522
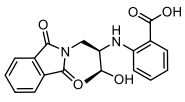	-11,65	-0,4480
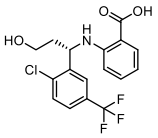	-11,62	-0,4647
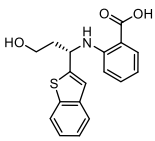	-11,52	-0,5009

Molécules	Docking score	LE
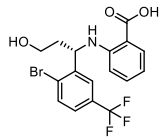	-11,44	-0,4576
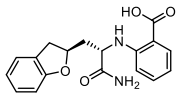	-11,43	-0,4764
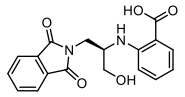	-11,42	-0,4566
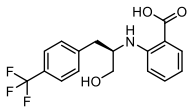	-11,40	-0,4749
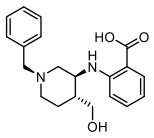	-11,32	-0,4529
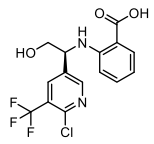	-11,30	-0,4707
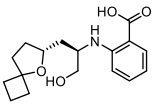	-11,29	-0,5134
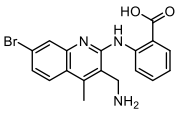	-11,18	-0,4658
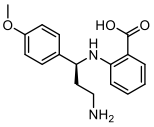	-11,14	-0,5065
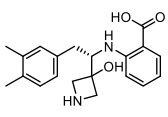	-11,10	-0,4439
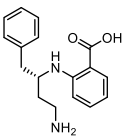	-11,05	-0,5261

Molécules	Docking score	LE
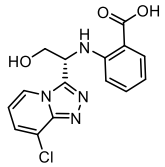	-10,92	-0,4746
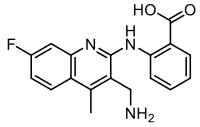	-10,88	-0,4534
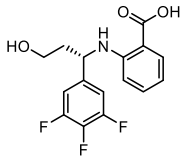	-10,87	-0,4725
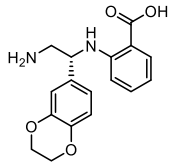	-10,77	-0,4683
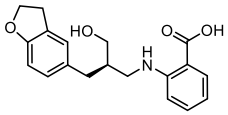	-10,70	-0,4460
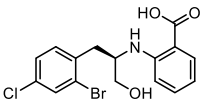	-10,62	-0,4827
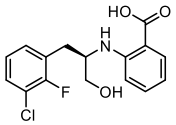	-10,61	-0,4822
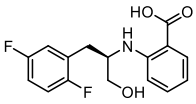	-10,53	-0,4786
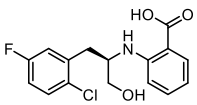	-10,51	-0,4778
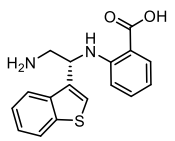	-10,23	-0,4649

2. Résultats du criblage virtuel basé sur les sous-structures de type acide 2-aminobenzoïque

Les scores de modélisations rapportés sont issus de l'arrimage SP de Glide.

Molécules	Docking score
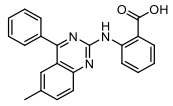	-14.76
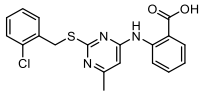	-14.64
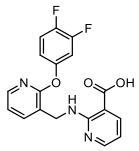	-14.02
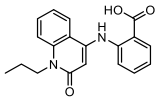	-13.78
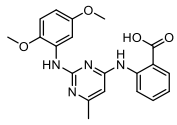	-12.9
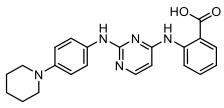	-12.59
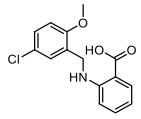	-12.29
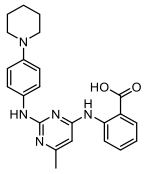	-12.15
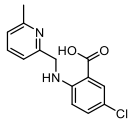	-11.63
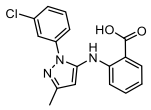	-11.53
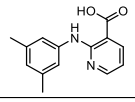	-11.52
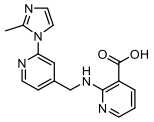	-11.48

Molécules	Docking score
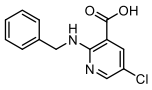	-11.24
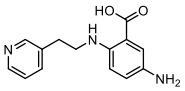	-11.23
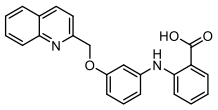	-11.01
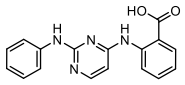	-10.92
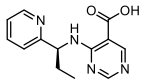	-10.76
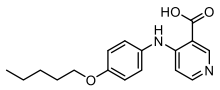	-10.68
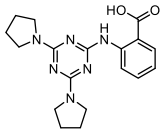	-10.52
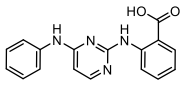	-10.22
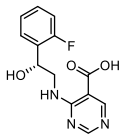	-10.21
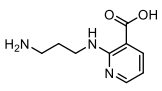	-9.375
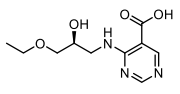	-6.922

ANNEXE C

« DESIGN AND SYNTHESIS OF A POTENT INHIBITOR OF PB1 WITH IMPROVED SELECTIVITY PROFILE OVER SMARCA2. » - PARTIE EXPÉRIMENTALE

Design and Synthesis of LM146, a Potent Inhibitor of PB1 with Improved Selectivity Profile over SMARCA2

Supporting Information

Léa Mélin,† Emily Gesner,§ Sarah Attwell,§ Olesya A. Kharenko,§ Edward H. van der Horst,§ Henrik C. Hansen,§ Alexandre Gagnon*†

† Département de chimie, Université du Québec à Montréal, C.P. 8888, Succ. Centre-Ville, Montréal, Québec, H3C 3P8, Canada

§ Zenith Epigenetics Ltd, Suite 300, 4820 Richard Road SW, Calgary, AB, T3E 6L1, Canad

TABLE OF CONTENT

1. Biological evaluation

a) Protein thermal shift assay (DSF)

N-terminally His-tagged recombinant bromodomains PB1(2) (Reaction Biology RD-11-218), PB1(4) (Reaction Biology RD-11-215), PB1(5) (Reaction Biology RD-11-216), and SMARCA2A (Reaction Biology RD-11-212) were incubated at a concentration of 10 μM with 100 μM of compound at a final DMSO concentration of 0.2% in the presence of 5× SYPRO orange protein stain (Life Technologies S-6650) for 30 min at 25 °C in 50 mM NaCl/50 mM HEPES buffer, pH 7.4. Melt curve experiments were run on an Applied Biosystems ViiA7 real-time PCR instrument. Melting temperatures (T_m) were calculated using Applied Biosystems Protein Thermal Shift Software v1.3. This assay was performed at Zenith Epigenetics Ltd, Calgary, Canada.

b) BromoMAX assay

Protocol description. T7 phage strains displaying bromodomains were grown in parallel in 24-well blocks in an E. coli host derived from the BL21 strain. E. coli were grown to log-phase and infected with T7 phage from a frozen stock (multiplicity of infection = 0.4) and incubated with shaking at 32°C until lysis (90-150 minutes). The lysates were centrifuged (5,000 x g) and filtered (0.2μm) to remove cell debris. Streptavidin-coated magnetic beads were treated with biotinylated small molecule or acetylated peptide ligands for 30 minutes at room temperature to generate affinity resins for bromodomain assays. The liganded beads were blocked with excess biotin and washed with blocking buffer (SeaBlock (Pierce), 1 % BSA, 0.05 % Tween 20, 1 mM DTT) to remove unbound ligand and to reduce non-specific phage binding. Binding reactions were assembled by combining bromodomains, liganded affinity beads, and test compounds in 1x binding buffer (16 % SeaBlock, 0.32x PBS, 0.02%BSA, 0.04 % Tween 20, 0.004% Sodium azide, 7.9 mM DTT). Test compounds were prepared as 1000X stocks in 100% DMSO and subsequently diluted 1:25 in monoethylene glycol (MEG). The compounds were then diluted directly into the assays such that the final concentrations of DMSO and MEG were 0.1% and 2.4%, respectively. All reactions were performed in polypropylene 384-well plates in a final volume of 0.02 ml. The assay plates were incubated at room temperature with shaking for 1 hour and the affinity beads were washed with wash buffer (1x PBS, 0.05% Tween 20). The beads were then re-suspended in elution buffer (1x PBS, 0.05% Tween 20, 2 μM non-biotinylated affinity ligand) and incubated at room temperature with shaking for 30 minutes. The bromodomain concentration in the eluates was measured by qPCR.

%Ctrl Calculation. LM146 was screened at 10 μM, and results for primary screen binding interactions are reported as '% Ctrl', where lower numbers indicate stronger hits in the matrix in **Table S1**.

$$\% \text{ Ctrl} = 100 \text{ x } \frac{test\ compound\ signal - positive\ control\ signal}{negative\ control\ signal - positive\ control\ signal}$$

With test compound = **LM146**, negative control = DMSO (100%Ctrl) and positive control = control compound (0%Ctrl).

Relationship between Binding Constant Distributions (Kds) & Single Concentration Primary Screen Values. Based on screening data from thousands of profiled compounds, a proportional relationship between primary screening results and corresponding compound/target affinities may be described. Evident in the correlation graph below is a range of binding constants (Kd values) for the indicated ranges of POC values with tighter binding (higher affinity) interactions associated with lower POC values and weaker binding (lower affinity) associated with higher POC values. This distribution of binding constants is characteristic of single concentration primary screens and underscores the importance of following up observed 'hits' or apparent high affinity interactions with quantitative binding constant determinations.

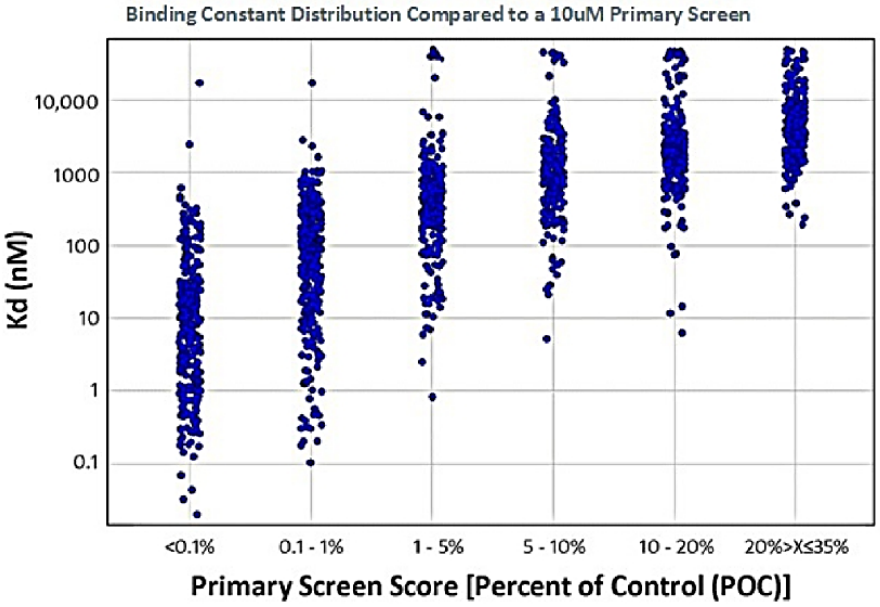

Figure S1. Data correlation between primary screening (10 μM concentration) and binding constants (Kd values). Binding constants are correlated with primary screening results, where lower POC values are associated with low Kd values (higher affinity interactions).

Additional data.

Table S1. Matrix of bromoMAX screen for **LM146** at 10 μM

Target	LM_146
Gene Symbol	%Ctrl @ 10000nM
ATAD2A	88
ATAD2B	78
BAZ2A	91
BAZ2B	88
BRD1	79
BRD2(1)	97
BRD2(2)	83
BRD3(1)	93
BRD3(2)	96
BRD4(1)	86
BRD4(2)	93
BRD7	70
BRD9	69
BRDT(1)	93
BRDT(2)	89
BRPF1	82
BRPF3	94
CECR2	65
CREBBP	70
EP300	89
FALZ	100
GCN5L2	76
PBRM1(2)	0
PBRM1(5)	0.1
PCAF	90
SMARCA2	0
SMARCA4	1.3
TAF1(2)	62
TAF1L(2)	91
TRIM24(PHD,Bromo.)	78
TRIM33(PHD,Bromo.)	100
WDR9(2)	56

%Ctrl Legend

0≤x<.1	1≤x<1	1≤x<10	10≤x<35	x≥35

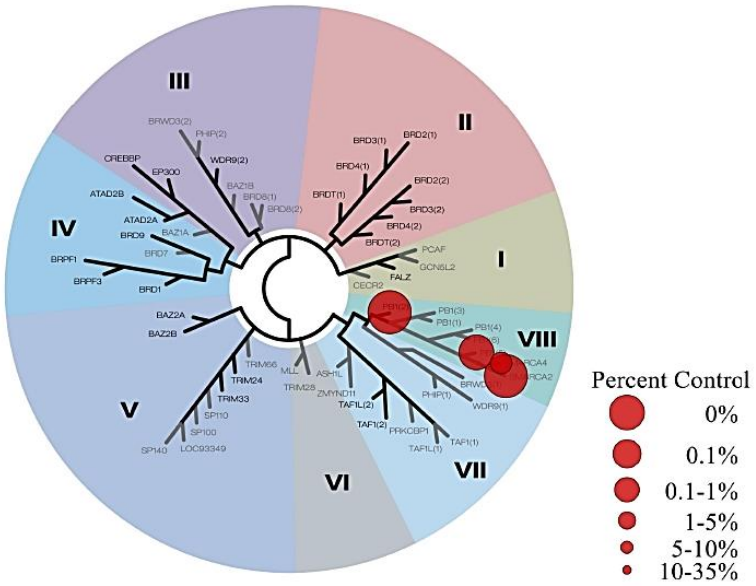

Figure S2. TREEspot™ bromodomain phylogenic tree for **LM146**.

c) BromoK$_d$ELECT assay

Protocol description. T7 phage strains displaying bromodomains were grown in parallel in 24-well blocks in an E. coli host derived from the BL21 strain. E. coli were grown to log-phase and infected with T7 phage from a frozen stock (multiplicity of infection = 0.4) and incubated with shaking at 32°C until lysis (90-150 minutes). The lysates were centrifuged (5,000 x g) and filtered (0.2μm) to remove cell debris. Streptavidin-coated magnetic beads were treated with biotinylated small molecule or acetylated peptide ligands for 30 minutes at room temperature to generate affinity resins for bromodomain assays. The liganded beads were blocked with excess biotin and washed with blocking buffer (SeaBlock (Pierce), 1 % BSA, 0.05 % Tween 20, 1 mM DTT) to remove unbound ligand and to reduce non-specific phage binding. Binding reactions were assembled by combining bromodomains, liganded affinity beads, and test compounds in 1x binding buffer (17% SeaBlock, 0.33x PBS, 0.04% Tween 20, 0.02% BSA, 0.004% Sodium azide, 7.4 mM DTT). Test compounds were prepared as 1000X stocks in 100% DMSO. Kds were determined using an 11-point 3-fold compound dilution series with one DMSO control point. All compounds for Kd measurements are distributed by acoustic transfer (non-contact dispensing) in 100% DMSO. The compounds were then diluted directly into the assays such that the final concentration of DMSO was 0.09%. All reactions performed in polypropylene 384-well plates. Each was a final volume of 0.02 ml. The assay plates were incubated at room temperature with shaking for 1 hour and the affinity beads were washed with wash buffer (1x PBS, 0.05% Tween 20). The beads were then re-suspended in elution buffer (1x PBS, 0.05% Tween 20, 2 μM non-biotinylated affinity ligand) and incubated at room temperature with shaking for 30 minutes. The bromodomain concentration in the eluates was measured by qPCR. This assay was performed at Eurofins DiscoverX, San Diego, USA.

Compound handling. An 11-point 3-fold serial dilution of each test compound was prepared in 100% DMSO at 1000x final test concentration. All compounds for Kd measurements are distributed by acoustic transfer (non-contact dispensing) in 100% DMSO. The compounds were then diluted directly into the assays such that the final concentration of DMSO was 0.09%. Most Kds were determined using a compound top concentration = 10,000 nM. If the initial Kd determined was < 0.169 nM (the lowest concentration tested), the measurement was repeated with a serial dilution starting at a lower top concentration.

Binding constants (Kds). Binding constants (Kds) were calculated with a standard dose-response curve using the Hill equation:

$$\text{Response} = \text{Background} + \frac{\text{Signal} - \text{Background}}{1 + \frac{\text{Kd(Hill Slope)}}{\text{Dose(Hill Slope)}}}$$

The Hill Slope was set to -1. Curves were fitted using a non-linear least square fit with the Levenberg-Marquardt algorithm.

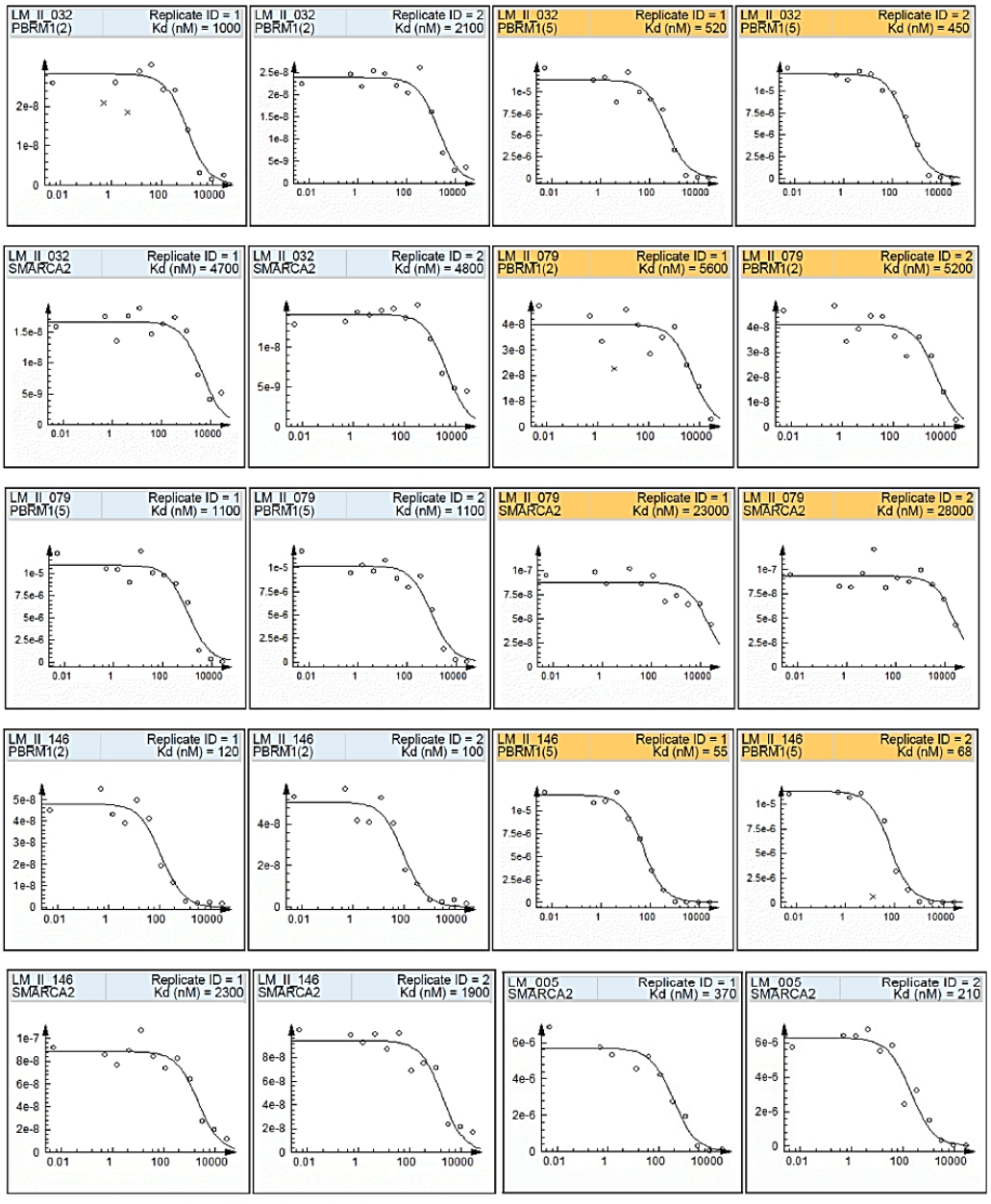

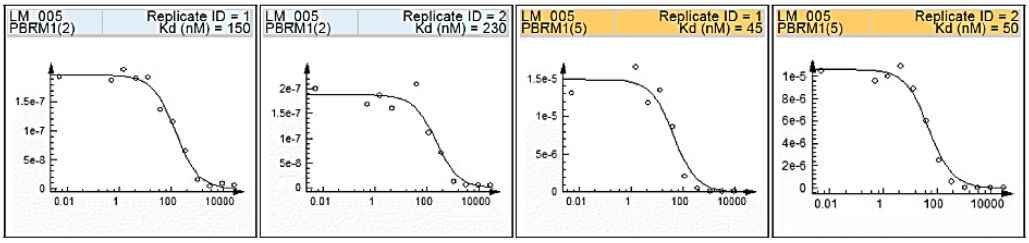

Figure S3. Additional Curve Images. The amount of bromodomain measured by qPCR (Signal; y-axis) is plotted against the corresponding compound concentration in nM in log10 scale (x-axis). Data points marked with an "x" were not used for Kd determination. LM_II_032 stands for compound **18**, LM_II_079 = compound **21**, LM_II_146 = **24** = **LM146** and LM_005 = **3**.

2. X-ray analysis

Protocol description. The data for **LM146**, crystallized from chloroform, were collected from a shock-cooled single crystal at 150 K on a Bruker Venture Metaljet κ-geometry diffractometer with a Metal Jet using Helios MX Mirror Optics as monochromator and a Bruker CMOS Photon III detector. The diffractometer was equipped with an Oxford Cryostream 700 low temperature device and used Ga *Kα* radiation (λ = 1.34139 Å). All data were integrated with SAINT and a multi-scan absorption correction using TWINABS was applied. The structure was solved by dual methods using XT and refined by full-matrix least-squares methods against F^2 by XL. Structure solution and refinement were performed within the graphical User Interface of OLEX2. All non-hydrogen atoms were refined with anisotropic displacement parameters. The hydrogen atoms were refined isotropically on calculated positions using a riding model with their U_{iso} values constrained to 1.5 times the U_{eq} of their pivot atoms for terminal sp^3 carbon atoms and 1.2 times for all other carbon atoms. Disordered moieties were refined using bond lengths restraints and displacement parameter restraints. This report and the CIF file were generated using FinalCif. The crystal structure was deposited in the Cambridge Crystallographic Data Centre CCDC (number 2070470).

Additional data.

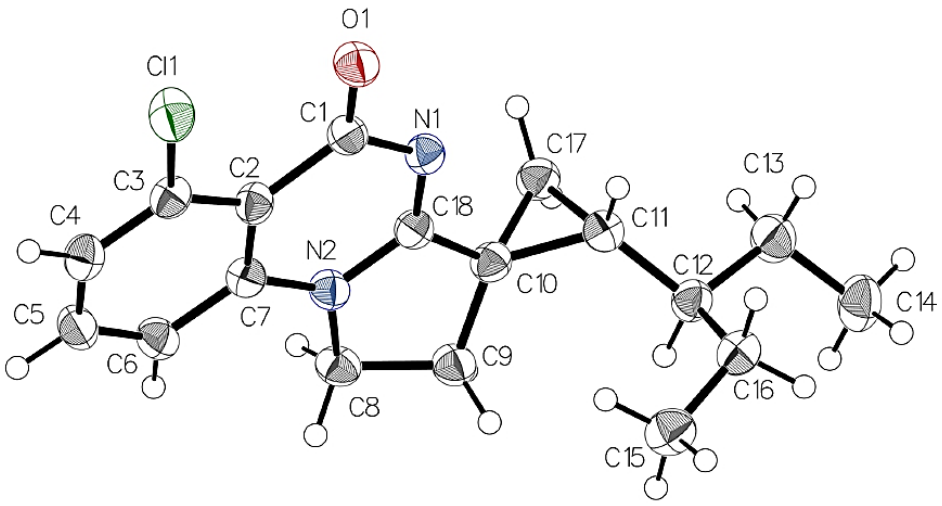

Figure S4. Thermal atomic displacement ellipsoid plot (Ortep) for LM146. Ellipsoids are drawn at the 50% probability level and hydrogen atoms are shown as spheres of arbitrary size. Cambridge Crystallographic Data Centre CCDC number 2070470.

Table S2. Crystal data and structure refinement for **LM146**

Empirical formula	$C_{18}H_{21}ClN_2O$
Formula weight	316.82
Temperature [K]	150
Crystal system	monoclinic
Space group (number)	$P2_1/c$ (14)
a [Å]	24.3485(10)
b [Å]	8.5492(3)
c [Å]	7.4732(3)
α [°]	90
β [°]	94.710(2)
γ [°]	90
Volume [Å^3]	1550.37(10)
Z	4
ρ_{calc} [g/cm^3]	1.357
μ [mm^{-1}]	1.449
F(000)	672
Crystal size [mm^3]	0.27×0.08×0.04
Crystal color	clear light colorless
Crystal shape	plate
Radiation	Ga K_α (λ=1.34139 Å)
2Θ range [°]	6.34 to 121.31 (0.77 Å)
Index ranges	0 ≤ h ≤ 31
	0 ≤ k ≤ 11
	-9 ≤ l ≤ 9
Reflections collected	3545
Independent reflections	3545
	R_{int} = 0.0755
	R_{sigma} = 0.0463
Completeness to θ = 53.594°	99.5 %
Data / Restraints / Parameters	3545/0/202
Goodness-of-fit on F^2	1.035
Final *R* indexes [$I \geq 2\sigma(I)$]	R_1 = 0.0580
	wR_2 = 0.1636
Final *R* indexes [all data]	R_1 = 0.0648
	wR_2 = 0.1735
Largest peak/hole [eÅ^3]	0.65/-0.29

Table S3. Atomic coordinates and U_{eq} [Å^2] for **LM146**

Atom	*x*	*y*	*z*	U_{eq}
Cl1	0.90977(3)	-0.08631(7)	0.53827(12)	0.0433(2)
O1	0.80626(8)	-0.0153(2)	0.3434(3)	0.0373(5)
N1	0.76591(8)	0.2230(2)	0.3167(3)	0.0294(5)
N2	0.81603(8)	0.4465(3)	0.4192(3)	0.0290(4)
C1	0.80971(10)	0.1255(3)	0.3711(4)	0.0293(5)
C2	0.86032(10)	0.1992(3)	0.4630(4)	0.0291(5)
C3	0.90749(10)	0.1167(3)	0.5330(4)	0.0301(5)
C4	0.95419(10)	0.1924(3)	0.6040(4)	0.0338(6)
H4	0.985416	0.133772	0.649495	0.041
C5	0.95560(10)	0.3554(3)	0.6091(4)	0.0348(6)
H5	0.988148	0.407422	0.655902	0.042
C6	0.91040(10)	0.4415(3)	0.5470(4)	0.0329(5)
H6	0.911306	0.552535	0.551994	0.039
C7	0.86282(10)	0.3632(3)	0.4762(4)	0.0294(5)
C8	0.80931(10)	0.6182(3)	0.4292(4)	0.0318(5)
H8A	0.828537	0.671743	0.334888	0.038
H8B	0.823391	0.658861	0.548262	0.038
C9	0.74669(10)	0.6387(3)	0.3982(4)	0.0336(6)
H9A	0.729941	0.650614	0.513787	0.040
H9B	0.737387	0.731539	0.322622	0.040
C10	0.72677(10)	0.4900(3)	0.3033(4)	0.0296(5)
C11	0.66688(10)	0.4392(3)	0.2733(4)	0.0310(5)
H11	0.661070	0.323802	0.282636	0.037
C12	0.61972(10)	0.5372(3)	0.3310(4)	0.0314(5)
H12	0.633418	0.646157	0.354062	0.038
C13	0.57303(12)	0.5425(4)	0.1791(4)	0.0422(7)
H13A	0.588803	0.573807	0.066486	0.051
H13B	0.557656	0.435953	0.161186	0.051
C14	0.52622(12)	0.6544(4)	0.2132(5)	0.0467(7)
H14A	0.500691	0.661544	0.105130	0.070
H14B	0.541386	0.758203	0.243173	0.070
H14C	0.506519	0.615313	0.313334	0.070
C15	0.63886(13)	0.4934(4)	0.6690(4)	0.0408(7)
H15A	0.673741	0.441229	0.649927	0.061
H15B	0.623074	0.447041	0.773287	0.061
H15C	0.645523	0.605075	0.690639	0.061
C16	0.59922(11)	0.4729(4)	0.5049(4)	0.0373(6)
H16A	0.564160	0.525662	0.526302	0.045
H16B	0.591279	0.360002	0.488605	0.045
C17	0.69778(10)	0.4882(3)	0.1154(4)	0.0337(6)
H17A	0.688129	0.590170	0.058336	0.040
H17B	0.708272	0.405627	0.031918	0.040
C18	0.77040(9)	0.3723(3)	0.3465(3)	0.0274(5)

Table S4. Bond lengths and angles for **LM146**

Atom–Atom	Length [Å]
Cl1–C3	1.737(3)
O1–C1	1.223(3)
N1–C1	1.388(3)
N1–C18	1.298(3)
N2–C7	1.381(3)
N2–C8	1.479(3)

N2–C18	1.354(3)
C1–C2	1.499(3)
C2–C3	1.411(3)
C2–C7	1.407(4)
C3–C4	1.377(4)
C4–H4	0.9500
C4–C5	1.394(4)
C5–H5	0.9500
C5–C6	1.372(4)
C6–H6	0.9500
C6–C7	1.404(3)
C8–H8A	0.9900
C8–H8B	0.9900
C8–C9	1.533(3)
C9–H9A	0.9900
C9–H9B	0.9900
C9–C10	1.515(4)
C10–C11	1.520(3)
C10–C17	1.519(4)
C10–C18	1.480(3)
C11–H11	1.0000
C11–C12	1.512(4)
C11–C17	1.509(4)
C12–H12	1.0000
C12–C13	1.540(4)
C12–C16	1.532(4)
C13–H13A	0.9900
C13–H13B	0.9900
C13–C14	1.525(4)
C14–H14A	0.9800
C14–H14B	0.9800
C14–H14C	0.9800
C15–H15A	0.9800
C15–H15B	0.9800
C15–H15C	0.9800
C15–C16	1.507(4)
C16–H16A	0.9900
C16–H16B	0.9900
C17–H17A	0.9900
C17–H17B	0.9900

Atom–Atom–Atom	**Angle [°]**
C18–N1–C1	119.2(2)
C7–N2–C8	126.0(2)
C18–N2–C7	120.7(2)
C18–N2–C8	113.3(2)
O1–C1–N1	120.1(2)
O1–C1–C2	122.2(2)
N1–C1–C2	117.7(2)
C3–C2–C1	125.0(2)
C7–C2–C1	118.7(2)
C7–C2–C3	116.3(2)
C2–C3–Cl1	122.08(19)
C4–C3–Cl1	115.95(19)
C4–C3–C2	122.0(2)
C3–C4–H4	120.1
C3–C4–C5	119.9(2)

C5–C4–H4	120.1
C4–C5–H5	119.7
C6–C5–C4	120.6(2)
C6–C5–H5	119.7
C5–C6–H6	120.5
C5–C6–C7	119.1(2)
C7–C6–H6	120.5
N2–C7–C2	117.6(2)
N2–C7–C6	120.3(2)
C6–C7–C2	122.1(2)
N2–C8–H8A	111.2
N2–C8–H8B	111.2
N2–C8–C9	102.63(19)
H8A–C8–H8B	109.2
C9–C8–H8A	111.2
C9–C8–H8B	111.2
C8–C9–H9A	110.8
C8–C9–H9B	110.8
H9A–C9–H9B	108.9
C10–C9–C8	104.5(2)
C10–C9–H9A	110.8
C10–C9–H9B	110.8
C9–C10–C11	125.1(2)
C9–C10–C17	123.2(2)
C17–C10–C11	59.56(17)
C18–C10–C9	105.8(2)
C18–C10–C11	120.0(2)
C18–C10–C17	117.8(2)
C10–C11–H11	114.3
C12–C11–C10	122.8(2)
C12–C11–H11	114.3
C17–C11–C10	60.17(17)
C17–C11–H11	114.3
C17–C11–C12	120.5(2)
C11–C12–H12	108.4
C11–C12–C13	109.8(2)
C11–C12–C16	110.6(2)
C13–C12–H12	108.4
C16–C12–H12	108.4
C16–C12–C13	111.3(2)
C12–C13–H13A	108.7
C12–C13–H13B	108.7
H13A–C13–H13B	107.6
C14–C13–C12	114.3(3)
C14–C13–H13A	108.7
C14–C13–H13B	108.7
C13–C14–H14A	109.5
C13–C14–H14B	109.5
C13–C14–H14C	109.5
H14A–C14–H14B	109.5
H14A–C14–H14C	109.5
H14B–C14–H14C	109.5
H15A–C15–H15B	109.5
H15A–C15–H15C	109.5
H15B–C15–H15C	109.5
C16–C15–H15A	109.5
C16–C15–H15B	109.5

C16–C15–H15C	109.5
C12–C16–H16A	108.6
C12–C16–H16B	108.6
C15–C16–C12	114.7(2)
C15–C16–H16A	108.6
C15–C16–H16B	108.6
H16A–C16–H16B	107.6
C10–C17–H17A	117.7
C10–C17–H17B	117.7
C11–C17–C10	60.27(17)
C11–C17–H17A	117.7
C11–C17–H17B	117.7
H17A–C17–H17B	114.9
N1–C18–N2	125.8(2)
N1–C18–C10	125.6(2)
N2–C18–C10	108.6(2)

Table S5. Torsion angles for **LM146**

Atom–Atom–Atom–Atom	Torsion Angle [°]
Cl1–C3–C4–C5	−178.6(2)
O1–C1–C2–C3	−2.8(4)
O1–C1–C2–C7	174.7(3)
N1–C1–C2–C3	177.3(3)
N1–C1–C2–C7	−5.2(4)
N2–C8–C9–C10	−21.7(3)
C1–N1–C18–N2	3.9(4)
C1–N1–C18–C10	−177.4(2)
C1–C2–C3–Cl1	−6.0(4)
C1–C2–C3–C4	175.1(3)
C1–C2–C7–N2	6.4(4)
C1–C2–C7–C6	−174.7(3)
C2–C3–C4–C5	0.4(4)
C3–C2–C7–N2	−176.0(2)
C3–C2–C7–C6	2.9(4)
C3–C4–C5–C6	1.3(4)
C4–C5–C6–C7	−0.8(4)
C5–C6–C7–N2	177.5(3)
C5–C6–C7–C2	−1.4(4)
C7–N2–C8–C9	−164.9(3)
C7–N2–C18–N1	−2.7(4)
C7–N2–C18–C10	178.4(2)
C7–C2–C3–Cl1	176.5(2)
C7–C2–C3–C4	−2.4(4)
C8–N2–C7–C2	177.1(2)
C8–N2–C7–C6	−1.8(4)
C8–N2–C18–N1	177.5(2)
C8–N2–C18–C10	−1.4(3)
C8–C9–C10–C11	168.1(3)
C8–C9–C10–C17	−118.1(3)
C8–C9–C10–C18	21.6(3)
C9–C10–C11–C12	2.2(4)
C9–C10–C11–C17	111.3(3)
C9–C10–C17–C11	−114.3(3)
C9–C10–C18–N1	168.0(3)
C9–C10–C18–N2	−13.1(3)

C10–C11–C12–C13	134.9(3)
C10–C11–C12–C16	−101.9(3)
C11–C10–C18–N1	19.5(4)
C11–C10–C18–N2	−161.7(2)
C11–C12–C13–C14	−172.9(3)
C11–C12–C16–C15	69.3(3)
C12–C11–C17–C10	112.7(3)
C13–C12–C16–C15	−168.4(3)
C16–C12–C13–C14	64.4(3)
C17–C10–C11–C12	−109.1(3)
C17–C10–C18–N1	−49.6(4)
C17–C10–C18–N2	129.3(2)
C17–C11–C12–C13	62.8(3)
C17–C11–C12–C16	−174.0(2)
C18–N1–C1–O1	−179.7(3)
C18–N1–C1–C2	0.2(4)
C18–N2–C7–C2	−2.7(4)
C18–N2–C7–C6	178.3(3)
C18–N2–C8–C9	14.9(3)
C18–C10–C11–C12	144.4(3)
C18–C10–C11–C17	−106.5(3)
C18–C10–C17–C11	110.3(3)

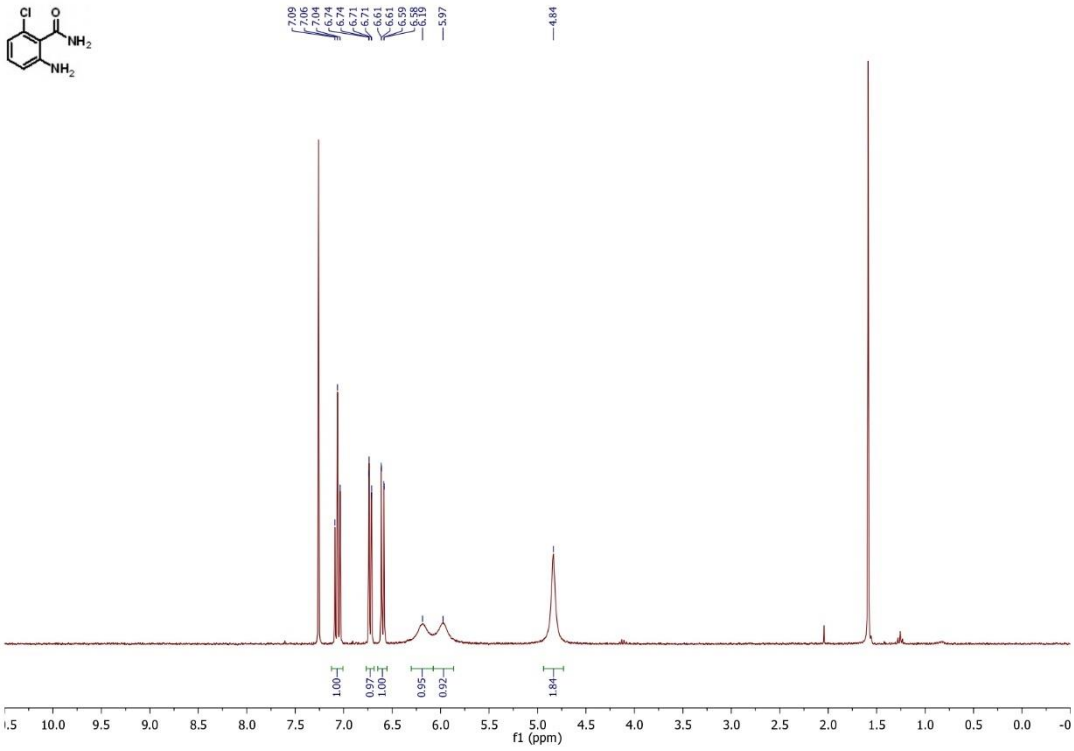
Cl
O
NH2
NH2
7.09
7.06
7.04
6.74
6.71
6.61
6.61
6.59
6.58
6.55
5.97
4.84
1.00
0.97
1.00
0.95
0.92
1.84
f1 (ppm)

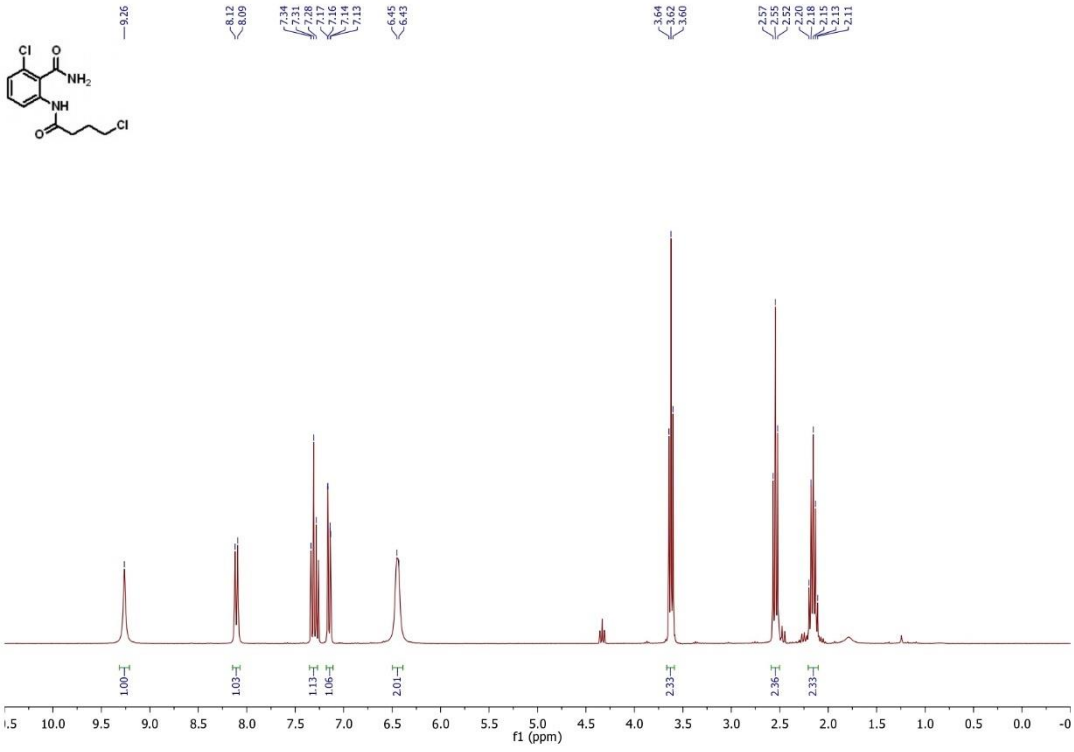
9.26
8.12
8.09
7.34
7.31
7.28
7.17
7.16
7.14
7.13
6.45
6.43
3.64
3.62
3.60
2.57
2.55
2.52
2.20
2.18
2.15
2.13
2.11
Cl
O
NH2
NH
O
Cl
1.00
1.03
1.13
1.06
2.01
2.33
2.36
2.33
f1 (ppm)

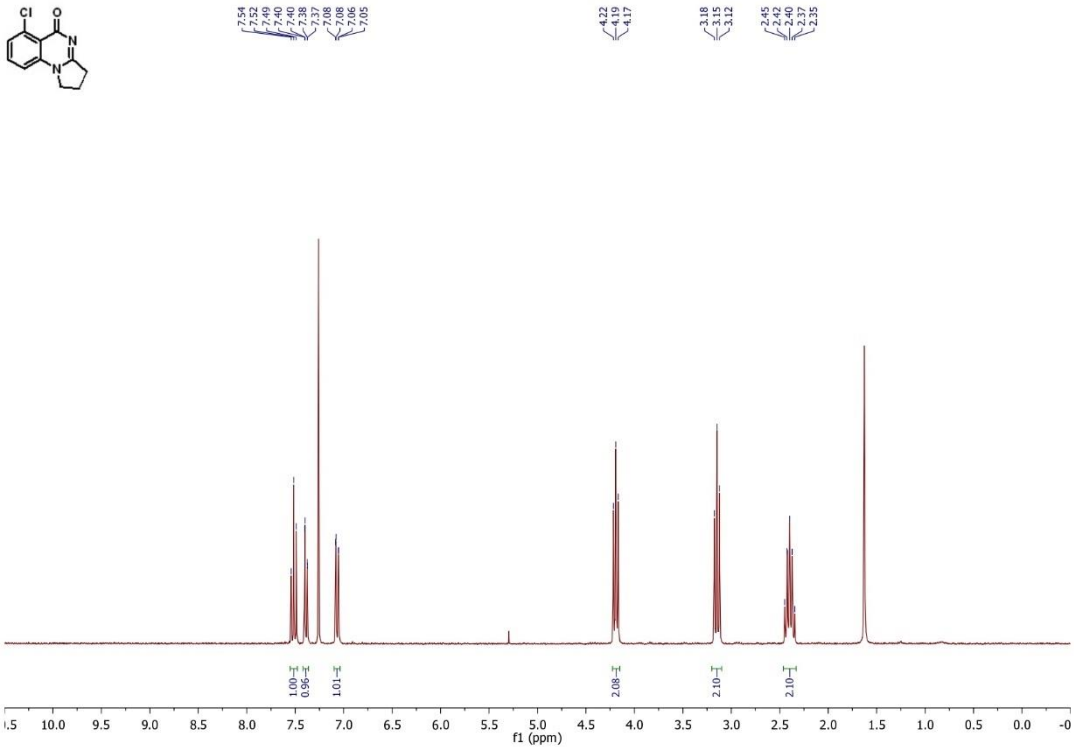
Cl
O
N
7.54
7.52
7.49
7.40
7.40
7.38
7.37
7.08
7.06
7.05
4.22
4.19
4.17
3.18
3.15
3.12
2.45
2.42
2.40
2.37
2.35
1.00
0.96
1.01
2.08
2.10
2.10
f1 (ppm)

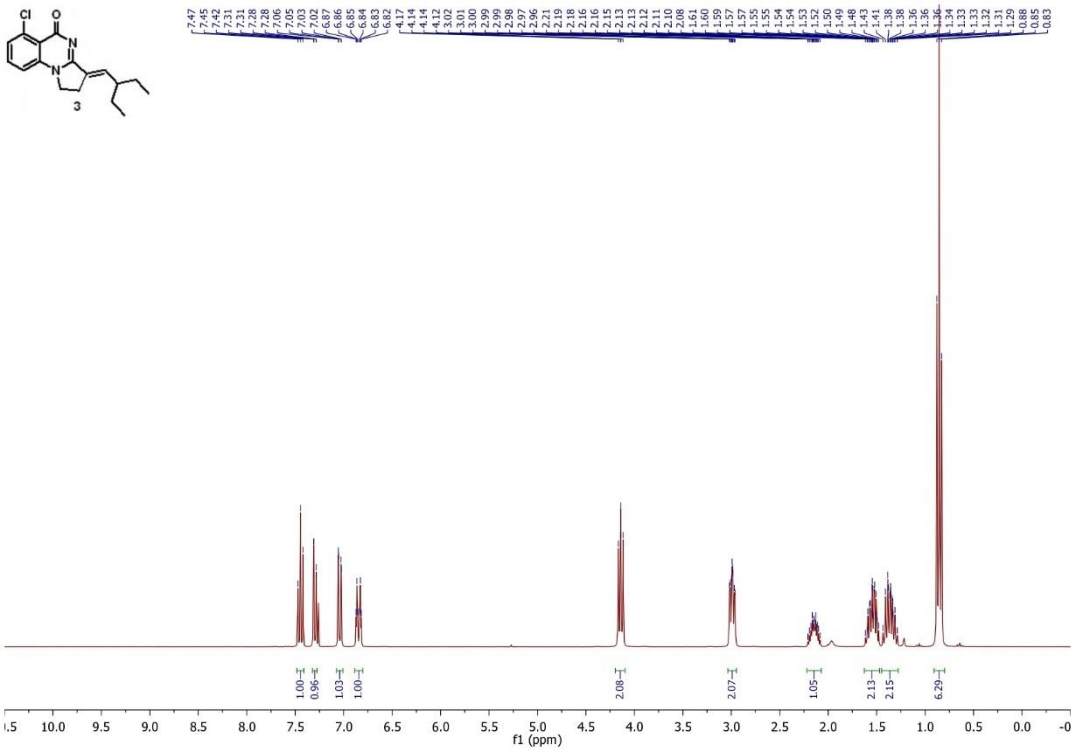
Cl
O
N
3
1.00
0.96
1.03
1.00
2.08
2.07
1.05
2.13
2.15
6.29
f1 (ppm)

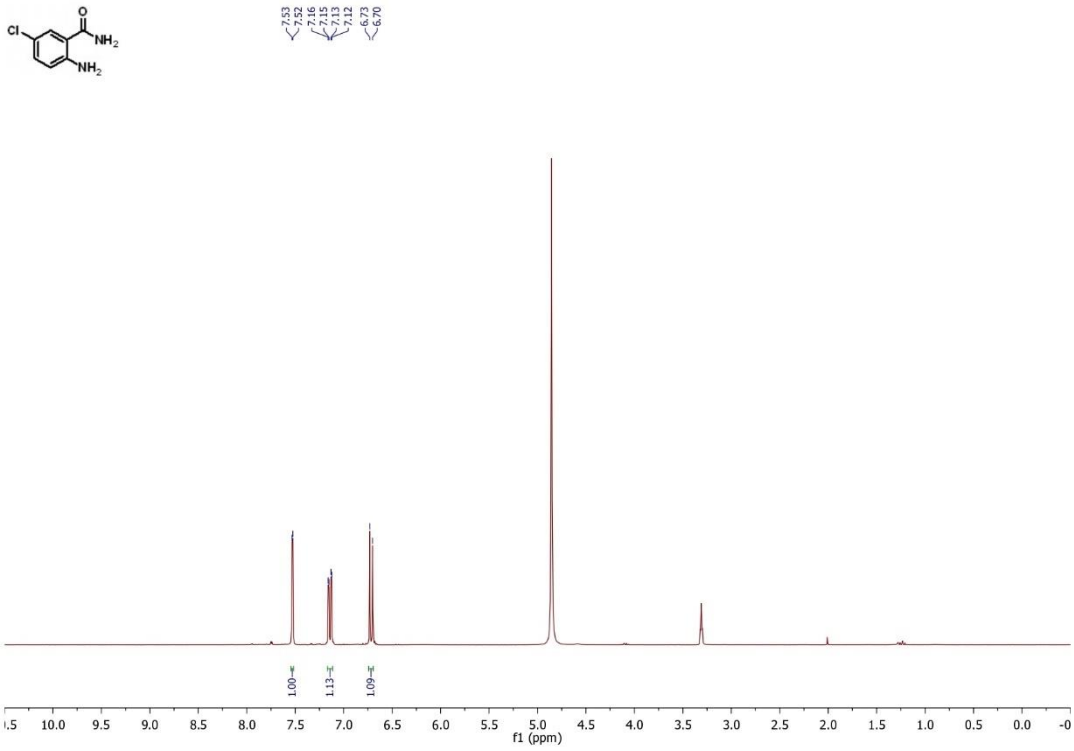
7.53
7.52
7.16
7.15
7.13
7.12
6.73
6.70
1.00
1.13
1.09
f1 (ppm)

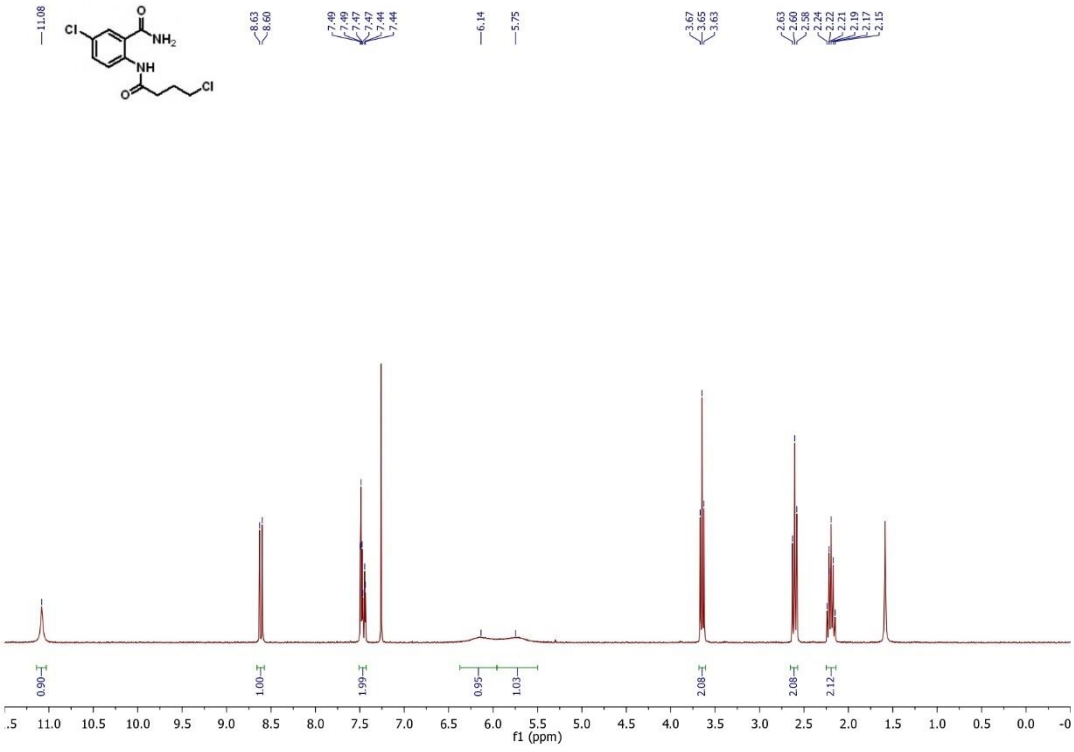
11.08
8.63
8.60
7.49
7.49
7.47
7.47
7.44
7.44
6.14
5.75
3.67
3.65
3.63
2.63
2.60
2.58
2.24
2.22
2.21
2.19
2.17
2.15
0.90
1.00
1.99
0.95
1.03
2.08
2.08
2.12
f1 (ppm)

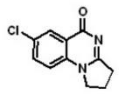

8.20
8.19
7.65
7.64
7.62
7.61
7.16
7.13
4.26
4.24
4.22
3.22
3.20
3.17
2.47
2.45
2.42
2.42
2.40
2.37
0.90
1.18
1.00
2.08
2.07
2.34
f1 (ppm)

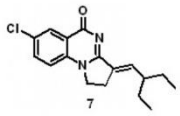
7

8.19
8.18
7.58
7.57
7.55
7.54
7.15
7.13
6.92
6.91
6.90
6.89
6.88
6.87
0.85
0.96
1.00
0.95
1.99
1.98
1.07
2.10
2.14
6.14
f1 (ppm)

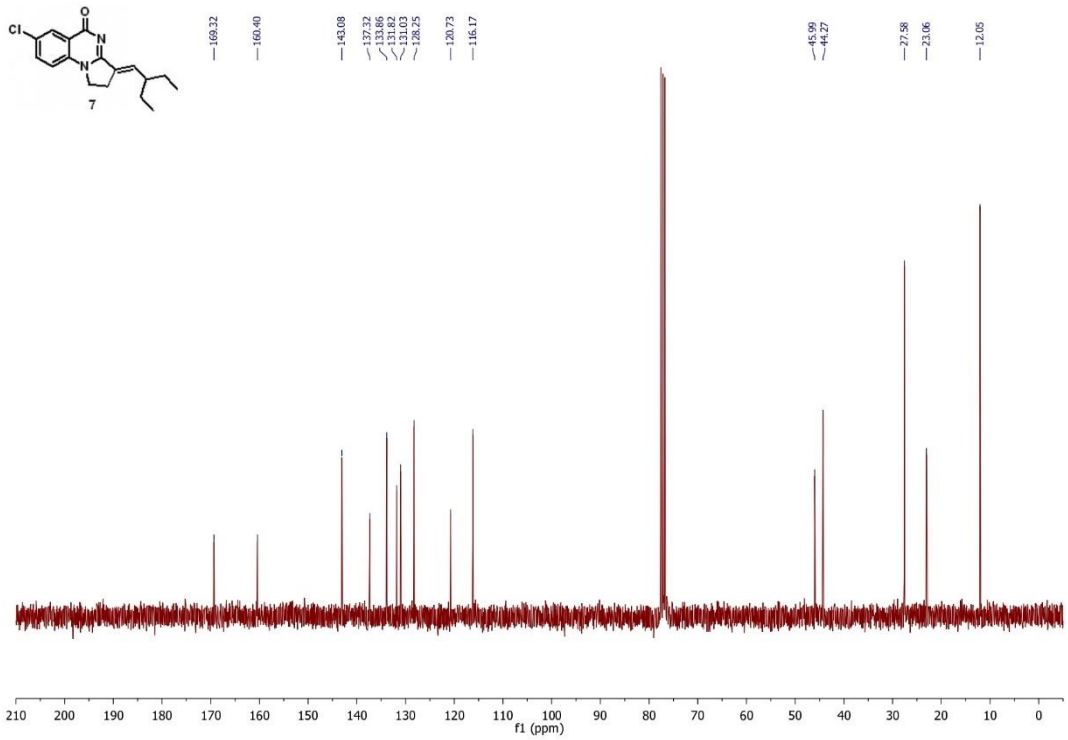
Cl
O
N
N
7
169.32
160.40
143.08
137.32
133.86
131.82
131.03
128.25
120.73
116.17
45.99
44.27
27.58
23.06
12.05
210 200 190 180 170 160 150 140 130 120 110 100 90 80 70 60 50 40 30 20 10 0
f1 (ppm)

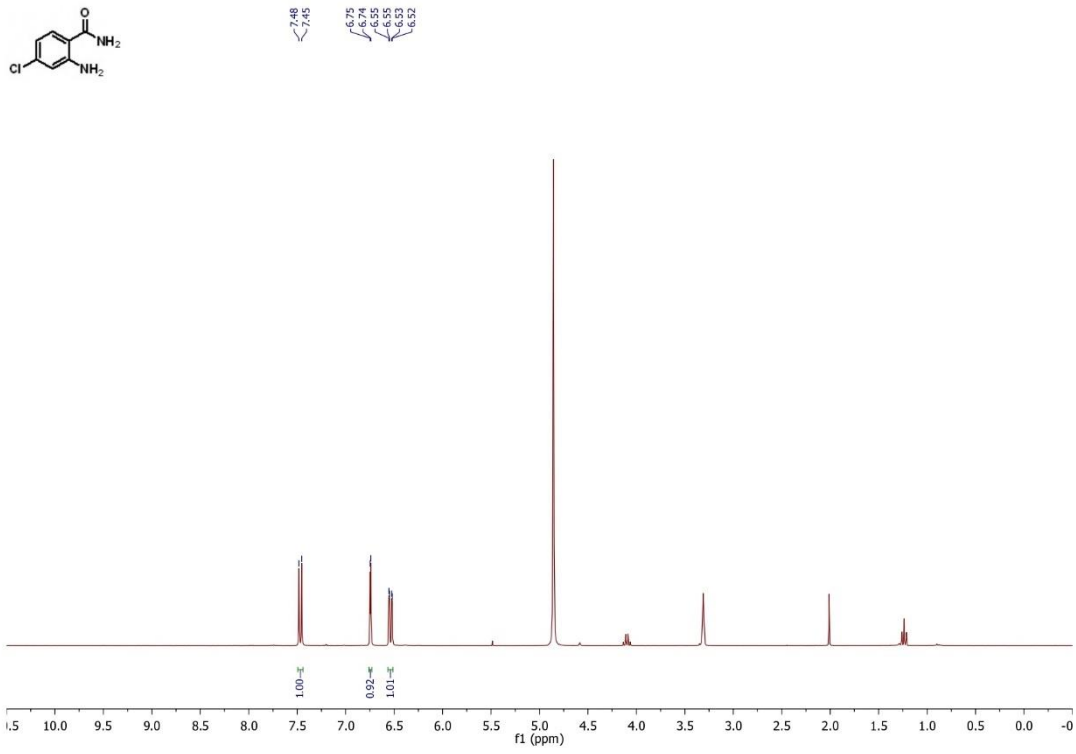
O
NH2
Cl
NH2
7.48
7.45
6.75
6.74
6.55
6.55
6.53
6.52
1.00
0.92
1.01
10.0 9.5 9.0 8.5 8.0 7.5 7.0 6.5 6.0 5.5 5.0 4.5 4.0 3.5 3.0 2.5 2.0 1.5 1.0 0.5 0.0 -0
f1 (ppm)

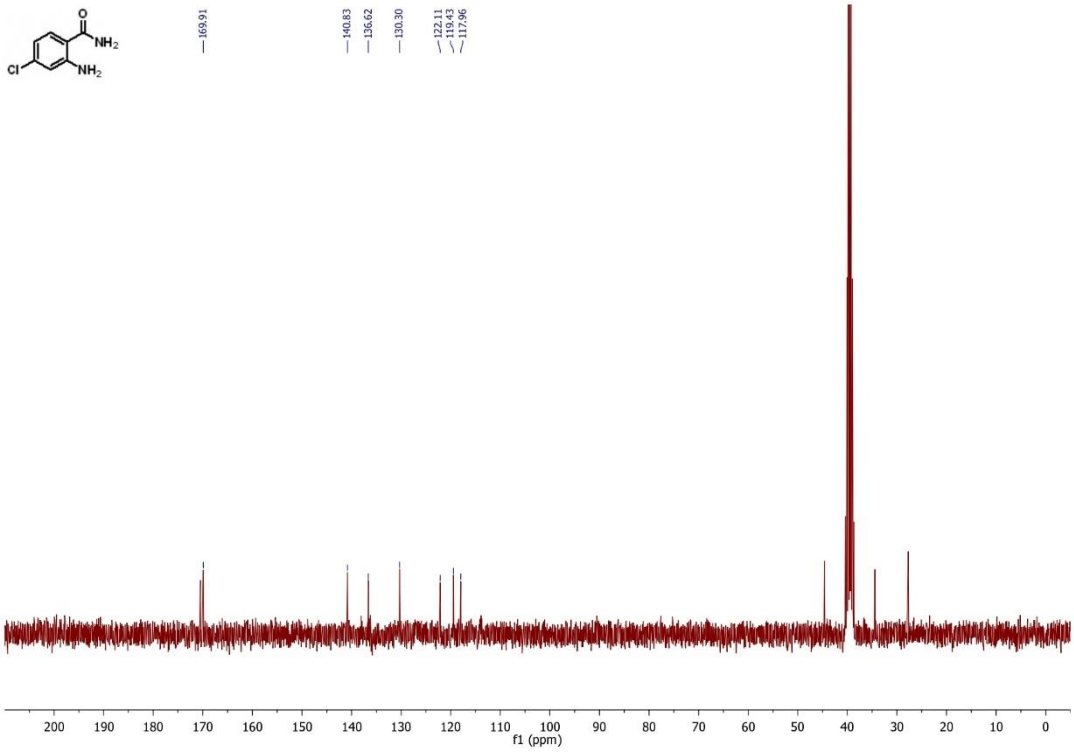
O
NH2
Cl
NH2
169.91
140.83
136.62
130.30
122.11
119.43
117.96
200 190 180 170 160 150 140 130 120 110 100 90 80 70 60 50 40 30 20 10 0
f1 (ppm)

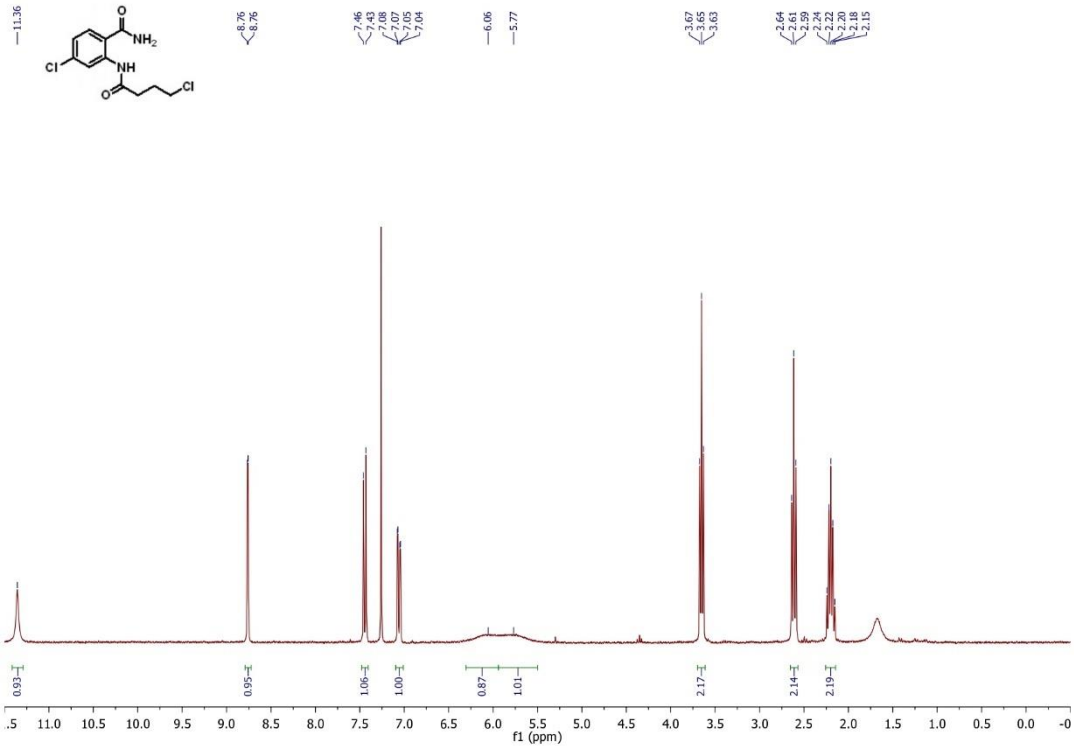
11.36
O
NH2
Cl
NH
O
Cl
8.76
8.76
7.46
7.43
7.08
7.07
7.05
7.04
6.06
5.77
3.67
3.65
3.63
2.64
2.61
2.59
2.24
2.22
2.20
2.18
2.15
0.93
0.95
1.06
1.00
0.87
1.01
2.17
2.14
2.19
11.0 10.5 10.0 9.5 9.0 8.5 8.0 7.5 7.0 6.5 6.0 5.5 5.0 4.5 4.0 3.5 3.0 2.5 2.0 1.5 1.0 0.5 0.0
f1 (ppm)

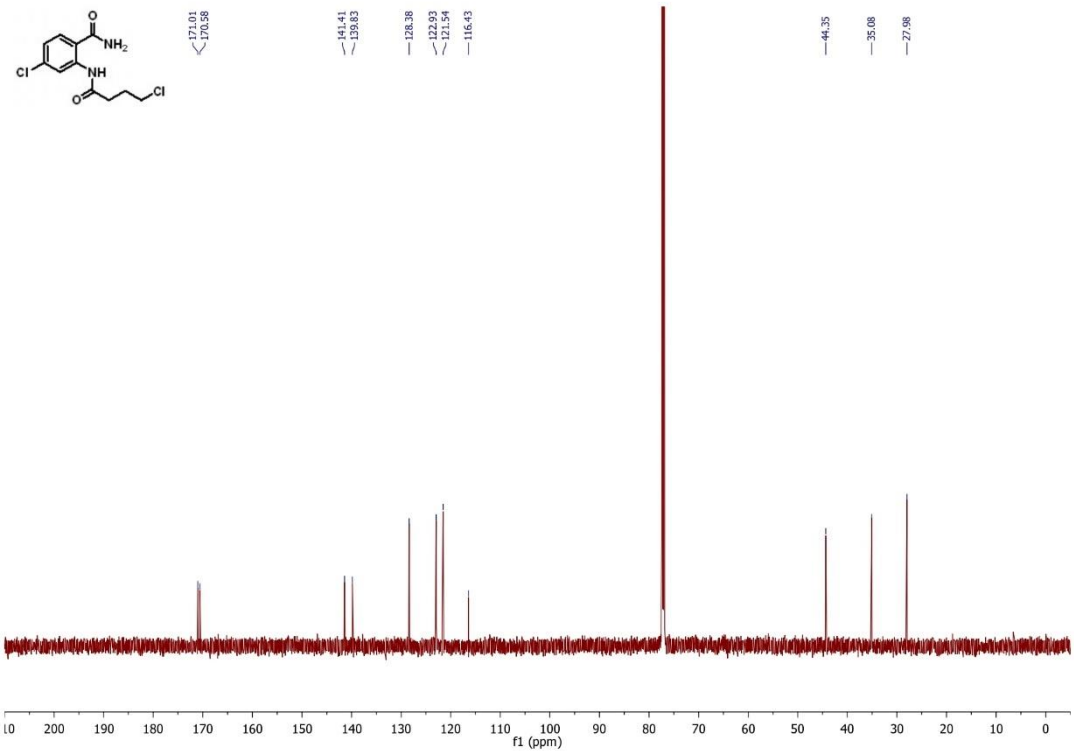
171.01
170.58
141.41
139.83
128.38
122.93
121.54
116.43
44.35
35.08
27.98
f1 (ppm)

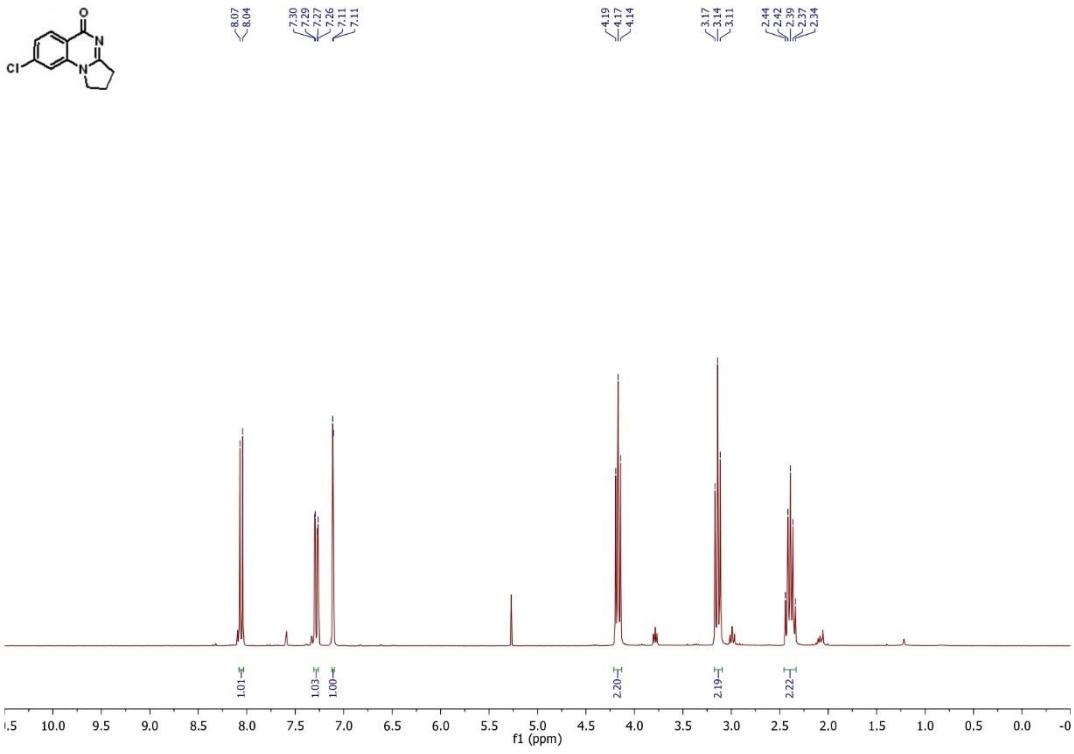
8.07
8.04
7.30
7.29
7.27
7.26
7.11
7.11
4.19
4.17
4.14
3.17
3.14
3.11
2.44
2.42
2.39
2.37
2.34
1.01
1.03
1.00
2.20
2.19
2.22
f1 (ppm)

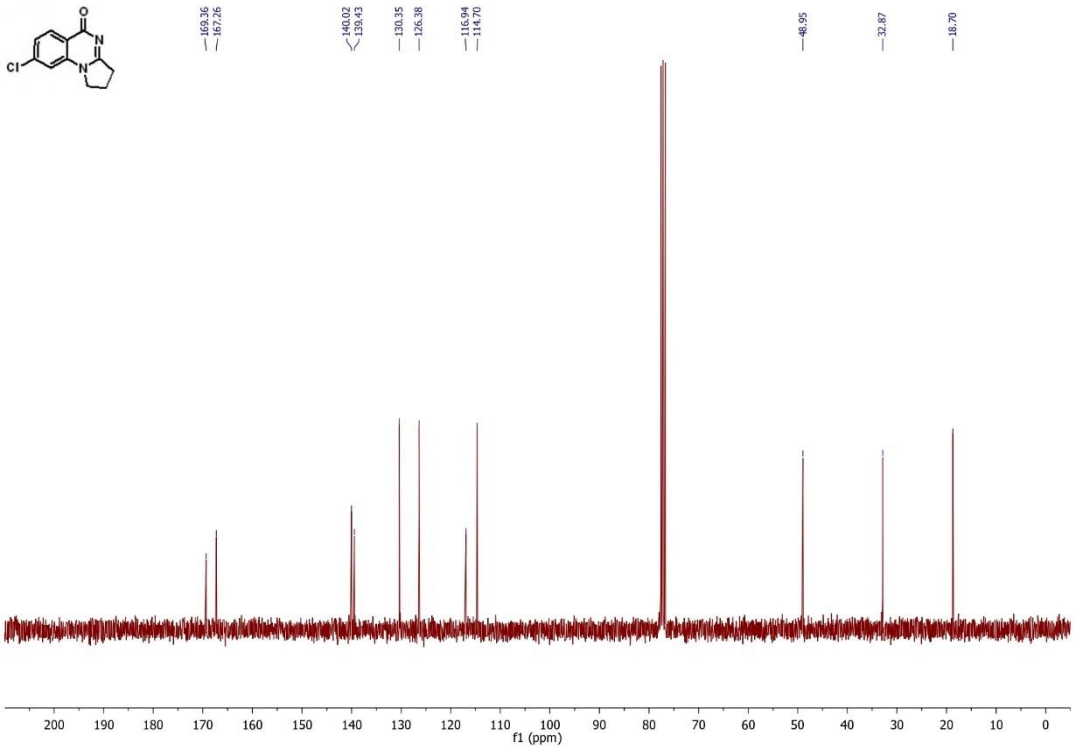
169.36
167.26
140.02
139.43
130.35
126.38
116.94
114.70
48.95
32.87
18.70
f1 (ppm)

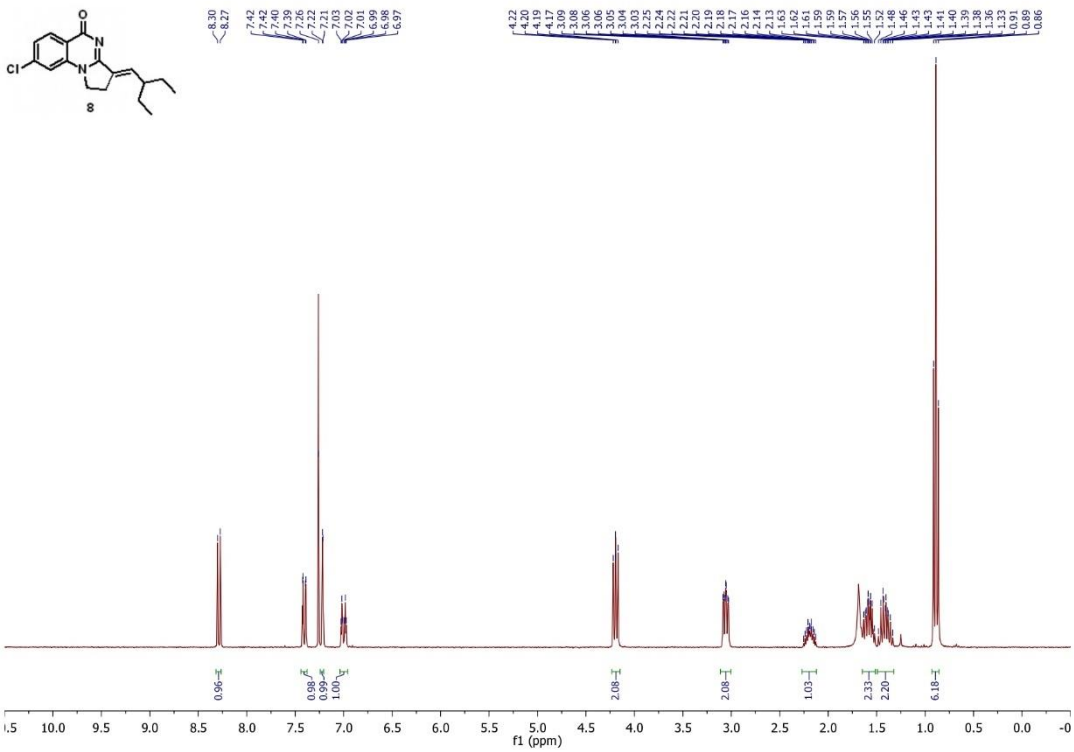
8
f1 (ppm)

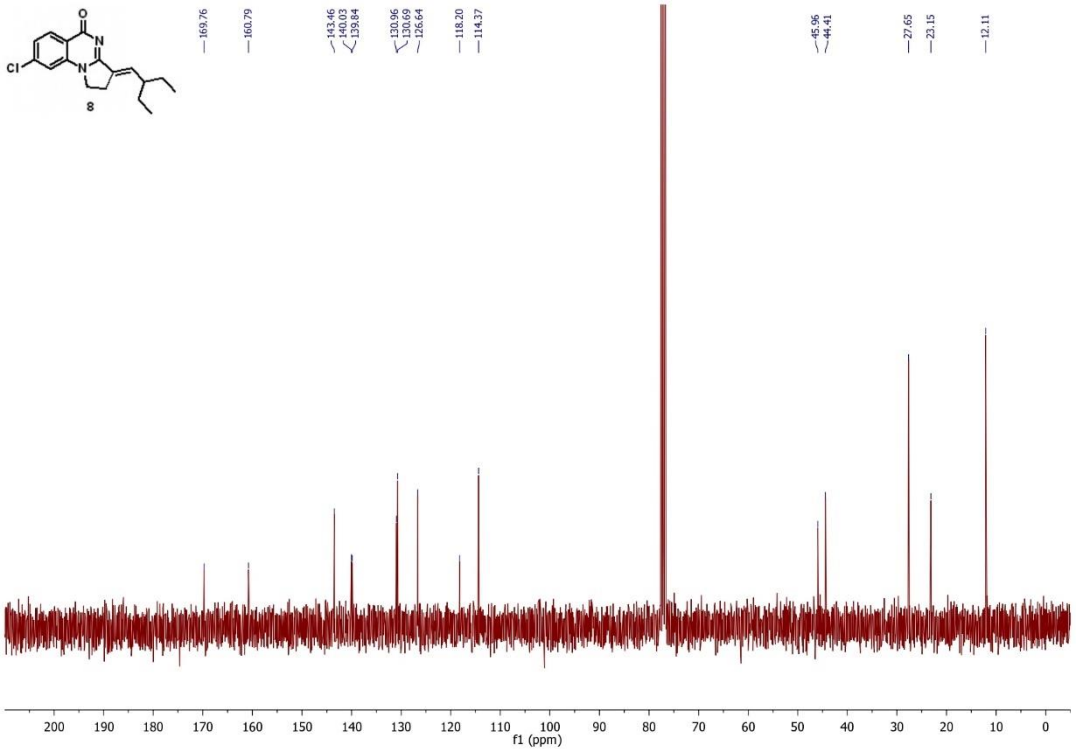
8
169.76
160.79
143.46
140.03
139.64
130.96
130.69
126.64
118.20
114.37
45.96
44.41
27.65
23.15
12.11
f1 (ppm)

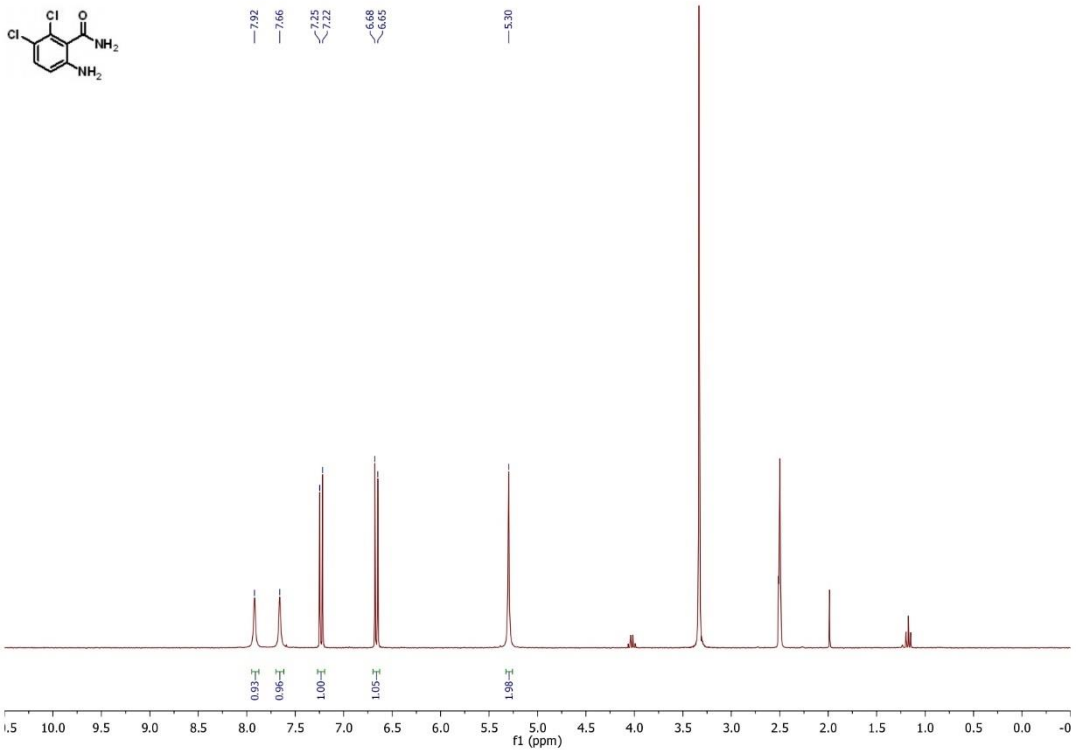
7.92
7.66
7.25
7.22
6.68
6.65
5.30
0.93
0.96
1.00
1.05
1.98
f1 (ppm)

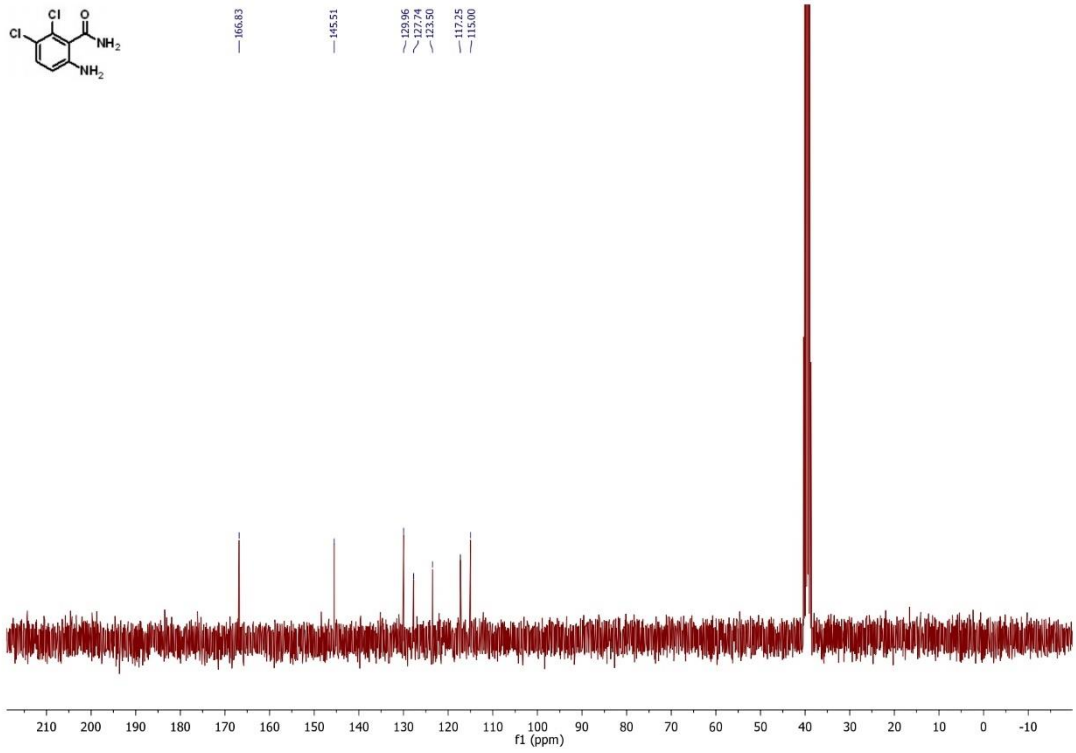
Cl
O
NH2
Cl
NH2
166.83
145.51
129.96
127.74
123.50
117.25
115.00
210 200 190 180 170 160 150 140 130 120 110 100 90 80 70 60 50 40 30 20 10 0 -10
f1 (ppm)

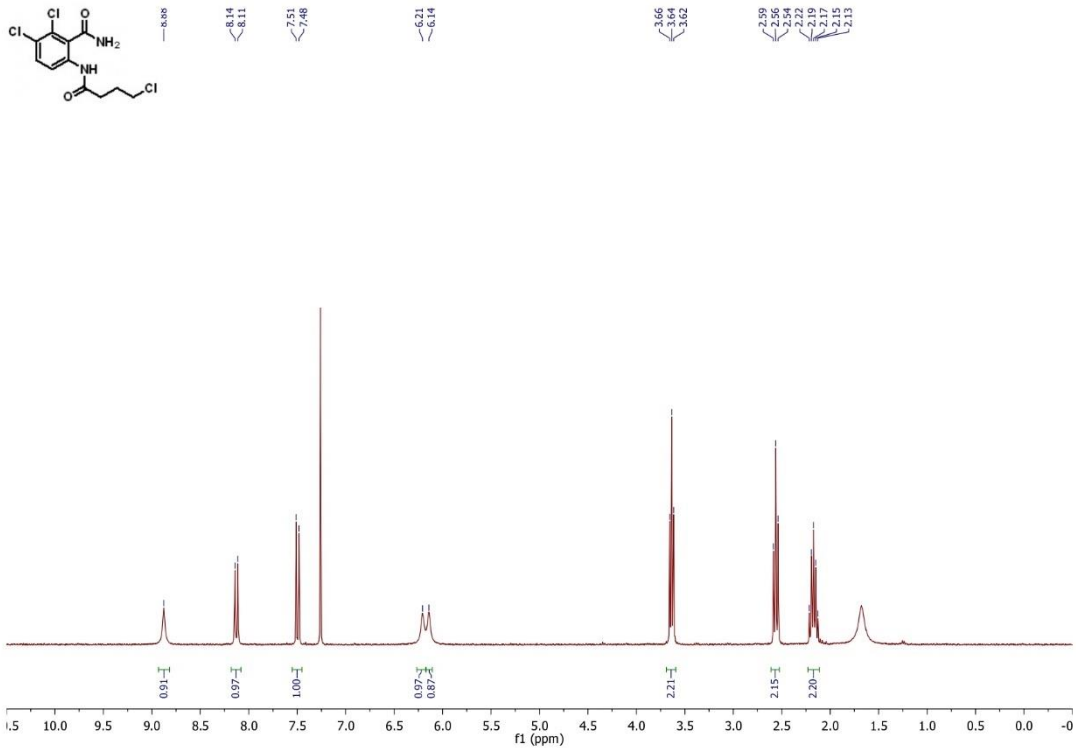
Cl
O
NH2
Cl
NH
O
Cl
8.88
8.14
8.11
7.51
7.48
6.21
6.14
3.66
3.64
3.62
2.59
2.56
2.54
2.22
2.19
2.17
2.15
2.13
0.91
0.97
1.00
0.97
0.87
2.21
2.15
2.20
10.0 9.5 9.0 8.5 8.0 7.5 7.0 6.5 6.0 5.5 5.0 4.5 4.0 3.5 3.0 2.5 2.0 1.5 1.0 0.5 0.0 -0
f1 (ppm)

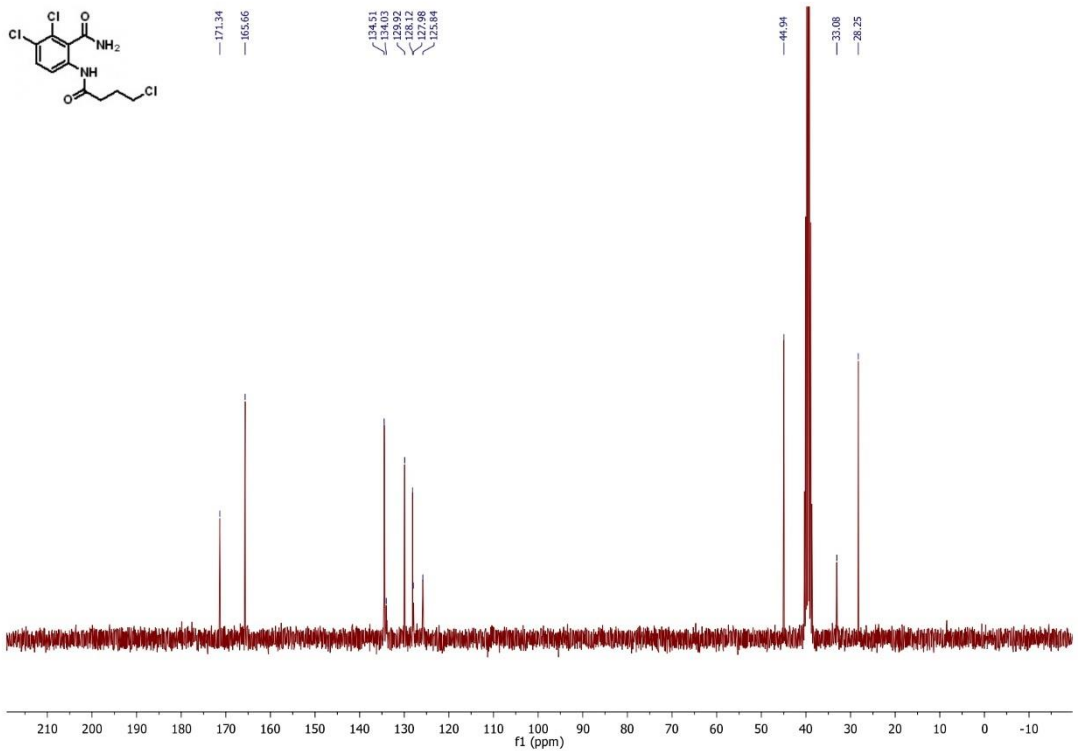
171.34
165.66
134.51
134.03
129.92
128.12
127.98
125.84
44.94
33.08
28.25
f1 (ppm)

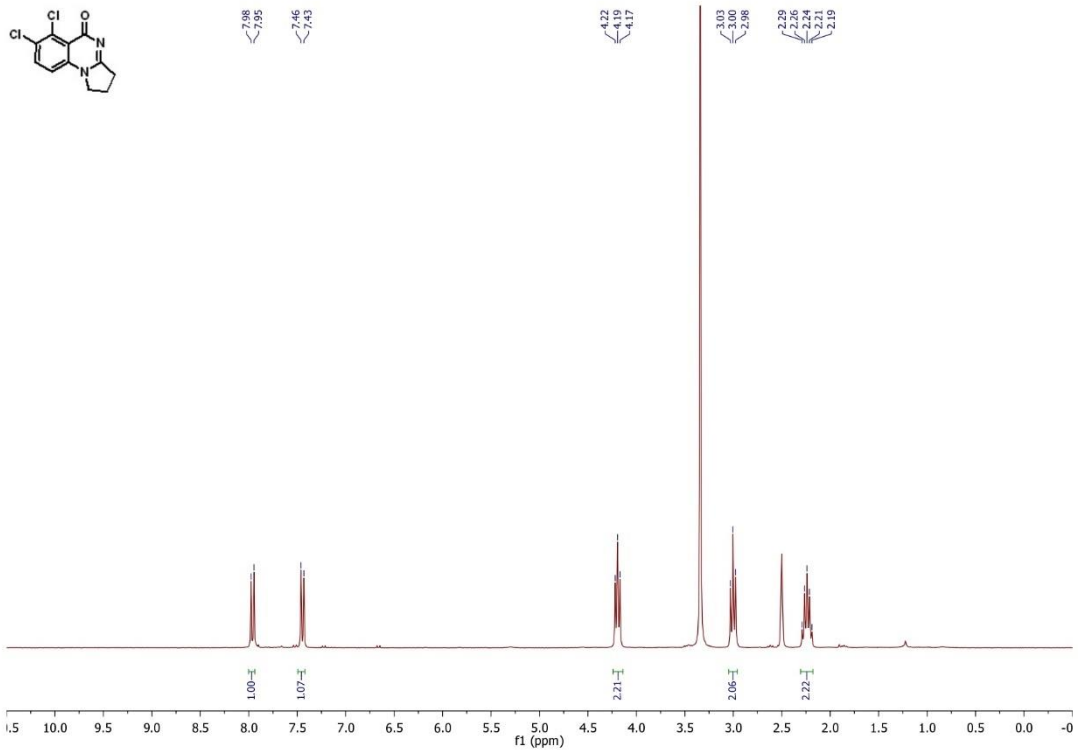
7.98
7.95
7.46
7.43
4.22
4.19
4.17
3.03
3.00
2.98
2.29
2.26
2.24
2.21
2.19
1.00
1.07
2.21
2.06
2.22
f1 (ppm)

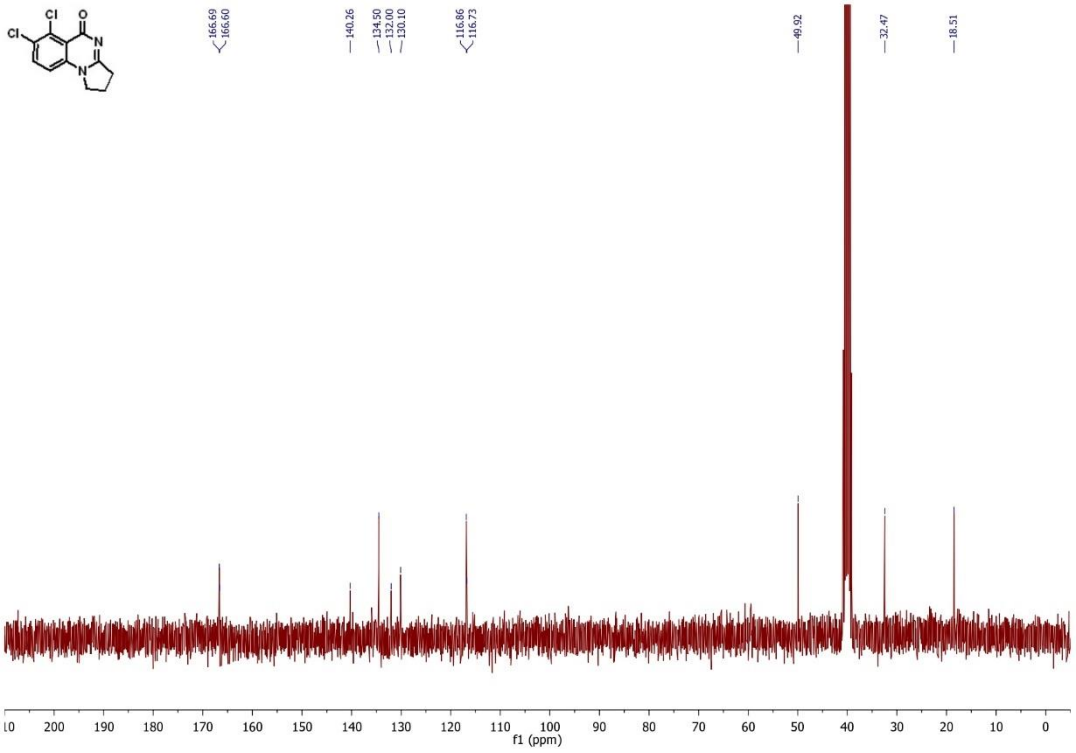
Cl
Cl
O
N
166.69
166.60
140.26
134.50
132.00
130.10
116.86
116.73
49.92
32.47
18.51
f1 (ppm)

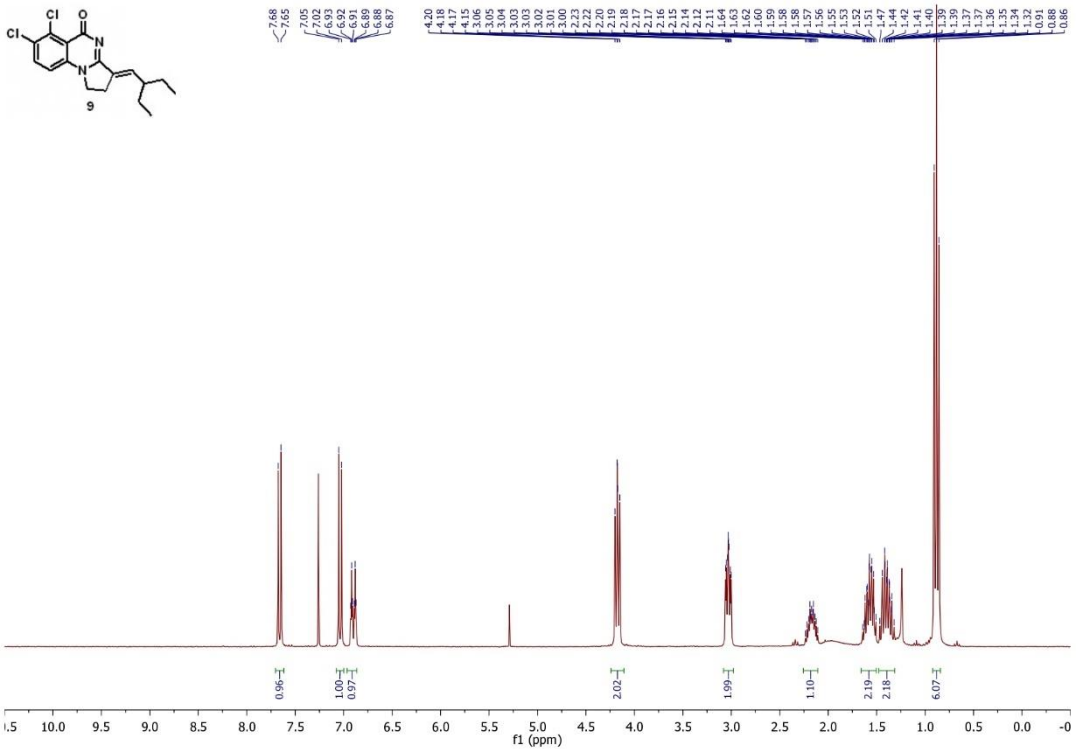
Cl
Cl
O
N
9
7.68
7.65
7.05
7.02
6.93
6.92
6.91
6.89
6.88
6.87
0.96
1.00
0.97
2.02
1.99
1.10
2.19
2.18
6.07
f1 (ppm)

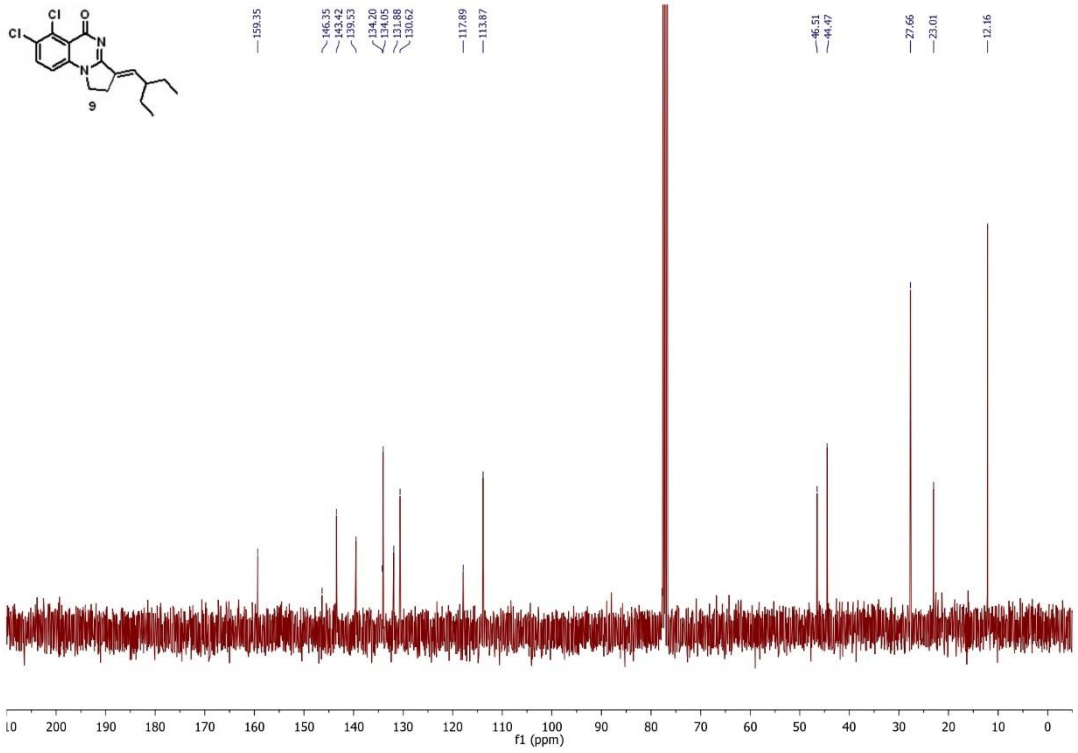
Cl
Cl
O
N
N
9
159.35
146.35
143.42
139.53
134.20
134.05
131.88
130.62
117.89
113.87
46.51
44.47
27.66
23.01
12.16
f1 (ppm)

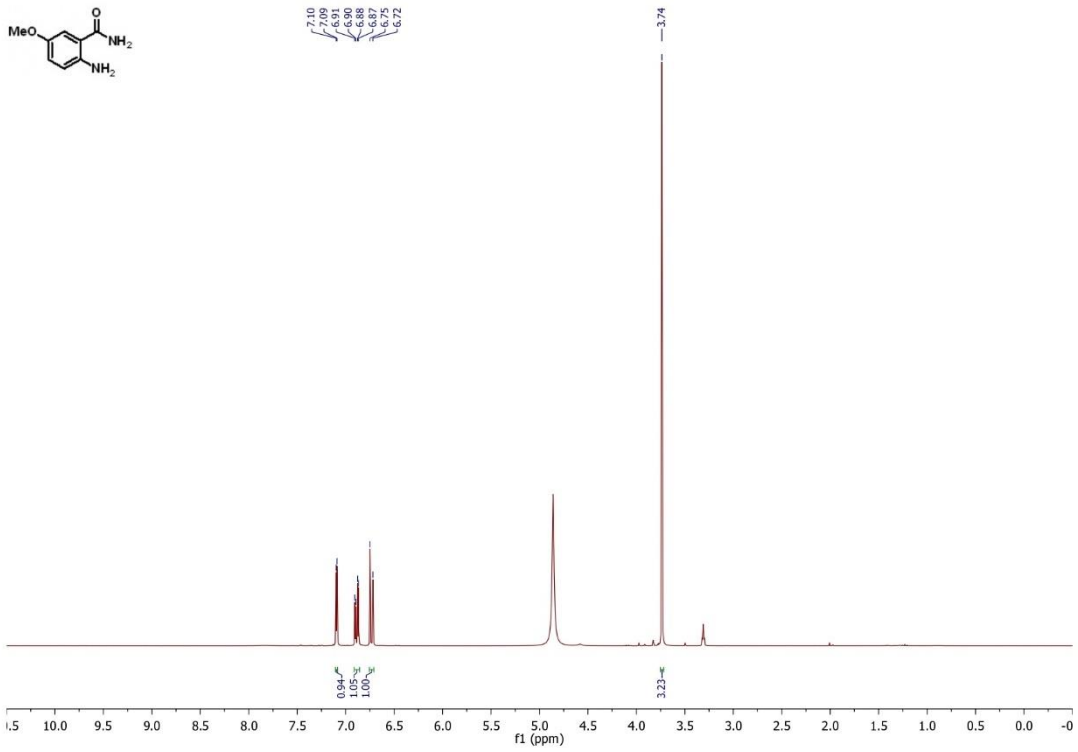
MeO
O
NH2
NH2
7.10
7.09
6.91
6.90
6.88
6.87
6.75
6.72
3.74
0.94
1.05
1.00
3.23
f1 (ppm)

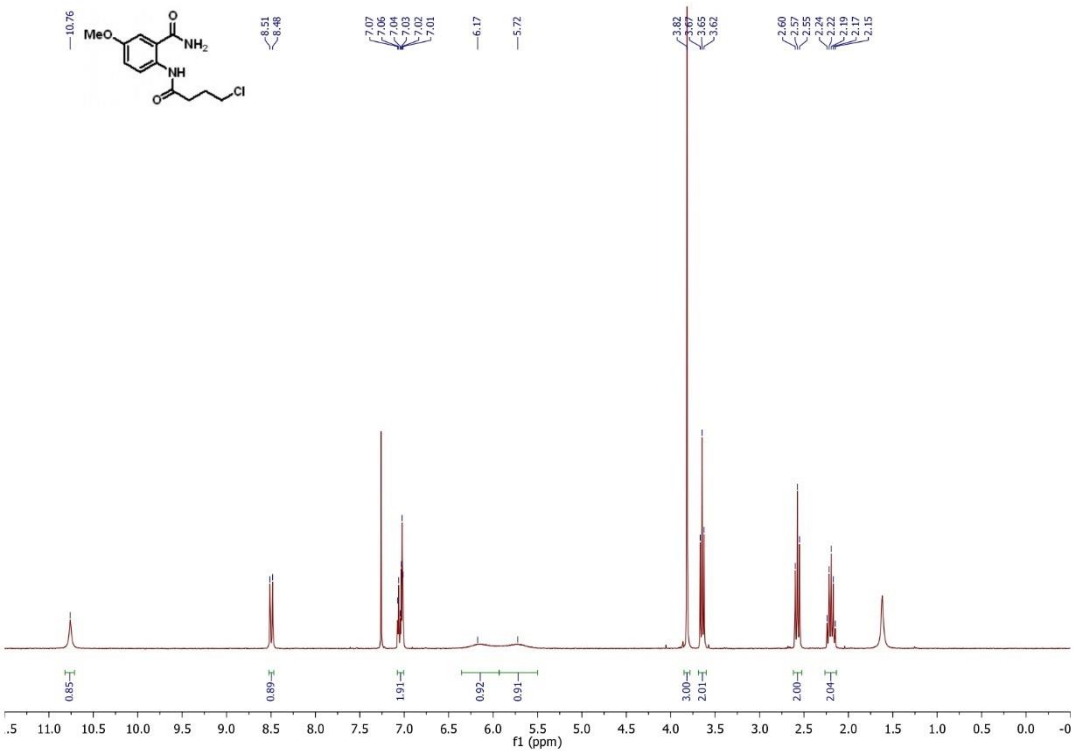
MeO
O
NH2
NH
O
Cl
10.76
8.51
8.48
7.07
7.06
7.04
7.03
7.02
7.01
6.17
5.72
3.82
3.67
3.65
3.62
2.60
2.57
2.55
2.24
2.22
2.19
2.17
2.15
0.85
0.89
1.91
0.92
0.91
3.00
2.01
2.00
2.04
f1 (ppm)

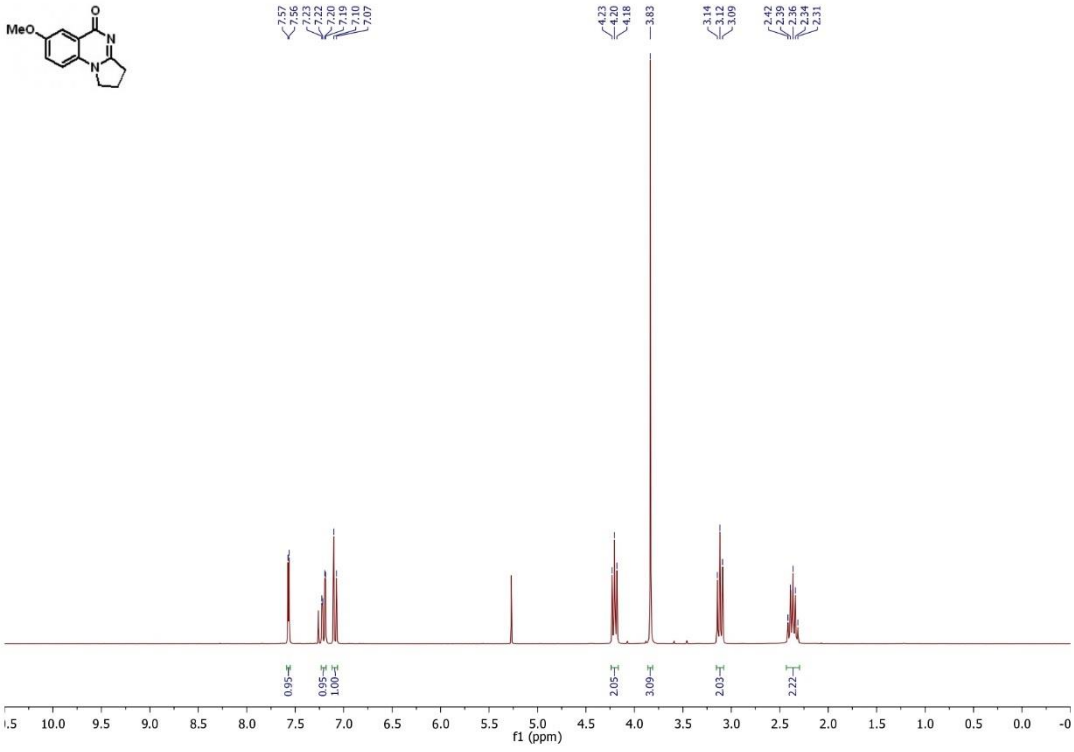
MeO
O
N
N
7.57
7.56
7.23
7.22
7.20
7.19
7.10
7.07
4.23
4.20
4.18
3.83
3.14
3.12
3.09
2.42
2.39
2.36
2.34
2.31
0.95
0.95
1.00
2.05
3.09
2.03
2.22
f1 (ppm)

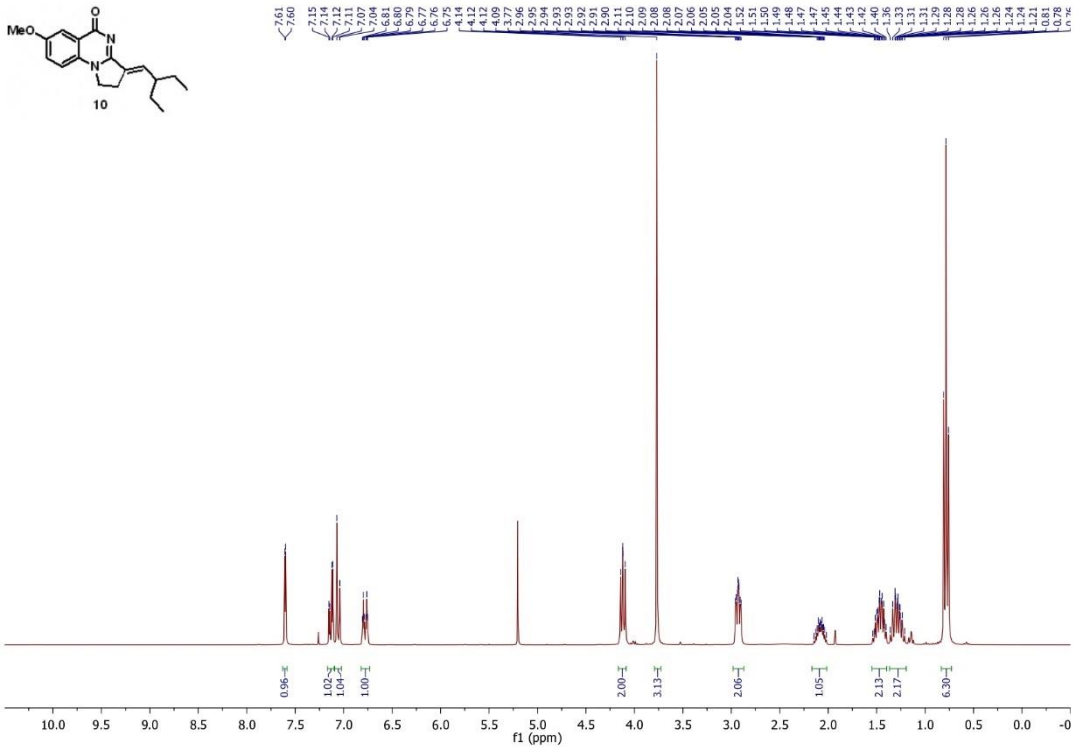
MeO
O
N
N
10
f1 (ppm)

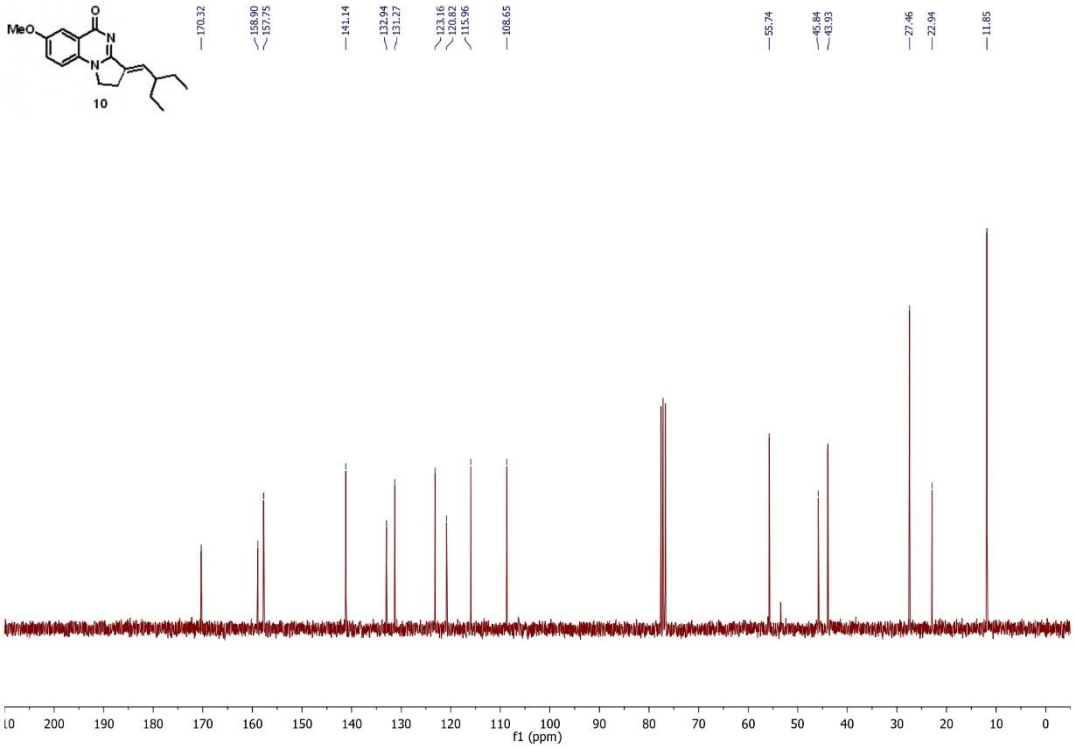
MeO
O
N
N
10
f1 (ppm)

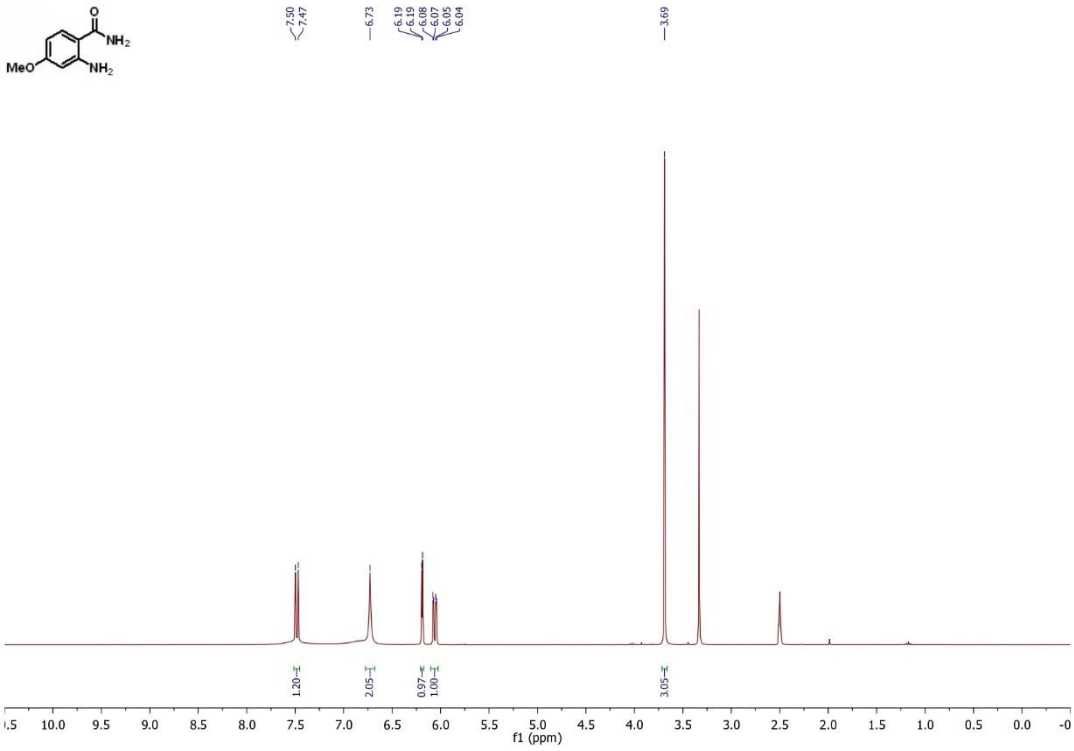
MeO
NH2
NH2
7.50
7.47
6.73
6.19
6.19
6.08
6.07
6.05
6.04
3.69
1.20
2.05
0.97
1.00
3.05
f1 (ppm)

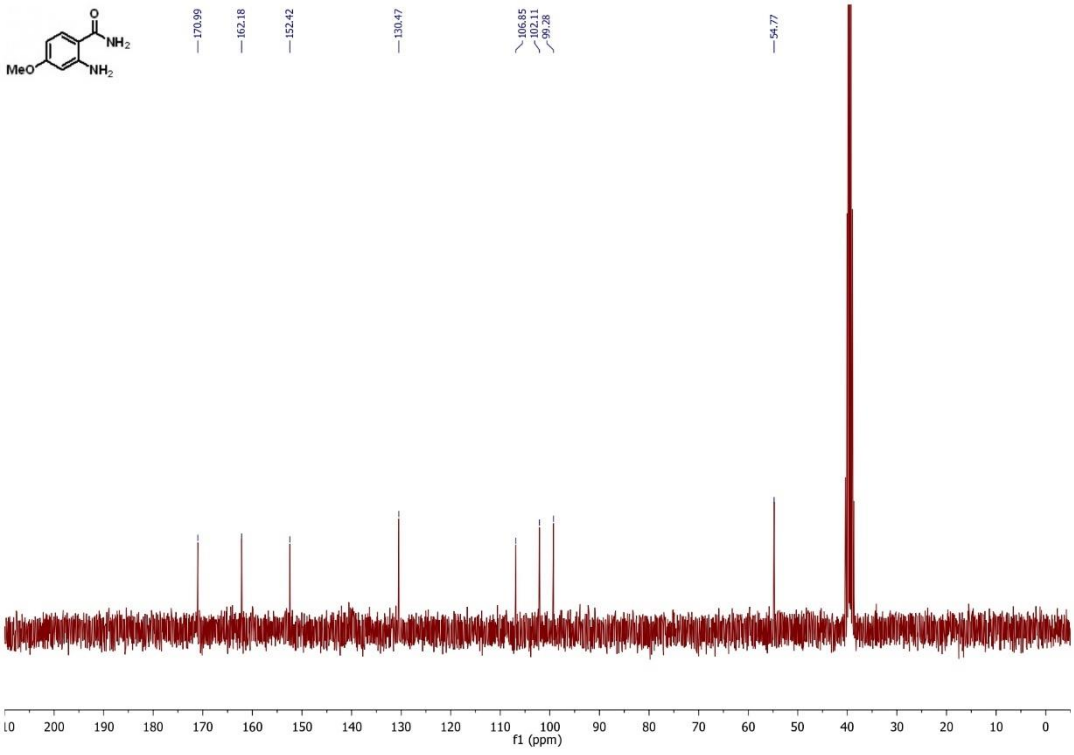
MeO
NH2
NH2
170.99
162.18
152.42
130.47
106.85
102.11
99.28
54.77
f1 (ppm)

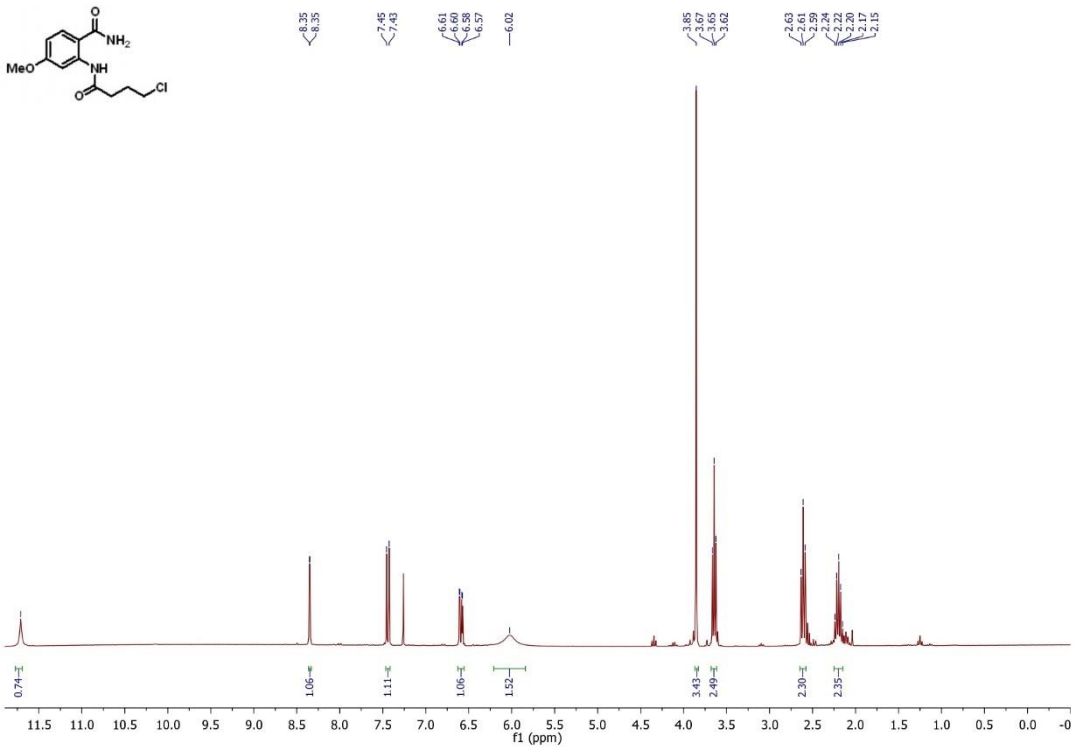
MeO
NH
NH2
O
Cl
8.35
8.35
7.45
7.43
6.61
6.60
6.58
6.57
6.02
3.85
3.67
3.65
3.62
2.63
2.61
2.59
2.24
2.22
2.20
2.17
2.15
0.74
1.06
1.11
1.06
1.52
3.43
2.49
2.30
2.35
f1 (ppm)

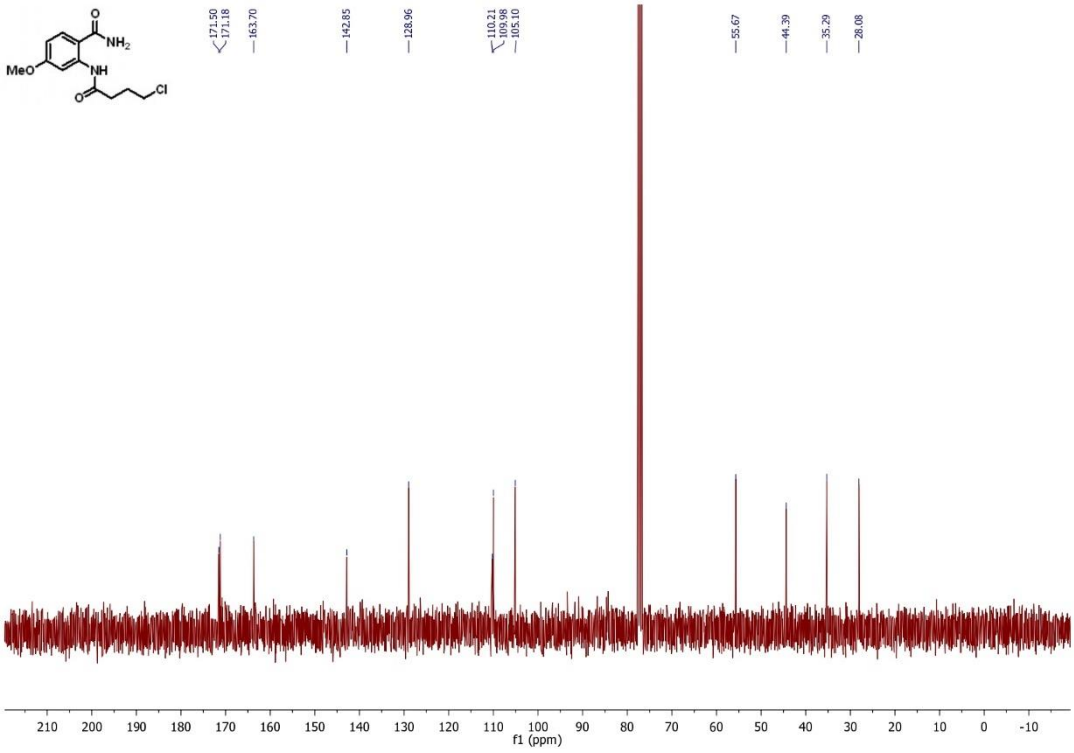
MeO
NH
NH2
O
Cl
171.50
171.18
163.70
142.85
128.96
110.21
109.98
105.10
55.67
44.39
35.29
28.08
f1 (ppm)

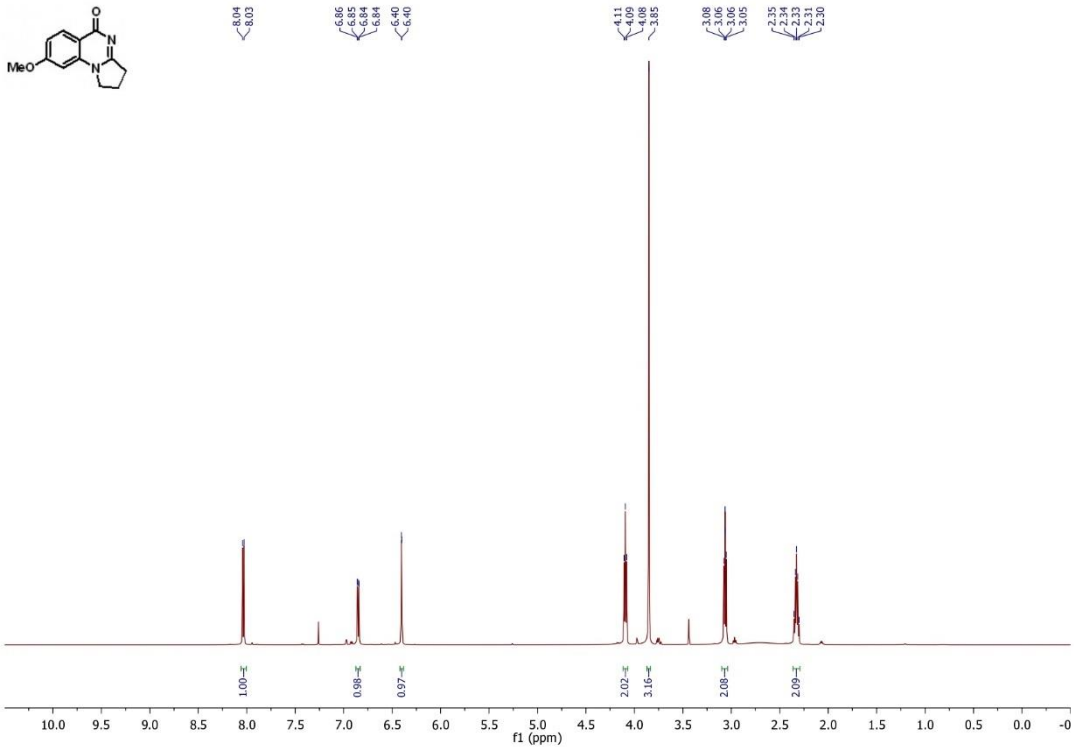
MeO
8.04
8.03
6.86
6.85
6.84
6.84
6.40
6.40
4.11
4.09
4.08
3.85
3.08
3.06
3.06
3.05
2.35
2.34
2.33
2.31
2.30
1.00
0.98
0.97
2.02
3.16
2.08
2.09
f1 (ppm)

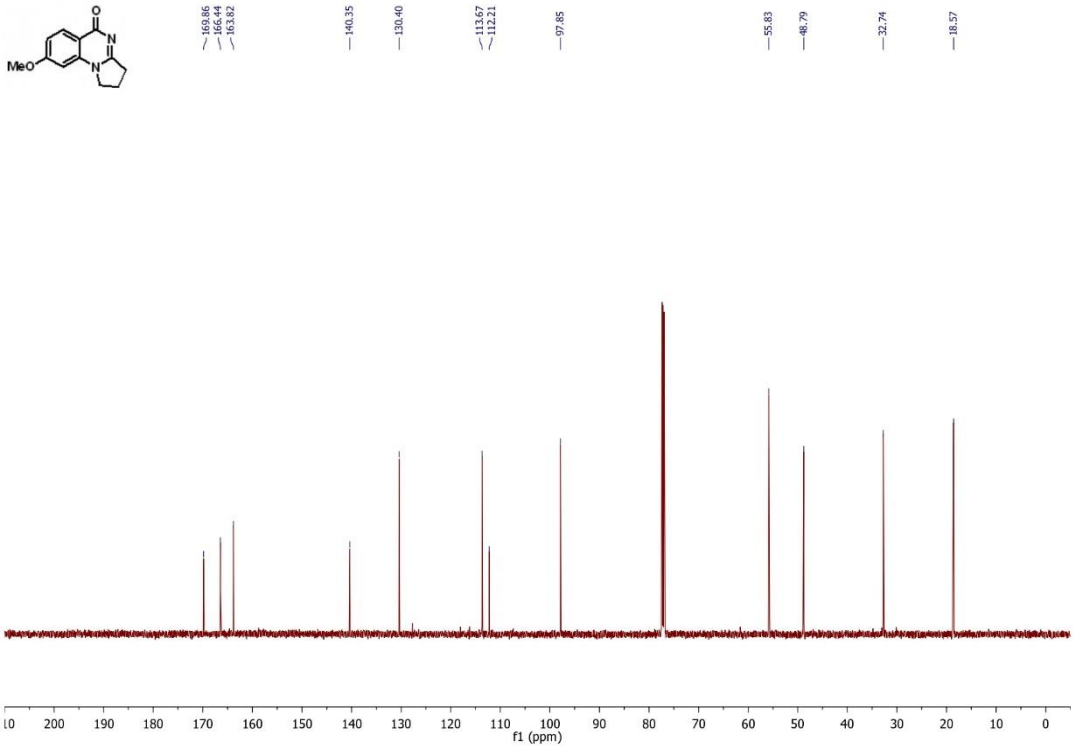
MeO
169.86
166.44
163.62
140.35
130.40
113.67
112.21
97.85
55.83
48.79
32.74
18.57
f1 (ppm)

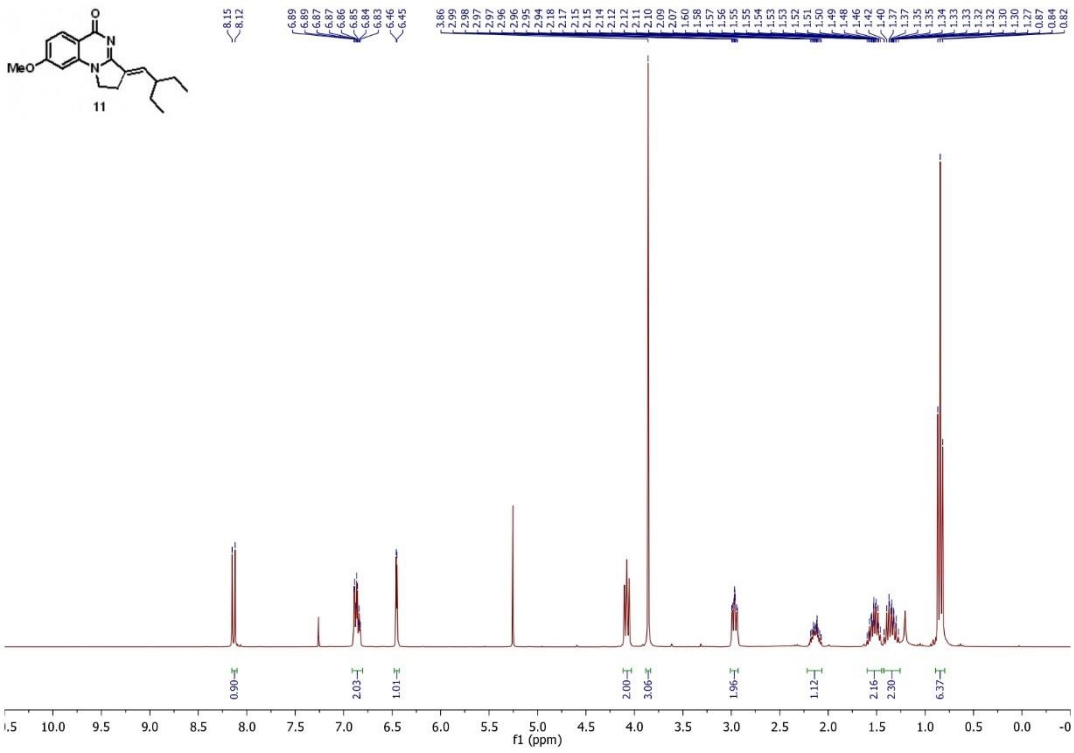
MeO
11
f1 (ppm)

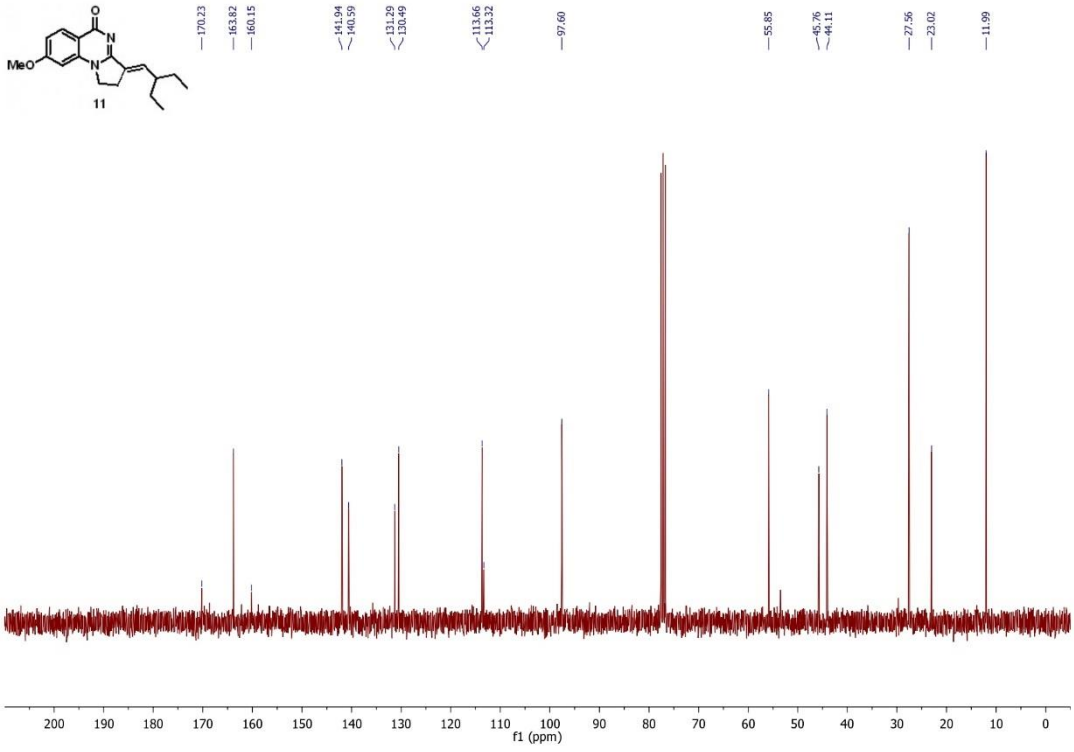
MeO
11
f1 (ppm)

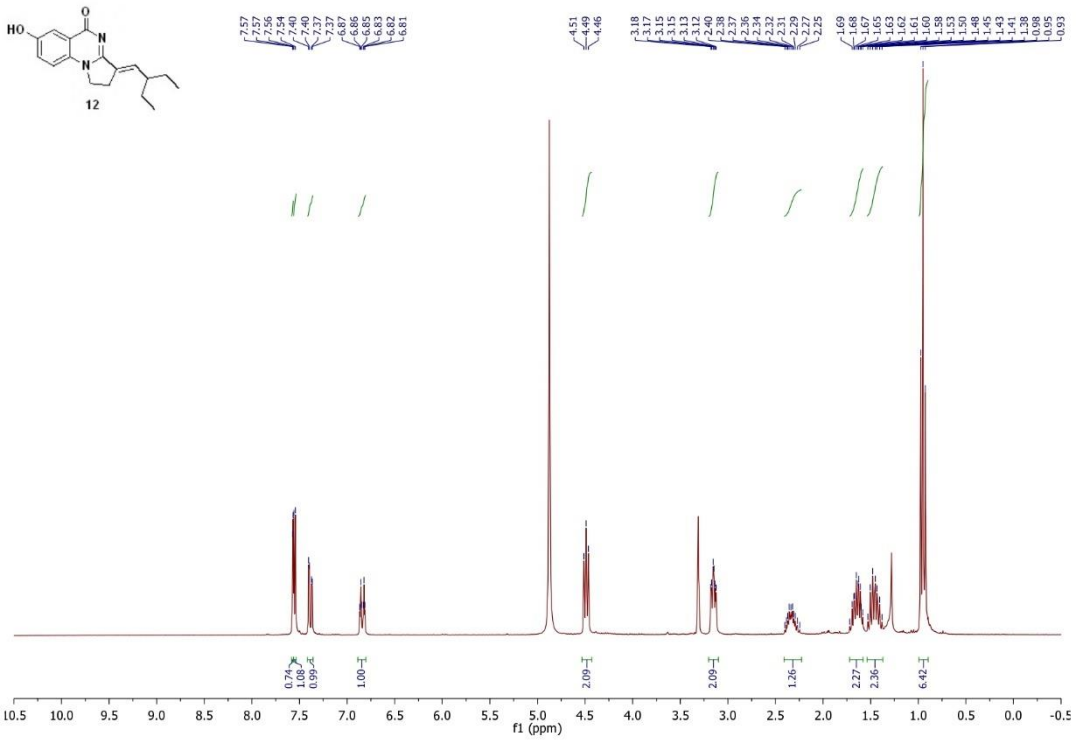
HO
O
N
N
12
f1 (ppm)

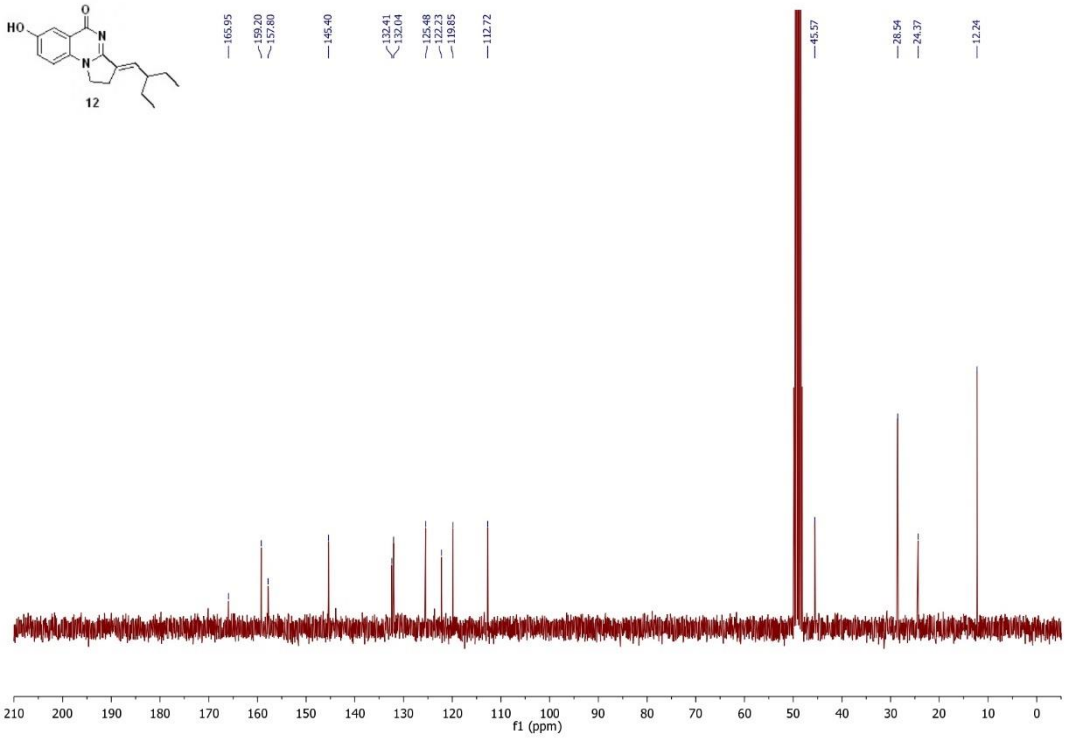
HO
O
N
N
12
f1 (ppm)

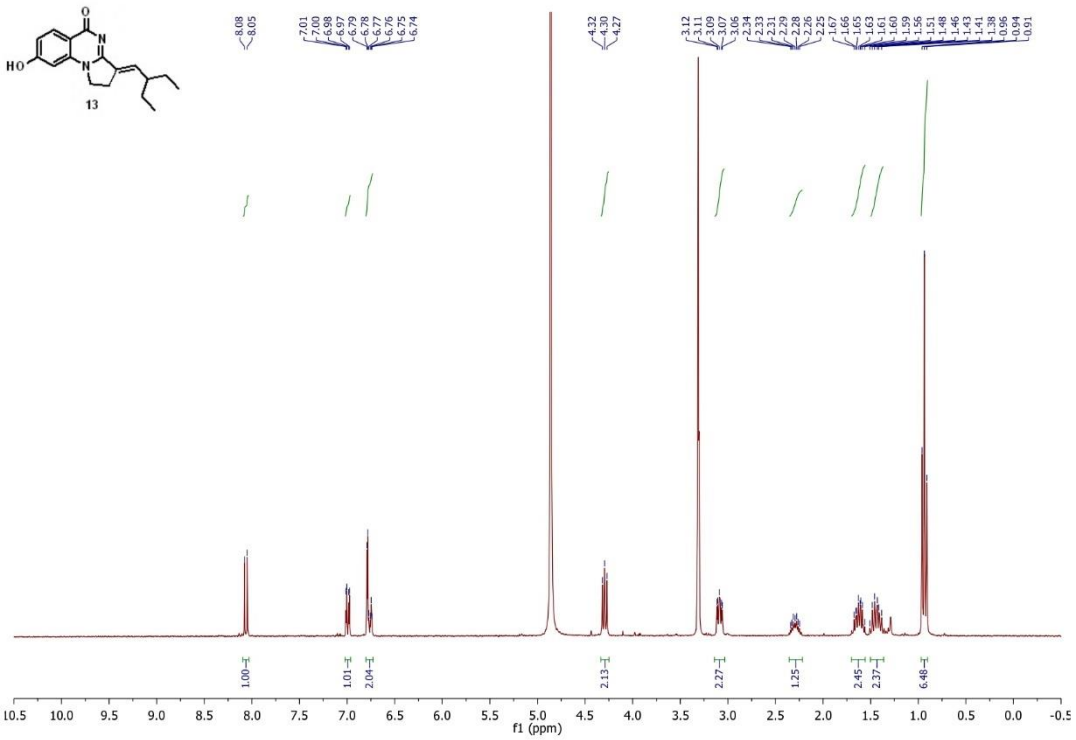
13
8.08
8.05
7.01
7.00
6.98
6.97
6.79
6.78
6.77
6.76
6.75
6.74
4.32
4.30
4.27
3.12
3.11
3.09
3.07
3.06
2.34
2.33
2.31
2.29
2.28
2.26
2.25
1.67
1.66
1.65
1.63
1.61
1.60
1.59
1.56
1.51
1.48
1.46
1.43
1.41
1.38
0.96
0.94
0.91
1.00
1.01
2.04
2.13
2.27
1.25
2.45
2.37
6.48
f1 (ppm)

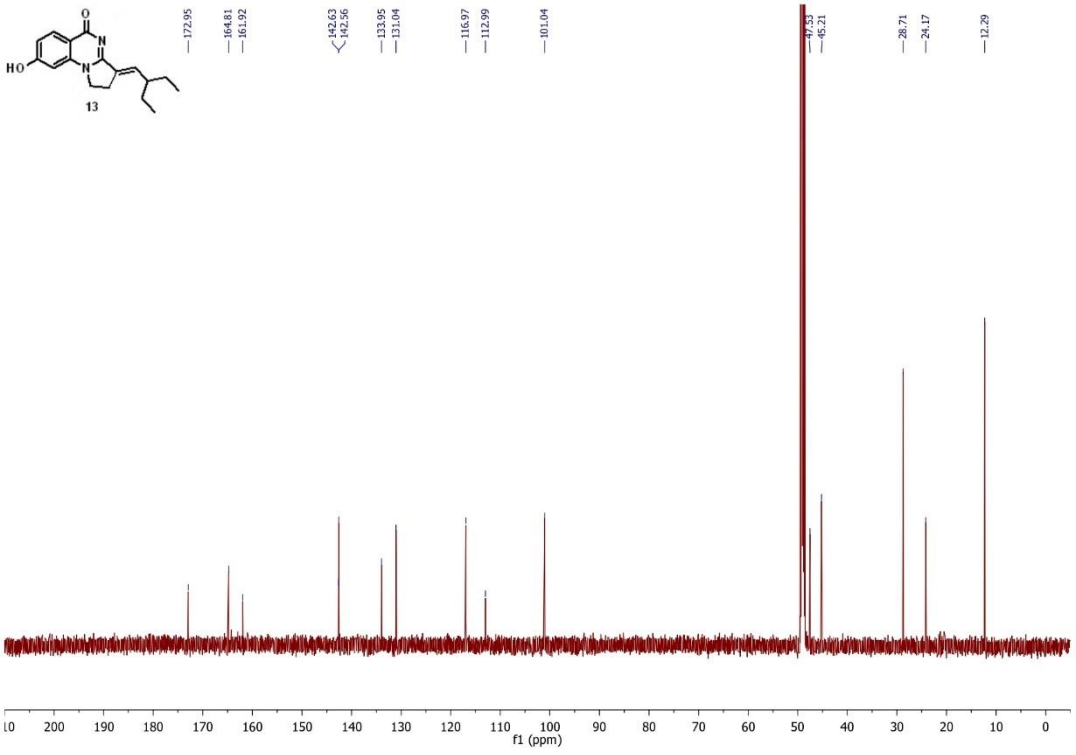
13
172.95
164.81
161.92
142.63
142.56
133.95
131.04
116.97
112.99
101.04
47.53
45.21
28.71
24.17
12.29
f1 (ppm)

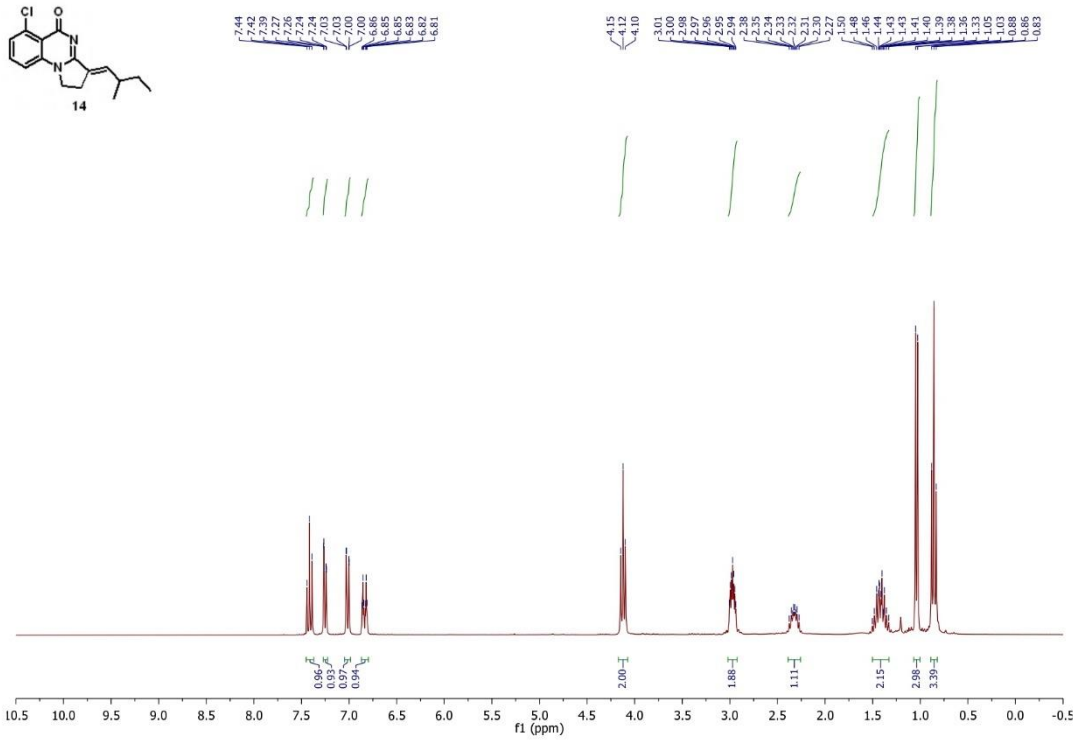
Cl
O
N
N
14
7.44
7.42
7.39
7.27
7.26
7.24
7.24
7.03
7.03
7.00
7.00
6.86
6.85
6.85
6.83
6.82
6.81
4.15
4.12
4.10
3.01
3.00
2.98
2.97
2.96
2.95
2.94
2.38
2.35
2.34
2.33
2.32
2.31
2.30
2.27
1.50
1.48
1.46
1.44
1.43
1.43
1.41
1.40
1.39
1.38
1.36
1.33
1.05
1.03
0.88
0.86
0.83
0.96
0.93
0.97
0.94
2.00
1.88
1.11
2.15
2.98
3.39
f1 (ppm)

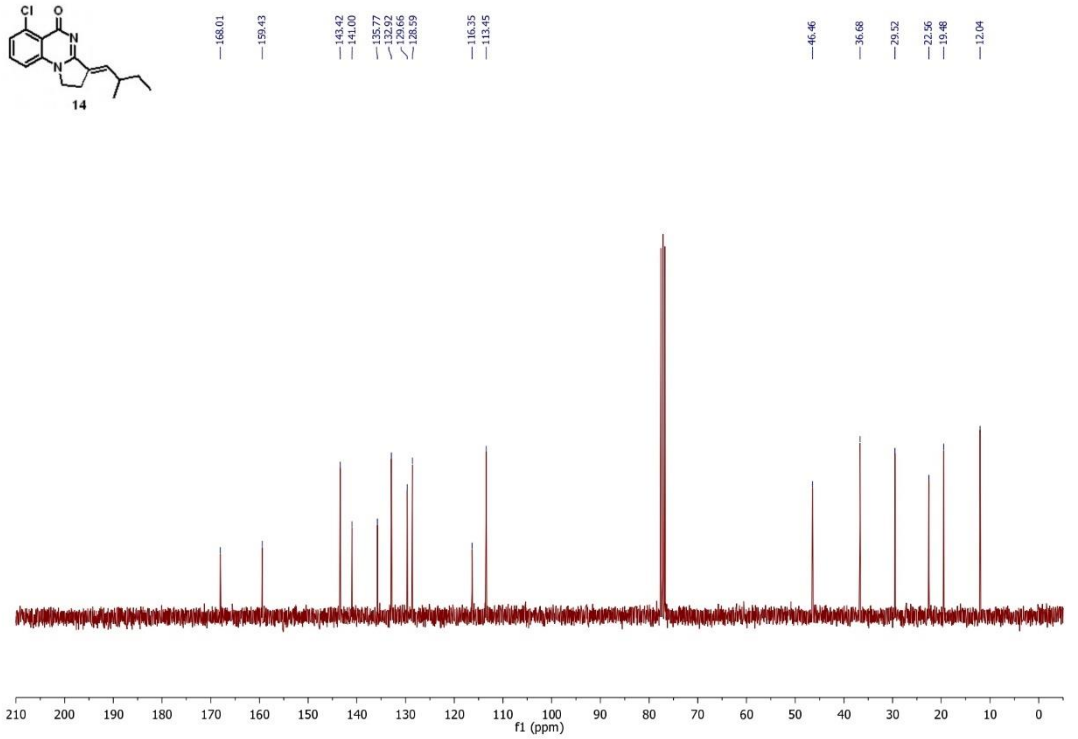
Cl
O
N
N
14
168.01
159.43
143.42
141.00
135.77
132.92
129.66
128.59
116.35
113.45
46.46
36.68
29.52
22.56
19.48
12.04
f1 (ppm)

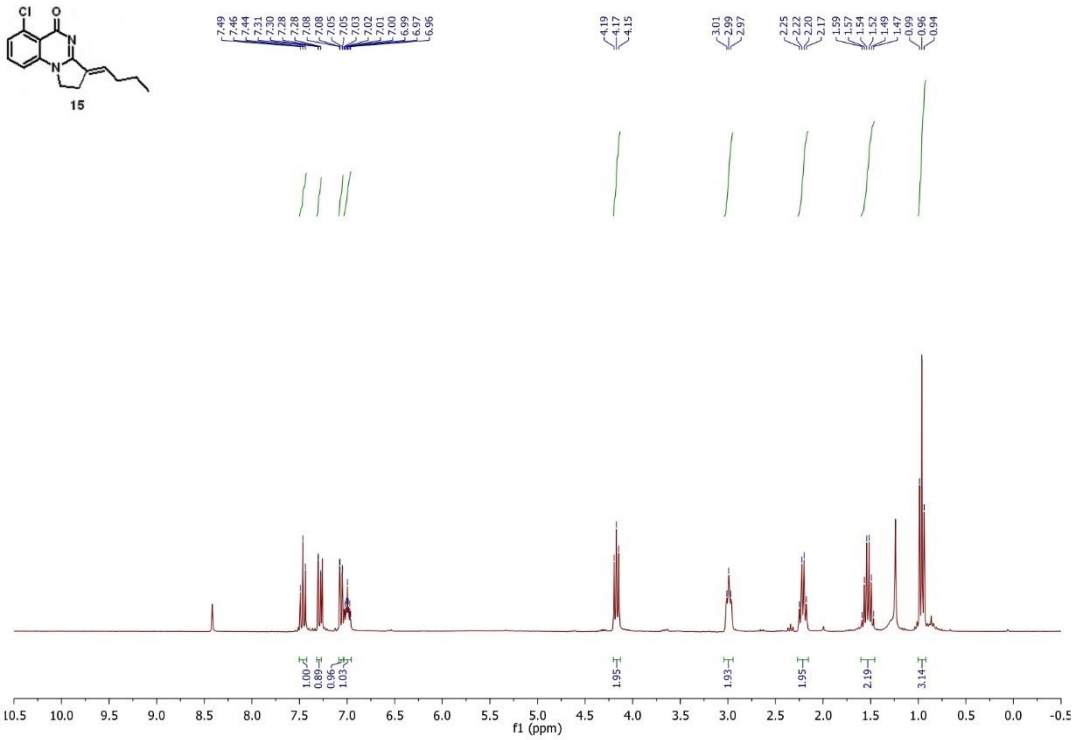
15
7.49
7.46
7.44
7.31
7.30
7.28
7.08
7.05
7.03
7.02
7.01
7.00
6.99
6.97
6.96
4.19
4.17
4.15
3.01
2.99
2.97
2.25
2.22
2.20
2.17
1.59
1.57
1.54
1.52
1.49
1.47
0.99
0.96
0.94
1.00
0.89
0.96
1.03
1.95
1.93
1.95
2.19
3.14
f1 (ppm)

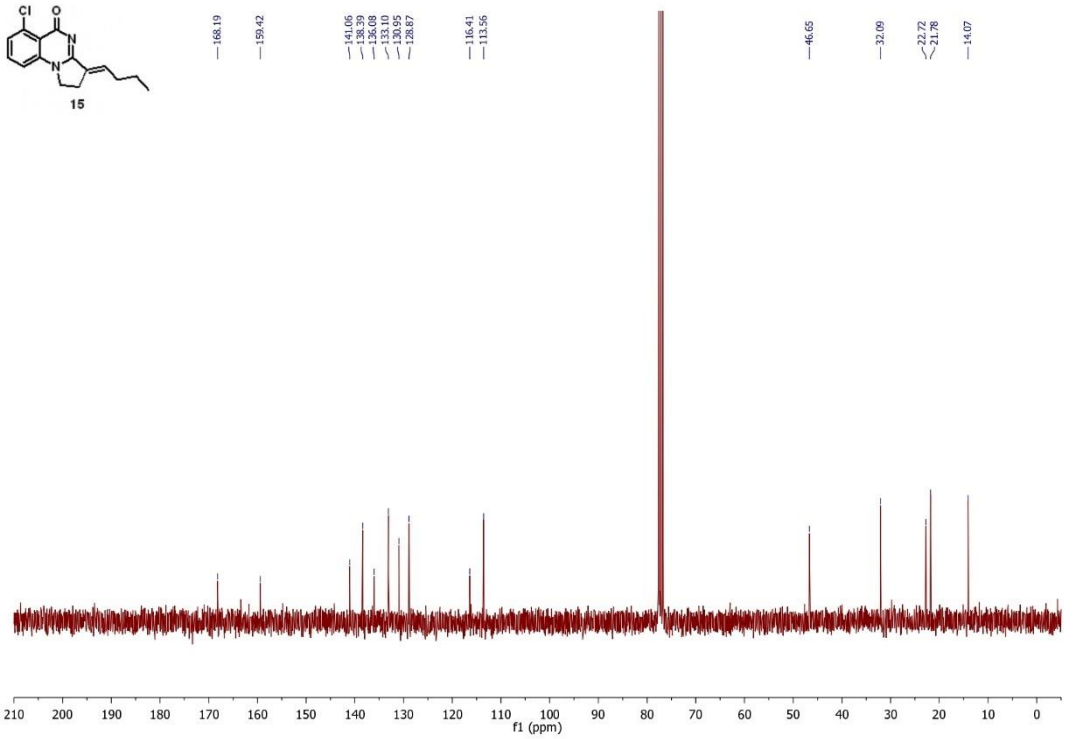
15
168.19
159.42
141.06
138.39
136.08
133.10
130.95
128.87
116.41
113.56
46.65
32.09
22.72
21.78
14.07
f1 (ppm)

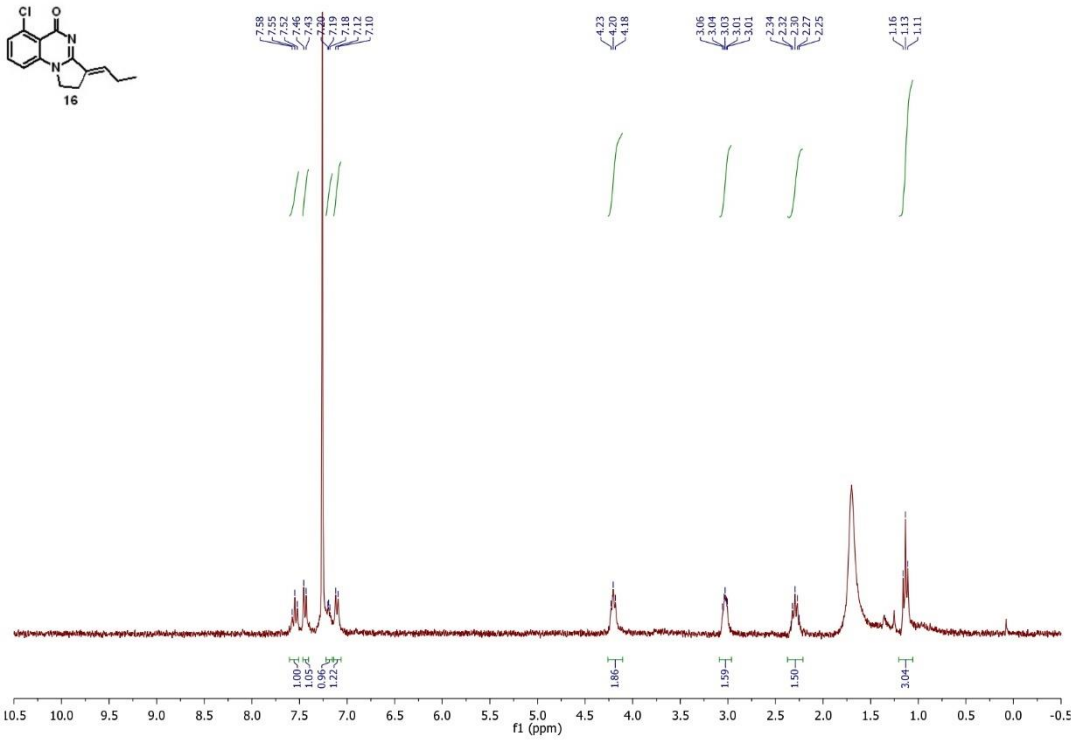
Cl
O
N
16
7.58
7.55
7.52
7.46
7.43
7.20
7.19
7.18
7.12
7.10
4.23
4.20
4.18
3.06
3.04
3.03
3.01
3.01
2.34
2.32
2.30
2.27
2.25
1.16
1.13
1.11
1.00
1.05
0.96
1.22
1.86
1.59
1.50
3.04
f1 (ppm)

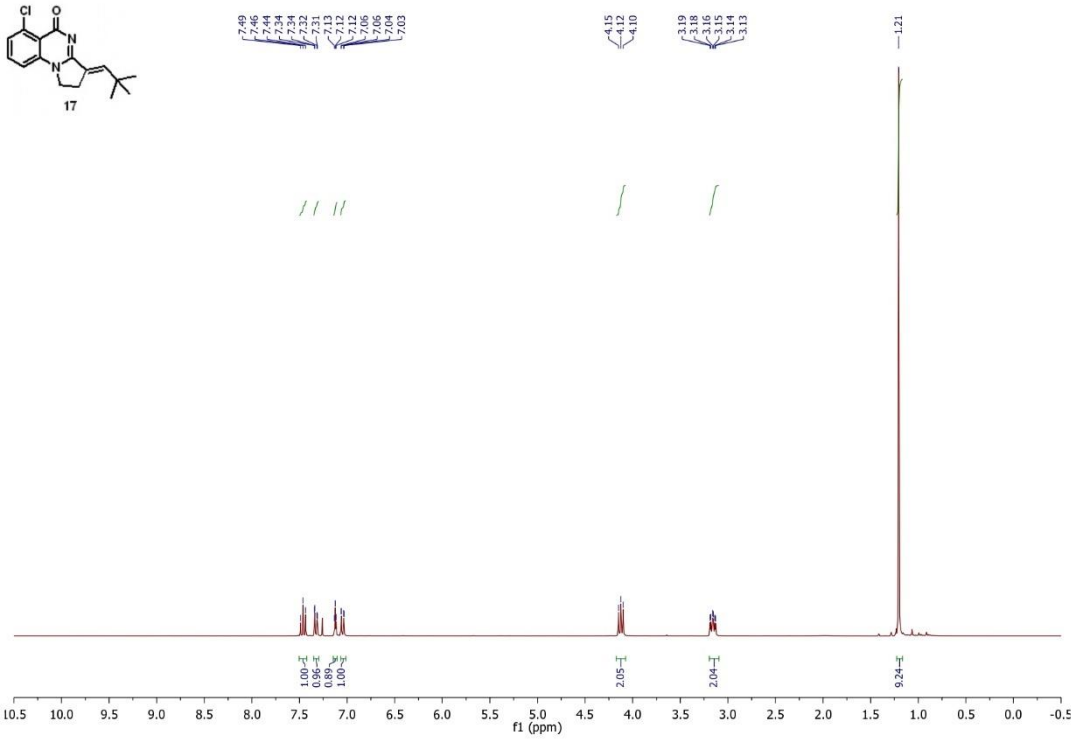
Cl
O
N
17
7.49
7.46
7.44
7.34
7.34
7.32
7.31
7.13
7.12
7.12
7.06
7.06
7.04
7.03
4.15
4.12
4.10
3.19
3.18
3.16
3.15
3.14
3.13
1.21
1.00
0.96
0.89
1.00
2.05
2.04
9.24
f1 (ppm)

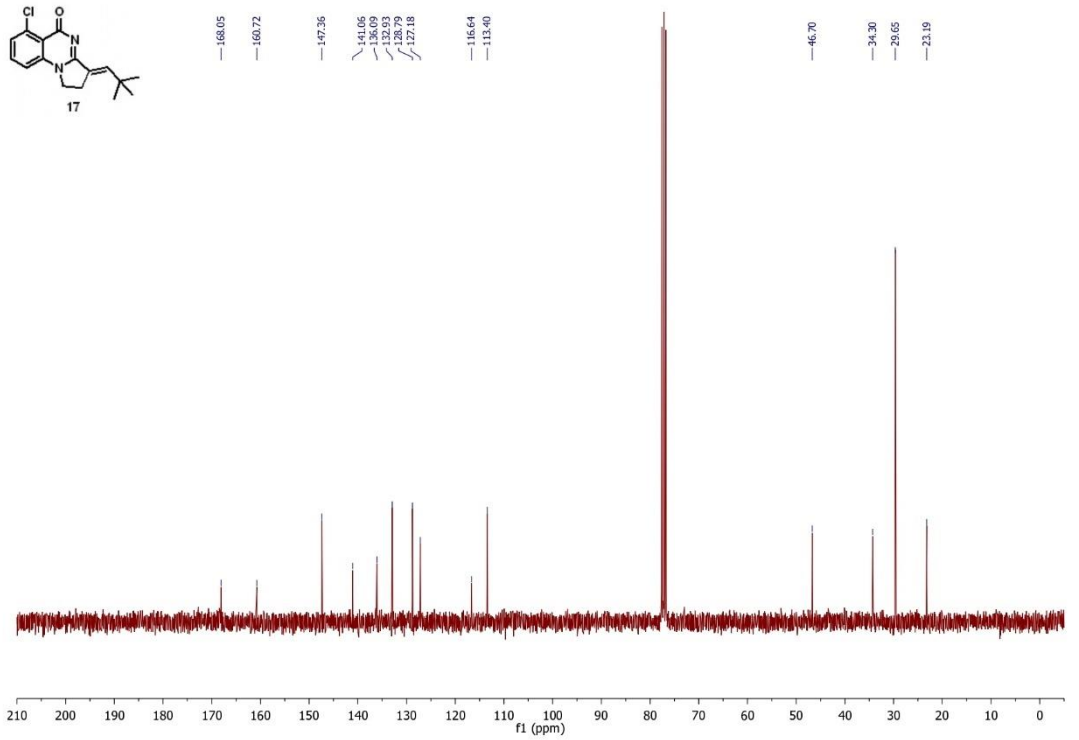
17
168.05
160.72
147.36
141.06
135.09
132.53
128.79
127.18
116.64
113.40
46.70
34.30
29.65
23.19
f1 (ppm)

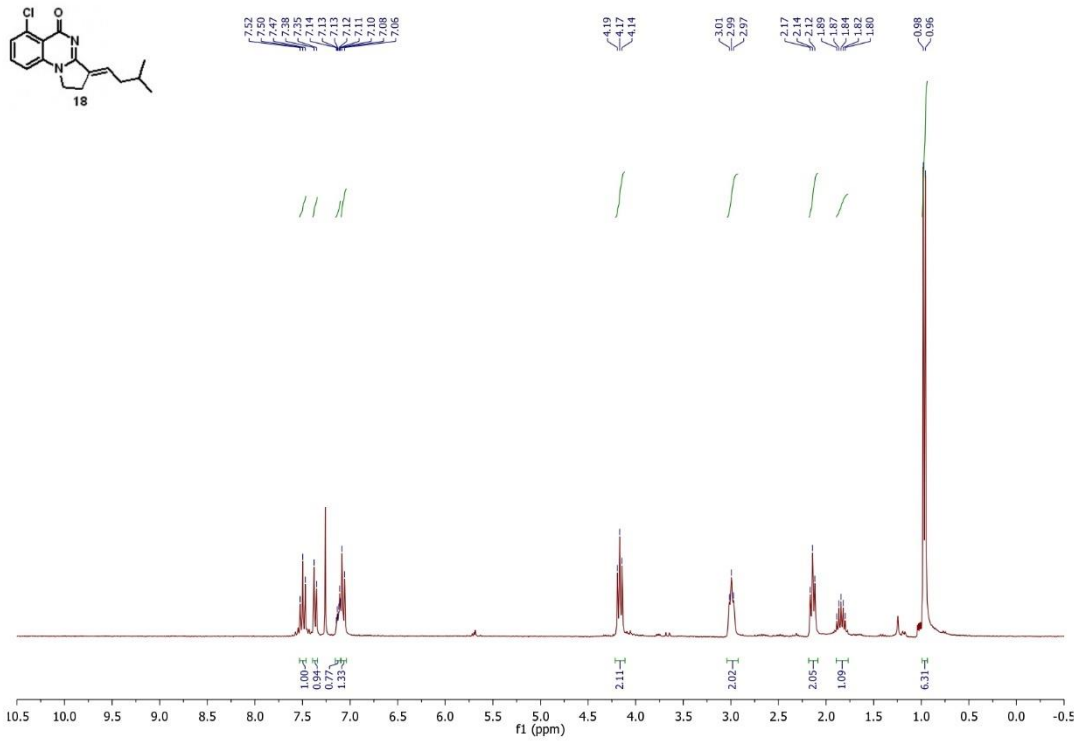
18
7.52
7.50
7.47
7.38
7.35
7.14
7.13
7.12
7.11
7.10
7.08
7.06
4.19
4.17
4.14
3.01
2.99
2.97
2.17
2.14
2.12
1.89
1.87
1.84
1.82
1.80
0.98
0.96
1.00
0.94
0.77
1.33
2.11
2.02
2.05
1.09
6.31
f1 (ppm)

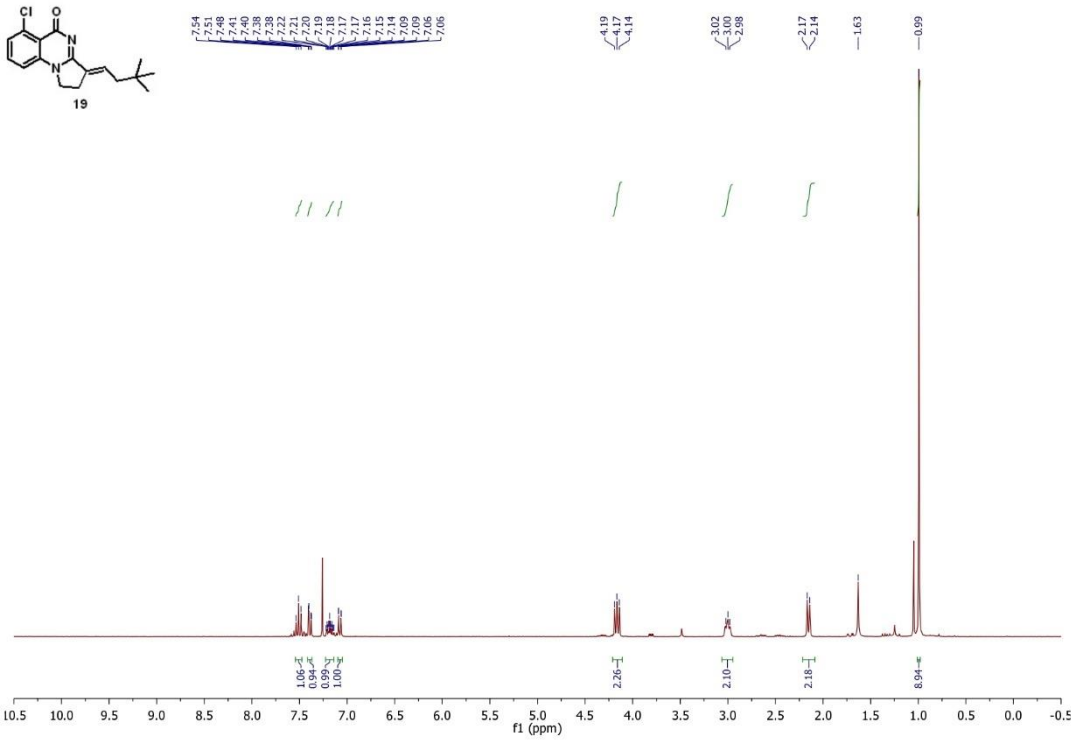
Cl
O
N
19
7.54
7.51
7.48
7.41
7.40
7.38
7.22
7.21
7.20
7.19
7.18
7.17
7.17
7.16
7.15
7.14
7.09
7.09
7.06
7.06
4.19
4.17
4.14
3.02
3.00
2.98
2.17
2.14
1.63
0.99
1.06
0.94
0.99
1.00
2.26
2.10
2.18
8.94
f1 (ppm)

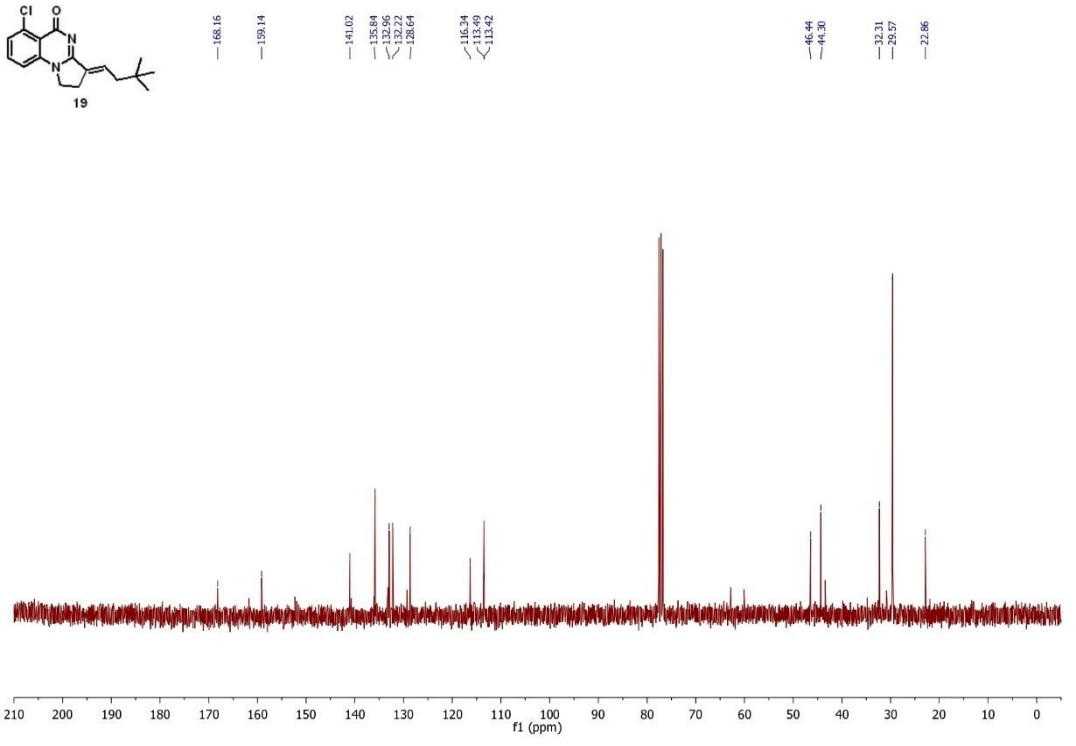
Cl
O
N
19
168.16
159.14
141.02
135.84
132.96
132.22
128.64
116.34
113.49
113.42
46.44
44.30
32.31
29.57
22.86
f1 (ppm)

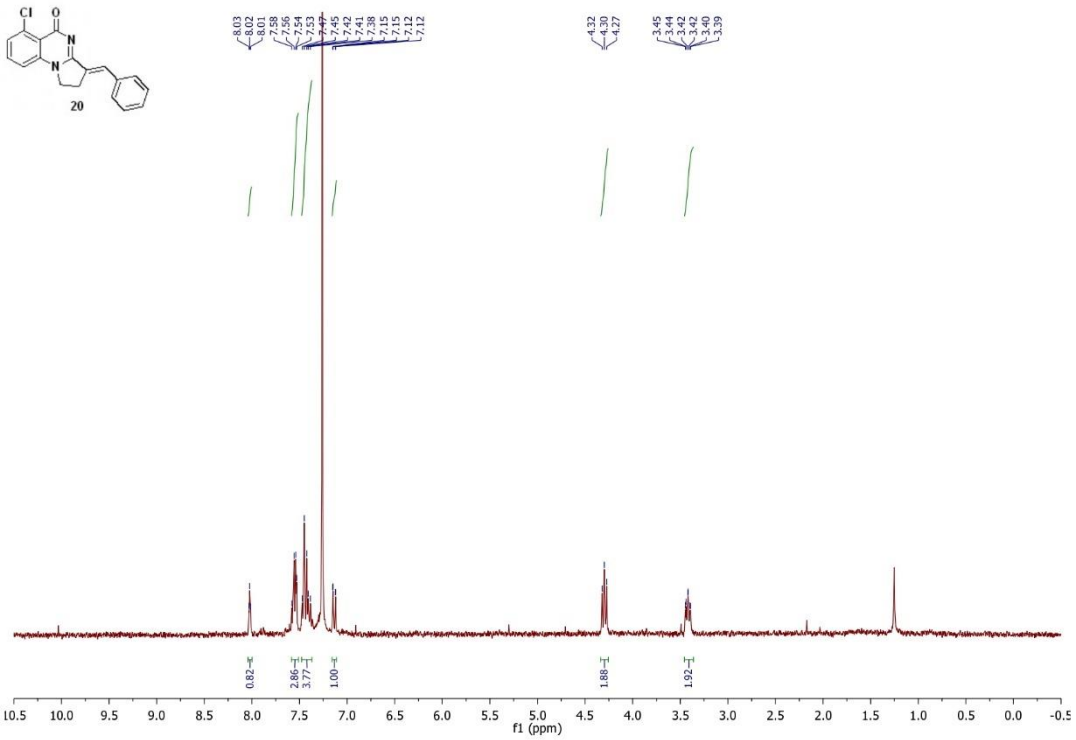
20
8.03
8.02
8.01
7.58
7.56
7.54
7.53
7.47
7.45
7.42
7.41
7.38
7.15
7.15
7.12
7.12
4.32
4.30
4.27
3.45
3.44
3.42
3.42
3.40
3.39
0.82
2.86
3.77
1.00
1.88
1.92
f1 (ppm)

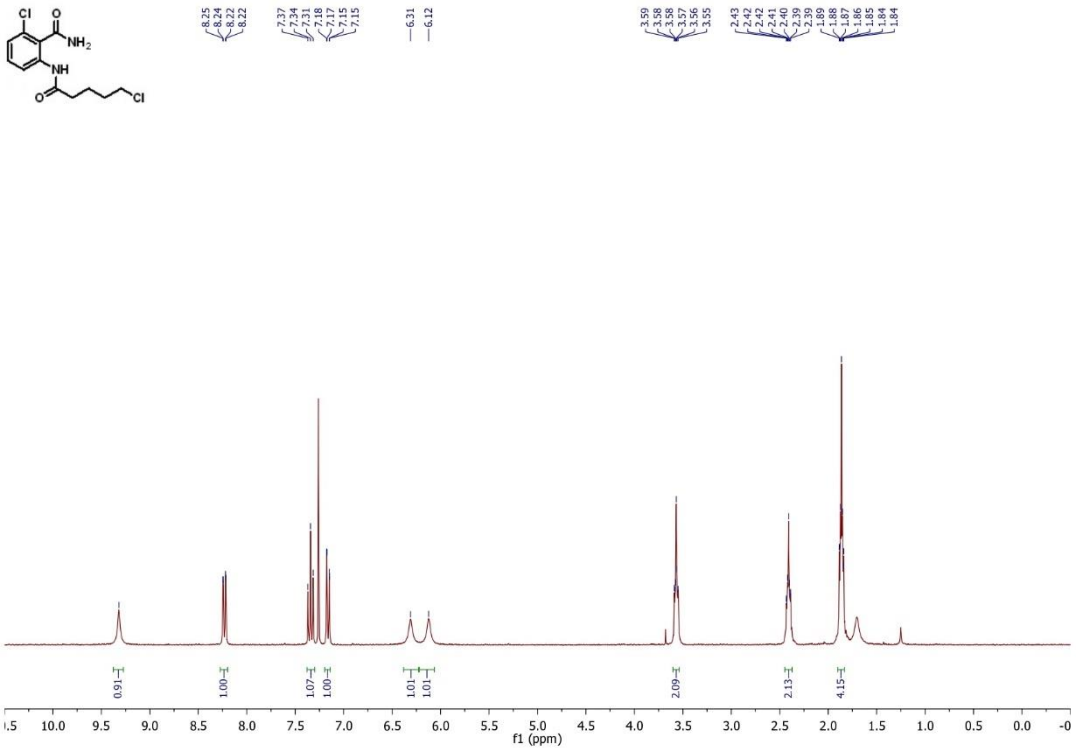
8.25
8.24
8.23
8.22
7.37
7.34
7.31
7.18
7.17
7.15
7.15
6.31
6.12
3.59
3.58
3.58
3.57
3.56
3.55
2.43
2.42
2.42
2.41
2.40
2.39
2.39
1.89
1.88
1.87
1.86
1.85
1.84
1.84
0.91
1.00
1.07
1.00
1.01
1.01
2.09
2.13
4.15
f1 (ppm)

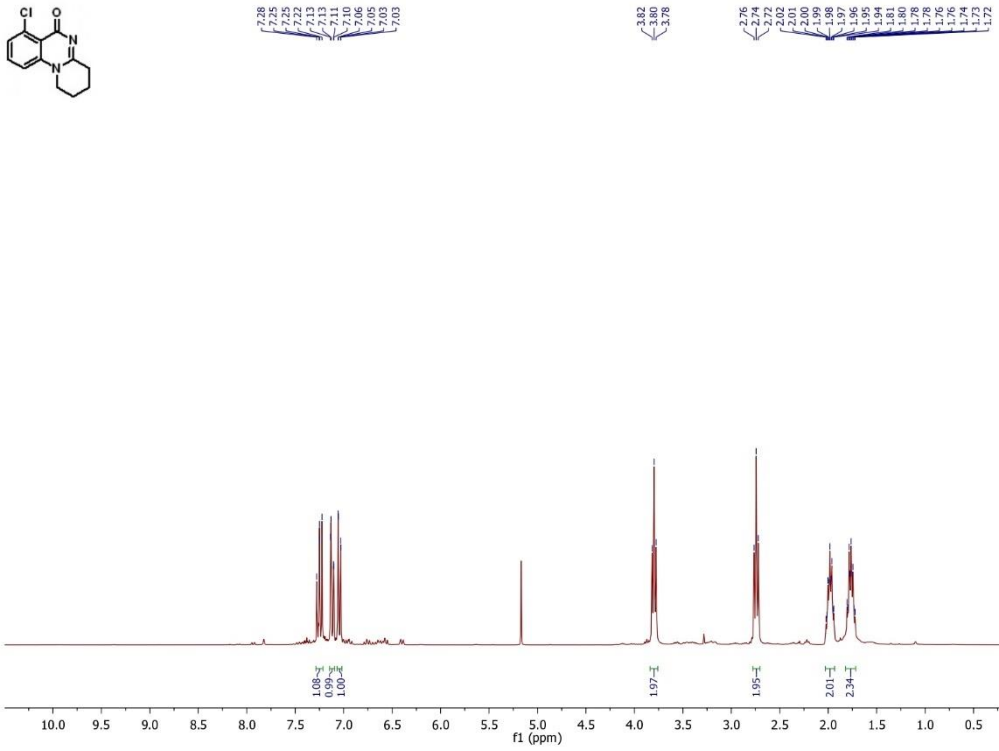
Cl
O
N
7.28
7.25
7.25
7.22
7.13
7.13
7.11
7.10
7.06
7.05
7.03
7.03
3.82
3.80
3.78
2.76
2.74
2.72
2.02
2.01
2.00
1.99
1.98
1.97
1.96
1.95
1.94
1.81
1.80
1.78
1.76
1.76
1.74
1.73
1.72
1.08
0.99
1.00
1.97
1.95
2.01
2.34
10.0 9.5 9.0 8.5 8.0 7.5 7.0 6.5 6.0 5.5 5.0 4.5 4.0 3.5 3.0 2.5 2.0 1.5 1.0 0.5 0.0 -0
f1 (ppm)

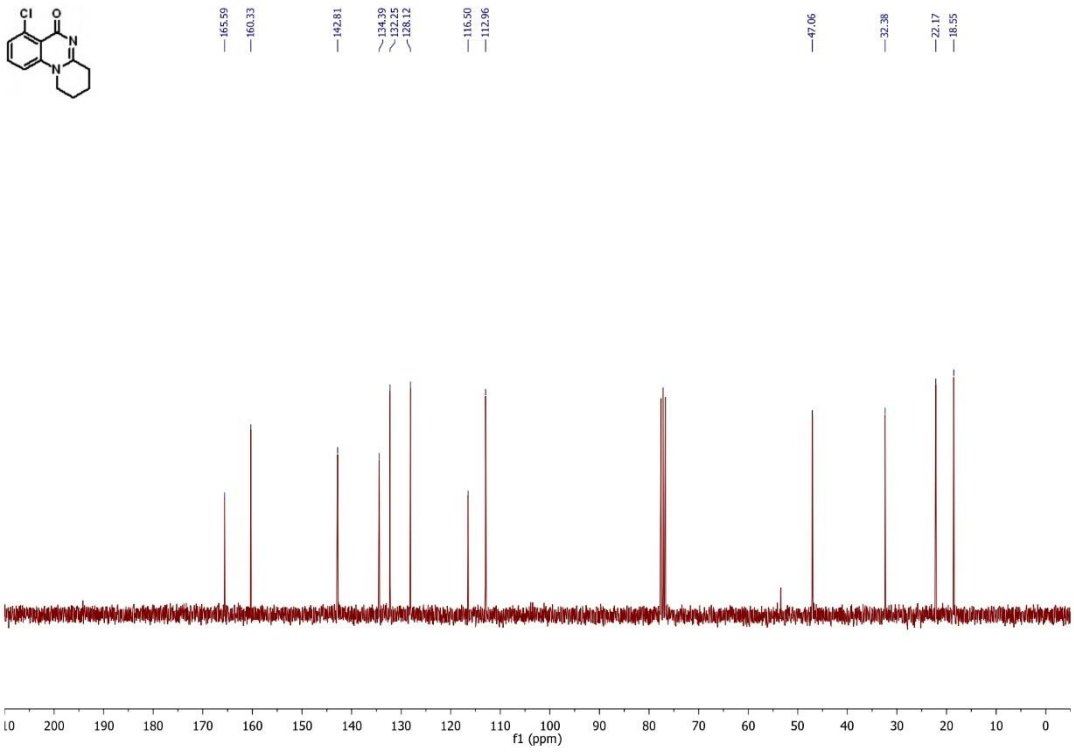
Cl
O
N
165.59
160.33
142.81
134.39
132.25
128.12
116.50
112.96
47.06
32.38
22.17
18.55
10 200 190 180 170 160 150 140 130 120 110 100 90 80 70 60 50 40 30 20 10 0
f1 (ppm)

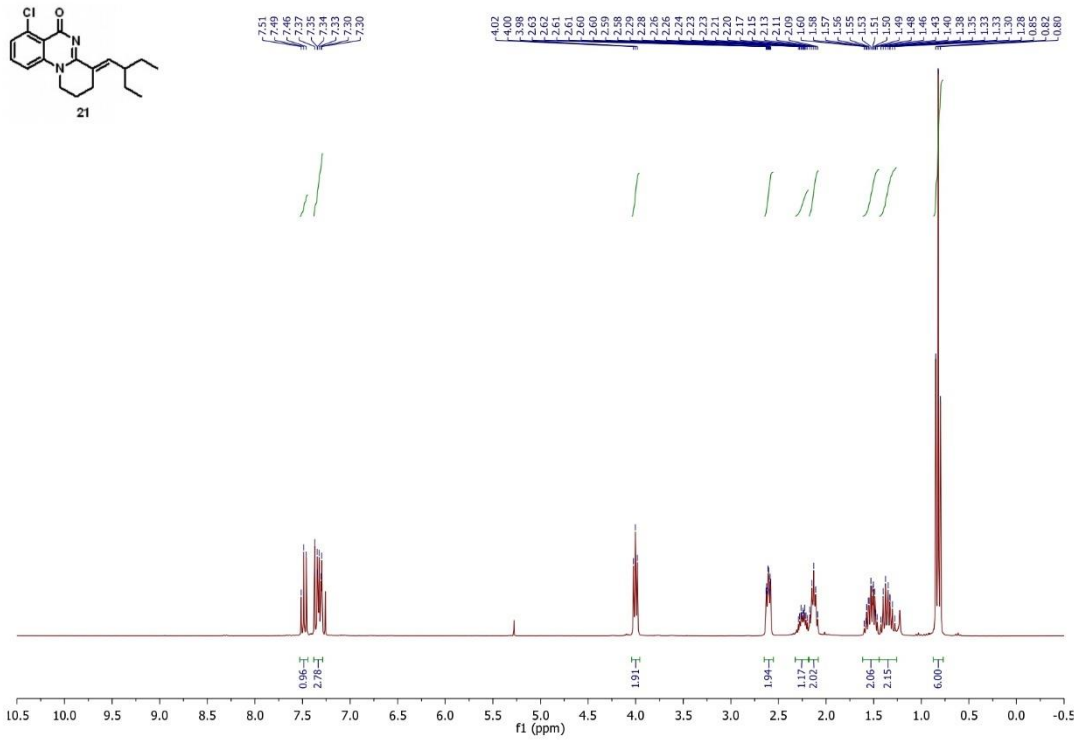
Cl
O
N
N
21
7.51
7.49
7.46
7.37
7.35
7.34
7.33
7.30
7.30
4.02
4.00
3.98
2.63
2.62
2.61
2.61
2.60
2.60
2.59
2.58
2.29
2.28
2.26
2.26
2.24
2.23
2.21
2.20
2.17
2.15
2.13
2.11
2.09
1.60
1.58
1.57
1.56
1.55
1.53
1.51
1.50
1.49
1.48
1.46
1.43
1.40
1.38
1.35
1.33
1.30
1.28
0.85
0.82
0.80
0.96
2.78
1.91
1.94
1.17
2.02
2.06
2.15
6.00
f1 (ppm)

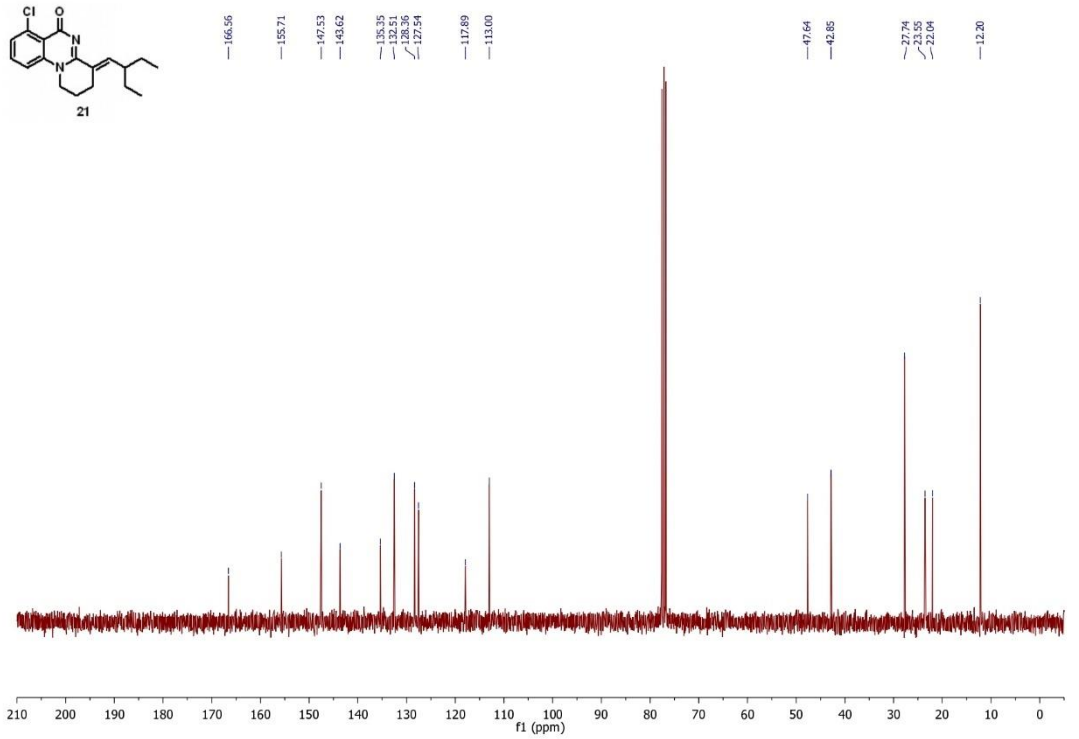
Cl
O
N
N
21
166.56
155.71
147.53
143.62
135.35
132.51
128.36
127.54
117.89
113.00
47.64
42.85
27.74
23.55
22.04
12.20
f1 (ppm)

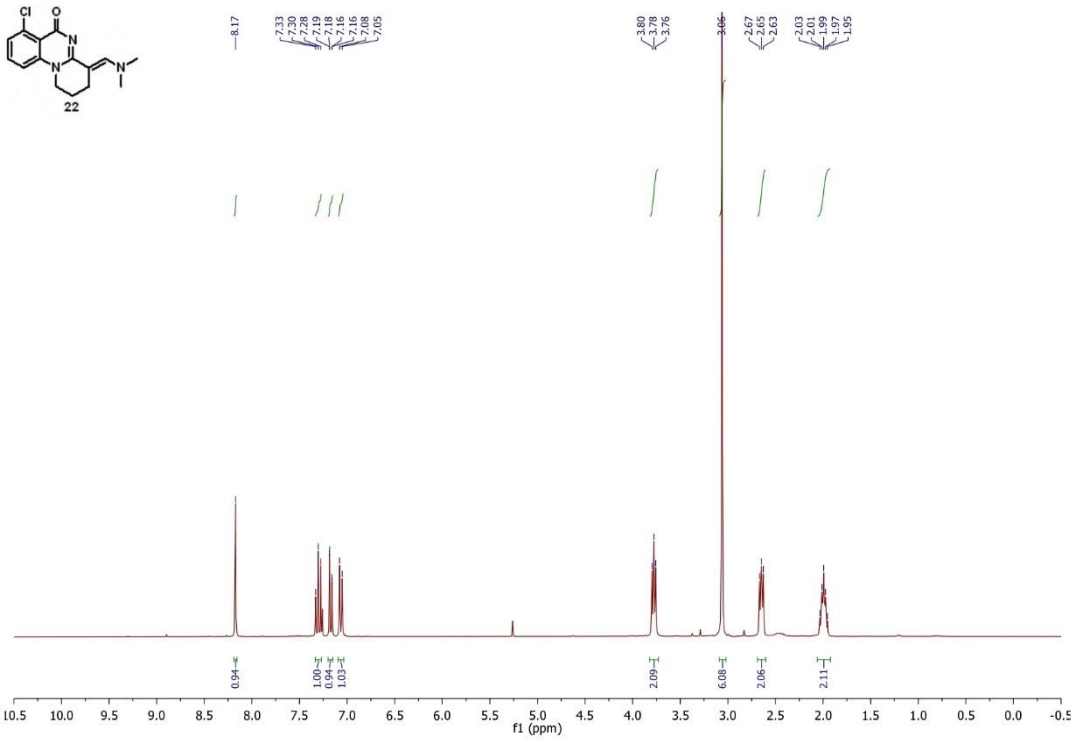
Cl
O
N
N
22
8.17
7.33
7.30
7.28
7.19
7.18
7.16
7.08
7.05
3.80
3.78
3.76
3.66
2.67
2.65
2.63
2.03
2.01
1.99
1.97
1.95
0.94
1.00
0.94
1.03
2.09
6.08
2.06
2.11
f1 (ppm)

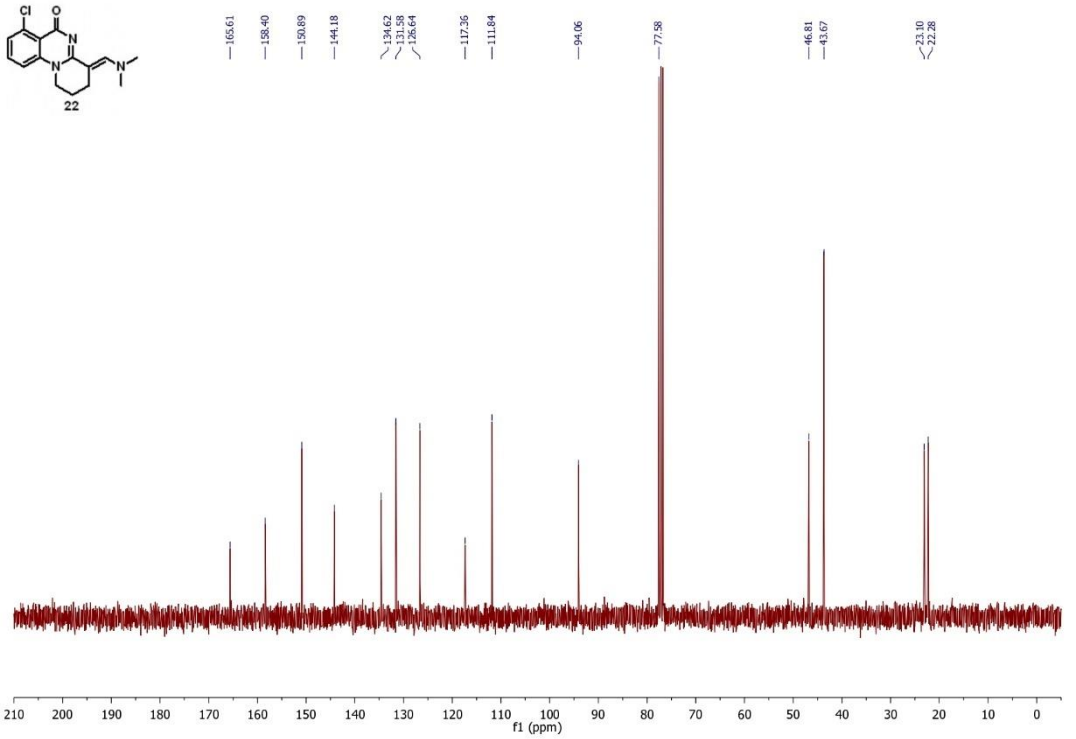
Cl
O
N
N
22
165.61
158.40
150.89
144.18
134.62
131.58
126.64
117.36
111.84
94.06
77.58
46.81
43.67
23.10
22.28
f1 (ppm)

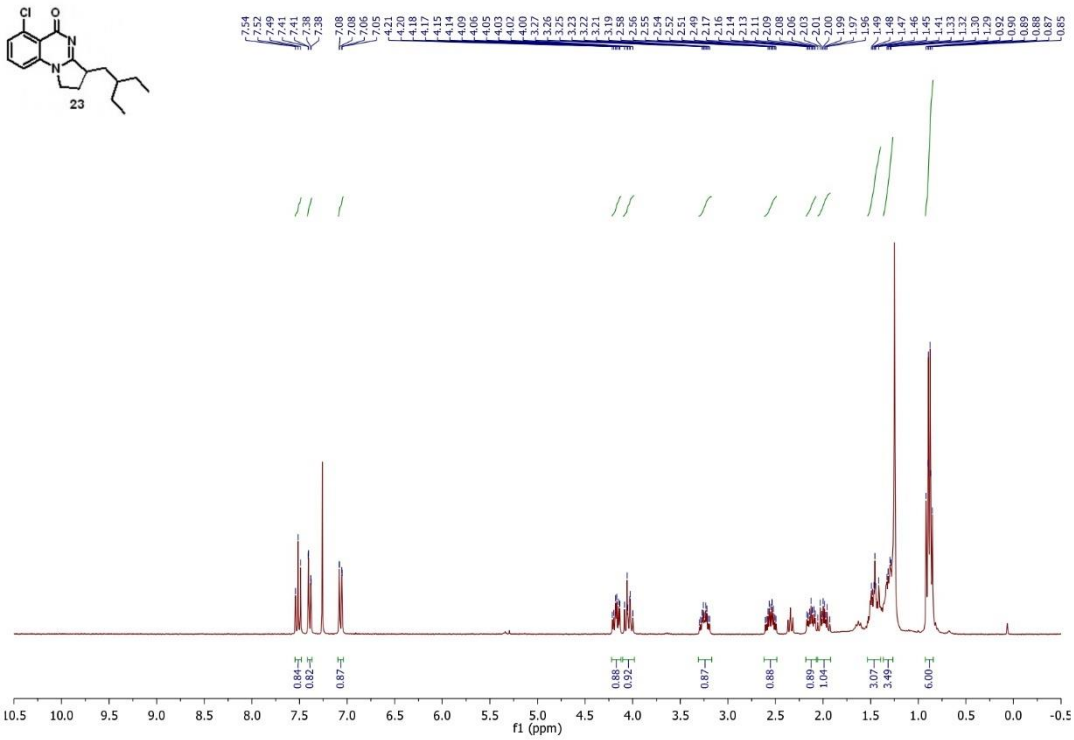
Cl
O
N
N
23
f1 (ppm)

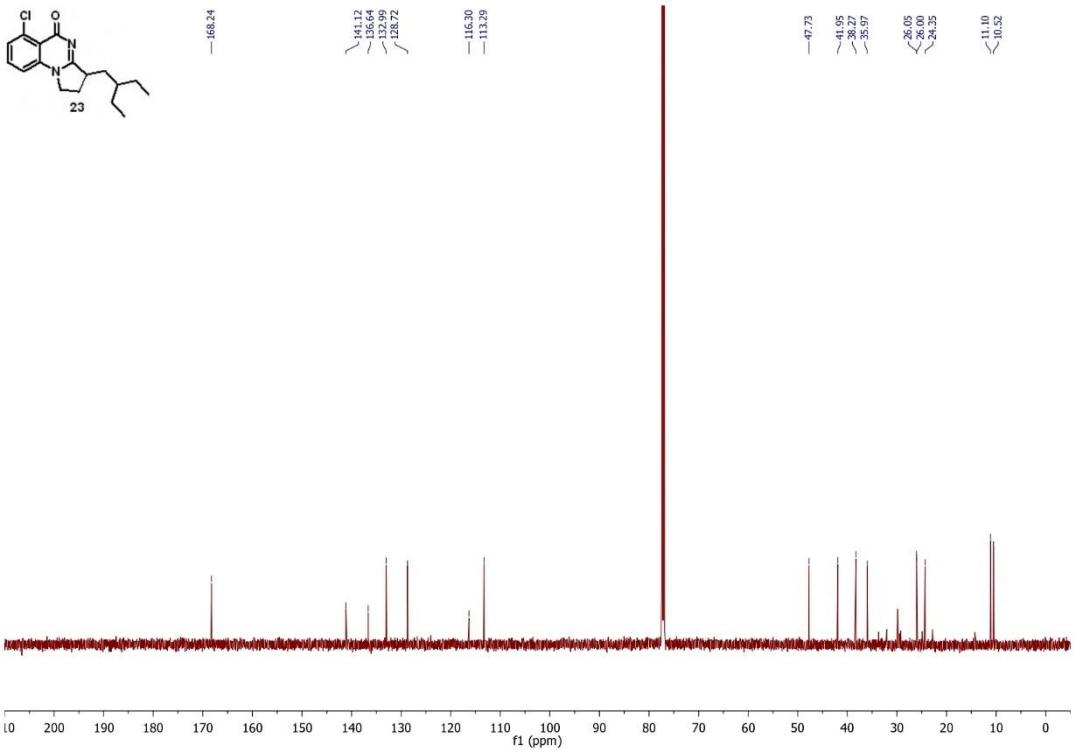
Cl
O
N
N
23
168.24
141.12
135.44
132.99
128.72
116.30
113.29
47.73
41.95
38.27
35.97
26.05
26.00
24.35
11.10
10.52
f1 (ppm)

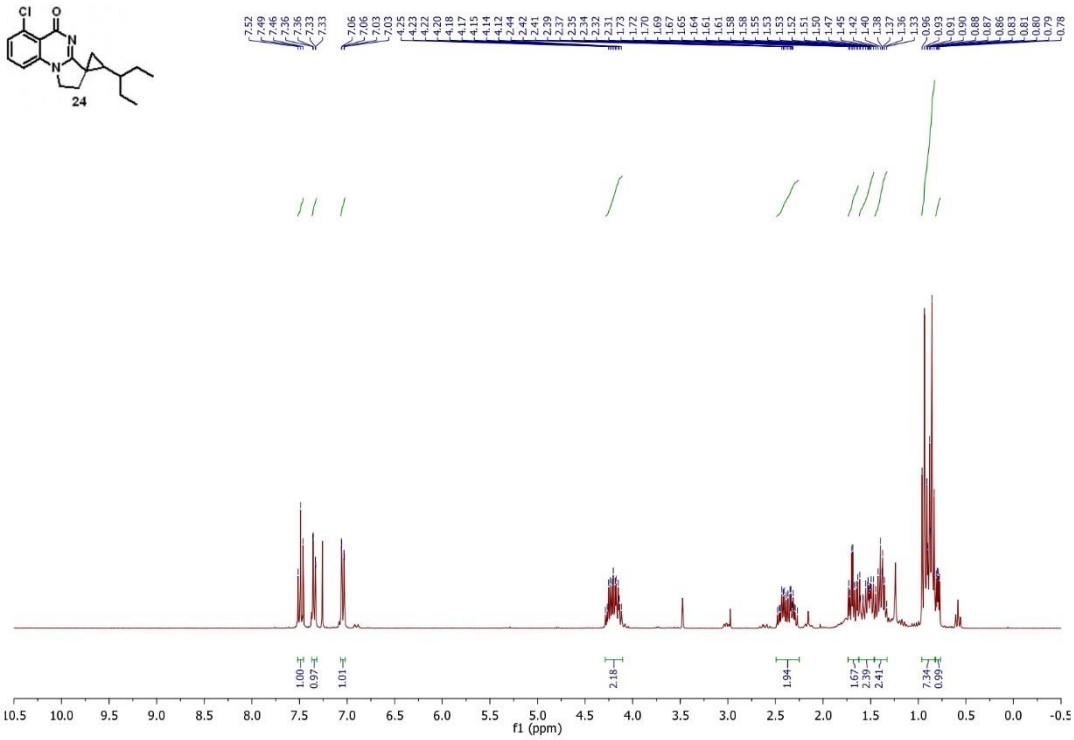
24
f1 (ppm)

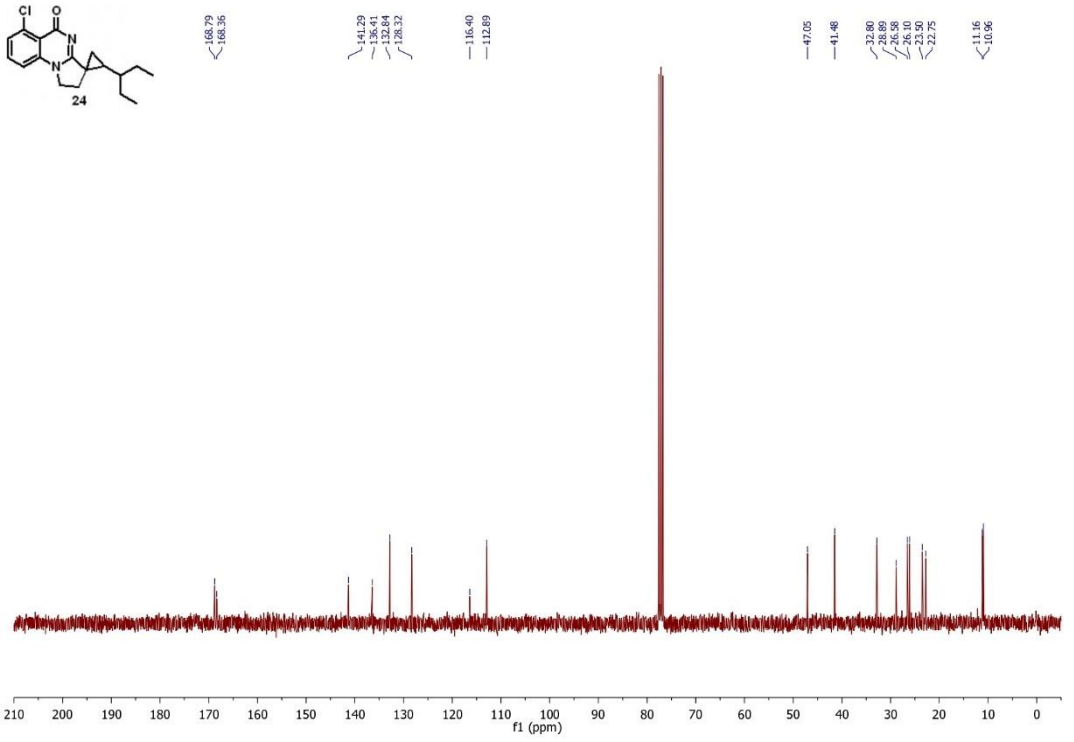
24
f1 (ppm)

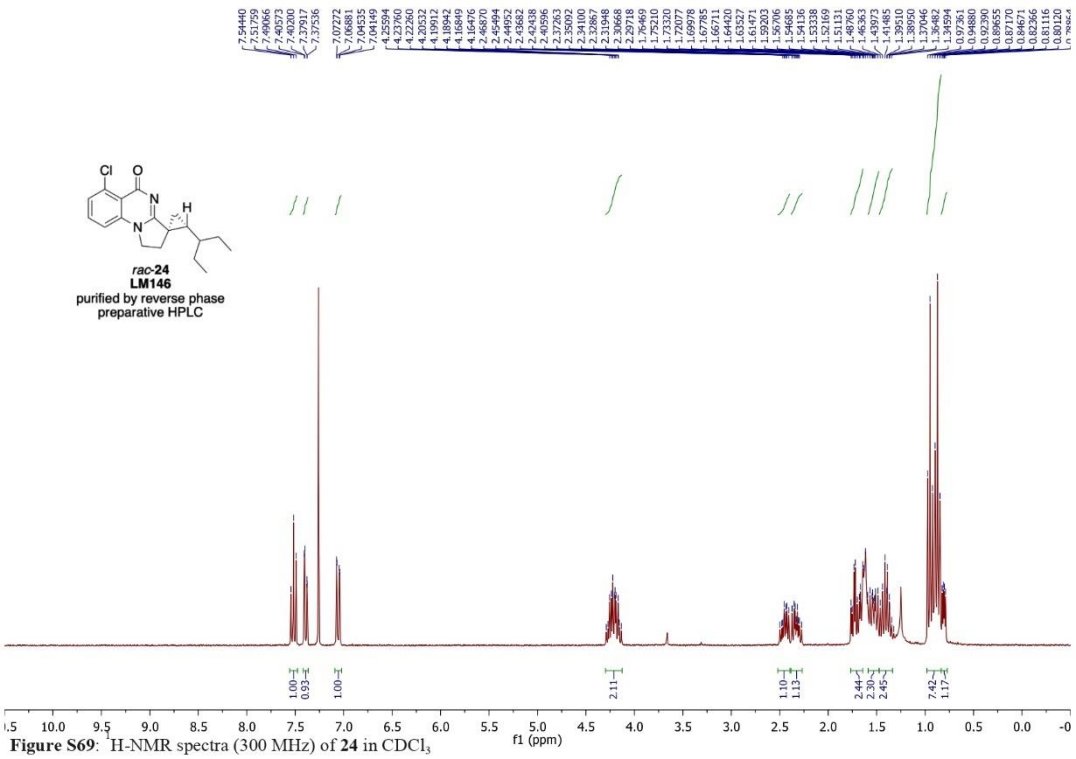

Figure S69: ^{1}H-NMR spectra (300 MHz) of **24** in $CDCl_3$

ANNEXE D

« SYNTHESIS OF NVS-BPTF-1 AND EVALUATION OF ITS IMPACT ON THE IMMUNOPROTEASOME. » - PARTIE EXPÉRIMENTALE

Mélin, L.; Calosing, C.; Kharenko, O.A.; Hansen, H.C.; Gagnon, A.

Supporting Information

Synthesis of NVS-BPTF-1 and Evaluation of its Impact on the Immunoproteasome

Léa Mélin,† Cyrus Calosing,§ Olesya A. Kharenko,§ Henrik C. Hansen,§ Alexandre Gagnon*†

† Département de chimie, Université du Québec à Montréal, C.P. 8888, Succ. Centre-Ville, Montréal, Québec, H3C 3P8, Canada

§ Zenith Epigenetics Ltd, Suite 300, 4820 Richard Road SW, Calgary, AB, T3E 6L1, Canada

Table of content

Mélin, L.; Calosing, C.; Kharenko, O.A.; Hansen, H.C.; Gagnon, A.

1. Biological Evaluation

a) AlphaScreen Assay

The AlphaScreen® Histidine (Nickel Chelate) Detection Kit (Perkin Elmer, 6760619M) was used according to the manufacturer's instructions. 100 nM N-terminally His-tagged BPTF (Active Motif) or 33 nM BRDBD1 (Genscript) and biotinylated tetra-acetylated histone H4 peptide (50 nM) (Millipore) were mixed in 50 mM HEPES, 100 mM NaCl, and 0.1% bovine serum albumin buffer, pH 7.4. Nickel chelate acceptor beads and streptavidin donor beads (PerkinElmer) were added to a final concentration of 2 µg/mL under green light. Serially diluted compounds were added to the reaction mixture in a white 96 well plate (Greiner) and assay plates were read at 570 nM on a Synergy H4 Plate Reader (Biotek) after 30 min incubation time. GraphPad Prism software was used to determine IC_{50} values.

b) Protein Thermal Denaturation Assay

5 µM of purified bromodomain proteins (BRD4BD1 and BPTF) were incubated with 100 µM of the compound or DMSO (0.2%) in the presence of 5X SYPRO® Orange (Molecular Probes) in 20 mM HEPES, pH 7.4, and 100 mM NaCl. Samples were incubated at room temperature for 30 min followed by the increase from 25 °C to 95 °C in a ViiA7 real-time PCR machine (Applied Biosystems). The melting temperatures were calculated using Protein Thermal Shift™ Software v1.0 (Life Technologies).

c) Proliferation Assay

Cells were purchased from ATCC and cultured according to supplier's protocol in 80 mL flasks. Once confluent cells were detached with trypsin, diluted 1:10 for B16F10, A549, BT549 and CAL51 and 1:6 for HCC70 and MDA453 then plated into 96 well plates. After overnight adherence, cells were treated with NVS-BPTF-1, AU1 or C620-0696 (Aobious) on Day 1 and Day 4. On day 7, the effect on proliferation was measured using CellTiter-Fluor™ Cell Viability Assay (Promega) and Synergy H4 Hybrid Microplate Reader (Biotek). Data was analyzed using GraphPad.

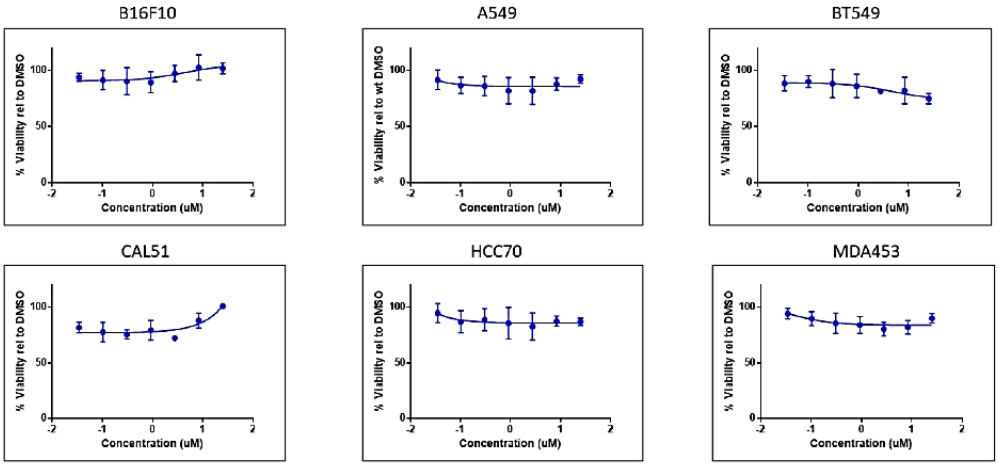

*Figure S1. Effect of BPTF bromodomain inhibition by **NVS-BPTF-1** on proliferation in mouse and human cell lines.*

d) siRNA Knockdown of Bptf in B16F10

B16F10 cells were plated 200,000 cells per well for 6 well plate. Dharmafect 1 (Dharmacon) was used to transfect ON-TARGETplus SMARTpool siRNA mouse Bptf (L-064332-01) or non-targeting pool (D-001810-10).

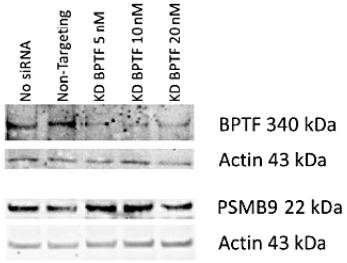

Figure S2. BPTF siRNA knockdown increases PSMB9 in B16F10 cells.

e) Measurement of Immunoproteasome Proteins by Western blot

B16F10, A549 and BT549 cells were plated and treated in 6 well plates, lysed with 300 µL RIPA buffer plus protease inhibitors then sonicated. Cell lysates were combined with LDS Loading Buffer and Sample Reducing Agent (Invitrogen). After 80 °C denaturation for 10 min, 10 µL of sample was loaded into NuPAGE 4-12% Bis-Tris gel and separated by electrophoresis at 100 V for 90 min then transferred onto nitrocellulose membrane. Antibodies against TAP1 (12341, Cell Signaling), TAP2 (PA5-37414, ThermoFisher). PSMB8 (13635, Cell Signaling), PSMB9 (PA1-1960, ThermoFisher) and goat anti-rabbit IgG peroxidase (EMD Millipore) were used. Supersignal West Femto Maximum Sensitivity Substrate (Thermo) and Universal Hood

II Gel Molecular Gel Imaging System (Biorad) were used for detection. Quantity One software was used for image processing.

f) RT-PCR of Mouse Psmb9

B16F10 cells were plated 25,000 cells per well in 96 well plates and cultured overnight. After treatment with NVS-BPTF-1, mRNA was isolated using Catcher PLUS (Invitrogen). Psmb9 (Mm00479004_m1) and Ppia endo control (Mm02342430_g1) were applied using RNA Ultrasense One Step qRT-PCR System and Viia7 (Life Technologies).

2. X-Ray Analysis

a) Protocol description

The data for **NVS-BPTF-1**, crystallized from DCM, were collected from a shock-cooled single crystal at 150 K on a Bruker Venture Metaljet κ-geometry diffractometer with a Metal Jet using Helios MX Mirror Optics as monochromator and a Bruker CMOS Photon III detector. The diffractometer was equipped with an Oxford Cryostream 700 low temperature device and used Ga K_α radiation (λ = 1.34139 Å). All data were integrated with *SAINT* and a multi-scan absorption correction using *SADABS* was applied. The structure was solved by dual methods using *XT* and refined by full-matrix least-squares methods against F^2 by *XL*. Structure solution and refinement cycles were performed within the graphical user interface of *OLEX2*. All non-hydrogen atoms were refined with anisotropic displacement parameters. The hydrogen atoms were refined isotropically on calculated positions using a riding model with their U_{iso} values constrained to 1.5 times the U_{eq} of their pivot atoms for terminal sp^3 carbon atoms and 1.2 times for all other carbon atoms. This report and the CIF file were generated using FinalCif. The crystal structure was deposited in the Cambridge Crystallographic Data Centre CCDC (number 2080173).

b) Additional Data

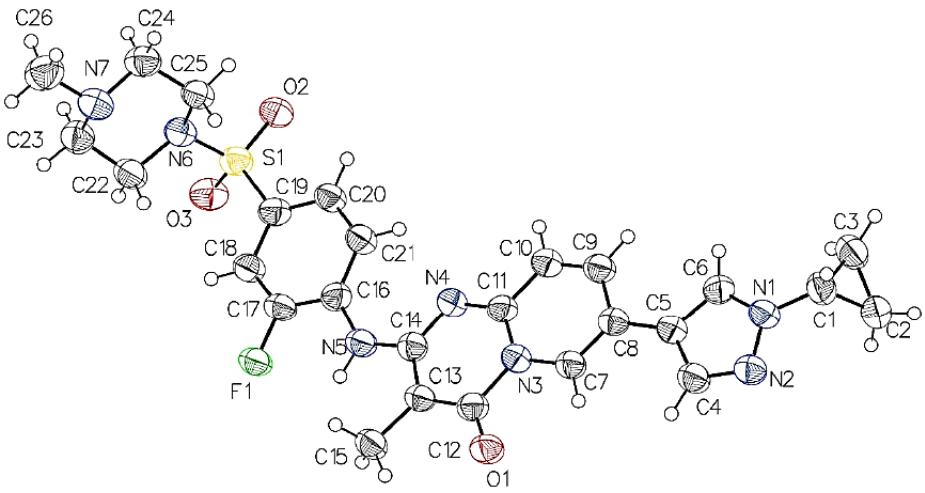

*Figure S3. Thermal atomic displacement ellipsoid plot (Ortep) for **NVS-BPTF-1**. Ellipsoids are drawn at the 50% probability level and hydrogen atoms are shown as spheres of arbitrary size.*

Table S1. Crystal data and structure refinement for ***NVS-BPTF-1.***

Empirical formula	$C_{26}H_{28}FN_7O_3S$
Formula weight	537.61
Temperature [K]	150
Crystal system	orthorhombic
Space group (number)	*Iba*2 (45)
a [Å]	15.8564(18)
b [Å]	43.448(5)
c [Å]	7.2000(9)
α [°]	90
β [°]	90
γ [°]	90
Volume [Å^3]	4960.2(10)
Z	8
ρ_{calc} [gcm^{-3}]	1.440
μ [mm^{-1}]	1.042
F(000)	2256
Crystal size [mm^3]	0.28×0.1×0.03
Crystal colour	clear light colourless
Crystal shape	plate
Radiation	Ga K_α (λ=1.34139 Å)
2Θ range [°]	5.16 to 110.02 (0.82 Å)
Index ranges	-19 ≤ h ≤ 15
	-52 ≤ k ≤ 53
	-8 ≤ l ≤ 8
Reflections collected	19529
Independent reflections	4465
	R_{int} = 0.0786
	R_{sigma} = 0.0705
Completeness to Θ = 53.594°	99.9 %
Data / Restraints / Parameters	4465/1/346
Goodness-of-fit on F^2	1.018
Final *R* indexes [I≥2σ(I)]	R_1 = 0.0586
	wR_2 = 0.1427
Final *R* indexes [all data]	R_1 = 0.0983
	wR_2 = 0.1717
Largest peak/hole [eÅ^{-3}]	0.29/-0.32
Flack X parameter	0.00(3)
Extinction coefficient	0.00057(14)

Table S2. Atomic coordinates and U_{eq} [Å^2] for ***NVS-BPTF-1.***

Atom	***x***	***y***	***z***	U_{eq}
S1	0.34117(8)	0.11773(3)	0.2683(3)	0.0528(4)
F1	0.63332(19)	0.16188(8)	0.3619(6)	0.0566(10)
O1	0.7225(2)	0.30515(10)	0.6912(7)	0.0572(12)
O2	0.2572(2)	0.13001(10)	0.2587(8)	0.0598(12)
O3	0.3767(3)	0.10278(10)	0.1087(7)	0.0603(12)
N1	0.4573(3)	0.42986(12)	0.8469(8)	0.0492(12)
N2	0.5432(3)	0.43189(12)	0.8561(8)	0.0546(13)
N3	0.5787(3)	0.30452(11)	0.6526(7)	0.0455(12)
N4	0.5062(3)	0.25949(10)	0.5507(7)	0.0471(13)

N5	0.5847(3)	0.21621(11)	0.4660(8)	0.0493(13)
H5	0.635765	0.209635	0.439175	0.059
N6	0.3403(3)	0.09159(11)	0.4333(8)	0.0511(13)
N7	0.3723(3)	0.05753(13)	0.7621(9)	0.0590(14)
C1	0.4068(4)	0.45634(13)	0.8913(11)	0.0541(16)
H1	0.402698	0.461976	1.025644	0.065
C2	0.4050(4)	0.48233(14)	0.7551(12)	0.0585(16)
H2A	0.439328	0.480315	0.640919	0.070
H2B	0.400509	0.503518	0.804741	0.070
C3	0.3301(4)	0.46162(15)	0.7759(13)	0.0643(18)
H3A	0.279493	0.470050	0.838233	0.077
H3B	0.318304	0.446853	0.674450	0.077
C4	0.5688(4)	0.40318(14)	0.8159(10)	0.0552(18)
H4	0.626335	0.397144	0.811896	0.066
C5	0.5019(3)	0.38319(12)	0.7807(10)	0.0453(13)
C6	0.4313(4)	0.40142(13)	0.8022(10)	0.0506(16)
H6	0.374399	0.394970	0.787980	0.061
C7	0.5767(3)	0.33490(14)	0.7060(10)	0.0481(15)
H7	0.628447	0.345252	0.729408	0.058
C8	0.5032(3)	0.35057(13)	0.7264(9)	0.0460(14)
C9	0.4269(4)	0.33385(15)	0.6910(10)	0.0507(15)
H9	0.373979	0.343773	0.706751	0.061
C10	0.4293(3)	0.30452(14)	0.6363(9)	0.0497(16)
H10	0.377722	0.294112	0.612926	0.060
C11	0.5066(3)	0.28821(13)	0.6117(10)	0.0470(14)
C12	0.6612(3)	0.28974(14)	0.6446(10)	0.0492(15)
C13	0.6587(3)	0.25915(14)	0.5849(9)	0.0468(14)
C14	0.5822(4)	0.24573(14)	0.5375(9)	0.0481(15)
C15	0.7402(4)	0.24147(15)	0.5828(10)	0.0539(16)
H15A	0.786117	0.254779	0.625978	0.081
H15B	0.752226	0.234530	0.455970	0.081
H15C	0.735513	0.223571	0.664957	0.081
C16	0.5214(3)	0.19506(13)	0.4287(10)	0.0471(14)
C17	0.5478(3)	0.16632(14)	0.3710(10)	0.0499(15)
C18	0.4957(4)	0.14254(13)	0.3210(9)	0.0500(16)
H18	0.517848	0.123470	0.278765	0.060
C19	0.4088(4)	0.14735(14)	0.3345(10)	0.0515(16)
C20	0.3788(3)	0.17559(14)	0.3989(9)	0.0503(15)
H20	0.319693	0.178648	0.411058	0.060
C21	0.4336(4)	0.19942(14)	0.4456(10)	0.0507(15)
H21	0.412006	0.218520	0.488733	0.061
C22	0.4190(4)	0.07370(15)	0.4551(11)	0.0574(17)
H22A	0.463680	0.086889	0.508837	0.069
H22B	0.438504	0.066239	0.332453	0.069
C23	0.4017(4)	0.04656(15)	0.5828(11)	0.0610(18)
H23A	0.358485	0.033038	0.526321	0.073
H23B	0.453961	0.034379	0.599341	0.073
C24	0.2927(4)	0.07384(16)	0.7383(12)	0.0617(18)
H24A	0.271593	0.080746	0.860784	0.074
H24B	0.250263	0.059788	0.683653	0.074
C25	0.3047(4)	0.10148(14)	0.6122(10)	0.0516(16)
H25A	0.249710	0.111734	0.591347	0.062
H25B	0.343089	0.116455	0.672010	0.062
C26	0.3620(5)	0.03200(18)	0.8901(14)	0.077(2)

H26A	0.315775	0.018797	0.847658	0.115
H26B	0.349035	0.039955	1.014204	0.115
H26C	0.414343	0.020018	0.894857	0.115

U_{eq} is defined as 1/3 of the trace of the orthogonalized U_{ij} tensor.

*Table S3. Bond lengths and angles for **NVS-BPTF-1.***

Atom–Atom	Length [Å]
S1–O2	1.436(4)
S1–O3	1.435(5)
S1–N6	1.644(6)
S1–C19	1.741(6)
F1–C17	1.371(6)
O1–C12	1.227(6)
N1–N2	1.367(6)
N1–C1	1.437(8)
N1–C6	1.342(8)
N2–C4	1.343(8)
N3–C7	1.375(7)
N3–C11	1.377(7)
N3–C12	1.458(7)
N4–C11	1.323(7)
N4–C14	1.349(7)
N5–H5	0.8800
N5–C14	1.383(7)
N5–C16	1.387(7)
N6–C22	1.479(7)
N6–C25	1.470(9)
N7–C23	1.453(10)
N7–C24	1.458(8)
N7–C26	1.451(10)
C1–H1	1.0000
C1–C2	1.496(10)
C1–C3	1.491(10)
C2–H2A	0.9900
C2–H2B	0.9900
C2–C3	1.497(9)
C3–H3A	0.9900
C3–H3B	0.9900
C4–H4	0.9500
C4–C5	1.394(8)
C5–C6	1.381(8)
C5–C8	1.470(7)
C6–H6	0.9500
C7–H7	0.9500
C7–C8	1.358(8)
C8–C9	1.435(8)
C9–H9	0.9500
C9–C10	1.335(9)
C10–H10	0.9500
C10–C11	1.426(8)
C12–C13	1.397(8)
C13–C14	1.388(8)
C13–C15	1.504(8)

C15–H15A	0.9800
C15–H15B	0.9800
C15–H15C	0.9800
C16–C17	1.381(8)
C16–C21	1.409(8)
C17–C18	1.371(8)
C18–H18	0.9500
C18–C19	1.397(8)
C19–C20	1.395(8)
C20–H20	0.9500
C20–C21	1.394(8)
C21–H21	0.9500
C22–H22A	0.9900
C22–H22B	0.9900
C22–C23	1.520(10)
C23–H23A	0.9900
C23–H23B	0.9900
C24–H24A	0.9900
C24–H24B	0.9900
C24–C25	1.517(9)
C25–H25A	0.9900
C25–H25B	0.9900
C26–H26A	0.9800
C26–H26B	0.9800
C26–H26C	0.9800

Atom–Atom–Atom	**Angle [°]**
O2–S1–N6	106.5(3)
O2–S1–C19	108.0(3)
O3–S1–O2	119.6(3)
O3–S1–N6	105.6(3)
O3–S1–C19	108.2(3)
N6–S1–C19	108.5(3)
N2–N1–C1	119.5(5)
C6–N1–N2	112.2(5)
C6–N1–C1	128.2(5)
C4–N2–N1	103.3(5)
C7–N3–C11	122.3(5)
C7–N3–C12	117.0(5)
C11–N3–C12	120.7(5)
C11–N4–C14	116.0(5)
C14–N5–H5	114.1
C14–N5–C16	131.8(5)
C16–N5–H5	114.1
C22–N6–S1	115.6(4)
C25–N6–S1	115.8(4)
C25–N6–C22	112.7(5)
C23–N7–C24	109.5(6)
C26–N7–C23	110.5(6)
C26–N7–C24	110.4(5)
N1–C1–H1	116.6
N1–C1–C2	118.0(6)
N1–C1–C3	117.0(6)
C2–C1–H1	116.6

C3–C1–H1	116.6
C3–C1–C2	60.1(5)
C1–C2–H2A	117.8
C1–C2–H2B	117.8
C1–C2–C3	59.8(4)
H2A–C2–H2B	114.9
C3–C2–H2A	117.8
C3–C2–H2B	117.8
C1–C3–C2	60.1(4)
C1–C3–H3A	117.8
C1–C3–H3B	117.8
C2–C3–H3A	117.8
C2–C3–H3B	117.8
H3A–C3–H3B	114.9
N2–C4–H4	123.6
N2–C4–C5	112.9(5)
C5–C4–H4	123.6
C4–C5–C8	129.7(5)
C6–C5–C4	103.8(5)
C6–C5–C8	126.4(5)
N1–C6–C5	107.8(5)
N1–C6–H6	126.1
C5–C6–H6	126.1
N3–C7–H7	119.0
C8–C7–N3	122.1(5)
C8–C7–H7	119.0
C7–C8–C5	121.6(5)
C7–C8–C9	116.8(5)
C9–C8–C5	121.6(5)
C8–C9–H9	119.6
C10–C9–C8	120.8(5)
C10–C9–H9	119.6
C9–C10–H10	118.8
C9–C10–C11	122.4(5)
C11–C10–H10	118.8
N3–C11–C10	115.6(5)
N4–C11–N3	124.0(5)
N4–C11–C10	120.4(5)
O1–C12–N3	117.3(5)
O1–C12–C13	128.7(5)
C13–C12–N3	113.9(5)
C12–C13–C15	117.7(5)
C14–C13–C12	120.0(5)
C14–C13–C15	122.3(5)
N4–C14–N5	117.6(5)
N4–C14–C13	125.2(6)
N5–C14–C13	117.2(5)
C13–C15–H15A	109.5
C13–C15–H15B	109.5
C13–C15–H15C	109.5
H15A–C15–H15B	109.5
H15A–C15–H15C	109.5
H15B–C15–H15C	109.5
N5–C16–C21	127.5(5)

C17–C16–N5	115.9(5)
C17–C16–C21	116.5(5)
F1–C17–C16	116.2(5)
C18–C17–F1	118.5(5)
C18–C17–C16	125.3(5)
C17–C18–H18	121.2
C17–C18–C19	117.6(5)
C19–C18–H18	121.2
C18–C19–S1	118.5(5)
C20–C19–S1	122.1(4)
C20–C19–C18	119.4(5)
C19–C20–H20	119.3
C21–C20–C19	121.4(5)
C21–C20–H20	119.3
C16–C21–H21	120.1
C20–C21–C16	119.7(5)
C20–C21–H21	120.1
N6–C22–H22A	110.0
N6–C22–H22B	110.0
N6–C22–C23	108.6(5)
H22A–C22–H22B	108.3
C23–C22–H22A	110.0
C23–C22–H22B	110.0
N7–C23–C22	109.9(6)
N7–C23–H23A	109.7
N7–C23–H23B	109.7
C22–C23–H23A	109.7
C22–C23–H23B	109.7
H23A–C23–H23B	108.2
N7–C24–H24A	109.6
N7–C24–H24B	109.6
N7–C24–C25	110.3(5)
H24A–C24–H24B	108.1
C25–C24–H24A	109.6
C25–C24–H24B	109.6
N6–C25–C24	109.9(5)
N6–C25–H25A	109.7
N6–C25–H25B	109.7
C24–C25–H25A	109.7
C24–C25–H25B	109.7
H25A–C25–H25B	108.2
N7–C26–H26A	109.5
N7–C26–H26B	109.5
N7–C26–H26C	109.5
H26A–C26–H26B	109.5
H26A–C26–H26C	109.5
H26B–C26–H26C	109.5

*Table S4. Torsion angles for **NVS-BPTF-1.***

Atom–Atom–Atom–Atom	Torsion Angle [°]
S1–N6–C22–C23	−168.3(5)
S1–N6–C25–C24	169.4(4)

S1–C19–C20–C21	−177.9(5)
F1–C17–C18–C19	178.9(6)
O1–C12–C13–C14	−179.9(6)
O1–C12–C13–C15	2.8(11)
O2–S1–N6–C22	174.3(5)
O2–S1–N6–C25	−50.8(5)
O2–S1–C19–C18	−168.6(6)
O2–S1–C19–C20	10.9(7)
O3–S1–N6–C22	46.2(5)
O3–S1–N6–C25	−178.9(4)
O3–S1–C19–C18	−37.8(6)
O3–S1–C19–C20	141.7(6)
N1–N2–C4–C5	0.3(8)
N1–C1–C2–C3	106.7(7)
N1–C1–C3–C2	−108.4(7)
N2–N1–C1–C2	72.7(8)
N2–N1–C1–C3	141.5(6)
N2–N1–C6–C5	0.2(8)
N2–C4–C5–C6	−0.2(8)
N2–C4–C5–C8	177.8(7)
N3–C7–C8–C5	−179.0(6)
N3–C7–C8–C9	0.5(10)
N3–C12–C13–C14	0.8(9)
N3–C12–C13–C15	−176.6(5)
N5–C16–C17–F1	1.6(9)
N5–C16–C17–C18	−177.6(6)
N5–C16–C21–C20	178.9(6)
N6–S1–C19–C18	76.4(6)
N6–S1–C19–C20	−104.1(6)
N6–C22–C23–N7	−59.0(7)
N7–C24–C25–N6	56.3(7)
C1–N1–N2–C4	177.0(6)
C1–N1–C6–C5	−176.8(6)
C4–C5–C6–N1	0.0(8)
C4–C5–C8–C7	1.2(11)
C4–C5–C8–C9	−178.3(7)
C5–C8–C9–C10	177.9(6)
C6–N1–N2–C4	−0.4(7)
C6–N1–C1–C2	−110.4(8)
C6–N1–C1–C3	−41.6(10)
C6–C5–C8–C7	178.8(7)
C6–C5–C8–C9	−0.7(11)
C7–N3–C11–N4	176.3(6)
C7–N3–C11–C10	−2.7(9)
C7–N3–C12–O1	2.1(8)
C7–N3–C12–C13	−178.5(6)
C7–C8–C9–C10	−1.6(10)
C8–C5–C6–N1	−178.1(6)
C8–C9–C10–C11	0.6(10)
C9–C10–C11–N3	1.5(9)
C9–C10–C11–N4	−177.5(7)
C11–N3–C7–C8	1.7(10)
C11–N3–C12–O1	−176.6(6)
C11–N3–C12–C13	2.8(8)

C11–N4–C14–N5	−177.0(6)
C11–N4–C14–C13	0.9(9)
C12–N3–C7–C8	−177.0(6)
C12–N3–C11–N4	−5.0(9)
C12–N3–C11–C10	176.0(5)
C12–C13–C14–N4	−2.8(10)
C12–C13–C14–N5	175.1(6)
C14–N4–C11–N3	3.0(9)
C14–N4–C11–C10	−178.0(6)
C14–N5–C16–C17	−174.7(7)
C14–N5–C16–C21	4.3(11)
C15–C13–C14–N4	174.4(6)
C15–C13–C14–N5	−7.6(9)
C16–N5–C14–N4	−11.7(10)
C16–N5–C14–C13	170.2(6)
C16–C17–C18–C19	−2.0(10)
C17–C16–C21–C20	−2.1(9)
C17–C18–C19–S1	179.0(5)
C17–C18–C19–C20	−0.6(10)
C18–C19–C20–C21	1.6(10)
C19–S1–N6–C22	−69.6(5)
C19–S1–N6–C25	65.2(5)
C19–C20–C21–C16	−0.3(10)
C21–C16–C17–F1	−177.5(5)
C21–C16–C17–C18	3.3(10)
C22–N6–C25–C24	−54.4(6)
C23–N7–C24–C25	−61.1(7)
C24–N7–C23–C22	62.8(7)
C25–N6–C22–C23	55.5(7)
C26–N7–C23–C22	−175.4(5)
C26–N7–C24–C25	177.1(6)

Table S5. Hydrogen bonds for ***NVS-BPTF-1.***

D–H···A [Å]	**d(D–H) [Å]**	**d(H···A) [Å]**	**d(D···A) [Å]**	**<(DHA) [°]**
N5–H5···F1	0.88	2.15	2.594(6)	110.7
C6–H6···O2$^{\#1}$	0.95	2.36	3.301(7)	169.8
C20–H20···O1$^{\#2}$	0.95	2.63	3.358(8)	133.2
C21–H21···N4	0.95	2.37	2.951(8)	119.4
C24–H24A···O3$^{\#3}$	0.99	2.62	3.236(9)	120.2
C25–H25B···F1$^{\#4}$	0.99	2.43	3.330(7)	150.8

Symmetry transformations used to generate equivalent atoms:
#1: 0.5-X, 0.5-Y, 0.5+Z; #2: -0.5+X, 0.5-Y, +Z; #3: +X, +Y, 1+Z; #4: 1.0-X, +Y, 0.5+Z

3. General Chemistry Methods

Unless otherwise stated, reactions were performed in non-flame dried glassware and commercial reagents were used without further purification. Anhydrous solvents were obtained using an encapsulated solvent purification system and were further dried over 4 Å molecular sieves. The evolution of reactions was monitored by analytical thin-layer chromatography

(TLC) using silica gel 60 F254 precoated plates visualized by ultraviolet radiation (254 nm). Flash chromatography was performed employing 230-400 mesh silica using the indicated solvent system according to standard techniques. Nuclear magnetic resonance spectra ^{1}H were recorded on a BrukerAvance-III 300 MHz or 600 MHz and ^{13}C were recorded on a BrukerAvance-III 75 MHz or 151 MHz spectrometer. Chemical shifts for ^{1}H-NMR spectra are recorded in parts per million from tetramethylsilane with the solvent resonance as the internal standard (chloroform-d, δ 7.26 ppm; methanol-d_4, δ 3.31 ppm, dimethysulfoxide-d_6, δ 2.50 ppm). Data is reported as follows: chemical shift, multiplicity (s = singlet, s(br) = broad singlet, d = doublet, t = triplet, q = quartet, quint = quintet, sext= sextet, m = multiplet, dd = doublet of doublet, dt = doublet of triplet, ddd = doublet of doublet of doublet, dtd = doublet of triplet of doublet), coupling constant *J* in Hz and integration. Chemical shifts for ^{13}C-NMR spectra are recorded in parts per million from tetramethylsilane using the solvent resonance as the internal standard (chloroform-d, δ 77.16 ppm; methanol-d_4, δ 49.00 ppm, dimethysulfoxide-d_6, δ 39.52 ppm). Purity was assessed on an Agilent 1260 infinity HPLC system equipped with an Agilent Eclipse Plus C18 (3.5 μM, 4.6 x 100 mm) column using a 20-minute gradient method (0 to 100% MeCN + 0.06% TFA in water + 0.06% TFA; the absorbance was measured at 254 nm). HRMS were performed on a TOF LCMS analyzer using the electrospray (ESI) mode.

4. Compound Synthesis and Characterization

1-((3-Fluoro-4-nitrophenyl)sulfonyl)-4-methylpiperazine (**11**)

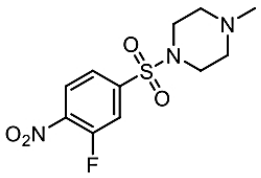

To a solution of 1-methylpiperazine **10** (0.17 mL, 1.5 mmol, 1 eq) in dry CH_2Cl_2 (12 mL) was added triethylamine (0.63 mL, 4.5 mmol, 3 eq). The solution was cooled to 0 °C and 3-fluoro-4-nitrobenzenesulfonyl chloride **9** (395 mg, 1.65 mmol, 1.1 eq) was added. The reaction mixture was slowly allowed to warm up to room temperature and stirred for 15 min. After being concentrated in vacuo, the crude material was purified by flash column chromatography (SiO_2, hexanes/EtOAc 20:80 to 0:100) to provide **11** as a yellow solid (253 mg, 0.834 mmol, 56%). ^{1}H-NMR (300 MHz, $CDCl_3$) δ 8.19 (dd, *J* = 8.7, 6.9 Hz, 1H), 7.71 – 7.64 (m, 2H), 3.11 (t, *J* = 5.0 Hz, 4H), 2.48 (t, *J* = 5.0 Hz, 4H), 2.27 (s, 3H); ^{13}C-NMR (75 MHz, $CDCl_3$) δ 157.00, 153.42,

143.04, 142.95, 127.16, 127.12, 123.78, 123.72, 118.35, 118.04, 53.99, 46.04, 45.79; ^{19}F-NMR (282 MHz, DMSO-d_6) δ -115.36, -115.39, -115.40, -115.42.

2-Fluoro-4-((4-methylpiperazin-1-yl)sulfonyl)aniline (**3**)

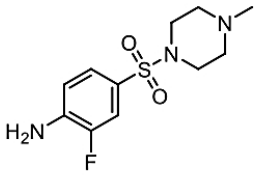

To a suspension of 1-((3-fluoro-4-nitrophenyl)sulfonyl)-4-methylpiperazine **11** (100 mg, 0.330 mmol, 1 eq) in ethanol (1.3 mL) was added three drops of $HCl_{conc.}$ and metallic iron powder (74 mg, 1.3 mmol, 4 eq). After heating at 79 °C for 1 h, the reaction mixture was cooled down to room temperature and quenched with a slow addition of saturated aqueous solution of $NaHCO_3$ (10 mL). The aqueous phase was extracted with EtOAc (3 x 10 mL). Combined organic phases were washed with water (1 x 20 mL), brine (1 x 20 mL), dried over Na_2SO_4, filtered and concentrated under reduced pressure to provide **3** (89 mg, 0.33 mmol, quant.) as a beige solid. ^{1}H-NMR (300 MHz, Methanol-d_4) δ 7.36 – 7.28 (m, 2H), 6.90 (t, J = 8.6 Hz, 1H), 2.99 (t, J = 5.1 Hz, 4H), 2.50 (t, J = 5.0 Hz, 4H), 2.26 (s, 3H); ^{13}C-NMR (75 MHz, $CDCl_3$) δ 125.38, 125.34, 123.54, 115.63, 115.54, 115.26, 54.12, 46.05, 45.79; ^{19}F-NMR (282 MHz, $CDCl_3$) δ -134.05, -134.08, -134.10, -134.11, -134.13.

1-Cyclopropyl-4-iodo-1*H*-pyrazole (**13**)

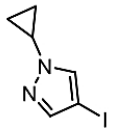

To a sealable tube were added 4-iodo-1*H*-pyrazole **12** (300 mg, 1.55 mmol, 1 eq), cyclopropylboronic acid (266 mg, 3.10 mmol, 2 eq), $Cu(OAc)_2$ (282 mg, 1.55 mmol, 1 eq), DMAP (757 mg, 6.20 mmol, 4 eq) and pyridine (0.314 mL, 3.88 mmol, 2.5 eq) in dioxane (15 mL). The resulting mixture was bubbled with oxygen for 1 min and then stirred at 100 °C for 16 h under oxygen atmosphere. Back to room temperature, a saturated aqueous solution of NH_4Cl was added. The aqueous phase was extracted with EtOAc (3 x 20 mL). Combined organic phases were washed with a saturated aqueous solution of NH_4Cl (2 x 40 mL), brine (1 x 40 mL), dried over Na_2SO_4, filtered and concentrated under reduced pressure. Purification by flash column chromatography (SiO_2, hexanes/EtOAc 95:5 to 85:15) provided **13** (347 mg, 1.48

mmol, 95%) as a transparent uncolored oil. ^{1}H-NMR (300 MHz, $CDCl_3$) δ 7.45 (s, 1H), 7.42 (s, 1H), 3.55 (tt, *J* = 7.3, 3.6 Hz, 1H), 1.10 – 1.01 (m, 2H), 1.01 – 0.92 (m, 2H); ^{13}C-NMR (75 MHz, $CDCl_3$) δ 144.23, 134.08, 55.66, 33.01, 6.56.

1-Cyclopropyl-4-(4,4,5,5-tetramethyl-1,3,2-dioxaborolan-2-yl)-1H-pyrazole (**14**)

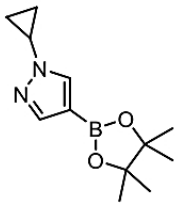

1-Cyclopropyl-4-iodo-1*H*-pyrazole **13** (463 mg, 1.98 mmol, 1 eq), bis(pinacolato)diboron (703 mg, 2.77 mmol, 1.4 eq), potassium acetate (777 mg, 7.77 mmol, 4 eq) and [1,1′-Bis(diphenylphosphino)ferrocene]dichloropalladium(II) in complex with dichloromethane (81 mg, 0.099 mmol, 0.05 eq) were combined in DMSO (7.5 mL). The mixture was purged with argon for 5 min and then heated at 80 °C for 3 h. After cooling the reaction mixture down to room temperature, the mixture was diluted with EtOAc (10 mL) and filtered over a plug of celite (rinsed with EtOAc 3 x). The filtrate obtained was washed with brine (2 x 20 mL), dried over Na_2SO_4, filtered and concentrated under reduced pressure. Purification by flash column chromatography (SiO_2, hexanes/EtOAc 80:20 to 50:50) provided **14** (383 mg, 1.63 mmol, 82%) as a transparent uncolored oil. ^{1}H-NMR (300 MHz, $CDCl_3$) δ 7.73 (s, 1H), 7.72 (s, 1H), 3.58 (tt, *J* = 7.4, 3.9 Hz, 1H), 1.29 (s, 12H), 1.12 – 1.05 (m, 2H), 1.03 – 0.95 (m, 2H); ^{13}C-NMR (75 MHz, $CDCl_3$) δ 145.52, 136.43, 83.37, 32.56, 24.88, 6.54.

Bis(2,4,6-trichlorophenyl) 2-methylmalonate (**23**)

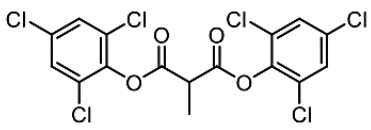

To a mixture of 2-methylmalonic acid **21** (250 mg, 2.12 mmol, 1 eq) and 2,4,6-trichlorophenol **22** (878 mg, 4.45 mmol, 2.1 eq) was added phosphoryl chloride (3.2 mL). The mixture was heated at 90 °C until hydrochloric acid emission stopped (approximately 3 h 30). Back at room temperature, the excess of $POCl_3$ was evaporated and the residue obtained was added to an ice-water mixture. The acidic aqueous phase was then slowly neutralized with a saturated aqueous solution of $NaHCO_3$ until pH = 7. The neutral aqueous phase was extracted with CH_2Cl_2 and combined organic phases were dried over Na_2SO_4, filtered and concentrated under reduced

pressure. Purification by flash column chromatography (SiO_2, hexanes/EtOAc 95:5 to 90:10) provided **23** (927 mg, 1.94 mmol, 92%) as a white solid. ^{1}H-NMR (300 MHz, $CDCl_3$) δ 7.40 (s, 4H), 4.16 (q, J = 7.3 Hz, 1H), 1.83 (d, J = 7.3 Hz, 3H); ^{13}C-NMR (75 MHz, $CDCl_3$) δ 165.39, 142.52, 132.69, 129.68, 128.87, 45.42, 14.39.

7-Bromo-2-hydroxy-3-methyl-4*H*-pyrido[1,2-*a*]pyrimidin-4-one (**17**)

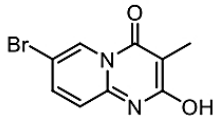

5-Bromopyridin-2-amine **15** (100 mg, 0.578 mmol, 1 eq) and bis(2,4,6-trichlorophenyl) 2-methylmalonate **23** (303 mg, 0.636 mmol, 1.1 eq) were combined in toluene (1 mL). The reaction mixture was stirred at 105 °C for 2 h, quickly leading to the apparition of a yellow precipitate. After cooling the mixture back to room temperature, the precipitate was filtered and rinsed first with toluene, then cold EtOH in order to provide **17** (122 mg, 0.478 mmol, 83%) as a yellow solid. ^{1}H-NMR (300 MHz, DMSO-d_6) δ 8.94 (d, J = 2.3 Hz, 1H), 8.07 (dd, J = 9.3, 2.3 Hz, 1H), 7.34 (d, J = 9.3 Hz, 1H), 1.91 (s, 3H).

7-Bromo-2-chloro-3-methyl-4*H*-pyrido[1,2-*a*]pyrimidin-4-one (**25**)

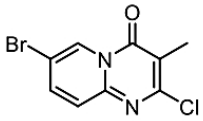

7-Bromo-2-hydroxy-3-methyl-4*H*-pyrido[1,2-*a*]pyrimidin-4-one **17** (67 mg, 0.26 mmol, 1 eq) and PCl_5 (135 mg, 0.650 mmol, 2.5 eq) were combined in $POCl_3$ (1 mL). The reaction mixture was stirred at 105 °C for 16 h. Back at room temperature, the mixture was poured onto ice. The acidic aqueous phase was then slowly neutralized with a saturated aqueous solution of $NaHCO_3$ until pH = 7. The precipitate obtained was filtered in order to provide **25** (54 mg, 0.20 mmol, 77%) as a beige solid. ^{1}H NMR (300 MHz, $CDCl_3$) δ 9.08 (dd, J = 2.2, 0.7 Hz, 1H), 7.75 (dd, J = 9.4, 2.2 Hz, 1H), 7.46 (dd, J = 9.4, 0.7 Hz, 1H), 2.34 (s, 3H); ^{13}C-NMR (75 MHz, $CDCl_3$) δ 157.02, 156.49, 146.46, 139.82, 127.55, 126.70, 112.87, 111.21, 13.65.

2-Chloro-7-(1-cyclopropyl-1*H*-pyrazol-4-yl)-3-methyl-4*H*-pyrido[1,2-*a*]pyrimidin-4-one (**27**)

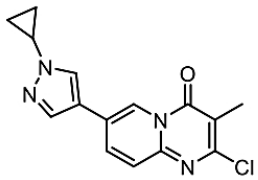

Under argon atmosphere were added 1-cyclopropyl-4-(4,4,5,5-tetramethyl-1,3,2-dioxaborolan-2-yl)-1*H*-pyrazole **14** (47 mg, 0.20 mmol, 1 eq), 7-bromo-2-chloro-3-methyl-4*H*-pyrido[1,2-*a*]pyrimidin-4-one **25** (54 mg, 0.20 mmol, 1 eq), $Pd(PPh_3)_4$ (23 mg, 0.020 mmol, 0.1 eq) and Na_2CO_3 (64 mg, 0.60 mmol, 3 eq) in a mixture of dioxane (1.2 mL) and water (0.3 mL). The reaction mixture was stirred at 80 °C under argon for 20 h. After cooling back to room temperature, the mixture was filtrated and rinsed with EtOAc. After addition of water to the filtrate, the aqueous phase was extracted with EtOAc (3 x). Combined organic phases were washed with brine (1 x 40 mL), dried over Na_2SO_4, filtered and concentrated under reduced pressure. Purification by flash column chromatography (SiO_2, hexanes/EtOAc 50:50 to 30:70) followed by a prep-TLC (hexanes/EtOAc 50:50, eluted 3 times) provided **27** (11 mg, 0.037 mmol, 19%) as a yellow solid. ^{1}H-NMR (300 MHz, DMSO-d_6) δ 9.01 (d, J = 2.1 Hz, 1H), 8.54 (s, 1H), 8.26 (dd, J = 9.2, 2.1 Hz, 1H), 8.07 (s, 1H), 7.67 (d, J = 9.2 Hz, 1H), 3.78 (tt, J = 7.4, 3.9 Hz, 1H), 2.22 (s, 3H), 1.14 – 1.06 (m, 2H), 1.06 – 0.96 (m, 2H).

7-(1-Cyclopropyl-1*H*-pyrazol-4-yl)-2-((2-fluoro-4-((4-methylpiperazin-1-yl)sulfonyl)phenyl)amino)-3-methyl-4*H*-pyrido[1,2-*a*]pyrimidin-4-one (**NVS-BPTF-1**)

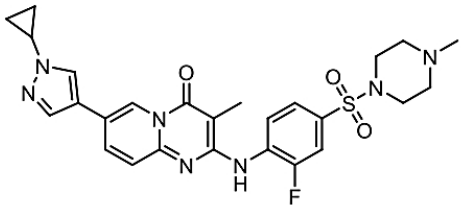

To a solution of 2-fluoro-4-((4-methylpiperazin-1-yl)sulfonyl)aniline **3** (9.3 mg, 0.034 mmol, 1 eq) in dry toluene (1 mL) was added 2-chloro-7-(1-cyclopropyl-1*H*-pyrazol-4-yl)-3-methyl-4*H*-pyrido[1,2-*a*]pyrimidin-4-one **27** (11 mg, 0.037 mmol, 1.1 eq), cesium carbonate (27 mg, 0.082 mmol, 2.4 eq) and a freshly prepared solution of $Pd(OAc)_2$/Rac-BINAP in dry toluene. This solution was obtained by stirring $Pd(OAc)_2$ (1 mg, 0.002 mmol, 0.06 eq) and Rac-BINAP (2 mg, 0.003 mmol, 0.09 eq) in dry toluene (0.3 mL) for 15 min with argon bubbling through

the mixture. The main reaction mixture was heated at 110 °C for 16 h, cooled down to room temperature, filtered over a plug of celite, rinsed with a mixture of CH_2Cl_2/MeOH (90:10) and concentrated under reduced pressure. Purification by flash column chromatography (SiO_2, CH_2Cl_2/MeOH 99:1 to 96:4) provided **NVS-BPTF-1** (10 mg, 0.019 mmol, 56%) as a light yellow solid. ^{1}H-NMR (300 MHz, $CDCl_3$) δ 9.11 (d, *J* = 2.1 Hz, 1H), 8.85 (t, *J* = 8.2 Hz, 1H), 7.84 – 7.79 (m, 3H), 7.59 – 7.48 (m, 3H), 6.87 (d, *J* = 4.8 Hz, 1H), 3.67 (tt, *J* = 7.3, 3.8 Hz, 1H), 3.08 (t, *J* = 5.0 Hz, 4H), 2.49 (t, *J* = 4.8 Hz, 4H), 2.29 (s, 3H), 2.27 (s, 3H), 1.26 – 1.16 (m, 2H), 1.15 – 1.05 (m, 2H); ^{13}C-NMR (75 MHz, $CDCl_3$) δ 157.89, 154.82, 147.26, 136.76, 135.19, 133.05, 132.93, 128.07, 127.99, 127.15, 125.09, 124.66, 122.32, 120.68, 120.61, 117.60, 114.68, 114.38, 94.13, 54.10, 46.05, 45.79, 33.23, 9.59, 6.74; ^{19}F-NMR (282 MHz, $CDCl_3$) δ -130.07, -130.08, -130.09, -130.11, -130.12, -130.13, -130.15; HPLC purity: >99%; IR (ATR)/ν (cm^{-1}): 3433, 3110, 2932, 2787, 1677, 1657, 1610, 1515, 1492, 1348, 1287, 1147, 1135, 942, 828, 732, 628; HRMS (ESI) calcd for $[C_{26}H_{28}FN_7O_3S + H]^+$: 538.20311, found 538.20451; T_{fus} = 239 °C.

5. NMR spectra

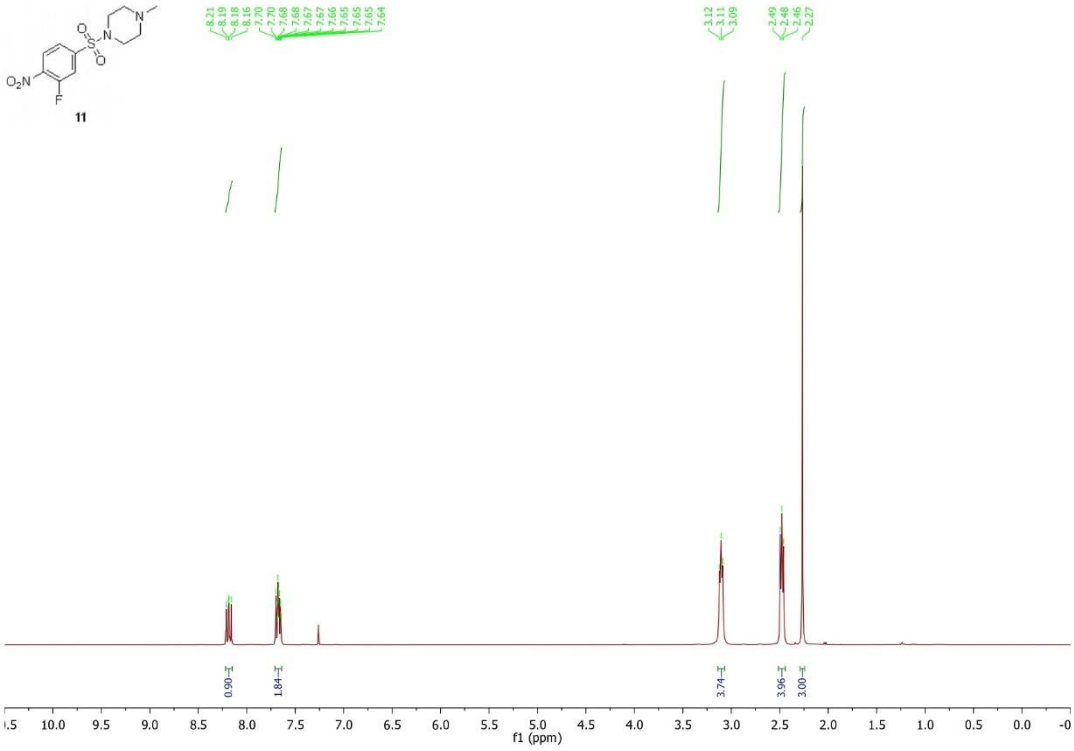
11
8.21
8.19
8.18
8.16
7.70
7.70
7.68
7.68
7.67
7.67
7.66
7.65
7.65
7.65
7.64
3.12
3.11
3.09
2.49
2.48
2.46
2.27
0.90
1.84
3.74
3.96
3.00
f1 (ppm)

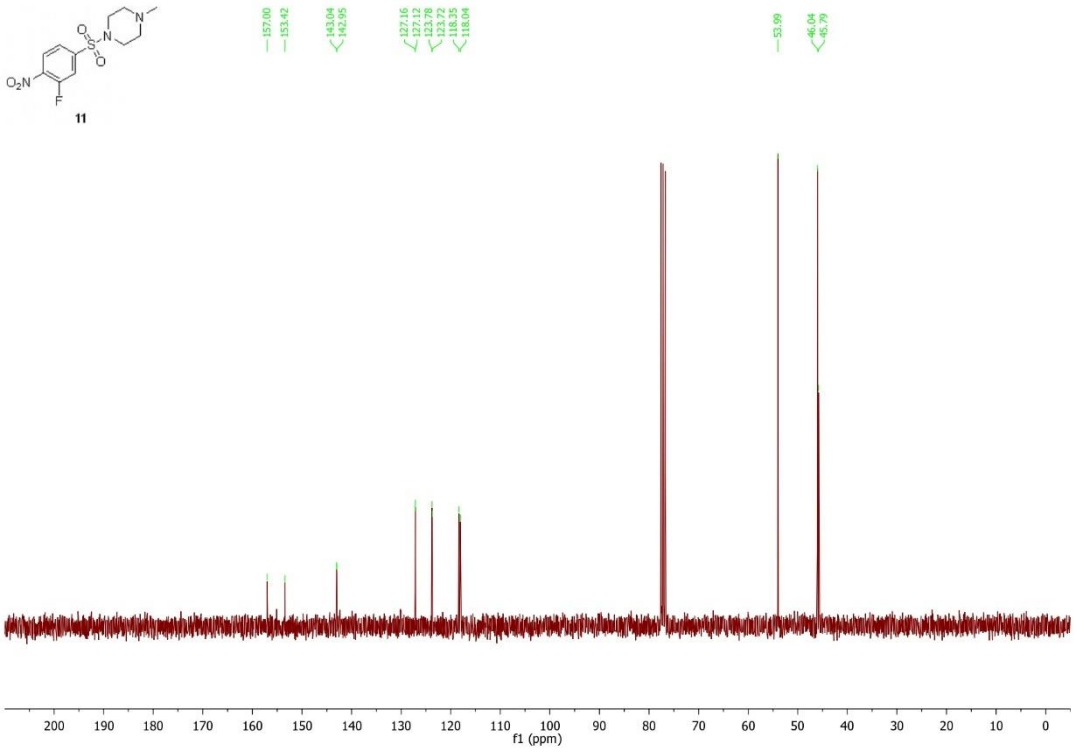
11
157.00
153.42
143.04
142.95
127.16
127.12
123.78
123.72
118.35
118.04
53.99
46.04
45.79
f1 (ppm)

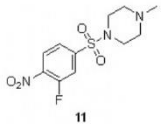

11

-115.36094
-115.39719
-115.39719
-115.42324
f1 (ppm)

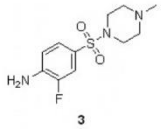

3

7.35
7.34
7.33
7.33
7.32
7.32
7.31
7.31
7.30
7.29
6.89
6.90
6.87
3.00
2.99
2.97
2.52
2.50
2.49
2.26
1.84
0.89
3.81
3.85
3.00
f1 (ppm)

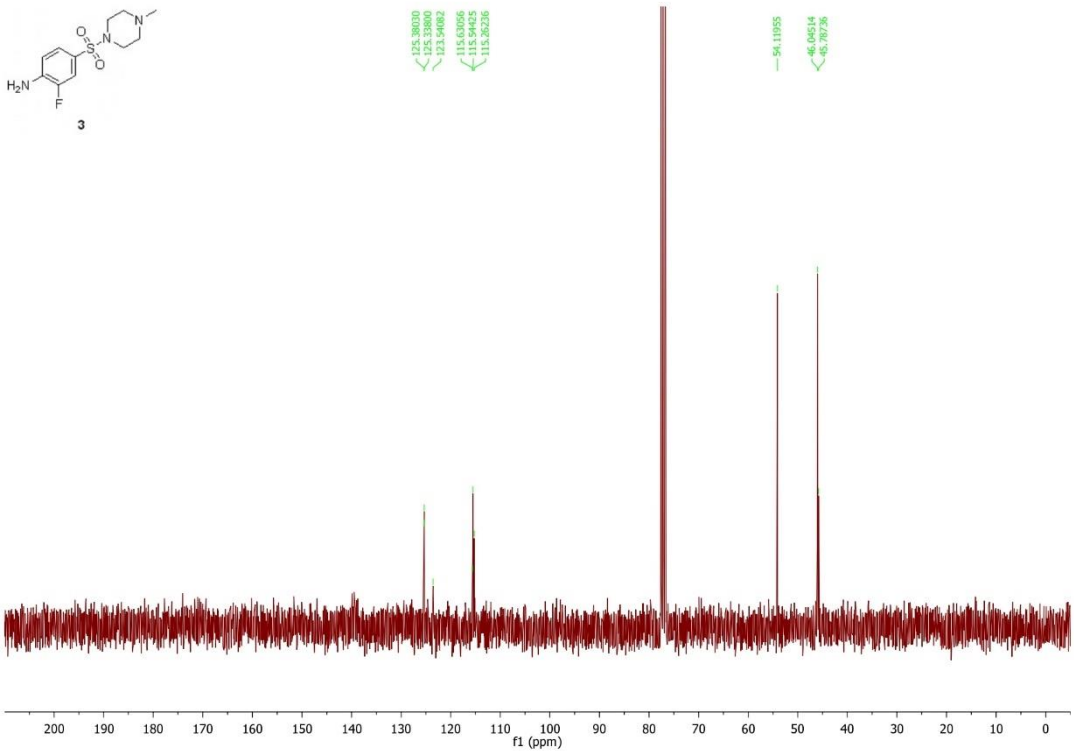
125.38030
125.33800
123.94682
115.63006
115.54425
115.46236
54.11955
46.04514
45.78736
3
200 190 180 170 160 150 140 130 120 110 100 90 80 70 60 50 40 30 20 10 0
f1 (ppm)

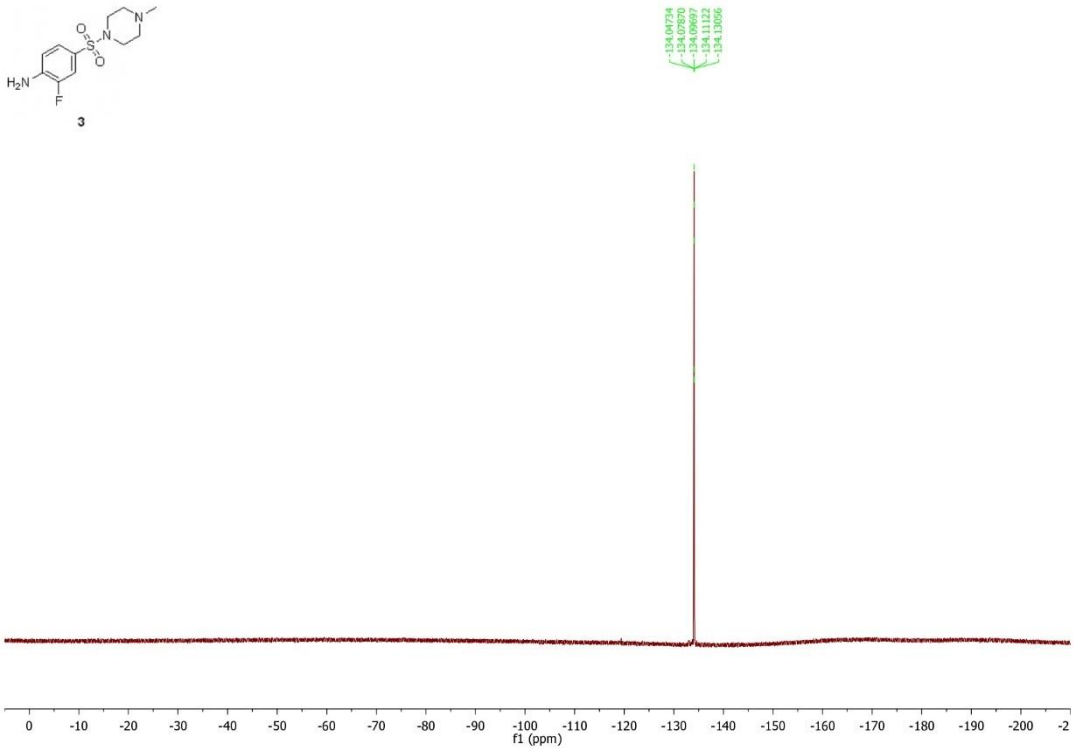
-134.04734
-134.07670
-134.09697
-134.11122
-134.13056
3
0 -10 -20 -30 -40 -50 -60 -70 -80 -90 -100 -110 -120 -130 -140 -150 -160 -170 -180 -190 -200 -2
f1 (ppm)

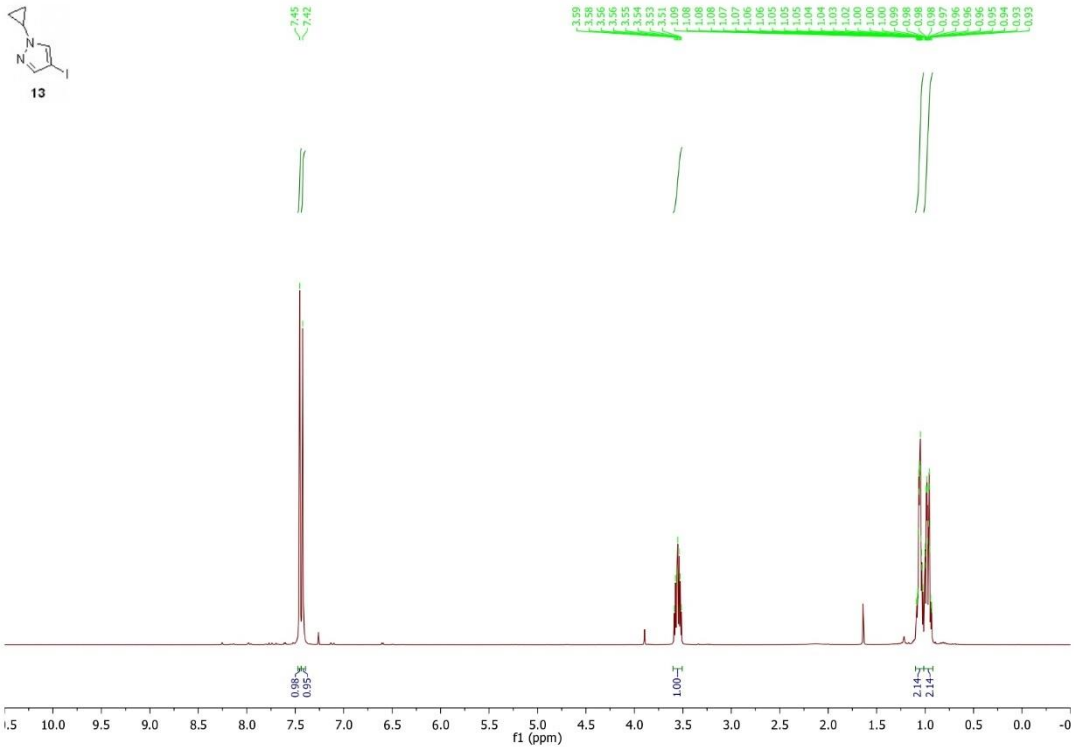
13
7.45
7.42
0.98
0.95
1.00
2.14
2.14
f1 (ppm)

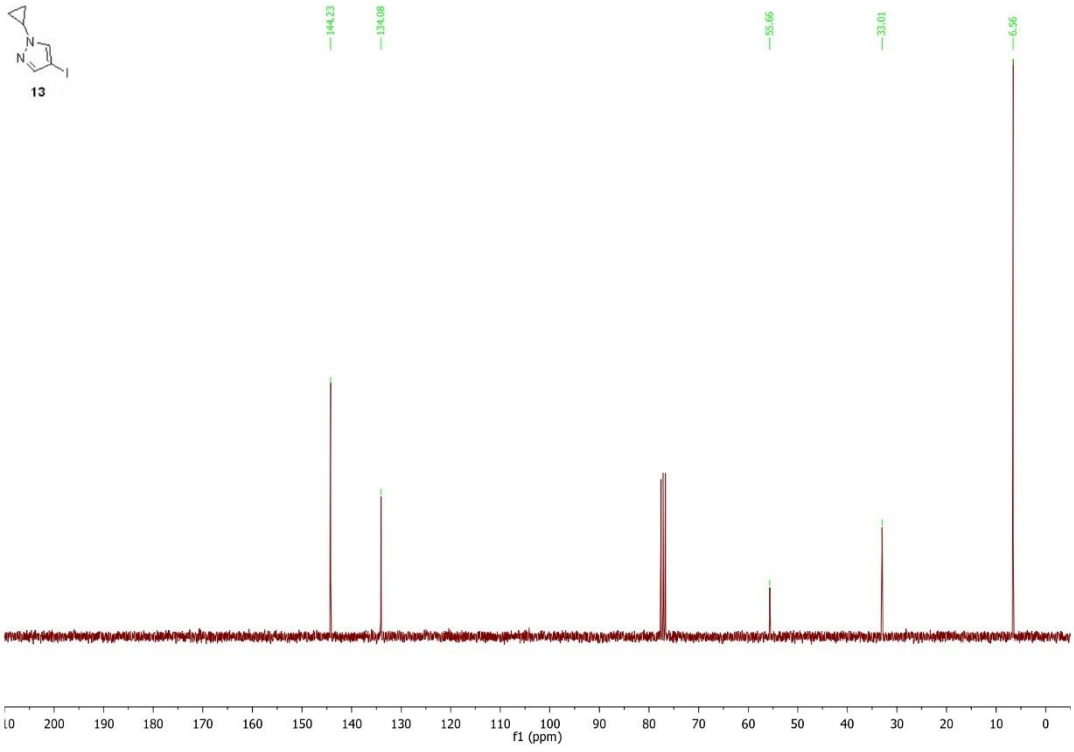
13
144.23
134.08
55.66
33.01
6.56
f1 (ppm)

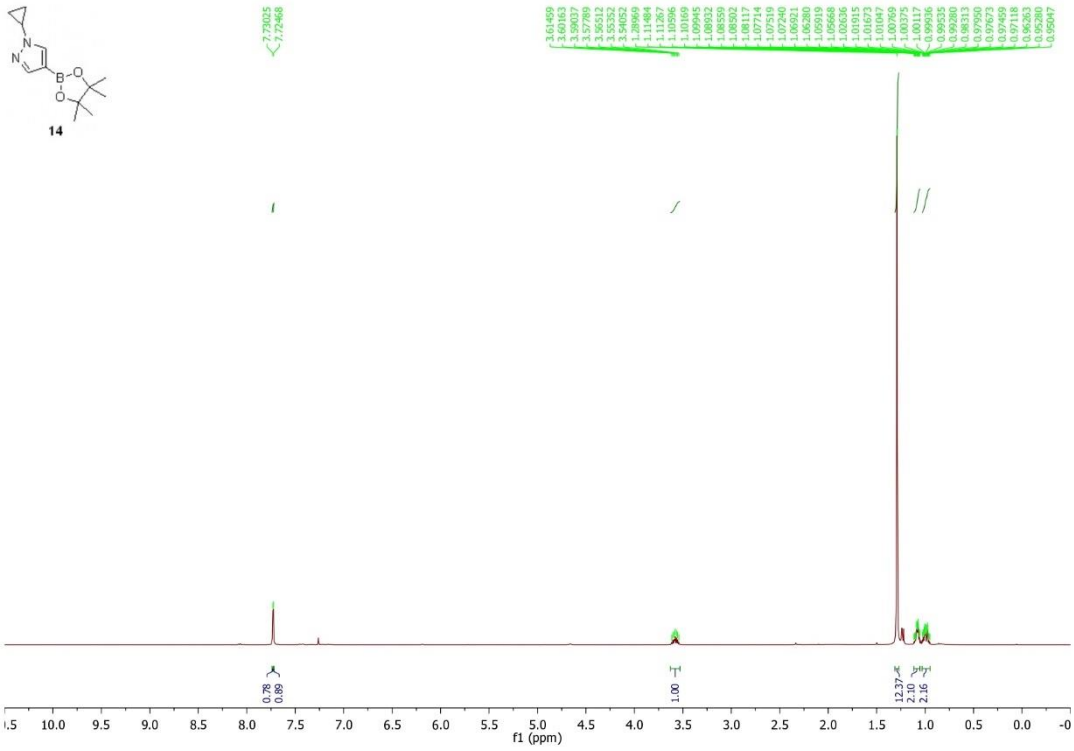
14
7.73025
7.72468
0.78
0.89
1.00
12.37
2.10
2.16
f1 (ppm)

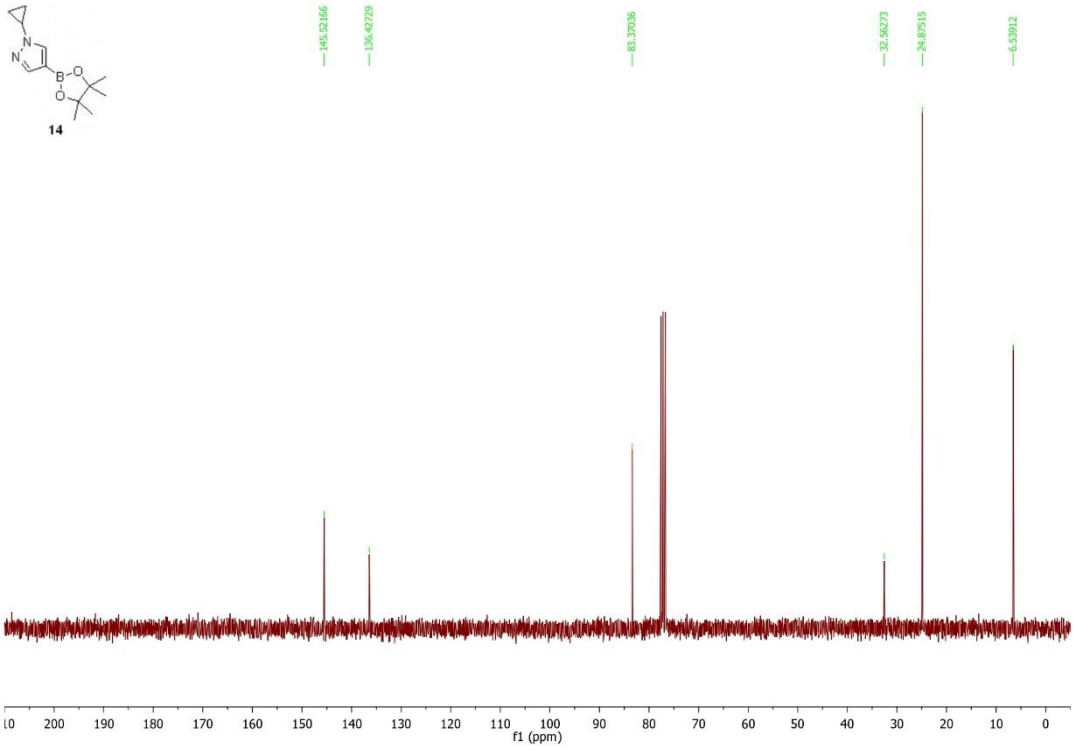
14
145.52166
136.42729
83.37036
32.56273
24.87515
6.53912
f1 (ppm)

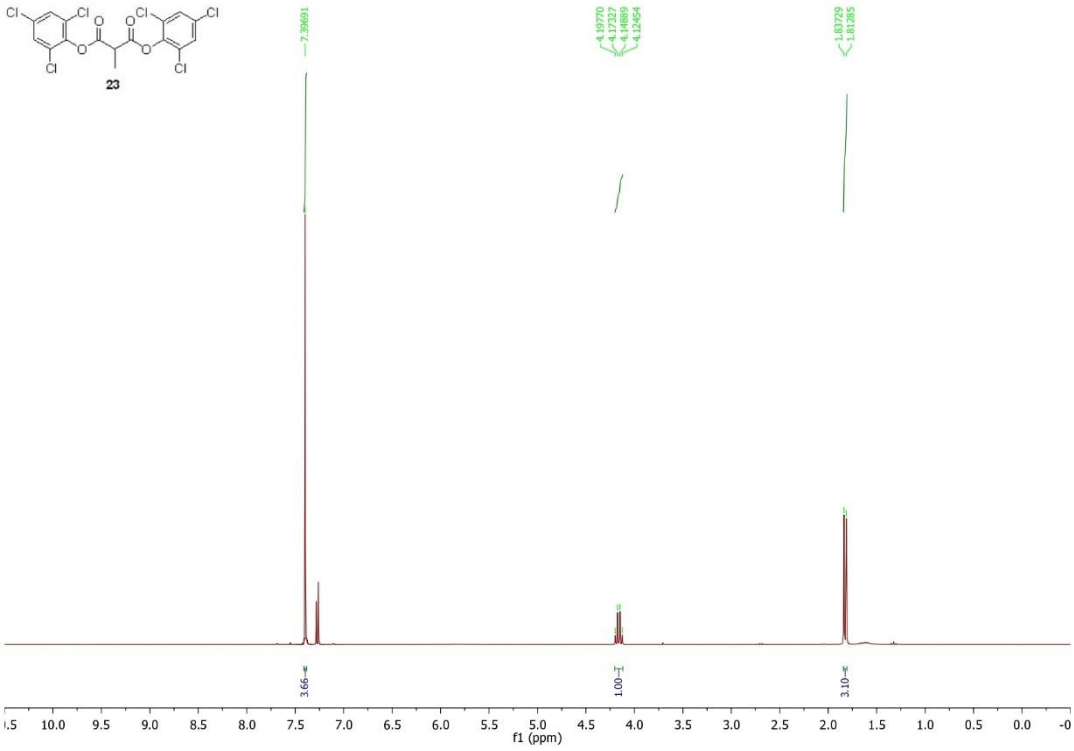
23
7.39691
4.19770
4.17327
4.14689
4.12454
1.83729
1.81285
3.66
1.00
3.10
f1 (ppm)

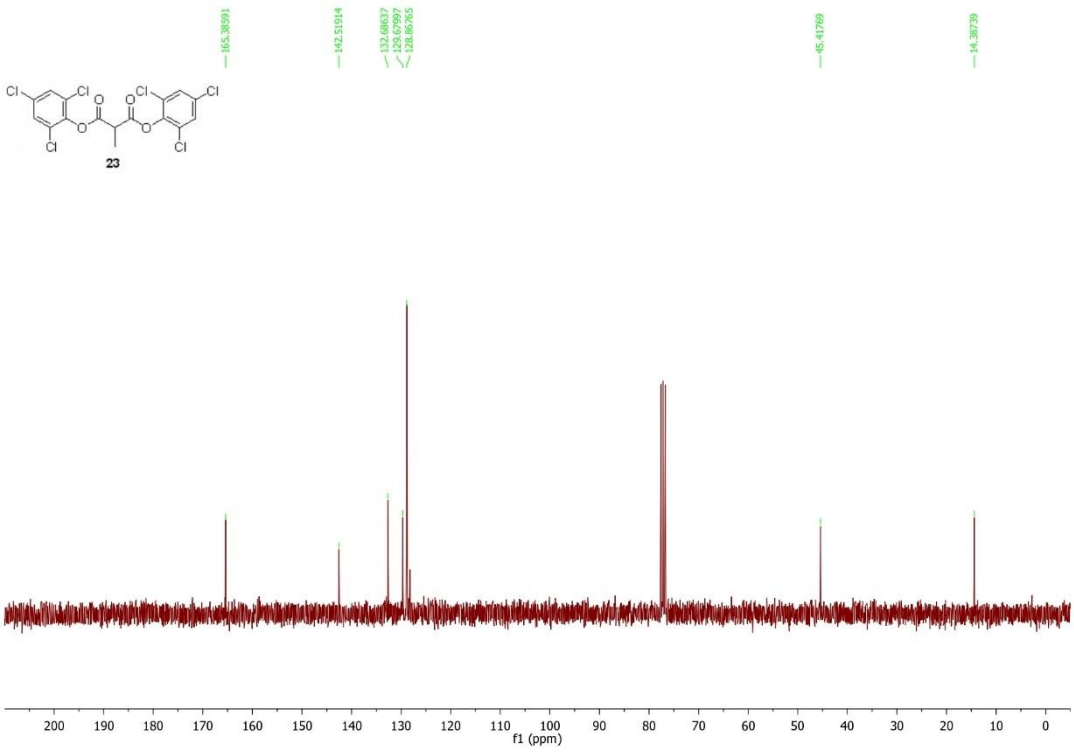
23
165.38591
142.51914
132.68637
129.67997
128.86765
45.41769
14.38739
f1 (ppm)

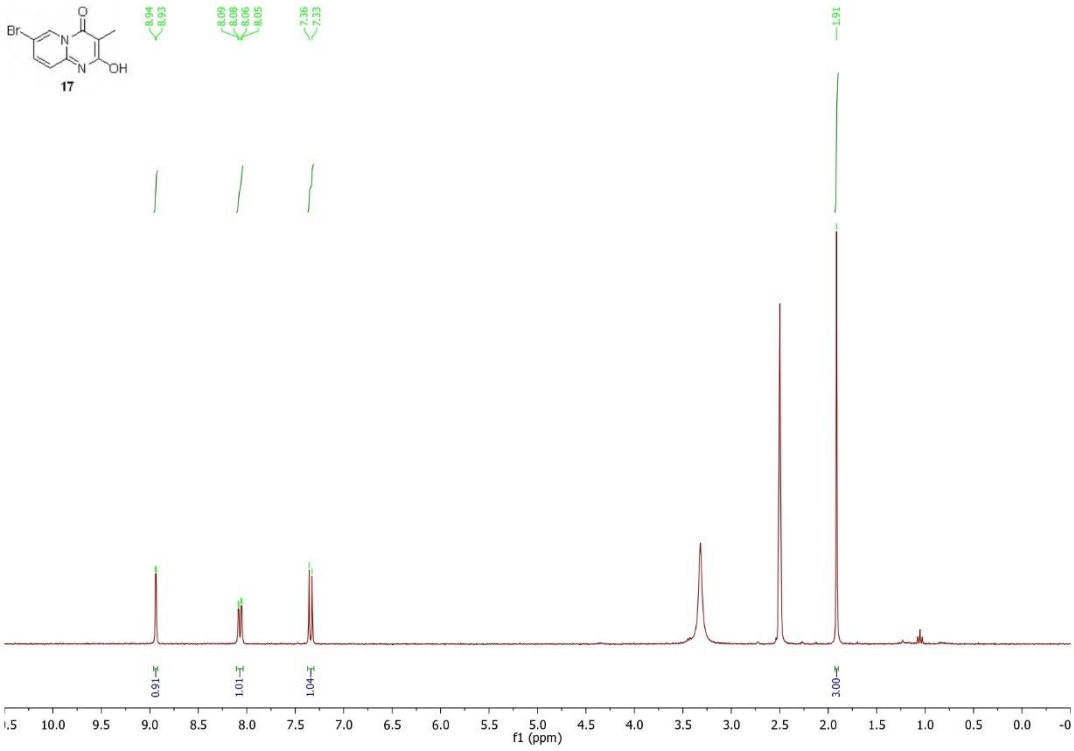
Br
O
N
N
OH
17
8.94
8.93
8.09
8.08
8.06
8.05
7.36
7.33
1.91
0.91
1.01
1.04
3.00
f1 (ppm)

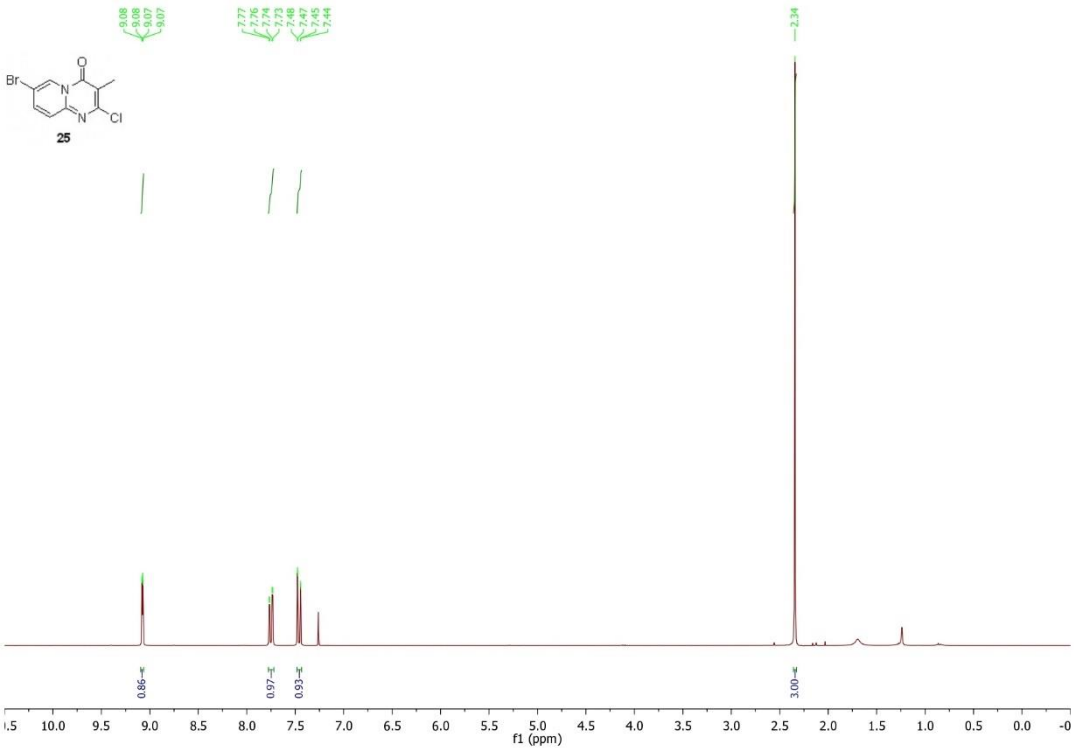
Br
O
N
N
Cl
25
9.08
9.08
9.07
9.07
7.77
7.76
7.74
7.73
7.48
7.47
7.45
7.44
2.34
0.86
0.97
0.93
3.00
f1 (ppm)

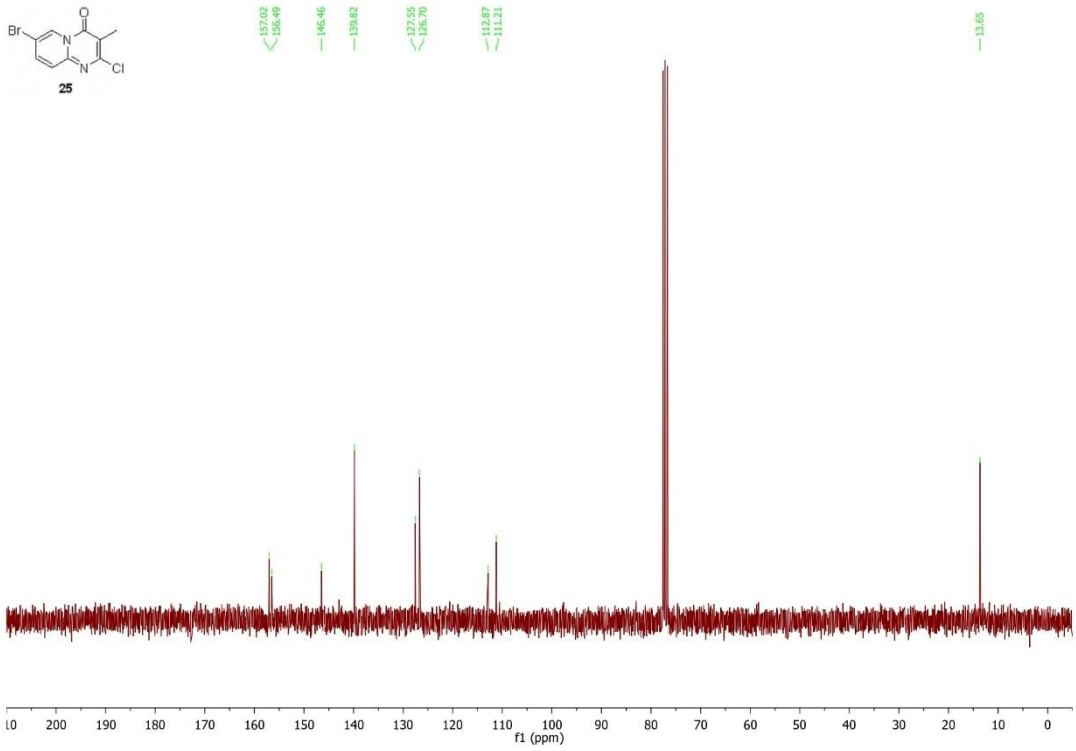
Br
N
O
N
Cl
25
157.02
156.49
146.46
139.82
127.55
126.70
112.87
111.21
13.65
f1 (ppm)

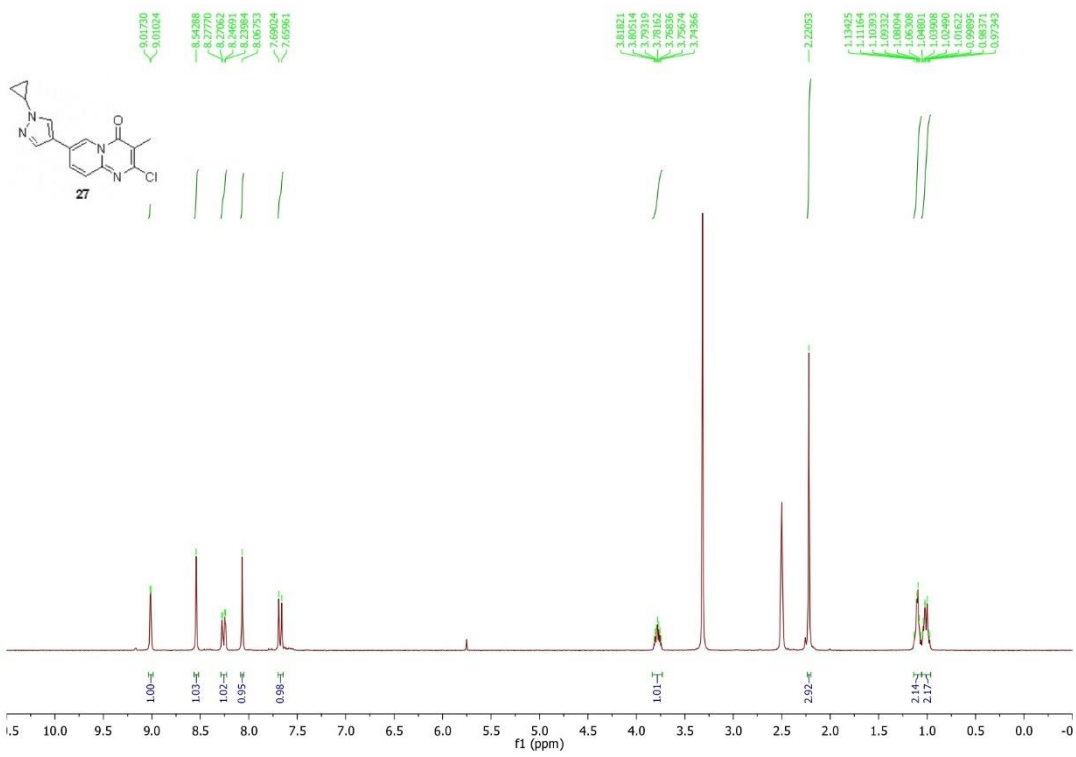
N
N
O
N
Cl
27
9.01730
9.01024
8.54288
8.27770
8.27062
8.24691
8.23984
8.06753
7.69024
7.68961
3.81821
3.80514
3.79319
3.78162
3.76836
3.75674
3.74366
2.22053
1.13425
1.11164
1.10393
1.09332
1.08094
1.06308
1.04601
1.03908
1.02969
1.01522
0.99095
0.98371
0.97343
1.00
1.03
1.02
0.95
0.98
1.01
2.92
2.14
2.17
f1 (ppm)

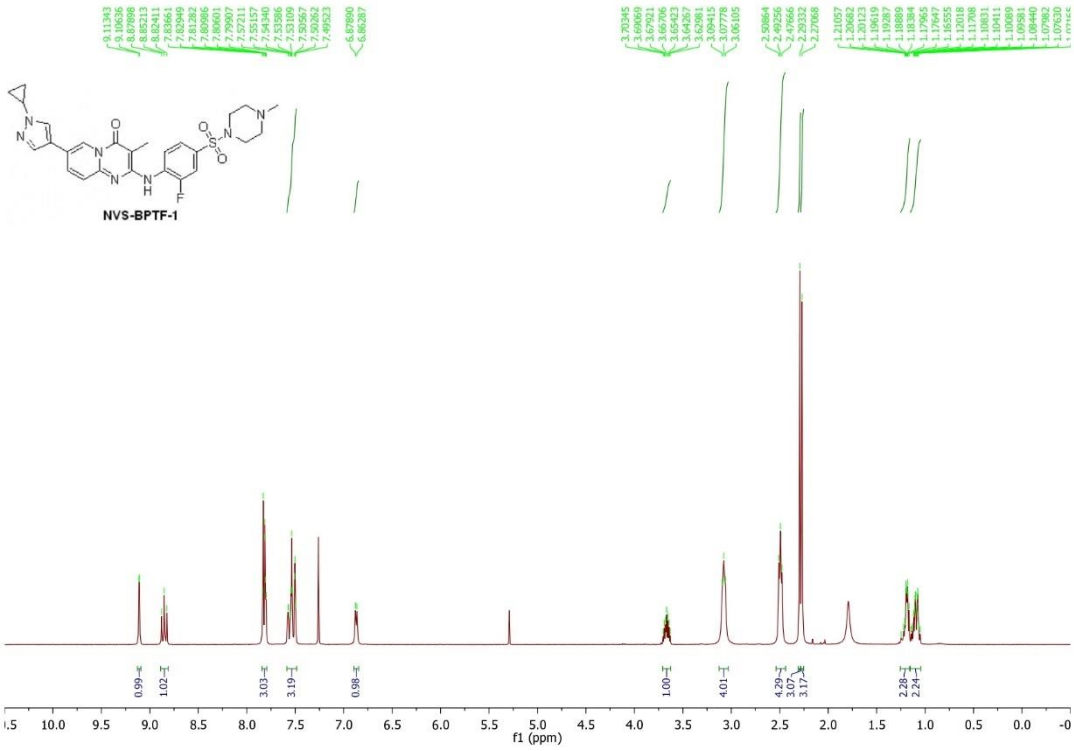
NVS-BPTF-1
f1 (ppm)

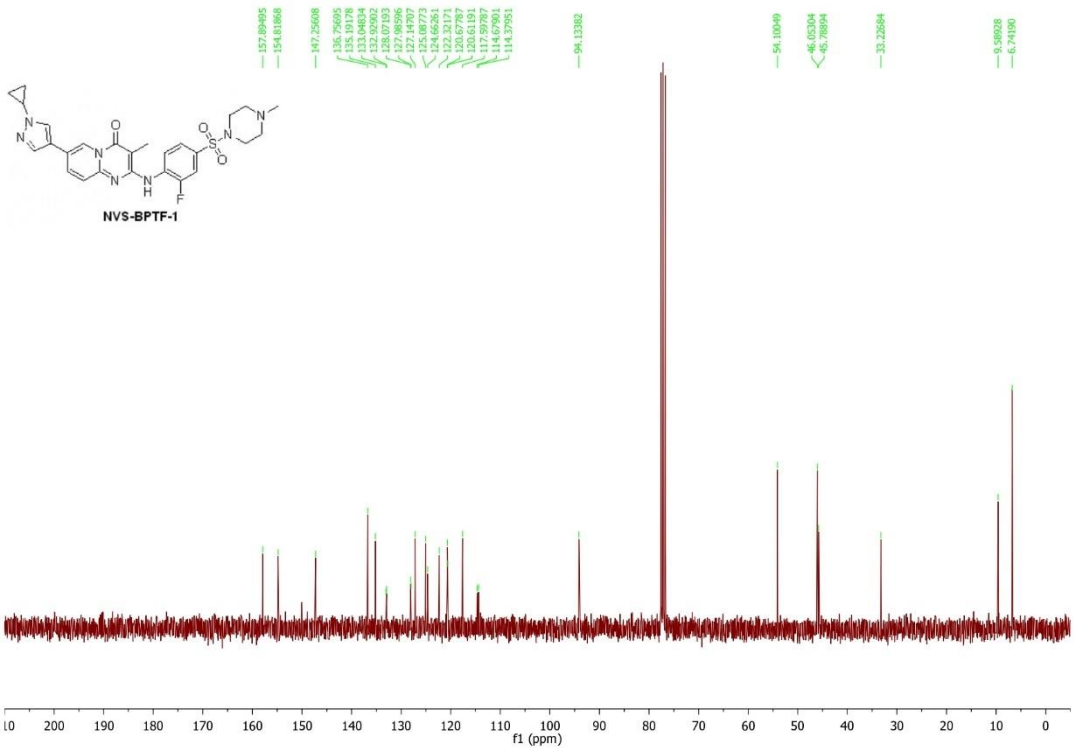
NVS-BPTF-1
f1 (ppm)

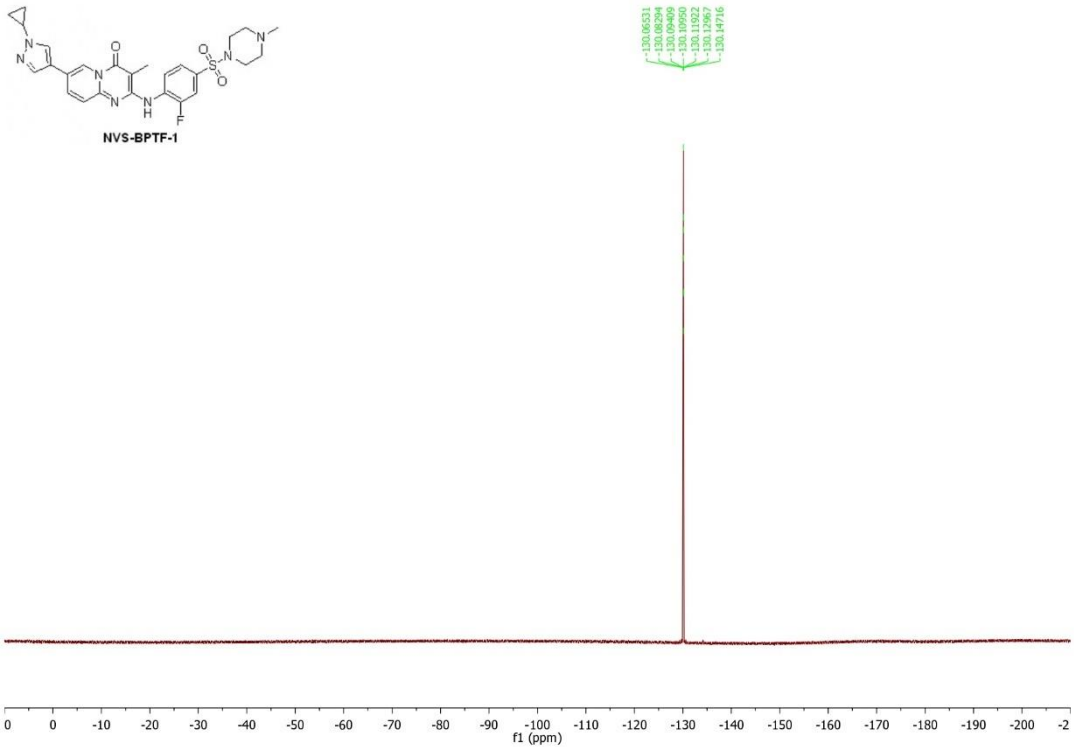
NVS-BPTF-1
-130.06531
-130.08294
-130.09409
-130.10950
-130.11922
-130.12987
-130.14716
0
0
-10
-20
-30
-40
-50
-60
-70
-80
-90
-100
-110
-120
-130
-140
-150
-160
-170
-180
-190
-200
-2
f1 (ppm)

BIBLIOGRAPHIE

(1) Willyard, C. New Human Gene Tally Reignites Debate. *Nature* **2018**, *558* (7710), 354–355. https://doi.org/10.1038/d41586-018-05462-w.

(2) Bianconi, E.; Piovesan, A.; Facchin, F.; Beraudi, A.; Casadei, R.; Frabetti, F.; Vitale, L.; Pelleri, M. C.; Tassani, S.; Piva, F.; Perez-Amodio, S.; Strippoli, P.; Canaider, S. An Estimation of the Number of Cells in the Human Body. *Ann Hum Biol* **2013**, *40* (6), 463–471. https://doi.org/10.3109/03014460.2013.807878.

(3) Shen-Orr, S. S.; Tibshirani, R.; Khatri, P.; Bodian, D. L.; Staedtler, F.; Perry, N. M.; Hastie, T.; Sarwal, M. M.; Davis, M. M.; Butte, A. J. Cell Type–Specific Gene Expression Differences in Complex Tissues. *Nature Methods* **2010**, *7* (4), 287–289. https://doi.org/10.1038/nmeth.1439.

(4) Buccitelli, C.; Selbach, M. MRNAs, Proteins and the Emerging Principles of Gene Expression Control. *Nat Rev Genet* **2020**, *21* (10), 630–644. https://doi.org/10.1038/s41576-020-0258-4.

(5) Davidson, E. *The Regulatory Genome*; Academic Press, 2006.

(6) Reményi, A.; Schöler, H. R.; Wilmanns, M. Combinatorial Control of Gene Expression. *Nature Structural & Molecular Biology* **2004**, *11* (9), 812–815. https://doi.org/10.1038/nsmb820.

(7) Sproul, D.; Gilbert, N.; Bickmore, W. A. The Role of Chromatin Structure in Regulating the Expression of Clustered Genes. *Nature Reviews Genetics* **2005**, *6* (10), 775–781. https://doi.org/10.1038/nrg1688.

(8) Roundtree, I. A.; Evans, M. E.; Pan, T.; He, C. Dynamic RNA Modifications in Gene Expression Regulation. *Cell* **2017**, *169* (7), 1187–1200. https://doi.org/10.1016/j.cell.2017.05.045.

(9) Sonenberg, N.; Hinnebusch, A. G. Regulation of Translation Initiation in Eukaryotes: Mechanisms and Biological Targets. *Cell* **2009**, *136* (4), 731–745. https://doi.org/10.1016/j.cell.2009.01.042.

(10) Mann, M.; Jensen, O. N. Proteomic Analysis of Post-Translational Modifications. *Nat Biotechnol* **2003**, *21* (3), 255–261. https://doi.org/10.1038/nbt0303-255.

(11) Cooper, G. M. Regulation of Transcription in Eukaryotes. *The Cell: A Molecular Approach. 2nd edition* **2000**.

(12) Swain, P. S.; Elowitz, M. B.; Siggia, E. D. Intrinsic and Extrinsic Contributions to Stochasticity in Gene Expression. *PNAS* **2002**, *99* (20), 12795–12800. https://doi.org/10.1073/pnas.162041399.

(13) Schvartzman, J. M.; Thompson, C. B.; Finley, L. W. S. Metabolic Regulation of Chromatin Modifications and Gene Expression. *Journal of Cell Biology* **2018**, *217* (7), 2247–2259. https://doi.org/10.1083/jcb.201803061.

(14) Mitchell, P.; Tjian, R. Transcriptional Regulation in Mammalian Cells by Sequence-Specific DNA Binding Proteins. *Science* **1989**, *245* (4916), 371–378. https://doi.org/10.1126/science.2667136.

(15) Lambert, S. A.; Jolma, A.; Campitelli, L. F.; Das, P. K.; Yin, Y.; Albu, M.; Chen, X.; Taipale, J.; Hughes, T. R.; Weirauch, M. T. The Human Transcription Factors. *Cell* **2018**, *172* (4), 650–665. https://doi.org/10.1016/j.cell.2018.01.029.

(16) Reese, J. C. Basal Transcription Factors. *Current Opinion in Genetics & Development* **2003**, *13* (2), 114–118. https://doi.org/10.1016/S0959-437X(03)00013-3.

(17) Orphanides, G.; Lagrange, T.; Reinberg, D. The General Transcription Factors of RNA Polymerase II. *Genes Dev.* **1996**, *10* (21), 2657–2683. https://doi.org/10.1101/gad.10.21.2657.

(18) Lodish, H.; Berk, A.; Zipursky, S. L.; Matsudaira, P.; Baltimore, D.; Darnell, J. Eukaryotic Transcription Activators and Repressors. *Molecular Cell Biology. 4th edition* **2000**.

(19) Nolis, I. K.; McKay, D. J.; Mantouvalou, E.; Lomvardas, S.; Merika, M.; Thanos, D. Transcription Factors Mediate Long-Range Enhancer–Promoter Interactions. *PNAS* **2009**, *106* (48), 20222–20227. https://doi.org/10.1073/pnas.0902454106.

(20) Levine, M.; Manley, J. L. Transcriptional Repression of Eukaryotic Promoters. *Cell* **1989**, *59* (3), 405–408. https://doi.org/10.1016/0092-8674(89)90024-X.

(21) Qian, Z.; Cai, Y.-D.; Li, Y. Automatic Transcription Factor Classifier Based on Functional Domain Composition. *Biochemical and Biophysical Research Communications* **2006**, *347* (1), 141–144. https://doi.org/10.1016/j.bbrc.2006.06.060.

(22) Stegmaier, P.; Kel, A. E.; Wingender, E. Systematic DNA-Binding Domain Classification of Transcription Factors. *Genome Inform* **2004**, *15* (2), 276–286.

(23) Pulverer, B. Getting Specific: Sequence-Specific DNA-Binding Transcription Factors. *Nat Rev Mol Cell Biol* **2005**, *6* (S1), S12–S12. https://doi.org/10.1038/nrm1800.

(24) Erijman, A.; Kozlowski, L.; Sohrabi-Jahromi, S.; Fishburn, J.; Warfield, L.; Schreiber, J.; Noble, W. S.; Söding, J.; Hahn, S. A High-Throughput Screen for Transcription Activation Domains Reveals Their Sequence Features and Permits Prediction by Deep Learning. *Molecular Cell* **2020**, *78* (5), 890-902.e6. https://doi.org/10.1016/j.molcel.2020.04.020.

(25) Triezenberg, S. Structure and Function of Transcriptional Activation Domains. *Current Opinion in Genetics & Development* **1995**, *5* (2), 190–196. https://doi.org/10.1016/0959-437X(95)80007-7.

(26) Boija, A.; Klein, I. A.; Sabari, B. R.; Dall'Agnese, A.; Coffey, E. L.; Zamudio, A. V.; Li, C. H.; Shrinivas, K.; Manteiga, J. C.; Hannett, N. M.; Abraham, B. J.; Afeyan, L. K.; Guo, Y. E.; Rimel, J. K.; Fant, C. B.; Schuijers, J.; Lee, T. I.; Taatjes, D. J.; Young, R. A. Transcription Factors Activate Genes through the Phase-Separation Capacity of Their Activation Domains. *Cell* **2018**, *175* (7), 1842-1855.e16. https://doi.org/10.1016/j.cell.2018.10.042.

(27) Ogryzko, V. V.; Schiltz, R. L.; Russanova, V.; Howard, B. H.; Nakatani, Y. The Transcriptional Coactivators P300 and CBP Are Histone Acetyltransferases. *Cell* **1996**, *87* (5), 953–959. https://doi.org/10.1016/S0092-8674(00)82001-2.

(28) Chiba, H.; Muramatsu, M.; Nomoto, A.; Kato, H. Two Human Homologues of Saccharomyces Cerevisiae SWI2/SNF2 and Drosophila Brahma Are Transcriptional Coactivators Cooperating with the Estrogen Receptor and the Retinoic Acid Receptor. *Nucleic Acids Res* **1994**, *22* (10), 1815–1820.

(29) Reiter, F.; Wienerroither, S.; Stark, A. Combinatorial Function of Transcription Factors and Cofactors. *Current Opinion in Genetics & Development* **2017**, *43*, 73–81. https://doi.org/10.1016/j.gde.2016.12.007.

(30) Amoutzias, G. D.; Robertson, D. L.; Peer, Y. V. de; Oliver, S. G. Choose Your Partners: Dimerization in Eukaryotic Transcription Factors. *Trends in Biochemical Sciences* **2008**, *33* (5), 220–229. https://doi.org/10.1016/j.tibs.2008.02.002.

(31) Pan, G.; Li, J.; Zhou, Y.; Zheng, H.; Pei, D.; Pan, G.; Li, J.; Zhou, Y.; Zheng, H.; Pei, D. A Negative Feedback Loop of Transcription Factors That Controls Stem Cell Pluripotency and Self‐renewal. *FASEB j.* **2006**, *20* (10), 1730–1732. https://doi.org/10.1096/fj.05-5543fje.

(32) Whiteside, S. T.; Goodbourn, S. Signal Transduction and Nuclear Targeting: Regulation of Transcription Factor Activity by Subcellular Localisation. *Journal of Cell Science* **1993**, *104* (4), 949–955.

(33) Mitsis, T.; Efthimiadou, A.; Bacopoulou, F.; Vlachakis, D.; Chrousos, G.; Eliopoulos, E. Transcription Factors and Evolution: An Integral Part of Gene Expression (Review). *World Acad Sci J* **2020**. https://doi.org/10.3892/wasj.2020.32.

(34) Hunter, T.; Karin, M. The Regulation of Transcription by Phosphorylation. *Cell* **1992**, *70* (3), 375–387. https://doi.org/10.1016/0092-8674(92)90162-6.

(35) Osório, J. Landscape and Mechanisms of Transcription Factor Cooperativity. *Nature Reviews Genetics* **2016**, *17* (1), 5–5. https://doi.org/10.1038/nrg.2015.11.

(36) Morgunova, E.; Taipale, J. Structural Perspective of Cooperative Transcription Factor Binding. *Curr Opin Struct Biol* **2017**, *47*, 1–8. https://doi.org/10.1016/j.sbi.2017.03.006.

(37) Fyodorov, D. V.; Zhou, B.-R.; Skoultchi, A. I.; Bai, Y. Emerging Roles of Linker Histones in Regulating Chromatin Structure and Function. *Nat Rev Mol Cell Biol* **2018**, *19* (3), 192–206. https://doi.org/10.1038/nrm.2017.94.

(38) Cooper, G. M. Chromosomes and Chromatin. *The Cell: A Molecular Approach. 2nd edition* **2000**.

(39) Quina, A. S.; Buschbeck, M.; Di Croce, L. Chromatin Structure and Epigenetics. *Biochemical Pharmacology* **2006**, *72* (11), 1563–1569. https://doi.org/10.1016/j.bcp.2006.06.016.

(40) Fischle, W.; Wang, Y.; Allis, C. D. Histone and Chromatin Cross-Talk. *Current Opinion in Cell Biology* **2003**, *15* (2), 172–183. https://doi.org/10.1016/S0955-0674(03)00013-9.

(41) Grunstein, M. Histone Acetylation in Chromatin Structure and Transcription. *Nature* **1997**, *389* (6649), 349–352. https://doi.org/10.1038/38664.

(42) Sterner, D. E.; Berger, S. L. Acetylation of Histones and Transcription-Related Factors. *Microbiol. Mol. Biol. Rev.* **2000**, *64* (2), 435–459. https://doi.org/10.1128/MMBR.64.2.435-459.2000.

(43) Eberharter, A.; Becker, P. B. Histone Acetylation: A Switch between Repressive and Permissive Chromatin. *EMBO Rep* **2002**, *3* (3), 224–229. https://doi.org/10.1093/embo-reports/kvf053.

(44) Greer, E. L.; Shi, Y. Histone Methylation: A Dynamic Mark in Health, Disease and Inheritance. *Nature Reviews Genetics* **2012**, *13* (5), 343–357. https://doi.org/10.1038/nrg3173.

(45) Hyun, K.; Jeon, J.; Park, K.; Kim, J. Writing, Erasing and Reading Histone Lysine Methylations. *Experimental & Molecular Medicine* **2017**, *49* (4), e324–e324. https://doi.org/10.1038/emm.2017.11.

(46) Smith, Z. D.; Meissner, A. DNA Methylation: Roles in Mammalian Development. *Nature Reviews Genetics* **2013**, *14* (3), 204–220. https://doi.org/10.1038/nrg3354.

(47) Moore, L. D.; Le, T.; Fan, G. DNA Methylation and Its Basic Function. *Neuropsychopharmacology* **2013**, *38* (1), 23–38. https://doi.org/10.1038/npp.2012.112.

(48) Rose, N. R.; Klose, R. J. Understanding the Relationship between DNA Methylation and Histone Lysine Methylation. *Biochimica et Biophysica Acta (BBA) -*

Gene Regulatory Mechanisms **2014**, *1839* (12), 1362–1372. https://doi.org/10.1016/j.bbagrm.2014.02.007.

(49) Richards, E. J.; Elgin, S. C. R. Epigenetic Codes for Heterochromatin Formation and Silencing: Rounding up the Usual Suspects. *Cell* **2002**, *108* (4), 489–500. https://doi.org/10.1016/s0092-8674(02)00644-x.

(50) Kouzarides, T. Chromatin Modifications and Their Function. *Cell* **2007**, *128* (4), 693–705. https://doi.org/10.1016/j.cell.2007.02.005.

(51) Längst, G.; Manelyte, L. Chromatin Remodelers: From Function to Dysfunction. *Genes (Basel)* **2015**, *6* (2), 299–324. https://doi.org/10.3390/genes6020299.

(52) Musselman, C. A.; Lalonde, M.-E.; Côté, J.; Kutateladze, T. G. Perceiving the Epigenetic Landscape through Histone Readers. *Nat Struct Mol Biol* **2012**, *19* (12), 1218–1227. https://doi.org/10.1038/nsmb.2436.

(53) Adams-Cioaba, M. A.; Min, J. Structure and Function of Histone Methylation Binding Proteins. *Biochem Cell Biol* **2009**, *87* (1), 93–105. https://doi.org/10.1139/O08-129.

(54) Clapier, C. R.; Cairns, B. R. The Biology of Chromatin Remodeling Complexes. *Annu. Rev. Biochem.* **2009**, *78* (1), 273–304. https://doi.org/10.1146/annurev.biochem.77.062706.153223.

(55) Saha, A.; Wittmeyer, J.; Cairns, B. R. Chromatin Remodelling: The Industrial Revolution of DNA around Histones. *Nat Rev Mol Cell Biol* **2006**, *7* (6), 437–447. https://doi.org/10.1038/nrm1945.

(56) Hendricks, K. B.; Shanahan, F.; Lees, E. Role for BRG1 in Cell Cycle Control and Tumor Suppression. *Mol Cell Biol* **2004**, *24* (1), 362–376. https://doi.org/10.1128/mcb.24.1.362-376.2004.

(57) de la Serna, I. L.; Carlson, K. A.; Imbalzano, A. N. Mammalian SWI/SNF Complexes Promote MyoD-Mediated Muscle Differentiation. *Nat Genet* **2001**, *27* (2), 187–190. https://doi.org/10.1038/84826.

(58) Lickert, H.; Takeuchi, J. K.; Von Both, I.; Walls, J. R.; McAuliffe, F.; Adamson, S. L.; Henkelman, R. M.; Wrana, J. L.; Rossant, J.; Bruneau, B. G. Baf60c Is Essential for Function of BAF Chromatin Remodelling Complexes in Heart Development. *Nature* **2004**, *432* (7013), 107–112. https://doi.org/10.1038/nature03071.

(59) Corey, L. L.; Weirich, C. S.; Benjamin, I. J.; Kingston, R. E. Localized Recruitment of a Chromatin-Remodeling Activity by an Activator in Vivo Drives Transcriptional Elongation. *Genes Dev.* **2003**, *17* (11), 1392–1401. https://doi.org/10.1101/gad.1071803.

(60) Zapater, A. G.; Mackowiak, S. D.; Guo, Y.; Jordan-Pla, A.; Friedländer, M. R.; Visa, N.; Farrants, A.-K. Ö. The SWI/SNF Subunits BRG1 Affects Alternative Splicing by Changing RNA Binding Factor Interactions with RNA. *bioRxiv* **2019**, 858852. https://doi.org/10.1101/858852.

(61) Swinstead, E. E.; Paakinaho, V.; Presman, D. M.; Hager, G. L. Pioneer Factors and ATP-Dependent Chromatin Remodeling Factors Interact Dynamically: A New Perspective. *BioEssays* **2016**, *38* (11), 1150–1157. https://doi.org/10.1002/bies.201600137.

(62) Zaret, K. S. Pioneer Transcription Factors Initiating Gene Network Changes. *Annu. Rev. Genet.* **2020**, *54* (1), 367–385. https://doi.org/10.1146/annurev-genet-030220-015007.

(63) Cirillo, L. A.; Lin, F. R.; Cuesta, I.; Friedman, D.; Jarnik, M.; Zaret, K. S. Opening of Compacted Chromatin by Early Developmental Transcription Factors HNF3 (FoxA) and GATA-4. *Mol Cell* **2002**, *9* (2), 279–289. https://doi.org/10.1016/s1097-2765(02)00459-8.

(64) Zaret, K. S.; Carroll, J. S. Pioneer Transcription Factors: Establishing Competence for Gene Expression. *Genes & Development* **2011**, *25* (21), 2227–2241. https://doi.org/10.1101/gad.176826.111.

(65) Mayran, A.; Drouin, J. Pioneer Transcription Factors Shape the Epigenetic Landscape. *Journal of Biological Chemistry* **2018**, *293* (36), 13795–13804. https://doi.org/10.1074/jbc.R117.001232.

(66) Vanzan, L.; Soldati, H.; Ythier, V.; Anand, S.; Francis, N.; Murr, R. High Throughput Screening Identifies SOX2 as a Super Pioneer Factor That Inhibits DNA

Methylation Maintenance at Its Binding Sites. *bioRxiv* **2020**, 2020.02.10.941682. https://doi.org/10.1101/2020.02.10.941682.

(67) Harvey, K.; Tapon, N. The Salvador–Warts–Hippo Pathway — an Emerging Tumour-Suppressor Network. *Nature Reviews Cancer* **2007**, *7* (3), 182–191. https://doi.org/10.1038/nrc2070.

(68) Gumbiner, B. M.; Kim, N.-G. The Hippo-YAP Signaling Pathway and Contact Inhibition of Growth. *J Cell Sci* **2014**, *127* (4), 709–717. https://doi.org/10.1242/jcs.140103.

(69) Meng, Z.; Moroishi, T.; Guan, K.-L. Mechanisms of Hippo Pathway Regulation. *Genes Dev* **2016**, *30* (1), 1–17. https://doi.org/10.1101/gad.274027.115.

(70) Yu, F.-X.; Guan, K.-L. The Hippo Pathway: Regulators and Regulations. *Genes Dev.* **2013**, *27* (4), 355–371. https://doi.org/10.1101/gad.210773.112.

(71) Cairns, L.; Tran, T.; Kavran, J. M. Structural Insights into the Regulation of Hippo Signaling. *ACS Chem. Biol.* **2017**, *12* (3), 601–610. https://doi.org/10.1021/acschembio.6b01058.

(72) Zhao, B.; Li, L.; Tumaneng, K.; Wang, C.-Y.; Guan, K.-L. A Coordinated Phosphorylation by Lats and CK1 Regulates YAP Stability through SCFβ-TRCP. *Genes Dev.* **2010**, *24* (1), 72–85. https://doi.org/10.1101/gad.1843810.

(73) Pavel, M.; Renna, M.; Park, S. J.; Menzies, F. M.; Ricketts, T.; Füllgrabe, J.; Ashkenazi, A.; Frake, R. A.; Lombarte, A. C.; Bento, C. F.; Franze, K.; Rubinsztein, D. C. Contact Inhibition Controls Cell Survival and Proliferation via YAP/TAZ-Autophagy Axis. *Nat Commun* **2018**, *9* (1), 2961. https://doi.org/10.1038/s41467-018-05388-x.

(74) Kim, M.-K.; Jang, J.-W.; Bae, S.-C. DNA Binding Partners of YAP/TAZ. *BMB Rep* **2018**, *51* (3), 126–133. https://doi.org/10.5483/bmbrep.2018.51.3.015.

(75) Wang, K. W.; Degerny, C. D.; Xu, M. X.; Yang, X.-J. Y.-J. YAP, TAZ, and Yorkie: A Conserved Family of Signal-Responsive Transcriptional Coregulators in Animal Development and Human DiseaseThis Paper Is One of a Selection of Papers Published in This Special Issue, Entitled CSBMCB's 51st Annual Meeting – Epigenetics and Chromatin Dynamics, and Has Undergone the Journal's Usual Peer

Review Process. *Biochemistry and Cell Biology* **2008**. https://doi.org/10.1139/O08-114.

(76) Pocaterra, A.; Romani, P.; Dupont, S. YAP/TAZ Functions and Their Regulation at a Glance. *J Cell Sci* **2020**, *133* (2). https://doi.org/10.1242/jcs.230425.

(77) Pan, D. The Hippo Signaling Pathway in Development and Cancer. *Dev Cell* **2010**, *19* (4), 491–505. https://doi.org/10.1016/j.devcel.2010.09.011.

(78) Xu, N.; Wu, M.-Z.; Deng, X.-T.; Ma, P.-C.; Li, Z.-H.; Liang, L.; Xia, M.-F.; Cui, D.; He, D.-D.; Zong, Y.; Xie, Z.; Song, X.-J. Inhibition of YAP/TAZ Activity in Spinal Cord Suppresses Neuropathic Pain. *J Neurosci* **2016**, *36* (39), 10128–10140. https://doi.org/10.1523/JNEUROSCI.0800-16.2016.

(79) Liu, F.; Lagares, D.; Choi, K. M.; Stopfer, L.; Marinković, A.; Vrbanac, V.; Probst, C. K.; Hiemer, S. E.; Sisson, T. H.; Horowitz, J. C.; Rosas, I. O.; Fredenburgh, L. E.; Feghali-Bostwick, C.; Varelas, X.; Tager, A. M.; Tschumperlin, D. J. Mechanosignaling through YAP and TAZ Drives Fibroblast Activation and Fibrosis. *Am J Physiol Lung Cell Mol Physiol* **2015**, *308* (4), L344-357. https://doi.org/10.1152/ajplung.00300.2014.

(80) Calses, P. C.; Crawford, J. J.; Lill, J. R.; Dey, A. Hippo Pathway in Cancer: Aberrant Regulation and Therapeutic Opportunities. *Trends in Cancer* **2019**, *5* (5), 297–307. https://doi.org/10.1016/j.trecan.2019.04.001.

(81) Han, Y. Analysis of the Role of the Hippo Pathway in Cancer. *Journal of Translational Medicine* **2019**, *17* (1), 116. https://doi.org/10.1186/s12967-019-1869-4.

(82) Wang, Y.; Xu, X.; Maglic, D.; Dill, M. T.; Mojumdar, K.; Ng, P. K.-S.; Jeong, K. J.; Tsang, Y. H.; Moreno, D.; Bhavana, V. H.; Peng, X.; Ge, Z.; Chen, H.; Li, J.; Chen, Z.; Zhang, H.; Han, L.; Du, D.; Creighton, C. J.; Mills, G. B.; Caesar-Johnson, S. J.; Demchok, J. A.; Felau, I.; Kasapi, M.; Ferguson, M. L.; Hutter, C. M.; Sofia, H. J.; Tarnuzzer, R.; Wang, Z.; Yang, L.; Zenklusen, J. C.; Zhang, J. (Julia); Chudamani, S.; Liu, J.; Lolla, L.; Naresh, R.; Pihl, T.; Sun, Q.; Wan, Y.; Wu, Y.; Cho, J.; DeFreitas, T.; Frazer, S.; Gehlenborg, N.; Getz, G.; Heiman, D. I.; Kim, J.; Lawrence, M. S.; Lin, P.; Meier, S.; Noble, M. S.; Saksena, G.; Voet, D.; Zhang, H.; Bernard, B.; Chambwe, N.; Dhankani, V.; Knijnenburg, T.; Kramer, R.; Leinonen, K.; Liu, Y.; Miller, M.; Reynolds, S.; Shmulevich, I.; Thorsson, V.; Zhang, W.; Akbani, R.; Broom, B. M.; Hegde, A. M.; Ju, Z.; Kanchi, R. S.; Korkut, A.; Li, J.; Liang, H.; Ling, S.; Liu, W.; Lu, Y.; Mills, G. B.; Ng, K.-S.; Rao, A.; Ryan, M.; Wang, J.; Weinstein, J. N.; Zhang, J.;

Abeshouse, A.; Armenia, J.; Chakravarty, D.; Chatila, W. K.; de Bruijn, I.; Gao, J.; Gross, B. E.; Heins, Z. J.; Kundra, R.; La, K.; Ladanyi, M.; Luna, A.; Nissan, M. G.; Ochoa, A.; Phillips, S. M.; Reznik, E.; Sanchez-Vega, F.; Sander, C.; Schultz, N.; Sheridan, R.; Sumer, S. O.; Sun, Y.; Taylor, B. S.; Wang, J.; Zhang, H.; Anur, P.; Peto, M.; Spellman, P.; Benz, C.; Stuart, J. M.; Wong, C. K.; Yau, C.; Hayes, D. N.; Parker, J. S.; Wilkerson, M. D.; Ally, A.; Balasundaram, M.; Bowlby, R.; Brooks, D.; Carlsen, R.; Chuah, E.; Dhalla, N.; Holt, R.; Jones, S. J. M.; Kasaian, K.; Lee, D.; Ma, Y.; Marra, M. A.; Mayo, M.; Moore, R. A.; Mungall, A. J.; Mungall, K.; Robertson, A. G.; Sadeghi, S.; Schein, J. E.; Sipahimalani, P.; Tam, A.; Thiessen, N.; Tse, K.; Wong, T.; Berger, A. C.; Beroukhim, R.; Cherniack, A. D.; Cibulskis, C.; Gabriel, S. B.; Gao, G. F.; Ha, G.; Meyerson, M.; Schumacher, S. E.; Shih, J.; Kucherlapati, M. H.; Kucherlapati, R. S.; Baylin, S.; Cope, L.; Danilova, L.; Bootwalla, M. S.; Lai, P. H.; Maglinte, D. T.; Van Den Berg, D. J.; Weisenberger, D. J.; Auman, J. T.; Balu, S.; Bodenheimer, T.; Fan, C.; Hoadley, K. A.; Hoyle, A. P.; Jefferys, S. R.; Jones, C. D.; Meng, S.; Mieczkowski, P. A.; Mose, L. E.; Perou, A. H.; Perou, C. M.; Roach, J.; Shi, Y.; Simons, J. V.; Skelly, T.; Soloway, M. G.; Tan, D.; Veluvolu, U.; Fan, H.; Hinoue, T.; Laird, P. W.; Shen, H.; Zhou, W.; Bellair, M.; Chang, K.; Covington, K.; Creighton, C. J.; Dinh, H.; Doddapaneni, H.; Donehower, L. A.; Drummond, J.; Gibbs, R. A.; Glenn, R.; Hale, W.; Han, Y.; Hu, J.; Korchina, V.; Lee, S.; Lewis, L.; Li, W.; Liu, X.; Morgan, M.; Morton, D.; Muzny, D.; Santibanez, J.; Sheth, M.; Shinbrot, E.; Wang, L.; Wang, M.; Wheeler, D. A.; Xi, L.; Zhao, F.; Hess, J.; Appelbaum, E. L.; Bailey, M.; Cordes, M. G.; Ding, L.; Fronick, C. C.; Fulton, L. A.; Fulton, R. S.; Kandoth, C.; Mardis, E. R.; McLellan, M. D.; Miller, C. A.; Schmidt, H. K.; Wilson, R. K.; Crain, D.; Curley, E.; Gardner, J.; Lau, K.; Mallery, D.; Morris, S.; Paulauskis, J.; Penny, R.; Shelton, C.; Shelton, T.; Sherman, M.; Thompson, E.; Yena, P.; Bowen, J.; Gastier-Foster, J. M.; Gerken, M.; Leraas, K. M.; Lichtenberg, T. M.; Ramirez, N. C.; Wise, L.; Zmuda, E.; Corcoran, N.; Costello, T.; Hovens, C.; Carvalho, A. L.; de Carvalho, A. C.; Fregnani, J. H.; Longatto-Filho, A.; Reis, R. M.; Scapulatempo-Neto, C.; Silveira, H. C. S.; Vidal, D. O.; Burnette, A.; Eschbacher, J.; Hermes, B.; Noss, A.; Singh, R.; Anderson, M. L.; Castro, P. D.; Ittmann, M.; Huntsman, D.; Kohl, B.; Le, X.; Thorp, R.; Andry, C.; Duffy, E. R.; Lyadov, V.; Paklina, O.; Setdikova, G.; Shabunin, A.; Tavobilov, M.; McPherson, C.; Warnick, R.; Berkowitz, R.; Cramer, D.; Feltmate, C.; Horowitz, N.; Kibel, A.; Muto, M.; Raut, C. P.; Malykh, A.; Barnholtz-Sloan, J. S.; Barrett, W.; Devine, K.; Fulop, J.; Ostrom, Q. T.; Shimmel, K.; Wolinsky, Y.; Sloan, A. E.; De Rose, A.; Giuliante, F.; Goodman, M.; Karlan, B. Y.; Hagedorn, C. H.; Eckman, J.; Harr, J.; Myers, J.; Tucker, K.; Zach, L. A.; Deyarmin, B.; Hu, H.; Kvecher, L.; Larson, C.; Mural, R. J.; Somiari, S.; Vicha, A.; Zelinka, T.; Bennett, J.; Iacocca, M.; Rabeno, B.; Swanson, P.; Latour, M.; Lacombe, L.; Têtu, B.; Bergeron, A.; McGraw, M.; Staugaitis, S. M.; Chabot, J.; Hibshoosh, H.; Sepulveda, A.; Su, T.; Wang, T.; Potapova, O.; Voronina, O.; Desjardins, L.; Mariani, O.; Roman-Roman, S.; Sastre, X.; Stern, M.-H.; Cheng, F.; Signoretti, S.; Berchuck, A.; Bigner, D.; Lipp, E.; Marks, J.; McCall, S.; McLendon, R.; Secord, A.; Sharp, A.; Behera, M.; Brat, D. J.; Chen, A.; Delman, K.; Force, S.; Khuri, F.; Magliocca, K.; Maithel, S.; Olson, J. J.;

Owonikoko, T.; Pickens, A.; Ramalingam, S.; Shin, D. M.; Sica, G.; Van Meir, E. G.; Zhang, H.; Eijckenboom, W.; Gillis, A.; Korpershoek, E.; Looijenga, L.; Oosterhuis, W.; Stoop, H.; van Kessel, K. E.; Zwarthoff, E. C.; Calatozzolo, C.; Cuppini, L.; Cuzzubbo, S.; DiMeco, F.; Finocchiaro, G.; Mattei, L.; Perin, A.; Pollo, B.; Chen, C.; Houck, J.; Lohavanichbutr, P.; Hartmann, A.; Stoehr, C.; Stoehr, R.; Taubert, H.; Wach, S.; Wullich, B.; Kycler, W.; Murawa, D.; Wiznerowicz, M.; Chung, K.; Edenfield, W. J.; Martin, J.; Baudin, E.; Bubley, G.; Bueno, R.; De Rienzo, A.; Richards, W. G.; Kalkanis, S.; Mikkelsen, T.; Noushmehr, H.; Scarpace, L.; Girard, N.; Aymerich, M.; Campo, E.; Giné, E.; Guillermo, A. L.; Van Bang, N.; Hanh, P. T.; Phu, B. D.; Tang, Y.; Colman, H.; Evason, K.; Dottino, P. R.; Martignetti, J. A.; Gabra, H.; Juhl, H.; Akeredolu, T.; Stepa, S.; Hoon, D.; Ahn, K.; Kang, K. J.; Beuschlein, F.; Breggia, A.; Birrer, M.; Bell, D.; Borad, M.; Bryce, A. H.; Castle, E.; Chandan, V.; Cheville, J.; Copland, J. A.; Farnell, M.; Flotte, T.; Giama, N.; Ho, T.; Kendrick, M.; Kocher, J.-P.; Kopp, K.; Moser, C.; Nagorney, D.; O'Brien, D.; O'Neill, B. P.; Patel, T.; Petersen, G.; Que, F.; Rivera, M.; Roberts, L.; Smallridge, R.; Smyrk, T.; Stanton, M.; Thompson, R. H.; Torbenson, M.; Yang, J. D.; Zhang, L.; Brimo, F.; Ajani, J. A.; Gonzalez, A. M. A.; Behrens, C.; Bondaruk, J.; Broaddus, R.; Czerniak, B.; Esmaeli, B.; Fujimoto, J.; Gershenwald, J.; Guo, C.; Lazar, A. J.; Logothetis, C.; Meric-Bernstam, F.; Moran, C.; Ramondetta, L.; Rice, D.; Sood, A.; Tamboli, P.; Thompson, T.; Troncoso, P.; Tsao, A.; Wistuba, I.; Carter, C.; Haydu, L.; Hersey, P.; Jakrot, V.; Kakavand, H.; Kefford, R.; Lee, K.; Long, G.; Mann, G.; Quinn, M.; Saw, R.; Scolyer, R.; Shannon, K.; Spillane, A.; Stretch, J.; Synott, M.; Thompson, J.; Wilmott, J.; Al-Ahmadie, H.; Chan, T. A.; Ghossein, R.; Gopalan, A.; Levine, D. A.; Reuter, V.; Singer, S.; Singh, B.; Tien, N. V.; Broudy, T.; Mirsaidi, C.; Nair, P.; Drwiega, P.; Miller, J.; Smith, J.; Zaren, H.; Park, J.-W.; Hung, N. P.; Kebebew, E.; Linehan, W. M.; Metwalli, A. R.; Pacak, K.; Pinto, P. A.; Schiffman, M.; Schmidt, L. S.; Vocke, C. D.; Wentzensen, N.; Worrell, R.; Yang, H.; Moncrieff, M.; Goparaju, C.; Melamed, J.; Pass, H.; Botnariuc, N.; Caraman, I.; Cernat, M.; Chemencedji, I.; Clipca, A.; Doruc, S.; Gorincioi, G.; Mura, S.; Pirtac, M.; Stancul, I.; Tcaciuc, D.; Albert, M.; Alexopoulou, I.; Arnaout, A.; Bartlett, J.; Engel, J.; Gilbert, S.; Parfitt, J.; Sekhon, H.; Thomas, G.; Rassl, D. M.; Rintoul, R. C.; Bifulco, C.; Tamakawa, R.; Urba, W.; Hayward, N.; Timmers, H.; Antenucci, A.; Facciolo, F.; Grazi, G.; Marino, M.; Merola, R.; de Krijger, R.; Gimenez-Roqueplo, A.-P.; Piché, A.; Chevalier, S.; McKercher, G.; Birsoy, K.; Barnett, G.; Brewer, C.; Farver, C.; Naska, T.; Pennell, N. A.; Raymond, D.; Schilero, C.; Smolenski, K.; Williams, F.; Morrison, C.; Borgia, J. A.; Liptay, M. J.; Pool, M.; Seder, C. W.; Junker, K.; Omberg, L.; Dinkin, M.; Manikhas, G.; Alvaro, D.; Bragazzi, M. C.; Cardinale, V.; Carpino, G.; Gaudio, E.; Chesla, D.; Cottingham, S.; Dubina, M.; Moiseenko, F.; Dhanasekaran, R.; Becker, K.-F.; Janssen, K.-P.; Slotta-Huspenina, J.; Abdel-Rahman, M. H.; Aziz, D.; Bell, S.; Cebulla, C. M.; Davis, A.; Duell, R.; Elder, J. B.; Hilty, J.; Kumar, B.; Lang, J.; Lehman, N. L.; Mandt, R.; Nguyen, P.; Pilarski, R.; Rai, K.; Schoenfield, L.; Senecal, K.; Wakely, P.; Hansen, P.; Lechan, R.; Powers, J.; Tischler, A.; Grizzle, W. E.; Sexton, K. C.; Kastl, A.; Henderson, J.; Porten, S.; Waldmann, J.; Fassnacht, M.; Asa, S. L.; Schadendorf, D.; Couce, M.; Graefen, M.;

Huland, H.; Sauter, G.; Schlomm, T.; Simon, R.; Tennstedt, P.; Olabode, O.; Nelson, M.; Bathe, O.; Carroll, P. R.; Chan, J. M.; Disaia, P.; Glenn, P.; Kelley, R. K.; Landen, C. N.; Phillips, J.; Prados, M.; Simko, J.; Smith-McCune, K.; VandenBerg, S.; Roggin, K.; Fehrenbach, A.; Kendler, A.; Sifri, S.; Steele, R.; Jimeno, A.; Carey, F.; Forgie, I.; Mannelli, M.; Carney, M.; Hernandez, B.; Campos, B.; Herold-Mende, C.; Jungk, C.; Unterberg, A.; von Deimling, A.; Bossler, A.; Galbraith, J.; Jacobus, L.; Knudson, M.; Knutson, T.; Ma, D.; Milhem, M.; Sigmund, R.; Godwin, A. K.; Madan, R.; Rosenthal, H. G.; Adebamowo, C.; Adebamowo, S. N.; Boussioutas, A.; Beer, D.; Giordano, T.; Mes-Masson, A.-M.; Saad, F.; Bocklage, T.; Landrum, L.; Mannel, R.; Moore, K.; Moxley, K.; Postier, R.; Walker, J.; Zuna, R.; Feldman, M.; Valdivieso, F.; Dhir, R.; Luketich, J.; Pinero, E. M. M.; Quintero-Aguilo, M.; Carlotti, C. G.; Dos Santos, J. S.; Kemp, R.; Sankarankuty, A.; Tirapelli, D.; Catto, J.; Agnew, K.; Swisher, E.; Creaney, J.; Robinson, B.; Shelley, C. S.; Godwin, E. M.; Kendall, S.; Shipman, C.; Bradford, C.; Carey, T.; Haddad, A.; Moyer, J.; Peterson, L.; Prince, M.; Rozek, L.; Wolf, G.; Bowman, R.; Fong, K. M.; Yang, I.; Korst, R.; Rathmell, W. K.; Fantacone-Campbell, J. L.; Hooke, J. A.; Kovatich, A. J.; Shriver, C. D.; DiPersio, J.; Drake, B.; Govindan, R.; Heath, S.; Ley, T.; Van Tine, B.; Westervelt, P.; Rubin, M. A.; Lee, J. I.; Aredes, N. D.; Mariamidze, A.; Camargo, F.; Liang, H. Comprehensive Molecular Characterization of the Hippo Signaling Pathway in Cancer. *Cell Reports* **2018**, *25* (5), 1304-1317.e5. https://doi.org/10.1016/j.celrep.2018.10.001.

(83) Lee, K.; Lee, K.-B.; Jung, H. Y.; Yi, N.-J.; Lee, K.-W.; Suh, K.-S.; Jang, J.-J. The Correlation between Poor Prognosis and Increased Yes-Associated Protein 1 Expression in Keratin 19 Expressing Hepatocellular Carcinomas and Cholangiocarcinomas. *BMC Cancer* **2017**, *17* (1), 441. https://doi.org/10.1186/s12885-017-3431-1.

(84) Corvaisier, M.; Bauzone, M.; Corfiotti, F.; Renaud, F.; Amrani, M. E.; Monté, D.; Truant, S.; Leteurtre, E.; Formstecher, P.; Van Seuningen, I.; Gespach, C.; Huet, G. Regulation of Cellular Quiescence by YAP/TAZ and Cyclin E1 in Colon Cancer Cells: Implication in Chemoresistance and Cancer Relapse. *Oncotarget* **2016**, *7* (35), 56699–56712. https://doi.org/10.18632/oncotarget.11057.

(85) Zhang, X.; George, J.; Deb, S.; Degoutin, J. L.; Takano, E. A.; Fox, S. B.; Bowtell, D. D. L.; Harvey, K. F. The Hippo Pathway Transcriptional Co-Activator, YAP, Is an Ovarian Cancer Oncogene. *Oncogene* **2011**, *30* (25), 2810–2822. https://doi.org/10.1038/onc.2011.8.

(86) Lo Sardo, F.; Strano, S.; Blandino, G. YAP and TAZ in Lung Cancer: Oncogenic Role and Clinical Targeting. *Cancers (Basel)* **2018**, *10* (5). https://doi.org/10.3390/cancers10050137.

(87) Marx, A.; Schumann, A.; Höflmayer, D.; Bady, E.; Hube-Magg, C.; Möller, K.; Tsourlakis, M. C.; Steurer, S.; Büscheck, F.; Eichenauer, T.; Clauditz, T. S.; Graefen, M.; Simon, R.; Sauter, G.; Izbicki, J. R.; Huland, H.; Heinzer, H.; Haese, A.; Schlomm, T.; Bernreuther, C.; Lebok, P.; Polonski, A. Up Regulation of the Hippo Signalling Effector YAP1 Is Linked to Early Biochemical Recurrence in Prostate Cancers. *Scientific Reports* **2020**, *10* (1), 8916. https://doi.org/10.1038/s41598-020-65772-w.

(88) Steinhardt, A. A.; Gayyed, M. F.; Klein, A. P.; Dong, J.; Maitra, A.; Pan, D.; Montgomery, E. A.; Anders, R. A. Expression of Yes-Associated Protein in Common Solid Tumors. *Human Pathology* **2008**, *39* (11), 1582–1589. https://doi.org/10.1016/j.humpath.2008.04.012.

(89) Overholtzer, M.; Zhang, J.; Smolen, G. A.; Muir, B.; Li, W.; Sgroi, D. C.; Deng, C.-X.; Brugge, J. S.; Haber, D. A. Transforming Properties of YAP, a Candidate Oncogene on the Chromosome 11q22 Amplicon. *PNAS* **2006**, *103* (33), 12405–12410. https://doi.org/10.1073/pnas.0605579103.

(90) Ling, H.-H.; Kuo, C.-C.; Lin, B.-X.; Huang, Y.-H.; Lin, C.-W. Elevation of YAP Promotes the Epithelial-Mesenchymal Transition and Tumor Aggressiveness in Colorectal Cancer. *Exp Cell Res* **2017**, *350* (1), 218–225. https://doi.org/10.1016/j.yexcr.2016.11.024.

(91) Camargo, F. D.; Gokhale, S.; Johnnidis, J. B.; Fu, D.; Bell, G. W.; Jaenisch, R.; Brummelkamp, T. R. YAP1 Increases Organ Size and Expands Undifferentiated Progenitor Cells. *Current Biology* **2007**, *17* (23), 2054–2060. https://doi.org/10.1016/j.cub.2007.10.039.

(92) Zhao, B.; Kim, J.; Ye, X.; Lai, Z.-C.; Guan, K.-L. Both TEAD-Binding and WW Domains Are Required for the Growth Stimulation and Oncogenic Transformation Activity of Yes-Associated Protein. *Cancer Res* **2009**, *69* (3), 1089–1098. https://doi.org/10.1158/0008-5472.CAN-08-2997.

(93) Galli, G. G.; Carrara, M.; Yuan, W.-C.; Valdes-Quezada, C.; Gurung, B.; Pepe-Mooney, B.; Zhang, T.; Geeven, G.; Gray, N. S.; de Laat, W.; Calogero, R. A.; Camargo, F. D. YAP Drives Growth by Controlling Transcriptional Pause Release from Dynamic Enhancers. *Mol Cell* **2015**, *60* (2), 328–337. https://doi.org/10.1016/j.molcel.2015.09.001.

(94) Zhou, Y.; Huang, T.; Cheng, A. S. L.; Yu, J.; Kang, W.; To, K. F. The TEAD Family and Its Oncogenic Role in Promoting Tumorigenesis. *International Journal of Molecular Sciences* **2016**, *17* (1), 138. https://doi.org/10.3390/ijms17010138.

(95) Xu, M. Z.; Chan, S. W.; Liu, A. M.; Wong, K. F.; Fan, S. T.; Chen, J.; Poon, R. T.; Zender, L.; Lowe, S. W.; Hong, W.; Luk, J. M. AXL Receptor Kinase Is a Mediator of YAP-Dependent Oncogenic Functions in Hepatocellular Carcinoma. *Oncogene* **2011**, *30* (10), 1229–1240. https://doi.org/10.1038/onc.2010.504.

(96) Liu-Chittenden, Y.; Huang, B.; Shim, J. S.; Chen, Q.; Lee, S.-J.; Anders, R. A.; Liu, J. O.; Pan, D. Genetic and Pharmacological Disruption of the TEAD–YAP Complex Suppresses the Oncogenic Activity of YAP. *Genes Dev.* **2012**, *26* (12), 1300–1305. https://doi.org/10.1101/gad.192856.112.

(97) Huh, H. D.; Kim, D. H.; Jeong, H.-S.; Park, H. W. Regulation of TEAD Transcription Factors in Cancer Biology. *Cells* **2019**, *8* (6). https://doi.org/10.3390/cells8060600.

(98) Zhao, B.; Ye, X.; Yu, J.; Li, L.; Li, W.; Li, S.; Yu, J.; Lin, J. D.; Wang, C.-Y.; Chinnaiyan, A. M.; Lai, Z.-C.; Guan, K.-L. TEAD Mediates YAP-Dependent Gene Induction and Growth Control. *Genes Dev* **2008**, *22* (14), 1962–1971. https://doi.org/10.1101/gad.1664408.

(99) Zanconato, F.; Forcato, M.; Battilana, G.; Azzolin, L.; Quaranta, E.; Bodega, B.; Rosato, A.; Bicciato, S.; Cordenonsi, M.; Piccolo, S. Genome-Wide Association between YAP/TAZ/TEAD and AP-1 at Enhancers Drives Oncogenic Growth. *Nat Cell Biol* **2015**, *17* (9), 1218–1227. https://doi.org/10.1038/ncb3216.

(100) Stein, C.; Bardet, A. F.; Roma, G.; Bergling, S.; Clay, I.; Ruchti, A.; Agarinis, C.; Schmelzle, T.; Bouwmeester, T.; Schübeler, D.; Bauer, A. YAP1 Exerts Its Transcriptional Control via TEAD-Mediated Activation of Enhancers. *PLoS Genet* **2015**, *11* (8), e1005465. https://doi.org/10.1371/journal.pgen.1005465.

(101) Lin, K. C.; Moroishi, T.; Meng, Z.; Jeong, H.-S.; Plouffe, S. W.; Sekido, Y.; Han, J.; Park, H. W.; Guan, K.-L. Regulation of Hippo Pathway Transcription Factor TEAD by P38 MAPK-Induced Cytoplasmic Translocation. *Nat Cell Biol* **2017**, *19* (8), 996–1002. https://doi.org/10.1038/ncb3581.

(102) Diepenbruck, M.; Waldmeier, L.; Ivanek, R.; Berninger, P.; Arnold, P.; van Nimwegen, E.; Christofori, G. Tead2 Expression Levels Control the Subcellular

Distribution of Yap and Taz, Zyxin Expression and Epithelial-Mesenchymal Transition. *J Cell Sci* **2014**, *127* (Pt 7), 1523–1536. https://doi.org/10.1242/jcs.139865.

(103) Lim, B.; Park, J.-L.; Kim, H.-J.; Park, Y.-K.; Kim, J.-H.; Sohn, H. A.; Noh, S.-M.; Song, K.-S.; Kim, W.-H.; Kim, Y. S.; Kim, S.-Y. Integrative Genomics Analysis Reveals the Multilevel Dysregulation and Oncogenic Characteristics of TEAD4 in Gastric Cancer. *Carcinogenesis* **2014**, *35* (5), 1020–1027. https://doi.org/10.1093/carcin/bgt409.

(104) Holden, J. K.; Cunningham, C. N. Targeting the Hippo Pathway and Cancer through the TEAD Family of Transcription Factors. *Cancers (Basel)* **2018**, *10* (3). https://doi.org/10.3390/cancers10030081.

(105) Knight, J. F.; Shepherd, C. J.; Rizzo, S.; Brewer, D.; Jhavar, S.; Dodson, A. R.; Cooper, C. S.; Eeles, R.; Falconer, A.; Kovacs, G.; Garrett, M. D.; Norman, A. R.; Shipley, J.; Hudson, D. L. TEAD1 and C-Cbl Are Novel Prostate Basal Cell Markers That Correlate with Poor Clinical Outcome in Prostate Cancer. *Br J Cancer* **2008**, *99* (11), 1849–1858. https://doi.org/10.1038/sj.bjc.6604774.

(106) Salem, O.; Hansen, C. G. The Hippo Pathway in Prostate Cancer. *Cells* **2019**, *8* (4). https://doi.org/10.3390/cells8040370.

(107) Zhao, B.; Li, L.; Wang, L.; Wang, C.-Y.; Yu, J.; Guan, K.-L. Cell Detachment Activates the Hippo Pathway via Cytoskeleton Reorganization to Induce Anoikis. *Genes Dev* **2012**, *26* (1), 54–68. https://doi.org/10.1101/gad.173435.111.

(108) Li, H.; He, F.; Zhao, X.; Zhang, Y.; Chu, X.; Hua, C.; Qu, Y.; Duan, Y.; Ming, L. YAP Inhibits the Apoptosis and Migration of Human Rectal Cancer Cells via Suppression of JNK-Drp1-Mitochondrial Fission-HtrA2/Omi Pathways. *CPB* **2017**, *44* (5), 2073–2089. https://doi.org/10.1159/000485946.

(109) Dong, J.; Feldmann, G.; Huang, J.; Wu, S.; Zhang, N.; Comerford, S. A.; Gayyed, M. F.; Anders, R. A.; Maitra, A.; Pan, D. Elucidation of a Universal Size-Control Mechanism in Drosophila and Mammals. *Cell* **2007**, *130* (6), 1120–1133. https://doi.org/10.1016/j.cell.2007.07.019.

(110) Boopathy, G. T. K.; Hong, W. Role of Hippo Pathway-YAP/TAZ Signaling in Angiogenesis. *Front. Cell Dev. Biol.* **2019**, *7*. https://doi.org/10.3389/fcell.2019.00049.

(111) Hayashi, H.; Higashi, T.; Yokoyama, N.; Kaida, T.; Sakamoto, K.; Fukushima, Y.; Ishimoto, T.; Kuroki, H.; Nitta, H.; Hashimoto, D.; Chikamoto, A.; Oki, E.; Beppu, T.; Baba, H. An Imbalance in TAZ and YAP Expression in Hepatocellular Carcinoma Confers Cancer Stem Cell-like Behaviors Contributing to Disease Progression. *Cancer Res* **2015**, *75* (22), 4985–4997. https://doi.org/10.1158/0008-5472.CAN-15-0291.

(112) Lamar, J. M.; Stern, P.; Liu, H.; Schindler, J. W.; Jiang, Z.-G.; Hynes, R. O. The Hippo Pathway Target, YAP, Promotes Metastasis through Its TEAD-Interaction Domain. *Proc Natl Acad Sci U S A* **2012**, *109* (37), E2441-2450. https://doi.org/10.1073/pnas.1212021109.

(113) Nguyen, C.; Yi, C. YAP/TAZ Signaling and Resistance to Cancer Therapy. *Trends Cancer* **2019**, *5* (5), 283–296. https://doi.org/10.1016/j.trecan.2019.02.010.

(114) Kim, M. H.; Kim, J. Role of YAP/TAZ Transcriptional Regulators in Resistance to Anti-Cancer Therapies. *Cell. Mol. Life Sci.* **2017**, *74* (8), 1457–1474. https://doi.org/10.1007/s00018-016-2412-x.

(115) Zanconato, F.; Cordenonsi, M.; Piccolo, S. YAP/TAZ at the Roots of Cancer. *Cancer Cell* **2016**, *29* (6), 783–803. https://doi.org/10.1016/j.ccell.2016.05.005.

(116) Warren, J. S. A.; Xiao, Y.; Lamar, J. M. YAP/TAZ Activation as a Target for Treating Metastatic Cancer. *Cancers (Basel)* **2018**, *10* (4). https://doi.org/10.3390/cancers10040115.

(117) Pobbati, A. V.; Hong, W. A Combat with the YAP/TAZ-TEAD Oncoproteins for Cancer Therapy. *Theranostics* **2020**, *10* (8), 3622–3635. https://doi.org/10.7150/thno.40889.

(118) Gibault, F.; Sturbaut, M.; Bailly, F.; Melnyk, P.; Cotelle, P. Targeting Transcriptional Enhanced Associate Domains (TEADs): Miniperspective. *J. Med. Chem.* **2018**, *61* (12), 5057–5072. https://doi.org/10.1021/acs.jmedchem.7b00879.

(119) Gaffney, C. J.; Oka, T.; Mazack, V.; Hilman, D.; Gat, U.; Muramatsu, T.; Inazawa, J.; Golden, A.; Carey, D. J.; Farooq, A.; Tromp, G.; Sudol, M. Identification, Basic Characterization and Evolutionary Analysis of Differentially Spliced MRNA Isoforms of Human YAP1 Gene. *Gene* **2012**, *509* (2), 215–222. https://doi.org/10.1016/j.gene.2012.08.025.

(120) Chen, Y.-A.; Lu, C.-Y.; Cheng, T.-Y.; Pan, S.-H.; Chen, H.-F.; Chang, N.-S. WW Domain-Containing Proteins YAP and TAZ in the Hippo Pathway as Key Regulators in Stemness Maintenance, Tissue Homeostasis, and Tumorigenesis. *Front. Oncol.* **2019**, *9*. https://doi.org/10.3389/fonc.2019.00060.

(121) Wang, C.; Zhu, X.; Feng, W.; Yu, Y.; Jeong, K.; Guo, W.; Lu, Y.; Mills, G. B. Verteporfin Inhibits YAP Function through Up-Regulating 14-3-3σ Sequestering YAP in the Cytoplasm. *Am J Cancer Res* **2016**, *6* (1), 27–37.

(122) Song, S.; Xie, M.; Scott, A. W.; Jin, J.; Ma, L.; Dong, X.; Skinner, H. D.; Johnson, R. L.; Ding, S.; Ajani, J. A. A Novel YAP1 Inhibitor Targets CSC-Enriched Radiation-Resistant Cells and Exerts Strong Antitumor Activity in Esophageal Adenocarcinoma. *Mol Cancer Ther* **2018**, *17* (2), 443–454. https://doi.org/10.1158/1535-7163.MCT-17-0560.

(123) Kandasamy, S.; Adhikary, G.; Rorke, E. A.; Friedberg, J. S.; Mickle, M. B.; Alexander, H. R.; Eckert, R. L. The YAP1 Signaling Inhibitors, Verteporfin and CA3, Suppress the Mesothelioma Cancer Stem Cell Phenotype. *Mol Cancer Res* **2020**, *18* (3), 343–351. https://doi.org/10.1158/1541-7786.MCR-19-0914.

(124) Dasari, V. R.; Mazack, V.; Feng, W.; Nash, J.; Carey, D. J.; Gogoi, R. Verteporfin Exhibits YAP-Independent Anti-Proliferative and Cytotoxic Effects in Endometrial Cancer Cells. *Oncotarget* **2017**, *8* (17), 28628–28640. https://doi.org/10.18632/oncotarget.15614.

(125) Jho, E. Dual Role of YAP: Oncoprotein and Tumor Suppressor. *J Thorac Dis* **2018**, *10* (Suppl 33), S3895–S3898. https://doi.org/10.21037/jtd.2018.10.70.

(126) Li, Z.; Zhao, B.; Wang, P.; Chen, F.; Dong, Z.; Yang, H.; Guan, K.-L.; Xu, Y. Structural Insights into the YAP and TEAD Complex. *Genes Dev.* **2010**, *24* (3), 235–240. https://doi.org/10.1101/gad.1865810.

(127) Mesrouze, Y.; Bokhovchuk, F.; Meyerhofer, M.; Fontana, P.; Zimmermann, C.; Martin, T.; Delaunay, C.; Erdmann, D.; Schmelzle, T.; Chène, P. Dissection of the Interaction between the Intrinsically Disordered YAP Protein and the Transcription Factor TEAD. *eLife* **2017**, *6*, e25068. https://doi.org/10.7554/eLife.25068.

(128) Zhou, Z.; Hu, T.; Xu, Z.; Lin, Z.; Zhang, Z.; Feng, T.; Zhu, L.; Rong, Y.; Shen, H.; Luk, J. M.; Zhang, X.; Qin, N. Targeting Hippo Pathway by Specific Interruption

of YAP-TEAD Interaction Using Cyclic YAP-like Peptides. *The FASEB Journal* **2015**, *29* (2), 724–732. https://doi.org/10.1096/fj.14-262980.

(129) Furet, P.; Salem, B.; Mesrouze, Y.; Schmelzle, T.; Lewis, I.; Kallen, J.; Chène, P. Structure-Based Design of Potent Linear Peptide Inhibitors of the YAP-TEAD Protein-Protein Interaction Derived from the YAP Omega-Loop Sequence. *Bioorganic & Medicinal Chemistry Letters* **2019**, *29* (16), 2316–2319. https://doi.org/10.1016/j.bmcl.2019.06.022.

(130) Crook, Z. R.; Sevilla, G. P.; Friend, D.; Brusniak, M.-Y.; Bandaranayake, A. D.; Clarke, M.; Gewe, M.; Mhyre, A. J.; Baker, D.; Strong, R. K.; Bradley, P.; Olson, J. M. Mammalian Display Screening of Diverse Cystine-Dense Peptides for Difficult to Drug Targets. *Nat Commun* **2017**, *8*. https://doi.org/10.1038/s41467-017-02098-8.

(131) Jiao, S.; Wang, H.; Shi, Z.; Dong, A.; Zhang, W.; Song, X.; He, F.; Wang, Y.; Zhang, Z.; Wang, W.; Wang, X.; Guo, T.; Li, P.; Zhao, Y.; Ji, H.; Zhang, L.; Zhou, Z. A Peptide Mimicking VGLL4 Function Acts as a YAP Antagonist Therapy against Gastric Cancer. *Cancer Cell* **2014**, *25* (2), 166–180. https://doi.org/10.1016/j.ccr.2014.01.010.

(132) Gibault, F.; Coevoet, M.; Sturbaut, M.; Farce, A.; Renault, N.; Allemand, F.; Guichou, J.-F.; Drucbert, A.-S.; Foulon, C.; Magnez, R.; Thuru, X.; Corvaisier, M.; Huet, G.; Chavatte, P.; Melnyk, P.; Bailly, F.; Cotelle, P. Toward the Discovery of a Novel Class of YAP–TEAD Interaction Inhibitors by Virtual Screening Approach Targeting YAP–TEAD Protein–Protein Interface. *Cancers (Basel)* **2018**, *10* (5). https://doi.org/10.3390/cancers10050140.

(133) Smith, S. A.; Sessions, R. B.; Shoemark, D. K.; Williams, C.; Ebrahimighaei, R.; McNeill, M. C.; Crump, M. P.; McKay, T. R.; Harris, G.; Newby, A. C.; Bond, M. Antiproliferative and Antimigratory Effects of a Novel YAP–TEAD Interaction Inhibitor Identified Using in Silico Molecular Docking. *J Med Chem* **2019**, *62* (3), 1291–1305. https://doi.org/10.1021/acs.jmedchem.8b01402.

(134) Crawford, J. J.; Bronner, S. M.; Zbieg, J. R. Hippo Pathway Inhibition by Blocking the YAP/TAZ–TEAD Interface: A Patent Review. *Expert Opinion on Therapeutic Patents* **2018**, *28* (12), 867–873. https://doi.org/10.1080/13543776.2018.1549226.

(135) Barth, M.; Contal, S.; Montalbetti, C.; Spitzer, L. New Compounds Inhibitors of the Yap/Taz-Tead Interaction and Their Use in the Treatment of Malignant Mesothelioma. WO/2017/064277, April 20, 2017.

(136) Qi, Y.; Yu, J.; Han, W.; Fan, X.; Qian, H.; Wei, H.; Tsai, Y. S.; Zhao, J.; Zhang, W.; Liu, Q.; Meng, S.; Wang, Y.; Wang, Z. A Splicing Isoform of TEAD4 Attenuates the Hippo–YAP Signalling to Inhibit Tumour Proliferation. *Nat Commun* **2016**, *7* (1), ncomms11840. https://doi.org/10.1038/ncomms11840.

(137) Chen, Z.; Friedrich, G. A.; Soriano, P. Transcriptional Enhancer Factor 1 Disruption by a Retroviral Gene Trap Leads to Heart Defects and Embryonic Lethality in Mice. *Genes Dev* **1994**, *8* (19), 2293–2301. https://doi.org/10.1101/gad.8.19.2293.

(138) Kaneko, K. J.; Kohn, M. J.; Liu, C.; DePamphilis, M. L. Transcription Factor TEAD2 Is Involved in Neural Tube Closure. *Genesis* **2007**, *45* (9), 577–587. https://doi.org/10.1002/dvg.20330.

(139) Sawada, A.; Kiyonari, H.; Ukita, K.; Nishioka, N.; Imuta, Y.; Sasaki, H. Redundant Roles of Tead1 and Tead2 in Notochord Development and the Regulation of Cell Proliferation and Survival. *Mol Cell Biol* **2008**, *28* (10), 3177–3189. https://doi.org/10.1128/MCB.01759-07.

(140) Yagi, R.; Kohn, M. J.; Karavanova, I.; Kaneko, K. J.; Vullhorst, D.; DePamphilis, M. L.; Buonanno, A. Transcription Factor TEAD4 Specifies the Trophectoderm Lineage at the Beginning of Mammalian Development. *Development* **2007**, *134* (21), 3827–3836. https://doi.org/10.1242/dev.010223.

(141) Jacquemin, P.; Sapin, V.; Alsat, E.; Evain-Brion, D.; Dollé, P.; Davidson, I. Differential Expression of the TEF Family of Transcription Factors in the Murine Placenta and during Differentiation of Primary Human Trophoblasts in Vitro. *Dev Dyn* **1998**, *212* (3), 423–436. https://doi.org/10.1002/(SICI)1097-0177(199807)212:3<423::AID-AJA10>3.0.CO;2-1.

(142) Mann, C. J.; Osborn, D. P. S.; Hughes, S. M. Vestigial-like-2b (VITO-1b) and Tead-3a (Tef-5a) Expression in Zebrafish Skeletal Muscle, Brain and Notochord. *Gene Expression Patterns* **2007**, *7* (8), 827–836. https://doi.org/10.1016/j.modgep.2007.08.001.

(143) Kakiuchi-Kiyota, S.; Schutten, M. M.; Zhong, Y.; Crawford, J. J.; Dey, A. Safety Considerations in the Development of Hippo Pathway Inhibitors in Cancers. *Front. Cell Dev. Biol.* **2019**, *7*. https://doi.org/10.3389/fcell.2019.00156.

(144) Shi, Z.; He, F.; Chen, M.; Hua, L.; Wang, W.; Jiao, S.; Zhou, Z. DNA-Binding Mechanism of the Hippo Pathway Transcription Factor TEAD4. *Oncogene* **2017**, *36* (30), 4362–4369. https://doi.org/10.1038/onc.2017.24.

(145) Chan, P.; Han, X.; Zheng, B.; DeRan, M.; Yu, J.; Jarugumilli, G. K.; Deng, H.; Pan, D.; Luo, X.; Wu, X. Autopalmitoylation of TEAD Proteins Regulates Transcriptional Output of the Hippo Pathway. *Nat Chem Biol* **2016**, *12* (4), 282–289. https://doi.org/10.1038/nchembio.2036.

(146) Li, Y.; Liu, S.; Ng, E. Y.; Li, R.; Poulsen, A.; Hill, J.; Pobbati, A. V.; Hung, A. W.; Hong, W.; Keller, T. H.; Kang, C. Structural and Ligand-Binding Analysis of the YAP-Binding Domain of Transcription Factor TEAD4. *Biochem J* **2018**, *475* (12), 2043–2055. https://doi.org/10.1042/BCJ20180225.

(147) Mesrouze, Y.; Meyerhofer, M.; Bokhovchuk, F.; Fontana, P.; Zimmermann, C.; Martin, T.; Delaunay, C.; Izaac, A.; Kallen, J.; Schmelzle, T.; Erdmann, D.; Chène, P. Effect of the Acylation of TEAD4 on Its Interaction with Co-Activators YAP and TAZ. *Protein Sci* **2017**, *26* (12), 2399–2409. https://doi.org/10.1002/pro.3312.

(148) Wu, X. TEAD Transcription Factor Autopalmitoylation Inhibitors. WO 2017/053706 Al, March 30, 2017.

(149) Noland, C. L.; Gierke, S.; Schnier, P. D.; Murray, J.; Sandoval, W. N.; Sagolla, M.; Dey, A.; Hannoush, R. N.; Fairbrother, W. J.; Cunningham, C. N. Palmitoylation of TEAD Transcription Factors Is Required for Their Stability and Function in Hippo Pathway Signaling. *Structure* **2016**, *24* (1), 179–186. https://doi.org/10.1016/j.str.2015.11.005.

(150) Kim, N.-G.; Gumbiner, B. M. Cell Contact and Nf2/Merlin-Dependent Regulation of TEAD Palmitoylation and Activity. *PNAS* **2019**, *116* (20), 9877–9882. https://doi.org/10.1073/pnas.1819400116.

(151) Pobbati, A. V.; Rubin, B. P. Protein-Protein Interaction Disruptors of the YAP/TAZ-TEAD Transcriptional Complex. *Molecules* **2020**, *25* (24). https://doi.org/10.3390/molecules25246001.

(152) Pobbati, A. V.; Han, X.; Hung, A. W.; Weiguang, S.; Huda, N.; Chen, G.-Y.; Kang, C.; Chia, C. S. B.; Luo, X.; Hong, W.; Poulsen, A. Targeting the Central Pocket in Human Transcription Factor TEAD as a Potential Cancer Therapeutic Strategy. *Structure* **2015**, *23* (11), 2076–2086. https://doi.org/10.1016/j.str.2015.09.009.

(153) Barth, M.; Contal, S.; Junien, J.-L.; Massardier, C.; Montalbetti, C.; Soude, A. Inhibitors of the Yap/Taz-Tead Interaction and Their Use in the Treatment of Cancer. WO/2020/070181, April 9, 2020.

(154) Holden, J. K.; Crawford, J. J.; Noland, C. L.; Schmidt, S.; Zbieg, J. R.; Lacap, J. A.; Zang, R.; Miller, G. M.; Zhang, Y.; Beroza, P.; Reja, R.; Lee, W.; Tom, J. Y. K.; Fong, R.; Steffek, M.; Clausen, S.; Hagenbeek, T. J.; Hu, T.; Zhou, Z.; Shen, H. C.; Cunningham, C. N. Small Molecule Dysregulation of TEAD Lipidation Induces a Dominant-Negative Inhibition of Hippo Pathway Signaling. *Cell Reports* **2020**, *31* (12). https://doi.org/10.1016/j.celrep.2020.107809.

(155) Kunig, V. B. K.; Potowski, M.; Akbarzadeh, M.; Škopić, M. K.; Smith, D. dos S.; Arendt, L.; Dormuth, I.; Adihou, H.; Andlovic, B.; Karatas, H.; Shaabani, S.; Zarganes‐Tzitzikas, T.; Neochoritis, C. G.; Zhang, R.; Groves, M.; Guéret, S. M.; Ottmann, C.; Rahnenführer, J.; Fried, R.; Dömling, A.; Brunschweiger, A. TEAD–YAP Interaction Inhibitors and MDM2 Binders from DNA-Encoded Indole-Focused Ugi Peptidomimetics. *Angewandte Chemie International Edition* **2020**, *59* (46), 20338–20342. https://doi.org/10.1002/anie.202006280.

(156) Amidon, B.; Syed, S.; Cavanaugh, J.; Frosch, H.; Natarajan, P.; Ecsedy, J.; McGovern, K.; Castro, A. C. Potent Small Molecule TEAD Inhibitors Targeting the Hippo Pathway Exhibit Antiproliferation in Vitro and Anti-Tumor Effect in Vivo. *Cancer Res* **2020**, *80* (16 Supplement), 2474–2474. https://doi.org/10.1158/1538-7445.AM2020-2474.

(157) Versele, M.; Candi, A.; Nijs, M.; Haeck, W.; Klaassen, H.; Smets, W.; Spieser, S.; Vanderhoydonck, B.; Marchand, A.; Chaltin, P.; Sansores, L.; Halder, G. Discovery of Novel Potent Allosteric Inhibitors of YAP/TAZ-TEAD Transcription for the Treatment of Multiple Solid Tumor Types Addicted to Hippo Signaling. *Cancer Res* **2020**, *80* (16 Supplement), 5229–5229. https://doi.org/10.1158/1538-7445.AM2020-5229.

(158) Lu, W.; Wang, J.; Li, Y.; Tao, H.; Xiong, H.; Lian, F.; Gao, J.; Ma, H.; Lu, T.; Zhang, D.; Ye, X.; Ding, H.; Yue, L.; Zhang, Y.; Tang, H.; Zhang, N.; Yang, Y.; Jiang, H.; Chen, K.; Zhou, B.; Luo, C. Discovery and Biological Evaluation of Vinylsulfonamide Derivatives as Highly Potent, Covalent TEAD Autopalmitoylation

Inhibitors. *European Journal of Medicinal Chemistry* **2019**, *184*, 111767. https://doi.org/10.1016/j.ejmech.2019.111767.

(159) Bum-Erdene, K.; Zhou, D.; Gonzalez-Gutierrez, G.; Ghozayel, M. K.; Si, Y.; Xu, D.; Shannon, H. E.; Bailey, B. J.; Corson, T. W.; Pollok, K. E.; Wells, C. D.; Meroueh, S. O. Small-Molecule Covalent Modification of Conserved Cysteine Leads to Allosteric Inhibition of the TEAD·Yap Protein-Protein Interaction. *Cell Chem Biol* **2019**, *26* (3), 378-389.e13. https://doi.org/10.1016/j.chembiol.2018.11.010.

(160) Kaneda, A.; Seike, T.; Danjo, T.; Nakajima, T.; Otsubo, N.; Yamaguchi, D.; Tsuji, Y.; Hamaguchi, K.; Yasunaga, M.; Nishiya, Y.; Suzuki, M.; Saito, J.; Yatsunami, R.; Nakamura, S.; Sekido, Y.; Mori, K. The Novel Potent TEAD Inhibitor, K-975, Inhibits YAP1/TAZ-TEAD Protein-Protein Interactions and Exerts an Anti-Tumor Effect on Malignant Pleural Mesothelioma. *Am J Cancer Res* **2020**, *10* (12), 4399–4415.

(161) Av, P.; T, M.; S, C.; H, K.; Sr, B.; Sm, G.; Pa, G.; G, H.; A, P.; S, S.; E, G.; H, S.; H, W.; W, H. Identification of Quinolinols as Activators of TEAD-Dependent Transcription. *ACS Chem Biol* **2019**, *14* (12), 2909–2921. https://doi.org/10.1021/acschembio.9b00786.

(162) Zeng, L.; Zhou, M.-M. Bromodomain: An Acetyl-Lysine Binding Domain. *FEBS Letters* **2002**, *513* (1), 124–128. https://doi.org/10.1016/S0014-5793(01)03309-9.

(163) Owen, D. J.; Ornaghi, P.; Yang, J. C.; Lowe, N.; Evans, P. R.; Ballario, P.; Neuhaus, D.; Filetici, P.; Travers, A. A. The Structural Basis for the Recognition of Acetylated Histone H4 by the Bromodomain of Histone Acetyltransferase Gcn5p. *EMBO J* **2000**, *19* (22), 6141–6149. https://doi.org/10.1093/emboj/19.22.6141.

(164) Zeng, L.; Zhang, Q.; Gerona-Navarro, G.; Moshkina, N.; Zhou, M.-M. Structural Basis of Site-Specific Histone Recognition by the Bromodomains of Human Coactivators PCAF and CBP/P300. *Structure* **2008**, *16* (4), 643–652. https://doi.org/10.1016/j.str.2008.01.010.

(165) Sanchez, R.; Zhou, M.-M. The Role of Human Bromodomains in Chromatin Biology and Gene Transcription. *Curr Opin Drug Discov Devel* **2009**, *12* (5), 659–665.

(166) Chandrasekaran, R.; Thompson, M. Expression, Purification and Characterization of Individual Bromodomains from Human Polybromo-1. *Protein*

Expression and Purification **2006**, *50* (1), 111–117. https://doi.org/10.1016/j.pep.2006.07.004.

(167) Jeanmougin, F.; Wurtz, J.-M.; Douarin, B. L.; Chambon, P.; Losson, R. The Bromodomain Revisited. *Trends in Biochemical Sciences* **1997**, *22* (5), 151–153. https://doi.org/10.1016/S0968-0004(97)01042-6.

(168) Filippakopoulos, P.; Picaud, S.; Mangos, M.; Keates, T.; Lambert, J.-P.; Barsyte-Lovejoy, D.; Felletar, I.; Volkmer, R.; Müller, S.; Pawson, T.; Gingras, A.-C.; Arrowsmith, C. H.; Knapp, S. Histone Recognition and Large-Scale Structural Analysis of the Human Bromodomain Family. *Cell* **2012**, *149* (1), 214–231. https://doi.org/10.1016/j.cell.2012.02.013.

(169) Fujisawa, T.; Filippakopoulos, P. Functions of Bromodomain-Containing Proteins and Their Roles in Homeostasis and Cancer. *Nature Reviews Molecular Cell Biology* **2017**, *18* (4), 246–262. https://doi.org/10.1038/nrm.2016.143.

(170) Ruthenburg, A. J.; Li, H.; Patel, D. J.; Allis, C. D. Multivalent Engagement of Chromatin Modifications by Linked Binding Modules. *Nat Rev Mol Cell Biol* **2007**, *8* (12), 983–994. https://doi.org/10.1038/nrm2298.

(171) Thompson, M. Polybromo-1: The Chromatin Targeting Subunit of the PBAF Complex. *Biochimie* **2009**, *91* (3), 309–319. https://doi.org/10.1016/j.biochi.2008.10.019.

(172) Kupitz, C.; Chandrasekaran, R.; Thompson, M. Kinetic Analysis of Acetylation-Dependent Pb1 Bromodomain-Histone Interactions. *Biophys Chem* **2008**, *136* (1), 7–12. https://doi.org/10.1016/j.bpc.2008.03.011.

(173) R, C.; M, T. Polybromo-1-Bromodomains Bind Histone H3 at Specific Acetyl-Lysine Positions. *Biochem Biophys Res Commun* **2007**, *355* (3), 661–666. https://doi.org/10.1016/j.bbrc.2007.01.193.

(174) Slaughter, M. J.; Shanle, E. K.; McFadden, A. W.; Hollis, E. S.; Suttle, L. E.; Strahl, B. D.; Davis, I. J. PBRM1 Bromodomains Variably Influence Nucleosome Interactions and Cellular Function. *J Biol Chem* **2018**, *293* (35), 13592–13603. https://doi.org/10.1074/jbc.RA118.003381.

(175) Ho, P. J.; Lloyd, S. M.; Bao, X. Unwinding Chromatin at the Right Places: How BAF Is Targeted to Specific Genomic Locations during Development. *Development* **2019**, *146* (19). https://doi.org/10.1242/dev.178780.

(176) Xue, Y.; Canman, J. C.; Lee, C. S.; Nie, Z.; Yang, D.; Moreno, G. T.; Young, M. K.; Salmon, E. D.; Wang, W. The Human SWI/SNF-B Chromatin-Remodeling Complex Is Related to Yeast Rsc and Localizes at Kinetochores of Mitotic Chromosomes. *Proc Natl Acad Sci U S A* **2000**, *97* (24), 13015–13020.

(177) Wang, Z.; Zhai, W.; Richardson, J. A.; Olson, E. N.; Meneses, J. J.; Firpo, M. T.; Kang, C.; Skarnes, W. C.; Tjian, R. Polybromo Protein BAF180 Functions in Mammalian Cardiac Chamber Maturation. *Genes Dev* **2004**, *18* (24), 3106–3116. https://doi.org/10.1101/gad.1238104.

(178) Kim, Y.; Hernández, M. A. S.; Herrema, H.; Delibasi, T.; Park, S. W. The Role of BRD7 in Embryo Development and Glucose Metabolism. *Journal of Cellular and Molecular Medicine* **2016**, *20* (8), 1561–1570. https://doi.org/10.1111/jcmm.12907.

(179) Morrison, A. J. Chromatin-Remodeling Links Metabolic Signaling to Gene Expression. *Molecular Metabolism* **2020**, *38*, 100973. https://doi.org/10.1016/j.molmet.2020.100973.

(180) Xu, F.; Flowers, S.; Moran, E. Essential Role of ARID2 Protein-Containing SWI/SNF Complex in Tissue-Specific Gene Expression *. *Journal of Biological Chemistry* **2012**, *287* (7), 5033–5041. https://doi.org/10.1074/jbc.M111.279968.

(181) Bajpai, R.; Chen, D. A.; Rada-Iglesias, A.; Zhang, J.; Xiong, Y.; Helms, J.; Chang, C.-P.; Zhao, Y.; Swigut, T.; Wysocka, J. CHD7 Cooperates with PBAF to Control Multipotent Neural Crest Formation. *Nature* **2010**, *463* (7283), 958–962. https://doi.org/10.1038/nature08733.

(182) Wei, Z.; Yoshihara, E.; He, N.; Hah, N.; Fan, W.; Pinto, A. F. M.; Huddy, T.; Wang, Y.; Ross, B.; Estepa, G.; Dai, Y.; Ding, N.; Sherman, M. H.; Fang, S.; Zhao, X.; Liddle, C.; Atkins, A. R.; Yu, R. T.; Downes, M.; Evans, R. M. Vitamin D Switches BAF Complexes to Protect β Cells. *Cell* **2018**, *173* (5), 1135-1149.e15. https://doi.org/10.1016/j.cell.2018.04.013.

(183) Nakayama, R. T.; Pulice, J. L.; Valencia, A. M.; McBride, M. J.; McKenzie, Z. M.; Gillespie, M. A.; Ku, W. L.; Teng, M.; Cui, K.; Williams, R. T.; Cassel, S. H.; Qing, H.; Widmer, C. J.; Demetri, G. D.; Irizarry, R. A.; Zhao, K.; Ranish, J. A.;

Kadoch, C. SMARCB1 Is Required for Widespread BAF Complex–Mediated Activation of Enhancers and Bivalent Promoters. *Nature Genetics* **2017**, *49* (11), 1613–1623. https://doi.org/10.1038/ng.3958.

(184) Raab, J. R.; Resnick, S.; Magnuson, T. Genome-Wide Transcriptional Regulation Mediated by Biochemically Distinct SWI/SNF Complexes. *PLOS Genetics* **2015**, *11* (12), e1005748. https://doi.org/10.1371/journal.pgen.1005748.

(185) Lemon, B.; Inouye, C.; King, D. S.; Tjian, R. Selectivity of Chromatin-Remodelling Cofactors for Ligand-Activated Transcription. *Nature* **2001**, *414* (6866), 924–928. https://doi.org/10.1038/414924a.

(186) Belandia, B.; Orford, R. L.; Hurst, H. C.; Parker, M. G. Targeting of SWI/SNF Chromatin Remodelling Complexes to Estrogen-Responsive Genes. *The EMBO Journal* **2002**, *21* (15), 4094–4103. https://doi.org/10.1093/emboj/cdf412.

(187) Porter, E. G.; Dykhuizen, E. C. Individual Bromodomains of Polybromo-1 Contribute to Chromatin Association and Tumor Suppression in Clear Cell Renal Carcinoma. *Journal of Biological Chemistry* **2017**, *292* (7), 2601–2610. https://doi.org/10.1074/jbc.M116.746875.

(188) Bettinger, B. T.; Gilbert, D. M.; Amberg, D. C. Actin up in the Nucleus. *Nature Reviews Molecular Cell Biology* **2004**, *5* (5), 410–415. https://doi.org/10.1038/nrm1370.

(189) Brownlee, P. M.; Chambers, A. L.; Cloney, R.; Bianchi, A.; Downs, J. A. BAF180 Promotes Cohesion and Prevents Genome Instability and Aneuploidy. *Cell Rep* **2014**, *6* (6), 973–981. https://doi.org/10.1016/j.celrep.2014.02.012.

(190) Niimi, A.; Chambers, A. L.; Downs, J. A.; Lehmann, A. R. A Role for Chromatin Remodellers in Replication of Damaged DNA. *Nucleic Acids Res* **2012**, *40* (15), 7393–7403. https://doi.org/10.1093/nar/gks453.

(191) Niimi, A.; Hopkins, S. R.; Downs, J. A.; Masutani, C. The BAH Domain of BAF180 Is Required for PCNA Ubiquitination. *Mutat Res* **2015**, *779*, 16–23. https://doi.org/10.1016/j.mrfmmm.2015.06.006.

(192) Kakarougkas, A.; Ismail, A.; Chambers, A. L.; Riballo, E.; Herbert, A. D.; Künzel, J.; Löbrich, M.; Jeggo, P. A.; Downs, J. A. Requirement for PBAF in Transcriptional Repression and Repair at DNA Breaks in Actively Transcribed

Regions of Chromatin. *Molecular Cell* **2014**, *55* (5), 723–732. https://doi.org/10.1016/j.molcel.2014.06.028.

(193) Huang, X.; Gao, X.; Diaz-Trelles, R.; Ruiz-Lozano, P.; Wang, Z. Coronary Development Is Regulated by ATP-Dependent SWI/SNF Chromatin Remodeling Component BAF180. *Dev Biol* **2008**, *319* (2), 258–266. https://doi.org/10.1016/j.ydbio.2008.04.020.

(194) Avgustinova, A.; Benitah, S. A. The Epigenetics of Tumour Initiation: Cancer Stem Cells and Their Chromatin. *Current Opinion in Genetics & Development* **2016**, *36*, 8–15. https://doi.org/10.1016/j.gde.2016.01.003.

(195) Shain, A. H.; Pollack, J. R. The Spectrum of SWI/SNF Mutations, Ubiquitous in Human Cancers. *PLoS One* **2013**, *8* (1). https://doi.org/10.1371/journal.pone.0055119.

(196) Kadoch, C.; Hargreaves, D. C.; Hodges, C.; Elias, L.; Ho, L.; Ranish, J.; Crabtree, G. R. Proteomic and Bioinformatic Analysis of MSWI/SNF (BAF) Complexes Reveals Extensive Roles in Human Malignancy. *Nat Genet* **2013**, *45* (6), 592–601. https://doi.org/10.1038/ng.2628.

(197) Hodges, C.; Kirkland, J. G.; Crabtree, G. R. The Many Roles of BAF (MSWI/SNF) and PBAF Complexes in Cancer. *Cold Spring Harb Perspect Med* **2016**, *6* (8), a026930. https://doi.org/10.1101/cshperspect.a026930.

(198) Varela, I.; Tarpey, P.; Raine, K.; Huang, D.; Ong, C. K.; Stephens, P.; Davies, H.; Jones, D.; Lin, M.-L.; Teague, J.; Bignell, G.; Butler, A.; Cho, J.; Dalgliesh, G. L.; Galappaththige, D.; Greenman, C.; Hardy, C.; Jia, M.; Latimer, C.; Lau, K. W.; Marshall, J.; McLaren, S.; Menzies, A.; Mudie, L.; Stebbings, L.; Largaespada, D. A.; Wessels, L. F. A.; Richard, S.; Kahnoski, R. J.; Anema, J.; Tuveson, D. A.; Perez-Mancera, P. A.; Mustonen, V.; Fischer, A.; Adams, D. J.; Rust, A.; Chan-on, W.; Subimerb, C.; Dykema, K.; Furge, K.; Campbell, P. J.; Teh, B. T.; Stratton, M. R.; Futreal, P. A. Exome Sequencing Identifies Frequent Mutation of the SWI/SNF Complex Gene PBRM1 in Renal Carcinoma. *Nature* **2011**, *469* (7331), 539–542. https://doi.org/10.1038/nature09639.

(199) Ibragimova, I.; Maradeo, M. E.; Dulaimi, E.; Cairns, P. Aberrant Promoter Hypermethylation of PBRM1, BAP1, SETD2, KDM6A and Other Chromatin-Modifying Genes Is Absent or Rare in Clear Cell RCC. *Epigenetics* **2013**, *8* (5), 486–493. https://doi.org/10.4161/epi.24552.

(200) Creighton, C. J.; Morgan, M.; Gunaratne, P. H.; Wheeler, D. A.; Gibbs, R. A.; Gordon Robertson, A.; Chu, A.; Beroukhim, R.; Cibulskis, K.; Signoretti, S.; Vandin Hsin-Ta Wu, F.; Raphael, B. J.; Verhaak, R. G. W.; Tamboli, P.; Torres-Garcia, W.; Akbani, R.; Weinstein, J. N.; Reuter, V.; Hsieh, J. J.; Rose Brannon, A.; Ari Hakimi, A.; Jacobsen, A.; Ciriello, G.; Reva, B.; Ricketts, C. J.; Marston Linehan, W.; Stuart, J. M.; Kimryn Rathmell, W.; Shen, H.; Laird, P. W.; Muzny, D.; Davis, C.; Morgan, M.; Xi, L.; Chang, K.; Kakkar, N.; Treviño, L. R.; Benton, S.; Reid, J. G.; Morton, D.; Doddapaneni, H.; Han, Y.; Lewis, L.; Dinh, H.; Kovar, C.; Zhu, Y.; Santibanez, J.; Wang, M.; Hale, W.; Kalra, D.; Creighton, C. J.; Wheeler, D. A.; Gibbs, R. A.; Getz, G.; Cibulskis, K.; Lawrence, M. S.; Sougnez, C.; Carter, S. L.; Sivachenko, A.; Lichtenstein, L.; Stewart, C.; Voet, D.; Fisher, S.; Gabriel, S. B.; Lander, E.; Beroukhim, R.; Schumacher, S. E.; Tabak, B.; Saksena, G.; Onofrio, R. C.; Carter, S. L.; Cherniack, A. D.; Gentry, J.; Ardlie, K.; Sougnez, C.; Getz, G.; Gabriel, S. B.; Meyerson, M.; Gordon Robertson, A.; Chu, A.; Chun, H.-J. E.; Mungall, A. J.; Sipahimalani, P.; Stoll, D.; Ally, A.; Balasundaram, M.; Butterfield, Y. S. N.; Carlsen, R.; Carter, C.; Chuah, E.; Coope, R. J. N.; Dhalla, N.; Gorski, S.; Guin, R.; Hirst, C.; Hirst, M.; Holt, R. A.; Lebovitz, C.; Lee, D.; Li, H. I.; Mayo, M.; Moore, R. A.; Pleasance, E.; Plettner, P.; Schein, J. E.; Shafiei, A.; Slobodan, J. R.; Tam, A.; Thiessen, N.; Varhol, R. J.; Wye, N.; Zhao, Y.; Birol, I.; Jones, S. J. M.; Marra, M. A.; Auman, J. T.; Tan, D.; Jones, C. D.; Hoadley, K. A.; Mieczkowski, P. A.; Mose, L. E.; Jefferys, S. R.; Topal, M. D.; Liquori, C.; Turman, Y. J.; Shi, Y.; Waring, S.; Buda, E.; Walsh, J.; Wu, J.; Bodenheimer, T.; Hoyle, A. P.; Simons, J. V.; Soloway, M. G.; Balu, S.; Parker, J. S.; Neil Hayes, D.; Perou, C. M.; Kucherlapati, R.; Park, P.; Shen, H.; Triche Jr, T.; Weisenberger, D. J.; Lai, P. H.; Bootwalla, M. S.; Maglinte, D. T.; Mahurkar, S.; Berman, B. P.; Van Den Berg, D. J.; Cope, L.; Baylin, S. B.; Laird, P. W.; Creighton, C. J.; Wheeler, D. A.; Getz, G.; Noble, M. S.; DiCara, D.; Zhang, H.; Cho, J.; Heiman, D. I.; Gehlenborg, N.; Voet, D.; Mallard, W.; Lin, P.; Frazer, S.; Stojanov, P.; Liu, Y.; Zhou, L.; Kim, J.; Lawrence, M. S.; Chin, L.; Vandin, F.; Wu, H.-T.; Raphael, B. J.; Benz, C.; Yau, C.; Reynolds, S. M.; Shmulevich, I.; Verhaak, R. G. W.; Torres-Garcia, W.; Vegesna, R.; Kim, H.; Zhang, W.; Cogdell, D.; Jonasch, E.; Ding, Z.; Lu, Y.; Akbani, R.; Zhang, N.; Unruh, A. K.; Casasent, T. D.; Wakefield, C.; Tsavachidou, D.; Chin, L.; Mills, G. B.; Weinstein, J. N.; Jacobsen, A.; Rose Brannon, A.; Ciriello, G.; Schultz, N.; Ari Hakimi, A.; Reva, B.; Antipin, Y.; Gao, J.; Cerami, E.; Gross, B.; Arman Aksoy, B.; Sinha, R.; Weinhold, N.; Onur Sumer, S.; Taylor, B. S.; Shen, R.; Ostrovnaya, I.; Hsieh, J. J.; Berger, M. F.; Ladanyi, M.; Sander, C.; Fei, S. S.; Stout, A.; Spellman, P. T.; Rubin, D. L.; Liu, T. T.; Stuart, J. M.; Ng, S.; Paull, E. O.; Carlin, D.; Goldstein, T.; Waltman, P.; Ellrott, K.; Zhu, J.; Haussler, D.; Gunaratne, P. H.; Xiao, W.; Shelton, C.; Gardner, J.; Penny, R.; Sherman, M.; Mallery, D.; Morris, S.; Paulauskis, J.; Burnett, K.; Shelton, T.; Signoretti, S.; Kaelin, W. G.; Choueiri, T.; Atkins, M. B.; Penny, R.; Burnett, K.; Mallery, D.; Curley, E.; Tickoo, S.; Reuter, V.; Kimryn Rathmell, W.; Thorne, L.; Boice, L.; Huang, M.; Fisher, J. C.; Marston Linehan, W.; Vocke, C. D.; Peterson, J.; Worrell, R.; Merino, M. J.; The Cancer Genome Atlas Research Network; Analysis working group: Baylor College of Medicine; BC Cancer

Agency; Broad Institute; Brigham & Women's Hospital; Brown University; The University of Texas MD Anderson Cancer Center; Memorial Sloan-Kettering Cancer Center; National Cancer Institute; University of California Santa Cruz; University of North Carolina, C. H.; University of Southern California; Genome sequencing centres: Baylor College of Medicine; Genome characterization centres: Broad Institute; Harvard Medical School; University of Southern California & Johns Hopkins University; Genome data analysis: Baylor College of Medicine; Buck Institute for Research on Aging; Institute for Systems Biology; Oregon Health & Science University; Stanford University; University of Houston; Biospecimen core resource: International Genomics Consortium; Tissue source sites: Brigham & Women's Hospital; Dana-Farber Cancer Institute; Georgetown University; International Genomics Consortium; University of North Carolina at Chapel Hill. Comprehensive Molecular Characterization of Clear Cell Renal Cell Carcinoma. *Nature* **2013**, *499* (7456), 43–49. https://doi.org/10.1038/nature12222.

(201) Hopson, S.; Thompson, M. J. BAF180: Its Roles in DNA Repair and Consequences in Cancer. *ACS Chem. Biol.* **2017**, *12* (10), 2482–2490. https://doi.org/10.1021/acschembio.7b00541.

(202) Misumi, K.; Hayashi, A.; Shibahara, J.; Arita, J.; Sakamoto, Y.; Hasegawa, K.; Kokudo, N.; Fukayama, M. Intrahepatic Cholangiocarcinoma Frequently Shows Loss of BAP1 and PBRM1 Expression, and Demonstrates Specific Clinicopathological and Genetic Characteristics with BAP1 Loss. *Histopathology* **2017**, *70* (5), 766–774. https://doi.org/10.1111/his.13127.

(203) Churi, C. R.; Shroff, R.; Wang, Y.; Rashid, A.; Kang, H. C.; Weatherly, J.; Zuo, M.; Zinner, R.; Hong, D.; Meric-Bernstam, F.; Janku, F.; Crane, C. H.; Mishra, L.; Vauthey, J.-N.; Wolff, R. A.; Mills, G.; Javle, M. Mutation Profiling in Cholangiocarcinoma: Prognostic and Therapeutic Implications. *PLoS One* **2014**, *9* (12), e115383. https://doi.org/10.1371/journal.pone.0115383.

(204) Xia, W.; Nagase, S.; Montia, A. G.; Kalachikov, S. M.; Keniry, M.; Su, T.; Memeo, L.; Hibshoosh, H.; Parsons, R. BAF180 Is a Critical Regulator of P21 Induction and a Tumor Suppressor Mutated in Breast Cancer. *Cancer Res* **2008**, *68* (6), 1667–1674. https://doi.org/10.1158/0008-5472.CAN-07-5276.

(205) Mo, D.; Li, C.; Liang, J.; Shi, Q.; Su, N.; Luo, S.; Zeng, T.; Li, X. Low PBRM1 Identifies Tumor Progression and Poor Prognosis in Breast Cancer. *Int J Clin Exp Pathol* **2015**, *8* (8), 9307–9313.

(206) Huang, L.; Peng, Y.; Zhong, G.; Xie, W.; Dong, W.; Wang, B.; Chen, X.; Gu, P.; He, W.; Wu, S.; Lin, T.; Huang, J. PBRM1 Suppresses Bladder Cancer by Cyclin B1 Induced Cell Cycle Arrest. *Oncotarget* **2015**, *6* (18), 16366–16378.

(207) Borczuk, A. C.; Pei, J.; Taub, R. N.; Levy, B.; Nahum, O.; Chen, J.; Chen, K.; Testa, J. R. Genome-Wide Analysis of Abdominal and Pleural Malignant Mesothelioma with DNA Arrays Reveals Both Common and Distinct Regions of Copy Number Alteration. *Cancer Biol Ther* **2016**, *17* (3), 328–335. https://doi.org/10.1080/15384047.2016.1145850.

(208) Brownlee, P. M.; Chambers, A. L.; Oliver, A. W.; Downs, J. A. Cancer and the Bromodomains of BAF180. *Biochemical Society Transactions* **2012**, *40* (2), 364–369. https://doi.org/10.1042/BST20110754.

(209) Liao, L.; Alicea-Velázquez, N. L.; Langbein, L.; Niu, X.; Cai, W.; Cho, E.-A.; Zhang, M.; Greer, C. B.; Yan, Q.; Cosgrove, M. S.; Yang, H. High Affinity Binding of H3K14ac through Collaboration of Bromodomains 2, 4 and 5 Is Critical for the Molecular and Tumor Suppressor Functions of PBRM1. *Mol Oncol* **2019**, *13* (4), 811–828. https://doi.org/10.1002/1878-0261.12434.

(210) Barbieri, I.; Cannizzaro, E.; Dawson, M. A. Bromodomains as Therapeutic Targets in Cancer. *Brief Funct Genomics* **2013**, *12* (3), 219–230. https://doi.org/10.1093/bfgp/elt007.

(211) Fedorov, O.; Castex, J.; Tallant, C.; Owen, D. R.; Martin, S.; Aldeghi, M.; Monteiro, O.; Filippakopoulos, P.; Picaud, S.; Trzupek, J. D.; Gerstenberger, B. S.; Bountra, C.; Willmann, D.; Wells, C.; Philpott, M.; Rogers, C.; Biggin, P. C.; Brennan, P. E.; Bunnage, M. E.; Schüle, R.; Günther, T.; Knapp, S.; Müller, S. Selective Targeting of the BRG/PB1 Bromodomains Impairs Embryonic and Trophoblast Stem Cell Maintenance. *Science Advances* **2015**, *1* (10), e1500723. https://doi.org/10.1126/sciadv.1500723.

(212) Aldeghi, M.; Ross, G. A.; Bodkin, M. J.; Essex, J. W.; Knapp, S.; Biggin, P. C. Large-Scale Analysis of Water Stability in Bromodomain Binding Pockets with Grand Canonical Monte Carlo. *Communications Chemistry* **2018**, *1* (1), 1–12. https://doi.org/10.1038/s42004-018-0019-x.

(213) Gerstenberger, B. S.; Trzupek, J. D.; Tallant, C.; Fedorov, O.; Filippakopoulos, P.; Brennan, P. E.; Fedele, V.; Martin, S.; Picaud, S.; Rogers, C.; Parikh, M.; Taylor, A.; Samas, B.; O'Mahony, A.; Berg, E.; Pallares, G.; Torrey, A. D.; Treiber, D. K.;

Samardjiev, I. J.; Nasipak, B. T.; Padilla-Benavides, T.; Wu, Q.; Imbalzano, A. N.; Nickerson, J. A.; Bunnage, M. E.; Müller, S.; Knapp, S.; Owen, D. R. Identification of a Chemical Probe for Family VIII Bromodomains through Optimization of a Fragment Hit. *J. Med. Chem.* **2016**, *59* (10), 4800–4811. https://doi.org/10.1021/acs.jmedchem.6b00012.

(214) Sutherell, C. L.; Tallant, C.; Monteiro, O. P.; Yapp, C.; Fuchs, J. E.; Fedorov, O.; Siejka, P.; Müller, S.; Knapp, S.; Brenton, J. D.; Brennan, P. E.; Ley, S. V. Identification and Development of 2,3-Dihydropyrrolo[1,2-a]Quinazolin-5(1H)-One Inhibitors Targeting Bromodomains within the Switch/Sucrose Nonfermenting Complex. *J Med Chem* **2016**, *59* (10), 5095–5101. https://doi.org/10.1021/acs.jmedchem.5b01997.

(215) Myrianthopoulos, V.; Gaboriaud-Kolar, N.; Tallant, C.; Hall, M.-L.; Grigoriou, S.; Brownlee, P. M.; Fedorov, O.; Rogers, C.; Heidenreich, D.; Wanior, M.; Drosos, N.; Mexia, N.; Savitsky, P.; Bagratuni, T.; Kastritis, E.; Terpos, E.; Filippakopoulos, P.; Müller, S.; Skaltsounis, A.-L.; Downs, J. A.; Knapp, S.; Mikros, E. Discovery and Optimization of a Selective Ligand for the Switch/Sucrose Nonfermenting-Related Bromodomains of Polybromo Protein-1 by the Use of Virtual Screening and Hydration Analysis. *J. Med. Chem.* **2016**, *59* (19), 8787–8803. https://doi.org/10.1021/acs.jmedchem.6b00355.

(216) Albrecht, B.; Cote, A.; Crawford, T.; Duplessis, M.; Good, A.; Leblanc, Y.; Magnuson, S.; Nasveschuk, C.; Romero, F. A.; Tang, Y.; Taylor, A. Therapeutic Pyridazine Compounds and Uses Thereof. WO/2016/138114, September 1, 2016.

(217) Wanior, M.; Preuss, F.; Ni, X.; Krämer, A.; Mathea, S.; Göbel, T.; Heidenreich, D.; Simonyi, S.; Kahnt, A. S.; Joerger, A. C.; Knapp, S. Pan-SMARCA/PB1 Bromodomain Inhibitors and Their Role in Regulating Adipogenesis. *J. Med. Chem.* **2020**, *63* (23), 14680–14699. https://doi.org/10.1021/acs.jmedchem.0c01242.

(218) Brehm, A.; Längst, G.; Kehle, J.; Clapier, C. R.; Imhof, A.; Eberharter, A.; Müller, J.; Becker, P. B. DMi-2 and ISWI Chromatin Remodelling Factors Have Distinct Nucleosome Binding and Mobilization Properties. *EMBO J* **2000**, *19* (16), 4332–4341. https://doi.org/10.1093/emboj/19.16.4332.

(219) Georgel, P. T.; Tsukiyama, T.; Wu, C. Role of Histone Tails in Nucleosome Remodeling by Drosophila NURF. *EMBO J* **1997**, *16* (15), 4717–4726. https://doi.org/10.1093/emboj/16.15.4717.

(220) Hamiche, A.; Sandaltzopoulos, R.; Gdula, D. A.; Wu, C. ATP-Dependent Histone Octamer Sliding Mediated by the Chromatin Remodeling Complex NURF. *Cell* **1999**, *97* (7), 833–842. https://doi.org/10.1016/s0092-8674(00)80796-5.

(221) Alkhatib, S. G.; Landry, J. W. The Nucleosome Remodeling Factor. *FEBS Lett* **2011**, *585* (20), 3197–3207. https://doi.org/10.1016/j.febslet.2011.09.003.

(222) Mizuguchi, G.; Tsukiyama, T.; Wisniewski, J.; Wu, C. Role of Nucleosome Remodeling Factor NURF in Transcriptional Activation of Chromatin. *Molecular Cell* **1997**, *1* (1), 141–150. https://doi.org/10.1016/S1097-2765(00)80015-5.

(223) Barak, O.; Lazzaro, M. A.; Lane, W. S.; Speicher, D. W.; Picketts, D. J.; Shiekhattar, R. Isolation of Human NURF: A Regulator of Engrailed Gene Expression. *EMBO J* **2003**, *22* (22), 6089–6100. https://doi.org/10.1093/emboj/cdg582.

(224) Xiao, H.; Sandaltzopoulos, R.; Wang, H.-M.; Hamiche, A.; Ranallo, R.; Lee, K.-M.; Fu, D.; Wu, C. Dual Functions of Largest NURF Subunit NURF301 in Nucleosome Sliding and Transcription Factor Interactions. *Molecular Cell* **2001**, *8* (3), 531–543. https://doi.org/10.1016/S1097-2765(01)00345-8.

(225) Badenhorst, P.; Voas, M.; Rebay, I.; Wu, C. Biological Functions of the ISWI Chromatin Remodeling Complex NURF. *Genes Dev* **2002**, *16* (24), 3186–3198. https://doi.org/10.1101/gad.1032202.

(226) Landry, J.; Sharov, A. A.; Piao, Y.; Sharova, L. V.; Xiao, H.; Southon, E.; Matta, J.; Tessarollo, L.; Zhang, Y. E.; Ko, M. S. H.; Kuehn, M. R.; Yamaguchi, T. P.; Wu, C. Essential Role of Chromatin Remodeling Protein Bptf in Early Mouse Embryos and Embryonic Stem Cells. *PLoS Genet* **2008**, *4* (10). https://doi.org/10.1371/journal.pgen.1000241.

(227) Goller, T.; Vauti, F.; Ramasamy, S.; Arnold, H.-H. Transcriptional Regulator BPTF/FAC1 Is Essential for Trophoblast Differentiation during Early Mouse Development. *Mol Cell Biol* **2008**, *28* (22), 6819–6827. https://doi.org/10.1128/MCB.01058-08.

(228) Frey, W. D.; Chaudhry, A.; Slepicka, P. F.; Ouellette, A. M.; Kirberger, S. E.; Pomerantz, W. C. K.; Hannon, G. J.; Dos Santos, C. O. BPTF Maintains Chromatin Accessibility and the Self-Renewal Capacity of Mammary Gland Stem Cells. *Stem Cell Reports* **2017**, *9* (1), 23–31. https://doi.org/10.1016/j.stemcr.2017.04.031.

(229) Koludrovic, D.; Laurette, P.; Strub, T.; Keime, C.; Coz, M. L.; Coassolo, S.; Mengus, G.; Larue, L.; Davidson, I. Chromatin-Remodelling Complex NURF Is Essential for Differentiation of Adult Melanocyte Stem Cells. *PLOS Genetics* **2015**, *11* (10), e1005555. https://doi.org/10.1371/journal.pgen.1005555.

(230) Landry, J. W.; Banerjee, S.; Taylor, B.; Aplan, P. D.; Singer, A.; Wu, C. Chromatin Remodeling Complex NURF Regulates Thymocyte Maturation. *Genes Dev* **2011**, *25* (3), 275–286. https://doi.org/10.1101/gad.2007311.

(231) Wu, B.; Wang, Y.; Wang, C.; Wang, G. G.; Wu, J.; Wan, Y. Y. BPTF Is Essential for T Cell Homeostasis and Function. *The Journal of Immunology* **2016**, *197* (11), 4325–4333. https://doi.org/10.4049/jimmunol.1600642.

(232) Jones, M. H.; Hamana, N.; Shimane, M. Identification and Characterization of BPTF, a Novel Bromodomain Transcription Factor. *Genomics* **2000**, *63* (1), 35–39. https://doi.org/10.1006/geno.1999.6070.

(233) Jordan-Sciutto, K. L.; Dragich, J. M.; Caltagarone, J.; Hall, D. J.; Bowser, R. Fetal Alz-50 Clone 1 (FAC1) Protein Interacts with the Myc-Associated Zinc Finger Protein (ZF87/MAZ) and Alters Its Transcriptional Activity. *Biochemistry* **2000**, *39* (12), 3206–3215. https://doi.org/10.1021/bi992211q.

(234) Strachan, G. D.; Morgan, K. L.; Otis, L. L.; Caltagarone, J.; Gittis, A.; Bowser, R.; Jordan-Sciutto, K. L. Fetal Alz-50 Clone 1 Interacts with the Human Orthologue of the Kelch-like Ech-Associated Protein. *Biochemistry* **2004**, *43* (38), 12113–12122. https://doi.org/10.1021/bi0494166.

(235) Wysocka, J.; Swigut, T.; Xiao, H.; Milne, T. A.; Kwon, S. Y.; Landry, J.; Kauer, M.; Tackett, A. J.; Chait, B. T.; Badenhorst, P.; Wu, C.; Allis, C. D. A PHD Finger of NURF Couples Histone H3 Lysine 4 Trimethylation with Chromatin Remodelling. *Nature* **2006**, *442* (7098), 86–90. https://doi.org/10.1038/nature04815.

(236) Ruthenburg, A. J.; Li, H.; Milne, T. A.; Dewell, S.; McGinty, R. K.; Yuen, M.; Ueberheide, B.; Dou, Y.; Muir, T. W.; Patel, D. J.; Allis, C. D. Recognition of a Mononucleosomal Histone Modification Pattern by BPTF via Multivalent Interactions. *Cell* **2011**, *145* (5), 692–706. https://doi.org/10.1016/j.cell.2011.03.053.

(237) Stankiewicz, P.; Khan, T. N.; Szafranski, P.; Slattery, L.; Streff, H.; Vetrini, F.; Bernstein, J. A.; Brown, C. W.; Rosenfeld, J. A.; Rednam, S.; Scollon, S.; Bergstrom, K. L.; Parsons, D. W.; Plon, S. E.; Vieira, M. W.; Quaio, C. R. D. C.; Baratela, W. A.

R.; Acosta Guio, J. C.; Armstrong, R.; Mehta, S. G.; Rump, P.; Pfundt, R.; Lewandowski, R.; Fernandes, E. M.; Shinde, D. N.; Tang, S.; Hoyer, J.; Zweier, C.; Reis, A.; Bacino, C. A.; Xiao, R.; Breman, A. M.; Smith, J. L.; Katsanis, N.; Bostwick, B.; Popp, B.; Davis, E. E.; Yang, Y. Haploinsufficiency of the Chromatin Remodeler BPTF Causes Syndromic Developmental and Speech Delay, Postnatal Microcephaly, and Dysmorphic Features. *Am J Hum Genet* **2017**, *101* (4), 503–515. https://doi.org/10.1016/j.ajhg.2017.08.014.

(238) Bown, N.; Cotterill, S.; Lastowska, M.; O'Neill, S.; Pearson, A. D.; Plantaz, D.; Meddeb, M.; Danglot, G.; Brinkschmidt, C.; Christiansen, H.; Laureys, G.; Speleman, F.; Nicholson, J.; Bernheim, A.; Betts, D. R.; Vandesompele, J.; Van Roy, N. Gain of Chromosome Arm 17q and Adverse Outcome in Patients with Neuroblastoma. *N Engl J Med* **1999**, *340* (25), 1954–1961. https://doi.org/10.1056/NEJM199906243402504.

(239) Xiao, S.; Liu, L.; Lu, X.; Long, J.; Zhou, X.; Fang, M. The Prognostic Significance of Bromodomain PHD-Finger Transcription Factor in Colorectal Carcinoma and Association with Vimentin and E-Cadherin. *J Cancer Res Clin Oncol* **2015**, *141* (8), 1465–1474. https://doi.org/10.1007/s00432-015-1937-y.

(240) Dai, M.; Lu, J.-J.; Guo, W.; Yu, W.; Wang, Q.; Tang, R.; Tang, Z.; Xiao, Y.; Li, Z.; Sun, W.; Sun, X.; Qin, Y.; Huang, W.; Deng, W.; Wu, T. BPTF Promotes Tumor Growth and Predicts Poor Prognosis in Lung Adenocarcinomas. *Oncotarget* **2015**, *6* (32), 33878–33892.

(241) Dar, A. A.; Nosrati, M.; Bezrookove, V.; de Semir, D.; Majid, S.; Thummala, S.; Sun, V.; Tong, S.; Leong, S. P. L.; Minor, D.; Billings, P. R.; Soroceanu, L.; Debs, R.; Miller, J. R.; Sagebiel, R. W.; Kashani-Sabet, M. The Role of BPTF in Melanoma Progression and in Response to BRAF-Targeted Therapy. *J Natl Cancer Inst* **2015**, *107* (5). https://doi.org/10.1093/jnci/djv034.

(242) Dar, A. A.; Majid, S.; Bezrookove, V.; Phan, B.; Ursu, S.; Nosrati, M.; Semir, D. D.; Sagebiel, R. W.; Miller, J. R.; Debs, R.; Cleaver, J. E.; Kashani-Sabet, M. BPTF Transduces MITF-Driven Prosurvival Signals in Melanoma Cells. *PNAS* **2016**, *113* (22), 6254–6258. https://doi.org/10.1073/pnas.1606027113.

(243) Buganim, Y.; Goldstein, I.; Lipson, D.; Milyavsky, M.; Polak-Charcon, S.; Mardoukh, C.; Solomon, H.; Kalo, E.; Madar, S.; Brosh, R.; Perelman, M.; Navon, R.; Goldfinger, N.; Barshack, I.; Yakhini, Z.; Rotter, V. A Novel Translocation Breakpoint within the BPTF Gene Is Associated with a Pre-Malignant Phenotype. *PLOS ONE* **2010**, *5* (3), e9657. https://doi.org/10.1371/journal.pone.0009657.

(244) Xiao, S.; Liu, L.; Fang, M.; Zhou, X.; Peng, X.; Long, J.; Lu, X. BPTF Associated with EMT Indicates Negative Prognosis in Patients with Hepatocellular Carcinoma. *Dig Dis Sci* **2015**, *60* (4), 910–918. https://doi.org/10.1007/s10620-014-3411-0.

(245) Mayes, K.; Qiu, Z.; Alhazmi, A.; Landry, J. W. ATP-Dependent Chromatin Remodeling Complexes as Novel Targets for Cancer Therapy. *Adv Cancer Res* **2014**, *121*, 183–233. https://doi.org/10.1016/B978-0-12-800249-0.00005-6.

(246) Zhao, X.; Zheng, F.; Li, Y.; Hao, J.; Tang, Z.; Tian, C.; Yang, Q.; Zhu, T.; Diao, C.; Zhang, C.; Chen, M.; Hu, S.; Guo, P.; Zhang, L.; Liao, Y.; Yu, W.; Chen, M.; Zou, L.; Guo, W.; Deng, W. BPTF Promotes Hepatocellular Carcinoma Growth by Modulating HTERT Signaling and Cancer Stem Cell Traits. *Redox Biol* **2018**, *20*, 427–441. https://doi.org/10.1016/j.redox.2018.10.018.

(247) Richart, L.; Carrillo-de Santa Pau, E.; Río-Machín, A.; de Andrés, M. P.; Cigudosa, J. C.; Lobo, V. J. S.-A.; Real, F. X. BPTF Is Required for C-MYC Transcriptional Activity and in Vivo Tumorigenesis. *Nature Communications* **2016**, *7* (1), 10153. https://doi.org/10.1038/ncomms10153.

(248) Richart, L.; Real, F. X.; Lobo, V. J. S.-A. C-MYC Partners with BPTF in Human Cancer. *Molecular & Cellular Oncology* **2016**, *3* (3), e1152346. https://doi.org/10.1080/23723556.2016.1152346.

(249) Green, A. L.; DeSisto, J.; Flannery, P.; Lemma, R.; Knox, A.; Lemieux, M.; Sanford, B.; O'Rourke, R.; Ramkissoon, S.; Jones, K.; Perry, J.; Hui, X.; Moroze, E.; Balakrishnan, I.; O'Neill, A. F.; Dunn, K.; DeRyckere, D.; Danis, E.; Safadi, A.; Gilani, A.; Hubbell-Engler, B.; Nuss, Z.; Mulcahy Levy, J. M.; Serkova, N.; Venkataraman, S.; Graham, D. K.; Foreman, N.; Ligon, K.; Jones, K.; Kung, A.; Vibhakar, R. BPTF Regulates Growth of Adult and Pediatric High-Grade Glioma through the MYC Pathway. *Oncogene* **2020**, *39* (11), 2305–2327. https://doi.org/10.1038/s41388-019-1125-7.

(250) Zahid, H.; Olson, N. M.; Pomerantz, W. C. K. Opportunity Knocks for Uncovering the New Function of an Understudied Nucleosome Remodeling Complex Member, the Bromodomain PHD Finger Transcription Factor, BPTF. *Current Opinion in Chemical Biology* **2021**, *63*, 57–67. https://doi.org/10.1016/j.cbpa.2021.02.003.

(251) Mayes, K.; Alkhatib, S. G.; Peterson, K.; Alhazmi, A.; Song, C.; Chan, V.; Blevins, T.; Roberts, M.; Dumur, C. I.; Wang, X.-Y.; Landry, J. W. BPTF Depletion

Enhances T-Cell-Mediated Antitumor Immunity. *Cancer Res* **2016**, *76* (21), 6183–6192. https://doi.org/10.1158/0008-5472.CAN-15-3125.

(252) Mayes, K.; Elsayed, Z.; Alhazmi, A.; Waters, M.; Alkhatib, S. G.; Roberts, M.; Song, C.; Peterson, K.; Chan, V.; Ailaney, N.; Malapati, P.; Blevins, T.; Lisnić, B.; Dumur, C. I.; Landry, J. W. BPTF Inhibits NK Cell Activity and the Abundance of Natural Cytotoxicity Receptor Co-Ligands. *Oncotarget* **2017**, *8* (38), 64344–64357. https://doi.org/10.18632/oncotarget.17834.

(253) Cochran, A. G.; Conery, A. R.; Sims, R. J. Bromodomains: A New Target Class for Drug Development. *Nature Reviews Drug Discovery* **2019**, *18* (8), 609–628. https://doi.org/10.1038/s41573-019-0030-7.

(254) Vidler, L. R.; Brown, N.; Knapp, S.; Hoelder, S. Druggability Analysis and Structural Classification of Bromodomain Acetyl-Lysine Binding Sites. *J Med Chem* **2012**, *55* (17), 7346–7359. https://doi.org/10.1021/jm300346w.

(255) Urick, A. K.; Hawk, L. M. L.; Cassel, M. K.; Mishra, N. K.; Liu, S.; Adhikari, N.; Zhang, W.; dos Santos, C. O.; Hall, J. L.; Pomerantz, W. C. K. Dual Screening of BPTF and Brd4 Using Protein-Observed Fluorine NMR Uncovers New Bromodomain Probe Molecules. *ACS Chem Biol* **2015**, *10* (10), 2246–2256. https://doi.org/10.1021/acschembio.5b00483.

(256) Elkins, J. M.; Fedele, V.; Szklarz, M.; Abdul Azeez, K. R.; Salah, E.; Mikolajczyk, J.; Romanov, S.; Sepetov, N.; Huang, X.-P.; Roth, B. L.; Al Haj Zen, A.; Fourches, D.; Muratov, E.; Tropsha, A.; Morris, J.; Teicher, B. A.; Kunkel, M.; Polley, E.; Lackey, K. E.; Atkinson, F. L.; Overington, J. P.; Bamborough, P.; Müller, S.; Price, D. J.; Willson, T. M.; Drewry, D. H.; Knapp, S.; Zuercher, W. J. Comprehensive Characterization of the Published Kinase Inhibitor Set. *Nat Biotechnol* **2016**, *34* (1), 95–103. https://doi.org/10.1038/nbt.3374.

(257) Kirberger, S. E.; Ycas, P. D.; Johnson, J. A.; Chen, C.; Ciccone, M. F.; Woo, R. W. L.; Urick, A. K.; Zahid, H.; Shi, K.; Aihara, H.; McAllister, S. D.; Kashani-Sabet, M.; Shi, J.; Dickson, A.; Santos, C. O. dos; Pomerantz, W. C. K. Selectivity, Ligand Deconstruction, and Cellular Activity Analysis of a BPTF Bromodomain Inhibitor. *Org. Biomol. Chem.* **2019**, *17* (7), 2020–2027. https://doi.org/10.1039/C8OB02599A.

(258) Zhang, D.; Han, J.; Lu, W.; Lian, F.; Wang, J.; Lu, T.; Tao, H.; Xiao, S.; Zhang, F.; Liu, Y.-C.; Liu, R.; Zhang, N.; Jiang, H.; Chen, K.; Zhao, C.; Luo, C. Discovery of Alkoxy Benzamide Derivatives as Novel BPTF Bromodomain Inhibitors via Structure-

Based Virtual Screening. *Bioorg Chem* **2019**, *86*, 494–500. https://doi.org/10.1016/j.bioorg.2019.01.035.

(259) Xu, J.; Wang, Q.; Leung, E. L. H.; Li, Y.; Fan, X.; Wu, Q.; Yao, X.; Liu, L. Compound C620-0696, a New Potent Inhibitor Targeting BPTF, the Chromatin-Remodeling Factor in Non-Small-Cell Lung Cancer. *Front. Med.* **2020**, *14* (1), 60–67. https://doi.org/10.1007/s11684-019-0694-8.

(260) TP-238 https://www.thesgc.org/chemical-probes/TP-238 (accessed Mar 29, 2021).

(261) NVS-BPTF-1 https://www.thesgc.org/chemical-probes/NVS-BPTF-1 (accessed Mar 12, 2021).

(262) Xiong, L.; Mao, X.; Guo, Y.; Zhou, Y.; Chen, M.; Chen, P.; Yang, S.; Li, L. Discovery of Selective BPTF Bromodomain Inhibitors by Screening and Structure-Based Optimization. *Biochemical and Biophysical Research Communications* **2021**, *545*, 125–131. https://doi.org/10.1016/j.bbrc.2021.01.067.

(263) Clark, D. E. What Has Virtual Screening Ever Done for Drug Discovery? *Expert Opinion on Drug Discovery* **2008**, *3* (8), 841–851. https://doi.org/10.1517/17460441.3.8.841.

(264) Yan, X. C.; Sanders, J. M.; Gao, Y.-D.; Tudor, M.; Haidle, A. M.; Klein, D. J.; Converso, A.; Lesburg, C. A.; Zang, Y.; Wood, H. B. Augmenting Hit Identification by Virtual Screening Techniques in Small Molecule Drug Discovery. *J. Chem. Inf. Model.* **2020**, *60* (9), 4144–4152. https://doi.org/10.1021/acs.jcim.0c00113.

(265) Pagadala, N. S.; Syed, K.; Tuszynski, J. Software for Molecular Docking: A Review. *Biophys Rev* **2017**, *9* (2), 91–102. https://doi.org/10.1007/s12551-016-0247-1.

(266) Abagyan, R.; Totrov, M.; Kuznetsov, D. ICM—A New Method for Protein Modeling and Design: Applications to Docking and Structure Prediction from the Distorted Native Conformation. *Journal of Computational Chemistry* **1994**, *15* (5), 488–506. https://doi.org/10.1002/jcc.540150503.

(267) Halgren, T. A. Merck Molecular Force Field. V. Extension of MMFF94 Using Experimental Data, Additional Computational Data, and Empirical Rules. *Journal of Computational Chemistry* **1996**, *17* (5–6), 616–641.

https://doi.org/10.1002/(SICI)1096-987X(199604)17:5/6<616::AID-JCC5>3.0.CO;2-X.

(268) Molsoft L.L.C.: ICM Docking and Screening http://www.molsoft.com/docking.html (accessed Mar 31, 2021).

(269) Abagyan, R.; Totrov, M. Biased Probability Monte Carlo Conformational Searches and Electrostatic Calculations for Peptides and Proteins. *J Mol Biol* **1994**, *235* (3), 983–1002. https://doi.org/10.1006/jmbi.1994.1052.

(270) Metropolis, N.; Rosenbluth, A. W.; Rosenbluth, M. N.; Teller, A. H.; Teller, E. Equation of State Calculations by Fast Computing Machines. *The Journal of Chemical Physics* **1953**, *21* (6), 1087–1092. https://doi.org/10.1063/1.1699114.

(271) Chen, H.; Lyne, P. D.; Giordanetto, F.; Lovell, T.; Li, J. On Evaluating Molecular-Docking Methods for Pose Prediction and Enrichment Factors. *J. Chem. Inf. Model.* **2006**, *46* (1), 401–415. https://doi.org/10.1021/ci0503255.

(272) Cross, J. B.; Thompson, D. C.; Rai, B. K.; Baber, J. C.; Fan, K. Y.; Hu, Y.; Humblet, C. Comparison of Several Molecular Docking Programs: Pose Prediction and Virtual Screening Accuracy. *J. Chem. Inf. Model.* **2009**, *49* (6), 1455–1474. https://doi.org/10.1021/ci900056c.

(273) Bursulaya, B. D.; Totrov, M.; Abagyan, R.; Brooks, C. L. Comparative Study of Several Algorithms for Flexible Ligand Docking. *J Comput Aided Mol Des* **2003**, *17* (11), 755–763. https://doi.org/10.1023/b:jcam.0000017496.76572.6f.

(274) Friesner, R. A.; Banks, J. L.; Murphy, R. B.; Halgren, T. A.; Klicic, J. J.; Mainz, D. T.; Repasky, M. P.; Knoll, E. H.; Shelley, M.; Perry, J. K.; Shaw, D. E.; Francis, P.; Shenkin, P. S. Glide: A New Approach for Rapid, Accurate Docking and Scoring. 1. Method and Assessment of Docking Accuracy. *J Med Chem* **2004**, *47* (7), 1739–1749. https://doi.org/10.1021/jm0306430.

(275) Halgren, T. A.; Murphy, R. B.; Friesner, R. A.; Beard, H. S.; Frye, L. L.; Pollard, W. T.; Banks, J. L. Glide: A New Approach for Rapid, Accurate Docking and Scoring. 2. Enrichment Factors in Database Screening. *J Med Chem* **2004**, *47* (7), 1750–1759. https://doi.org/10.1021/jm030644s.

(276) Jorgensen, W. L.; Maxwell, D. S.; Tirado-Rives, J. Development and Testing of the OPLS All-Atom Force Field on Conformational Energetics and Properties of

Organic Liquids. *J. Am. Chem. Soc.* **1996**, *118* (45), 11225–11236. https://doi.org/10.1021/ja9621760.

(277) Eldridge, M. D.; Murray, C. W.; Auton, T. R.; Paolini, G. V.; Mee, R. P. Empirical Scoring Functions: I. The Development of a Fast Empirical Scoring Function to Estimate the Binding Affinity of Ligands in Receptor Complexes. *J Comput Aided Mol Des* **1997**, *11* (5), 425–445. https://doi.org/10.1023/a:1007996124545.

(278) Friesner, R. A.; Murphy, R. B.; Repasky, M. P.; Frye, L. L.; Greenwood, J. R.; Halgren, T. A.; Sanschagrin, P. C.; Mainz, D. T. Extra Precision Glide: Docking and Scoring Incorporating a Model of Hydrophobic Enclosure for Protein−Ligand Complexes. *J. Med. Chem.* **2006**, *49* (21), 6177–6196. https://doi.org/10.1021/jm051256o.

(279) Wang, L.; Wu, Y.; Deng, Y.; Kim, B.; Pierce, L.; Krilov, G.; Lupyan, D.; Robinson, S.; Dahlgren, M. K.; Greenwood, J.; Romero, D. L.; Masse, C.; Knight, J. L.; Steinbrecher, T.; Beuming, T.; Damm, W.; Harder, E.; Sherman, W.; Brewer, M.; Wester, R.; Murcko, M.; Frye, L.; Farid, R.; Lin, T.; Mobley, D. L.; Jorgensen, W. L.; Berne, B. J.; Friesner, R. A.; Abel, R. Accurate and Reliable Prediction of Relative Ligand Binding Potency in Prospective Drug Discovery by Way of a Modern Free-Energy Calculation Protocol and Force Field. *J. Am. Chem. Soc.* **2015**, *137* (7), 2695–2703. https://doi.org/10.1021/ja512751q.

(280) Schindler, C. E. M.; Baumann, H.; Blum, A.; Böse, D.; Buchstaller, H.-P.; Burgdorf, L.; Cappel, D.; Chekler, E.; Czodrowski, P.; Dorsch, D.; Eguida, M. K. I.; Follows, B.; Fuchß, T.; Grädler, U.; Gunera, J.; Johnson, T.; Jorand Lebrun, C.; Karra, S.; Klein, M.; Knehans, T.; Koetzner, L.; Krier, M.; Leiendecker, M.; Leuthner, B.; Li, L.; Mochalkin, I.; Musil, D.; Neagu, C.; Rippmann, F.; Schiemann, K.; Schulz, R.; Steinbrecher, T.; Tanzer, E.-M.; Unzue Lopez, A.; Viacava Follis, A.; Wegener, A.; Kuhn, D. Large-Scale Assessment of Binding Free Energy Calculations in Active Drug Discovery Projects. *J. Chem. Inf. Model.* **2020**, *60* (11), 5457–5474. https://doi.org/10.1021/acs.jcim.0c00900.

(281) *Free Energy Calculations: Theory and Applications in Chemistry and Biology*; Chipot, C., Pohorille, A., Eds.; Springer Series in Chemical Physics; Springer-Verlag: Berlin Heidelberg, 2007. https://doi.org/10.1007/978-3-540-38448-9.

(282) Zwanzig, R. W. High‐Temperature Equation of State by a Perturbation Method. I. Nonpolar Gases. *J. Chem. Phys.* **1954**, *22* (8), 1420–1426. https://doi.org/10.1063/1.1740409.

(283) Simplício, A. L.; Clancy, J. M.; Gilmer, J. F. Prodrugs for Amines. *Molecules* **2008**, *13* (3), 519–547. https://doi.org/10.3390/molecules13030519.